

**Computational studies on δ -branch G protein-coupled P2Y and
related orphan receptors**

Kumulative Dissertation

zur

Erlangung des Doktorgrades (Dr. rer. nat.)

der

Mathematisch-Naturwissenschaftlichen Fakultät

der

Rheinischen Friedrich-Wilhelms-Universität Bonn

vorgelegt von

Alexander Neumann

aus St. Roslawl

Bonn, 2023

Angefertigt mit Genehmigung der Mathematisch-Naturwissenschaftlichen Fakultät
der Rheinischen Friedrich-Wilhelms-Universität Bonn.

1. Gutachterin: Prof. Dr. Christa E. Müller

2. Gutachter: Prof. Dr. Finn Hansen

Tag der Promotion: 25.04.2023

Erscheinungsjahr: 2023

Contents

1. Overview	1
2. Introduction	4
2.1. G Protein-Coupled Receptors	4
2.2. Computer-Aided Drug Discovery.....	8
2.3. X-Ray Crystal Structures and Homology Modeling	11
2.4. Pharmacological Assessment	14
2.4.1. Intracellular Calcium Mobilization Assay	14
2.4.2. β -Arrestin Recruitment Assay	14
2.5. Mutagenesis Studies	15
2.6. Tool Compounds	16
3. P2Y₁-like Nucleotide Receptors - Structures, Molecular Modeling, Mutagenesis, and Oligomerization	19
3.1. Introduction	19
3.2. Publication.....	19
3.3. Summary and Outlook.....	52
4. Molecular Recognition of Agonists and Antagonists by the Nucleotide-Activated G Protein Coupled P2Y₂ Receptor	53
4.1. Introduction	53
4.2. Publication.....	53
4.3. Supporting Information	70
4.4. Summary and Outlook.....	81
5. Ligand Binding and Activation of UTP-Activated G Protein-Coupled P2Y₂ and P2Y₄ Receptors Elucidated by Mutagenesis, Pharmacological and Computational Studies	82
5.1. Introduction	82
5.2. Publication.....	82
5.3. Supporting Information	103

5.4. Summary and Outlook.....	118
6. Discovery of P2Y₂ Receptor Antagonist Scaffolds through Virtual High-Throughput Screening	119
6.1. Introduction	119
6.2. Publication.....	119
6.3. Supporting Information	132
6.4. Summary and Outlook.....	145
7. Development of Potent and Selective Antagonists for the UTP-Activated P2Y₄ Receptor	146
7.1. Introduction	146
7.2. Publication.....	146
7.3. Supporting Information	166
7.4. Summary and Outlook.....	167
8. Computational Investigations on the Binding Mode of Ligands for the Cannabinoid-Activated G Protein-Coupled Receptor GPR18	168
8.1. Introduction	168
8.2. Publication.....	168
8.3. Supporting Information	188
8.4. Summary and Outlook.....	201
9. Conclusions	202
10. Abbreviations.....	209
11. References	211
12. Acknowledgments	219
13. Curriculum Vitae	221
14. Publications.....	223
14.1. Research Publications.....	223
14.2. Reviews.....	223

14.3. Conference Presentations.....	224
15. Declaration (Eidesstattliche Erklärung).....	225

1. Overview

The human P2Y receptor (P2YR) family of G protein-coupled receptors (GPCRs) comprises eight subtypes which can be further subdivided into two groups: P2Y₁-like (P2Y₁, P2Y₂, P2Y₄, P2Y₆, P2Y₁₁) and P2Y₁₂-like (P2Y₁₂, P2Y₁₃, P2Y₁₄). These transmembrane-spanning receptors belonging to the δ -branch of rhodopsin-like GPCRs are ubiquitously expressed in the human body and are involved in a plethora of physiological processes and pathological conditions making them an attractive target for drug intervention. Endogenously, P2Y receptors are activated by mono- (ADP, ATP, UDP, UTP) and dinucleotides (e.g., Ap₄A), or by nucleotide sugars such as uridine 5'-diphosphoglucose. The presence of phosphate groups in the endogenous ligands poses an obstacle from a drug design perspective: At the physiological pH value of 7.4 phosphate groups are negatively charged which decreases oral bioavailability of the compounds and their analogues. Since the di- and triphosphate groups are important to form selective, high-quality interactions with the receptor, discovery of lead compounds for drug development lacking charged functionalities with favorable physicochemical and pharmacokinetic properties represents a major challenge.

The aim of this work was the elucidation of the three-dimensional architecture of P2Y and P2Y-related receptors and their complexes. Based on binding mode predictions from molecular docking studies of ligands at homology models of the receptors, structure-activity relationships (SARs) were investigated, and key interactions were identified through computational modeling supported by pharmacological assessment. The scientific process was reported in six publications – one extensive review and five primary research articles. After a general introduction (**Section 2**), each publication is presented in **Sections 3-8** accompanied by an outline of the individual findings.

The review “P2Y₁-like nucleotide receptors — Structures, molecular modeling, mutagenesis, and oligomerization” covered in **Section 3** of this work links findings from computer-aided drug discovery (CADD) approaches to in vitro assessment of P2YR subtype mutants with their respective agonists and antagonists. It introduces the P2YR family with respect to their degree of sequence similarity and their endogenous nucleotide ligands. The gathered information provides insights into the three-dimensional context between ligand binding and key interactions with the target as well as the hetero-oligomerization of different P2YRs altering their pharmacological profile.

These results will facilitate the understanding of P2YR architecture including their interaction hot-spots and that of other GPCRs.

The subject of **Section 4** is the investigation of ligand binding modes at the human P2Y₂R supported by mutagenesis studies. Endogenous nucleotide agonists and the P2Y₂-selective antagonist AR-C118925 were docked at an updated homology model of P2Y₂R. Based on the results, receptor mutants were created for pharmacological assessment. Complete loss of receptor activation by the endogenous agonist UTP or a significant decrease in potency confirmed the predicted involvement of those residues in the binding of the ligand hence defining the orthosteric binding site of P2Y₂R. This report contributed to the understanding of different nucleotide binding modes, namely of those with a pharmacological agonist or antagonist profile, at P2YRs and will therefore contribute to future drug development for those targets.

To further elucidate the binding mode of agonists and antagonists at purinergic GPCRs, two P2YR subtypes with the highest sequence similarity in the receptor family, namely P2Y₂- and P2Y₄Rs, were chosen for subsequent mutagenesis studies which are the subject of **Section 5**. Several key interactions between nucleotide agonists and anthraquinone antagonists were identified that are consistent with the proposed binding modes. Orthosteric and allosteric binding modes of anthraquinone-based antagonists were connected to the size of both receptors' binding pockets which will contribute to future design of selective compounds.

The collected findings on the binding mode of the selective P2Y₂R antagonist AR-C118925 are compiled for a virtual screening (VS) campaign "Discovery of P2Y₂ Receptor Antagonist Scaffolds through Virtual High-Throughput Screening" which is the subject of **Section 6**. 3.2 million molecules of the ZINC database were virtually screened and a selection of fifty-eight compounds has been purchased for pharmacological evaluation. The VS campaign led to the discovery of the first three novel drug-like scaffolds which represent perfect starting points for future drug development. The provided SAR and predicted binding modes can further be used for structure-guided ligand optimization.

Investigation of anthraquinone-based antagonists of the P2Y₄R subtype is presented in **Section 7**. An in-house synthesized library of anthraquinones related to the promiscuous compound Reactive Blue 2 (RB-2) was screened for their inhibition of

human P2Y₄R as well as other P2YR subtypes which led to the discovery of several selective and potent P2Y₄R antagonists with IC₅₀ values in the nanomolar range. The SARs are further elucidated with molecular docking studies of RB-2 and the most potent selective antagonists at the generated homology model of human P2Y₄R.

The subject of **Section 8** is the cannabinoid-activated orphan receptor GPR18. Given the interest of our group in the development of ligands and tool compounds for this scarcely investigated receptor, a homology model based on the human P2Y₁R and two other receptors was generated to investigate the binding mode of GPR18 ligands. Molecular docking studies followed by 200 ns molecular dynamics (MD) simulations of the apo-form and two different antagonist-bound complex revealed important interaction patterns that help stabilizing the inactive form of the target receptor. The collected and analyzed predictions on the binding mode of the highly lipophilic compounds represent a valuable framework for the design of selective compounds targeting the scarcely investigated GPR18.

Altogether, the findings of this work can be summarized as follows:

- i) Characterization of P2Y₁-like receptor structures including the identification of residues important for ligand recognition and binding
- ii) SAR elucidation of P2YR ligands and their respective binding modes by mutagenesis and molecular docking studies
- iii) Discovery of novel drug-like P2Y₂R antagonist scaffolds through a structure-based virtual screening campaign of 3.2 million compounds at a validated homology model
- iv) Tracing of interaction patterns in a highly lipophilic binding pocket between the P2YR-related GPCR GPR18 and its antagonists

This work will therefore contribute to the holistic understanding of these incredibly important drug targets and provide a groundwork for further development of future tool compounds for target validation studies and drug candidate design.

2. Introduction

2.1. G Protein-Coupled Receptors

GPCRs belong to one of the most investigated drug targets largely due to their ubiquitous expression in the human body and their central involvement with physiological processes.¹ They are activated by a plethora of chemically diverse endogenous ligands and transmit extracellular triggers to the intracellular lumen by several pathways. Most importantly, the accessibility of the exposed, druggable binding site allows intervention with their signaling by small molecules without the need of a difficult-to-achieve cell penetration. Their druggability has contributed to their popularity as a target class for therapeutic intervention which is reflected by the fact that around one-third of drugs approved by the Food and Drug Administration (FDA) act on GPCRs.²

The purine- and pyrimidine sensitive P2YR family belongs to the δ -branch of GPCRs and is part of a series of purinergic receptors activated by various nucleosides and nucleotides. The P1 receptors, a GPCR family consisting of four members (A_1 , A_{2A} , A_{2B} , A_3), are activated by adenosine and AMP, whereas the P2 receptors are responsive to purine and pyrimidine di- and triphosphates. P2 is subdivided into two groups: the seven-membered P2X (ligand-gated cation channels P2X1-7), and the P2Y group (GPCRs). The P2YR family consists of eight members: P2Y₁, P2Y₂, P2Y₄, P2Y₆ and P2Y₁₁ which belong to the P2Y₁-like group, and P2Y₁₂, P2Y₁₃, P2Y₁₄ that belong to the P2Y₁₂-like group.

One focus of this work is placed on two receptor subtypes of the P2Y₁-like group, namely P2Y₂- and P2Y₄Rs. While human P2Y₂R is endogenously activated by the nucleotides ATP and UTP, human P2Y₄R is only sensitive towards UTP and is antagonized by ATP. They are the closest related receptors in the P2YR family, sharing a sequence identity of 48%, and a sequence similarity of 61%.

While P2Y₂R is extensively expressed in the endocrine, immune, and reproductive systems, cardiac and skeletal muscle, lung, and proximal digestive tract, P2Y₄R was found to be expressed in brain, lung, heart, skin, and the gastrointestinal tract.³⁻⁵ The involvement of both receptors in pathological conditions identified them as a potential drug target for pharmaceutical intervention for the treatment of various diseases including cancer, inflammation, and neuro-degenerative diseases.⁵⁻⁸

Since the first reported observation of purinergic signaling evoking biological response in 1929 and the proposition of a distinct family of purinergic receptors in 1976, substantial research efforts have been directed at the development of compounds acting at purinergic receptors.⁹⁻¹¹ Although significant progress has been made for several receptors, only a moderate number of partially unselective ligands with unfavorable physicochemical properties for P2Y₂- and P2Y₄Rs has been reported.^{12,13}

A major subject of this work is the elucidation of differences in the conserved binding site responsible for the discrimination between the nucleotides ATP and UTP. Furthermore, computational prediction of novel antagonist scaffolds targeting P2Y₂R was performed, and a selection of compounds was assessed for their activity. The obtained insights will become a cornerstone for future design of selective drugs targeting those receptors.

Further focus of this work is put on another member of the δ -branch of GPCRs, human GPR18. To date, despite several attempts, no endogenous ligand was paired with this receptor, granting GPR18 the formal status of an 'orphan receptor'. In the past, resolvin D2 and *N*-arachidonoylglycine (NAGly) has been proposed as the endogenous ligands of GPR18.¹⁴⁻¹⁷ Unfortunately, other groups were not able to reproduce the activation of GPR18 in β -arrestin recruitment assays.¹⁸ Although GPR18 shares low sequence homology with the cannabinoid receptors CB₁ and CB₂, it displays overlapping pharmacology with them as they are all activated by the natural lipophilic cannabinoid Δ^9 -tetrahydrocannabinol (THC).

GPR18 is expressed in the gastrointestinal tract, testis, bone marrow, and the lymphoid tissues indicating involvement in immunomodulatory processes.^{15,19-24} Further, small molecules acting at GPR18 possess pharmaceutical relevance as drugs for the treatment of inflammation and cancer.²⁵⁻²⁸

However, rational drug design of GPR18 ligands is impeded as its mechanisms of activation and signaling are poorly understood. Knowledge about the binding of ligands and their interactions with the target would contribute to elucidation of essential features required to trigger the desired therapeutic outcome. In the present work, docking and MD studies were performed to study the behavior of known binders of GPR18. Since no X-ray crystal structure of human GPR18 is available, a homology model based on human P2Y₁R, murine μ -opioid receptor, and the zebrafish

lysophosphatidic acid receptor LPA6 as templated was generated. The preceding insights on putative binding sites of P2Y₂- and P2Y₄Rs and the architecture of GPCRs in general contributed to the assessment of the quality of the model and binding mode predictions.

Ligands of the receptors investigated in this work (P2Y₂R, P2Y₄R, GPR18) represent opposite extremes on the chemical spectrum: The nucleotides contain a triphosphate group which is exceptionally hydrophilic as it is negatively charged at the physiological pH. THC, on the other hand, is a highly lipophilic compound with only two heteroatoms which may engage in H-bond interactions. Therefore, it is very likely that protein binding of THC is driven by lipophilic interactions similar to the binding of other alkyl group containing compounds like retinol.²⁹ Structures of the discussed compounds are depicted in **Figure 1**.

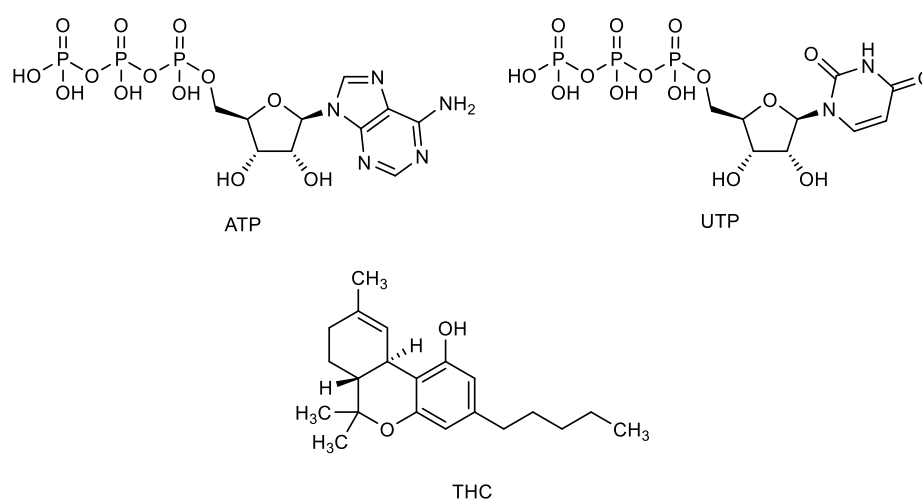


Figure 1. Structures of nucleotide triphosphates acting at human P2Y₂- and P2Y₄Rs, and Δ⁹-tetrahydrocannabinol (THC).

Both hydrophilic and lipophilic extremes represent a challenging task from a drug discovery and lead optimization perspective. Exogenously applied drugs containing negatively charged phosphate groups are incapable to permeate the phospholipid bilayer of cells resulting in poor bioavailability. Additionally, phosphate groups are prone to hydrolyzation by phosphatase enzymes leading to decreased stability of the molecules. Replacement of the phosphate chain with bioisosteric groups results in most cases in a decrease of potency due to the fact that proper geometric interaction of the oxygens with the amino acid residues of the target generally plays an important

role in the bioactivity of the compound.^{30,31} Hence, mimicry of phosphate groups has been one of the most challenging objectives in medicinal chemistry in the past decades without a general guideline for success.^{32,33} In contrast, compounds displaying high lipophilicity are accompanied by a range of parameters affecting the attractiveness of a compound, including membrane permeability, selectivity, solubility, and toxicity.^{34,35} Yet, compounds with high lipophilicity, such as THC and other lipophilic cannabinoids, can exhibit target promiscuity resulting in selectivity issues and adverse side effects.^{36,37}

For all those reasons, detailed insights and understanding of ligand binding modes are required for the design of novel tool compounds and drug candidates for these pharmaceutically relevant targets. The involvement of P2Y₂R, P2Y₄R and GPR18 in inflammation processes could provide the opportunity of future discovery of multitarget-directed ligands for the treatment of a high range of diseases.^{38–40}

2.2. Computer-Aided Drug Discovery

The advent of the information age has led to paradigm shifts in areas relying on innovation including the drug discovery process in pharmaceutical companies and research facilities around the world. The trial-and-error strategy has been steadily displaced by rational and decision-driven drug design as it is cost-efficient and resource-friendly whilst still providing high-quality information for fast follow-up.^{41,42} The ambitious goal to predict potent drug candidates before those are synthesized led to the emergence of a whole new field of technologies that have set themselves the task to support and accelerate the decision-making process during research and development.

Among those innovations, computer-aided drug discovery (CADD) is the area of data generation and processing aimed to support hit identification, compound evolution, prediction of physicochemical and pharmacological properties, and assessment of the pharmacokinetic fate of a drug after application, contributing to every phase of drug development.¹² Furthermore, CADD is widely used to predict potential development dead ends and toxicity issues ahead of time.^{43,44} CADD methods can be applied to prefilter molecule sets for metabolically instable substructures and compounds with a tendency to be identified as false positives from in vitro screens, the so-called pan-assay interference compounds (PAINS).

In general, CADD methods can be subdivided into two fields: structure-based drug discovery (SBDD) and ligand-based drug discovery (LBDD). While SBDD is applied to predict the orientation of a molecule within a 3D replication of the target (e.g., protein, DNA, RNA) to assess its interactions within the binding site, LBDD revolves around identifying bioactive molecules by relying on information about structures of known binders and non-binders agnostic of details to the target's architecture. Here, insights and knowledge resulting from both perspectives adds valuable information to the SAR between a ligand and its addressed target structure. Both aim to discuss and elucidate what key features of the molecules lead to its binding and effect at the target. The resulting information can be used to elaborate on possible structural modifications of the lead molecule to fine-tune compound parameters and properties during the optimization process.

The guiding questions during lead compound identification and optimization are how to differentiate active from inactive compounds and how to improve the properties of a lead structure. In order to address those, knowledge about a ligand's binding mode – the placement and orientation of the molecule at the target – is indispensable to make informed decisions.

Molecular docking is a CADD method that aims to predict the preferred orientation of a molecule at a (predefined) binding site of the target forming a stable complex with favorable interactions. The prediction is not limited to a particular molecule size as it can be used for the prediction of the binding mode of a single ion up to the docking of a whole macromolecule (e.g., protein, DNA, RNA) at another target structure.

This method is subsequently accompanied by the scoring of the complex which provides a quantitative numerical value assessing the quality of the formed interactions between target and docked molecule. In turn, this score value can be used to rank the so-called “poses”, different conformations of the molecule inside the binding site of the target, to detect the best docking predictions forming high-quality interactions. By transferring this premise to a set of different molecules, molecular docking with subsequent scoring can therefore be used to screen for compounds with the best interaction qualities with the target resulting in stable complexes for hit identification. This procedure of *in silico* screening of large molecule libraries usually containing hundred thousands to millions of individual entries named “virtual screening” (VS) can be applied to select a set of molecules that are likely to interact with the investigated target.⁴⁵ After docking and scoring, only the top-ranking percentage of molecules is examined for potential hit candidates to be synthesized or commercially acquired for *in vitro* confirmation as those are deemed to form favorable interactions within the target binding site. Its appeal of differentiating potentially active versus inactive chemotypes without the necessity of the physical possession of the samples makes VS a cost-efficient and valuable method for enrichment of interesting chemistry for follow up.

While standard high-throughput screening (HTS) campaigns usually deliver hit rates far less than 1%, VS can improve the rate up to 40% depending on the target class.^{46,47} To compensate for the poor hit rates, HTS requires the screening of million-sized compound collections to provide sufficient numbers of chemotypes as hits for the progression of drug discovery campaigns. The physical libraries come with prohibitive

costs involving the maintenance and acquisition of the molecules, and the execution of the screening assays. In order to save resources, smaller institutions and companies can therefore use VS to bypass the setup of in-house libraries by focusing on commercially available compounds. After performing the screening with virtual products, the best candidates can be cherry-picked providing control over the chemical diversity of the set. A smaller sample size usually in the range of fifty to a few hundred compounds is ordered from a chemical compound supplier and validated in vitro and/or in vivo assays.

It should be mentioned that although the scoring of a generated set of poses is a prerequisite for an objective processing of the data, it requires further assessment by medicinal and computational chemists. One of those is the validation of the docking protocol that is usually performed if the investigated structure contains a co-crystallized ligand. This ligand is redocked at the target and the generated poses are compared to the native X-ray complex. Under the premise that the best scoring pose should result in a congruent conformation with the investigated ligand, the root-mean-square deviation (RMSD) for the corresponding atom pairs of the native and predicted poses is calculated. For drug-like compounds RMSD values between 1 to 2 Å, depending on the size of the ligand and internal standards, are considered as adequate for docking protocol validation.⁴⁸

Furthermore, detailed assessment of the generated poses by visual inspection can be performed to compensate for inaccuracies and deficiencies of the docking method or modeling setup. This can be achieved by visually evaluating the complex of ligand and target including the binding pocket space occupation, shape complementarity, hydrogen bond network, interactions with key residues, intramolecular angle torsions, molecular overlap with known binders, conserved water molecules, and protonation state of the complex.⁴⁹ Usually this step is applied to detect poses that receive a too high estimation since the scoring function cannot include the above mentioned parameters into the numerical value based on quantification of the target-ligand interaction qualities.

Another challenge for the application of molecular docking is the conformational change of both ligand and target during the binding event. The revised concept of a “lock-and-key” model where the receptor remains rigid during ligand binding allows fast processing and generation of poses.^{50,51} Its successor, the induced-fit hypothesis, is

more compatible as it covers additional experimental observations e.g. allosteric modulation of target activity. The induced-fit hypothesis describes that upon binding of a molecule, both the target and the ligand adapt to each other and mutually undergo conformational changes.⁵² And although the induced-fit model is more universal, it comes with some challenges for molecular docking. Mainly, the consequence of investigating both the ligand, which is handled flexible per standard in most docking protocols, and the target requires additional computation and assessment. The procedure involves iteration cycles of ligand positioning and rearrangement of the target during the adaptation event. Sampling of possible side chain conformations and protein backbone can therefore easily result in a combinatorial explosion of calculations which requires extensive computing resources compared to docking of a flexible ligand at a rigid target.

In theory, all combinations of ligand and target being rigid/flexible possess a *raison d'être* depending on the investigated scenario. While semiflexible docking (target remains rigid, ligands handled as flexible) delivers better results for soluble targets with a high share of hydrophilic surface areas, full flexible docking (both target and ligands are flexible) is better suited for targets that undergo significant conformational changes during the ligand binding event like membrane-bound receptors and transporters.⁵³ Therefore, in regards to this work, the full flexible induced-fit docking (IFD) protocol was applied on a series of membrane-bound GPCRs to take the conformational flexibility of those receptors into account and to explore a broader range of possible binding modes of ligands.

Yet, although several progresses have been made in the past decades, *in silico* methods have not reached the level of satisfactorily predicting drug candidates based purely on calculations and therefore still have to rely on experimental *in vitro* and *in vivo* validation.

2.3. X-Ray Crystal Structures and Homology Modeling

One major obstacle for CADD remains the availability of elucidated target structures. Although huge advances have been made in the past decades, high-resolution X-ray crystal structures remain a luxury of the few. This is especially true for the class of GPCRs: As membrane-bound receptors they pose several challenges for crystallization efforts such as the high flexibility of their loop regions, presence of

several conformations beyond that of active and inactive states, dependency on the lipid environment and the presence of interacting proteins, and crystal sizes generated in a lipidic cubic phase matrix being too small for high-resolution structure determination even in modern microfocus synchrotron beamlines.^{54–57}

In the past years, advances in electron cryo-microscopy (cryo-EM) have led to the emergence of this method for the elucidation of GPCR structures. After the first determination of a GPCR structure by cryo-EM in 2017, a boom of GPCR structure elucidation was observed.^{58–60} Cryo-EM offers certain benefits compared to X-ray crystallography: It can be performed on proteins containing highly flexible regions eliminating the need of truncation of N- and/or C-terminal domains, and does not necessarily require structure stabilization by mutation or thermostabilization with fusion partners (e.g. apocytochrome b₅₆₂RIL, T4 lysozyme) allowing the determination of native wild type protein structures. As a result, the majority of the previously intractable GPCRs structures are nowadays solved by cryo-EM while X-ray crystallography takes the second place.⁵⁴

To date, six X-ray crystal structures of the P2YR family are available: two of P2Y₁R (PDB-IDs: 4XNV, 4XNW) and four of P2Y₁₂R (PDB-IDs: 4PY0, 4PXZ, 4NTJ, 7PP1).⁶¹ Therefore, structure-based investigation at other receptors without any structural information, including those in the focus of this work, namely P2Y₂- and P2Y₄Rs, and GPR18, requires a workaround to generate 3D models of target structures for further analysis. The application of computational methods to generate models based on template structures provides the so-called 'homology models' for this purpose if no target structure is available.

The two major premises of homology modeling (also known as 'comparative modeling') are (i) that the 3D structure of a macromolecule (e.g. protein) is determined by its amino acid sequence and (ii) the overall structure of a target class is evolutionary conserved leading to similar folding of related receptors sharing even low sequence similarity.^{62,63} The latter aspect is of particular interest as insights gained from molecular modeling of receptors in the same branch can provide valuable insights to common key features and architecture (e.g. P2Y₂R, P2Y₄R, and GPR18 belong to the δ -branch of GPCRs).

Prior to the homology modeling, the amino acid sequence of a protein of interest has to be aligned to one or more resolved template structure sequences. The sequence

similarity (percentage of amino acids sharing resemblance in their side chain features in the alignment) and sequence identity (percentage of amino acids with exact matching), as well as absence of alignment gaps in conserved regions (e.g., transmembrane regions), allow the evaluation of the quality of generated models. Several bioinformatic tools, such as Clustal Omega and Blast, are available to the public to perform multiple sequence alignment with the subsequent assessment of sequence similarity and identity.^{64–66}

For the sake of completeness, it should be mentioned that de novo generation of models without the need of a particular template structure, like in the case of homology modeling, represents an alternative to the abovementioned approach. Those neural network-based methods such as RoseTTAFold, and DeepMind's AlphaFold 1 and 2 which received broad media coverage in the past years, rely on deep learning algorithms to identify smaller features of a protein structure within a data set containing over 170,000 entries.^{67–70} The collected features are processed into data containing 3D information coupled to an amino acid sequence which can be used to predict the structure of a given protein sequence. To date, over two hundred million structures can be publicly accessed via the AlphaFold database (<https://alphafold.ebi.ac.uk/>) operated by DeepMind and EMBL's European Bioinformatics Institute (EMBL-EBI).

Although the de novo methods provide accurate models for protein classes with high coverage of solved structures, their prediction quality drops for those with less available data, such as highly flexible membrane-bound receptors and transporters, intrinsically disordered proteins, and multi-chain protein complexes.^{71,72} To put this into perspective: AlphaFold 2 was trained with over 170,000 protein structures of which only 370 represented determined GPCR structures in various conformations (less than 0.22%). Moreover, template-based homology modeling was described to outperform neural network-based methods especially in regards to the highly flexible loop regions which play a crucial role in ligand recognition of several GPCRs.⁷³

2.4. Pharmacological Assessment

As mentioned above, computational methods heavily rely on subsequent in vitro and/or in vivo validation of the results as a source for follow up. In the case of VS, the major goal is to predict small molecules which bind at the target of interest. After selection and acquisition of most promising candidates, the compounds are assessed in functional assays for their potency. Functional assays are used to investigate the ligand-mediated effects on a target structure by measuring changes in intracellular messenger concentration of signaling pathways, protein expression, ion flux, or enzyme activity. Two functional assays, calcium mobilization and β -arrestin recruitment assay, were applied in this work for pharmacological assessment of investigated ligands.

2.4.1. Intracellular Calcium Mobilization Assay

The activation of a G_q or G_i protein-coupled receptor leads to the dissociation of the G protein heterotrimer. The respective G_α and $G_{\beta\gamma}$ subunits separately modulate the activity of several enzymes and ion channels of their pathways. Upon dissociation, $G_{\beta\gamma}$ activates phospholipase C (PLC) which mediates the hydrolysis of PIP_2 (phosphatidylinositol 4,5-bisphosphate) to IP_3 (inositol 1,4,5-trisphosphate) and DAG (diacyl glycerol).⁷⁴ IP_3 , in turn, induces the release of intracellular Ca^{2+} from the endoplasmic reticulum into the cytosol through activation of IP_3 receptors.

The intracellular calcium mobilization assay is a cell-based second messenger assay based on complex formation of intracellular calcium with a calcium-sensitive fluorescent dye resulting in increased fluorescence intensity. Therefore, it is used to measure intracellular Ca^{2+} flux resulting from the activation of a GPCR by an agonist.⁷⁵

2.4.2. β -Arrestin Recruitment Assay

β -Arrestin belongs to the four-membered family of cytosolic arrestin proteins that are ubiquitously expressed in all cell types of vertebrates and participate in GPCR desensitization, signaling, and intracellular trafficking.^{76,77} Alongside the agonist-induced G protein mediated signaling, β -arrestin mediated signaling pathways act as multifunctional adaptors for many GPCRs. Since the β -arrestin activity is independent of the G-protein coupling of the receptor, β -arrestin recruitment assays became an essential tool in drug discovery, especially for cases where the G-protein coupling or

the endogenous ligand is unknown. Further, as agonist-induced activation of GPCRs can selectively trigger one of the two mentioned pathways leading to different pharmacological outcomes relevant for the treatment of a disease, β -arrestin recruitment assays can be used to screen for the so-called 'biased' ligands with the preferred pathway to avoid undesired effects associated with other pathways.⁷⁸

The functional β -arrestin recruitment assay employed in this work was developed based on galactosidase enzyme complementation technology from DiscoverX®.⁷⁹ In this setup, GPCR cell lines co-express two inactive β -galactosidase enzyme fragments: an enzyme acceptor (EA) tagged to β -arrestin (β -arrestin-EA), and an enzyme donor fragment, ProLink™ (PK), tagged to a GPCR (GPCR-PK). Agonist-induced receptor activation leads to the recruitment of β -arrestin-EA, resulting in the formation of a fully functional β -galactosidase by enzyme fragment complementation. The resulting active β -galactosidase hydrolyzes a substrate to generate a chemiluminescence signal that can be measured and quantified.

2.5. Mutagenesis Studies

The application of functional assays can be expanded to elucidate SARs of a protein-ligand complex and to identify important interactions in the binding site. Subsequently, it is a powerful tool to corroborate the binding mode and binding position of a ligand if no X-ray crystal structure of the complex is available.

During the ligand binding event conformational changes by both ligand and target structure take place which results in the formation of hydrophilic and lipophilic interactions in the binding site. The subsequent enthalpic and entropic effects determine the binding affinity of the ligand which can be quantified as a measurement for the strength of the binding interactions. In general, those interactions can be investigated in two ways: First, chemical modification of the ligand to explore the impacts of replacements, additions, or removals of molecule parts. Second, modification of the target binding site by site-directed mutagenesis where one or multiple residues are replaced. Both approaches aim to investigate the role of features in ligand binding and their contribution to the recognition and potency of the ligand.

A rational investigation of replacement at both the ligand and the target structure can provide valuable insights on interaction partners between the small molecule and the target structure. Given a proposed binding mode from docking studies where an

aromatic ring system of a ligand interacts with a phenylalanine in a binding subpocket, two scenarios can be pursued to investigate the coherence of the proposed binding mode: Systematic investigation of close analogs with varying aromatic and non-aromatic ring systems (e.g. exchange of a naphthyl group for an indolyl and cyclohexyl group, respectively), and the introduction of single point mutations (e.g. exchange of the phenylalanine residue for alanine, valine, and tyrosine, respectively). Changes in ligand potency in the stated scenarios would allow conclusions which of the interactions (lipophilic or aromatic) contributes to the overall binding affinity of the ligand. Ultimately, the results can support or dismiss the initial binding mode hypothesis.

Insights into the binding mode and SARs of a ligand are a crucial element for the compound optimization and potency improvement as they allow the design and prediction of improved candidates. Identified key interactions between receptor and ligands can additionally serve as a filter for VS campaigns in which vital pharmacophore features of a compound can be set as constraint for the directed generation of docking poses. The resulting conformations display the needed chemical functionalities shared by known binders, hence enriching the likelihood to discover hit molecules.^{80,81}

In the present work mutagenesis studies were applied to investigate the binding mode of ligands to gain insights on compound selectivity and location of the binding sites. Especially ligand recognition and binding site differences of the closely related P2Y₂- and P2Y₄Rs will provide valuable information for future discovery of selective drugs.

2.6. Tool Compounds

Selectivity of agonists and antagonists is important for studying the roles of drug targets in physiology and pathophysiology in target validation campaigns. Yet, as mentioned above, only few unselective agonists and antagonists acting at human P2Y₂- and P2Y₄Rs has been reported.

Anthraquinones were reported to promiscuously antagonize purinergic receptors, kinases, and endonucleotidases likely due to the negatively charged sulfonate groups imitating the phosphate chain of the endogenous nucleotide ligands.⁸² Likewise, polysulfonated anthraquinone derivatives face the same pharmacological and physicochemical problems as their agonist counterparts, namely poor bioavailability

and selectivity issues, which limits them to the scope of tool compounds. Derived from reactive blue 2 (RB-2) and suramin (see **Figure 2**), several potent P2Y₄R antagonists have been investigated in this work for their putative binding modes.

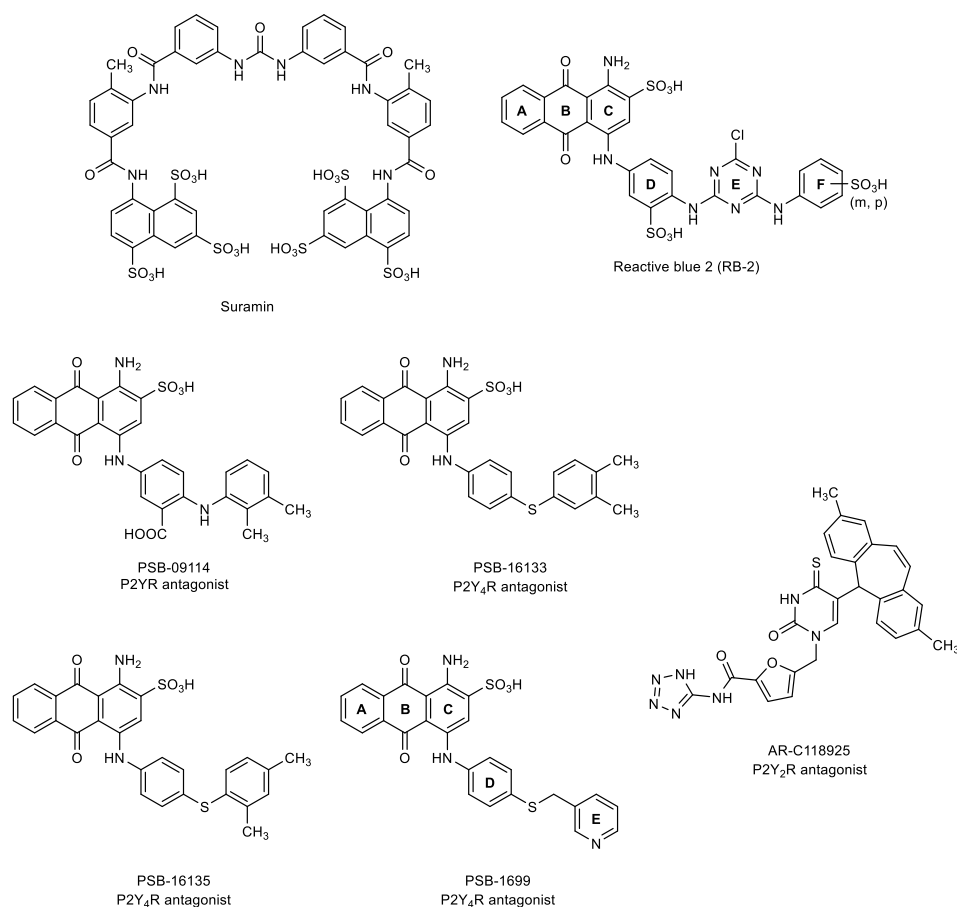


Figure 2. Structures of purinergic receptor antagonists.

AR-C118925 is a P2Y₂R selective antagonist which was developed by AstraZeneca.⁸² The endogenous ligands ATP and UTP were considered as starting points for the drug discovery campaign which can still be recognized in the thiouracil motif. Introduction of lipophilic substituents in position five of the uracil ring led to the shift from agonism to antagonism. The replacement of the ribose moiety by a chemically less complicated furan group, and the introduction of the tetrazole as a phosphate group bioisoster resulted in AR-C118925. Although AR-C118925 displayed good P2Y₂R selectivity over other purinergic receptors, the compound exhibited moderate permeability in Caco2 cell experiments which indicates poor oral bioavailability.⁸³

As for GPR18, synthetic imidazothiazinone derivatives were reported as antagonists.^{84,85} The scaffold emerged from a β -arrestin assay HTS campaign with THC as agonist. The subsequent optimization of the most potent hit molecule PSB-CB-5 lead to the development of the GPR18 selective antagonist PSB-CB-27 (see **Figure 3**).

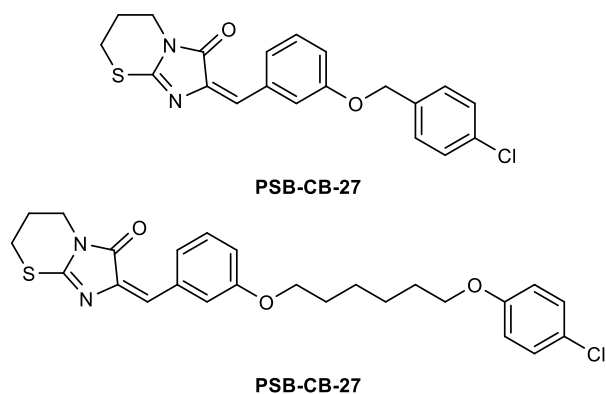


Figure 3. Structures of GPR18 antagonists.

Subsequently, the identification of an initial hit molecule requires optimization in order to increase the selectivity and/or affinity of the compound. Again, the prediction of promising molecule decorations or replacements can profit from structure-based approaches to enable rational strategies for compound evolution. Results of this work will therefore greatly contribute to the understanding of the targets' binding sites and aid in future projects aiming to discover and develop novel tool compounds and drug candidates to study and address the receptors.

3. P2Y₁-like Nucleotide Receptors - Structures, Molecular Modeling, Mutagenesis, and Oligomerization

3.1. Introduction

As initiative of this work to elucidate the binding mode of agonists and antagonists at P2YRs, available data on mutagenesis studies of P2Y₁-like receptors (P2Y_{1,2,4,6,11}) was collected and analyzed. This review provides a comprehensive overview on key residues involved in ligand binding and recognition, as well as the effects of mutants on ligand potency. Complementary sequence analysis contributed to the holistic understanding of the receptor architectures and conserved residues. Particular emphasis was put on agonistic and antagonistic nucleotide binding modes. A computational MD simulation study of P2Y₁R proposed the involvement of an ionic lock between an aspartic acid and an arginine residue in agonist-induced receptor activation.⁸⁶ Therefore, structural features in other P2YR subtypes were assessed for their capability to form analogous interactions as strategic targeting points for the design of drug candidates. Further, a breakdown on hetero-oligomerization of P2YRs with other GPCRs and P2YR subtypes was conducted to the obtain an overall picture on the complex pharmacology of those receptors.

3.2. Publication

OVERVIEW



WILEY

P2Y₁-like nucleotide receptors—Structures, molecular modeling, mutagenesis, and oligomerization

Alexander Neumann^{1,2} | Christa E. Müller^{1,2} | Vigneshwaran Namasivayam¹

¹Department of Pharmaceutical and Medicinal Chemistry, PharmaCenter Bonn, Pharmaceutical Institute, Pharmaceutical Sciences Bonn (PSB), University of Bonn, Bonn, Germany

²Research Training Group 1873, University of Bonn, Bonn, Germany

Correspondence

Vigneshwaran Namasivayam, Department of Pharmaceutical and Medicinal Chemistry, PharmaCenter Bonn, Pharmaceutical Institute, Pharmaceutical Sciences Bonn (PSB), University of Bonn, Bonn, Germany.
Email: vnamasiv@uni-bonn.de

Funding information

Deutsche Forschungsgemeinschaft, Grant/Award Number: Research Training Group 1873

Abstract

The P2Y receptors (P2YRs) are G protein-coupled receptors (GPCRs) consisting of eight members, subdivided into two groups, P2Y₁- and P2Y₁₂-like receptor subtypes. They are activated by extracellular nucleotides and represent current (P2Y₂, P2Y₁₂) or potential future drug targets. The chemical nature of the highly polar endogenous agonists represents a challenge in the discovery and design of potent and bioavailable compounds. A number of mutants and several homology models of P2YR subtypes have been created and updated on the basis of the recently published X-ray crystal structures of the human P2Y₁ and P2Y₁₂Rs. The models were used for prediction of the binding sites of agonists and antagonists, and mutants were constructed for confirmation. Pharmacological data on mutants published for the P2Y₁-like receptors (P2Y₁, P2Y₂, P2Y₄, P2Y₆, and P2Y₁₁R) were evaluated to analyze the role of specific amino acids and that of corresponding amino acid residues in related P2Y receptor subtypes. In several P2YR subtypes, an ionic lock between extracellular loop 2 and transmembrane region VII was postulated to be essential for agonist-induced receptor activation. Mutagenesis and homology modeling data suggest that the nucleotide antagonist (1'*R*,2'*S*,4'*S*,5'*S*)-4-(2-iodo-6-methylaminopurin-9-yl)-1-[(phosphato)methyl]-2-(phosphato)bicyclo[3.1.0]hexane (MRS2500), which was co-crystallized with the human P2Y₁R, binds differently from agonistic nucleotides to a site partly overlapping with that of orthosteric agonists. Hetero-oligomerization of P2YRs with other P2YR subtypes or other GPCRs may allosterically modulate receptor-ligand interactions and/or G protein coupling. The collected information will contribute to the understanding of the architecture of P2Y₁-like nucleotide receptors and will consequently be useful for the design of novel agonists and antagonists.

This article is categorized under:

Molecular and Statistical Mechanics > Free Energy Methods

Structure and Mechanism > Computational Biochemistry and Biophysics

Molecular and Statistical Mechanics > Molecular Interactions

This is an open access article under the terms of the Creative Commons Attribution-NonCommercial-NoDerivs License, which permits use and distribution in any medium, provided the original work is properly cited, the use is non-commercial and no modifications or adaptations are made.

© 2020 Rheinische Friedrich-Wilhelms-Universität Bonn. *WIREs Computational Molecular Science* published by Wiley Periodicals, Inc.

Software > Molecular Modeling

KEYWORDS

GPCRs, molecular modeling, mutagenesis, P2Y receptors

1 | INTRODUCTION

G protein-coupled receptors (GPCRs) are cell surface receptors that are involved in physiological functions and pathological processes. Therefore, they can be easily accessed by modulators and represent important targets for drug therapy. GPCRs contain seven transmembrane-spanning α -helices. The N-terminus is exposed towards the extracellular space, while the C-terminus is located in the intracellular lumen with three loops each connecting the α -helices intracellularly (ICL1-3) and extracellularly (ECL1-3). GPCRs can be subdivided into six classes: A (rhodopsin-like, the largest family), B (secretin-like), C (glutamate), D (fungal mating pheromone receptors), E (cyclic AMP receptors), and F (frizzled).¹⁻⁴ Several GPCRs from the A and B families contain an eighth α -helix in the C-terminus.^{5,6} Class A GPCRs can further be subdivided into four branches: α , β , γ , and δ .^{7,8} The α -branch includes five subgroups: prostaglandin, amine, opsin, melatonin, and adenosine receptors. The β -branch includes receptors which recognize and bind peptides. The γ -branch comprises the SOG (somatostatin, opioid, and galanin), the MCH (melanin-concentrating hormone), and chemokine receptors. The δ -branch consists of four sub-branches which contains Mas-related (receptors related to the MAS1 proto-oncogene), glycoprotein, olfactory as well as many orphan receptors. The purinergic receptor family is classified into P1 receptors activated by adenosine (α -branch), and P2 receptors activated by nucleotides. The P2 receptors are further subdivided into ATP-gated ionotropic P2X receptors (P2XR) and the δ -class metabotropic G protein-coupled P2Y receptors (P2YRs). P2XRs are ion channels permeable for Na^+ , K^+ , and Ca^{2+} ions.^{9,10} Seven different subunits exist (P2X1-P2X7) which form homo- or heterotrimeric channels. Based on their sequence similarity and G-protein selectivity, the human P2YRs are grouped into two families: the G_q protein-coupled “P2Y₁-like” receptors (P2Y₁, P2Y₂, P2Y₄, P2Y₆, and P2Y₁₁) and the G_i protein-coupled “P2Y₁₂-like” receptors (P2Y₁₂, P2Y₁₃, and P2Y₁₄).

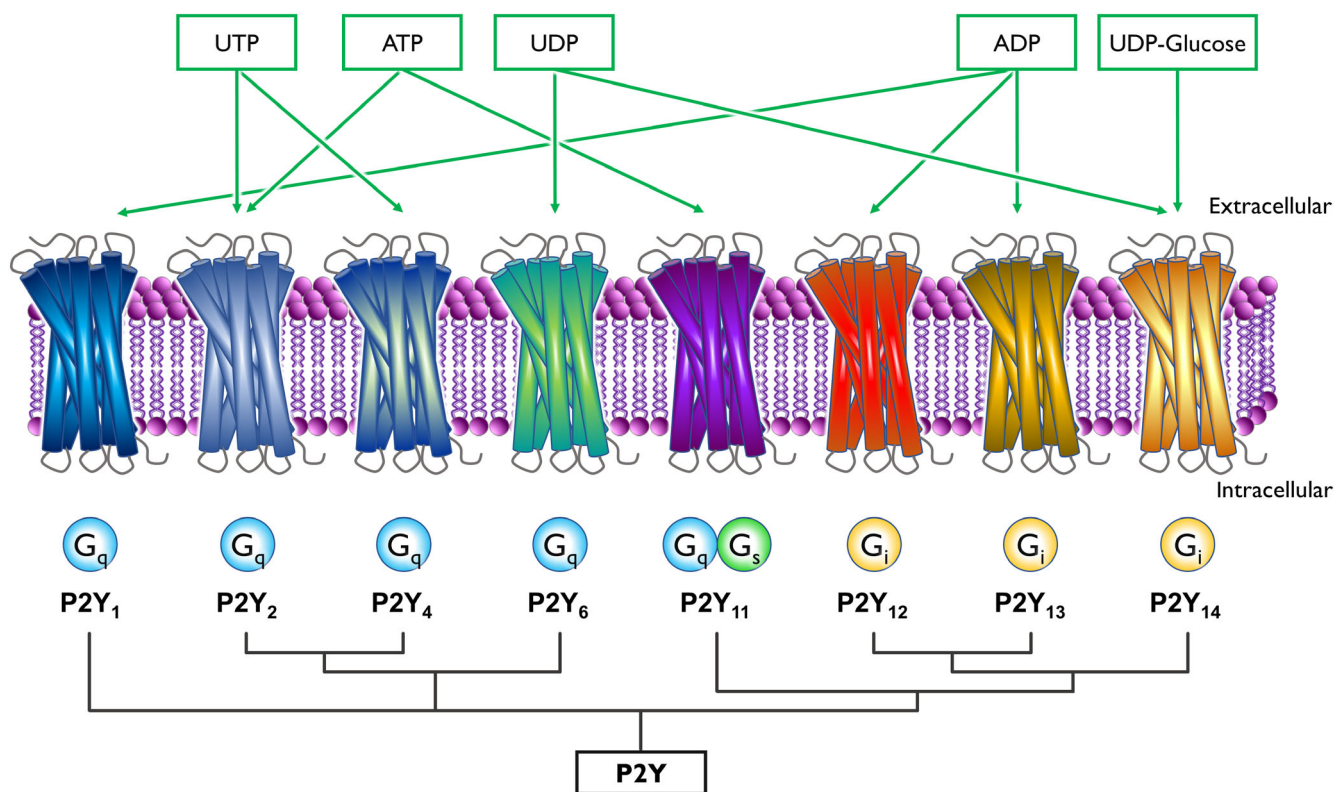


FIGURE 1 Schematic presentation of P2YRs embedded in a phospholipid bilayer and their preferred endogenous agonists. A phylogenetic tree shows the degree of their relationship. The endogenous agonists activating the respective receptor at physiologically relevant concentrations and the G protein coupling are shown at the top. Phylogenetic analysis was generated using Clustal Omega¹¹⁻¹³

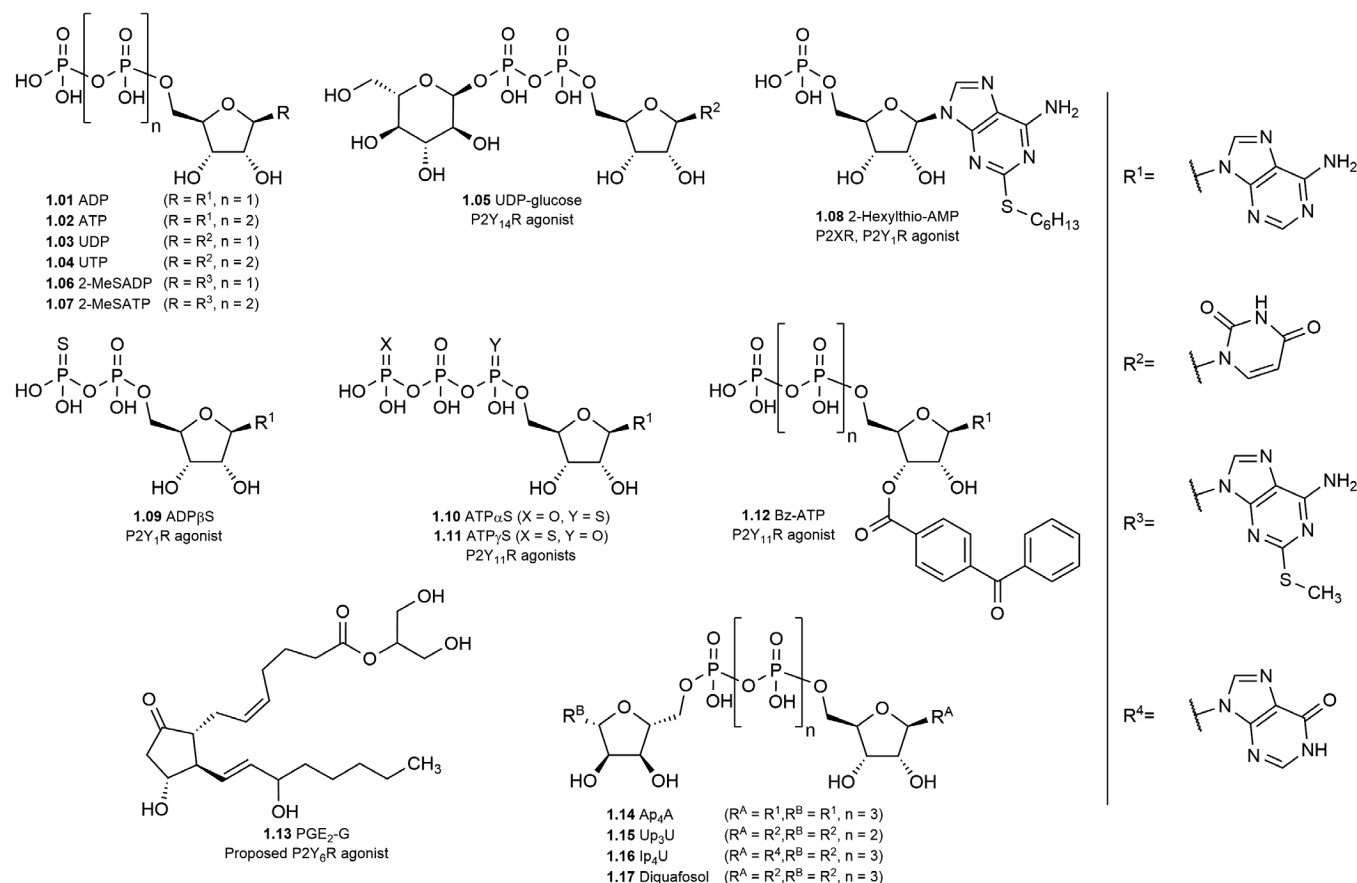


FIGURE 2 Structures of selected (proposed) P2Y receptor agonists

receptors (P2Y₁₂, P2Y₁₃, and P2Y₁₄) (see Figure 1).^{14,15} The P2Y₁₁R couples additionally to G_s proteins besides its ability to activate G_q proteins. P2Y₁, P2Y₁₂, and P2Y₁₃Rs are activated by ADP (**1.01**, for structures see Figure 2) but not by ATP (**1.02**) at physiologically relevant concentrations, whereas the uracil nucleotide UDP (**1.03**) is an endogenous agonist of the P2Y₆R. The P2Y₂R is sensitive toward both nucleotides, ATP and UTP (**1.04**). The human P2Y₄R is activated by UTP. UDP-glucose (**1.05**), as well other UDP-sugars including UDP-galactose, UDP-glucuronic acid, UDP-*N*-acetylglucosamine, and UDP itself were reported to act as physiological P2Y₁₄R agonists.^{16,17} P2YRs contain four conserved cysteine residues, one each in the N-terminus, in helix III, in the ECL2, and in helix VII. Most often they form two disulfide bridges, one between helix III and ECL2, and another one between the N-terminus and helix VII. Similarities between members of class A GPCRs include an NSxxNPxxY motif (where x represents any amino acid) in transmembrane region (TM) VII and a DRY or D(E)RY(F) motif at the intracellularly orientated end of TMIII.

Agonists of the P2Y₁-like receptors (**1.01–1.17**) are shown in Figure 2, structures of P2Y₁-like receptor antagonists (**2.01–2.15**) in Figures 3 and 4, and P2Y₁₂R antagonists (**3.01–3.05**) and adenosine receptor ligands (**4.01–4.03**) in Figure 5.

P2Y₁-like receptors are currently in the focus as novel drug targets, in particular for inflammatory-related conditions including neurodegenerative diseases.¹⁵ The P2Y₂R agonist diquafosol (**1.17**) is approved for the treatment of dry eye disease in Japan and other Asian countries including Korea, Thailand, and Vietnam.¹⁸ The P2Y₁₂R is blocked by anti-thrombotic drugs such as ticagrelor (**3.01**), cangrelor (**3.02**), clopidogrel (**3.03**), and prasugrel (**3.04**) (see Figure 5 for structures). However, there is still a lack of selective, bioavailable ligands suitable for target validation studies of several P2YR subtypes, which limits drug development.¹⁹ The recently published X-Ray crystal structures of the P2Y₁R and the P2Y₁₂R provide a solid basis for computer-aided approaches towards rational ligand design and drug discovery.^{20,21} For P2Y₁, P2Y₂, and P2Y₁₁Rs a considerable number of mutagenesis studies has been published, which are useful for predicting the orthosteric binding site. However, only a few studies on P2Y₄ and P2Y₆R mutants have been reported. Therefore, it will be useful to investigate if the results obtained for one subtype could be translated to corresponding residues in other P2YRs. This review article summarizes and evaluates mutagenesis studies of P2Y₁-like receptors with regard to residues presumably interacting with receptor agonists. It combines computational chemistry and mutagenesis approaches for predicting the three-dimensional structure of the receptors.

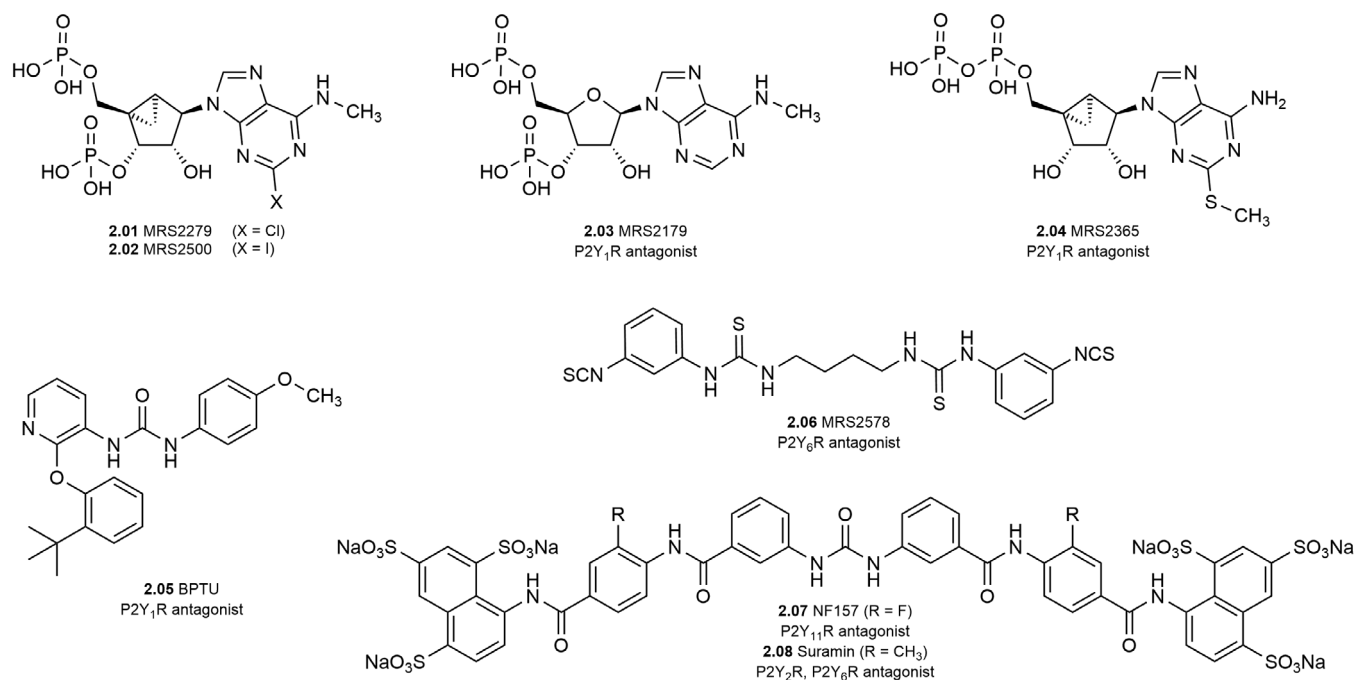


FIGURE 3 Structures of selected P2YR antagonists

2 | MUTANTS OF THE HUMAN P2Y₁-LIKE RECEPTORS

Rational drug design makes use of various methods and tools, including pharmacophore modeling, homology modeling, molecular dynamics (MD) simulations, and docking studies. Mutagenesis (see Box 1) is a powerful tool to modify single or multiple amino acid residues or to construct chimeric receptors. Subsequent testing of the amino acid residues' role and function provides valuable insights. These studies are typically based on multiple sequence alignment of the receptor of interest preferably with related structures to determine conserved and non-conserved residues. Sequence alignment of the five P2Y₁-like receptors is presented in Figure 6. Highly conserved residues often play a role in

BOX 1 MUTAGENESIS

Mutagenesis describes the process of gene information altering and can be subdivided into two groups: random and directed mutagenesis. Random mutagenesis occurs naturally or can be enforced by exposure to mutagens (e.g., UV-light, ionizing radiation, chemicals, and viruses). In contrast, the directed methods involve the substitution, insertion, deletion, or addition of a single mutation or whole sequences at a specific site, or a combination of those with the purpose of creating a gene with desired properties. Site-directed mutagenesis therefore became a commonly used investigative tool in the field of protein function studies and drug design. Docking studies on X-ray crystal structures or homology models allow predictions of the ligand binding mode at a desired target but require validation by pharmacological data. Here, gene alteration can be used to engineer proteins with single or multiple amino acid changes. Through exchange of the side chain functionality (lipophilic, hydrophilic, charged, aromatic, ...) of the amino acids, predicted interactions between the ligand and the protein can be confirmed or discarded. An example is the prediction of a ligand containing a phenyl moiety binding in a lipophilic cavity at a target protein. The mutation of a phenylalanine in the cavity to valine decreases the potency of the ligand, while no such effect is observed if the phenylalanine is mutated to tyrosine. This observation may imply that π - π interactions between the phenyl moiety of the ligand and the protein are important for its activity. The knowledge of key interactions and the spatial environment in the ligand binding site is indispensable for rational drug design and ligand optimization to minimize time and material costs.

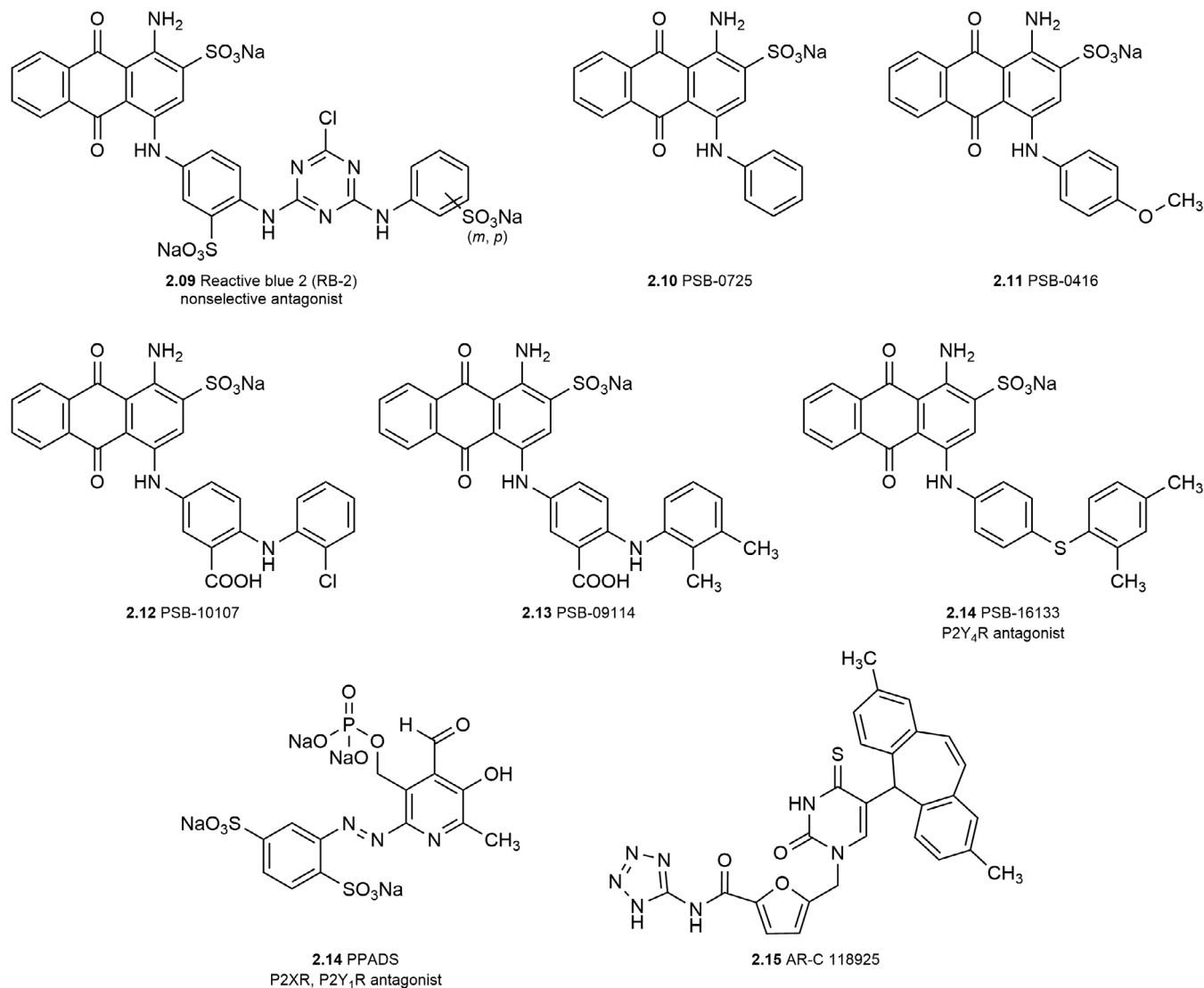


FIGURE 4 Structures of selected P2YR antagonists

receptor function, targeting of those in mutagenesis studies has been a successful approach for identifying key residues responsible for agonist-induced receptor activation. Small changes in the binding site or modification of extracellular residues important for initial ligand binding can be crucial for ligand specificity.

To rationalize the effects of a mutation on the receptor-ligand interaction, 3D models are helpful visualization tools which can be utilized for explaining structure-activity relationships (SARs).^{22,23} With the publication of the X-ray crystal structure of bovine rhodopsin, the first GPCR X-Ray crystal structure had become available as a template for generating homology models of other GPCR structures including P2YRs.²⁴ Subsequent publications of X-Ray crystal structures of GPCRs with higher sequence identity and similarity to P2YRs, including the β_1 -adrenergic receptor (α -branch of rhodopsin-like receptors), the adenosine A_{2A} receptor (α -branch), and, finally, the P2Y₁ and P2Y₁₂Rs belonging to the P2YR family of the δ -branch of class A GPCRs, provided more closely related crystal structures as templates for homology modeling.^{25–29} Refinement of the models, based on newly published mutagenesis data, crystal structures, and MD simulations led to improved models, which can be extended to the further applications including virtual screening and SAR studies.

2.1 | P2Y₁R mutants

Several single point mutations, truncations, and chimeric receptors have been reported for the P2Y₁R. Mutations and their effects on agonist and antagonist potency, as well as residues important for protein-protein interactions are

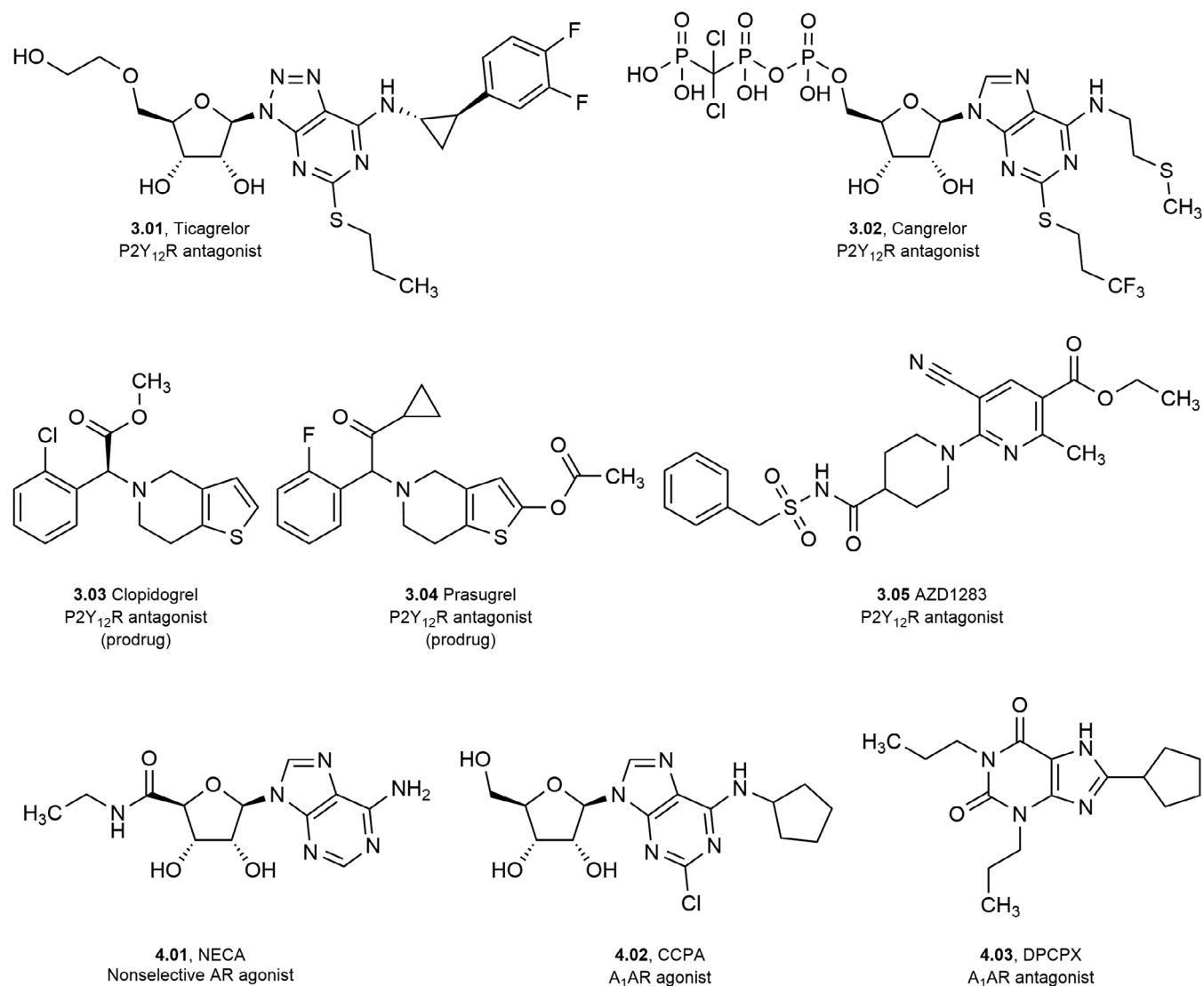


FIGURE 5 Structures of selected P2Y₁₂R antagonists and A₁AR agonists and antagonists

summarized in Figure 7. In the following chapters, we will use the 3-letter amino acid code for specific residues, the 1-letter code for mutants, and the full names for general amino acid annotations.

2.1.1 | Ligand recognition

Jacobson et al. were one of the first research groups who performed mutagenesis studies on the human P2Y₁R to identify residues participating in agonist-induced receptor activation.³⁰ Based on a molecular modeling study and sequence alignment of P2YRs with other GPCR sequences, 16 receptor mutants (15 single residue mutants and 1 double mutant) were created and EC₅₀ values of three agonists, 2-MeSADP (**1.06**), 2-MeSATP (**1.07**), and 2-hexylthio-AMP (**1.08**), were determined. The mutations R128A, R310A, and S314A as well as the double mutation R310S_S314R led to a complete abolishment of receptor activation by the three selected agonists. Among them, for the agonist 2-MeSATP a high impact (>100-fold decrease) was observed for the mutants K280A, Q307A, R310K, a moderate impact (>10-fold decrease) for H132A, Y136A, T221A, T222A, H277A and a low impact (<10-fold decrease) for F131A, F226A, S314T, and S317A. Comparable results were observed for the other two agonists, 2-MeSADP and 2-hexylthio-AMP. The role of Arg310 was further investigated by switching the amino acid residues between Arg310 and Ser314, due to hydrophilic interactions with the residues. The constructed double mutant R310S_S314R failed to restore receptor activity, indicating that the

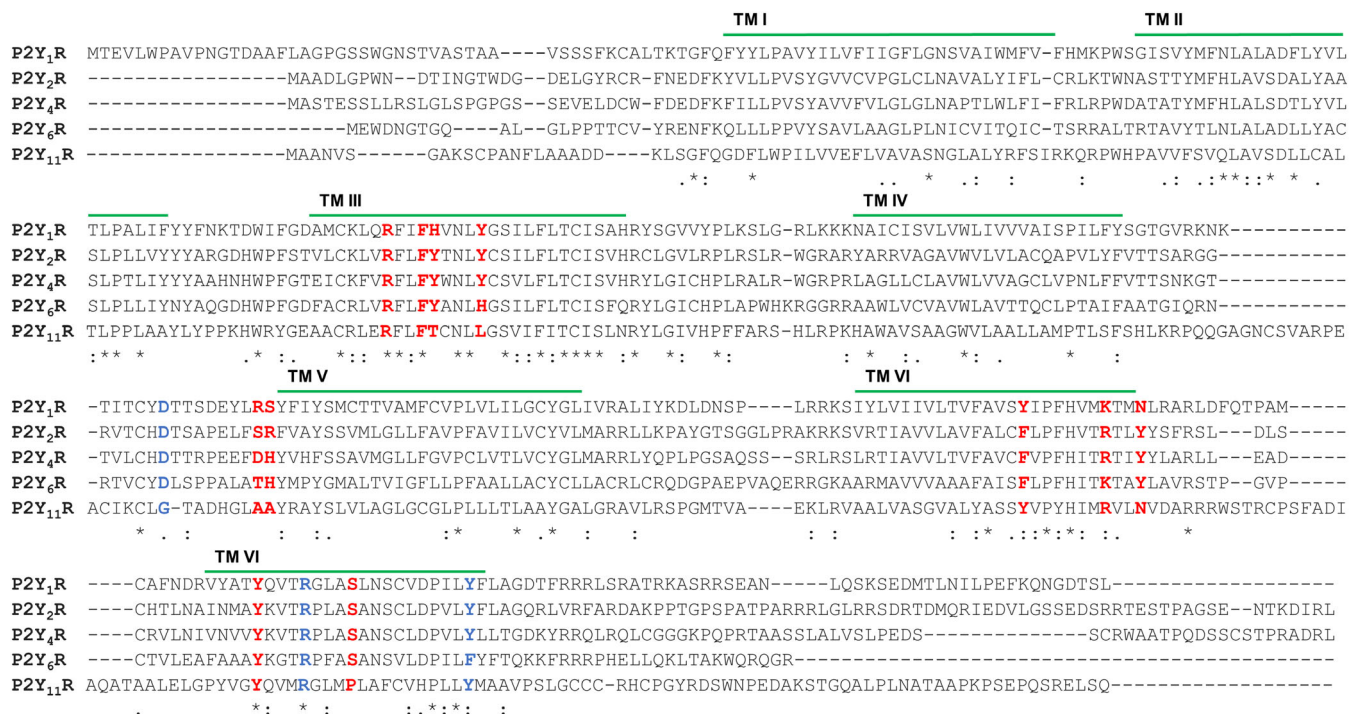


FIGURE 6 Sequence alignment of the human P2Y₁-like receptor subtypes. Residues important for agonist-induced receptor activation predicted by MD simulations are highlighted in blue. Amino acid residues mutated in more than one receptor subtype are highlighted in red. Multiple sequence alignment was generated using Clustal Omega. MD, molecular dynamics

conformation of Arg310 plays a key role in receptor function. Nucleoside diphosphates were typically 5- to 10-fold more potent than the corresponding triphosphates. 2-MeSADP was found to be around 400 times more potent than 2-hexylthio-AMP. The results suggested that several charged amino acids (His132, Lys280, His277, and Arg310) may interact with the phosphate chain of the agonists.

Out of the 15 mutants constructed by Jacobson et al., 11 mutants were further investigated for their effects on the potencies of agonists and antagonists and to support the molecular modeling studies.³¹ Similar results were obtained: K280A, Q307A, and R310K mutations resulted in a high decrease in potency (over 100-fold) for 2-MeSADP. F131A, H132A, Y136A, T222A, F226A, H277A, and S314T led to a moderate decrease (5- to 60-fold) in potency. The T221A and the S317A mutations had virtually no effect on the potency of 2-MeSADP. Additionally, modulatory effects of mutations toward recognition of the antagonist MRS2179 (**2.03**) were observed: the H132A, Y136A, and T222A mutation led to a two- to three-fold reduction in antagonist potency and therefore appeared to have a modulatory role in recognition of the antagonist **2.03**. Substitution of Ser314 with threonine reduced the affinity of the antagonist, indicating specific steric requirements for antagonist binding. Two extracellular disulfide bridges were confirmed to be essential for receptor activation and receptor membrane trafficking: one between Cys42 (N-terminus) and Cys296 (ECL2), and the second one between Cys124 (ECL1) and Cys202 (ECL2).³² Mutations of the cysteine residues (C42A, C124A, C202A, C296A) resulted in receptors which were no longer activated by agonists. Thus, the disulfide bridges are essential for stable receptor conformation and functionality. Asp204 is likely to be involved in the activation of the P2Y₁R, whereupon Glu209 and Arg287 are probably participating in the ligand recognition process. Since Asp204 is not likely to interact with the phosphate chain of the nucleotide agonist but rather plays a role in receptor activation, interactions with other residues are feasible. A large decrease in potency of 2-MeSADP and 2-MeSATP was observed upon mutation of further residues of the extracellular loop regions (D204A/N/E, E209A, R287A/K/Q/E). The double mutants E209R_R287E and E209A_R287A led to an almost complete lack of response even at high agonist concentrations (up to 100 μM). Moderate effects were determined for the mutants R195A, K196A, K198A, D208A, E209D/Q/R R212A (ECL2), and R285A, D289A, D300A, R301A (ECL3).

Systematic analysis of multiple sequence alignments of the P2Y receptors, and first homology modeling-aided analysis attempts based on the bovine rhodopsin X-ray crystal structure led to the creation of several additional mutants which were further investigated by Costanzi et al.³³ A high impact on agonist potency was observed for the single

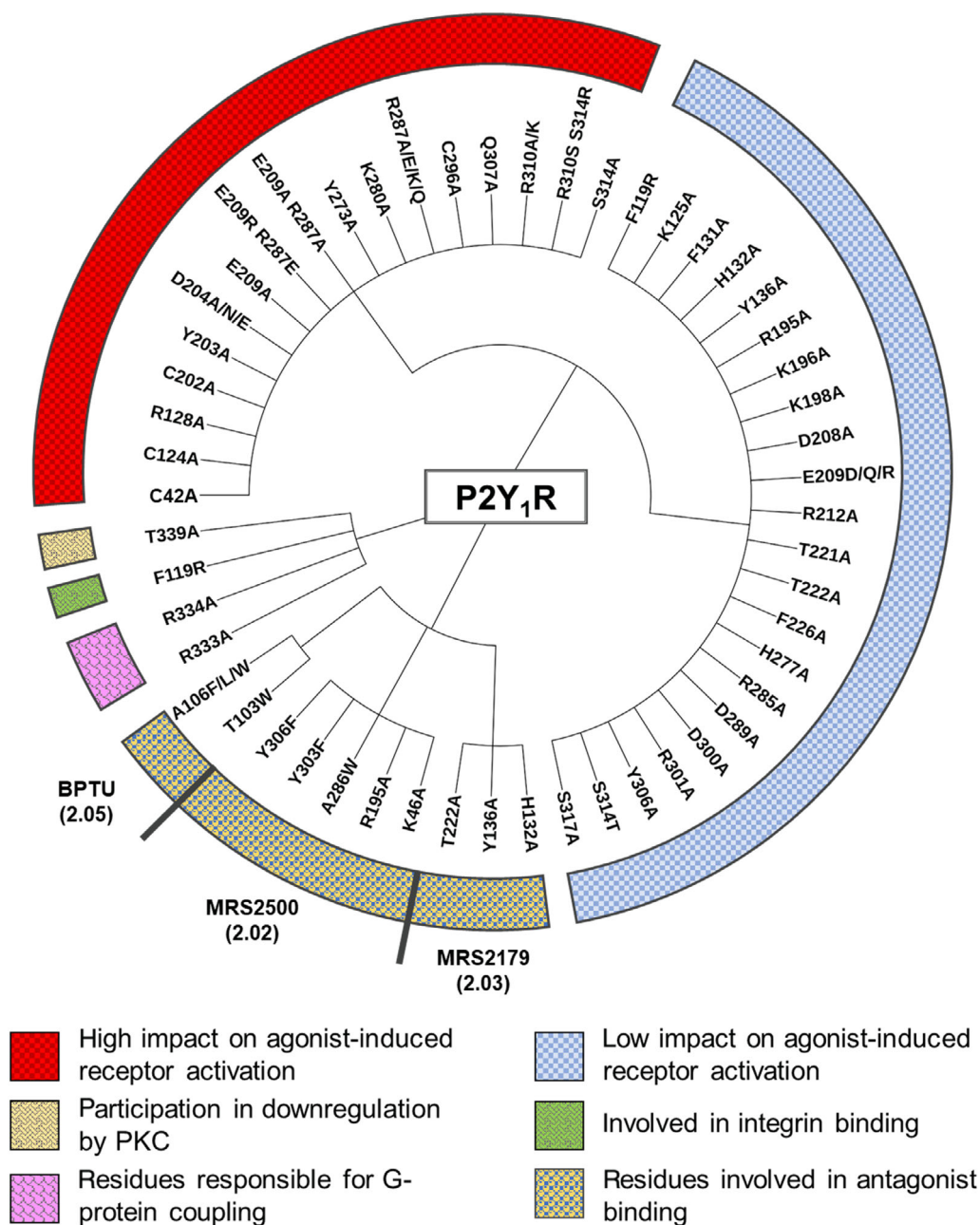


FIGURE 7 Schematic diagram of available mutagenesis data of the human P2Y₁R, and effects of mutations on agonist and antagonist potencies. High impact was defined as at least 10-fold change in the potency of the agonist. Changes below a 10-fold difference in potency of the agonist were defined as low impact

mutations R128A, R310A, S314A, C124A, C202A, E209A, and R287A/E resulting in a complete loss of receptor activation. The mutants K280A, Q307A, R310K, D204N/E, R287Q, H277A, and C296A showed a significant decrease in potency (80- to 4,000-fold). Comparatively low effects (less than five-fold change) on the potency of 2-MeSADP was observed for F131A, H132A, Y136A, T221A, T222A, F226A, S314T, S317A, K125A, R195A, K196A, K198A, D204A, D208A, E209D, E209Q, E209R, R212A, R287K, D289A, D300A, and R301A, respectively. The potency of the agonist 2-MeSADP and that of the antagonist MRS2578 (**2.06**) were additionally studied on mutants of Tyr203, Tyr273, and Tyr306. A dramatic loss of 2-MeSADP-induced receptor activation was observed for the single mutants Y203A and Y273A, whereas the Y273A mutation had no major effect on the binding affinity of either the agonist 2-MeSADP or the antagonist **2.06** as determined by radioligand binding versus the antagonist radioligand [³H]MRS2279 (**2.01**). Thus, Tyr273 might play a key role in receptor activation. No significant changes were observed regarding the inhibitory potency of antagonist **2.06**.

In the publication of the P2Y₁R X-ray crystal structures, Zhang et al. reported on additional structure-guided mutagenesis of residues which were interacting with the co-crystallized antagonists MRS2500 (**2.02**) and BPTU (**2.05**).²³ The single mutants K46A, R195A, A286W, Y303F, and Y306F resulted in a more than 10-fold decrease in potency of the antagonist **2.02**, which binds close to the orthosteric site, but no effect was observed on the potency of the allosteric antagonists BPTU, that binds at the periphery of the receptor close to the lipid membrane. A significant decrease (over 50-fold) in BPTU potency was found for the single mutation of amino acid residues present in TMII (T103W, A106W, A106F, and A106L). Contrary, the mutations in TMII had no impact on the potency of the agonist 2-MeSADP and nucleotide antagonist, **2.02**. The single mutants K46A, R195A, A286W, Y303F, and Y306F had diverse effects on the potency of the agonist 2-MeSADP and the nucleotide antagonist **2.02**. Significant decrease in the potency of antagonist **2.02** was determined for these mutants and only minor effects on the potency of 2-MeSADP were observed. These results indicated different binding interactions for the agonist 2-MeSADP as compared to the antagonist **2.02**. A cavity close to the orthosteric binding site most likely accommodates a phosphate group of **2.02**. Further analysis is presented in the section “Molecular modelling of P2Y₁-like receptors.”

Guo et al. performed mutagenesis on residues likely participating in agonist-induced receptor activation. While only moderate decreases in the potency of 2-MeSADP could be observed for the F131A, F226A, and K280R single mutants, over 100-fold decreases in potency were observed for the H132A, H277A, K280A, Q307A, and R310K mutants.³⁴

2.1.2 | C-Terminus

The truncation of the C-terminus (Δ Thr330-Leu373) of the P2Y₁R resulted in a complete loss of inositol phosphate generation and Ca²⁺ mobilization, indicating that it was required for G_q protein activation.³⁵ In a study performed by Ding et al., the domain between Arg340 and Leu373 showed no participation in G_q coupling of the P2Y₁R. The C-terminus of the P2Y₁R was reported to regulate the inactivation gating of the transient inward (T_{in}) ion channel studied in oocytes through the interaction of the region Arg340-Leu359 with the channel.³⁶ The amino acid residues exchanged in the double mutant R333A_R334A are located in the BBXXB (B representing basic amino acid residues and X any non-basic amino acid residue) motif of the C-terminus, that is commonly involved in G_q coupling. This double mutant displayed a similar behavior regarding inositol phosphate generation and Ca²⁺ mobilization as the truncated P2Y₁R receptor, indicating key roles for Arg333 and Arg334 in G_q protein-coupling.

In another study, Fam et al. investigated the role of threonine and serine residues in the C-terminus regarding their role in the receptor downregulation by protein kinase C (PKC).³⁷ The truncation of the predicted C-terminus at or beyond Leu335 resulted in no functional receptor expression. Ca²⁺ responses were not suppressed by the PKC activator phorbol-12-myristate-13-acetate (PMA) in the P2Y₁R truncated at Leu335 or Ala338. Receptors truncated at residue Ala342 were still expressed and activated by an agonist, but inhibition of Ca²⁺ mobilization by PMA was dramatically reduced. The T339A mutant in the receptor truncated at Ala342, or the wild-type (*wt*) receptor eliminated Ca²⁺ response depression by PMA after agonist-induced activation. Therefore, the authors concluded that Thr339 is required for PKC-dependent downregulation of Ca²⁺ responses, whereas Thr330, Ser336, and Ser343 are not involved in PKC-dependent downregulation.

Ser352 and Ser354 in the C-terminus of the human P2Y₁R were found to be critical residues for agonist-induced receptor internalization.³⁸ The single mutants S352A, S354A, T358A, the double mutant S352A_S354A, as well as a mutant, in which all threonine and serine residues following Thr339 in the C-terminus were mutated to alanine, were constructed. Ser352 and Ser354 are the residues that are phosphorylated.

Results of the whole set of P2Y₁R mutants involved in agonist and antagonist recognition are summarized in Figure 8, where the respective positions of the mutated residues were colored in the cylindrical presentation of the P2Y₁R X-ray crystal structure (PDB-ID: 4XNW). The mostly mutated regions included TMIII, V, VI, and VII, as well as ECL2. Several charged residues most likely interact with the phosphate chain of the ligand, while aromatic residues interact with the nucleobase as identified by mutagenesis data and confirmed by X-ray crystal structures. Interaction patterns seem rather complex as residues distant from the predicted orthosteric binding site which cannot directly interact with the ligands, still modulate receptor functionality (e.g., disulfide bridges maintaining proper receptor structure).

2.1.3 | Role of the extracellular domains

Hoffmann et al. investigated the role of extracellular domains in agonist recognition and ligand preferences.³⁹ In their study, the extracellular loops and the N-terminus of the human P2Y₁R for those of the rat P2Y₆R were exchanged.

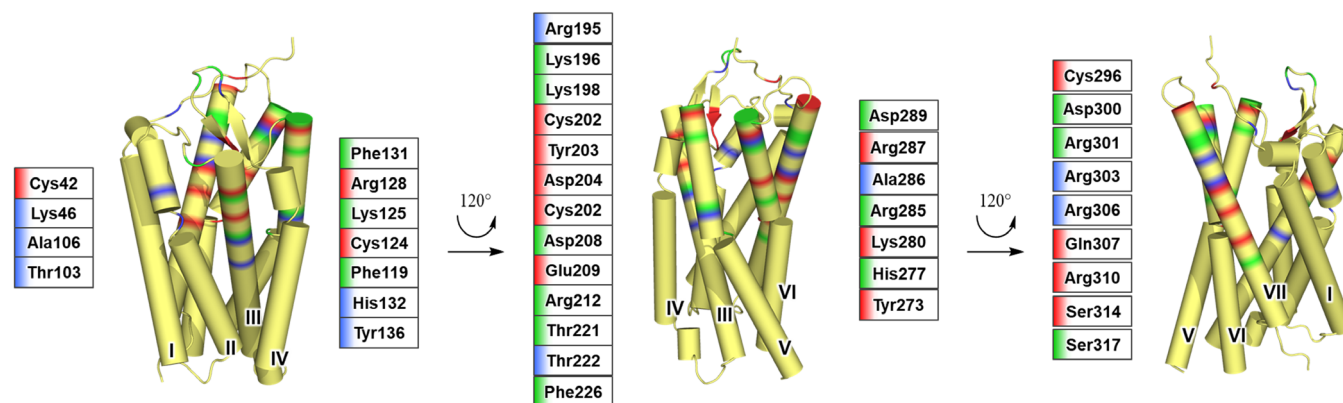


FIGURE 8 Schematic presentation of mutated residues depicted in the X-ray crystal structure of the human P2Y₁R (PDB: 4XNW). Transmembrane regions are presented as cylinders. Roman numbers indicate the transmembrane regions. Mutations of residues highlighted in red led to a large decrease in potency or complete abolishment of the receptor's ability to be activated by agonists. Mutation of green colored residues had no or low impact on agonist potency. Blue highlighted residues were shown to participate in the binding of different antagonists

While the P2Y₁R is activated by adenine nucleotides (ADP > ATP), the P2Y₆R is activated by the uracil nucleotide UDP. UDP itself showed a maximum effect of 32% at the human P2Y₁R compared to the rat P2Y₆R (=100%). Exchange of the *N*-terminal residues 37–46 of the P2Y₁R by the analogous sequence of the rat P2Y₆R resulted in a chimeric receptor with a poor cell surface expression level (6% of wt) which was still activated by the ADP derivative 2-MeSADP, although it displayed a 7,000-fold decrease in potency. The other two constructs with a mutated sequence (residues 37–51, and 37–61, respectively) were not activated by high concentrations of the agonist 2-MeSADP (up to 100 μM). However, a strong gain in UDP potency was observed for the chimeric receptor whose amino acid sequence 37–61 had been exchanged for that of the rat P2Y₆R.

Sequence exchange of the ECL1 of the P2Y₁R (Tyr111-Met123) by the corresponding residues of the P2Y₆R resulted in a 330-fold decrease in the potency of 2-MeSADP. Chimeric receptors with a shorter ECL1 sequence replaced (residues Tyr111-Ile118) led to a similarly high, 460-fold decrease in potency. An extended sequence exchange of residues in the P2Y₁R for P2Y₆R residues (Tyr111-Val133) had no further significant impact on the potency of 2-MeSADP. Even ECL1 exchanges including Tyr110 (residues Tyr110-Ile118, Tyr110-Met123, and Tyr110-Val133) resulted in mutants that were not activated by 2-MeSADP at high concentrations (up to 100 μM). The exchange of larger TMIII regions of the P2Y₁R showed a trend toward higher acceptance of UDP as an agonist.

Exchange of the ECL2 (residues Thr192-Tyr210) in the human P2Y₁R by that of the rat P2Y₆R resulted in a dramatic reduction in the potency of 2-MeSADP (6500-fold decrease). Partial exchange (residues Thr192-Ser213, Thr192-Phe215, Thr192-Met225) led to significantly diminished receptor surface expression levels and a complete loss of 2-MeSADP-induced receptor stimulation, as well as unchanged low activation by UDP.

Among the five constructed chimeric mutants of ECL3 exchanges (Ile274-Phe298, Leu284-Phe298, Leu284-Tyr303, Leu284-Gln307, and Leu284-Ala313), the chimeric receptor, in which P2Y₁R residues Leu284-Phe298 were exchanged for the analogous residues of the rat P2Y₆R, was activated by 2-MeSADP (60-fold decrease in potency) and demonstrated 50% of the maximal effect of UDP compared to the rat P2Y₆R.

To further investigate the role of the amino acid clusters responsible for agonist recognition and agonist-induced receptor activation, combinational chimeras were constructed. The double constructs Tyr110-Val133/Leu284-Phe298 (Construct 1) and Ser37-Val61/Tyr110-Val133 (Construct 2), and the triple constructs Ser37-Val61/Tyr110-Val133/Leu284-Phe298 (Construct 3), and Ser37-Val61/Tyr111-Val133/Leu284-Phe298 (Construct 4), could not be activated by 2-MeSADP. Construct 2, Construct 3, and Construct 4 demonstrated increased acceptance of UDP as an agonist with 3- to 6.5-fold increase in potency (maximal effect of 90, 92, 86%, respectively). The double constructs Tyr111-Val133/Leu284-Phe298 (Construct 5), Ser37-Val61/Tyr111-Val133 (Construct 6), and Ser37-Val61/Leu284-Phe298 (Construct 7) were activated by 2-MeSADP albeit a dramatic drop in potency was observed. It can be deduced that the ECL2 plays a major role in ligand recognition and acceptance. Although residues of TM regions involved in interactions with 2-MeSADP were not mutated, major differences in potency of 2-MeSADP and UDP were determined in the chimeric receptors. This is supported by the key role of the conserved disulfide bridges which likely influence the flexibility and proper folding of ECL2.

To investigate the role of residues involved in agonist binding and recognition, Hillmann et al. created human P2Y₂R mutants to test their effects on the potency of various agonists and antagonists.⁴³ R272A led to a dramatic decrease in the potency of the tested agonists UTP, ATP, Ap₄A (diadenosine tetraphosphate), and Ip₄U (**1.16**), (350-, 185-, 4,400-, and 3,500-fold, respectively), similar to the S296A mutant (2000- to 3,700-fold decrease). A three- to five-fold decrease in ATP potency was observed in the double mutant R177A_R180A as well as in the single point mutants R177A, R180A, and Y118A. The Y118A mutant also led to a three-fold decrease in Ap₄A potency. The single mutants R194H and Y198A showed no significant changes in agonist potency. The created mutants were used to further investigate the binding mode of the anthraquinone-derived antagonists Reactive Blue 2 (RB-2, **2.09**) and PSB-0416 (**2.11**). The mutation of Tyr114 to alanine resulted in an over 50-fold decrease in the potency of RB-2, whereas the double mutant R177A_R180A and the single mutant Y198A resulted in a moderate 10- and 4-fold decrease in potency. For the smaller antagonist **2.11** no significant changes could be observed in the mutants.

Additional studies focused on the putative orthosteric binding pocket of the human P2Y₂R and investigated additional charged and aromatic residues of the TM regions and the ECL2.⁴⁴ The single mutants R110A, R265A, Y288A, and R292A led to complete abolishment of receptor activation by UTP. In addition to these mutants, the Y114F, R194A, F261A, and Y288F mutants were no longer activated by the agonist Ap₄A. Decreased UTP potency was observed for the F111A, Y114F, H184A, S193A R194A/H, F261A, Y268F, Y269F, and Y288F mutants, while the mutant Y114A had only a low impact on UTP potency. A significant decrease in Ap₄A potency was observed for F111A, Y114A, H184A, S193A, R194H, Y268F, and Y269F. This data is consistent with results from previous P2Y₁R mutagenesis studies as the corresponding residues showed similar effects on the potencies of agonists. For all of those residues, participation in agonist binding in the orthosteric binding site or an effect on the flexibility of ECL2 was hypothesized on the basis of an updated homology model combined with docking studies. The results of all mutagenesis studies involving the residues that are important for agonist binding are summarized in Figure 10.

In addition to investigation of agonists, a selected set of anthraquinone-(AQ-) derived antagonists (**2.11–2.13**) and the thiouracil derivative AR-C118925 (**2.16**), a P2Y₂R-selective competitive antagonist, were tested on all of those mutants, that could be activated by UTP.^{45–47} A trend toward increased potency of **2.11–2.13** was observed for the mutants Y114A, Y114F, R194H, F261A, Y268F, and Y288F, indicating an orthosteric binding mode of these AQ derivatives.

The mutations Y114A, Y114F, and R194H had a significant effect on the smaller AQ derivative **2.11**, whereas the larger derivatives **2.12** and **2.13** showed no significant changes in potency at those and other mutants. The mutants Y114F and R194H led to an increased potency of **2.13** indicating an orthosteric binding mode of medium-sized anthraquinone derivatives, since Tyr114 is placed deeply in the putative orthosteric binding pocket. Complete abolishment of inhibition by RB-2 was observed for the mutants F111A, H184A, R194H, F261A, and Y269F, and a significant drop in potency was found for the mutant Y114A leading to the assumption, that the large RB-2 possesses a different binding mode than the smaller AQ derivatives.

2.2.2 | Role of the extracellular domains

In another mutagenesis study, Asp97 was mutated to glutamic acid for investigating the role of the RGD motif present in the ECL1 of the P2Y₂R, as the RGD motif is rare in the extracellular loop regions of GPCRs and shared by the P2Y₂R, P2Y₆R and the histamine receptor H₂.^{48,49} The D97E mutant required ~1,000-fold higher concentrations of the agonist UTP (785 μM) for receptor activation, compared to the *wt* receptor as determined in Ca²⁺ mobilization assays (0.85 μM). Another study demonstrated that the RGD motif in the ECL1 acted as an integrin-binding domain, and it was also required by the P2Y₂R to activate G_q and G₁₂, but not for G_q activation.⁴⁸ The authors postulated that the P2Y₂R forms a complex with the integrins α_vβ₃ and α_vβ₅. The α_v integrin complex formation is required for the P2Y₂R to access heterotrimeric G proteins involved in chemotaxis. In the study of Erb et al. regarding the integrin-binding motives of the human P2Y₁R and P2Y₂R, mutants of the ECL1 were created. Since the RGD97 integrin-binding motif is not present in the human P2Y₁R, the two aspartic acid-containing motifs KTD116 and FGD121 in the ECL1 of the P2Y₁R were selected for mutagenesis experiments. The mutations D116E and D121E resulted in similar Ca²⁺ mobilization ability compared to the *wt*, whereupon F119R resulted in a 34-fold decrease in ADP potency.

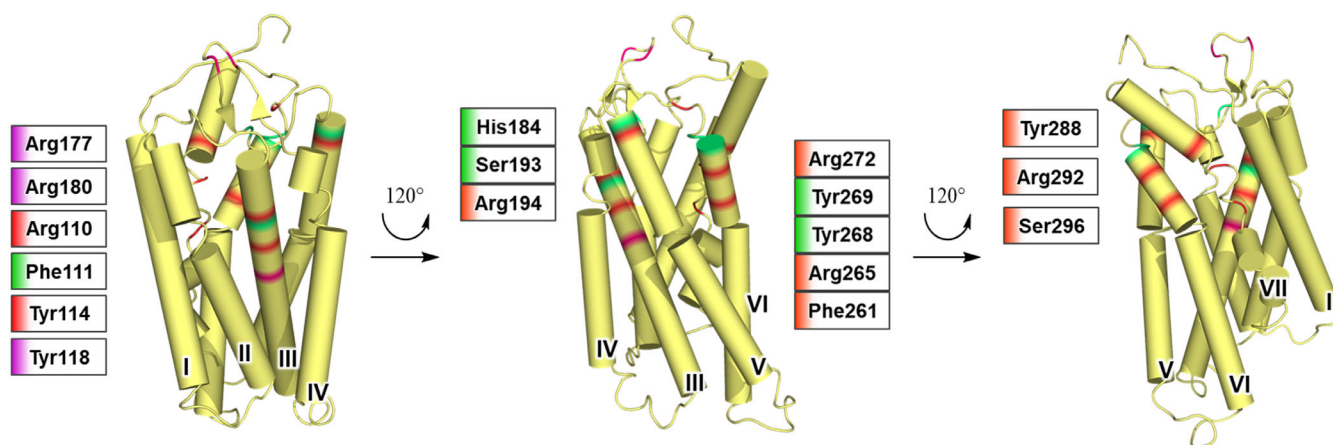


FIGURE 10 Schematic presentation of mutated residues in the human P2Y₂R homology model based on the human P2Y₁R X-ray crystal structure. Transmembrane regions are presented as cylinders. Mutations of residues highlighted in red led to a large decrease in potency or complete abolishment of the receptor's ability to be activated by agonists. Mutation of green colored residues had a moderate impact on agonist potency. Purple-colored mutants led to a decrease in potency only for ATP

2.2.3 | Role of the intracellular domains

The triple mutant S243A_T344A_S356A on ICL3 and the C-terminus was created to test the hypothesis that phosphorylation of the P2Y₂R may be implicated in agonist-induced desensitization.⁵⁰ The triple mutant led to reduced phosphorylation of the receptor upon activation with agonists but had no effect on the receptor's ability to activate calcium mobilization.

2.3 | P2Y₄R mutants

The role of the ECL2 of the human and the rat P2Y₄R was studied by Herold et al.⁵¹ While the human P2Y₄R is activated solely by UTP at physiological concentrations, the rat P2Y₄R can be activated by ATP as well as by UTP. Several chimeras targeting TM regions and ECLs of the human P2Y₄R were exchanged for the corresponding sequences of the rat receptor. Out of the 10 chimeras constructed, only those containing the rat ECL2, and the triple mutant S177N_V183I_R190L resulted in receptors which responded to high concentrations of ATP (13- to 100-fold decrease in potency compared to the rat *wt* P2Y₄R). Although ATP was somewhat active on the single point mutants S177N, V183I, and R190L, EC₅₀ values could not be determined due to its low potency. ATP had no agonistic effect on the N178A and K179N mutants.

In a study of the agonist-promoted regulation of the P2Y₄R and P2Y₆R, several residues of the C-terminus and the ICL3 of the P2Y₄R and the P2Y₆R were investigated.⁵² The mutant S243A failed to inhibit agonist-induced internalization. C-terminus-capped versions of the *wt* P2Y₄R were created including deletion from Ala332, Asp343, and Asp355 upward, respectively. The P2Y₄R/Ala332 and P2Y₄R/Asp343 truncated receptors no longer showed the effect of agonist-induced loss of cell surface P2Y₄R expression or desensitization. The exchange of the C-terminus of the P2Y₆R for that of the P2Y₄R failed to confer agonist-induced loss of surface receptors, indicating the additional participation of intracellular loops in the regulation of P2Y₄R desensitization. Since the C-terminus contains 11 serine and threonine residues as potential amino acids for phosphorylation, additional single and multiple point mutations were performed. The triple mutant S333A_S334A_S339A and the double mutant S333A_S334A, as well as the full-length C-terminus with serines and threonines mutated to alanine, had a greatly reduced capacity to undergo agonist-promoted internalization. Mutation of individual serine residues led to the conclusion that Ser333 and Ser334 are key regulatory residues in agonist-induced phosphorylation, desensitization, and internalization of the P2Y₄R.

Results for the mutant S243A of the human P2Y₄R led to the construction of the A237S mutant of the human P2Y₆R. However, the A237S single mutant failed to confer the capacity at P2Y₆R to undergo rapid agonist-dependent loss of surface receptors.

Four hydrophobic residues near the C-terminus and two basic residues were found to be involved in the apical targeting of the P2Y₄R in epithelial cell models: a valine (Val338) and three leucine residues (Leu335, Leu337, and Leu340) were found to disrupt the apical targeting and promote basolateral targeting if mutated to alanine.⁵³ To investigate the role of charged residues in the apical targeting sequence, the amino acid residues arginine, glutamate, and lysine were mutated to alanine, resulting in four receptor mutants lacking the selected residue in the C-terminus. Mutation of the glutamate and aspartate residues to alanine had no effect on targeting, while mutation of lysine and arginine to alanine had a low but still significant impact. The study concluded that the apical targeting signal of the P2Y₄R is sequence-independent, as confirmed by inversion of a 23 amino acids sequence (Cys321-Asp343) of the C-terminus. Similar results were published for the P2Y₁R.⁵⁴

2.4 | P2Y₆R mutants

Brüser et al. performed mutagenesis and molecular modeling studies to delineate the binding modes of the glyceryl ester of prostaglandin E₂ (PGE₂-G, **1.13**) and UDP, after identification of PGE₂-G as a potent endogenous agonist of the human P2Y₆R (EC₅₀ ≈ 1 pM).⁵⁵ Four residues were mutated to alanine: Tyr75, Phe252, Tyr262, and Arg287. The mutants Y262A and R287A led to a complete loss of the IP₁ accumulation response to UDP-induced receptor activation, while Y75A led to a two-fold decrease. Complete abolishment of activation by PGE₂-G was observed for the Y75A, F252A and R287A mutants. Mutagenesis data and docking studies led to the postulation of a binding pocket close to TMIII, VI and VII for both agonists, whereupon PGE₂-G appeared to extend further with its glycerol ester moiety toward TMV.

2.5 | P2Y₁₁R mutants

Based on homology modeling utilizing the bovine rhodopsin X-ray crystal structure and comparison with previously published P2Y₁R mutagenesis data, several P2Y₁₁R mutants were created and tested for their response toward the endogenous P2Y₁₁R agonist ATP and its stable analog ATP γ S.⁵⁶ The ability of ATP to trigger a calcium signal due to receptor activation was nearly abolished for the mutants R106A and R307A. Analogous mutations in the human P2Y₁R (Arg128 and Arg310) and the human P2Y₂R (Arg110 and Arg292) had also been essential for ligand recognition by those receptors. Furthermore, mutant Y261A (analogous to P2Y₁R's Tyr273) was not activated by ATP. A significant decrease in ATP potency was observed for E186A, R268A, and R268Q (10-, 750-, and 40-fold decrease, respectively). A small effect was measured for F109I and A313N. The agonist ATP γ S was tested on the mutants E186I, R268A, and R268Q with similar results.

The residues Glu186 and Arg268 were additionally investigated with respect to their recognition of the *R*- and *S*-isomers of ATP α S (**1.10**). The R268A mutant and the E186A_R268Q double mutant had the highest effect on the stereospecificity of the *S*- and *R*-isomers (20- and 10-fold, and 100- and 50-fold decrease, respectively), while the potency of either isomer did not differ strongly for the mutants E186A and R268Q.⁵⁷ Hetero-oligomerization of the P2Y₁₁R with the P2Y₁R was studied using the R268A mutant of P2Y₁₁R, which prohibited the functional interaction of the P2Y₁₁R with the P2Y₁R. The association of the P2Y₁R with the P2Y₁₁R influenced the ligand selectivity of the P2Y₁₁R.⁵⁸

The mutant A87T is a common single nucleotide polymorphism (SNP) of the P2Y₁₁R which is associated with an increased risk of acute myocardial infarction and increased levels of C-reactive protein, indicating involvement in inflammatory reactions.⁵⁹ The P2Y₁₁R A87T polymorphism was present in 19.8% of controls and in 22.9% of acute myocardial infarction patients.⁶⁰ Alongside the A87T polymorphism, eight other single mutations with lower frequencies in cohort (≤ 0.0075) from nine narcolepsy with cataplexy patients were studied. The mutants A64T, S166G, V272M, and A87T had no significant effect on potency of benzoylbenzoyl-ATP (Bz-ATP, **1.12**), a P2Y₁₁R agonist. Significant effects were measured in the R86C, E186K, Y261C and Y321H single mutants (9- to 28-fold decreases in potency). The R307W mutant was no longer activated by high concentrations of 100 μ M Bz-ATP, indicating a key role in the recognition of Bz-ATP. Haas et al. studied the A87T mutant alongside the A87S/Y mutants in the presence of P2Y₁R. The A87T mutant was not activated by Bz-ATP, in the presence of P2Y₁R while the A87S/Y mutants displayed a similar level of activation as the *wt* receptor. The potency of 2-MeSADP decreased almost 10-fold for the A87T mutant, with no drastic changes for the other mutants. ATP induced similar levels of activation for all mutants of the *wt* receptor. The effects of P2Y₁/P2Y₁₁R heterodimerization are further discussed in the Section 6.

2.6 | Assessment of mutants

GPCRdb is a database for GPCRs, which provides analysis tools, diagrams, and annotations of X-ray crystal structures, mutants, and reference sequence alignments.^{3,4} The visual presentation of the data using the integrated web tools of GPCRdb has allowed a straightforward comparison of the P2Y₁-like receptors. In the following discussion, the Ballesteros–Weinstein numbering system will be applied.⁶¹ We decided to limit that numbering system to this section to keep the previous sections reader-friendly, but highlight the analogy of the compared residues in the following discussion.

The analysis of the receptor sequences provides information about their phylogenetic relationships (see Table 1). Multiple sequence alignment and phylogenetic analysis revealed that the P2Y₂R and the P2Y₄R are the most closely related receptors within the P2Y₁-like subgroup (see Figure 1).^{11–13} The human P2Y₁₁R shares the lowest similarity and identity with the other four receptor subtypes. No rat or mouse P2Y₁₁R orthologs have been identified, indicating a recent evolutionary separation of the P2Y₁₁R from the other P2YR subtypes.⁶² Despite low sequence identities, homology and mutagenesis studies of analogous counterparts in the other P2YR subtypes allowed prediction of binding sites and mode of activation (e.g., prediction of allosteric (P2Y₄R) and orthosteric agonist and antagonist binding sites (P2Y₂R) based on crystallized complexes of the human P2Y₁R and P2Y₁₂R). Since no crystal structure of agonist-bound P2Y₁-like receptors is available at this point, mutagenesis data, homology modeling approaches, MD simulations or a combination of the above methods have to be used for predicting the binding poses of agonists and the activation mechanism of the receptors.

Arg128^{3,29} (P2Y₁R), Arg110^{3,29} (P2Y₂R), and Arg106^{3,29} (P2Y₁₁R) were found to be essential for agonist-induced receptor activation. Homology modeling and mutagenesis studies of the human P2Y₂R indicate an interaction of the ribose moiety of UTP and Ap₄A with Arg110.⁴⁴ However, mutation of Arg110 in the murine P2Y₂R showed little effect on agonist potency. The difference in the role of this residue in different species is not fully understood yet. The environment could influence the properties of the arginine, resulting in preference toward different agonists and antagonists.^{40,41}

Mutation of residues Phe131^{3,32} (P2Y₁R) and Phe109^{3,32} (P2Y₁₁R) had no impact on agonist potency. His132^{3,33} (P2Y₁R) is not conserved in the P2Y₁-like receptor subtypes: the analogous position is occupied by tyrosine in the P2Y₂R, P2Y₄R, P2Y₆R subtypes, and by threonine in the P2Y₁₁R. Mutation of His132 led to a significant decrease in potency of the agonist 2-MeSADP, and the mutation of the analogous residue Tyr114 (P2Y₂R) reduced the potency of the endogenous agonist UTP. Interestingly both mutations Y114A and Y114F resulted in a complete loss of response to Ap₄A.

The mutants Tyr136^{3,37} (P2Y₁R) and Tyr118^{3,37} (P2Y₂R) had a moderate or low impact on agonist potency. The impact was higher for the Tyr136 mutant, while Tyr118 had only a low impact on ATP and Ap₄A potency but no significant difference was observed for UTP. Alongside His132 and Thr222 in the human P2Y₁R, Tyr136 appears to be involved in binding of the antagonist **2.03**.³¹

Arg212^{5,33} and Ser213^{5,34} are placed in the upper third part of the P2Y₁R. The respective positions are swapped in the P2Y₂R: Ser193^{5,33} and Arg194^{5,34}. While the mutant R212A showed no effect on agonist potency, complete loss of activation by Ap₄A was observed for the mutant R194A, and decreased Ap₄A and UTP potencies were determined for the R194H mutant. Homology modeling approaches predicted a potential ionic lock between Arg194 and Glu190 (P2Y₂R). Interestingly, the triad of Arg212, Arg285, and Asp289 formed an ionic lock in the X-ray crystal structure of the human P2Y₁R. Based on this observation, the higher impact on P2Y₂R agonists was explained with a possibly modulated flexibility of the ECL2 in the mutants, leading to different effects on adenine and uracil-based nucleotides. Mutation of Ser193 led to decreased potency of UTP and Ap₄A possibly due to the same mechanism.

Tyr273^{6,48} (P2Y₁R) was postulated to participate in agonist-induced signal transduction, while the mutation Y273A had no effect on agonist or antagonist binding affinity. The analogous P2Y₁₁R Y261A mutation could not be activated by agonist anymore, indicating a conserved role for P2Y₁R and P2Y₁₁R. Mutations of Phe252^{6,48} (P2Y₆R) showed no significant effect on UDP potency, but greatly impaired P2Y₆R activation by PGE₂-G.

The three basic residues Lys280^{6,55} (P2Y₁R), Arg265^{6,55} (P2Y₂R), and Arg268^{6,55} (P2Y₁₁R) were investigated in all the receptors for their effects on agonist potency. Each mutation resulted in an immense drop in potency for the respective agonists. In the homology model complex of the human P2Y₂R with UTP or Ap₄A, ionic interactions between Arg265 and the phosphate chain were observed. Additional interactions with the nucleotide base are feasible. Mutation of the rat P2Y₂R's Arg264^{6,55} to leucine had no effect on agonist potency. Therefore, it is possible, that the environment

	P2Y ₁	P2Y ₂	P2Y ₄	P2Y ₆	P2Y ₁₁
P2Y ₁		28	32	28	25
P2Y ₂	<i>44</i>		48	31	22
P2Y ₄	<i>47</i>	<i>61</i>		33	25
P2Y ₆	<i>41</i>	<i>41</i>	<i>43</i>		19
P2Y ₁₁	<i>42</i>	<i>35</i>	<i>38</i>	<i>30</i>	

TABLE 1 Similarity and identity (%) of P2Y₁-like receptors after multiple sequence alignment performed by the integrated web tool of the GPCRdb

Note: Similarities are shown on the lower left side of the table (entries in italics), and identities on the upper-right side (entries in bold).

around the arginine in both receptors induces different rotamers resulting in different interaction patterns, or modulates its role in receptor activation.

Asn283^{6,58} (P2Y₁R), Tyr268^{6,58} (P2Y₂R), and Tyr262^{6,58} (P2Y₆R) are placed close to the predicted orthosteric binding pocket of the receptors. Asn283 (P2Y₁R) was not observed to interact with the agonists 2-MeSADP, 2-MeSATP and **1.08**, but with antagonist **2.02**. Mutant Y268F (P2Y₂R) revealed significant decreases in the potency of the agonists UTP and Ap₄A. Mutation of Tyr262 (P2Y₆R) to alanine led to a complete abolishment of response induced by UDP. Thus, the role of residues in position 6.58 seems to be receptor subtype-specific.

Tyr306^{7,35} (P2Y₁R) is involved in binding of the antagonist **2.02**. Tyr288^{7,35} (P2Y₂R) was mutated to alanine and phenylalanine, both leading to severe effects on UTP and Ap₄A potencies. However, only weak interactions of Tyr288 (P2Y₄R) with UTP were observed in docking studies based on the homology model of the human P2Y₂R. A role in initial ligand recognition and guidance toward the binding pocket were proposed.⁴⁴

The key role of the highly conserved arginine in TMVII will be discussed in detail in the Section 4. The mutation of Arg310^{7,39} (P2Y₁R), Arg292^{7,39} (P2Y₂R), Arg287^{7,39} (P2Y₆R), or Arg307^{7,39} (P2Y₁₁R) in all cases led to a complete loss of activation by agonists (UTP/Ap₄A, UDP, and ATP, respectively). The arginine likely forms an ionic lock with an aspartic acid residue from the ECL2 in the cases of the P2Y₁R (Asp204), P2Y₂R (Asp185), and P2Y₄R (Asp187), as indicated by homology modeling. No similar interactions have been proposed in previous homology models of the human P2Y₆R and P2Y₁₁R, probably because they were created before the P2Y₁R or P2Y₁₂R X-ray crystal structures had been published. Docking and MD simulations revealed that agonists interact with one or both residues, and eventually break the ionic lock, while allosteric and orthosteric antagonists seem to stabilize the ionic lock thus preventing agonist-induced receptor activation.

Ser314^{7,45} (P2Y₁R) and Ser296^{7,45} (P2Y₂R) were mutated revealing their important role in receptor activation. X-ray crystal structures (P2Y₁R)²⁷ and docking studies on the homology model (P2Y₂R)⁴⁴ showed no interactions with ligands. Therefore, it is concluded that these serine residues in TMVII have a role in signal transduction which needs further research as it cannot be interpreted based on the published data.

Tyr324^{7,53} (P2Y₁R) underwent a molecular switch in MD simulations which resulted in the formation of a continuous water channel inside the receptor. The homologous amino acid residues have not been mutated in the other P2Y₁-like receptor subtypes and therefore discussions are limited to computational results. Among the five subtypes of P2YRs, tyrosine is not highly conserved, as it is substituted by phenylalanine (Phe301) in the P2Y₆R.

To investigate the role of ECL2 in agonist recognition and its effect on agonist potency, its mutations were studied on several GPCRs, including P2Y₁R and P2Y₄R.^{39,51,63–65} Several attributes of the ECL2 were characterized for several GPCRs, including subtype-selective recognition and binding of ligands, conversion of antagonist to agonist upon mutation, and different conformational changes during binding of agonists, antagonists, and inverse agonists.^{66–69} Within the P2Y₁-like receptor family, only a single cysteine is conserved in the ECL2 (see Figure 6). Exchanges of ECL2 and ECL3 in the human P2Y₁R by those of rat P2Y₆R led to the acceptance of UDP as an agonist and also had a high impact on the potency of ADP. Arginine is present in the ECL2 of P2Y₁-like receptors and might play a role in the recognition and binding of agonists.⁷⁰ The distribution pattern and number of arginine residues is heterogeneous within the P2Y₁-like subclass. Frequently observed residues present in the ECL2 of GPCRs have been reported previously: glutamate residues in ECL2 were found to be responsible for ligand recognition of the human A_{2A}R.⁷¹ It is likely that not a single residue is responsible for the ability to distinguish between agonists, but rather the conformation induced by the composition of several residues.⁷² Several residues in the ECL3 of the M₃ muscarinic acetylcholine receptor were found to have functional importance in the stabilization of the active state of the receptor.⁷³ Although computational approaches have vastly improved in the recent decades, prediction of ECL2 structure remains a difficult task if no resolved loop structure of any related receptor structure is available.⁷⁴

The comparison of the sequences of the ECL2 within the P2Y₁-like receptors reveals high similarity between P2Y₁, P2Y₂, P2Y₄, and P2Y₆, and in particular high similarity between P2Y₁ and P2Y₆ on the one hand, and P2Y₂ and P2Y₄R on the other hand (see Table 2). The low similarity and identity of P2Y₁₁R's ECL2 compared to those of the other receptor subtypes can be explained by its extended size; while the ECL2 of P2Y₁R consists of 24 residues and the ECL2 of P2Y₂R, P2Y₄R, and P2Y₆R consist of 23 residues, the ECL2 of P2Y₁₁R is extended to 34 residues. A very different tertiary structure of the P2Y₁₁R ECL2 as compared to that of the other subtypes can be expected. Additionally, no aspartic acid which might contribute to the receptor activation mechanism is present in a key position within the ECL2 of the P2Y₁₁R. The P2Y_{1,2,4,6} subtypes possess a characteristic aspartic acid two positions apart from a highly conserved cysteine. The analogous residue is changed to glycine in the P2Y₁₁R. The aspartic acid of the ECL2 is expected to form an ionic lock with arginine in TMVII, as observed by MD simulation utilizing the X-ray crystal structure of human P2Y₁R.⁷⁵ Agonists used to break the ionic lock, resulting in drifting apart of the involved aspartic acid and arginine, while two antagonists that interact with different binding sites stabilized the ionic lock and prevented receptor activation. Homology models of P2Y₂R and P2Y₄R and docking studies of agonists and antagonists revealed interactions with those conserved aspartic acid and arginine residues, indicating a similar mode of activation and inhibition for the three receptor subtypes P2Y₁, P2Y₂, and P2Y₄. No homology model of human P2Y₆R has been published to this date to confirm these relatively new findings. Even though one aspartic acid is present in the P2Y₁₁R's ECL2 (Asp196), its position close to TMV indicates a different mode of activation.

2.7 | Extracellular loop 2

A role for the ECL2 has been described in agonist and antagonist recognition for the human P2Y₁R and P2Y₄R.^{32,39,51} While the highly conserved disulfide bridge among the P2Y₁-like receptors between ECL2 and TMIII was proven to be essential for agonist-induced receptor activation, mutants of other residues within the ECL2 had a negative impact on agonist potencies. Obviously, an acidic residue (e.g., aspartic acid) in ECL2 which is participating in receptor activation, confirmed by mutagenesis data and MD simulations (see below), plays a key role in ECL2 for proper receptor activation.

3 | X-RAY CRYSTAL STRUCTURES

GPCRs are transmembrane proteins which undergo spontaneous conformational changes between active and inactive states. The structural flexibility, the scarcity of hydrophilic regions necessary for crystallization, and poor solubility outside the cell membrane impede all stages of obtaining diffraction-quality protein crystals including protein expression, purification, and crystallization. Recent progress in the field of protein engineering and technology contributed to an increased number of structure determinations of human GPCRs in the past decades. The methods include the introduction of thermostabilized fusion proteins, lipidic cubic phase crystallization, point mutations for protein stabilization, and truncations of the flexible N- and C-termini.^{76,77} Finally, structure determination of GPCRs has greatly benefitted from technological advances of 3D cryo-electron microscopy (cryo-EM).⁷⁸ Cryo-EM provides detailed insights to fully functional macromolecular complexes in different functional states without the necessity of crystallization which has led to the structure determination of several GPCRs often in complex with G proteins with reasonable resolutions.^{79,80}

3.1 | X-ray crystal structure of the human P2Y₁R

Zhang et al. recently published the X-ray crystal structure of the human P2Y₁R in complex with the antagonists MRS2500 (**2.02**; PDB-ID: 4XNW, resolution: 2.7 Å) and BPTU (**2.05**; PDB-ID: 4XNV, resolution: 2.2 Å), making the P2Y₁R the first of the P2Y₁-like receptors whose crystal structure was solved.²⁷ Two disulfide bridges are observed, connecting the N-terminus to TM VII (Cys42 to Cys296) and TMIII to ECL2 (Cys124 to Cys202), and both had been proven to be essential for agonist-induced receptor activation. ECL2 reveals a hairpin structure, containing two β-sheet regions.

The GPCR D[E]RY motif of TMIII typical for class A GPCRs is replaced by an HRY motif in the P2Y₁R. This difference to other class A GPCRs results in a missing salt bridge between D[E]^{3,49} and R^{3,50}. In contrast, H148^{3,49} repels R149^{3,50}, resulting in a different conformation of the C-terminus compared to other class A GPCR structures. An ionic lock is present in both X-ray crystal structures between Asp204^{ECL2} and Arg310^{TMVII}, indicating that in the inactive state of the receptor an ionic lock between both residues is present. In addition, another salt bridge between TMV (Arg214) and TMVI (Arg285 and Asp289) can be observed in both X-ray crystal structures.

TABLE 2 Similarity and identity (%) of the ECL2 after multiple sequence alignment of P2Y₁-like receptors performed by the integrated web tool of GPCRdb

	P2Y ₁ (24 AAS)	P2Y ₂ (23 AAS)	P2Y ₄ (23 AAS)	P2Y ₆ (23 AAS)	P2Y ₁₁ (34 AAS)
P2Y ₁		30	30	35	10
P2Y ₂	<i>50</i>		58	37	6
P2Y ₄	<i>45</i>	<i>68</i>		21	6
P2Y ₆	<i>65</i>	<i>47</i>	<i>42</i>		3
P2Y ₁₁	<i>16</i>	<i>10</i>	<i>6</i>	<i>10</i>	

Note: The number of amino acid residues in the ECL2 is presented in brackets below the receptor designation. Similarities are on the lower-left side of the table (entries in italics), and identities on the upper-right (entries in bold).

The X-ray crystal structures were obtained from engineered constructs of the human P2Y₁R. Construct 1 in complex with **2.02** was crystallized with an inserted sequence Met1-Glu54 of rubredoxin as a fusion partner between Lys247 and Pro253 within the ICL3.⁷⁶ Construct 2 in complex with **2.02**, included the sequence Ala23-Leu128 of the thermostabilized apocytochrome b(562)RIL (BRIL) prior to amino acid residue Ala8 of the P2Y₁R sequence.⁸¹ For further improved protein yield and stability, an additional mutation D320^{7.49}N was introduced to the P2Y₁R.

Overall, both resolved P2Y₁R X-ray crystal structures are similar, with a C_α RMSD between both of 0.9 Å with minor differences between TMI and II. Antagonist **2.02** occupies a binding pocket in the upper third part of the receptor consisting of residues of the N-terminus, ECL2 and TMVI and VII. This nucleotide antagonist was reported to be P2Y₁R-selective, interacting with amino acids that differ from those interacting with agonists as shown by mutagenesis studies.^{82,83} The adenine ring of **2.02** binds between Arg287 and Leu44. The N⁶-hydrogen atom and N7 of adenine form hydrogen bonds with Asn283. The 2-iodo group binds in a subpocket formed by the N-terminus and interacts with the backbone of Cys42 through hydrophobic interactions. The N⁶-methyl group occupies another subpocket consisting of residues of TMVI and VII, where it is stabilized through hydrophobic interactions with Ala286 and Asn299. Tyr203 interacts with the (N)-methanocarba ribose ring through hydrophobic interactions. The 3'-phosphate forms hydrogen bonds with Tyr110 and Tyr303 and shows additional ionic interactions with Lys34 and Arg195. The 5'-phosphate forms hydrogen bonds with Thr205 and Tyr306 and additional ionic interactions with Arg310. The binding mode was confirmed by mutagenesis studies and supported by SAR studies of analogs. The observations from mutagenesis studies and the X-ray crystal structure indicate that the antagonist BPTU does not interact with the same residues as the antagonist **2.02**. The nucleotide analog binds close to the orthosteric binding site, which is observed in the agonist-bound X-ray crystal structure of the P2Y₁₂R. It appears likely that a second, partly overlapping, nucleotide binding site exists in the P2Y₁R, consisting of residues from the N-terminus, ECL2, and TMVI and VII. The binding cavity for nucleotide agonists is blocked in the P2Y₁R X-ray crystal structure in complex with the nucleotide antagonist **2.02** due to the extension of ECL2 into the orthosteric binding site upon binding of the antagonist **2.02**. Thus, the antagonist **2.02** may be characterized as an allosteric antagonist that binds above the presumed orthosteric site occupied by nucleotide agonists (see below).

The urea derivative BPTU was identified as a noncompetitive P2Y₁R-selective antagonist, which binds in the transmembrane interface of TMI, II and III, where it exhibits aromatic and hydrophobic interactions.⁸⁴ Interestingly previous studies had predicted a competitive binding mechanism for BPTU and its derivatives.⁸⁵ The only hydrophilic interactions can be observed between the nitrogen atoms of the urea group and Leu102. For the pyridyl ring, hydrophobic interactions can be observed with Ala106 and Phe119. A hydrophobic binding pocket formed by Thr103, Met123, Leu126, and Trp127 accommodates the benzene ring of the phenoxy group. The *tert*-butyl moiety forms hydrophobic interactions with Leu102. For the ureidophenyl ring, π - π interactions with Phe62 and Phe66 can be observed. Again, these observations are consistent with mutagenesis data and SARs of derivatives and analogs of antagonist BPTU.

3.2 | X-ray structure of the human P2Y₁₂R

The intracellular C-terminal region of the P2Y₁R misses helix VIII which is observed in the human P2Y₁₂R X-ray crystal structure. The C_α RMSD between the P2Y₁R X-ray crystal structure and both, the agonist-bound and the antagonist-bound P2Y₁₂R X-ray crystal structures within the helical bundle is 2.2 and 2.6 Å, respectively.^{28,29} The main differences between the TM regions of the P2Y₁R and the P2Y₁₂R can be observed for TMIII, V, VI. The extracellular region of

TMIII is shifted by over 5 Å toward the TMVII in the P2Y₁R compared to the P2Y₁₂R. This shift is likely induced by different conformations of ECL2. The TMV region of the P2Y₁R is displaced by over 4 Å compared to the P2Y₁₂R, probably due to a highly conserved proline (Pro229^{5,50}) in TMV, which is replaced by asparagine in the antagonist-bound P2Y₁₂R (Asn201^{5,50}). The tip of TMVI in the P2Y₁R lies in a position intermediate between the agonist- and antagonist-bound P2Y₁₂R X-ray crystal structures.

Similar to the P2Y₁R, the P2Y₁₂R X-ray crystal structures were obtained from engineered proteins. Both agonist-bound and the antagonist-bound X-ray diffraction data, were collected from a P2Y₁₂R-BRIL construct, in which the thermostabilized BRIL was inserted into the ICL3 between the residues Thr223 and Arg224, with an additional D294^{7,49}N mutation for increased expression and protein stability.

4 | MOLECULAR MECHANISM OF P2Y₁R ACTIVATION

With the publication of two different antagonist-bound structures of the human P2Y₁R, and two agonist-bound and one antagonist-bound P2Y₁₂R X-ray crystal structures, structural information on two diverse P2Y receptor subtypes have become available (PDB-ID: 4XNW, 4XNV, 4NTJ, 4PXZ, 4PY0) (see Figure 11).^{27–29} Even with a set of different X-ray crystal structures, which actually only represent a snapshot of a receptor's state induced by external forces, and the previously published mutagenesis data, the mechanism of receptor activation is still incompletely understood.

In a recently published study by Yuan et al. MD simulation of the human P2Y₁R was performed to investigate the mode of agonist-induced P2Y₁R activation and antagonist-induced inhibition.⁷⁵ In the process, ADP was placed extracellularly in the proximity of the P2Y₁R. After 6 × 2 μs all-atom long-timescale MD simulations of the system, the putative binding mode of the endogenous agonist was determined in the upper third part of the receptor, interacting with Tyr303 (π-π-interactions with the purine moiety and H-bond network interactions of the ribose through bulk water molecules) and forming several strong interactions via the phosphate chain with various negatively charged residues (Lys41, Lys46, Arg195, and Arg287), which was consistent with previously published mutagenesis data.

Additionally, 2 μs MD simulations for each antagonist, **2.02** and BPTU, with the P2Y₁R complex were performed. Antagonist **2.02** interacted with Tyr303 through hydrogen-π-interactions. The 3'-phosphate formed an ionic lock with Lys46 and Arg195, and the 5'-phosphate formed an ionic lock with Arg287 and Arg310. K46A, R195A, and Y303F were confirmed as interaction partners by mutagenesis, since mutation had a negative impact on the potency of nucleotide antagonist **2.02**.⁵⁰ The urea derivative antagonist BPTU bound distantly from the putative agonist (ADP) binding site, forming hydrophobic interactions with Phe62, Phe66, Leu102, Pro105, Phe119, Met123, and Leu126. The binding site of the antagonist was consistent with the X-ray crystal structure.

An ionic lock between Asp204^{ECL2} and Arg310^{TMVII} was confirmed to play an essential role in receptor activation.^{30–32,34} ADP broke the ionic lock, while both antagonists **2.02** and BPTU used in MD simulations stabilized the ionic lock. D204A/N/E mutants led to a complete loss of agonist-induced receptor activation.³² The role of Arg310 in receptor activation had been previously investigated: R310A and the double mutant R310S_S314R resulted in complete abolishment of receptor activation, whereupon the R310K mutant resulted in 10- to 100-fold decrease in potency.^{30,34} The analysis revealed an increase in the solvent accessible surface area (SASA) between both of the antagonist states (3,300–3,500 Å²) as compared to the agonist-bound states (3,800 and 4,050 Å²). Therefore, breaking of the ionic lock was postulated to lead to a water influx and thus to a rotamer shift of Tyr324^{TMVII} forming a continuous water channel inside the receptor which leads to receptor activation. A significant movement of TMIII, V, VI, and VII (~2, 4, 7, and 5 Å, respectively) was observed during ADP-induced receptor activation compared to the antagonist-bound inactive states. The distances between the TM helices III, VI, and VII were particularly increased, from 5 to 12 Å in the inactive state to 14–16 Å in the active state. TMIII, VI, and VII were reported to play an essential role in GPCR activation through direct contact with the G_α subunit.^{86,87}

While Arg310 is highly conserved within the P2Y₁-like receptor subclass, Asp204 is exchanged for glycine in the human P2Y₁₁R and Tyr324 for phenylalanine in the human P2Y₆R. The P2Y₁, P2Y₂, and P2Y₄ receptors share the same analogous residues that form the ionic lock, and the rotamer shifting of Tyr324, indicating a similar mode of activation (see Figure 12). While P2Y₁, P2Y₂, P2Y₄, and P2Y₆ possess extracellular loops of almost the same length, the ECL2 of P2Y₁₁ contains 10 additional residues. A similar mode of activation of the P2Y₁₁R cannot be dismissed, since other residues possibly eligible for the formation of an ionic lock with Arg310 are present in the ECL2 (e.g., Glu186, Asp196), but other forms of ionic locks are also feasible.

Homology models of P2Y₂R and P2Y₄R exhibited an analogous ionic lock composition of arginine and aspartic acid between ECL2 and TMVII, possibly allowing a similar mode of receptor activation after agonist binding. Agonists as well as antagonists were docked into the models and interacted with one or both residues.⁸⁸ Mutation of Arg292 in the human P2Y₂R led to a complete loss of activation by the agonists UTP and Ap₄A.⁴⁴

An updated homology model of the human P2Y₆R is available, but no interactions similar to the ionic lock have been described.⁵⁵ Since both key residues are present within its sequence, it is likely that the P2Y₆R is activated similarly to the P2Y₁R, P2Y₂R, and P2Y₄R.

5 | MOLECULAR MODELING OF P2Y₁-LIKE RECEPTORS

5.1 | Assessment of homology models

The possibilities and reliability of computer-aided receptor modeling have enormously grown over the past decade. While the tools and algorithms have improved significantly, the combination with high-resolution crystal structures of various receptors have made molecular modeling a versatile tool for studies on receptors and rational design of novel tool compounds and drugs. Prior to the publication of the first P2YR X-ray crystal structure, several homology modeling attempts based on structures of distantly related receptors (e.g., bovine rhodopsin, CXCR4) were published and evaluated, supported by mutagenesis data.^{33,43,56,89–92} Mutagenesis and computational chemistry contributed to the development of several potent P2Y₁R and P2Y₁₂R agonists and antagonist.⁹²

With the publication of the crystal structures of the human P2Y₁₂R in 2014 and of the human P2Y₁R in 2015, structures of the P2YR family have become available as a more reliable basis for homology modeling. Together with a wide range of synthesized compounds, mutagenesis data and MD simulations, more well-grounded and improved homology modeling have become feasible.

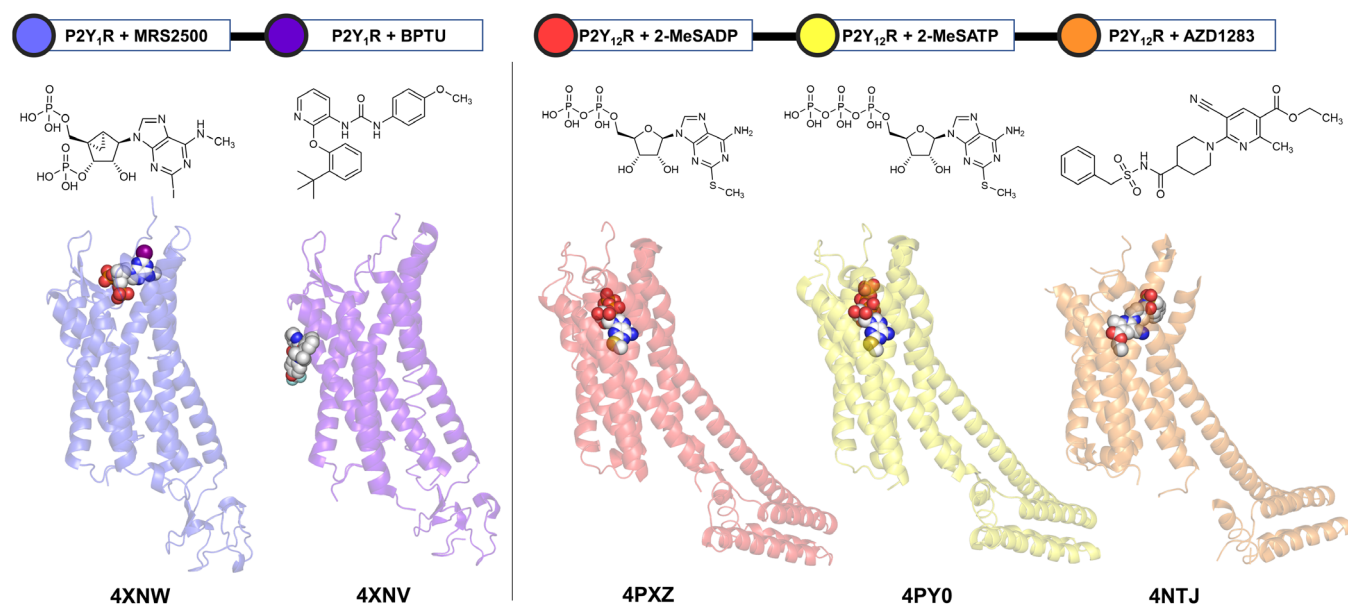


FIGURE 11 Cartoon-style presentation of published X-ray crystal structures of P2YRs and their respective PDB-ID. On the left side, both of the antagonist-bound structures of the human P2Y₁R are shown in complex with **2.02** (MRS2500, PDB-ID: 4XNW) in light blue, and with **2.05** (BPTU, PDB-ID: 4XNV) in violet blue. On the right side, the three available structures of the P2Y₁₂R are shown: in red the complex with the agonist 2-MeSADP (2-MeSADP, PDB-ID: 4PXZ), in yellow the complex with the agonist 2-MeSATP (**1.07**, PDB-ID: 4PY0), and in orange the complex with a competitive antagonist **3.05** (AZD1283, PDB-ID: 4NTJ). The receptors are presented as cartoon models, the co-crystallized atoms of the ligands are presented as spheres: carbon atoms are colored in white, nitrogen in blue, oxygen atoms in red, phosphorus atoms in orange, sulfur atoms in yellow, iodine atoms in purple

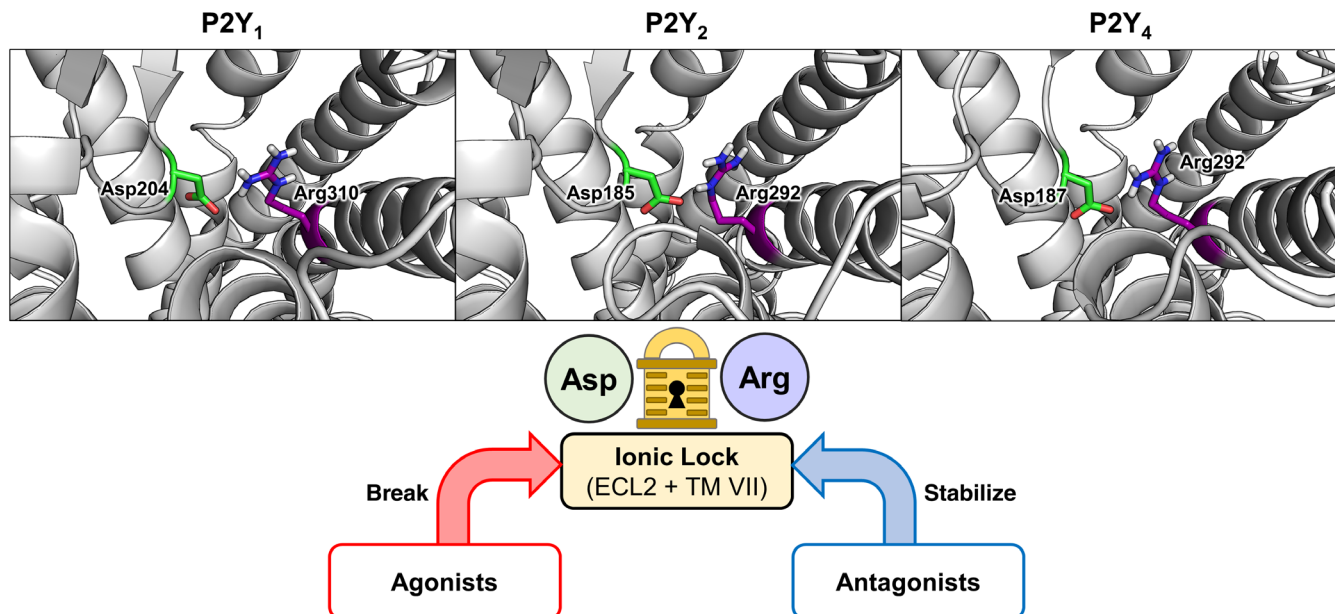


FIGURE 12 Comparison of residues between ECL2 and TMVII which might play a role in receptor activation. P2Y₁R data was taken from the X-ray crystal structure (PDB-ID: 4XNW), P2Y₂R and P2Y₄R data from published homology models based on the P2Y₁R structure.^{44,88} The ionic lock could be induced by rotamer library selection. Ionic contact is presented by dashed lines

5.1.1 | P2Y₁R

Prior to the published X-ray crystal structure of human P2Y₁R, approaches in homology modeling of the receptor had been pursued. A bovine rhodopsin-based model of the human P2Y₁R was evaluated together with mutagenesis data and docking studies.³³ Docking of agonists and antagonists revealed interactions with positively charged residues Arg128, Lys280, and Arg310 possibly through salt bridges between ligands and receptor. Tyr273 was proposed to transmit a rotation—induced upon binding of the agonist—to the lower part of the helix. Mutagenesis data and calculations suggested a similar binding mode of agonist ADP and nucleotide antagonist **2.01**. Now we know that of the agonist 2-MeSADP binds in a lipophilic binding pocket formed by TMIII, IV and V in the human P2Y₁₂R X-ray crystal structure, the docking studies into the homology model of human P2Y₁R proposed a binding site between TMI, II and VII, resulting in a “turned” orientation. Although no related structures as templates for homology modeling were determined, Constanzi et al. identified several charged residues interacting with the phosphate groups. This example shows that homology models approach without related structures can be useful to elucidate bindings modes and interactions. With ongoing structure determinations of more closely related structures, those models can be improved for additional binding mode predictions.

An optimized model was later used for docking-based QSAR analysis of 45 published P2Y₁R antagonists.⁸⁹ The QSAR studies yielded reasonable correlation coefficients and good internal predictivities, which were higher than those obtained on the basis of docking scores and free binding energy predictions. The nucleotide base was oriented toward the orthosteric binding pocket of TMIII, IV, and V with the phosphate side chain reaching toward several positively charged residues. In contrast to the later published P2Y₁R X-ray crystal structure, the nucleobase of antagonist **2.2** was accommodated in a hydrophobic binding pocket consisting of residues of TMVI and VII, and did not bind in the putative orthosteric binding site.

5.1.2 | P2Y₂R

The combinatorial assessment of the human P2Y₂R allowed studies on the binding mode of agonists and antagonists within the P2Y₁-like receptors. The first combinatorial analysis of mutagenesis-guided homology modeling was performed using the X-ray crystal structure of bovine rhodopsin.⁴³ A binding pocket was identified in the upper third part of the receptor using docking and MD simulations. The MD simulations observed gliding of the agonists toward their binding site consisting of high number of serine and threonine amino acids, as well as three positively charged residues

(His262, Arg265, and Arg292.). Additionally, two anthraquinone derivatives RB-2 and PSB-0725 (**2.10**) were docked for the first time and bound in the same binding site as the agonists, but interacted with different residues. A gatekeeper role of Arg272 in the extended binding pocket for ligands was postulated, where it was proposed to initially interact with negatively charged ligands (e.g., phosphate groups of nucleotides).

Rafehi et al. mutated residues are most likely to be involved in agonist and antagonist recognition and performed docking studies on the P2Y₁R-based homology model.⁴⁴ After the publication of the binding mode of 2-MeSADP in complex with the X-ray crystal structure of the human P2Y₁₂R, UTP and Ap₄A were docked to an improved homology model of the human P2Y₂R, resulting in binding poses which were consistent with mutagenesis data of previous and recent studies. This study presented the first approach of predicting the agonist binding mode in the improved homology model based on the antagonist-bound X-ray crystal structure of human P2Y₁R. The nucleobase of UTP and one of Ap₄A were postulated to bind inside the TM regions in an aromatic binding pocket, where π - π interactions with Tyr114 and Phe261 could be observed. The 3'-hydroxyl group of the ribose moiety of UTP was observed to form hydrogen bonding interactions with Arg110 and possibly with Asp185 of the ECL2. Several charged residues were observed to form salt bridges with the phosphate groups of UTP and Ap₄A: the α -phosphate group may interact with Arg265 and Lys289, a β -phosphate group with Tyr268, Tyr269, Arg272, Lys289, and the γ -phosphate group was predicted to interact with Arg177, Asp185, Arg272, Lys289, and Arg292. The δ -phosphate group of Ap₄A was predicted to form additional ionic interactions with Arg26, Arg177, and Lys289. It was shown that the transfer of the agonist binding mode of the human P2Y₁₂R can lead to mutagenesis-confirmed orthosteric ligand binding site predictions for more distantly related receptor subtypes.

The docking of the selective P2Y₂R antagonist AR-C118925 (**2.16**) revealed a hydrophobic binding pocket in the orthosteric binding site beneath ECL2, which is thought to be occupied by its tricyclic dibenzocycloheptenyl moiety. QSAR studies performed on precursors of **2.16** revealed several interactions which might contribute to the high selectivity of **2.16** for the P2Y₂R.^{45,47} The thiouracil moiety was accommodated between Arg265 and Arg292, where cation- π -interactions may stabilize the substituted uracil base in the binding pocket. Tyr114, Phe261, and Tyr288 likely allowed further interactions with the thio group. A subpocket consisting of Asp185, Thr186, and Tyr268 hosted the furan moiety. The amide linker may interact with Tyr268 and Asn285. The tetrazolate group, which is a carboxylate and phosphate bioisostere, most likely forms ionic salt bridges with the residues Arg24, His184, and/or Arg272. Based on mutagenesis data and the observation of a highly lipophilic binding pocket representing the orthosteric site, an orthosteric binding mode for anthraquinone derivatives was proposed, although no docking was shown.

5.1.3 | P2Y₄R

Docking studies were performed on the P2Y₁R-based homology model of the human P2Y₄R.⁸⁸ A synthesized library of anthraquinone derivatives and RB-2 were docked into the model of the P2Y₄R and found to be interacting with several residues of ECL2 and TMV and VI. The antagonists bound above the expected orthosteric agonist binding site. The sulfonate group interacted with Lys34, Lys289, Arg292, and possibly with Asp187. The interaction with Asp187 and Arg292 of the P2Y₄-analogous ionic lock may play an especially key role in receptor activation leading to receptor inactivity of the antagonist-bound complex. RB-2 was accommodated in the same binding cavity, but its anthraquinone moiety was found to be exposed to the extracellular lumen due to its large size compared to the other studied smaller anthraquinone derivatives (see Figure 13). The high potency and selectivity of the best compounds described in that study were explained by hydrophobic and aromatic interactions of the terminally substituted phenyl ring and the thio-linker connecting the terminal phenyl rings, as well as due to potential interactions of the terminal sulfonate of ring F with Arg265.

5.1.4 | P2Y₆R

A rhodopsin-based homology model of the P2Y₆R was studied by MD simulations with a selection of several ligands.⁹³ A 10 ns MD simulation in a fully hydrated phospholipid (dioleoylphosphatidylcholine, DOPC) bilayer was used to refine the model. A β -hairpin structure similar to that observed in the P2Y₁R X-ray crystal structure was found after MD simulations. The phosphate moiety of UDP bound to a positively charged sub-pocket formed by three cationic residues Arg103, Lys259, and Arg287. Ser291 was involved in the coordination of O² of the uridine moiety of UDP. Analogous residues (Ser314 (P2Y₁R), Ser296 (P2Y₂R)) were confirmed by mutagenesis to be essential for receptor activation

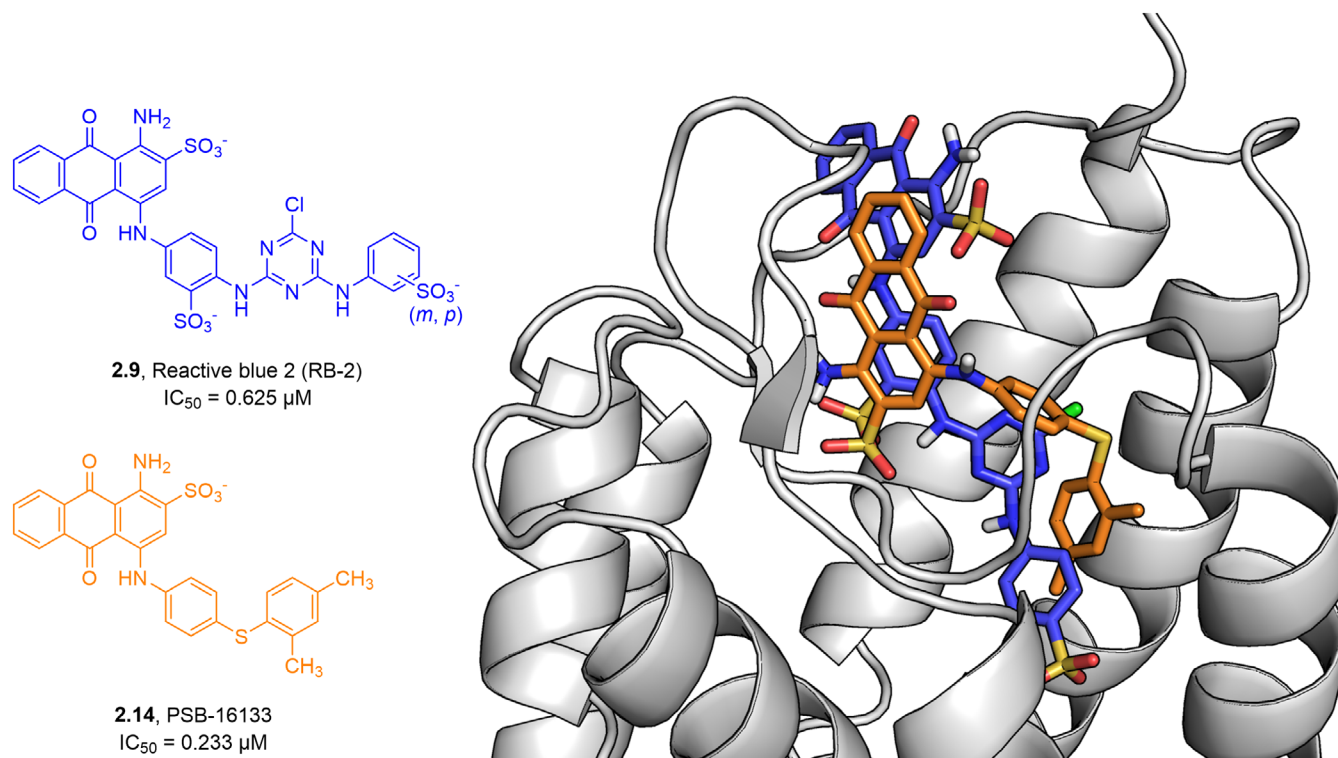


FIGURE 13 Overlay of RB-2 (**2.9**) and the smaller anthraquinone derivative PSB-16133 (**2.14**) in complex with the homology model of the human P2Y₄R. The receptor is presented in cartoon style. The helices are colored in red, the extracellular loops in green, and the β-sheet of ECL2 in yellow. The antagonists are presented as stick models. RB-2 is colored in blue, the smaller, most potent anthraquinone derivative PSB-16133 is colored in orange

in their respective receptors. An ionic lock was found between Arg103 (TMIII) and Asp179 (ECL2), which was stable for 10 ns MD simulations but was broken in MD simulations of the P2Y₆R-UDP complex.

An updated P2Y₆R model based on the X-ray crystal structure of P2Y₁R and P2Y₁₂R, as well as several supplementary templates, was recently used to predict the binding sites of UDP and prostaglandin E₂ glyceryl ester (PGE₂-G, **1.13**).⁵⁵ The docking studies suggested a binding pocket for UDP between TMIII, VI and VII, similar to those predicted for the P2Y₁R and P2Y₂R. The uridine moiety was oriented toward TMIII. The ribose moiety interacted with Arg287. The diphosphate group pointed toward TM VI. PGE₂-G was predicted to bind close to TMII and to interact with the Tyr75, Phe252 and Arg287. The glycerol moiety of PGE₂-G extended toward TMV and VI. The docking studies suggested a shared, overlapping orthosteric binding pocket for UDP and PGE₂-G. Since the prostaglandin derivative as well as the P2YRs are involved in inflammatory processes, the proinflammatory effect of the prostaglandins might be partially mediated by P2YRs.⁹⁴ However, the correlation between proinflammatory effects of prostaglandins and P2YR activation is rather complex, as prostaglandin E₂ itself impairs P2YR signaling.^{95,96} Moreover, the finding that PGE₂-G can act as a cognate P2Y₆R agonist still awaits independent confirmation.

5.1.5 | P2Y₁₁R

Based on the bovine rhodopsin X-ray crystal structure and a previously predicted model of the human P2Y₁R complex with ATP, a model of the human P2Y₁₁R was constructed.⁵⁶ Loop modeling with constraints forming an ionic lock between Asp196 and Arg275 was performed to generate the missing loops. Ligand-residue interactions were postulated for Arg106, Phe109, Ser206, Arg268, Arg307, and Met310. Arg106, Tyr261, Arg268, Arg307, and Ala313 were confirmed to participate in ligand recognition by mutagenesis studies. Glu186 in the ECL2 (analogous to the key residue Asp204 in P2Y₁R) proved to be significant for ligand recognition. A lipophilic binding pocket analogous to the nucleobase

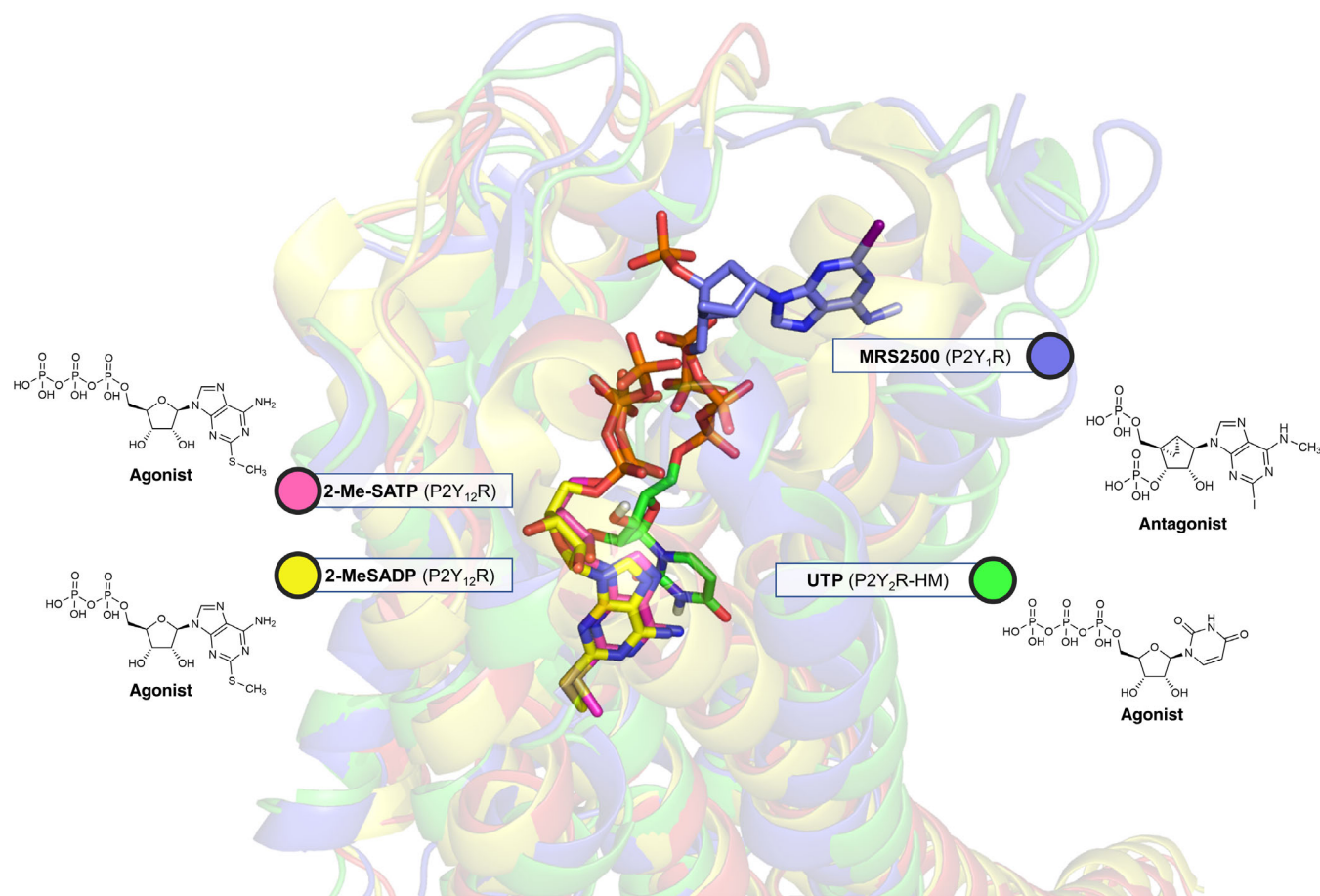


FIGURE 14 Overlay of the agonist-bound X-ray crystal structures of the human P2Y₁₂R, the nucleotide antagonist-bound X-ray crystal structure of human P2Y₁R, as well as the proposed binding mode of UTP in complex with the homology model of human P2Y₂R. The P2Y₁₂R complex with the agonist 2-MeSADP is colored in yellow, the P2Y₁₂R complex with agonist 2-MeSATP is colored in red, the P2Y₁R complex with antagonist MRS2500 (**2.2**) is colored in blue, the homology model P2Y₂R complex with agonist UTP is colored in green. The ligands are shown as stick models and the carbon atoms are colored respective to their receptor. Nitrogen atoms are colored in blue, oxygen in red, phosphorus in orange, sulfur in yellow. The β - and γ -phosphate groups of the UTP bind close to a region occupied by the 5'-phosphate group of the P2Y₁ antagonist MRS2500 (**2.2**)

binding pocket recognized in the P2Y₂R (see above) was confirmed between TMII, III and VII consisting of Leu82, Phe109, Leu133, Pro311, and Ala313. Compared to the P2Y₁R-based homology model of the P2Y₂R, the nucleobase of ATP bound in the proximity of the predicted hydrophobic binding pocket.

5.2 | Binding mode of nucleotides

The docking studies, MD simulations and the mutagenesis data suggested that the 5'-phosphate group of the antagonist MRS2500 (**2.02**) shares a binding pocket with the β - and γ -phosphate groups of the agonistic nucleotides, while the nucleoside residues are suggested to bind to very different regions (see Figure 14). The agonists seem to bind in a “deeper” binding pocket compared to **2.02**, similar to the binding mode of the agonists 2-MeSADP and 2-MeSATP in the P2Y₁₂R X-ray crystal structure. Whereas the nucleotide analog **2.02**, which is a P2Y₁R antagonist binds on top of ECL2 and stabilizes the ionic lock, agonists can enter the receptor, and their nucleobase binds in a lipophilic cavity formed by several aromatic and lipophilic residues. The phosphate groups project toward the extracellular lumen and form hydrophilic interactions and salt bridges with charged residues. These findings could explain the increase in potency of agonists upon introducing lipophilic groups (e.g., 2-thiomethyl moiety into ADP or ATP) in the case of the P2YR subtypes accepting adenine nucleotides.

6 | OLIGOMERIZATION OF P2Y₁Rs

Oligomerization of GPCRs forming heteromeric or homomeric structures is based on protein–protein interaction. This has been observed for different GPCR families and it can lead to altered binding and functional properties.^{97–99} Thus, an oligomeric complex involving P2Y₁Rs may display properties differing from those of its single receptor form, for example, showing increased or decreased potencies of agonists or antagonists, functionality gains or losses, and even altered G protein-coupling (see Figure 15). Heteromers consist of different GPCRs interacting with each other in close proximity leading to reciprocal allosteric modulation. The mechanism of heteromerization between two membrane proteins can involve the interaction of intracellular domains, the interaction between transmembrane domains or a combination of both.^{100,101} In the past decades, protein–protein complexes have become of interest as drug targets.^{102–105} The progress in computational medicinal chemistry has provided new possibilities in predicting the 3D-structures of proteins and has allowed MD simulations predicting protein–protein interactions. The resulting dimers or oligomers can further be used for the design of selective allosteric modulators of the macromolecular complexes or as a basis for virtual screening approaches (see Box 2).^{106,107}

Several oligomers of P2Y₁Rs have been reported (see Figure 15). The P2Y₁R was found to form heteromers when coexpressed in HEK293 cells together with the P2Y₁₁R.⁵⁸ This interaction promoted agonist-induced internalization of the P2Y₁₁R which does not undergo endocytosis by itself. The study suggested that the P2Y₁₁-selective agonist Bz-ATP (**1.12**) and the P2Y₁-selective antagonist MRS2179 (**2.03**) bind to their respective receptor, and the selectivity of both receptors is modulated by heteromerization. In the presence of the P2Y₁R, the P2Y₁₁R was no longer inhibited by the selective P2Y₁₁R antagonist NF157 (**2.07**), a derivative of the unselective P2Y receptor antagonist suramin (**2.08**). Moreover, antagonist MRS2179 (**2.03**) inhibited the activation of the P2Y₁₁R induced by Bz-ATP. The authors concluded that Bz-ATP induces a specific receptor conformation which has modulatory effects by its interaction with the P2Y₁.

P2Y₁R and P2Y₁₂R modulate the activity of neurons via the two-pore potassium K_{2P} (two-pore domain potassium) channels as observed in tsA201 cells transfected with the P2Y₁R, the P2Y₁₂R, or both, and with or without the K_{2P} channel.¹¹⁵ ADP inhibited evoked currents of the K_{2P} channels possibly through binding to the P2Y₁₂R. The P2Y₁₂R antagonist cangrelor (**3.02**) had no significant effect on ion channel activity. ATP, which is an agonist of the P2Y₁R but not of the P2Y₁₂R subtype, had no effect on cells expressing only the K_{2P} ion channels but showed inhibitory effects when P2Y₁R and P2Y₁₂R were coexpressed, with a similar time-course as ADP. These results suggest that the P2Y₁₂R inhibits K_{2P} currents through co-activation of P2Y₁Rs. The P2Y₁R inhibited K_{2P} ion channel activity after activation by ADP. The inhibition was reversed after treatment with the P2Y₁R-selective antagonist **2.3**. K_{2P} ion channel currents were suppressed by both G_{q/11}- and G_i-coupled receptors. In summary, when P2Y₁R and P2Y₁₂R were coexpressed, the pharmacological profile could be compared to that of the P2Y₁₂R, while G protein-coupling was comparable to cells expressing only P2Y₁R, indicating hetero-oligomerization of P2Y₁R and P2Y₁₂R.

Agonist-induced hetero-oligomerization of the P2Y₁R and the adenosine A₁ receptor (A₁AR) was confirmed by bioluminescence resonance energy transfer (BRET) technology when coexpressed in HEK293T cells.^{116,117} The P2Y₁R agonist ADPβS revealed a 400-fold increase in potency toward the A₁AR when tested on cells expressing both receptors, while binding of the AR agonist NECA (**4.01**) and the A₁AR-selective antagonist DPCPX (**4.03**) was reduced. These

BOX 2 VIRTUAL SCREENING

The introduction of virtual screening marked a paradigm shift in drug discovery. The increasing number of published X-ray crystal structures and improvement in computer-aided homology modeling has allowed rational approaches based on ligand docking. Virtual screening attempts prior as well as post to the publication of the X-ray crystal structure of the human P2Y₁R led to the discovery of new orthosteric and allosteric antagonists for the P2Y₁R.^{108–111} To this date, only pharmacophore model-based virtual screening studies have been published for P2Y receptors. No virtual receptor structure-based screening attempts on human P2Y₁-like receptors have been reported in the literature. Virtual high throughput screening (vHTS) is a structure-based approach for the discovery of new scaffolds for drug design.¹¹² Combination of the recently published X-ray crystal structures and updated homology model with vHTS could be of great interest for future drug development.^{113,114}

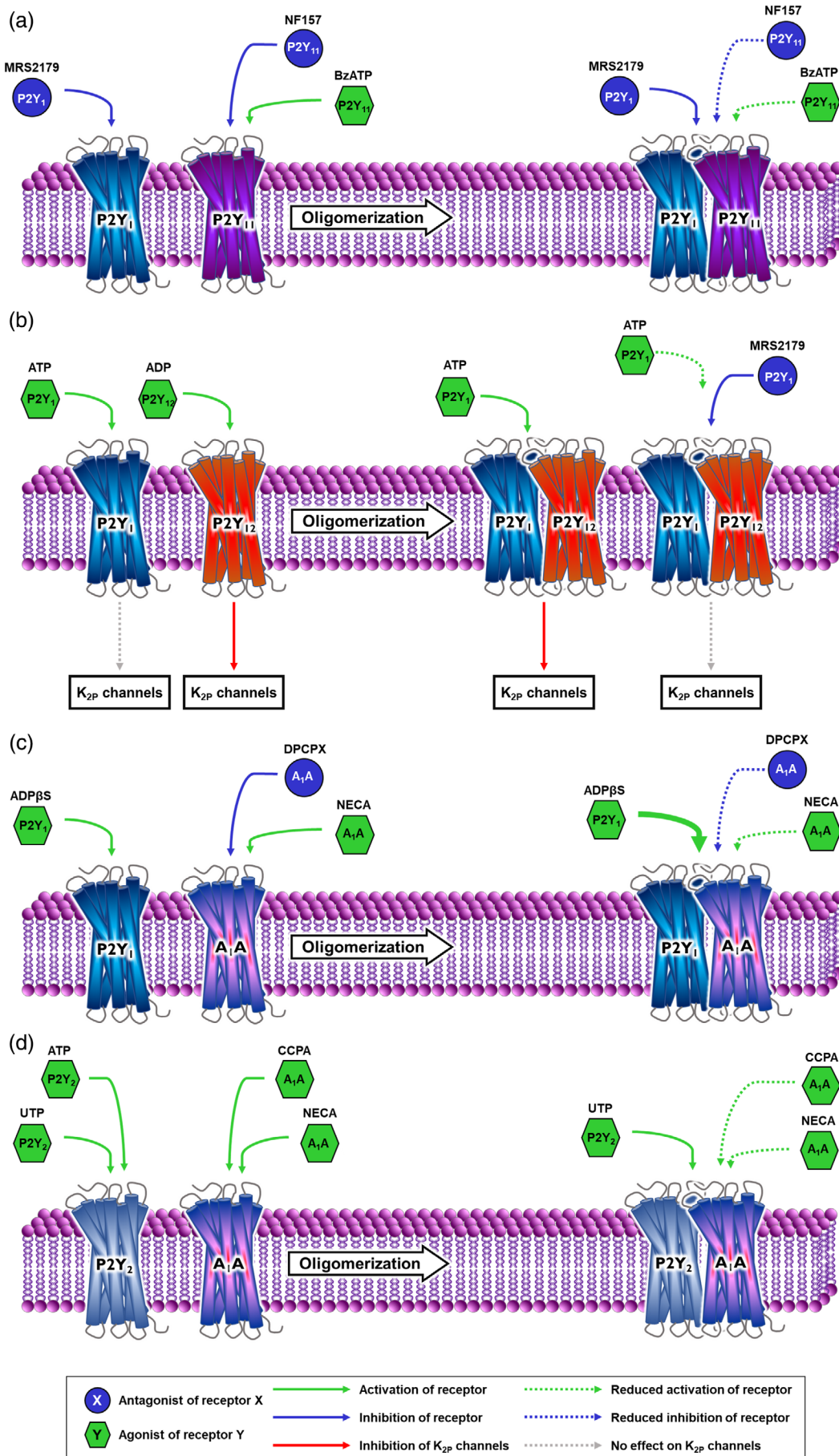


FIGURE 15 Legend on next page.

results indicated that ADP β S bound to the heteromer, altering its pharmacology toward that of the P2Y₁R, and inhibited the activity of adenylate cyclase via the G_{i/o} protein pathway.

Suzuki et al. investigated the heteromerization of A₁AR and P2Y₂R and its pharmacological effects when coexpressed in HEK293T cells.¹¹⁸ P2Y₂R agonists UTP and ATP reduced the binding of the AR agonist NECA (**4.01**) to A₁AR, indicating a direct association of both receptors, as cells expressing only A₁AR showed no significant changes in NECA potency in the presence of P2Y₂R agonists. Hence the heterooligomers possessed different pharmacological properties than the homomeric receptors. ADP β S, a nucleotide that does not bind to the P2Y₂R, had no effect on the binding of NECA. UTP showed inhibitory effects on the activation of cells transfected with both receptors by the selective A₁AR agonist CCPA (**4.2**). These results suggested that UTP interferes with G protein-coupling of the A₁AR in cells coexpressing A₁AR and P2Y₂R. The G_{q/11}-protein-coupled pathway was enhanced by the simultaneous addition of ADP β S and UTP and interfered with signaling via G_{i/o}.

The P2Y₄R was found to form homodimers, and the P2Y₆R homomers as well as monomers.¹¹⁹ Hetero-oligomers of the P2Y₄R were formed only with the P2Y₆R, although P2Y₄R and P2Y₆R possess domains that might enable them to interact with all P2Y₁-like receptors subtypes.

So far, the oligomerization of GPCRs and in particular P2Y receptors still incompletely understood and requires extensive research efforts. It adds another level of complexity to GPCR pharmacology and offers possibilities for selective pharmacological intervention.

7 | CONCLUSION

Mutagenesis and computational chemistry provide a favorable combination to predict binding sites for GPCRs lacking a X-ray crystal structure. However, a X-ray crystal structure of a related receptor should be available to obtain reliable results. So far, 38 mutants with 52 annotations have been created for the human P2Y₁R, 22 mutants with 25 annotations for the human P2Y₂R, and 8 mutants with 11 annotations for the P2Y₁₁R; each was tested for its effects on the potency of agonists and/or antagonists. While an acceptable amount of data on the human P2Y₁R and P2Y₂R is available, only scarce mutagenesis studies have been published for the other three P2Y₁-like receptor subtypes, P2Y₄, P2Y₆ and P2Y₁₁. Homology modeling has been successful in pinpointing key interactions for the P2Y_{2,4,6,11}R subtypes, specifically in combination with the recently published X-ray crystal structures of human P2Y₁R and P2Y₁₂R. The molecular mode of receptor activation postulated on the basis of long-term MD simulations involves the disruption of an ionic lock between an aspartic acid residue of ECL2 and an arginine from TMVII for the P2Y₁R, P2Y₂R, and P2Y₄R, while a similar mode of activation is feasible for P2Y₆R and P2Y₁₁R, but additional data and updated receptor models are required to confirm this assumption. Docking of agonists and antagonists confirmed interactions with the proposed key residues; agonists appear to weaken the salt bridge between both residues thereby breaking the ionic lock, while antagonists stabilize the ionic lock and thus prevent receptor activation. It appears that the ECL2 has a major role in ligand recognition and binding.

Pharmacophore-based virtual screening led to the discovery of *N,N'*-bis-aryurea derivatives as P2Y₁R antagonists. With progressing research on protein-protein interactions, oligomerization of GPCRs, and the consequences of association of homo- or hetero-oligomers for the pharmacological properties of the receptors, receptor complexes will likely become interesting targets for research and the development of new classes of molecules which alter oligomer formation and allosterically modulate receptor function. The P2Y₁-like receptors represent promising targets for the treatment of a number of common diseases, including inflammation and neurodegeneration. The synergistic combination of mutagenesis and computational chemistry will be useful for systematic search and rational design of future drugs acting at these receptors.

FIGURE 15 Oligomerization of P2Y receptors. (a) Oligomerization of P2Y₁R with P2Y₁₁R and the resulting impact on the pharmacological profile of the P2Y₁₁R. (b) Dimerization of P2Y₁R and P2Y₁₂R modulates the responses of the receptors toward K_{2P} ion channels when coexpressed in the same cell line. The profile of the dimers is similar to the pharmacological profile of the P2Y₁₂R, while the G protein-coupling seems to be comparable to that of the P2Y₁R. Oligomerization of the adenosine A₁ receptor with the P2Y₁R (c) and the P2Y₂R (d). The oligomeric A₁AR/P2YR exhibits a preference for the corresponding P2YR agonists, whereas the potency of A₁AR agonist and agonists is reduced

ACKNOWLEDGMENTS

A.N. and C.E.M. were supported by the German Research Foundation (DFG, Research Training group GRK 1873).

CONFLICT OF INTEREST

The authors have declared no conflicts of interest for this article.

AUTHOR CONTRIBUTIONS

Alexander Neumann: Data curation-equal; formal analysis-equal; writing-review & editing-equal. **Christa Müller:** Funding acquisition-lead; supervision-equal; writing-review & editing-equal. **Vigneshwaran Namasivayam:** Conceptualization-equal; supervision-equal; writing-review & editing-equal.

ORCID

Alexander Neumann  <https://orcid.org/0000-0002-1446-4389>

Christa E. Müller  <https://orcid.org/0000-0002-0013-6624>

Vigneshwaran Namasivayam  <https://orcid.org/0000-0003-3031-3377>

RELATED WIRES ARTICLES

[Optimization of protein models](#)

[Reversing cancer multidrug resistance: insights into the efflux by ABC transports from in silico studies](#)

[About P-glycoprotein: a new drugable domain is emerging from structural data](#)

[Computer-aided drug design in new druggable targets for the next generation of immune-oncology therapies](#)

FURTHER READING

Ferré S, Casadó V, Devi LA, et al. G protein-coupled receptor oligomerization revisited: functional and pharmacological perspectives. *Pharmacol Rev.* 2014;66:413–434. <https://doi.org/10.1124/pr.113.008052>.

Thal DM, Glukhova A, Sexton PM, Christopoulos A. Structural insights into G-protein-coupled receptor allostery. *Nature.* 2018;559:45–53. <https://doi.org/10.1038/s41586-018-0259-z>.

Gacasan SB, Baker DL, Parrill AL. G protein-coupled receptors: the evolution of structural insight. *AIMS Biophys.* 2017;4:491–527. <https://doi.org/10.3934/biophy.2017.3.491>.

Burnstock G. Purinergic signalling: therapeutic developments. *Front Pharmacol.* 2017;8:661. <https://doi.org/10.3389/fphar.2017.00661>.

von Kügelgen I. Pharmacology of P2Y receptors. *Brain Res Bull.* 2019;151:12–24. <https://doi.org/10.1016/j.brainresbull.2019.03.010>.

Rafehi M, Müller CE. Tools and drugs for uracil nucleotide-activated P2Y receptors. *Pharmacol Ther.* 2018;190:24–80. <https://doi.org/10.1016/j.pharmthera.2018.04.002>.

REFERENCES

1. Attwood TK, Findlay JB. Fingerprinting G-protein-coupled receptors. *Protein Eng.* 1994;7:195–203.
2. Foord SM, Bonner TI, Neubig RR, et al. International Union of Pharmacology. XLVI. G protein-coupled receptor list. *Pharmacol Rev.* 2005;57:279–288. <https://doi.org/10.1124/pr.57.2.5>.
3. Isberg V, Mordalski S, Munk C, et al. GPCRdb: an information system for G protein-coupled receptors. *Nucleic Acids Res.* 2017;45:2936. <https://doi.org/10.1093/nar/gkw1218>.
4. Munk C, Isberg V, Mordalski S, et al. GPCRdb: the G protein-coupled receptor database - an introduction. *Br J Pharmacol.* 2016;173:2195–2207. <https://doi.org/10.1111/bph.13509>.
5. Conner M, Hicks MR, Dafforn T, et al. Functional and biophysical analysis of the C-terminus of the CGRP-receptor; a family B GPCR. *Biochemistry.* 2008;47:8434–8444. <https://doi.org/10.1021/bi8004126>.
6. Katritch V, Cherezov V, Stevens RC. Structure-function of the G protein-coupled receptor superfamily. *Annu Rev Pharmacol Toxicol.* 2013;53:531–556. <https://doi.org/10.1146/annurev-pharmtox-032112-135923>.
7. Schiöth HB, Fredriksson R. The GRAFS classification system of G-protein coupled receptors in comparative perspective. *Gen Comp Endocrinol.* 2005;142:94–101. <https://doi.org/10.1016/j.ygcen.2004.12.018>.
8. Latek D, Modzelewska A, Trzaskowski B, Palczewski K, Filipek S. G protein-coupled receptors — recent advances. *Acta Biochim Pol.* 2012;59:515–529.
9. Coddou C, Stojilkovic SS, Huidobro-Toro JP. Allosteric modulation of ATP-gated P2X receptor channels. *Rev Neurosci.* 2011;22:335–354. <https://doi.org/10.1515/RNS.2011.014>.
10. Hausmann R, Kless A, Schmalzing G. Key sites for P2X receptor function and multimerization: overview of mutagenesis studies on a structural basis. *Curr Med Chem.* 2015;22:799–818.
11. Sievers F, Higgins DG. Clustal omega. *Curr Protoc Bioinformatics.* 2014;48:3.13.1–3.13.16. <https://doi.org/10.1002/0471250953.bi0313s48>.

12. Sievers F, Higgins DG. Clustal Omega, accurate alignment of very large numbers of sequences. *Methods Mol Biol.* 2014;1079:105–116. https://doi.org/10.1007/978-1-62703-646-7_6.
13. Sievers F, Wilm A, Dineen D, et al. Fast, scalable generation of high-quality protein multiple sequence alignments using Clustal Omega. *Mol Syst Biol.* 2011;7:539. <https://doi.org/10.1038/msb.2011.75>.
14. Erb L, Weisman GA. Coupling of P2Y receptors to G proteins and other signaling pathways. *Wiley Interdiscip Rev Membr Transp Signal.* 2012;1:789–803. <https://doi.org/10.1002/wmts.62>.
15. von Kügelgen I, Hoffmann K. Pharmacology and structure of P2Y receptors. *Neuropharmacology.* 2016;104:50–61. <https://doi.org/10.1016/j.neuropharm.2015.10.030>.
16. Brunschweiler A, Müller CE. P2 receptors activated by uracil nucleotides—an update. *Curr Med Chem.* 2006;13:289–312.
17. Chambers JK, Macdonald LE, Sarau HM, et al. A G protein-coupled receptor for UDP-glucose. *J Biol Chem.* 2000;275:10767–10771.
18. Xu P, Feng X, Luan H, et al. Current knowledge on the nucleotide agonists for the P2Y2 receptor. *Bioorg Med Chem.* 2018;26:366–375. <https://doi.org/10.1016/j.bmc.2017.11.043>.
19. Rafehi M, Müller CE. Tools and drugs for uracil nucleotide-activated P2Y receptors. *Pharmacol Ther.* 2018;190:24–80. <https://doi.org/10.1016/j.pharmthera.2018.04.002>.
20. Ciancetta A, O'Connor RD, Paoletta S, Jacobson KA. Demystifying P2Y1 receptor ligand recognition through docking and molecular dynamics analyses. *J Chem Inf Model.* 2017;57:3104–3123. <https://doi.org/10.1021/acs.jcim.7b00528>.
21. Ciancetta A, Jacobson KA. Breakthrough in GPCR crystallography and its impact on computer-aided drug design. *Methods Mol Biol.* 2018;1705:45–72. https://doi.org/10.1007/978-1-4939-7465-8_3.
22. Jacobson KA, Gao Z-G, Paoletta S, et al. John Daly Lecture: structure-guided drug design for adenosine and P2Y receptors. *Comput Struct Biotechnol J.* 2015;13:286–298. <https://doi.org/10.1016/j.csbj.2014.10.004>.
23. Jacobson KA, Müller CE. Medicinal chemistry of adenosine, P2Y and P2X receptors. *Neuropharmacology.* 2016;104:31–49. <https://doi.org/10.1016/j.neuropharm.2015.12.001>.
24. Palczewski K, Kumasaka T, Hori T, et al. Crystal structure of rhodopsin: a G protein-coupled receptor. *Science.* 2000;289:739–745.
25. Rasmussen SGF, Choi H-J, Rosenbaum DM, et al. Crystal structure of the human beta2 adrenergic G-protein-coupled receptor. *Nature.* 2007;450:383–387. <https://doi.org/10.1038/nature06325>.
26. Jaakola V-P, Griffith MT, Hanson MA, et al. The 2.6 angstrom crystal structure of a human A2A adenosine receptor bound to an antagonist. *Science.* 2008;322:1211–1217. <https://doi.org/10.1126/science.1164772>.
27. Zhang J, Zhang K, Gao Z-G, et al. Agonist-bound structure of the human P2Y12 receptor. *Nature.* 2014;509:119–122. <https://doi.org/10.1038/nature13288>.
28. Zhang D, Gao Z-G, Zhang K, et al. Two disparate ligand-binding sites in the human P2Y1 receptor. *Nature.* 2015;520:317–321. <https://doi.org/10.1038/nature14287>.
29. Zhang K, Zhang J, Gao Z-G, et al. Structure of the human P2Y12 receptor in complex with an antithrombotic drug. *Nature.* 2014;509:115–118. <https://doi.org/10.1038/nature13083>.
30. Jiang Q, Guo D, Lee BX, et al. A mutational analysis of residues essential for ligand recognition at the human P2Y1 receptor. *Mol Pharmacol.* 1997;52:499–507.
31. Moro S, Guo D, Camaioni E, Boyer JL, Harden TK, Jacobson KA. Human P2Y1 receptor: molecular modeling and site-directed mutagenesis as tools to identify agonist and antagonist recognition sites. *J Med Chem.* 1998;41:1456–1466. <https://doi.org/10.1021/jm970684u>.
32. Hoffmann C, Moro S, Nicholas RA, Harden TK, Jacobson KA. The role of amino acids in extracellular loops of the human P2Y1 receptor in surface expression and activation processes. *J Biol Chem.* 1999;274:14639–14647.
33. Costanzi S, Mamedova L, Gao Z-G, Jacobson KA. Architecture of P2Y nucleotide receptors: structural comparison based on sequence analysis, mutagenesis, and homology modeling. *J Med Chem.* 2004;47:5393–5404. <https://doi.org/10.1021/jm049914c>.
34. Guo D, von Kügelgen I, Moro S, Kim Y-C, Jacobson KA. Evidence for the recognition of non-nucleotide antagonists within the transmembrane domains of the human P2Y(1) receptor. *Drug Dev Res.* 2002;57:173–181. <https://doi.org/10.1002/ddr.10145>.
35. Ding Z, Tuluc F, Bandivadekar KR, Zhang L, Jin J, Kunapuli SP. Arg333 and Arg334 in the COOH terminus of the human P2Y1 receptor are crucial for Gq coupling. *Am J Physiol Cell Physiol.* 2005;288:C559–C567. <https://doi.org/10.1152/ajpcell.00401.2004>.
36. Lee SY, Wolff SC, Nicholas RA, O'Grady SM. P2Y receptors modulate ion channel function through interactions involving the C-terminal domain. *Mol Pharmacol.* 2003;63:878–885.
37. Fam SR, Gallagher CJ, Kalia LV, Salter MW. Differential frequency dependence of P2Y1- and P2Y2- mediated Ca²⁺ signaling in astrocytes. *J Neurosci.* 2003;23:4437–4444.
38. Qi A-D, Houston-Cohen D, Naruszewicz I, Harden TK, Nicholas RA. Ser352 and Ser354 in the carboxyl terminus of the human P2Y(1) receptor are required for agonist-promoted phosphorylation and internalization in MDCK cells. *Br J Pharmacol.* 2011;162:1304–1313. <https://doi.org/10.1111/j.1476-5381.2010.01135.x>.
39. Hoffmann C, Soltysiak K, West PL, Jacobson KA. Shift in purine/pyrimidine base recognition upon exchanging extracellular domains in P2Y 1/6 chimeric receptors. *Biochem Pharmacol.* 2004;68:2075–2086. <https://doi.org/10.1016/j.bcp.2004.07.014>.
40. Wildman SS, Unwin RJ, King BF. Extended pharmacological profiles of rat P2Y2 and rat P2Y4 receptors and their sensitivity to extracellular H⁺ and Zn²⁺ ions. *Br J Pharmacol.* 2003;140:1177–1186. <https://doi.org/10.1038/sj.bjp.0705544>.
41. Erb L, Garrad R, Wang Y, Quinn T, Turner JT, Weisman GA. Site-directed mutagenesis of P2U purinoceptors. Positively charged amino acids in transmembrane helices 6 and 7 affect agonist potency and specificity. *J Biol Chem.* 1995;270:4185–4188.

42. Ibuka S, Matsumoto S, Fujii S, Kikuchi A. The P2Y2 receptor promotes Wnt3a- and EGF-induced epithelial tubular formation by IEC6 cells by binding to integrins. *J Cell Sci.* 2015;128:2156–2168. <https://doi.org/10.1242/jcs.169060>.
43. Hillmann P, Ko G-Y, Spinrath A, et al. Key determinants of nucleotide-activated G protein-coupled P2Y(2) receptor function revealed by chemical and pharmacological experiments, mutagenesis and homology modeling. *J Med Chem.* 2009;52:2762–2775. <https://doi.org/10.1021/jm801442p>.
44. Rafehi M, Neumann A, Baqi Y, et al. Molecular recognition of agonists and antagonists by the nucleotide-activated G protein-coupled P2Y2 receptor. *J Med Chem.* 2017;60:8425–8440. <https://doi.org/10.1021/acs.jmedchem.7b00854>.
45. Kindon N, Davis A, Dougall I, et al. From UTP to AR-C118925, the discovery of a potent non nucleotide antagonist of the P2Y2 receptor. *Bioorg Med Chem Lett.* 2017;27:4849–4853. <https://doi.org/10.1016/j.bmcl.2017.09.043>.
46. Muoboghare MO, Drummond RM, Kennedy C. Characterisation of P2Y2 receptors in human vascular endothelial cells using AR-C118925XX, a competitive and selective P2Y2 antagonist. *Br J Pharmacol.* 2019;176:2894–2904. <https://doi.org/10.1111/bph.14715>.
47. Rafehi M, Burbiel JC, Attah IY, Abdelrahman A, Müller CE. Synthesis, characterization, and in vitro evaluation of the selective P2Y2 receptor antagonist AR-C118925. *Purinergic Signal.* 2017;13:89–103. <https://doi.org/10.1007/s11302-016-9542-3>.
48. Erb L, Liu J, Ockerhausen J, et al. An RGD sequence in the P2Y(2) receptor interacts with alpha(V)beta(3) integrins and is required for G(o)-mediated signal transduction. *J Cell Biol.* 2001;153:491–501.
49. Liao Z, Seye CI, Weisman GA, Erb L. The P2Y2 nucleotide receptor requires interaction with alpha v integrins to access and activate G12. *J Cell Sci.* 2007;120:1654–1662. <https://doi.org/10.1242/jcs.03441>.
50. Flores RV, Hernández-Pérez MG, Aquino E, Garrad RC, Weisman GA, Gonzalez FA. Agonist-induced phosphorylation and desensitization of the P2Y2 nucleotide receptor. *Mol Cell Biochem.* 2005;280:35–45. <https://doi.org/10.1007/s11010-005-8050-5>.
51. Herold CL, Qi A-D, Harden TK, Nicholas RA. Agonist versus antagonist action of ATP at the P2Y4 receptor is determined by the second extracellular loop. *J Biol Chem.* 2004;279:11456–11464. <https://doi.org/10.1074/jbc.M301734200>.
52. Brinson AE, Harden TK. Differential regulation of the uridine nucleotide-activated P2Y4 and P2Y6 receptors. SER-333 and SER-334 in the carboxyl terminus are involved in agonist-dependent phosphorylation desensitization and internalization of the P2Y4 receptor. *J Biol Chem.* 2001;276:11939–11948. <https://doi.org/10.1074/jbc.M009909200>.
53. DuBose DR, Wolff SC, Qi AD, Naruszewicz I, Nicholas RA. Apical targeting of the P2Y(4) receptor is directed by hydrophobic and basic residues in the cytoplasmic tail. *Am J Physiol Cell Physiol.* 2013;304(3):C228–C239. <https://doi.org/10.1152/ajpcell.00251.2012>.
54. Wolff SC, Qi A-D, Harden TK, Nicholas RA. Charged residues in the C-terminus of the P2Y1 receptor constitute a basolateral-sorting signal. *J Cell Sci.* 2010;123:2512–2520. <https://doi.org/10.1242/jcs.060723>.
55. Brüser A, Zimmermann A, Crews BC, et al. Prostaglandin E2 glyceryl ester is an endogenous agonist of the nucleotide receptor P2Y6. *Sci Rep.* 2017;7:2380. <https://doi.org/10.1038/s41598-017-02414-8>.
56. Zylberg J, Ecke D, Fischer B, Reiser G. Structure and ligand-binding site characteristics of the human P2Y11 nucleotide receptor deduced from computational modelling and mutational analysis. *Biochem J.* 2007;405:277–286. <https://doi.org/10.1042/BJ20061728>.
57. Ecke D, Fischer B, Reiser G. Diastereoselectivity of the P2Y11 nucleotide receptor: mutational analysis. *Br J Pharmacol.* 2008;155:1250–1255. <https://doi.org/10.1038/bjp.2008.352>.
58. Ecke D, Hanck T, Tulapurkar ME, et al. Hetero-oligomerization of the P2Y11 receptor with the P2Y1 receptor controls the internalization and ligand selectivity of the P2Y11 receptor. *Biochem J.* 2008;409:107–116. <https://doi.org/10.1042/BJ20070671>.
59. Haas M, Shaaban A, Reiser G. Alanine-(87)-threonine polymorphism impairs signaling and internalization of the human P2Y11 receptor, when co-expressed with the P2Y1 receptor. *J Neurochem.* 2014;129:602–613. <https://doi.org/10.1111/jnc.12666>.
60. Amisten S, Melander O, Wihlborg A-K, Berglund G, Erlinge D. Increased risk of acute myocardial infarction and elevated levels of C-reactive protein in carriers of the Thr-87 variant of the ATP receptor P2Y11. *Eur Heart J.* 2007;28:13–18. <https://doi.org/10.1093/eurheartj/ehl410>.
61. Ballesteros JA, Weinstein H. Analysis and refinement of criteria for predicting the structure and relative orientations of transmembrane helical domains. *Biophys J.* 1992;62:107–109. [https://doi.org/10.1016/S0006-3495\(92\)81794-0](https://doi.org/10.1016/S0006-3495(92)81794-0).
62. Dreisig K, Kornum BR. A critical look at the function of the P2Y11 receptor. *Purinergic Signal.* 2016;12:427–437. <https://doi.org/10.1007/s11302-016-9514-7>.
63. Chao TH, Ember JA, Wang M, Bayon Y, Hugli TE, Ye RD. Role of the second extracellular loop of human C3a receptor in agonist binding and receptor function. *J Biol Chem.* 1999;274:9721–9728.
64. Brunskole I, Strasser A, Seifert R, Buschauer A. Role of the second and third extracellular loops of the histamine H(4) receptor in receptor activation. *Naunyn Schmiedebergs Arch Pharmacol.* 2011;384:301–317. <https://doi.org/10.1007/s00210-011-0673-3>.
65. Wifling D, Bernhardt G, Dove S, Buschauer A. The extracellular loop 2 (ECL2) of the human histamine H4 receptor substantially contributes to ligand binding and constitutive activity. *PLoS One.* 2015;10:e0117185. <https://doi.org/10.1371/journal.pone.0117185>.
66. Zhao MM, Hwa J, Perez DM. Identification of critical extracellular loop residues involved in alpha 1-adrenergic receptor subtype-selective antagonist binding. *Mol Pharmacol.* 1996;50:1118–1126.
67. Ott TR, Troskie BE, Roeske RW, Illing N, Flanagan CA, Millar RP. Two mutations in extracellular loop 2 of the human GnRH receptor convert an antagonist to an agonist. *Mol Endocrinol.* 2002;16:1079–1088. <https://doi.org/10.1210/mend.16.5.0824>.
68. Banères J-L, Mesnier D, Martin A, Joubert L, Dumuis A, Bockaert J. Molecular characterization of a purified 5-HT4 receptor: a structural basis for drug efficacy. *J Biol Chem.* 2005;280:20253–20260. <https://doi.org/10.1074/jbc.M412009200>.
69. Wheatley M, Wootten D, Conner MT, et al. Lifting the lid on GPCRs: the role of extracellular loops. *Br J Pharmacol.* 2012;165:1688–1703. <https://doi.org/10.1111/j.1476-5381.2011.01629.x>.

70. Shiraki K, Hirano A, Kita Y, Koyama AH, Arakawa T. Potential application of arginine in interaction analysis. *Drug Discov Ther.* 2010;4:326–333.
71. Kim J, Jiang Q, Glashofer M, Yehle S, Wess J, Jacobson KA. Glutamate residues in the second extracellular loop of the human A2a adenosine receptor are required for ligand recognition. *Mol Pharmacol.* 1996;49:683–691.
72. Bertalovitz AC, Ahn KH, Kendall DA. Ligand binding sensitivity of the extracellular loop two of the cannabinoid receptor 1. *Drug Dev Res.* 2010;71:404–411. <https://doi.org/10.1002/ddr.20388>.
73. Scarselli M, Li B, Kim S-K, Wess J. Multiple residues in the second extracellular loop are critical for M3 muscarinic acetylcholine receptor activation. *J Biol Chem.* 2007;282:7385–7396. <https://doi.org/10.1074/jbc.M610394200>.
74. Kmiecik S, Jamroz M, Kolinski M. Structure prediction of the second extracellular loop in G-protein-coupled receptors. *Biophys J.* 2014;106:2408–2416. <https://doi.org/10.1016/j.bpj.2014.04.022>.
75. Yuan S, Chan HCS, Vogel H, Filipek S, Stevens RC, Palczewski K. The molecular mechanism of P2Y1 receptor activation. *Angew Chem Int Ed Engl.* 2016;55:10331–10335. <https://doi.org/10.1002/anie.201605147>.
76. Chun E, Thompson AA, Liu W, et al. Fusion partner toolchest for the stabilization and crystallization of G protein-coupled receptors. *Structure.* 2012;20:967–976. <https://doi.org/10.1016/j.str.2012.04.010>.
77. Topiol S. X-ray structural information of GPCRs in drug design: what are the limitations and where do we go? *Expert Opin Drug Discov.* 2013;8:607–620. <https://doi.org/10.1517/17460441.2013.783815>.
78. Nogales E, Scheres SHW. Cryo-EM: a unique tool for the visualization of macromolecular complexity. *Mol Cell.* 2015;58:677–689. <https://doi.org/10.1016/j.molcel.2015.02.019>.
79. García-Nafria J, Lee Y, Bai X, Carpenter B, Tate CG. Cryo-EM structure of the adenosine A2A receptor coupled to an engineered heterotrimeric G protein. *Elife.* 2018;7. <https://doi.org/10.7554/eLife.35946>.
80. Zhang Y, Sun B, Feng D, et al. Cryo-EM structure of the activated GLP-1 receptor in complex with a G protein. *Nature.* 2017;546:248–253. <https://doi.org/10.1038/nature22394>.
81. Chu R, Takei J, Knowlton JR, et al. Redesign of a four-helix bundle protein by phage display coupled with proteolysis and structural characterization by NMR and X-ray crystallography. *J Mol Biol.* 2002;323:253–262.
82. Kim HS, Ohno M, Xu B, et al. 2-Substitution of adenine nucleotide analogues containing a bicyclo3.1.0hexane ring system locked in a northern conformation: enhanced potency as P2Y1 receptor antagonists. *J Med Chem.* 2003;46:4974–4987. <https://doi.org/10.1021/jm030127>.
83. Hechler B, Nonne C, Roh EJ, et al. MRS2500 2-iodo-N6-methyl-(N)-methanocarpa-2'-deoxyadenosine-3',5'-bisphosphate, a potent, selective, and stable antagonist of the platelet P2Y1 receptor with strong antithrombotic activity in mice. *J Pharmacol Exp Ther.* 2006;316:556–563. <https://doi.org/10.1124/jpet.105.094037>.
84. Chao H, Turdi H, Herpin TF, et al. Discovery of 2-(phenoxy)pyridine-3-phenylureas as small molecule P2Y1 antagonists. *J Med Chem.* 2013;56:1704–1714. <https://doi.org/10.1021/jm301708u>.
85. Qiao JX, Wang TC, Ruel R, et al. Conformationally constrained ortho-anilino diaryl ureas: discovery of 1-(2-[1'-neopentylspiroindoline-3,4'-piperidine-1-yl]phenyl)-3-(4-[trifluoromethoxy]phenyl)urea, a potent, selective, and bioavailable P2Y1 antagonist. *J Med Chem.* 2013;56:9275–9295. <https://doi.org/10.1021/jm4013906>.
86. Flock T, Ravarani CNJ, Sun D, et al. Universal allosteric mechanism for G α activation by GPCRs. *Nature.* 2015;524:173–179. <https://doi.org/10.1038/nature14663>.
87. Trzaskowski B, Latek D, Yuan S, Ghoshdastider U, Debinski A, Filipek S. Action of molecular switches in GPCRs—theoretical and experimental studies. *Curr Med Chem.* 2012;19:1090–1109.
88. Rafehi M, Malik EM, Neumann A, et al. Development of potent and selective antagonists for the UTP-activated P2Y4 receptor. *J Med Chem.* 2017;60:3020–3038. <https://doi.org/10.1021/acs.jmedchem.7b00030>.
89. Jacobson KA, Jayasekara MPS, Costanzi S. Molecular structure of P2Y receptors: mutagenesis, modeling, and chemical probes. *Wiley Interdiscip Rev Membr Transp Signal.* 2012;1:815–827. <https://doi.org/10.1002/wmts.68>.
90. Ivanov AA, Ko H, Cosyn L, et al. Molecular modeling of the human P2Y2 receptor and design of a selective agonist, 2'-amino-2'-deoxy-2-thiouridine 5'-triphosphate. *J Med Chem.* 2007;50:1166–1176. <https://doi.org/10.1021/jm060903o>.
91. Costanzi S, Tikhonova IG, Ohno M, et al. P2Y1 antagonists: combining receptor-based modeling and QSAR for a quantitative prediction of the biological activity based on consensus scoring. *J Med Chem.* 2007;50:3229–3241. <https://doi.org/10.1021/jm0700971>.
92. Deflorian F, Jacobson KA. Comparison of three GPCR structural templates for modeling of the P2Y12 nucleotide receptor. *J Comput Aided Mol Des.* 2011;25:329–338. <https://doi.org/10.1007/s10822-011-9423-3>.
93. Costanzi S, Joshi BV, Maddileti S, et al. Human P2Y(6) receptor: molecular modeling leads to the rational design of a novel agonist based on a unique conformational preference. *J Med Chem.* 2005;48:8108–8111. <https://doi.org/10.1021/jm050911p>.
94. Aitken H, Poyser NL, Hollingsworth M. The effects of P2Y receptor agonists and adenosine on prostaglandin production by the guinea-pig uterus. *Br J Pharmacol.* 2001;132:709–721. <https://doi.org/10.1038/sj.bjp.0703848>.
95. Través PG, Pimentel-Santillana M, Carrasquero LMG, et al. Selective impairment of P2Y signaling by prostaglandin E2 in macrophages: implications for Ca $^{2+}$ -dependent responses. *J Immunol.* 2013;190:4226–4235. <https://doi.org/10.4049/jimmunol.1203029>.
96. Ouzounoglou E, Kalamatianos D, Emmanouilidou E, et al. In silico modeling of the effects of alpha-synuclein oligomerization on dopaminergic neuronal homeostasis. *BMC Syst Biol.* 2014;8:54. <https://doi.org/10.1186/1752-0509-8-54>.
97. Kroeger KM, Pflieger KDG, Eidne KA. G-protein coupled receptor oligomerization in neuroendocrine pathways. *Front Neuroendocrinol.* 2003;24:254–278.

98. Gahbauer S, Böckmann RA. Membrane-mediated oligomerization of G protein coupled receptors and its implications for GPCR function. *Front Physiol.* 2016;7:494. <https://doi.org/10.3389/fphys.2016.00494>.
99. Gabizon R, Friedler A. Allosteric modulation of protein oligomerization: an emerging approach to drug design. *Front Chem.* 2014;2:9. <https://doi.org/10.3389/fchem.2014.00009>.
100. Ferré S, Casadó V, Devi LA, et al. G protein-coupled receptor oligomerization revisited: functional and pharmacological perspectives. *Pharmacol Rev.* 2014;66:413–434. <https://doi.org/10.1124/pr.113.008052>.
101. Bastos-Aristizabal S, Kozlov G, Gehring K. Structural insight into the dimerization of human protein disulfide isomerase. *Protein Sci.* 2014;23:618–626. <https://doi.org/10.1002/pro.2444>.
102. Assimon VA, Gillies AT, Rauch JN, Gestwicki JE. Hsp70 protein complexes as drug targets. *Curr Pharm Des.* 2013;19:404–417. <https://doi.org/10.2174/138161213804143699>.
103. Goncarenco A, Li M, Simonetti FL, Shoemaker BA, Panchenko AR. Exploring protein-protein interactions as drug targets for anti-cancer therapy with in silico workflows. *Methods Mol Biol.* 1647;2017:221–236. https://doi.org/10.1007/978-1-4939-7201-2_15.
104. Villoutreix BO, Kuenemann MA, Poyet J-L, et al. Drug-like protein-protein interaction modulators: challenges and opportunities for drug discovery and chemical biology. *Mol Inform.* 2014;33:414–437. <https://doi.org/10.1002/minf.201400040>.
105. Feng Y, Wang Q, Wang T. Drug target protein-protein interaction networks: a systematic perspective. *Biomed Res Int.* 2017;2017:1–13. <https://doi.org/10.1155/2017/1289259>.
106. Kaczor AA, Rutkowska E, Bartuzi D, Targowska-Duda KM, Matosiuk D, Selent J. Computational methods for studying G protein-coupled receptors (GPCRs). *Methods Cell Biol.* 2016;132:359–399. <https://doi.org/10.1016/bs.mcb.2015.11.002>.
107. Taddese B, Simpson LM, Wall ID, et al. G-protein-coupled receptor dynamics: dimerization and activation models compared with experiment. *Biochem Soc Trans.* 2012;40:394–399. <https://doi.org/10.1042/BST20110755>.
108. Zhang X, Lu F, Chen Y-K, et al. Discovery of potential orthosteric and allosteric antagonists of P2Y1R from Chinese herbs by molecular simulation methods. *Evid Based Complement Alternat Med.* 2016;2016:1–12. <https://doi.org/10.1155/2016/4320201>.
109. Yi F, Le Sun XL-J, Peng Y, Liu H-B, He C-N, Xiao P-G. In silico approach for anti-thrombosis drug discovery: P2Y1R structure-based TCMs screening. *Front Pharmacol.* 2016;7:531. <https://doi.org/10.3389/fphar.2016.00531>.
110. Jacobson KA. Structure-based approaches to ligands for G-protein-coupled adenosine and P2Y receptors, from small molecules to nanoconjugates. *J Med Chem.* 2013;56:3749–3767. <https://doi.org/10.1021/jm400422s>.
111. Hiramoto T, Nonaka Y, Inoue K, et al. Identification of endogenous surrogate ligands for human P2Y receptors through an in silico search. *J Pharmacol Sci.* 2004;95:81–93.
112. Subramaniam S, Mehrotra M, Gupta D. Virtual high throughput screening (vHTS)—a perspective. *Bioinformation.* 2008;3:14–17.
113. Leelananda SP, Lindert S. Computational methods in drug discovery. *Beilstein J Org Chem.* 2016;12:2694–2718. <https://doi.org/10.3762/bjoc.12.267>.
114. Srivastava P, Tiwari A. Critical role of computer simulations in drug discovery and development. *Curr Top Med Chem.* 2017;17:2422–2432. <https://doi.org/10.2174/1568026617666170403113541>.
115. Shrestha SS, Parmar M, Kennedy C, Bushell TJ. Two-pore potassium ion channels are inhibited by both G(q/11)- and G(i)-coupled P2Y receptors. *Mol Cell Neurosci.* 2010;43:363–369. <https://doi.org/10.1016/j.mcn.2010.01.003>.
116. Yoshioka K, Saitoh O, Nakata H. Heteromeric association creates a P2Y-like adenosine receptor. *Proc Natl Acad Sci USA.* 2001;98:7617–7622. <https://doi.org/10.1073/pnas.121587098>.
117. Yoshioka K, Saitoh O, Nakata H. Agonist-promoted heteromeric oligomerization between adenosine A(1) and P2Y(1) receptors in living cells. *FEBS Lett.* 2002;523:147–151.
118. Suzuki T, Namba K, Tsuga H, Nakata H. Regulation of pharmacology by hetero-oligomerization between A1 adenosine receptor and P2Y2 receptor. *Biochem Biophys Res Commun.* 2006;351:559–565. <https://doi.org/10.1016/j.bbrc.2006.10.075>.
119. D'Ambrosi N, Iafrate M, Saba E, Rosa P, Volonté C. Comparative analysis of P2Y4 and P2Y6 receptor architecture in native and transfected neuronal systems. *Biochim Biophys Acta.* 2007;1768:1592–1599. <https://doi.org/10.1016/j.bbame.2007.03.020>.

How to cite this article: Neumann A, Müller CE, Namasivayam V. P2Y₁-like nucleotide receptors—Structures, molecular modeling, mutagenesis, and oligomerization. *WIREs Comput Mol Sci.* 2020;10:e1464. <https://doi.org/10.1002/wcms.1464>

3.3. Summary and Outlook

This review collected research data on pharmacological effects of P2YR mutants and hetero-oligomerization with other receptors. The findings suggest that endogenous nucleotides bind in the upper third part of the receptor similar to the binding mode of agonists at human P2Y₁₂R. Contrary to the binding mode of the P2Y₁R nucleotide antagonist MRS2500 in which the nucleobase is exposed to the extracellular lumen, endogenous agonists likely occupy a lipophilic binding site underneath extracellular loop 2 (ECL2). Yet, the β - and γ -phosphate groups of agonists overlap with the 5'-phosphate of MRS2500. Furthermore, ionic locks between an aspartic acid in ECL2 and an arginine in transmembrane 7 (TM7) analogous to the proposed for P2Y₁R were observed in homology models of human P2Y₂- and P2Y₄Rs. They likely represent central elements in agonist-induced receptor activation and are therefore of great interest for the future design of (tool) compounds. Knowledge about the topology of the binding site and about the ligand conformation amassed in this review will be a useful resource for rational compound evolution and computational SBDD.

4. Molecular Recognition of Agonists and Antagonists by the Nucleotide-Activated G Protein-Coupled P2Y₂ Receptor

4.1. Introduction

Unfortunately, only a low number of compounds acting at P2Y₂R is available. Most of them display unfavorable properties such as charged groups (e.g., sulfonic acid in anthraquinone derivatives) resulting in poor oral bioavailability making them unattractive as lead structures. Yet, in order to design and discover novel drugs and tool compounds to perform target validation studies of this pharmacologically relevant receptor, knowledge about potential binding sites is required. Since no X-ray crystal structure of human P2Y₂R has been published so far, a homology model was created for SBDD. In order to elucidate and confirm the binding mode hypothesis of nucleotide agonists at P2Y₂R, several residues were selected for site-directed mutagenesis. Based on insights summarized in **Section 3** and molecular docking studies at an updated homology model of human P2Y₂R, fifteen charged and lipophilic residues predicted to interact with nucleotides in the putative orthosteric binding site were mutated and pharmacologically assessed with agonists (UTP and Ap₄A) and antagonists (anthraquinone derivatives and AR-C118925). The aim of this study was the determination of the orthosteric binding site utilizing the impact of mutants on ligand potency as surrogate parameter, as well as the elucidation of agonist and antagonist binding modes. The updated homology P2Y₂R model based on the more closely related P2Y₁R and P2Y₁₂R X-ray crystal structures as templates represents an improved basis for structure-based computational approaches compared to the previously published model based on bovine rhodopsin.

4.2. Publication

Molecular Recognition of Agonists and Antagonists by the Nucleotide-Activated G Protein-Coupled P2Y₂ Receptor

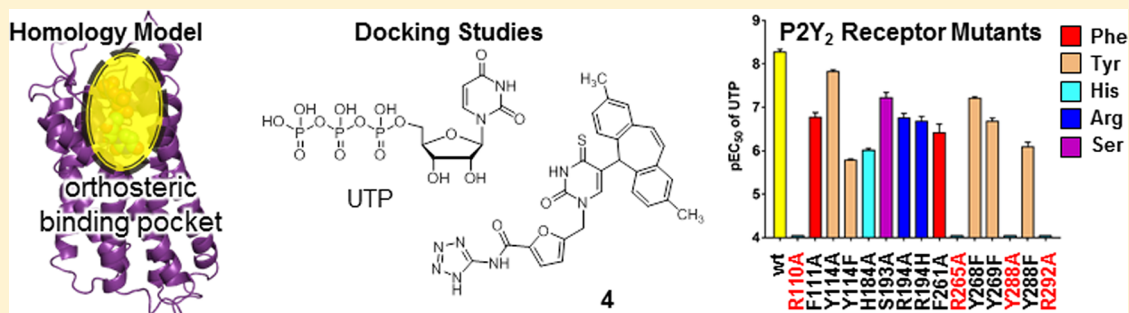
Muhammad Rafehi,^{†,‡,§} Alexander Neumann,^{†,‡,§} Younis Baqi,[§] Enas M. Malik,^{†,§} Michael Wiese,[‡] Vigneshwaran Namasivayam,^{†,‡} and Christa E. Müller^{*,†,§}

[†]PharmaCenter Bonn, Pharmaceutical Institute, Pharmaceutical Sciences Bonn (PSB), Pharmaceutical Chemistry I, University of Bonn, 53121 Bonn, Germany

[‡]PharmaCenter Bonn, Pharmaceutical Institute, Pharmaceutical Chemistry II, University of Bonn, 53121 Bonn, Germany

[§]Department of Chemistry, Faculty of Science, Sultan Qaboos University, PO Box 36, Postal Code 123, Muscat, Oman

S Supporting Information



ABSTRACT: A homology model of the nucleotide-activated P2Y₂R was created based on the X-ray structures of the P2Y₁ receptor. Docking studies were performed, and receptor mutants were created to probe the identified binding interactions. Mutation of residues predicted to interact with the ribose (Arg110) and the phosphates of the nucleotide agonists (Arg265, Arg292) or that contribute indirectly to binding (Tyr288) abolished activity. The Y114F, R194A, and F261A mutations led to inactivity of diadenosine tetraphosphate and to a reduced response of UTP. Significant reduction in agonist potency was observed for all other receptor mutants (Phe111, His184, Ser193, Phe261, Tyr268, Tyr269) predicted to be involved in agonist recognition. An ionic lock between Asp185 and Arg292 that is probably involved in receptor activation interacts with the phosphate groups. The antagonist AR-C118925 and anthraquinones likely bind to the orthosteric site. The updated homology models will be useful for virtual screening and drug design.

INTRODUCTION

The P2Y₂R is a subtype of the P2Y receptor family of G protein-coupled receptors. Its endogenous agonists are uridine-5'-triphosphate (UTP, **1**, Figure 1) and adenosine-5'-triphosphate (ATP, **2**), which activate the receptor with similar potencies in the midnanomolar range.^{1–3} Upon receptor stimulation, phospholipase C_β is activated via G_{α_{q/11}} proteins.⁴ This leads to the hydrolysis of phosphatidylinositol-4,5-bisphosphate (PIP₂), producing the second messengers inositol trisphosphate (IP₃) and diacylglycerol. IP₃ mediates the release of calcium ions from intracellular stores, which can be detected in vitro using calcium-sensitive fluorescent dyes. In addition to G_{α_{q/11}}, the P2Y₂R was also shown to couple to G_o, G₁₂, and G₁₆.^{5–7} Expression of P2Y₂R mRNA was found in a wide range of different human organs and tissues, with particularly high expression levels in skeletal muscle and heart and moderate levels in the lung, intestine, placenta, spleen, bone marrow, immune cells, and different regions of the brain.⁸ The P2Y₂R is involved in various pathological processes, and P2Y₂R ligands have been proposed as novel therapeutic agents. The P2Y₂R

agonist P¹,P⁴-di(uridine-5')-tetraphosphate (diquafosol) is already marketed as a symptomatic therapy for dry eye syndrome in Japan. Moreover, P2Y₂R agonists may be useful for the treatment of cystic fibrosis. Knockout mice deficient in the P2Y₂R showed defective chloride secretion in airway epithelium in response to ATP and UTP.⁹ P2Y₂R agonism might thus compensate for the malfunctioning of the Cl[−] channel cystic fibrosis transmembrane conductance regulator in cystic fibrosis patients. Cardioprotective effects in cultured rat cardiomyocytes and a reduction of postischemic myocardial damage in mice were observed with the selective P2Y₂R agonist uridine-5'-tetraphosphate δ-phenyl ester (MRS2768).¹⁰ The P2Y₂R was shown to enhance α-secretase-dependent amyloid precursor protein processing to a nonamyloidogenic product in astrocytoma cells.¹¹ This prevents the processing via β- and γ-secretase to amyloid-β, the main component of the plaques

Received: June 11, 2017

Published: September 22, 2017

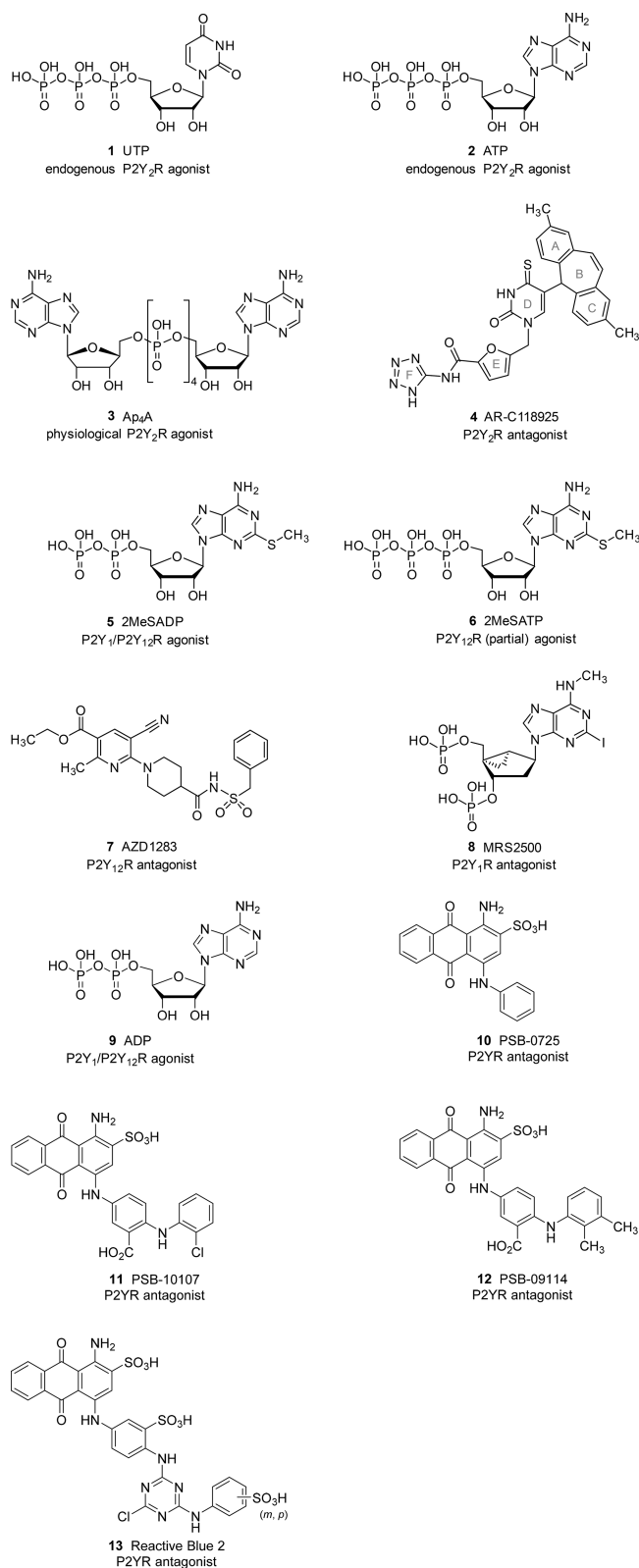


Figure 1. Structures of selected P2Y₂R ligands.

associated with Alzheimer's disease. Thus, P2Y₂R agonists may be useful for the treatment of neurodegenerative disorders.¹¹

P2Y₂R antagonists, on the other hand, may be used to combat cancer and inflammation because P2Y₂R activation has pro-inflammatory, pro-proliferative, and pro-metastatic effects. The P2Y₂R appears to activate cytosolic phospholipase A₂,

which in turn promotes the release of arachidonic acid and subsequent synthesis of prostaglandins and leukotrienes.^{12,13} It is also involved in the proliferation, migration, adhesion, and infiltration of immune cells.^{5,14–19} P2Y₂R activation was reported to lead to the proliferation of different tumor and nontumor cells and to the induction of cell cycle progression in vascular smooth muscle cells.^{20–25} Furthermore, P2Y₂Rs located on endothelial cell membranes were found to open the endothelial barrier following activation by ATP secreted from platelets. The P2Y₂R thereby permits cancer cell transendothelial migration from the bloodstream into surrounding tissue, where it can form secondary tumor sites.²⁶ Patients suffering from nephrogenic diabetes insipidus acquired through the chronic use of lithium, for example, in a bipolar disorder therapy, could benefit from P2Y₂R antagonists as well. In support of this hypothesis is the observation that the P2Y₂R is expressed in collecting ducts of the kidney, where it opposes the actions of antidiuretic hormone (arginine vasopressin) and thus reduces water reuptake.²⁷

Despite its great potential as a drug target, only few P2Y₂R-selective agonists and very few antagonists are available. Moreover, they have severe limitations, e.g., low metabolic stability, high polarity due to negative charges, moderate potency, and/or low selectivity.^{28–31} This is unfortunate, as they could be used as pharmacological tools to characterize this receptor further or serve as lead compounds for drug design. A comprehensive knowledge of the ligand binding site would undoubtedly be of great value for the development of potent and selective ligands. However, an X-ray structure of the P2Y₂R has not been published. Fortunately, for the related P2Y₁ and P2Y₁₂R subtypes, X-ray structures have recently become available.^{32–34}

To provide insights into the structure of the orthosteric P2Y₂R ligand binding site, we constructed a preliminary model based on the X-ray structures of the P2Y₁R. The agonists UTP (1) and the dinucleotide P¹,P⁴-di(adenosine-5')-tetrphosphate (Ap₄A, 3) were docked into the model. Docking studies were also conducted with 4 (AR-C118925), one of the few relatively potent and selective competitive P2Y₂R antagonists available to date,^{28–31,35–37} and several different antagonists possessing an anthraquinone scaffold. This led to the prediction of amino acid residues in the orthosteric binding site of the P2Y₂R that may interact with these ligands. To provide experimental evidence for the validation and improvement of the model, we subsequently conducted a site-directed mutagenesis study exchanging residues thought to contribute to the putative orthosteric site. The mutated receptors were expressed in 1321N1 astrocytoma cells, and the effects of the mutations were assessed by measuring the potency of structurally diverse agonists and antagonists in fluorescence-based calcium mobilization assays. The obtained pharmacological data support our model and have provided a basis for its refinement. The updated P2Y₂R homology models will be useful for virtual screening and the design of superior ligands and drug candidates, in particular antagonists, for this promising new drug target.

RESULTS AND DISCUSSION

Homology Model of the Human P2Y₂ Receptor. We previously reported a homology model of the human P2Y₂R that was based on the crystal structure of bovine rhodopsin.³ However, the sequence homology between the human P2Y₂R and rhodopsin is relatively low (17.9% identity, 33.2%

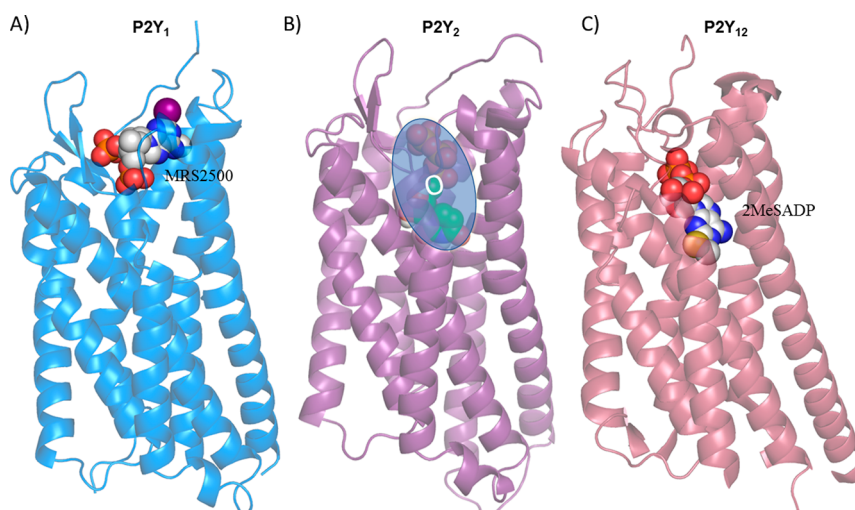


Figure 2. Homology model of the human P2Y₂R. (A) X-ray structure of the human P2Y₁R, which was used as a template for generating the homology model of the human P2Y₂R. The P2Y₁R antagonist **8** binds to a site only partially overlapping with the agonist binding site of the P2Y₁₂R as determined by X-ray crystallography. (B) Homology model of the human P2Y₂R based on the human P2Y₁R crystal structure. The putative orthosteric binding site in complex with UTP is schematically indicated and denoted as “O”. (C) Human P2Y₁₂R X-ray structure in complex with the agonist **5**, shown for comparison of the orthosteric binding sites. Receptors are represented as cartoon models, and the co-crystallized atoms of the ligands are depicted as spheres.

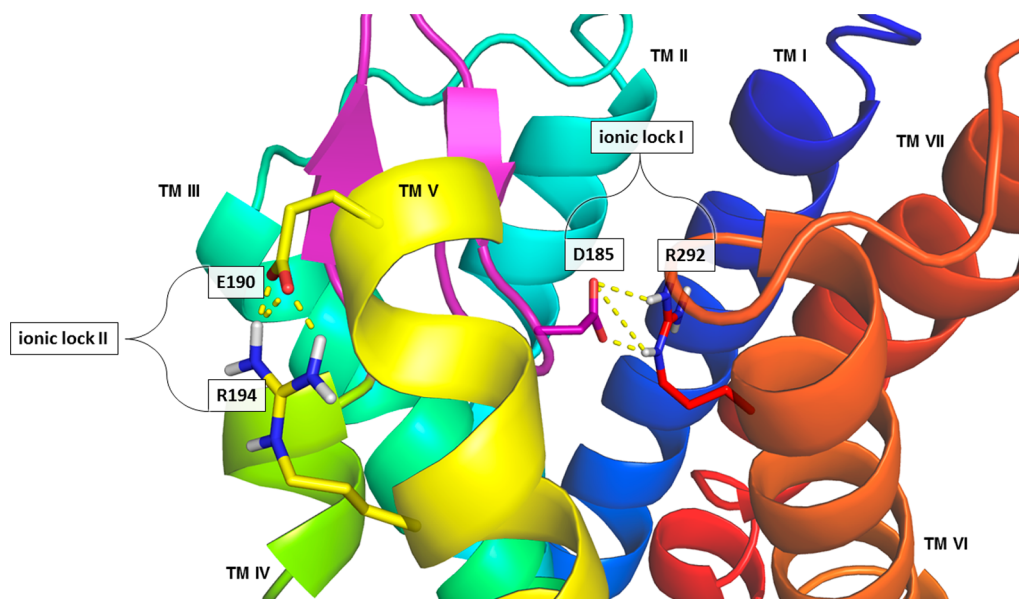


Figure 3. Homology model of the human P2Y₂R with the ionic lock I formed between Asp185 and Arg292 and the ionic lock II formed between Glu190 and Arg194. The receptor is represented as a cartoon model.

similarity), but X-ray structures of closely related GPCRs were not available at that time. The very first structure obtained for a P2YR subtype was the crystal structure of the human P2Y₁₂R. The overall sequence identity and similarity between the human P2Y₂R and the human P2Y₁₂R is 22.8% and 41.9%, respectively. The human P2Y₁₂R was crystallized in complex with the agonist **5** (2MeSADP; PDB 4PXZ), the proposed partial agonist **6** (2MeSATP; PDB 4PY0), and the antagonist **7** (AZD1283; PDB 4NTJ).^{33,34} Shortly after the release of the human P2Y₁₂R crystal structures, the structure of the human P2Y₁R in complex with the antagonist **8** (MRS2500; PDB 4XNW) was published.³² The latter P2YR subtype shares an even greater sequence homology (36.3% identity and 54.1% similarity) with the P2Y₂R than the P2Y₁₂R and therefore should be more suitable as a template for generating a P2Y₂R

homology model. The sequence alignments are shown in Figure S1 of the Supporting Information. We developed a homology model of the human P2Y₂R based on the P2Y₁R structure to refine the structure and analysis of the residues involved in ligand recognition and interaction. However, in this model, the extracellular loop 2 (ECL2) projected into the putative orthosteric binding site transformed from the P2Y₁R crystal structure and thereby impeded computational docking of orthosteric agonists. To insert the ligands into the putative orthosteric binding site during molecular docking, we attempted loop modeling by creating the possible side chain rotamers of the amino acids present in the ECL2. This was achieved by using the rotamer library tool implemented in Molecular Operating Environment (MOE, 2014.09, Chemical Computing Group Inc., Montreal, Canada). The amino acid

side chains in a receptor tend to exist in a limited number of low energy conformations. The side chain prediction methods select rotamers on the basis of the receptor sequence and the backbone coordinates by using a defined energy function and search strategy. Specifically, different rotamers of the amino acids Thr188, Arg265, and Arg272 were studied, and the models that showed the lowest energy rotamer conformations, and additionally the largest volume in the putative orthosteric binding pocket of the human P2Y₂R were selected (Figure 2). An orthosteric binding site comparable to the binding site identified in the crystal structure of the human P2Y₁₂R (PDB 4PXZ) in complex with the agonist **5** was identified in the thus created P2Y₂R model that was generated based on the human P2Y₁R crystal structure (see Figure 2). Moreover, it is analogous to the orthosteric binding site observed in a molecular dynamics simulation study of the human P2Y₁R in complex with the agonist ADP (**9**).³⁸

According to molecular dynamics simulations aimed at finding the molecular mechanism of P2Y₁R activation, an ionic lock is present between Asp204 and Arg310 that stabilizes the inactive state of the P2Y₁R.³⁸ In these molecular dynamics simulations of the human P2Y₁R in complex with the agonist ADP (**9**), the ionic lock was broken. This resulted in an increased solvent-accessible surface area and water influx that was proposed to lead to receptor activation.³⁸ In the P2Y₂R, a similar mechanism of activation as in the P2Y₁R is conceivable. The analogous residues Asp185 and Arg292 are likely to form an ionic lock (designated “ionic lock I”, see Figure 3). The strong electrostatic interactions between the phosphate groups of the P2Y₂R agonists UTP and ATP and the amino acids Asp185 and Arg292 will likely break the ionic lock I between those two amino acids. This probably leads to an analogous mode of activation as proposed for the P2Y₁R. In our homology model of the human P2Y₂R, an additional ionic lock (designated “ionic lock II”, see Figure 3) between Glu190 and Arg194 in TM V is formed. The proposed strong ionic interaction between Glu190 and Arg194 is underscored by the severe effects on agonist recognition we observed when mutating Arg194 (see [Pharmacological Assessment and Docking of Agonists on Mutated P2Y₂R](#)). The ionic lock II so far appears to be unique for the P2Y₂R. It possibly plays a role in the orientation of the ECL2 and thus may allow Asp185 in ECL2 to form interactions with ligands in the orthosteric binding site. The residue Arg212 of the P2Y₁R that is analogous to Arg194 in the P2Y₂R forms a different ionic lock between Asp289 and Arg285 in TM VI of the P2Y₁R. The same type of interaction is not possible in the P2Y₂R because there is no residue comparable to Asp289 (P2Y₁R) in the P2Y₂R sequence; the analogous residue to Arg285 in the P2Y₁R is Ser270 in the P2Y₂R.

Site-Directed Mutagenesis. To confirm and refine the created homology model of the human P2Y₂R, amino acid residues were suggested for subsequent mutagenesis studies. Several mutants of the human P2Y₂R had been previously published.^{3,6,39–43} However, only few residues postulated to participate in the orthosteric binding of the endogenous agonists ATP and UTP have been reported. An early study was performed by Erb et al. on the murine P2Y₂R, in which they investigated the role of the basic amino acid residues Lys107, Arg110, His262, Arg265, Lys289, and Arg292 for receptor activation.⁴³ These are conserved in the human P2Y₂R and therefore suitable for hypothesis generation and comparison of trends between murine and human orthologues. In

previous mutagenesis work undertaken in our laboratory, some of these along with additional basic residues (Arg177, Arg180, Arg194, His262, Arg265, Arg272, Lys289, Arg292) had been mutated in the human P2Y₂R.³ These were assumed to interact with the negatively charged phosphate chain of the nucleotide agonists. In addition, several aromatic residues (Tyr114, Tyr118, Tyr198) in proximity to the presumed binding pocket had also been exchanged.³ These results were re-evaluated and implemented in the present mutagenesis work to study the binding of structurally diverse agonists and antagonists of the human P2Y₂R. On the basis of an analysis of the putative orthosteric site in our homology model and preliminary docking simulations, a variety of additional basic and aromatic residues were selected for mutagenesis to probe our hypothesis that they are engaged in direct interactions with UTP (**1**), Ap₄A (**3**), or **4** in the orthosteric ligand binding site. Furthermore, residues in the ECL2 or in its vicinity that may be responsible for agonist recognition were mutated.

In total, 12 new single mutations were engineered into the sequence of the human P2Y₂R. Three additional P2Y₂R mutants that had previously been created in our laboratory, Y114A, R194A, and R194H,³ were also included in the subsequent assessment of agonists and antagonists. The mutants were chosen based on the results from preliminary docking simulations and analysis of the binding site of our human P2Y₂R model. Arginine, histidine, and serine residues were mutated to alanine to identify the key role of these functional amino acid residues. Arg194 was additionally mutated to histidine to maintain a positive charge which would allow studying its effects on the ionic lock. The aromatic residues phenylalanine and tyrosine were mutated to alanine, and tyrosine was additionally mutated to phenylalanine to study their interactions with the ligands as observed in the docking simulations. All P2Y₂R mutations investigated in the present study are depicted in Figure 4. The DNA sequences for the mutated P2Y₂Rs were cloned into the pLXSN retroviral expression vector featuring an hemagglutinin (HA) epitope sequence at the N-terminus of the receptor. Exceptions were R194A and R194H, two of the receptor mutants that had been previously created:³ the vector used for these was pcDNA3.1 and they did not contain an HA-tag. All mutated receptors were expressed in 1321N1 astrocytoma cells, which do not respond to nucleotides and are thus suitable for P2 receptor expression. Subsequently, the mutated receptors were studied in calcium mobilization assays.

Receptor Expression. It was required to confirm that the mutated receptors that showed no response to agonists in the calcium mobilization assays were actually present in the cell membrane. Moreover, the EC₅₀ values determined in a test system for GPCR agonists are dependent on the receptor expression levels.^{44,45} Therefore, the cell surface expression of the receptor mutants was determined using enzyme-linked immunosorbent assays (ELISA). The expression of all mutated receptors was found to be similar to that of the wild-type (wt) P2Y₂R (for more details, refer to Supporting Information, Figure S5), except for Y114A (180% of wt), Y268F (200% of wt), and Y269F (180% of wt). A receptor density twice as high should nevertheless not affect the EC₅₀ value to such an extent that it prevented a direct comparison between the two. In support of this is a previous observation by our group, where several 1321N1 astrocytoma cell lines recombinantly expressing different levels of wt P2Y₂R were created and compared. The EC₅₀ value of UTP did not differ significantly (less than 2-fold,

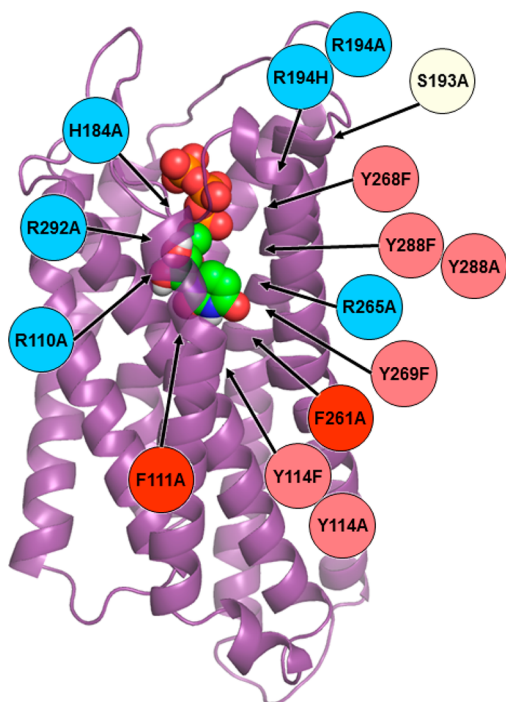


Figure 4. Assumed pose of the cognate P2Y₂R agonist UTP (1) docked into the putative binding pocket of the human P2Y₂R model. The amino acid residues selected for site-directed mutagenesis are indicated. Basic residues are colored in blue, phenylalanine in dark red, tyrosine in light red, and serine in white.

i.e., 80.4 ± 6.4 nM versus 59.0 ± 4.6 nM) for two cell lines expressing the wt P2Y₂R with receptor expression levels differing by a factor of 2.³

Pharmacological Assessment and Docking of Agonists on Mutated P2Y₂Rs. Subsequently, the effect of the mutations on the potency of two structurally diverse physiological agonists, UTP (1) and the dinucleotide Ap₄A (3), were investigated. Figure 5 shows exemplarily the dose-response curves obtained in fluorescence-based calcium mobilization assays of UTP on a selection of mutated

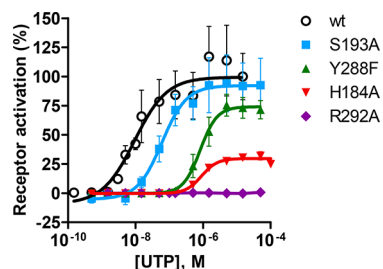


Figure 5. Dose–response curves of UTP at the wt P2Y₂R and at selected mutants expressed in 1321N1 astrocytoma cells, determined using a fluorescence-based calcium mobilization assay. EC₅₀ values \pm standard error of the mean of UTP are: wt, 5.61 ± 0.85 nM; S193A, 70.6 ± 19.7 nM; Y288F, 911 ± 218 nM; H184A, 996 ± 98 nM ($n \geq 4$). In each experiment, activation of the intrinsically expressed M₃ muscarinic acetylcholine receptor by carbachol (100 μ M) served as a control and reference standard. The upper plateau for each curve was normalized to the carbachol signal. Subsequently, the upper plateau for the wt curve was set at 100% and the maximal effects observed for the different receptor mutants was calculated in relation to that of the wt receptor.

P2Y₂Rs. The potencies for both UTP and Ap₄A on all mutated P2Y₂Rs are summarized as bar charts in Figure 6. A table listing

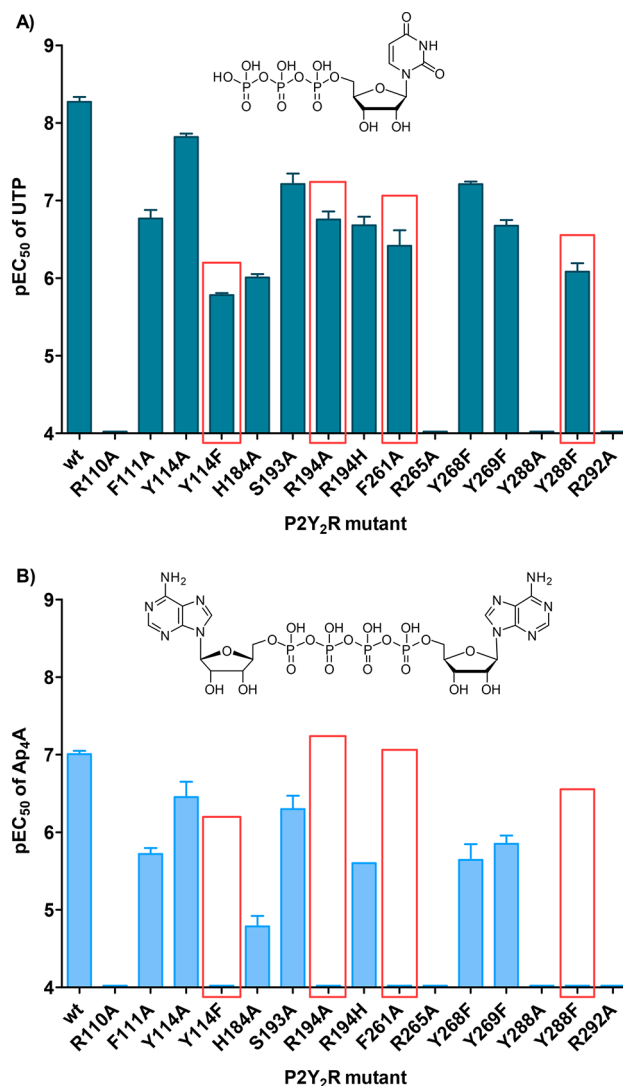


Figure 6. Potencies of the agonists UTP (A) and Ap₄A (B) on the wt and mutated P2Y₂R expressed in 1321N1 astrocytoma cells, determined using a fluorescence-based calcium mobilization assay ($n \geq 4$). Shown are the negative logarithms of the mean EC₅₀ values. The EC₅₀ values are listed in Supporting Information, Table S1. The data for each mutant was compared to that of the wt receptor using one-way ANOVA with Dunnett's post-test. The differences were found to be statistically significant, with $p < 0.001$ for all mutations. The only exception was Y114A, for which $p < 0.05$ for UTP (A) and $p < 0.01$ for Ap₄A (B) were obtained. The mutants, for which a large difference in potency between UTP and Ap₄A was observed, are highlighted in red. The efficacies of the mutant receptors were similar to that of the wt receptor, except for H184A (25% efficacy) and Y268F (36% efficacy).

the EC₅₀ values is found in the Supporting Information (Table S1). Radioligand binding studies could not be performed because no radioligand for the P2Y₂R is currently available.

As shown in Figure 6, each of the 15 mutations caused a significant decrease in the potencies of both agonists UTP and Ap₄A. The mutations R110A, R265A, Y288A, and R292A even resulted in receptor mutants that were completely insensitive to both agonists. Y114F, R194A, F261A, and Y288F also caused

complete receptor unresponsiveness to Ap₄A, while UTP was still able to activate these receptor mutants.

As a next step, the agonists UTP (1) and Ap₄A (4) were docked into the human P2Y₂R model to predict their binding poses. All available structural information, including the results from our new mutagenesis studies, was taken into account. The docking and glide scores from the induced-fit molecular docking experiments and results from previously published site-directed mutagenesis studies^{3,43,46–49} were also included. However, most previous studies had been performed on the human P2Y₁R and are only partly transferable to the P2Y₂R. Published results from P2Y₁R mutagenesis studies may nevertheless be useful for a detailed analysis of the putative P2Y₂R orthosteric binding site. As illustrated in Figure 7A, UTP, located in the orthosteric site of the receptor, binds primarily through strong electrostatic and hydrogen bonding interactions. According to our model, the triphosphate group of

UTP is bound to Arg177, Asp185, Arg265, Tyr268, Tyr269, Arg272, Lys289, and Arg292. The α -phosphate group is proposed to form interactions with Arg265 and Lys289. The β -phosphate group likely interacts with Tyr268, Tyr269, Arg272, and Lys289. The γ -phosphate group is predicted to interact with Arg177, Asp185, Arg272, Lys289, and Arg292. Further hydrogen bond interaction could be observed in the model of the human P2Y₂R-UTP complex between the γ -phosphate of UTP and His184, which are located 3.6 Å apart. The 3'-hydroxyl group of the ribose moiety of UTP probably forms hydrogen bond interactions with Arg110 and possibly with Asp185 of the ECL2. Our docking results suggest that the uracil ring of UTP is stacked between the aromatic residues Tyr114 and Phe261 and forms π - π interactions. Tyr118 could interact with O⁴ through hydrogen bonding (see Figure 7).

The potency determined for UTP in our cell line expressing the wt P2Y₂R was in the low nanomolar range ($EC_{50} = 5.61$ nM). At four receptor mutants, R110A, R265A, R292A, and Y288A, the activity of UTP was completely abolished (Figure 6), although they were clearly expressed in the cell membrane (see Supporting Information, Figure S5). Interestingly, Arg110 had previously been mutated to Leu in the murine P2Y₂R by Erb and co-workers,⁴³ which had little effect on the potency of UTP and ATP. The strong effect observed in our mutagenesis study when mutating Arg110 to Ala in the human orthologue is possibly a result of species differences. According to our homology model, the three arginine residues were predicted to form hydrogen bonds with the ribose moiety (Arg110) and the phosphate groups of UTP (Arg265 and Arg292). Arg292 was already reported previously to play a key role in agonist-induced receptor activation.^{38,43} Tyr288, on the other hand, likely forms interactions with Arg265 and contributes to the binding of the phosphate groups or guides the nucleobase for binding into the orthosteric binding pocket through aromatic π - π interactions. The Y288F mutant, which displayed a 150-fold decrease in potency, might prevent these interactions. The residues Tyr114 and Phe261 (300- and 100-fold decrease in potency, respectively) form strong π - π interactions with the uracil ring of UTP. The mutant F261A cannot form such interactions, resulting in a significant loss of potency for UTP. The hydroxyl group of Tyr114, which is missing in the Y114F mutant, might play a major role in stabilizing the binding pocket or in guiding the agonists toward the binding pocket, which would explain the almost 300-fold decrease in potency observed with Y114F. For Y114A, only a small effect on the potency was observed. This could possibly be due to additional space, which allows more flexibility for the agonists and thereby compensates for the loss of the π - π interactions. The mutation of His184 to alanine resulted in a >100-fold decrease in potency, although we did not observe interactions between His184 and UTP in its putative binding pose. However, His184 present in the ECL2 might still form interactions with agonists due to the flexibility of the extracellular loop region.

The potency of UTP was decreased by 10–50-fold for R194A, R194H, Y268F, S193A, F111A, and Y269F. The mutation of Arg194 to alanine or histidine resulted in a moderate loss of potency. The position of Arg194 in the upper part of TM V could be important for the flexibility of ECL2. In our previously published model,³ we could observe the ionic lock II between Arg194 and Glu190, whereupon a backbone interaction of Arg194 with the main chain of Glu190 is also possible. The role of the ECL2 in ligand affinity and agonist efficacy through direct or indirect interactions has been

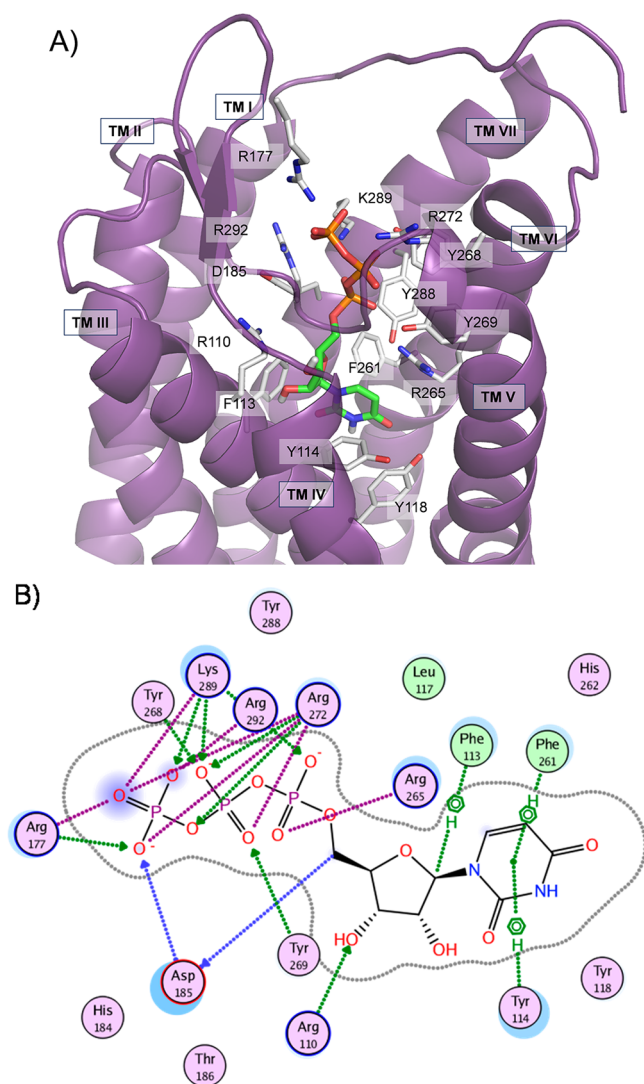


Figure 7. Suggested binding mode of UTP in the human P2Y₂R. (A) Docked pose of UTP with the important residues in the binding pocket shown. (B) 2D interaction diagram. The human P2Y₂R (purple) is displayed in cartoon representation, the amino acid residues (white) and UTP (green) are shown as stick models. Oxygen atoms are colored in red, nitrogen atoms in blue, and phosphorus atoms in orange.

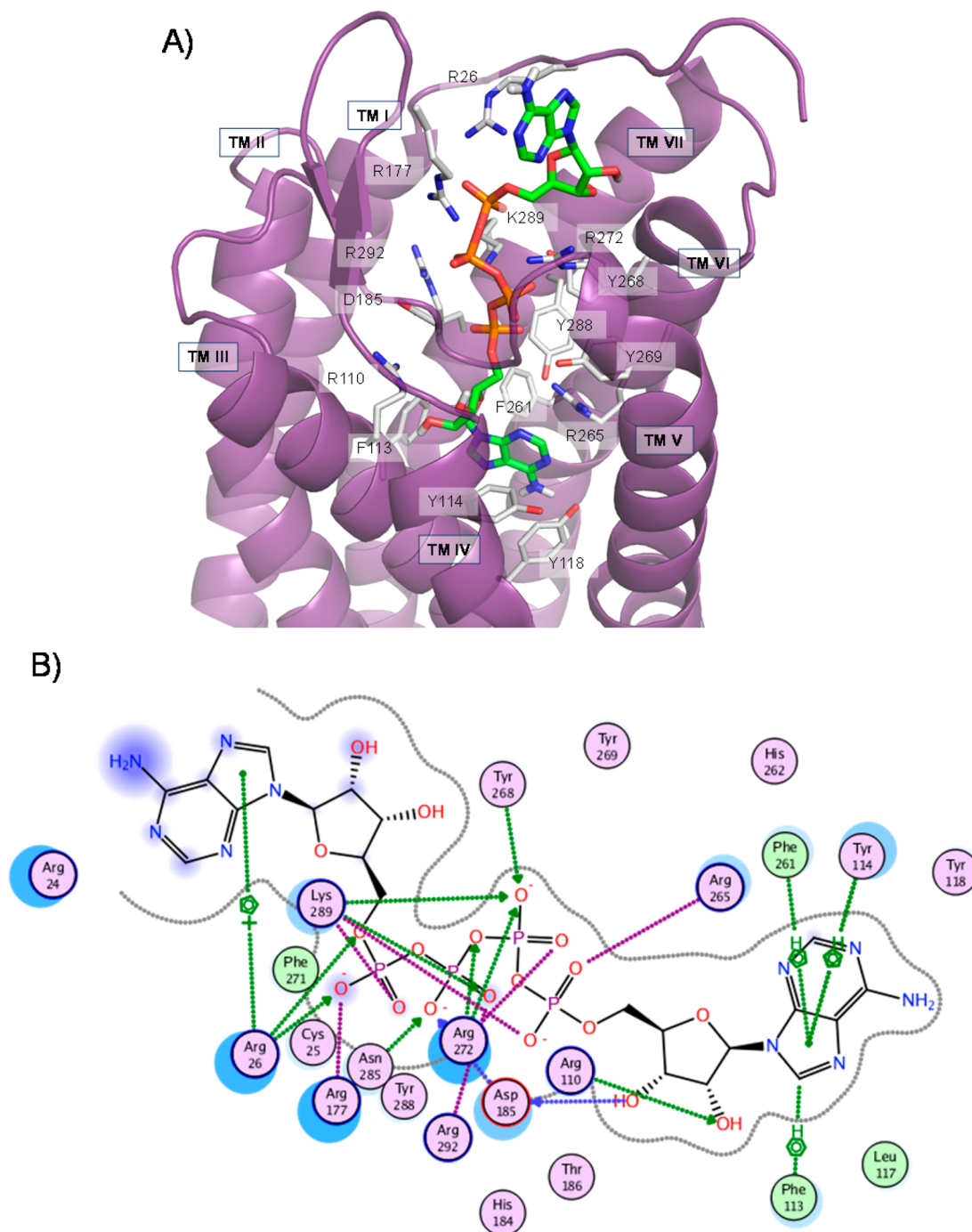


Figure 8. Putative binding mode of Ap₄A (4) in the human P2Y₂R. (A) Docked pose of Ap₄A with the important residues in the binding pocket shown. (B) 2D interaction diagram (see Figure 7 for color code).

reported previously for other GPCRs including the P2Y₄R.^{50–52} As no direct interactions were observed for Ser193, we expect it to play a role in receptor activation.

According to our model, the orientation of one of the adenosine moieties of the symmetrical dinucleotide Ap₄A (4) in the orthosteric site is identical to that of ATP (2). While Ap₄A can have more interactions than ATP, it may also lead to reduced receptor flexibility,³ and therefore, less induced movements will be possible within the active site upon binding of Ap₄A. The molecule has to adopt a specific conformation to fit into the binding site (Figure 8): in our homology model, the α -, β -, and γ -phosphate groups of Ap₄A form interactions with

the same set of residues as UTP, i.e., Arg177, Asp185, Arg265, Tyr268, Tyr269, Arg272, Lys289, and Arg292. The δ -phosphate group forms additional electrostatic interactions with Arg26, Arg177, and Lys289. The 2'-hydroxyl group of the first ribose moiety that binds to the orthosteric site forms similar interactions as UTP with Arg110 and interacts with the backbone of Asp185. The first adenine base is oriented toward a similar direction as UTP and stacked between Tyr114 and Phe261 through π - π interactions with additional stabilization by Phe113. In comparison to the uracil ring of UTP, the adenine ring of Ap₄A is larger in size and forms stronger aromatic interactions with the residues Tyr114 and Phe261.

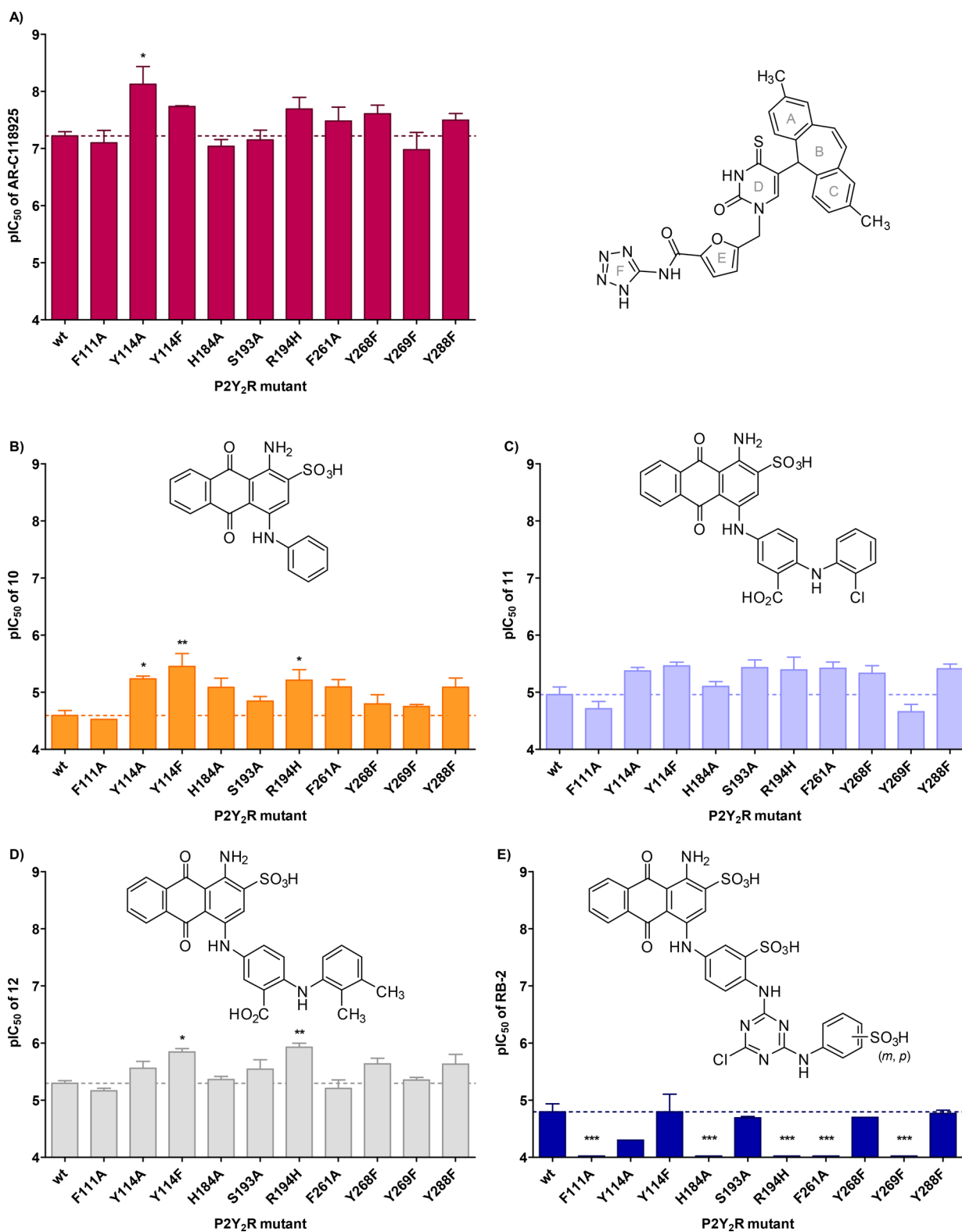


Figure 9. Potencies of structurally diverse antagonists on the wt and mutated P2Y₂Rs in 1321N1 astrocytoma cells determined using a fluorescence-based calcium mobilization assay ($n \geq 3$). Receptor activation was achieved using UTP at a concentration that represented the EC₈₀ at the respective mutant. Shown are the negative logarithms of the mean IC₅₀ values. The IC₅₀ values are listed in Supporting Information, Table S2. Each mutant was compared to the wt P2Y₂R using one-way ANOVA with Dunnett's post-test; * $p < 0.05$, ** $p < 0.01$, *** $p < 0.001$.

The second nucleobase is oriented toward the extracellular space of the receptor, possibly forming a cation- π interaction with Arg26 of the highly flexible N-terminus.

Our findings suggest a different binding mode for the P2Y₂ agonist UTP than that observed for the nucleotide antagonist **8**, which was co-crystallized with the human P2Y₁R. Compound **8** binds in the upper part of the receptor, on the very top, above

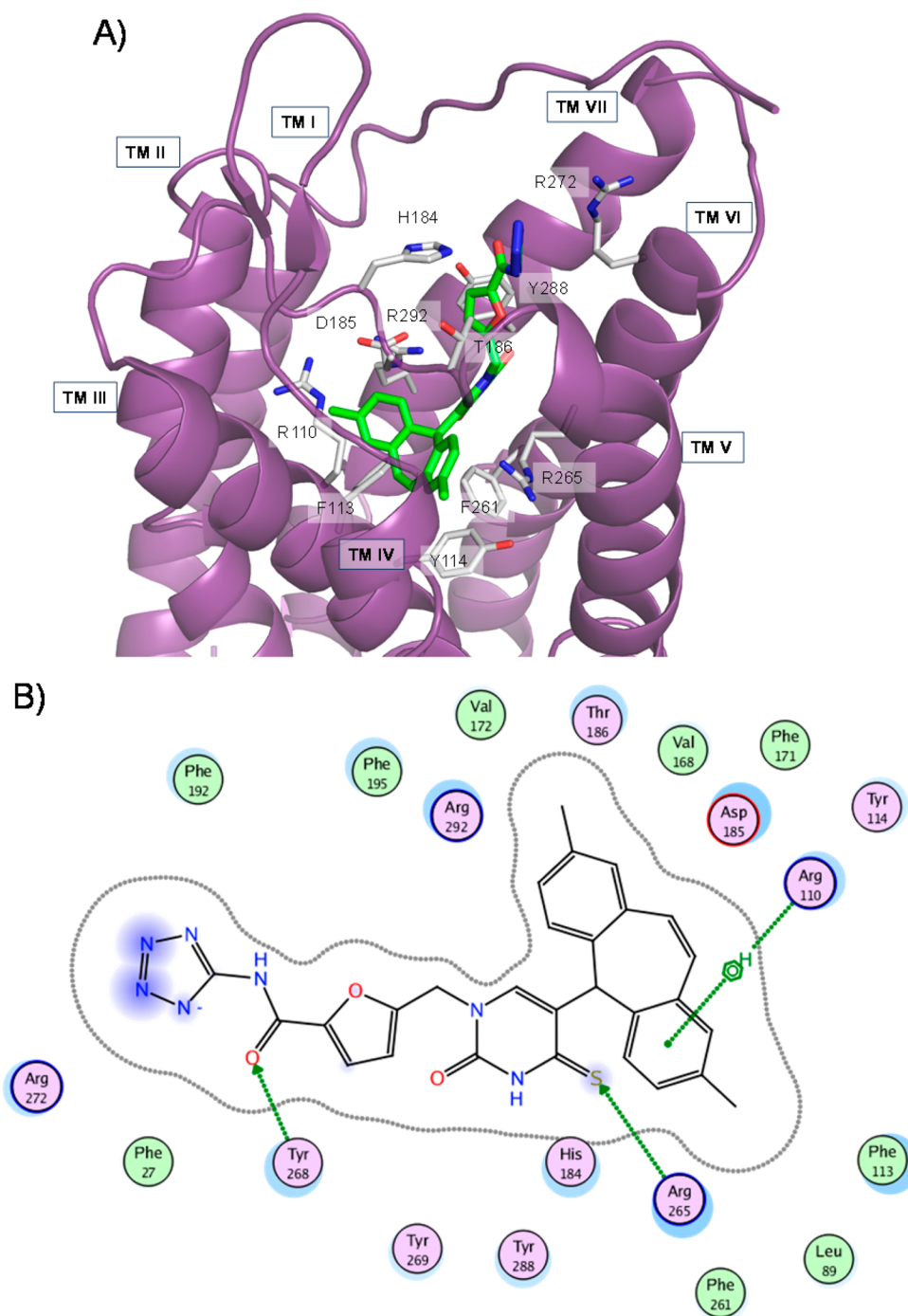


Figure 10. Putative binding mode of **4** in the human P2Y₂R. (A) Docked pose of **4** with the important residues in the binding pocket shown. (B) 2D interaction diagram (see Figure 7 for color code).

ECL2, and interacts with residues from the N-terminus, ECL2 and TM VII. Mutagenesis studies confirmed different interaction patterns for the nucleotide antagonist **8** as compared to the nucleotide agonist **5**. While the mutants K46A, R195A, A286W, Y303F, and Y306F affected the potency of antagonist **8** (23-, 8-, 45-, 156- and 129-fold decrease in potency, respectively), these had only a minor or at least a much lower effect on the potency of the agonist **5** (~2-fold for K46A, R195A, A286W, and Y303F, and ~10-fold for Y306F), indicating different binding interactions of both nucleotides, **5** and **8**.³² Our P2Y₂R models suggested that analogous residues, which affected the potency of the antagonist **8** in the P2Y₁R, are

too distant to have direct interactions with UTP. However, mutation of P2Y₂R's Tyr288, which is analogous to P2Y₁R's Tyr306, affected the potency of the agonist UTP when mutated to phenylalanine. Similar results were observed for the potency of the agonist **5** on the P2Y₁R, which supports our findings. Moreover, molecular dynamics simulation studies had indicated a similar binding site and mode for the agonist ADP at the P2Y₁R as we have now identified for agonists at the P2Y₂R.³⁸

For the dinucleotide Ap₄A, the determined potencies were generally 10–100-fold lower at the wt P2Y₂R and the mutants. Its potency appeared to be affected by the mutations in a similar manner as observed for UTP. Exceptions were Y114F,

R194A, F261A, and Y288F, for which a complete loss of potency was observed with Ap₄A but not with UTP. Because Ap₄A features an adenine moiety that contains an extended π -ring system, it is likely to form more interactions with residues in the ligand binding site than uracil. Y114F and F261A therefore affected the potency of Ap₄A more strongly than that of UTP. This can be explained by the fact that both are in the vicinity of the first adenine moiety. The docking and mutagenesis data suggest that the right orientation of the base in the binding pocket is determined by certain aromatic (Phe113, Tyr114, Phe261) and hydrophilic (Arg265) residues, which are important for receptor activation by Ap₄A. Mutation of Arg194 to His decreased the potency by 25-fold, while mutation to Ala resulted in a complete loss of activity. It appears likely that Arg194 in the ECL2 plays a key role in Ap₄A recognition. The R194H mutant is still capable of forming ionic lock II. Thus, this mutation only led to a decrease in potency. In contrast, the R194A mutant cannot form ionic lock II, and consequently Ap₄A displayed a complete loss of potency. The complete abolishment of receptor activation for the agonist Ap₄A and the 50-fold decrease for UTP confirm a strong ionic interaction between Glu190 and Arg194 that influences the binding interaction of agonists. Because of the flexibility of the extracellularly oriented domains additional similar binding modes for the second adenine and the ribose moiety of Ap₄A are conceivable. Further mutagenesis studies of the extracellular domains and the N-terminus would be required to predict the exact binding interactions. Our results suggest that the P2Y₂R features a nucleotide binding pocket for the agonists UTP and Ap₄A that is similar to the binding pocket of agonist **5** in the crystallized complex of the human P2Y₁₂R³⁴ as well as the proposed binding pocket for ADP in the human P2Y₁R as predicted by molecular dynamics simulation.³⁸

Pharmacological Assessment and Docking of Antagonists. Next, we assessed a selection of structurally diverse antagonists on the P2Y₂R mutants. These included the potent and selective P2Y₂R antagonist **4** (see Figure 1 for structures).³⁵ In addition, we tested three anthraquinone derivatives synthesized by our group,^{53–55} **10** (PSB-0725), **11** (PSB-10107), and **12** (PSB-09114), that were found to show P2Y₂R-antagonist activity with IC₅₀ values in the low micromolar range. The moderately potent, nonselective, commercially available P2Y receptor antagonist **13** (Reactive Blue 2, RB-2)^{28–31} was also assessed. Compound **13** consists of a mixture of two constitutional isomers with the sulfonate group at the terminal phenyl ring located in the *meta*- or *para*-position (Figure 1).^{56,57} These antagonists were assessed in fluorescence-based calcium mobilization assays on the wt P2Y₂R and the P2Y₂R mutants to determine potential effects of the mutations on the compounds' potencies. The pharmacological assessment of antagonists in functional assays requires receptor stimulation by an agonist. Because several of the mutants (R110A, R265A, Y288A, and R292A) were completely insensitive to the endogenous agonist UTP, it was not possible to test antagonists on those receptors. Therefore, only the mutated receptors that still responded to UTP could be studied (see Figure 9).

The competitive³⁵ P2Y₂R-selective antagonist **4** showed no dramatic changes in potency at the tested mutants. Only Y114A led to a significant increase in potency. Although not significant, the mutants Y114F, R194H, F261A, Y268F, and Y288F showed a trend toward increased potency (up to 3-fold).

To investigate the binding interactions of **4** with the P2Y₂R, an induced-fit docking simulation was carried out. The putative binding pose and interactions of **4** are shown in Figure 10. In the simulation study, the tricyclic dibenzocycloheptenyl moiety was anchored inside the binding cleft formed by Leu89, Arg110, Phe113, Tyr114, Val168, Phe171, Val172, Phe195, and Phe261. In particular, Arg110 was observed to form a strong cation– π interaction with ring C of **4** (see Figure 10). The methyl substituents of rings A and C are proposed to form hydrophobic interactions with Leu89, Phe113, Val168, Phe171, and Phe195, respectively. We believe that this strong hydrophobic interaction and anchoring inside the binding pocket confers high P2Y₂R potency to this antagonist. According to our model, the thiouracil moiety (ring D) is placed between the two basic residues Arg265 and Arg292, where cation– π interactions may stabilize the substituted thiouracil base in the binding pocket. The proximity of Tyr114, Phe261, and Tyr288 likely allows further interactions with S⁴. This may account for the requirement of a thio-group in **4** to achieve high potency.³⁵ Replacement of S⁴ by oxygen led to a 20-fold decrease in potency.³⁵ The furan ring is probably extended to the subpocket formed by Asp185, Thr186, and Tyr268. The carbonyl group of the amide may form a hydrogen bond interaction with the hydroxyl group of Tyr268. Visual inspection of rotamers implicated a potential participation of Asn285 in interactions with the amide linkers. The tetrazolate group that is deprotonated at a physiological pH value of 7.4 was found to be in close proximity to the basic amino acid residues His184 and Arg272, which would thus be able to form ionic salt bridges.

The tested anthraquinone antagonist **10** displayed an increase in potency at the mutants Y114A, Y114F, and R194H. The larger anthraquinone derivative **11** showed an increase in potency on some of the tested receptor mutants, which, however, did not reach the level of statistical significance. The potency of its analogue **12** was significantly enhanced for Y114F and R194H. We expect the mutations Y114A and Y114F to increase the lipophilicity of the binding pocket and provide additional flexibility for ligand binding. Both factors could be a reason for the observed increase in potency for the anthraquinone derivatives **10–12**. The increased potency caused by the R194H mutation could be explained by the induction of a conformation of the ECL2 that could be beneficial for the guidance of the anthraquinone derivatives into the binding pocket. Because Tyr114 plays an important role in agonist recognition, and mutation of this residue also influences the potency of the anthraquinone derivatives, we assume binding to the orthosteric site for **10–12** with similar binding modes for these three antagonists. Pharmacological data could, however, not confirm binding of the anthraquinone moiety or the aromatic substituents of **10–12** in the lipophilic binding pocket that is occupied by the tricyclic ring system of **4**.

The large anthraquinone derivative **13** showed a different interaction pattern than the smaller derivatives **10–12**. It displayed a loss in potency at the mutants F111A, H184A, R194H, F261A, and Y269F. Thus, **13** appears to have a different binding mode. The three sulfonic acid groups of **13** may interact with different basic residues, and several alternative binding modes are conceivable. Previous mutagenesis data showed a decrease in potency of **13** for the double mutant R177A_R180A of the ECL2.³ This further suggests complex binding modes and mechanisms of receptor blockade for **13**.

In summary, the residues that were mutated and could be assessed for antagonist activity do not, with a few exceptions, play a major role in the binding of the antagonists other than 13. It is reasonable to assume that the four residues, for which the mutation resulted in a complete loss of agonist potency, may also be involved in the binding of competitive antagonists. Unfortunately, they could not be assessed in this study. A radioligand–receptor binding assay would be a suitable test system, however, at present no P2Y₂R radioligand is available.

■ COMPARISON WITH PREVIOUS MODELS

In comparison to our previously published P2Y₂R homology model,³ the new model presented here is refined to match previous and new mutagenesis data and, most importantly, it is based on the recently obtained crystal structure of the P2Y₁R and compared to the agonist-bound structure of the P2Y₁₂R. These two receptors belong to the same GPCR subfamily as the P2Y₂R and are thus suitable templates. The overall root-mean-square deviation (RMSD) of atomic positions of the previously published and the present, P2Y₁R-based P2Y₂R homology model was 5.7 Å. The largest discrepancies were seen with respect to the ECL2 and the intracellular loop 3. In our previous model, the ECL2 was almost planar and drifted down toward the center of the TM regions. The present model has higher similarities with the P2Y₁R crystal structure that contains two β -sheets pointing outward from the receptor. Interestingly, both models included the ionic lock I, formed by Asp185 and Arg292. Our new model suggests that Arg272 directly interacts with the phosphate side chain of the nucleotides. This is in contrast to the previous assumption that Arg272 is merely guiding the agonists toward the putative binding pocket. Additional interactions with the δ -phosphate could explain the higher impact of the R272A mutation on tetraphosphate dinucleotides compared to triphosphate mononucleotides: >4000-fold versus 350-fold loss in potency, respectively.³ The refined putative binding mode of UTP is also compatible with the molecular mode of activation deduced from molecular dynamics simulations of the P2Y₁R.³⁸ The combination of the recently published P2Y₁R crystal structure and molecular dynamics simulations has led to a much more reliable model of the human P2Y₂R with regard to the binding mode of agonists. We determined a putative lipophilic binding pocket for the base moiety of the nucleotides, a strong interaction of Arg110 with the ribose moiety, and a proposed hydrophilic binding pocket for the phosphate chain. Finally, interactions of the negatively charged phosphate groups with the residues Asp185 and Arg292 were observed, which are most likely important for agonist-induced receptor activation. This may explain why only nucleotides, but not nucleosides, can activate the receptor.

In a pioneering P2Y₂R mutagenesis study by Erb et al.,⁴³ a few residues of the murine P2Y₂R had been mutated to investigate the binding mode of agonists. The K289R mutant had led to a shift in agonist potencies, which was increased for the nucleoside diphosphates ADP and UDP but significantly decreased for the nucleoside triphosphates UTP and ATP.⁴³ Our P2Y₁R-based model suggests hydrogen bonding interactions of Lys289 with the phosphate groups and particularly strong ionic interactions with the γ -phosphate. The larger size of arginine in comparison to lysine likely leads to a steric clash with the γ -phosphate of nucleoside triphosphates and to a conformation that favors binding of nucleoside diphosphates.

■ CONCLUSIONS

We created a homology model of the human P2Y₂R based on the crystal structure of the P2Y₁R and compared the proposed orthosteric site to the agonist-bound crystal structure of the P2Y₁₂R. The endogenous ligand UTP, the dinucleotide Ap₄A, and the competitive antagonist 4 were docked into the putative orthosteric site. Fifteen cell lines were created, each expressing the P2Y₂R with a different mutation affecting residues that were presumed to contribute to the ligand binding site. The effects on the potency of the agonists UTP and Ap₄A as well as five structurally diverse antagonists were determined using fluorescence-based calcium mobilization assays. We observed a significant decrease in potency, or in several cases even a complete loss of response, for the agonists by those mutations affecting residues that were predicted to form strong interactions with agonists in the putative binding pocket (Arg110, Arg265, and Tyr288) and for amino acid residues probably involved in receptor activation (in particular Arg292). In addition, residues contributing to nucleobase recognition (Tyr114, Arg194, Phe261, Tyr288) were found to form interactions with the agonists in our homology model. Further mutagenesis studies of the extracellular domains and the N-terminus could be useful to confirm the proposed binding site and molecular interactions for the second adenine moiety of Ap₄A. Previously presumed binding modes of agonists at the P2Y₂R were revised by utilizing the recently published P2Y₁R crystal structure and molecular dynamics simulations. The participation of the ECL2 in agonist recognition and binding was supported by our model. Our docking simulations propose an orthosteric mode of antagonism for 4, which is in accordance with experimental data.³⁵ Furthermore, our results suggest the participation of Tyr114 and Tyr288 in the binding of anthraquinone-derived antagonists, thereby implying orthosteric antagonism. The experimental data correlate well with our homology model and have provided a basis for its refinement. The updated homology models of the P2Y₂R will be useful for the design of superior ligands and drug candidates. The predicted docking modes of the investigated ligands in the created models will allow virtual screening approaches, which have recently been shown to be highly useful in the search for novel ligands for GPCRs.^{58,59}

■ EXPERIMENTAL SECTION

Test Compounds. UTP and Ap₄A were purchased from Sigma-Aldrich (Munich, Germany). Compound 13 was obtained from Alexis Biochem. The antagonists 4, 10, and 12 were synthesized in our laboratory as previously reported.^{35,53–55} Compound 11 was synthesized in analogy to published procedures.^{54,55,60}

The purities of isolated products were determined by ESI–mass spectra obtained on an LC–MS instrument (Applied Biosystems API 2000 LC–MS/MS, HPLC Agilent 1100) using the following procedure: the compounds were dissolved at a concentration of 0.5 mg/mL in H₂O:MeOH = 1:1 containing 2 mM NH₄CH₃COO. Then, 10 μ L of the sample was injected into an HPLC column (Phenomenex Luna 3 μ C18, 50 mm \times 2.00 mm). Elution was performed with a gradient of water:methanol (containing 2 mM NH₄CH₃COO) from 90:10 to 0:100 starting the gradient immediately at a flow rate of 250 μ L/min for 15 min followed by washing with 100% methanol for another 15 min. UV absorption was detected from 200 to 950 nm using a diode array detector. The purity of the compounds proved to be \geq 95%.

Sodium 1-Amino-4-[4-(2-chlorophenylamino)-3-carboxyphenylamino]-9,10-dioxo-9,10-dihydroanthracene-2-sulfonate (11). To a suspension of 2-(2-chlorophenylamino)-5-nitrobenzoic acid⁶⁰ (146 mg, 0.5 mmol) in a mixture of ethanol (1.5 mL)

and water (0.4 mL), iron powder (325 mg, 5 mmol) and hydrochloric acid (37%, 0.006 mL) were added. The mixture was refluxed at 120 °C, and the reaction was completed after 17.5 h (as monitored by TLC). After cooling to room temperature, the mixture was filtered through Celite to remove solid materials, including iron catalyst, and washed with ethanol (3 mL), followed by ethyl acetate (3 mL). The filtrate was collected in a microwave reaction tube (10 mL), evaporated under reduced pressure, yielding 46 mg of the desired intermediate product (5-amino-2-(2-chlorophenylamino)benzoic acid) and used as such for the next step. The intermediate was treated with 1-amino-4-bromoanthraquinone-2-sulfonate (45.8 mg, 0.113 mmol) and phosphate buffer solution composed of Na₂HPO₄ (pH 9.6) (4.0 mL) and NaH₂PO₄ (pH 4.2) (1.0 mL) and finely powdered elemental copper (5 mg, 0.08 mmol) as a catalyst. The microwave tube was then capped and irradiated in a CEM Focused microwave synthesizer type Discover at 100 W and 120 °C for 5 min. The reaction mixture was cooled to rt and added to 100 mL of water. The aqueous solution was extracted with dichloromethane (2 × 150 mL). The volume of the aqueous layer was then reduced by rotary evaporation to ca. 50 mL. Purification was performed by flash column chromatography using a column packed with RP-18 silica gel and applying a gradient of acetone/water (5%, 20% and finally 40%).^{54,55} The combined product-containing fractions were evaporated under vacuum to remove the acetone and reduce the water volume (ca. 20 mL). The remaining water was subsequently removed by lyophilization to yield 1.3 mg of compound 11. Analytical data: mp >300 °C, blue powder. ¹H NMR: δ 7.35 (m, 4H, 5'-H, 6'-H, 4''-H, 5''-H), 7.55 (dd, J = 7.9 and 1.55 Hz, 1H, 6''-H), 7.58 (dd, J = 7.9 and 1.3 Hz, 1H, 5''-H), 7.83 (m, 3H, 5-H, 8-H, 2'-H), 7.85 (s, 1H, 3-H), 8.27 (m, 2H, 6-H, 7-H), 10.20 (br, 2H, 1-NH₂), 12.17 (br, 1H, 4-NH). ¹³C NMR: δ 109.1, 110.6, 113.5, 115.3, 121.6, 122.5, 123.3, 126.0, 126.1, 127.8, 128.8, 129.7, 131.4, 132.8, 133.1, 133.8, 134.3, 140.6, 142.6, 143.19, 144.3, 144.8, 169.5 (CO₂H), 181.8 (C-9), 182.1 (C10). LC-MS (*m/z*): 564 [M - Na]⁺, 562 [M - Na]⁻, 581 [M - Na + NH₄⁺]⁺. Purity determined by HPLC-UV (220–700 nm) ESI-MS: 95%.

Materials. Dulbecco's Modified Eagle Medium (DMEM), trypsin-EDTA (ethylenediaminetetraacetic acid), fluo-4-acetoxymethyl ester, lipofectamine 2000, and penicillin/streptomycin were purchased from Life Technologies GmbH (Darmstadt, Germany). The hemagglutinin-(HA)-specific mouse monoclonal antibody (HA.11) was obtained from Covance, Berkeley, CA, USA. Fetal bovine serum, bovine serum albumin, Pluronic F-127, and the peroxidase-conjugated goat antimouse IgG antibody were purchased from Sigma-Aldrich (Munich, Germany), G418 from AppliChem (Darmstadt, Germany), Corning 3340 microplates from Corning (Tewksbury, Massachusetts, USA), and 12-well plates from Greiner BioOne (Frickenhäuser, Germany). The restriction enzymes, Q5 DNA polymerase and T4 DNA ligase were purchased from New England BioLabs (Frankfurt am Main, Germany), Pyrobest DNA polymerase from TaKaRa Bio Inc. (Kusatsu, Japan), and ABTS (2,2'-azino-bis-3-ethylbenzothiazoline-6-sulfonic acid) chromophore solution from Merck (Darmstadt, Germany).

Site-Directed Mutagenesis. The coding sequence for the human P2Y₂R (UniProt ID: P41231) was cloned into the pUC19 vector. Point mutations were subsequently introduced using whole-plasmid recombination polymerase chain reaction (PCR)⁶¹ according to the following protocol: 30 s at 98 °C, followed by 30 cycles each consisting of 10 s at 98 °C, 40 s at 60 °C, and 5 min at 72 °C. The PCR reaction was concluded with an additional 10 min at 72 °C. Following purification, the wt receptor template DNA was removed from the PCR product through digestion with DpnI. Competent *Escherichia coli* were subsequently transformed with the PCR product and spread onto agar plates. The cDNA was isolated from individual clones and sent for sequencing (GATC Biotech, Cologne, Germany). Subsequently, it was amplified and cloned into the retroviral expression vector pLXSN⁶² containing the influenza virus HA-epitope at the N-terminus of the receptor. It had been shown previously that the HA-tag does not alter the pharmacological properties of the P2Y₂R.^{3,63}

Retroviral Transfection of 1321N1 Astrocytoma Cells.

Retroviral transfection was performed as previously described.³ Briefly, the sequence coding for the wt or mutated P2Y₂R was cloned into the pLXSN retroviral vector, amplified, purified, and sequenced prior to the transfection of GP^{env} AM-12 packaging cells together with vesicular stomatitis virus G protein DNA using lipofectamine 2000. After 16 h, 3 mL of DMEM containing 10% fetal bovine serum, 1% of a penicillin/streptomycin solution (final concentrations: penicillin = 100 U/mL, streptomycin = 0.1 mg/mL), and sodium butyrate (5 mM) was added to the packaging cells. They were kept at 32 °C with 5% CO₂ for 48 h, during which the viral vectors containing the receptor sequences were produced and released into the surrounding medium. These were harvested, filtered (45 μm filter pore diameter), and added to 1321N1 astrocytoma cells, as these do not intrinsically express P2Y receptors at a detectable level. Polybrene solution (6 μL, 4 mg/mL in H₂O, sterile filtered) was added. After 2.5 h, the virus-containing medium was discarded and DMEM supplemented with 10% fetal bovine serum and 1% of a penicillin/streptomycin solution (final concentrations: penicillin = 100 U/mL, streptomycin = 0.1 mg/mL) was added to the cells. These were incubated for 48 h, after which successfully transfected cells were selected for Geneticin resistance by adding G418 (200 μg/mL) to the medium.

Cell Culturing. 1321N1 human astrocytoma cells transfected with the coding sequence for the wt or mutated P2Y₂R were grown in DMEM supplemented with 10% fetal bovine serum, 1% of a penicillin/streptomycin solution (final concentrations: penicillin = 100 U/mL, streptomycin = 0.1 mg/mL), and 200 μg/mL G418. The cells were kept at 37 °C in humidified air containing 10% CO₂. The cells were maintained in the exponential growth phase and regularly tested for mycoplasma contamination.

Calcium Mobilization Assays. 1321N1 human astrocytoma cells transfected with the coding sequence for the wt or mutated P2Y₂R were employed. Approximately 24 h prior to testing, the nutrient medium was discarded and the cells rinsed with phosphate-buffered saline (PBS; 137 mM NaCl, 2.7 mM KCl, 4.3 mM Na₂HPO₄, and 1.47 mM KH₂PO₄, pH 7.4) before detachment using trypsin-EDTA. The cells were then suspended in DMEM with the supplements described under "cell culturing" and dispensed into sterile, black with clear-bottom 96-well polystyrene microplates with lid (Corning 3340) at a density of 50000 cells per well. The microplates were incubated overnight at 37 °C in humidified air with 10% CO₂, during which the cells adhered to the coated bottom of the wells.

Test compounds were investigated by measuring their inhibition of P2Y₂R-mediated intracellular calcium mobilization using a FlexStation 3 (Molecular Devices GmbH, Biberach an der Riss, Germany) microplate reader. At the start of the assay, the plated cells were incubated with fluo-4 acetoxymethyl ester (0.3% of a 1 mM solution in dimethyl sulfoxide) and Pluronic F-127 (0.3% of a 25% (m/v) solution in dimethyl sulfoxide) in Hank's Balanced Salt Solution (HBSS) buffer for 1 h. Excess dye was subsequently removed, and HBSS buffer was given to the cells. For the assessment of UTP and Ap₄A, different concentrations of the agonists were injected by the microplate reader. When testing antagonists, the cells were preincubated with the test compound for 30 min, and the physiological agonist UTP at a concentration that corresponded to its EC₈₀ value in the respective cell line was injected. The final volume was 200 μL per well in all cases. Fluorescence intensity was measured at 525 nm following excitation at 488 nm. EC₅₀ values for agonists and IC₅₀ values for antagonists were calculated by nonlinear regression using Prism 5.0 (GraphPad Software, San Diego, CA, USA). Nontransfected 1321N1 astrocytoma cells showed no response to UTP (data not shown). 1321N1 astrocytoma cells intrinsically express the M₃ muscarinic acetylcholine receptor, which is also coupled to Gα_{q/11} and causes an increase in the intracellular free calcium ion concentration. In each assay, the effect of the M₃ receptor agonist carbachol at 100 μM, at which it shows a maximal response (data not shown), was measured and used as a reference to compare the maximum receptor activation. For R194A and R194H, the efficacy could not be determined.

Cell Surface Enzyme-Linked Immunosorbent Assay. The cell surface enzyme-linked immunosorbent assay (ELISA) was performed

as described before.³ One day prior to the assay, 1321N1 astrocytoma cells expressing the wt or mutant P2Y₂R were seeded into 12-well plates in duplicates at a density of 300000 cells per well and incubated at 37 °C overnight. The entire ELISA except for antibody incubations and the substrate reaction was done on ice and using 500 μL of cooled buffers and solutions. Upon removal of the nutrient medium, the cells were washed with PBS and cell surfaces were blocked using 1% bovine serum albumin (BSA) dissolved in PBS. The cells were subsequently incubated for 1 h at room temperature with 300 μL of a 1:500 dilution of HA-specific mouse monoclonal antibody (HA.11) solution in DMEM supplemented with 1% BSA, 10 μM 2-[4-(2-hydroxyethyl)-piperazin-1-yl]ethanesulfonic acid (HEPES), and 1 μM CaCl₂, and adjusted to pH 7.0. The cells were washed three times with PBS, fixed using 4% paraformaldehyde solution for 5 min, washed again, and blocked with 1% BSA in PBS for 10 min. After 1 h of incubation with peroxidase-conjugated goat antimouse IgG antibody at a 1:2500 dilution in DMEM with the supplements described above, the cells were washed four times with PBS and incubated with 300 μL of 2,2'-azino-bis-3-ethylbenzothiazoline-6-sulfonic acid (ABTS) chromophore solution for 45 min at room temperature. Subsequently, 170 μL of the substrate were transferred to a 96-well plate, and absorbance was measured at 405 nm using a PHERAstar microplate reader (BMG Laboratory Technologies, Offenburg, Germany).

Homology Modeling. The crystal structures of the human P2Y₁R (PDB 4XNW) bound to the nucleotide antagonist **8** and of the human P2Y₁₂R (PDBs 4PXZ and 4NTJ) co-crystallized with the agonist **6** and the antagonist **7**, respectively, were downloaded from the Research Collaboratory for Structural Bioinformatics (RCSB) Protein Data Bank (PDB).⁶⁴ The crystal structure of human P2Y₁R was used as a template for generating homology models of the human P2Y₂R sequence (accession number: P41231) retrieved from the UniProt sequence database (<http://www.uniprot.org>).⁶⁵ The sequences of the human P2Y₁R and P2Y₁₂R were aligned with that of the human P2Y₂R using Clustal Omega and AlignMe.^{66,67} With the human P2Y₂R as a template, we generated 500 models using the standard comparative modeling by the automodel class available for MODELER. To ensure correct tertiary protein structure, we introduced disulfide bridges between Cys25 and Cys278 as well as between Cys106 and Cys183. The best model was selected on the basis of Discrete Optimized Protein Energy (DOPE) scores calculated for the models.^{68,69} The generated models were analyzed, and the best model of the human P2Y₂R was used for molecular docking studies based on the DOPE- and GA341-score, PROSA II Z-score, and Ramachandran plots.

Docking Studies. Prior to docking, the homology model of the human P2Y₂R was prepared using the Protein Preparation Wizard module implemented in Schrödinger.^{70,71} In the first step for protein preparation, we preprocessed the structure using the standard protocol which included the assigning of bond orders using the CCD database, the adding of hydrogens, the creating of disulfide bonds, and the generating of het states using the implemented Epik module for prediction of the structure protonation state at physiological pH of 7.4. The second step involved H-bond assignment optimization by considering sample water orientations and by using the PROPKA package to determine the protein protonation state at pH 7.4. In the third and final protein preparation step, we performed restrained minimization, covering only heavy atoms, to 0.30 Å RMSD using the Liquid Simulations Version 3 (OPLS3) force field.

Rotamers of side chains were examined using the rotamer library module implemented in Molecular Operating Environment (MOE 2014.09, Chemical Computing Group Inc., Montreal, Canada). The orthosteric binding site was identified using the SiteFinder module from MOE 2014.09. For predicting the binding mode, the agonists UTP and Ap₄A as well as the antagonists **4**, **10**–**12**, and **13** were docked into the predicted orthosteric binding site of the receptor. Docking was performed using Induced Fit Docking (IFD) and Glide as implemented in Schrödinger release 2016.^{70–72} In the first step of IFD, Glide ligand docking were performed by removing the side chains of the amino acids in the selected binding pocket. In the second phase of docking, the Prime was applied to refine the nearby residues and optimize the side chains. In the final docking phase, the ligand was

redocked into all induced fit protein structures that were within 30 kcal/mol of the lowest energy structure by using the Glide XP scoring function. A receptor grid center was specified on the basis of the transformed position of the orthosteric agonist **5** from the human P2Y₁₂R structure, with the cubic grid side length of 10 Å. We thus limited the possible docking area, and we therefore cannot completely exclude that other binding areas outside of the selected one might also qualify as potential binding sites.

During the docking simulations, the receptor and the ligands were selected flexible during docking. Following docking, the resulting poses of the best model was selected using the IFD scores and Prime Energy as representative values. The conformations of the docked ligands within an energy window of 2.5 kcal/mol were considered. For Glide docking, the following standard parameters were selected: receptor van der Waals scaling, 0.50; ligand van der Waals scaling, 0.50; a maximum of 20 poses per ligand. Residues within 5.0 Å of the ligand poses were refined, and the side chains were optimized. The best docking pose was selected based on the IFD score and Prime Energy values.

■ ASSOCIATED CONTENT

📄 Supporting Information

The Supporting Information is available free of charge on the ACS Publications website at DOI: 10.1021/acs.jmedchem.7b00854.

Sequence alignment of the P2Y₂R and P2Y₁R; sequence–structure compatibility and Ramachandran diagram of the P2Y₂R model; model showing residues mutated in this study; cell surface expression of the mutated receptors; table with potencies of agonists and antagonists (PDF)

Molecular formula strings (CSV)

P2Y₂ homology model (PDB)

■ AUTHOR INFORMATION

Corresponding Author

*Phone: +49-228-73-2301. Fax: +49-228-73-2567. E-mail: christa.mueller@uni-bonn.de.

ORCID

Muhammad Rafehi: 0000-0002-4314-4800

Enas M. Malik: 0000-0003-4563-3584

Christa E. Müller: 0000-0002-0013-6624

Author Contributions

#M.R. and A.N. contributed equally.

Notes

The authors declare no competing financial interest.

■ ACKNOWLEDGMENTS

This study was supported by the Ministry for Innovation, Science, Research and Technology of the State of North Rhine-Westphalia through the NRW International Graduate Research School Biotech-Pharma (M.R., C.E.M.). A.N. and C.E.M. were supported by the German Research Foundation (DFG, Research Training group GRK 1873). Y.B. is grateful for an SQU grant (SR/SCI/CHEM/15/01). E.M.M. thanks The Deutscher Akademischer Austauschdienst (DAAD) for a Ph.D. scholarship. We also thank Schrödinger Inc. for providing the evaluation license.

■ ABBREVIATIONS USED

ADP, adenosine-5'-diphosphate; Ap₄A, P¹,P⁴-di(adenosine-5')-tetraphosphate; ATP, adenosine-5'-triphosphate; BSA, bovine serum albumin; DMEM, Dulbecco's Modified Eagle Medium; ECL, extracellular loop; EDTA, ethylenediaminetetraacetic

acid; ELISA, enzyme-linked immunosorbent assay; GPCR, G protein-coupled receptor; HA, hemagglutinin; HBSS, Hank's Balanced Salt Solution; IFD, induced fit docking; MeS, methylthio; P2Y₂R, P2Y₂ receptor; PBS, phosphate-buffered saline; PCR, polymerase chain reaction; PDB, Protein Data Bank; PSB, Pharmaceutical Sciences Bonn; RB-2, Reactive blue 2; TM, transmembrane region; UTP, uridine-5'-triphosphate; Wt, wild-type

REFERENCES

- (1) Nicholas, R. A.; Watt, W. C.; Lazarowski, E. R.; Li, Q.; Harden, K. Uridine nucleotide selectivity of three phospholipase C-activating P2 receptors: Identification of a UDP-selective, a UTP-selective, and an ATP- and UTP-specific receptor. *Mol. Pharmacol.* **1996**, *50*, 224–229.
- (2) Jacobson, K. A.; Costanzi, S.; Ivanov, A. A.; Tchilibon, S.; Besada, P.; Gao, Z.-G.; Maddileti, S.; Harden, T. K. Structure activity and molecular modeling analyses of ribose- and base-modified uridine 5'-triphosphate analogues at the human P2Y₂ and P2Y₄ receptors. *Biochem. Pharmacol.* **2006**, *71*, 540–549.
- (3) Hillmann, P.; Ko, G. Y.; Spinrath, A.; Raulf, A.; von Kügelgen, I.; Wolff, S. C.; Nicholas, R. A.; Kostenis, E.; Holtje, H. D.; Müller, C. E. Key determinants of nucleotide-activated G protein-coupled P2Y(2) receptor function revealed by chemical and pharmacological experiments, mutagenesis and homology modeling. *J. Med. Chem.* **2009**, *52*, 2762–2775.
- (4) Murthy, K. S.; Makhlof, G. M. Coexpression of ligand-gated P2X and G protein-coupled P2Y receptors in smooth muscle. Preferential activation of P2Y receptors coupled to phospholipase C (PLC)-beta1 via Galphaq/11 and to PLC-beta3 via Gbetagamma3. *J. Biol. Chem.* **1998**, *273*, 4695–4704.
- (5) Bagchi, S.; Liao, Z.; Gonzalez, F. A.; Chorna, N. E.; Seye, C. I.; Weisman, G. A.; Erb, L. The P2Y₂ nucleotide receptor interacts with v integrins to activate G_o and induce cell migration. *J. Biol. Chem.* **2005**, *280*, 39050–39057.
- (6) Liao, Z.; Seye, C. I.; Weisman, G. A.; Erb, L. The P2Y₂ nucleotide receptor requires interaction with alpha v integrins to access and activate G₁₂. *J. Cell Sci.* **2007**, *120*, 1654–1662.
- (7) Baltensperger, K.; Porzig, H. The P_{2U} purinoceptor obligatorily engages the heterotrimeric G protein G₁₆ to mobilize intracellular Ca²⁺ in human erythroleukemia cells. *J. Biol. Chem.* **1997**, *272*, 10151–10159.
- (8) Moore, D. J.; Chambers, J. K.; Wahlin, J. P.; Tan, K. B.; Moore, G. B.; Jenkins, O.; Emson, P. C.; Murdock, P. R. Expression pattern of human P2Y receptor subtypes, a quantitative reverse transcription-polymerase chain reaction study. *Biochim. Biophys. Acta, Gene Struct. Expression* **2001**, *1521*, 107–119.
- (9) Cressman, V. L.; Lazarowski, E.; Homolya, L.; Boucher, R. C.; Koller, B. H.; Grubb, B. R. Effect of loss of P2Y(2) receptor gene expression on nucleotide regulation of murine epithelial Cl⁻ transport. *J. Biol. Chem.* **1999**, *274*, 26461–26468.
- (10) Hochhauser, E.; Cohen, R.; Waldman, M.; Maksin, A.; Isak, A.; Aravot, D.; Jayasekara, P. S.; Müller, C. E.; Jacobson, K. A.; Shainberg, A. P2Y receptor agonist with enhanced stability protects the heart from ischemic damage in vitro and in vivo. *Purinergic Signalling* **2013**, *9*, 633–642.
- (11) Camden, J. M.; Schrader, A. M.; Camden, R. E.; Gonzalez, F. A.; Erb, L.; Seye, C. I.; Weisman, G. A. P2Y₂ nucleotide receptors enhance alpha-secretase-dependent amyloid precursor protein processing. *J. Biol. Chem.* **2005**, *280*, 18696–18702.
- (12) Xing, M.; Firestein, B. L.; Shen, G. H.; Insel, P. A. Dual role of protein kinase C in the regulation of cPLA2-mediated arachidonic acid release by P2U receptors in MDCK-D1 cells, involvement of MAP kinase-dependent and -independent pathways. *J. Clin. Invest.* **1997**, *99*, 805–814.
- (13) Welch, B. D.; Carlson, N. G.; Shi, H.; Myatt, L.; Kishore, B. K. P2Y₂ receptor-stimulated release of prostaglandin E₂ by rat inner medullary collecting duct preparations. *Am. J. Physiol. Renal. Physiol.* **2003**, *285*, F711–721.
- (14) Schuchardt, M.; Prüfer, J.; Prüfer, N.; Wiedon, A.; Huang, T.; Chebli, M.; Jankowski, V.; Jankowski, J.; Schäfer-Korting, M.; Zidek, W.; van der Giet, M.; Tölle, M. The endothelium-derived contracting factor uridine adenosine tetraphosphate induces P2Y(2)-mediated pro-inflammatory signaling by monocyte chemoattractant protein-1 formation. *J. Mol. Med.* **2011**, *89*, 799–810.
- (15) Seye, C. I.; Yu, N.; Jain, R.; Kong, Q.; Minor, T.; Newton, J.; Erb, L.; Gonzalez, F. A.; Weisman, G. A. The P2Y₂ nucleotide receptor mediates UTP-induced vascular cell adhesion molecule-1 expression in coronary artery endothelial cells. *J. Biol. Chem.* **2003**, *278*, 24960–24965.
- (16) Kaczmarek, E.; Erb, L.; Koziak, K.; Jarzyna, R.; Wink, M. R.; Guckelberger, O.; Blusztajn, K.; Trinkaus-Randall, V.; Weisman, G. A.; Robson, S. C. Modulation of endothelial cell migration by extracellular nucleotides, involvement of focal adhesion kinase and phosphatidylinositol 3-kinase-mediated pathways. *Thromb. Haemostasis* **2005**, *93*, 735–742.
- (17) Abbracchio, M. P.; Burnstock, G.; Boeynaems, J. M.; Barnard, E. A.; Boyer, J. L.; Kennedy, C.; Knight, G. E.; Fumagalli, M.; Gachet, C.; Jacobson, K. A.; Weisman, G. A. International Union of Pharmacology LVIII, update on the P2Y G protein-coupled nucleotide receptors, from molecular mechanisms and pathophysiology to therapy. *Pharmacol. Rev.* **2006**, *58*, 281–341.
- (18) Müller, T.; Robaye, B.; Vieira, R. P.; Ferrari, D.; Grimm, M.; Jakob, T.; Martin, S. F.; Di Virgilio, F.; Boeynaems, J. M.; Virchow, J. C.; Idzko, M. The purinergic receptor P2Y₂ receptor mediates chemotaxis of dendritic cells and eosinophils in allergic lung inflammation. *Allergy* **2010**, *65*, 1545–1553.
- (19) Ayata, C. K.; Ganai, S. C.; Hockenjos, B.; Willim, K.; Vieira, R. P.; Grimm, M.; Robaye, B.; Boeynaems, J. M.; Di Virgilio, F.; Pellegatti, P.; Diefenbach, A.; Idzko, M.; Hasselblatt, P. Purinergic P2Y₂ receptors promote neutrophil infiltration and hepatocyte death in mice with acute liver injury. *Gastroenterology* **2012**, *143*, 1620–1629.
- (20) Tu, M. T.; Luo, S. F.; Wang, C. C.; Chien, C. S.; Chiu, C. T.; Lin, C. C.; Yang, C. M. P2Y(2) receptor-mediated proliferation of C(6) glioma cells via activation of Ras/Raf/MEK/MAPK pathway. *Br. J. Pharmacol.* **2000**, *129*, 1481–1489.
- (21) Muscella, A.; Elia, M. G.; Greco, S.; Storelli, C.; Marsigliante, S. Activation of P2Y₂ receptor induces c-FOS protein through a pathway involving mitogen-activated protein kinases and phosphoinositide 3-kinases in HeLa cells. *J. Cell. Physiol.* **2003**, *195*, 234–240.
- (22) Schafer, R.; Sedehizade, F.; Welte, T.; Reiser, G. ATP- and UTP-activated P2Y receptors differently regulate proliferation of human lung epithelial tumor cells. *Am. J. Physiol. Lung Cell Mol. Physiol.* **2003**, *285*, L376–385.
- (23) Weisman, G. A.; Wang, M.; Kong, Q.; Chorna, N. E.; Neary, J. T.; Sun, G. Y.; González, F. A.; Seye, C. I.; Erb, L. Molecular determinants of P2Y₂ nucleotide receptor function, implications for proliferative and inflammatory pathways in astrocytes. *Mol. Neurobiol.* **2005**, *31*, 169–183.
- (24) Malam-Souley, R.; Seye, C.; Gadeau, A. P.; Loirand, G.; Pillois, X.; Campan, M.; Pacaud, P.; Desgranges, C. Nucleotide receptor P_{2U} partially mediates ATP-induced cell cycle progression of aortic smooth muscle cells. *J. Cell. Physiol.* **1996**, *166*, 57–65.
- (25) Miyagi, Y.; Kobayashi, S.; Ahmed, A.; Nishimura, J.; Fukui, M.; Kanaide, H. P_{2U} purinergic activation leads to the cell cycle progression from the G1 to the S and M phases but not from the G₀ to G₁ phase in vascular smooth muscle cells in primary culture. *Biochem. Biophys. Res. Commun.* **1996**, *222*, 652–658.
- (26) Schumacher, D.; Strilic, B.; Sivaraj, K. K.; Wettschureck, N.; Offermanns, S. Platelet-Derived Nucleotides Promote Tumor-Cell Transendothelial Migration and Metastasis via P2Y₂ Receptor. *Cancer Cell* **2013**, *24*, 130–137.
- (27) Kishore, B. K.; Carlson, N. G.; Ecelbarger, C. M.; Kohan, D. E.; Müller, C. E.; Nelson, R. D.; Peti-Peterdi, J.; Zhang, Y. Targeting renal purinergic signalling for the treatment of lithium-induced nephrogenic diabetes insipidus. *Acta Physiol.* **2015**, *214*, 176–188.

- (28) Conroy, S.; Kondon, N.; Kellam, B.; Stocks, M. J. Drug-like antagonists of P2Y receptors -from lead identification to drug development. *J. Med. Chem.* **2016**, *59*, 9981–10005.
- (29) Brunschweiler, A.; Müller, C. E. P2 receptors activated by uracil nucleotides—an update. *Curr. Med. Chem.* **2006**, *12*, 763–771.
- (30) Von Kügelgen, I.; Hoffmann, K. Pharmacology and structure of P2Y receptors. *Neuropharmacology* **2016**, *104*, 50–61.
- (31) Jacobson, K. A.; Müller, C. E. Medicinal chemistry of adenosine, P2Y and P2X receptors. *Neuropharmacology* **2016**, *104*, 31–49.
- (32) Zhang, D.; Gao, Z. G.; Zhang, K.; Kiselev, E.; Crane, S.; Wang, J.; Paoletta, S.; Yi, C.; Ma, L.; Zhang, W.; Han, G. W.; Liu, H.; Cherezov, V.; Katritch, V.; Jiang, H.; Stevens, R. C.; Jacobson, K. A.; Zhao, Q.; Wu, B. Two disparate ligand-binding sites in the human P2Y₁ receptor. *Nature* **2015**, *520*, 317–321.
- (33) Zhang, K.; Zhang, J.; Gao, Z. G.; Zhang, D.; Zhu, L.; Han, G. W.; Moss, S. M.; Paoletta, S.; Kiselev, E.; Lu, W.; Fenalti, G.; Zhang, W.; Müller, C. E.; Yang, H.; Jiang, H.; Cherezov, V.; Katritch, V.; Jacobson, K. A.; Stevens, R. C.; Wu, B.; Zhao, Q. Structure of the human P2Y₁₂ receptor in complex with an antithrombotic drug. *Nature* **2014**, *509*, 115–118.
- (34) Zhang, J.; Zhang, K.; Gao, Z. G.; Paoletta, S.; Zhang, D.; Han, G. W.; Li, T.; Ma, L.; Zhang, W.; Müller, C. E.; Yang, H.; Jiang, H.; Cherezov, V.; Katritch, V.; Jacobson, K. A.; Stevens, R. C.; Wu, B.; Zhao, Q. Agonist-bound structure of the human P2Y₁₂ receptor. *Nature* **2014**, *509*, 119–122.
- (35) Rafahi, M.; Burbiel, J. C.; Attah, I. Y.; Abdelrahman, A.; Müller, C. E. Synthesis, characterization, and in vitro evaluation of the selective P2Y₂ receptor antagonist AR-C118925. *Purinergic Signalling* **2017**, *13*, 89–103.
- (36) Meghani, P. The design of P2Y₂ antagonists for the treatment of inflammatory diseases. *American Chemical Society Division of Medicinal Chemistry Abstracts of 224th ACS National Meeting, Boston, MA, USA*; American Chemical Society: Washington, DC, 2002.
- (37) Kondon, N.; Meghani, P.; Thom, S. N. C. Novel Compounds. WO1999002501 A1, 1998.
- (38) Yuan, S.; Chan, H. C.; Vogel, H.; Filipek, S.; Stevens, R. C.; Palczewski, K. The molecular mechanism of P2Y₁ receptor activation. *Angew. Chem., Int. Ed.* **2016**, *55*, 10331–10335.
- (39) Flores, R. V.; Hernández-Pérez, M. G.; Aquino, E.; Garrad, R. C.; Weisman, G. A.; Gonzalez, F. A. Agonist-induced phosphorylation and desensitization of the P2Y₂ nucleotide receptor. *Mol. Cell. Biochem.* **2005**, *280*, 35–45.
- (40) Qi, A. D.; Wolff, S. C.; Nicholas, R. A. The apical targeting signal of the P2Y₂ receptor is located in its first extracellular loop. *J. Biol. Chem.* **2005**, *280*, 29169–29175.
- (41) Ibuka, S.; Matsumoto, S.; Fujii, S.; Kikuchi, A. The P2Y₂ receptor promotes Wnt3a- and EGF-induced epithelial tubular formation by IEC6 cells by binding to integrins. *J. Cell Sci.* **2015**, *128*, 2156–2168.
- (42) Erb, L.; Liu, J.; Ockerhausen, J.; Kong, Q.; Garrad, R. C.; Griffin, K.; Neal, C.; Krugh, B.; Santiago-Pérez, L. I.; González, F. A.; Gresham, H. D.; Turner, J. T.; Weisman, G. A. An RGD sequence in the P2Y(2) receptor interacts with alpha(V)beta(3) integrins and is required for G(o)-mediated signal transduction. *J. Cell Biol.* **2001**, *153*, 491–501.
- (43) Erb, L.; Garrad, R.; Wang, Y.; Quinn, T.; Turner, J. T.; Weisman, G. A. Site-directed mutagenesis of P_{2U} purinoceptors. *J. Biol. Chem.* **1995**, *270*, 4185–4188.
- (44) Kinzer-Ursem, T. L.; Linderman, J. J. Both ligand- and cell-specific parameters control ligand agonism in a kinetic model of G protein coupled receptor signaling. *PLoS Comput. Biol.* **2007**, *3*, e6.
- (45) Kenakin, T. Differences between natural and recombinant G protein coupled receptor systems with varying receptor/G protein stoichiometry. *Trends Pharmacol. Sci.* **1997**, *18*, 456–464.
- (46) Hoffmann, C.; Moro, S.; Nicholas, R. A.; Harden, T. K.; Jacobson, K. A. The role of amino acids in extracellular loops of the human P2Y₁ receptor in surface expression and activation processes. *J. Biol. Chem.* **1999**, *274*, 14639–14647.
- (47) Moro, S.; Guo, D.; Camaioni, E.; Boyer, J. L.; Harden, T. K.; Jacobson, K. A. Human P2Y₁ receptor: Molecular modeling and site-directed mutagenesis as tools to identify agonist and antagonist recognition sites. *J. Med. Chem.* **1998**, *41*, 1456–1466.
- (48) Costanzi, S.; Mamedova, L.; Gao, Z. G.; Jacobson, K. A. Architecture of P2Y nucleotide receptors: Structural comparison based on sequence analysis, mutagenesis, and homology modeling. *J. Med. Chem.* **2004**, *47*, 5393–5404.
- (49) Moro, S.; Hoffmann, C.; Jacobson, K. A. Role of the extracellular loops of G protein-coupled receptors in ligand recognition: a molecular modeling study of the human P2Y₁ receptor. *Biochemistry* **1999**, *38*, 3498–3507.
- (50) Nguyen, A. T.; Baltos, J. A.; Thomas, T.; Nguyen, T. D.; Muñoz, L. L.; Gregory, K. J.; White, P. J.; Sexton, P. M.; Christopoulos, A.; May, L. T. Extracellular loop 2 of the adenosine A₁ receptor has a key role in orthosteric ligand affinity and agonist efficacy. *Mol. Pharmacol.* **2016**, *90*, 703–714.
- (51) Herold, C. L.; Qi, A. D.; Harden, T. K.; Nicholas, R. A. Agonists versus antagonist action of ATP at the P2Y₄ receptor is determined by the second extracellular loop. *J. Biol. Chem.* **2004**, *279*, 11456–11464.
- (52) Wifling, D.; Bernhardt, G.; Dove, S.; Buschauer, A. The extracellular loop 2 (ECL2) of the human histamine H4 receptor substantially contributes to ligand binding and constitutive activity. *PLoS One* **2015**, *10*, e0117185.
- (53) Weyler, S.; Baqi, Y.; Hillmann, P.; Kaulich, M.; Hunder, A. M.; Müller, I. A.; Müller, C. E. Combinatorial synthesis of anilinoanthraquinone derivatives and evaluation as non-nucleotide-derived P2Y₂ receptor antagonists. *Bioorg. Med. Chem. Lett.* **2008**, *18*, 223–227.
- (54) Baqi, Y.; Müller, C. E. Synthesis of alkyl- and aryl-amino-substituted anthraquinone derivatives by microwave-assisted copper(0)-catalyzed Ullmann coupling reactions. *Nat. Protoc.* **2010**, *5*, 945–953.
- (55) Baqi, Y.; Müller, C. E. Rapid and efficient microwave-assisted copper(0)-catalyzed Ullmann coupling reaction: general access to anilinoanthraquinone derivatives. *Org. Lett.* **2007**, *9*, 1271–1274.
- (56) Baqi, Y. Ecto-nucleotidase inhibitors: recent developments in drug discovery. *Mini-Rev. Med. Chem.* **2015**, *15*, 21–33.
- (57) Baqi, Y. Anthraquinone as a privileged scaffold in drug discovery targeting nucleotide binding proteins. *Drug Discovery Today* **2016**, *21*, 1571–1577.
- (58) Costanzi, S.; Santhosh Kumar, T.; Balasubramanian, R.; Kendall Harden, T.; Jacobson, K. A. Virtual screening leads to the discovery of novel non-nucleotide P2Y₁ receptor antagonists. *Bioorg. Med. Chem.* **2012**, *20*, 5254–5261.
- (59) Gutiérrez-de-Terán, H.; Sallander, J.; Sotelo, E. Structure-based rational design of adenosine receptor ligands. *Curr. Top. Med. Chem.* **2017**, *17*, 40–58.
- (60) Baqi, Y.; Müller, C. E. Catalyst-free microwave-assisted amination of 2-chloro-5-nitrobenzoic acid. *J. Org. Chem.* **2007**, *72*, 5908–5911.
- (61) Reikofski, J.; Tao, B. Y. Polymerase chain reaction (PCR) techniques for site-directed mutagenesis. *Biotechnol. Adv.* **1992**, *10*, 535–547.
- (62) Miller, A. D.; Rosman, G. J. Improved retroviral vectors for gene transfer and expression. *Biotechniques* **1989**, *7*, 980–982 984–986, 989–990.
- (63) Sromek, S. M.; Harden, T. K. Agonist-induced internalization of the P2Y₂ receptor. *Mol. Pharmacol.* **1998**, *54*, 485–494.
- (64) Berman, H. M.; Westbrook, J.; Feng, Z.; Gilliland, G.; Bhat, T. N.; Weissig, H.; Shindyalov, I. N.; Bourne, P. E. The Protein Data Bank. *Nucleic Acids Res.* **2000**, *28*, 235–242.
- (65) UniProt. UniProt: a hub for protein information. *Nucleic Acids Res.* **2015**, *43*, D204–D212.
- (66) Sievers, F.; Wilm, A.; Dineen, D.; Gibson, T. J.; Karplus, K.; Li, W.; Lopez, R.; McWilliam, H.; Remmert, M.; Söding, J.; Thompson, J. D.; Higgins, D. G. Fast, scalable generation of high-quality protein multiple sequence alignments using Clustal Omega. *Mol. Syst. Biol.* **2011**, *7*, 539.

(67) Stamm, M.; Staritzbichler, R.; Khafizov, K.; Forrest, L. R. AlignMe - a membrane protein sequence alignment web server. *Nucleic Acids Res.* **2014**, *42*, W246–W251.

(68) Sali, A.; Blundell, T. L. Comparative protein modelling by satisfaction of spatial restraints. *J. Mol. Biol.* **1993**, *234*, 779–815.

(69) Webb, B.; Sali, A. Protein structure modeling with MODELLER. *Methods Mol. Biol.* **2014**, *1137*, 1–15.

(70) Friesner, R. A.; Banks, J. L.; Murphy, R. B.; Halgren, T. A.; Klicic, J. J.; Mainz, D. T.; Repasky, M. P.; Knoll, E. H.; Shaw, D. E.; Shelley, M.; Perry, J. K.; Francis, P.; Shenkin, P. S. Glide, A new approach for rapid, accurate docking and scoring. 1. Method and assessment of docking accuracy. *J. Med. Chem.* **2004**, *47*, 1739–1749.

(71) Halgren, T. A.; Murphy, R. B.; Friesner, R. A.; Beard, H. S.; Frye, L. L.; Pollard, W. T.; Banks, J. L. Glide, a new approach for rapid, accurate docking and scoring. 2. Enrichment factors in database screening. *J. Med. Chem.* **2004**, *47*, 1750–1759.

(72) Sherman, W.; Day, T.; Jacobson, M. P.; Friesner, R. A.; Farid, R. Novel procedure for modeling ligand/receptor induced fit effects. *J. Med. Chem.* **2006**, *49*, 534–553.

4.3. Supporting Information

The Supporting Information and the homology model of human P2Y₂R can be accessed free of charge online at:

<https://pubs.acs.org/doi/10.1021/acs.jmedchem.7b00854>.

Supporting Information

**Molecular recognition of agonists and antagonists
by the nucleotide-activated G protein-coupled P2Y₂ receptor**

Muhammad Rafehi,^{1,#} Alexander Neumann,^{1,#} Younis Baqi,³ Enas M. Malik,¹ Michael Wiese,² Vigneshwaran Namasivayam,^{1,2} Christa E. Müller^{1,*}

Table of contents

P2Y ₂ R homology model.....	S2
Figure S1. Sequence alignment of the P2Y ₂ R and P2Y ₁ R.....	S2
Figure S2. Ramachandran diagram of the P2Y ₂ R model	S3
Figure S3. Sequence-structure compatibility of the P2Y ₂ R model	S4
Figure S4. Space-fill model of residues mutated in this study	S5
Receptor expression	S6
Figure S5. Cell surface expression of the mutated P2Y ₂ Rs	S6
Pharmacological assessments of mutated P2Y ₂ Rs.....	S7
Table S1. Potencies of the agonists UTP and Ap ₄ A on the wt and mutant P2Y ₂ Rs	S7
Table S2. Potencies of various antagonists on the wt and mutant P2Y ₂ Rs	S9
References	S10

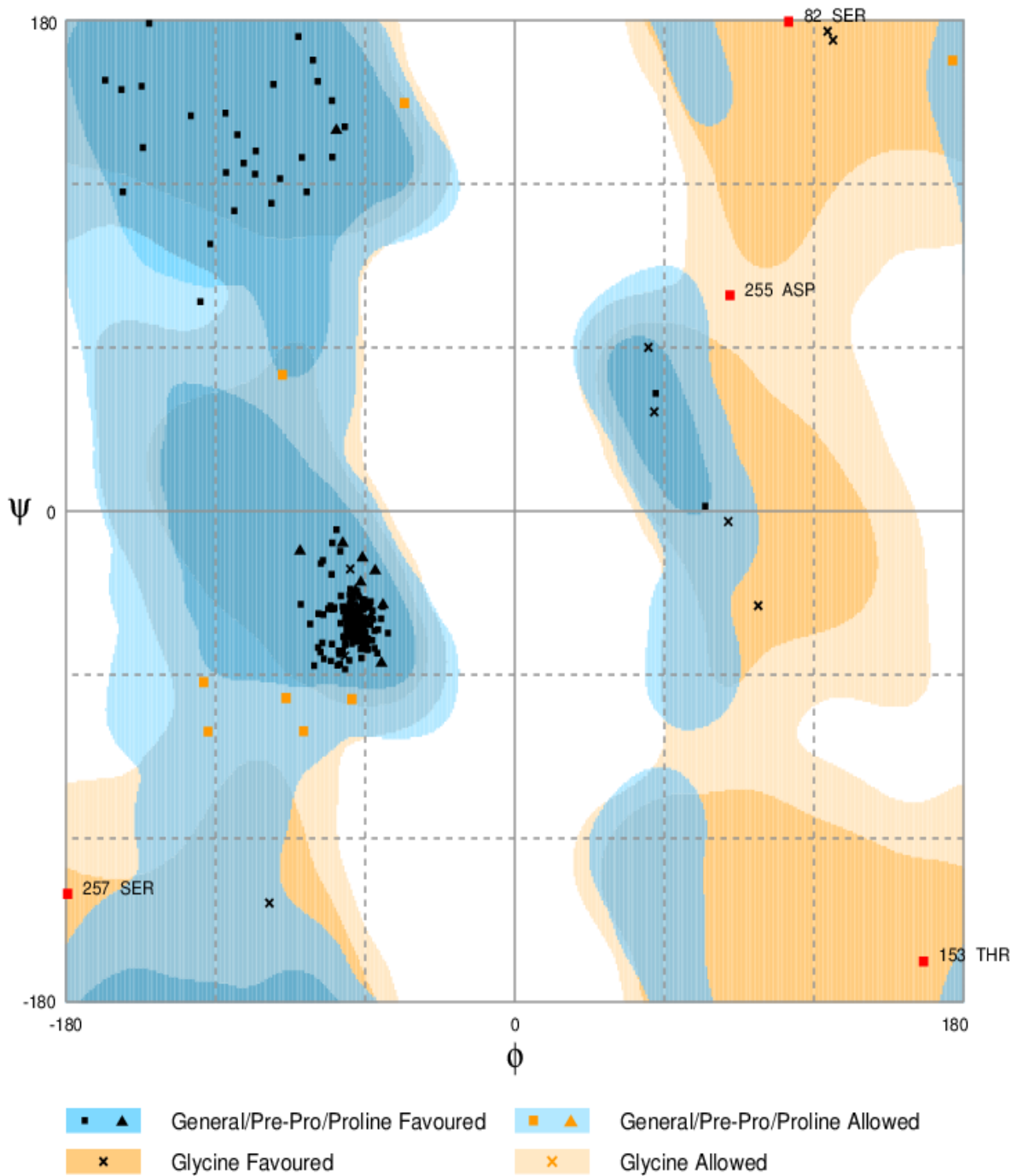


Figure S2. Ramachandran diagram of the human P2Y₂R model: 98.0 % of all residues map to most favored regions.

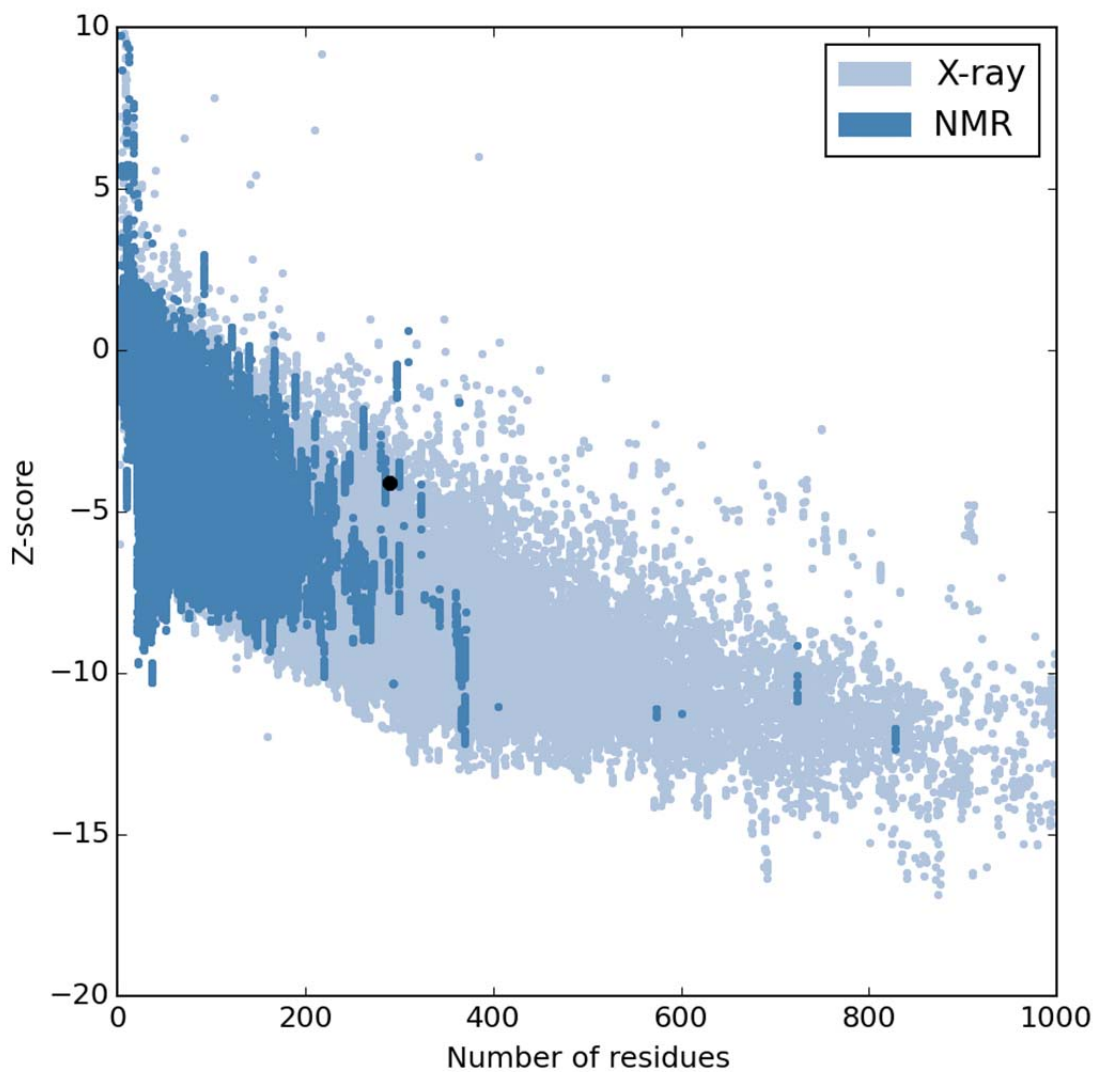


Figure S3. Sequence-structure compatibility of the human P2Y₂R model. A PROSA II Z-score profile of NMR and X-ray reference structures is shown that contains the P2Y₂R model (black circle) yielding a Z-score of -4.1.

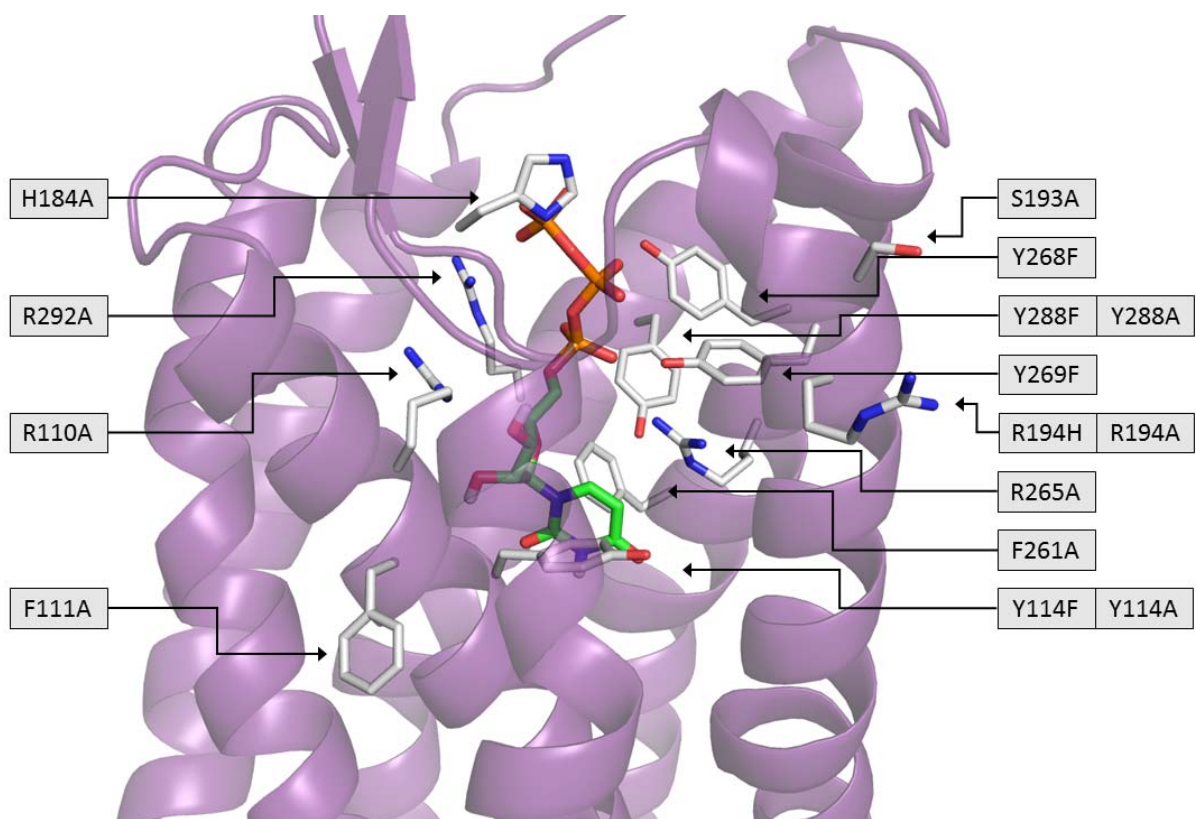


Figure S4. Amino acid residues mutated in this study, presented in the homology model of the human P2Y₂R in complex with uridine-5'-triphosphate (UTP, **1**). Side chains are presented as sticks. Oxygen is colored in red, nitrogen in blue.

Receptor expression

Cell surface expression for the wild-type (wt) and mutated receptors was confirmed and quantified using enzyme-linked immunosorbent assays (ELISA), with the exception of the mutants R194A and R194H. The cell lines for these receptor mutations had been created in a previous study¹ and did not contain a hemagglutinin (HA)-tag. Results are shown in Figure S5.

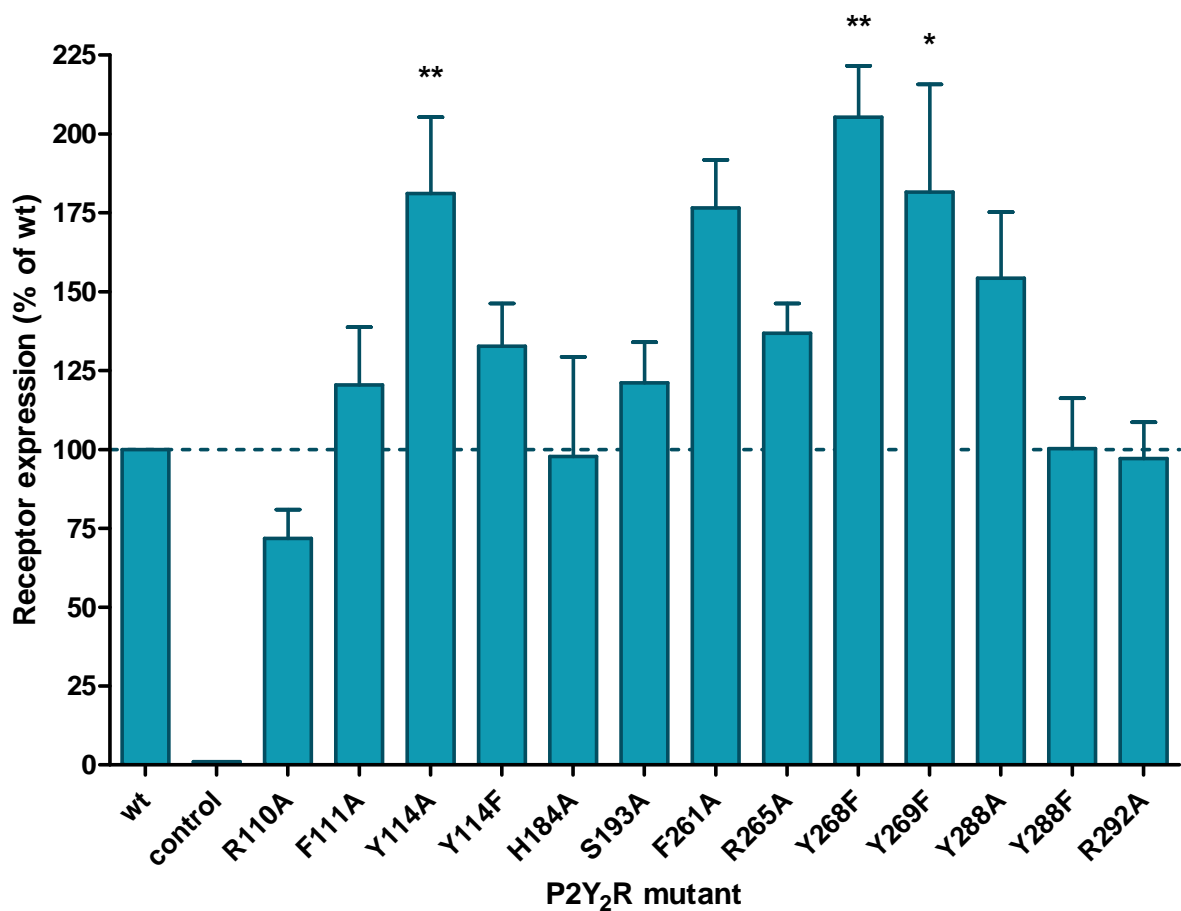


Figure S5. Cell surface expression of the mutated P2Y₂Rs in stably transfected 1321N1 astrocytoma cells determined by ELISA. The mean expression levels of at least 3 independent experiments are shown for the mutated receptors, normalized to that of the wt receptor; error bar represent SEM values. Non-transfected 1321N1 astrocytoma cells were used as a control. Each mutant was compared to the wt using one-way ANOVA with Dunnett's post-test; * $p < 0.05$, ** $p < 0.01$.

Pharmacological assessment of mutated P2Y₂ receptors

To provide experimental evidence for the support and refinement of our homology model, the effect of different mutations in the putative orthosteric site of the human P2Y₂R on the potencies of the agonists UTP (**1**) and *P*¹,*P*⁴-di(adenosine-5')-tetrphosphate (Ap₄A, **3**) as well as various antagonists was determined using calcium mobilization assays. The EC₅₀ values for the agonists are found in Table S1.

Table S1. Potencies of the agonists UTP (**1**) and Ap₄A (**3**) at the wt and mutant human P2Y₂Rs, determined using a fluorescence-based calcium mobilization assay in transfected 1321N1 astrocytoma cells (n ≥ 4). The cell surface expression of the mutant receptors relative to the expression of the wt receptor is also shown.

P2Y ₂ R mutant	EC ₅₀ ± SEM (nM)		Receptor expression (% of wt)
	UTP (1)	Ap ₄ A (3)	
wt	5.61 ± 0.85	100.0 ± 0.1	100
R110A	> 100,000	> 100,000	72
F111A	186 ± 40	1,986 ± 324	120
Y114A	15.9 ± 2.0	593 ± 257	181
Y114F	1,662 ± 93	> 100,000	133
H184A	996 ± 98	18,100 ± 5900	98
S193A	70.6 ± 19.7	618 ± 202	121
R194A	254 ± 62	> 100,000	n.d. ^a
R194H	304 ± 74	≈ 2,500	n.d. ^a

F261A	496 ± 172	> 100,000	177
R265A	> 100,000	> 100,000	137
Y268F	62.3 ± 5.0	3,160 ± 1,490	205
Y269F	221 ± 36	1,520 ± 290	182
Y288A	≥ 100,000	> 100,000	154
Y288F	911 ± 218	≥ 100,000	100
R292A	> 50,000	> 50,000	97

^an.d., not determined, as no HA-tag was present and determination of receptor expression via ELISA was therefore not possible.

Several different antagonists were also determined on the mutated P2Y₂Rs using calcium mobilization assays. In the assessment of antagonists, receptors were stimulated with UTP at a concentration that corresponded to its EC₈₀ value. Some of the mutations led to an abolishment of the response to UTP, and the assessment of antagonists was in these cases not possible. The IC₅₀ values for the antagonists are found in Table S2.

Table S2. Potencies of various antagonists on the wt and mutant human P2Y₂Rs determined using a fluorescence-based calcium mobilization assay in transfected 1321N1 astrocytoma cells (n ≥ 3). Antagonist assessments were done at a concentration of the agonist UTP that corresponded to its EC₈₀ value.

P2Y ₂ R mutant	IC ₅₀ ± SEM (μM)				
	AR-C118925 (4)	PSB-0725 (10)	PSB-10107 (11)	PSB-09114 (12)	Reactive Blue 2 (13)
wt	0.0629 ± 0.0117	26.4 ± 5.1	12.2 ± 3.9	5.10 ± 0.52	22.1 ± 5.9
F111A	0.110 ± 0.043	≈ 30	21.2 ± 5.8	6.97 ± 0.64	> 100
Y114A	0.0143 ± 0.008	5.93 ± 0.73	4.34 ± 0.60	2.99 ± 0.91	≈ 50
Y114F	0.0184 ± 0.0005	4.69 ± 2.56	3.59 ± 0.57	1.47 ± 0.21	29.7 ± 14.5
H184A	0.103 ± 0.030	9.32 ± 3.35	8.36 ± 1.54	4.43 ± 0.48	≈ 100
S193A	0.0829 ± 0.0337	14.7 ± 2.6	4.18 ± 0.94	3.40 ± 0.98	20.5 ± 1.1
R194H	0.0261 ± 0.0077	7.87 ± 2.92	5.82 ± 2.52	1.21 ± 0.18	> 100
F261A	0.0483 ± 0.0198	9.90 ± 2.54	4.23 ± 1.19	7.06 ± 2.65	≈ 100
Y268F	0.0315 ± 0.0089	20.7 ± 7.6	5.30 ± 1.41	2.43 ± 0.51	≈ 20
Y269F	0.279 ± 0.141	17.9 ± 1.5	25.5 ± 9.2	4.48 ± 0.44	> 100
Y288F	0.0345 ± 0.0100	9.79 ± 3.13	4.03 ± 0.78	2.76 ± 1.18	17.4 ± 2.4

References

1. Hillmann, P.; Ko, G. Y.; Spinrath, A.; Raulf, A.; von Kügelgen, I.; Wolff, S. C.; Nicholas, R. A.; Kostenis, E.; Höltje, H. D.; Müller, C. E. Key determinants of nucleotide-activated G protein-coupled P2Y₂ receptor function revealed by chemical and pharmacological experiments, mutagenesis and homology modeling. *J. Med. Chem.* **2009**, *52*, 2762-2775.

4.4. Summary and Outlook

In this study, several charged and lipophilic residues buried underneath ECL2 were successfully predicted to interact with nucleotide agonists and confirmed by fluorescence-based calcium mobilization assays. Use of the closely related P2Y₁- and P2Y₁₂Rs X-ray crystal structures improved the overall quality of the human P2Y₂R homology model and provided a better understanding of the cartography of the residues forming the orthosteric binding site. The comprehensive analysis identified key interactions between the nucleobase of agonists with aromatic residues, as well as differences between the recognition of UTP and Ap₄A. These findings are of immense importance for the design of selective and potent drugs targeting P2Y₂R. Furthermore, presence of the Asp^{ECL2}-Arg^{TM7} ionic lock postulated to be important in P2Y₁R activation was also observed in P2Y₂R indicating analogous functionality. Interestingly, a residue distant to the orthosteric binding site as it faces the phospholipid layer and the extracellular lumen, namely Arg194, was found to affect the potency of the investigated agonists and antagonist RB-2. The homology model suggests the presence of a second ionic lock Glu190-Arg194 that likely modifies the flexibility of ECL2 resulting in reduced potency or loss of receptor activation in the case of Ap₄A. This information added a further level of complexity to the conformational changes of the receptor upon activation which have to be considered during assessment of computational predictions. The investigated anthraquinone-based antagonists displayed heterogeneous behavior at the cloned receptor mutants which hints different binding modes. Among them, RB-2 was found to interact with several residues involved in agonist recognition indicating binding close to or at the orthosteric binding site.

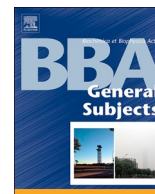
In summary, the optimized and experimentally validated model provided insights on the binding mode of ligands and the architecture of the binding site which in turn are invaluable information for virtual screening campaigns.

5. Ligand Binding and Activation of UTP-Activated G Protein-Coupled P2Y₂ and P2Y₄ Receptors Elucidated by Mutagenesis, Pharmacological and Computational Studies

5.1. Introduction

Among the P2YR subtypes, P2Y₂- and P2Y₄Rs are the closest related receptors with a sequence similarity of 68% and sequence identity of 58%. Especially the putative orthosteric binding site responsible for the binding of endogenous nucleotide agonists is highly conserved which represents a major challenge for the design of selective compounds targeting those receptors. In order to enable the design of selective and potent ligands for both receptors, structural traits of both binding sites were computationally and pharmacologically investigated in this study for variances. For this, effects of site-directed mutagenesis on the potency and efficacy of selected agonists and antagonists were measured in calcium mobilization assays on human wildtype and mutant P2Y₂- and P2Y₄Rs expressed in 1321N1 astrocytoma cells to determine locations of key interactions between receptor and ligand. Especially the differences in ATP and UTP recognition were of interest, as human P2Y₂R is activated by both ATP and UTP, whereas human P2Y₄R is exclusively activated by UTP. Additionally, to supplement future design of potent and selective P2Y₂R/P2Y₄R antagonists with information, binding modes of anthraquinone derivatives were extensively analyzed to elucidate differences between orthosteric and allosteric ligand behavior.

5.2. Publication



Ligand binding and activation of UTP-activated G protein-coupled P2Y₂ and P2Y₄ receptors elucidated by mutagenesis, pharmacological and computational studies

Isaac Y. Attah^{a,1,2}, Alexander Neumann^{a,2}, Haneen Al-Hroub^a, Muhammad Rafehi^a, Younis Baqi^{a,b}, Vigneshwaran Namasivayam^a, Christa E. Müller^{a,*}

^a PharmaCenter Bonn, Pharmaceutical Institute, Pharmaceutical Sciences Bonn (PSB), Pharmaceutical & Medicinal Chemistry, University of Bonn, Germany

^b Department of Chemistry, Faculty of Science, Sultan Qaboos University, PO Box 36, Postal Code 123 Muscat, Oman

ARTICLE INFO

Keywords:

Agonists
Antagonists
Anthraquinone
ATP
Docking
Homology Modeling
Nucleotide
P2Y receptors
Site-directed mutagenesis
UTP

ABSTRACT

The nucleotide receptors P2Y₂ and P2Y₄ are the most closely related G protein-coupled receptors (GPCRs) of the P2Y receptor (P2YR) family. Both subtypes couple to G_q proteins and are activated by the pyrimidine nucleotide UTP, but only P2Y₂R is also activated by the purine nucleotide ATP. Agonists and antagonists of both receptor subtypes have potential as drugs e.g. for neurodegenerative and inflammatory diseases. So far, potent and selective, “drug-like” ligands for both receptors are scarce, but would be required for target validation and as lead structures for drug development. Structural information on the receptors is lacking since no X-ray structures or cryo-electron microscopy images are available. Thus, we performed receptor homology modeling and docking studies combined with mutagenesis experiments on both receptors to address the question how ligand binding selectivity for these closely related P2YR subtypes can be achieved. The orthosteric binding site of P2Y₂R appeared to be more spacious than that of P2Y₄R. Mutation of Y197 to alanine in P2Y₄R resulted in a gain of ATP sensitivity. Anthraquinone-derived antagonists are likely to bind to the orthosteric or an allosteric site depending on their substitution pattern and the nature of the orthosteric binding site of the respective P2YR subtype. These insights into the architecture of P2Y₂- and P2Y₄Rs and their interactions with structurally diverse agonists and antagonist provide a solid basis for the future design of potent and selective ligands.

1. Introduction

P2Y receptors (P2YRs) are G protein-coupled receptors (GPCRs) activated by adenine and/or uracil nucleotides. Eight different P2YR subtypes exist which are sub-grouped into P2Y₁-like (P2Y₁, P2Y₂, P2Y₄, P2Y₆, and P2Y₁₁) and P2Y₁₂-like (P2Y₁₂, P2Y₁₃, and P2Y₁₄) receptors [1,2]. The P2Y₁, P2Y₁₂, and P2Y₁₃Rs are activated by ADP, P2Y₂R is activated by both ATP and UTP, P2Y₄R by UTP, P2Y₆R by UDP, and

P2Y₁₄R by both UDP and UDP-glucose [3]. The P2Y₁, P2Y₂, P2Y₄, and P2Y₆Rs couple to G_q proteins, P2Y₁₁ couples to both G_q and G_s proteins, while the P2Y₁₂-like receptor subtypes couple to G_{i/o} proteins. Upon receptor activation by an agonist, G_q proteins stimulate the release of intracellular calcium through the phospholipase C pathway, while G_s and G_i proteins lead to the activation and inhibition of adenylyl cyclase, respectively, thereby modulating intracellular cAMP levels.

P2YRs are widely distributed in the human body and represent

Abbreviations: 2-MeSADP, 2-methylthioadenosine-5'-O-diphosphate; 2-MeSATP, 2-methylthioadenosine-5'-O-triphosphate; ABTS, 2,2'-azino-bis-3-ethylbenzothiazoline-6-sulfonic acid; AP₄A, diadenosine tetraphosphate; AQ, anthraquinone; AR-C118925, 5-[[5-(2,8-dimethyl-5H-dibenzo[a,d]cyclohept-5-yl)-3,4-dihydro-2-oxo-4-thioxo-1(2H)-pyrimidinyl)methyl]-N-(1H-tetrazol-5-yl)-2-furancarboxamide; BSA, bovine serum albumin; DMEM, Dulbecco's Modified Eagle's Medium; DMSO, dimethyl sulfoxide; ECL, extracellular loop; EDTA, ethylenediaminetetraacetic acid; ELISA, enzyme-linked immunosorbent assay; FBS, fetal bovine serum; fluo-4 AM, fluo-4 acetoxymethyl ester; GPCR, G protein-coupled receptor; HA, hemagglutinin; HBSS, Hank's balanced salt solution; hP2Y₂R, human P2Y₂ receptor; hP2Y₄R, human P2Y₄ receptor; hP2Y_xR, human P2Y_x receptor; IFD, induced fit docking; MRS4062, (((2R,3S,4R,5R)-3,4-dihydroxy-5-((Z)-2-oxo-4-((3-phenylpropoxy)imino)-3,4-dihydropyrimidin-1-(2H)-yl)tetrahydrofuran-2-yl)methyl)triphosphoric acid; PBS, phosphate-buffered saline; RB-2, Reactive blue 2; TM, transmembrane

* Corresponding author at: Pharmazeutisches Institut, Pharmazeutische Chemie I, An der Immenburg 4, D-53121 Bonn, Germany.

E-mail address: christa.mueller@uni-bonn.de (C.E. Müller).

¹ Present address: Department of Biomedical Sciences, School of Health and Allied Sciences, University of Cape Coast, Cape Coast, Ghana.

² Equal contribution.

<https://doi.org/10.1016/j.bbagen.2019.129501>

Received 15 October 2019; Received in revised form 17 November 2019; Accepted 3 December 2019

Available online 05 December 2019

0304-4165/© 2019 Elsevier B.V. All rights reserved.

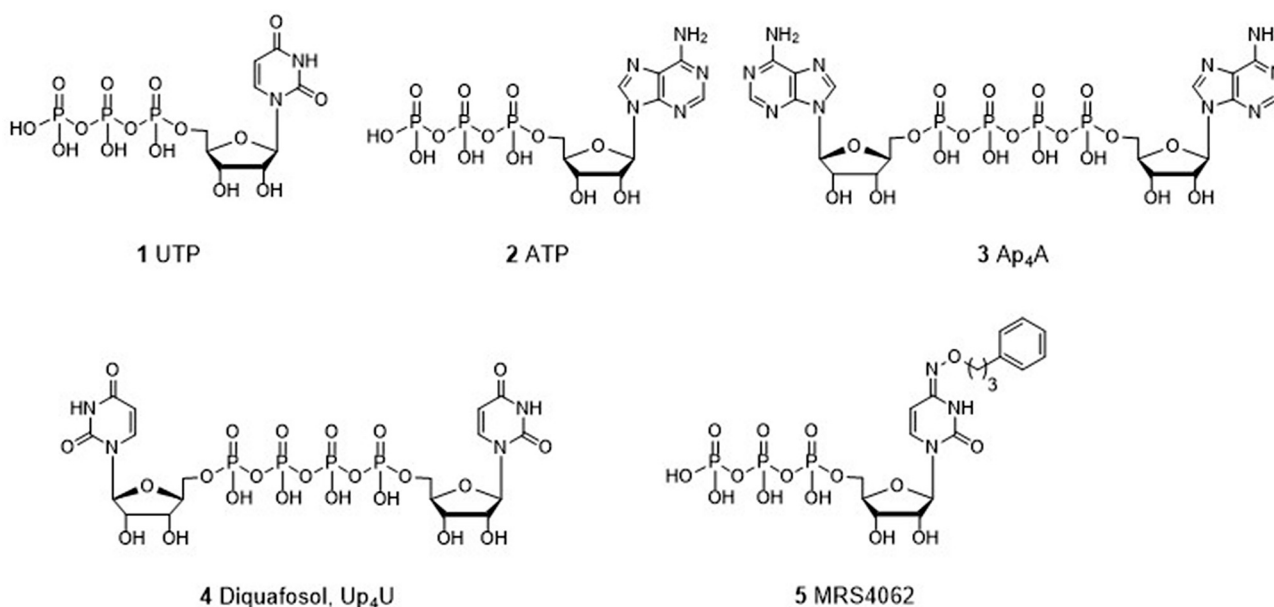


Fig. 1. Structures of selected P2Y receptor agonists.

(potential) therapeutic targets for several diseases including thrombosis, inflammation, neurodegenerative diseases and cancer [4,5]. For instance, several antagonists of the ADP-activated P2Y₁₂R are marketed as antithrombotic drugs, namely clopidogrel, prasugrel, cangrelor and ticagrelor [6–8]. However, at present there are no drugs available for the uracil-activated P2Y₄, P2Y₆ and P2Y₁₄ receptors and only one (diquafosol) for the P2Y₂R [9–11]. In the present study, we focused on the closely related P2Y₂ and P2Y₄ receptor subtypes.

The P2Y₂R is the only member of the P2Y receptor family that is activated by both UTP (1) and ATP (2) (see Fig. 1) with comparable potencies and efficacies [2,12]. It is additionally activated by dinucleotides such as Ap₄A (3) [13]. P2Y₂R is widely expressed in the body, e.g. in brain, lungs, heart, liver, stomach, skeletal muscle, spleen and bone marrow [14–16]. Agonists of the P2Y₂R have been proposed for the treatment of cystic fibrosis, chronic bronchitis, viral infections, myocardial infarction and Alzheimer's disease (AD) [17]. Diquafosol (Up₄A, 4), a P2Y₂R agonist, is in fact used for treating dry eye disease in Asia [18–22]. In AD, activation of P2Y₂R expressed in microglia mediates phagocytosis and degradation of the insoluble fibrillar β -amyloid and oligomeric β -amyloid aggregates that are neurotoxic [23]. Moreover, activation of the P2Y₂R mediates an increase in α -secretase-dependent non-amyloidogenic cleavage of the amyloid precursor protein (APP). P2Y₂R agonists have also been reported to be cardio-protective during hypoxia and myocardial infarction in cultured rat cardiomyocytes and *in vivo* in mice [24,25].

Antagonists of the P2Y₂R, on the other hand, may be useful as drugs for preventing cancer metastasis and for the treatment of obesity, diabetes insipidus and inflammatory conditions including asthma [5,23,26–31]. Only few antagonists have been reported so far that can be utilized as pharmacological tools for studying the P2Y₂R. These include the non-selective P2YR antagonist reactive blue 2 (RB-2, 6) and the selective P2Y₂R antagonist AR-C118925 (7) (for structures see Fig. 2) [32–34].

The P2Y₂R is closely related to the P2Y₄R. Both receptors share the highest amino acid sequence identity among the human (h) P2YR subtypes (53%), compared to sequence identities of 34% for P2Y₂/P2Y₁, 38% for P2Y₂/P2Y₆ and 21% for P2Y₂/P2Y₁₂.

The P2Y₄R is widely distributed in the body, including brain, lung and intestine. It regulates chloride secretion in the jejunum. In the brain, it is involved in regulating the production and secretion of amyloid precursor proteins [35–38]. Agonists for the P2Y₄R are

therefore, like those for the P2Y₂R, of interest as drugs for the treatment of cystic fibrosis [39] and AD [3]. In AD, activation of microglial P2Y₄R leads to pinocytosis of soluble A β _{1–42} from the neuronal extracellular environment and thus prevents A β accumulation which would eventually result in synaptic dysfunction [23,40]. Antagonists of the P2Y₄R might be used for the treatment of diarrhea caused by bacterial infections [39] and for the treatment of diabetic neuropathy [41]. P2Y₄R antagonists have also been reported to be protective in early stage of myocardial infarct [42,43].

The human P2Y₄R (*h*P2Y₄R) is activated by UTP (1) and blocked by ATP (2) and Ap₄A (3). In contrast, ATP is a full agonist at the rat P2Y₄R. MRS4062 (5), an N⁴-phenylpropoxy-substituted cytosine-5'-triphosphate derivative, was reported to be a selective agonist of *h*P2Y₄R (EC₅₀ = 0.023 μ M) with 28- and 38-fold selectivity over P2Y₂R and P2Y₆R, respectively [44]. Few antagonists have been described for the P2Y₄R so far. Those commonly used as pharmacological tools include the non-selective P2YR antagonist RB-2 (6) and pyridoxal phosphate-6-azophenyl-2',4'-disulfonic acid (PPADS, 8) [45,46]. Recently, the anthraquinone (AQ) derivatives PSB-09114 (9), PSB-16133 (10), PSB-16135 (11), and PSB-1699 (12) have been reported as antagonists of the P2Y₄R displaying moderate potency and selectivity [47].

Despite their therapeutic potential, selective, orally bioavailable agonists and antagonists for P2Y₂- and P2Y₄R are hardly available. In order to be able to design ligands, knowledge of the topography of the binding site(s) of these receptors is required. To this end, we employed molecular modeling and site-directed mutagenesis studies. While the X-ray crystallographic structures of the P2Y₂- and P2Y₄R are not available, those of the P2YR subtypes P2Y₁ and P2Y₁₂ have been published, which can serve as templates for homology modeling [48,49]. Recently, our group published a P2Y₂R homology model based on the crystal structures of *h*P2Y₁R. Preliminary data from site-directed mutagenesis studies in combination with docking studies for UTP, Ap₄A and AR-C118925 using that model shed light on key interactions with amino acids in the orthosteric binding pocket of the P2Y₂R structure [50]. The docking results suggested a binding mode for agonists similar to that of 2Me-SADP and 2Me-SATP in *h*P2Y₁₂R [2], which differs from the binding mode of the nucleotide antagonist MRS2500 (13) in complex with *h*P2Y₁R [49]. Moreover, we published a homology model of *h*P2Y₄R and used it to predict the binding site of AQ antagonists [47].

In the present study, we performed site-directed mutagenesis to specifically address the question, how selective ligand binding at the

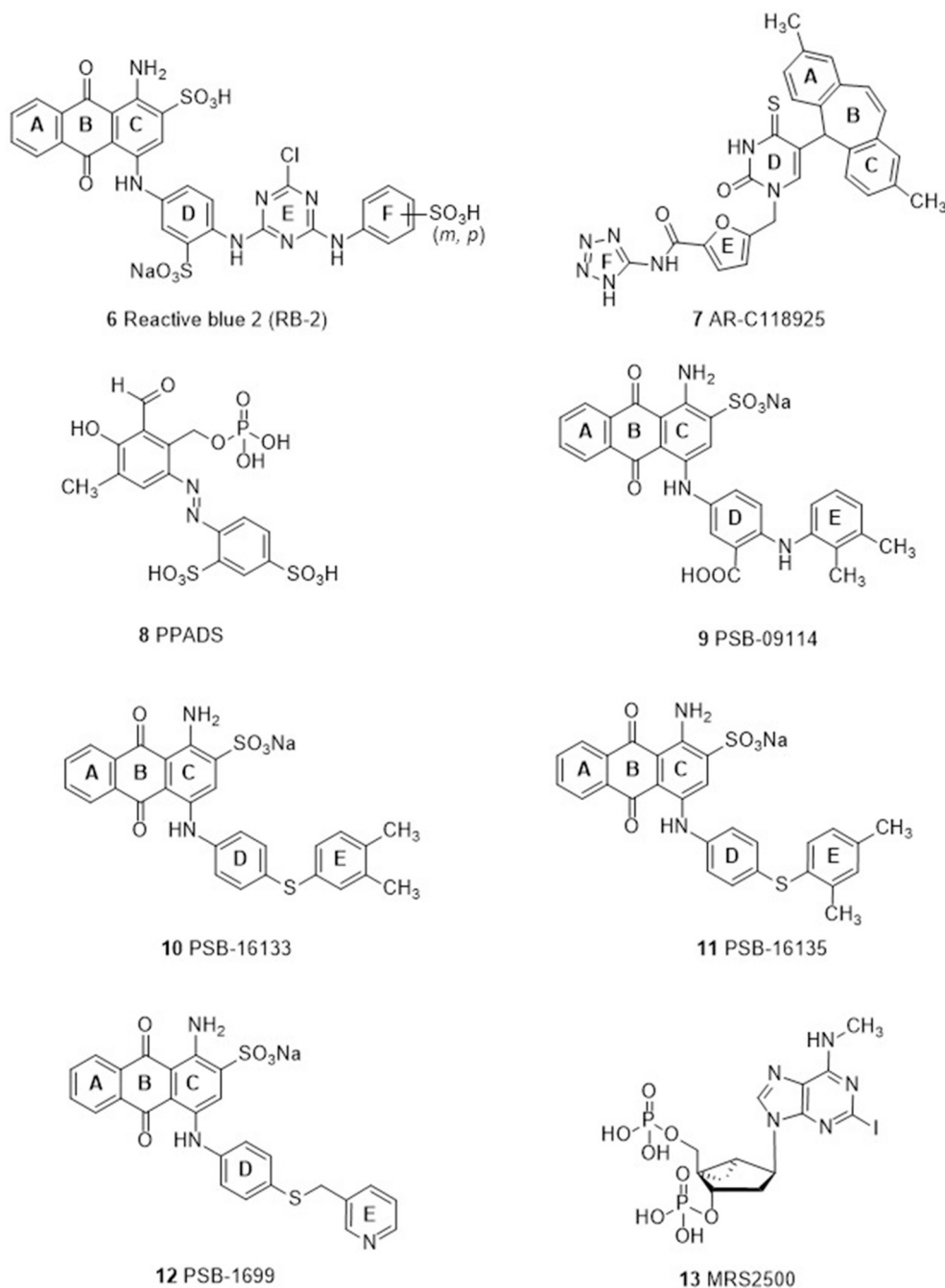


Fig. 2. Structures of selected P2YR antagonists.

closely related P2Y receptor subtypes P2Y₂ and P2Y₄ can be achieved. We investigated agonist binding modes, and agonist discrimination, e.g. ATP versus UTP, as well as binding modes of antagonists.

2. Materials and methods

2.1. Materials

The restriction enzymes and T4 DNA ligase were obtained from New England BioLabs (Frankfurt am Main, Germany) while the DNA polymerase Pyrobest was purchased from TaKaRa Bio Inc. (Saint-Germain-en-Laye, France). All primers used in the current work were synthesized by MWG Biotech (Ebersberg, Germany). The agar for cloning and the chromophore solution 2,2'-azino-bis-3-ethylbenzothiazoline-6-sulfonic acid (ABTS) were purchased from Calbiochem (Darmstadt, Germany).

Dulbecco's Modified Eagle Medium (DMEM), penicillin/streptomycin, trypsin-EDTA (ethylenediaminetetraacetic acid), and lipofectamine 2000 were obtained from Life Technologies GmbH (Darmstadt, Germany). Fluo-4 acetoxymethyl ester (Fluo-4-AM) was obtained from Invitrogen/Thermo Fisher (Merelbeke, Belgium) while gentamicin (G418) was from PAN Biotech (Aidenbach, Germany). Fetal bovine serum (FBS) was purchased from Sigma-Aldrich (Taufkirchen, Germany). The hemagglutinin-(HA)-specific mouse monoclonal antibody (HA.11) was obtained from Covance, Berkeley, CA, USA. Ap₄A was and UTP were bought from Sigma-Aldrich (Steinheim, Germany) and ATP from ROTH, Carl Roth GmbH (Karlsruhe, Germany). MRS4062 was bought from Tocris Bioscience (Bristol, UK) and carbachol from Alfa Aesar Thermo Fisher GmbH (Kandel, Germany). Corning 3340 microplates were purchased from Corning Life Sciences (Tewksbury, Massachusetts, USA), and 24-well plates for ELISA assays from Sarstedt AG & Co. (Nuembrecht, Germany).

2.2. Homology modeling

Previously, we reported on homology models for *hP2Y₂*- and *hP2Y₄*Rs [47,50]. Both had been based on the X-ray crystal structure of *hP2Y₁*R in complex with the nucleotide antagonist MRS2500 (PDB-ID: 4XNW). These were used as starting points in the present study [49].

2.3. Docking studies

The previously published procedure was used for docking studies with the Induced Fit Docking and Glide Docking modules implemented in the Schrödinger software package release 2016 [51]. To limit docking to the putative orthosteric binding site, the aspartic acid residues Asp185^{ECL2} (P2Y₂R) and Asp187^{ECL2} (P2Y₄R), residues assumed to be involved in receptor activation as discussed below, were selected as the receptor center. The putative orthosteric binding site was derived from the X-ray crystal structure of *hP2Y₁₂*R in complex with the orthosteric agonists 2-methylthio-ADP (2MeSADP) and 2-methylthio-ATP (2MeSATP) (PDB-IDs: 4PXZ, 4PYO) [52]. Ligands were docked into a box with a side length of 25.0 Å around the aspartic acid residue Asp185^{ECL2} (P2Y₂R) and Asp187^{ECL2} (P2Y₄R). The best docking pose was selected based on the induced fit docking (IFD) score and Prime Energy values.

In the case of the agonist MRS4062 (5) no conclusive docking position in the P2Y₄R was achievable due to steric hindrance by Tyr116^{3.33}. Therefore, we introduced a computational Y116^{3.33}A mutant to increase the space of the binding cavity, and docked MRS4062 using the published procedure. The best docking pose was selected, and the Y116^{3.33}A mutation was subsequently reverted. The Tyr116^{3.33} rotamer with the lowest energy value was selected for the final docking pose.

During docking of the AQ-derived antagonists, the highest-ranked protein complex of P2Y₂R with PSB-16133 (10) was considered as a template for further dockings, since we expected the ligands to have a similar binding mode with respect to the induced rotamers. The ligands were subsequently redocked with the most reasonable docking pose using extra precision (XP) glide docking. The top scoring docking poses were evaluated with their scores and Prime Energy.

2.4. Site-directed mutagenesis studies

The sequences of *hP2Y₂* (ID P41231) and *hP2Y₄*Rs (ID P51582) used for site-directed mutagenesis studies were taken from the Uniprot database [53]. Whole plasmid recombinant polymerase chain reaction (PCR) using the appropriate primers was performed using the puc19 vector to introduce the desired point mutations. PCR was performed as follows: 30 s at 98 °C, 30 cycles, each consisting of 10 s at 98 °C, 40 s at the appropriate annealing temperatures (°C), and 5 min of primer extension at 72 °C. The PCR products were treated with *DpnI* to digest the template plasmid, then purified and used to transform competent *E. coli* bacteria. For each receptor, wildtype (wt) or mutant, cDNA was isolated from individual clones and recombinantly cloned into the mammalian retroviral vector pLXSN with the influenza hemagglutinin (HA) epitope attached to the N-terminus. All DNA sequencing data were generated by GATC Biotech (Cologne, Germany), confirming the expected sequences.

2.5. Retroviral transfection

One day before transfection, 1.5×10^6 GP + envAM12 packaging cells were seeded into a small 25 cm² cell culture flask with Dulbecco's Modified Eagle's Medium (DMEM) medium supplemented with 10% FBS and 100 U/mL penicillin G and 100 µg/mL streptomycin. A few hours before the transfection, the medium was changed to 6.25 µL of DMEM medium containing only 10% FBS. Transfection involved the delivery of a total of 10 µg DNA - 6.25 µg of receptor-containing plasmid-DNA and 3.75 µg of the vesicular stomatitis virus G protein (VSV-G) - into the packaging cells using Lipofectamine 2000. After incubating the transfected cells at 37 °C for 12–15 h, the medium was changed to 3 mL

DMEM supplemented with 10% FBS, 100 U/mL penicillin G, 100 µg/mL streptomycin and 5 mM of a sterile aqueous solution of sodium butyrate. The cells were then incubated at 32 °C with 5% CO₂ for 48 h. About 24 h before infection, 5×10^5 1321 N1 astrocytoma cells were seeded into a 25 cm² flask containing DMEM medium with 10% FBS, 100 U/mL penicillin G and 100 µg/mL streptomycin, and incubated at 37 °C. On the day of infection, the medium was removed from the astrocytoma cells and discarded. The medium (containing viruses) was removed from the GP + envAM12 cells, filtered through a 0.22 µm filter onto the astrocytoma cells followed by 6 µL of sterilized polybrene solution (4 mg/mL in water). The astrocytoma cells were then incubated at 37 °C for 2½ h after which the medium was exchanged for 5 mL of DMEM medium containing 10% FBS, 100 U/mL penicillin G and 100 µg/mL streptomycin. The medium was replaced after 48 h of incubation by DMEM with 10% FBS, 100 U/mL penicillin G, 100 µg/mL streptomycin and 800 µg/mL G418 for selection of cells expressing the receptor.

2.6. Cell culture

The 1321 N1 astrocytoma cells were cultured in DMEM supplemented with 1% ultraglutamine, 10% FBS, 100 U/mL penicillin G, and 100 µg/mL streptomycin. They were stably transfected with either the wt or mutant P2Y₂ or P2Y₄R. The DMEM medium described above was further supplemented with 800 µg/mL G418. The GP + envAM12 packaging cells were maintained in HXM (hypoxanthine, xanthine, mycophenolic acid) media containing DMEM supplemented with 1% ultraglutamine, 10% FBS, 100 U/mL penicillin G, 100 µg/mL streptomycin, 15 µg/mL hypoxanthine, 250 µg/mL xanthine, 25 µg/mL mycophenolic acid, and 200 µg/mL hygromycin B. All cells were grown at 37 °C in 96% humidified air.

2.7. Cell surface enzyme-linked immunosorbent assay (ELISA)

The 1321 N1 astrocytoma cell-line expressing the various wt or mutant receptors were seeded in duplicates at a density of 150,000 cells per well into a 12-well plate 24 h before the assay. The medium was removed and the cells were washed with phosphate-buffered saline (PBS). 500 µL of 1% bovine serum albumin (BSA) in PBS was added for 5 min to block non-specific cell surface binding. Next, 300 µL of a 1:1000 dilution of the hemagglutinin (HA)-specific mouse monoclonal antibody (HA.11) solution in DMEM containing 1% BSA was added to each well and the mixture was incubated at room temperature (rt) for 1 h. The cells were washed three times with 500 µL of PBS, fixed with 500 µL of 4% paraformaldehyde in PBS, pH 7.3, washed again with 500 µL of PBS and blocked with 500 µL of 1% BSA in PBS for 10 min. The cells were then incubated at rt. for 1 h with 300 µL of peroxidase-conjugated goat anti-mouse IgG antibody of a 1:2500 dilution ratio in DMEM supplemented with 1% BSA. After further washing with 500 µL PBS for four times, the cells were incubated with 300 µL of the substrate, ABTS solution, for 45 min at rt. Finally, 170 µL aliquots of the supernatant ABTS solution were then transferred into a 96-well plate, and the absorbance was measured at 405 nm by a PHERAstar microplate reader (BMG Laboratory Technologies, Offenburg, Germany). The whole assay, except for the addition of antibodies and the substrate reaction, was performed on ice and with freshly prepared cold buffers.

2.8. Calcium mobilization assay

About 16–24 h before the assay, the growth medium was removed from a T175 mL flask with approximately 80–90% cell confluency. The cells were washed with PBS (containing 137 mM NaCl, 2.7 mM KCl, 4.3 mM Na₂HPO₄, and 1.47 mM KH₂PO₄, at pH 7.3). Then, they were detached with trypsin-EDTA and re-suspended in supplemented DMEM (see above). To each well of the sterile black 96-well polystyrene plate with a transparent flat bottom (Corning 3340), about 60,000 cells in 200 µL DMEM growth medium were added and subsequently incubated at 37 °C, 96% humidity and 10% CO₂. Prior to the assay, the growth medium was removed completely and the adherent cells were incubated

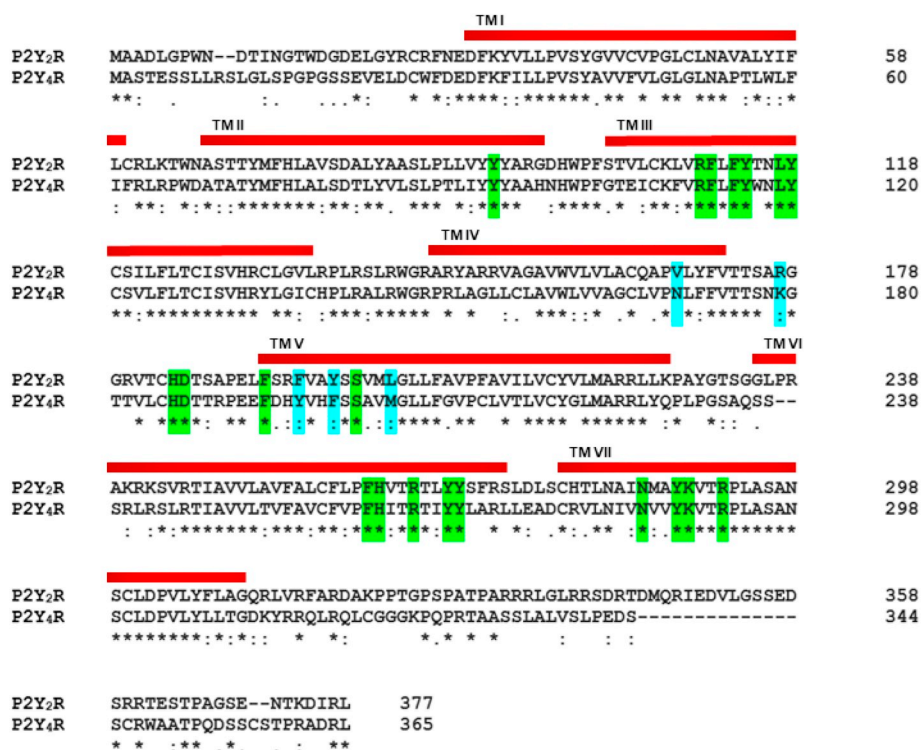


Fig. 3. Sequence alignment of hP2Y₂R and hP2Y₄R. Transmembrane regions (denoted as ‘TM’) are indicated by red bars. Identical residues of the putative orthosteric binding site are highlighted in green, non-identical residues are highlighted in blue.

with 40 μL of loading dye, consisting of 15 μL of fluo-4 acetoxymethyl ester (1 mM solution in dimethyl sulfoxide (DMSO)) and 15 μL Pluronic F-127 (25% w/v in DMSO) in 4970 μL Hank’s balanced salt solution (HBSS) buffer, in each well, for 1 h. After incubation, the excess dye was removed, and cells were further incubated in HBSS buffer at rt for 30 min before the addition of agonists. For assessment of antagonist potencies, the cells were pre-incubated with the antagonists in HBSS buffer during the 30 min incubation before addition of the agonist at its EC₈₀ concentration. All dilutions used for concentration–response curves were performed on a log-scale. The final volume in each well was 200 μL, and the final DMSO concentration was 0.5%. The measurement of fluorescence intensities was performed on a Novostar plate reader (BMG LabTechnologies, Offenburg, Germany) at 520 nm for 30 s at 0.4 s intervals after excitation at 485 nm. For all assays, 100 μM carbachol, inducing intracellular Ca²⁺ release by activating the natively expressed G_q protein-coupled muscarinic M₃ receptor (M₃R) in 1321 N1 astrocytoma cells, was used as a positive control. The maximal carbachol response was set at 100% and employed for normalization of all other responses.

3. Results and discussions

3.1. Molecular modeling

Sequence alignment as well as previously published homology models of the hP2Y₂R and the hP2Y₄R were employed to predict residues of interest that were selected for site-directed mutagenesis studies [47,50]. While several mutagenesis studies of human and rat P2Y₂R have been reported, only limited data is available for P2Y₄R [12,50,54]. A comparative study between N-terminus and extracellular loop 2 (ECL2) of the hP2Y₄R (activated by UTP) and the rat P2Y₄R (activated by both UTP and ATP) was previously performed by studying chimeric receptors [55]. Ten chimeras of the hP2Y₄R, in which the extra- and intracellular regions were exchanged for those of the rat P2Y₄R, had been constructed. The amino acid residues Asn177^{ECL2}, Ile183^{ECL2}, and Leu190^{ECL2} were reported to contribute to the acceptance of ATP as an agonist by the hP2Y₄R

chimera, in which the ECL2 was exchanged for that of the rat P2Y₄R.

Although hP2Y₂R and hP2Y₄R share only a moderate sequence identity (53%), the predicted orthosteric binding pocket is rather conserved, except for three residues (see Fig. 3): Tyr197^{5.35} of P2Y₄R is replaced by phenylalanine in P2Y₂R, Val204^{5.42} is replaced by methionine, and Met205^{5.43} by leucine. Tyr197^{5.35} is conserved in the human, rat and mouse P2Y₄R, while the corresponding phenylalanine is conserved in the human, rat, and mouse P2Y₂R (see Fig. S1 in Supplementary Information). Val204^{5.42} is not highly conserved, as it is exchanged for isoleucine in the mouse P2Y₄R. Met205^{5.43}, on the other hand, is conserved in P2Y₄R of all three species. This leads to the conclusion that either a single or multiple mutations or other contributors like the ECL2 itself may be responsible for agonist discrimination.

3.1.1. Docking studies at the P2Y₂R

We previously reported on the binding mode of UTP in hP2Y₄R based on a homology model [50]. The endogenous agonist UTP is proposed to bind in the upper third part of the receptor in a cleft formed by side-chains of TM III, VI and VII, as it is common for many GPCRs (see Fig. 4) [49,56]. The phosphate groups are proposed to interact with positively charged amino acid residues (arginine, lysine, histidine). The nucleobase likely binds in a lipophilic binding cavity formed by phenylalanine and tyrosine residues. Docking studies of UTP into the homology model of hP2Y₂R propose a similar binding mode. For detailed discussion of interactions see below (Section 3.5.1).

Based on previously published docking studies of the agonist UTP into the homology model of hP2Y₂R, and the predicted binding mode of UTP in the homology model of hP2Y₄R, we selected 14 amino acid residues (five of P2Y₂R and nine of P2Y₄R) for site-directed mutagenesis.

3.1.1.1. P2Y₂R. Molecular dynamics simulation studies suggested an ionic lock between an aspartic acid residue in the extracellular loop 2 (ECL2) and an arginine in TM VII to play a key role in P2Y₁R activation; agonists were proposed to break the ionic lock between Asp204^{ECL2} and Arg310^{7.39}, while antagonists were predicted to stabilize the interaction

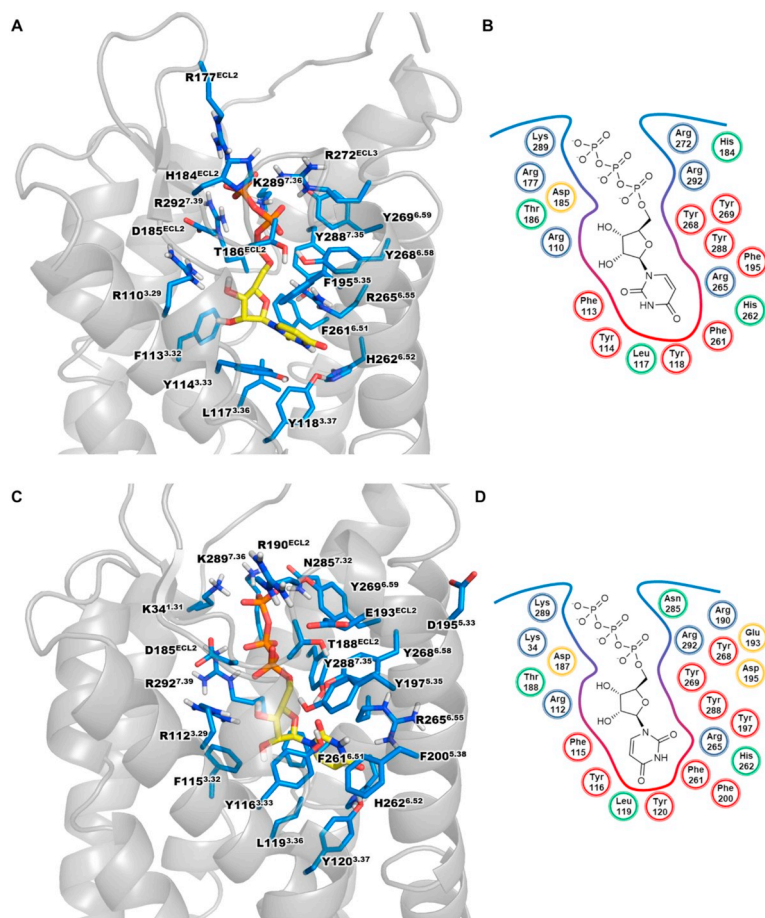


Fig. 4. Putative binding mode of UTP in the homology models of *hP2Y₂*- (A and B) and *hP2Y₄*Rs (C and D). **A.** Docked pose of UTP with the important residues in the binding pocket is shown. **B.** Schematic 2D representation of the binding pocket. **C.** Docked pose of UTP in *hP2Y₄*R homology model. **D.** Schematic 2D representation of the UTP-*P2Y₄*R complex. *P2Y₂*- and *P2Y₄*Rs (gray) are displayed in cartoon representation, the amino acid residues (blue) and UTP (yellow) are shown as stick models; oxygen atoms are colored in red, nitrogen atoms in blue, phosphorus atoms in orange (A, C). Charged, basic residues are colored in blue, aromatic residues in red, the conserved aspartic acid residue in the ECL2 involved in an ionic lock with Arg292^{7.39} is depicted in yellow, other residues in the binding pocket in green (B, D).

thereby preventing receptor activation [57]. Mutagenesis studies on *hP2Y₁*R had shown that both residues play key roles in agonist-induced receptor activation [58]. In our previous studies we were able to confirm *P2Y₂*-Arg292^{7.39} as an important residue for agonist function, which is the analogous residue to *P2Y₁*-Arg310^{7.39}. To further investigate the role of an ionic lock between ECL2 and TM VII in *P2Y₂*R, we selected the *P2Y₂*-D185^{ECL2}A mutant. *P2Y₂*-R110^{5.29}A, a previously published mutant [50] was additionally investigated in this study for possible consequences on *P2Y₂*R interaction with the recently published agonist MRS4062 [44]. *P2Y₂*-Phe113^{3.32} is predicted to be part of the orthosteric binding site of *P2Y₂*R. Therefore, it was mutated to alanine and tyrosine, respectively, to investigate its interactions with the nucleobases of the agonists. *P2Y₂*-Phe195^{5.35}, corresponding to Tyr197^{5.35} in *hP2Y₄*R, is located close to the ECL2 in the upper part of TM V. These represent non-conserved residues in the predicted orthosteric binding pocket of *P2Y₂*- and *P2Y₄*Rs, which might play a role in the acceptance of UTP versus ATP.

3.1.1.2. *P2Y₄*R. For mutation of *hP2Y₄*R, Asn170^{4.60} was selected as it is close to the putative orthosteric binding site and replaced by Val168^{4.60} in *P2Y₂*R. Arg194^{ECL2} was found to play a role in ligand recognition by *P2Y₂*R even though it is distant from the putative orthosteric binding site [50]. It was concluded, that Arg194^{ECL2} may form a salt bridge with Glu190^{ECL2} forming a second ionic lock close to the TMV and ECL2, that modifies the flexibility of the loop, resulting in decreased potency of agonists. Therefore, we decided to investigate Arg190^{ECL2}, Glu193^{ECL2} and Asp195^{5.33} in *P2Y₄*R as those amino acid residues may form an analogous ionic lock in *P2Y₄*R. Finally, Tyr197^{5.35} and Phe200^{5.38} of *P2Y₄*R were selected as candidates for mutagenesis studies, as they are close to the putative orthosteric binding site and not conserved between the two related *P2Y*R subtypes.

All mutants selected for mutagenesis in the present study are

presented in Fig. 5. New and published mutagenesis data for *P2Y₂*- and *P2Y₄*Rs were taken into account for the analysis and prediction of binding modes of agonists and antagonists. The mutants were recombinantly expressed in 1321 N1 astrocytoma cells, and their effects on selected ligands were investigated by calcium mobilization studies. Four agonists, UTP (1), ATP (2), Ap₄A (3), and MRS4062 (5) were evaluated. The investigated antagonists included AR-C118925 (7), and the AQ derivatives RB-2 (6), PSB-09114 (9), PSB-16133 (10), PSB-16135 (11), and PSB-1699 (12). The ligand selection was based on structural diversity, differences in size, and unique pharmacological profiles, i.e. selectivity for either receptor subtype.

3.2. Site-directed mutagenesis studies

The coding sequences of *P2Y₂*- and the *P2Y₄*Rs were cloned into the plasmid vector pUC19, and using whole plasmid PCR, the desired point mutations were introduced. From pUC19, the cDNAs were cloned into the pLXSN retroviral expression vector featuring a hemagglutinin (HA) epitope sequence at the N-terminus of the receptors. The wt and mutant receptors were then stably transfected into 1321 N1 astrocytoma cells. Since expression levels can directly affect the potency of GPCR agonists in functional assays [59,60], these were determined by enzyme-linked immunosorbent assay (ELISA) using an antibody against the HA-tag. Previous reports had shown that the HA-tag does not interfere with ligand-receptor pharmacology [12,50]. All data were normalized to the expression of the wt receptor (see Fig. 6 and Appendix Table S1 for expression values). Cell surface expression of the *P2Y₂*R mutants was between 16% and 125% relative to that of the wt receptor (100%). The receptor with the lowest expression was the *P2Y₂*R-F113^{3.32}Y mutant (16 ± 1%), which is a highly conserved amino acid among the two investigated *P2Y*R subtypes (see Fig. 6). In contrast to F113^{3.32}Y, the *P2Y₂*R-mutant F113^{3.32}A showed high expression

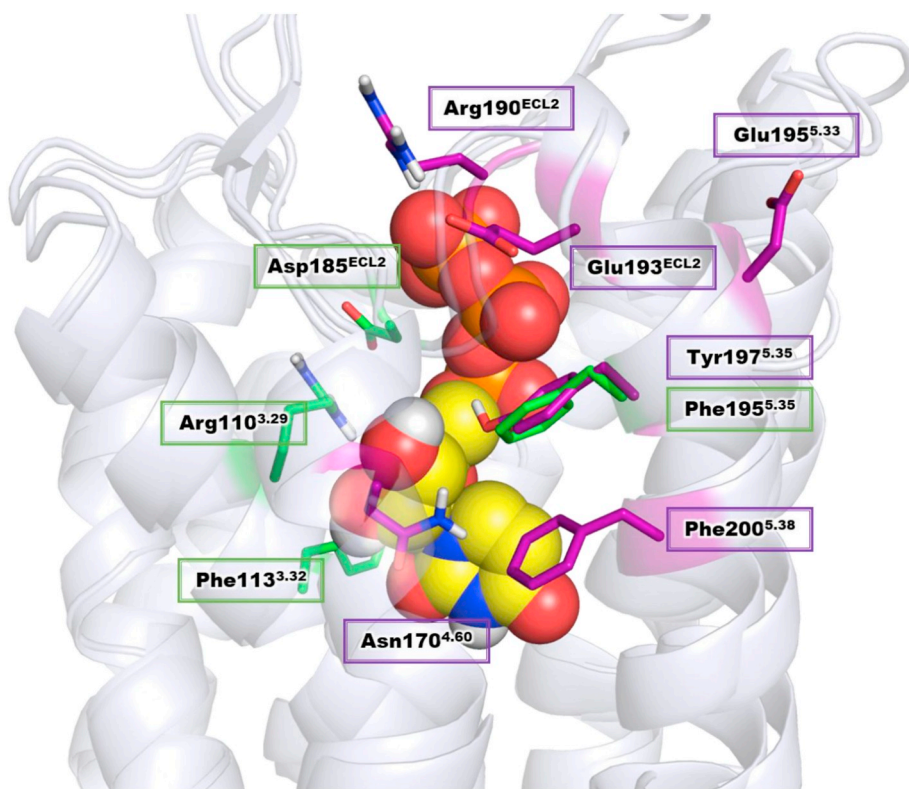


Fig. 5. Putative binding mode of UTP in the homology model of *hP2Y₂R* in overlay with the homology model of *hP2Y₄R* used for selection of amino acid residues for mutagenesis. *P2Y₂*- and the *P2Y₄R* are displayed in cartoon representation, the amino acid residues of *P2Y₂*- (green) and *P2Y₄R*s (purple) to be mutated are shown as stick models, UTP as spheres. Carbon atoms are colored in yellow, hydrogen atoms in white, oxygen atoms in red, nitrogen atoms in blue, and phosphorus atoms in orange.

(125 ± 10%). *P2Y₂R*-R110^{3.29}A mutant displayed a high cell surface expression (74 ± 4%) similar as in a previous study [50]. Cell surface expression of the *P2Y₄R* mutants was between 56 ± 2% (Y197^{5.35}A) and 144 ± 6% (F200^{5.38}Y) relative to that of the wt *P2Y₄R* (100%).

3.3. Analysis of agonist activities

Four agonists, UTP (1), ATP (2), Ap₄A (3) and MRS4062 (5), were selected for testing at the receptors based on their structures and their pharmacology. UTP activates both receptor subtypes. ATP and Ap₄A only activate *P2Y₂R* while MRS4062 was reported to be selective for *P2Y₄R*.

The ligands were assessed by measuring intracellular calcium concentrations using the fluorescent calcium-chelating dye Fluo-4. 1321 N1 Astrocytoma cells natively express the muscarinic M₃R which is also G_q protein-coupled and therefore, like the *P2Y₂*- and *P2Y₄R*s, leads to intracellular calcium release upon activation. Carbachol, a muscarinic M₃R agonist was therefore used as an internal standard to which all data were normalized. In addition, data for all agonist efficacies at each mutant were normalized to UTP efficacy at the corresponding wt receptors. Concentration–response curves are shown in Figs. 7, 9 and 10, pEC₅₀ values and efficacies are presented in Figs. 8 and 11 while EC₅₀ values are collected in Tables S2 and S3 of Supplementary Information.

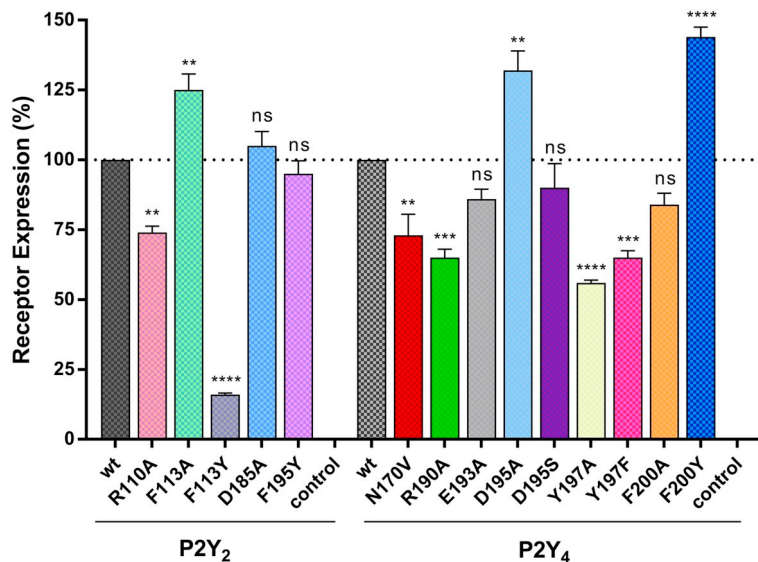


Fig. 6. Cell surface receptor expression levels as determined by ELISA using antibodies interacting with the HA tag fused to the N-terminus of *P2Y₂*- and *P2Y₄R*s. Data represent means ± SEM of 3–4 independent experiments (in duplicates). Expression rates of the mutants were determined relative to that of the wt (100%). Statistical analysis was done using one-way ANOVA with Dunnett's post-hoc test: ns not significant; * *p* ≤ .05; ** *p* ≤ .01; *** *p* ≤ .001; **** *p* ≤ .0001.

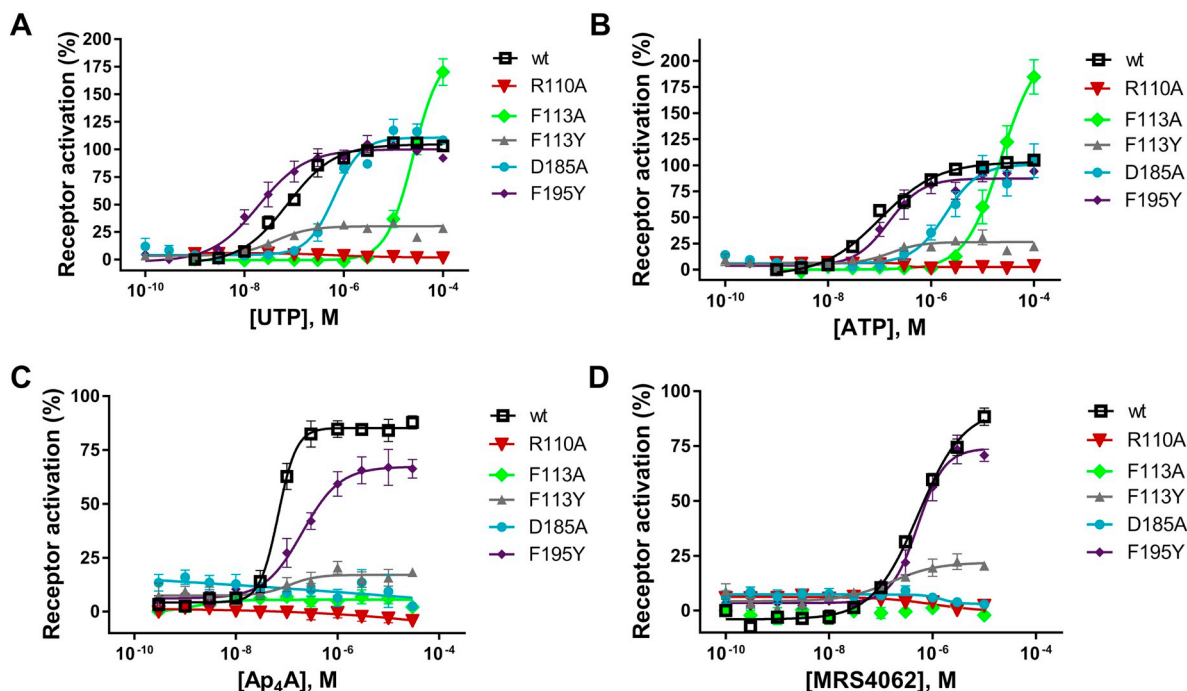


Fig. 7. Concentration–response curves of (A) UTP (B) ATP (C) Ap₄A and (D) MRS4062 determined by calcium mobilization assays on the wt and mutant P2Y₂R_s expressed in 1321 N1 astrocytoma cells. Each data point represents the mean \pm SEM of 4–6 independent determinations each in duplicates. EC₅₀ values are reported in Supplementary Information, Table S2.

3.3.1. Evaluation of agonists at the P2Y₂R

3.3.1.1. UTP. UTP (1) displayed an EC₅₀ value of $0.0822 \pm 0.0059 \mu\text{M}$ at hP2Y₂R, which is consistent with previous reports in calcium assays [12,50]. We observed a rightward shift of the concentration–response curves for most of the mutants relative to the wt receptor, except for the F195^{5.35}Y mutant at which UTP showed an EC₅₀ value of $0.0233 \pm 0.0064 \mu\text{M}$ (see Figs. 7 and 8; Table S2). There was no significant difference ($p > .05$) between the potencies at the wt and the F113^{3.32}Y receptor mutant despite its comparatively lower expression level (16% of the wt P2Y₂R). The R110^{3.29}A mutation resulted in a complete loss of receptor activation for all four tested agonists. The potency of UTP decreased by 300-fold at the F113^{3.32}A mutant (EC₅₀ $25.0 \pm 2.7 \mu\text{M}$, $p \leq .0001$, ****) whereas at the D185^{ECL2}A mutant it decreased 7-fold compared to that at the wt P2Y₂R ($0.606 \pm 0.076 \mu\text{M}$ vs $0.0822 \pm 0.0059 \mu\text{M}$). There was a 3-fold increase in UTP potency at the F195^{5.35}Y mutant (EC₅₀ $0.0233 \pm 0.0064 \mu\text{M}$, $p \leq .01$, **). The efficacies of UTP at the P2Y₂ mutants ranged between 33% and 170% compared to the wt P2Y₂R. A significant change in UTP efficacy was observed for the F113^{3.32}A ($170 \pm 12\%$, $p \leq .0001$, ****) and the F113^{3.32}Y ($33 \pm 2\%$, $p \leq .0001$, ****) mutants compared to the wt receptor (see Fig. 8).

3.3.1.2. ATP. ATP (2) was about equipotent to UTP at the wt hP2Y₂R (EC₅₀ $0.102 \pm 0.010 \mu\text{M}$) with nearly the same efficacy (see Table S2). Similar to UTP, concentration–response curves were slightly rightward-shifted for ATP at most of the mutants (i.e. F113^{3.32}A, F113^{3.32}Y, D185^{ECL2}A and F195^{5.35}Y), with significant differences in potencies (see Figs. 7 and 8). Like UTP, ATP was completely inactive at the R110^{3.29}A mutant although this mutant was highly expressed. Disruption of the ionic lock in the D185^{ECL2}A mutant led to a 21-fold reduction in ATP potency (EC₅₀ $2.160 \pm 0.454 \mu\text{M}$, $p \leq .0001$, ****) relative to the wt P2Y₂R. Also, the receptor mutants F113^{3.32}A and F113^{3.32}Y showed appreciable differences in ATP activity as compared to the wt P2Y₂R. At F113^{3.32}A, ATP (2) was 200-fold less potent (EC₅₀ $20.5 \pm 4.2 \mu\text{M}$, $p \leq .0001$, ****) compared to the wt receptor, whereas the F113^{3.32}Y mutation resulted in only a 2-fold, non-significant decrease in potency (EC₅₀ $0.219 \pm 0.044 \mu\text{M}$). In addition, the efficacy of ATP (2) was significantly different at the F113^{3.32}A

($185 \pm 16\%$, $p \leq .0001$, ****) and the F113^{3.32}Y ($31 \pm 7\%$, $p \leq .0001$, ****) mutants compared to that at the wt P2Y₂R (set at 100%). Residues Arg110^{3.29}, Phe113^{3.32} and to a lesser extent Asp185^{ECL2} were observed to be important for P2Y₂R activation by UTP and ATP.

3.3.1.3. Ap₄A. The EC₅₀ value of Ap₄A (3) at the wt P2Y₂R amounted to $0.0695 \pm 0.0065 \mu\text{M}$ with 88% efficacy compared to UTP, similar to the previously reported values [50]. Ap₄A was completely inactive at most of the P2Y₂R mutants (i.e. R110^{3.29}A, F113^{3.32}A, F113^{3.32}Y and D185^{ECL2}A) except for the F195^{5.35}Y mutant, at which it showed a 3-fold decrease in potency (EC₅₀ $0.194 \pm 0.043 \mu\text{M}$, $p \leq .001$, **), and a moderate reduction in efficacy to $67 \pm 8\%$ ($p \leq .05$, *) (see Figs. 7 and 8).

3.3.1.4. MRS4062. The wt P2Y₂R was activated by the P2Y₄R agonist MRS4062 (5) with an EC₅₀ value of $0.535 \pm 0.044 \mu\text{M}$ and $88 \pm 4\%$ efficacy compared to UTP. MRS4062 was 10-fold more potent at the F113^{3.32}Y receptor mutant (EC₅₀ $0.0546 \pm 0.0145 \mu\text{M}$, $p \leq .0001$, ****), 3-fold more potent at the F195^{5.35}Y receptor mutant (EC₅₀ $0.178 \pm 0.027 \mu\text{M}$, $p \leq .001$, ***) and completely inactive at all other investigated P2Y₂R mutants (Figs. 7 and 8). MRS4062 showed reduced efficacies at the F113^{3.32}Y mutant ($20 \pm 2\%$, $p \leq .0001$, ****) and at the F195^{5.35}Y mutant ($71 \pm 3\%$, $p \leq .001$, ***) compared to the wt P2Y₂R.

3.3.2. Evaluation of agonists at the P2Y₄R

3.3.2.1. UTP. UTP displayed an EC₅₀ value of $0.135 \pm 0.025 \mu\text{M}$ at the wt hP2Y₄R. At the P2Y₄R mutants, UTP showed no significantly different potency, except for the R190^{ECL2}A mutant where it displayed a 15-fold decrease (EC₅₀ $1.98 \pm 0.20 \mu\text{M}$, $p \leq .0001$, ****, see Figs. 9 and 10 and Table S3). However, differences in agonist efficacies were observed for several mutants (Fig. 11). Notably, there was a slight decrease in UTP potency at the Y197^{5.35}A ($0.411 \pm 0.056 \mu\text{M}$, 3-fold) and the F200^{5.38}A ($0.284 \pm 0.018 \mu\text{M}$, 2-fold) mutants with significantly reduced efficacy to $56 \pm 6\%$ ($p \leq .001$, ***) and $24 \pm 5\%$ ($p \leq .0001$, ****), respectively. UTP was least potent at the R190^{ECL2}A mutant with a 15-fold decrease (EC₅₀ $1.98 \pm 0.20 \mu\text{M}$, $p \leq .0001$, ****) and only $53 \pm 6\%$ efficacy ($p \leq .001$, ***) compared to the wt P2Y₄R (100%).

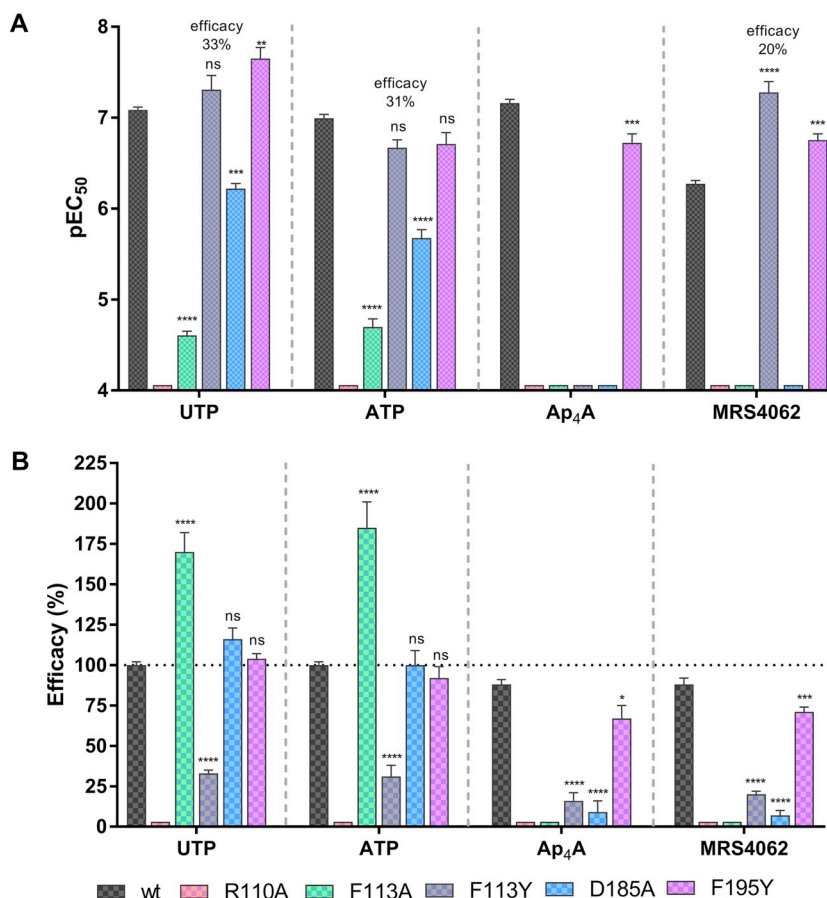


Fig. 8. A. Potencies and B. efficacies of the selected P2Y agonists determined in calcium mobilization assays on human wt and mutant P2Y₂Rs expressed in 1321 N1 astrocytoma cells. Data represent means ± SEM (n = 4–6) performed in duplicates. One-way ANOVA with Dunnett's post-hoc test: ns not significant; * p ≤ .05; ** p ≤ .01; *** p ≤ .001; **** p ≤ .0001.

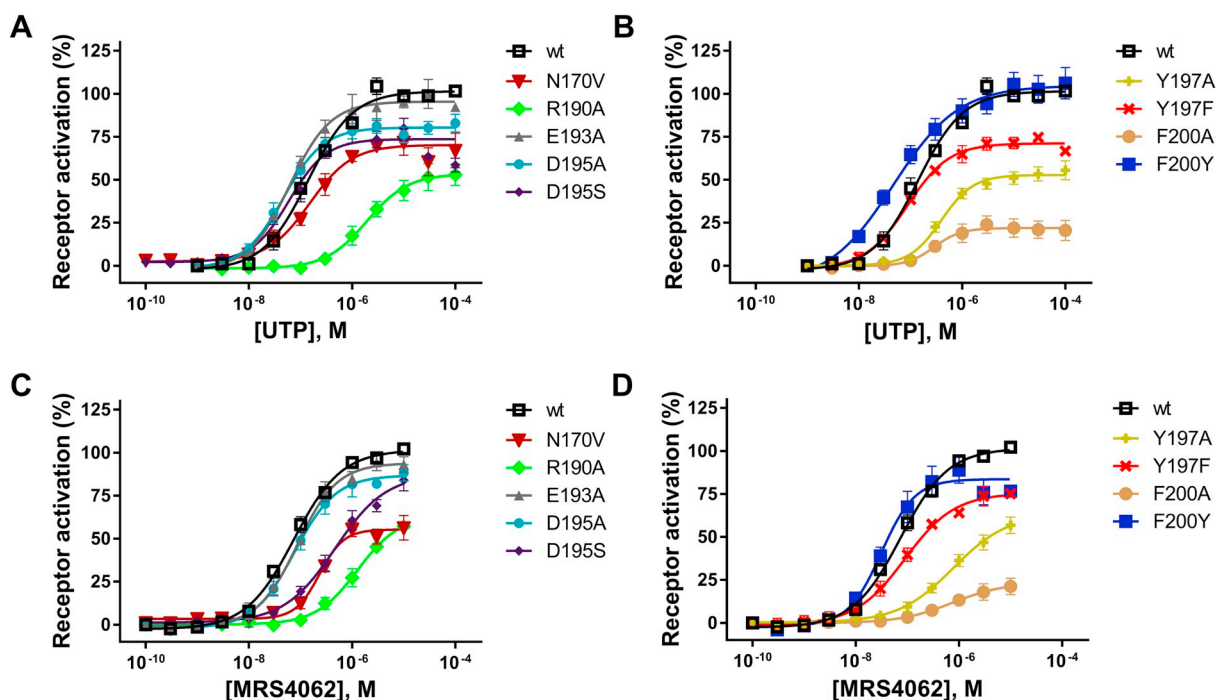


Fig. 9. Concentration–response curves of UTP (A and B) and MRS4062 (C and D) determined by calcium mobilization assays on the P2Y₄Rs (wt and mutants) expressed in 1321 N1 astrocytoma cells. Each data point represents means ± SEM of 4–6 independent determinations each in duplicates. EC₅₀ values are reported in Supplementary Table S3, pEC₅₀ values are shown in Fig. 11.

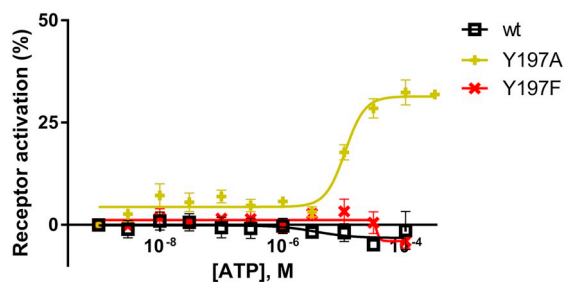


Fig. 10. Concentration–response curves of ATP on the wt P2Y₄R and the P2Y₄R mutants Y197^{5.35}A and Y197^{5.35}F expressed in 1321 N1 astrocytoma cells as determined in calcium mobilization assays. Replacement of Tyr197^{5.35} in the wt P2Y₄R by alanine (Y197^{5.35}A), but not by phenylalanine (Y197^{5.35}F), led to a receptor mutant that could be activated by ATP (EC₅₀ 11.9 ± 1.6 μM) with an efficacy of 32 ± 3% compared to the maximal effect of UTP (100%). Each data point represents means ± SEM of 4–6 independent determinations each in duplicates. EC₅₀ values are reported in Supplementary Table S3, pEC₅₀ values are shown in Fig. 11.

3.3.2.2. ATP. ATP was inactive at the wt P2Y₄R as previously described [2,12]. Interestingly, ATP showed some activity at the P2Y₄R mutant Y197^{5.35}A with an EC₅₀ value of 11.9 ± 1.6 μM and an efficacy of 32 ± 3%, while it was inactive at all other investigated P2Y₄R mutants (see Figs. 9 and 10, Table S3).

3.3.2.3. Ap₄A. In agreement with previous reports, Ap₄A (3) was completely inactive as an agonist at the wt hP2Y₄R, and the same was observed for its mutants (see Table S3 of Supplementary information) [2,12].

3.3.2.4. MRS4062. MRS4062 (5) was found in our experiments to be 7-fold selective for the wt P2Y₄R (0.0761 ± 0.0100 μM, 100% efficacy) versus the wt P2Y₂R (0.535 ± 0.044 μM, 88% efficacy) essentially confirming originally published data [44]. The potency of MRS4062 was significantly reduced at the R190^{ECL2A} mutant (EC₅₀ 1.24 ± 0.28 μM, 16-fold), the Y197^{5.35}A mutant (EC₅₀ 0.757 ± 0.068 μM, 10-fold), and the F200^{5.38}A (EC₅₀ 0.694 ± 0.069 μM, 9-fold) as compared to the wt P2Y₄R. The efficacies at these mutants were also significantly decreased to 57% (p ≤ .001, ***) for the R190^{ECL2A} and the Y197^{5.35}A mutants, and to 21 ± 5% for the F200^{5.38}A mutant (p ≤ .0001, ****). MRS4062 showed also reduced efficacy at the N170^{4.60}V receptor mutant (56 ± 7%, p ≤ .0001, ****) although its potency was unchanged compared to the wt P2Y₄R (see Figs. 9 and 11, Table S3).

3.4. Evaluation of antagonist potencies

Selected antagonists were tested in calcium assays at the wt P2Y₂- and P2Y₄R and their mutants. Recombinant 1321 N1 cells were pre-incubated with different concentrations of antagonist followed by receptor stimulation by agonist at its EC₈₀ concentration to obtain concentration-dependent inhibition curves. We tested the non-selective P2YR antagonist RB-2 (6), the related, but smaller AQ derivatives PSB-09144 (9), PSB-16133 (10), PSB-16135 (11) and PSB-1699 (12), as well as ARC118925 (7) [34], a potent and selective P2Y₂R antagonist derived from UTP. These antagonists have been proposed to bind to the orthosteric site of P2Y₂R [50]. In contrast, at P2Y₄R, RB-2 and some other AQ derivatives were reported to bind to an allosteric pocket in close proximity to the orthosteric site, based on a computational study [47]. However, experimental evidence for this hypothesis is still lacking and the individual

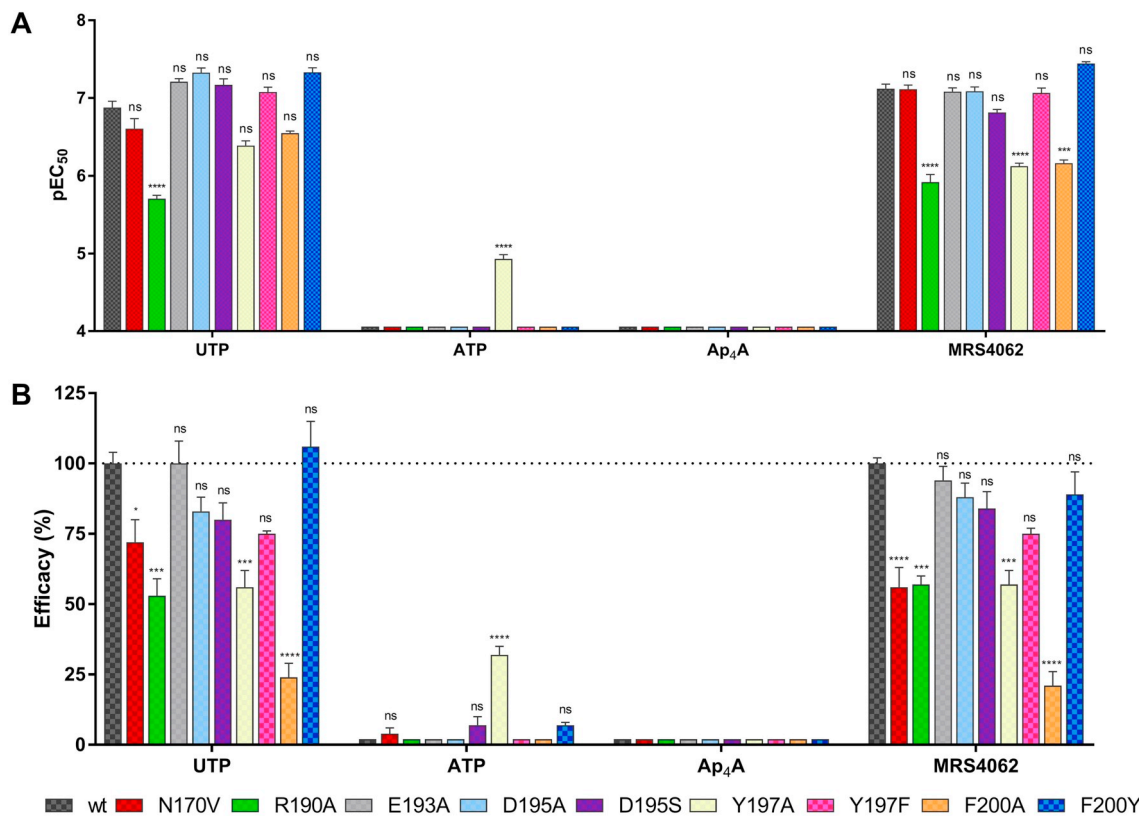


Fig. 11. A. Potencies and B. efficacies of selected P2Y agonists determined in calcium mobilization assays at the wt P2Y₄R and its mutants expressed in 1321 N1 astrocytoma cells. EC₅₀ values are presented in Supplementary Table S3. Data represent means ± SEM from 4 to 6 separate experiments performed in duplicates. Statistical analysis was done by one-way ANOVA with Dunnett's post-hoc test: ns not significant; * p ≤ .05; ** p ≤ .01; *** p ≤ .001; **** p ≤ .0001.

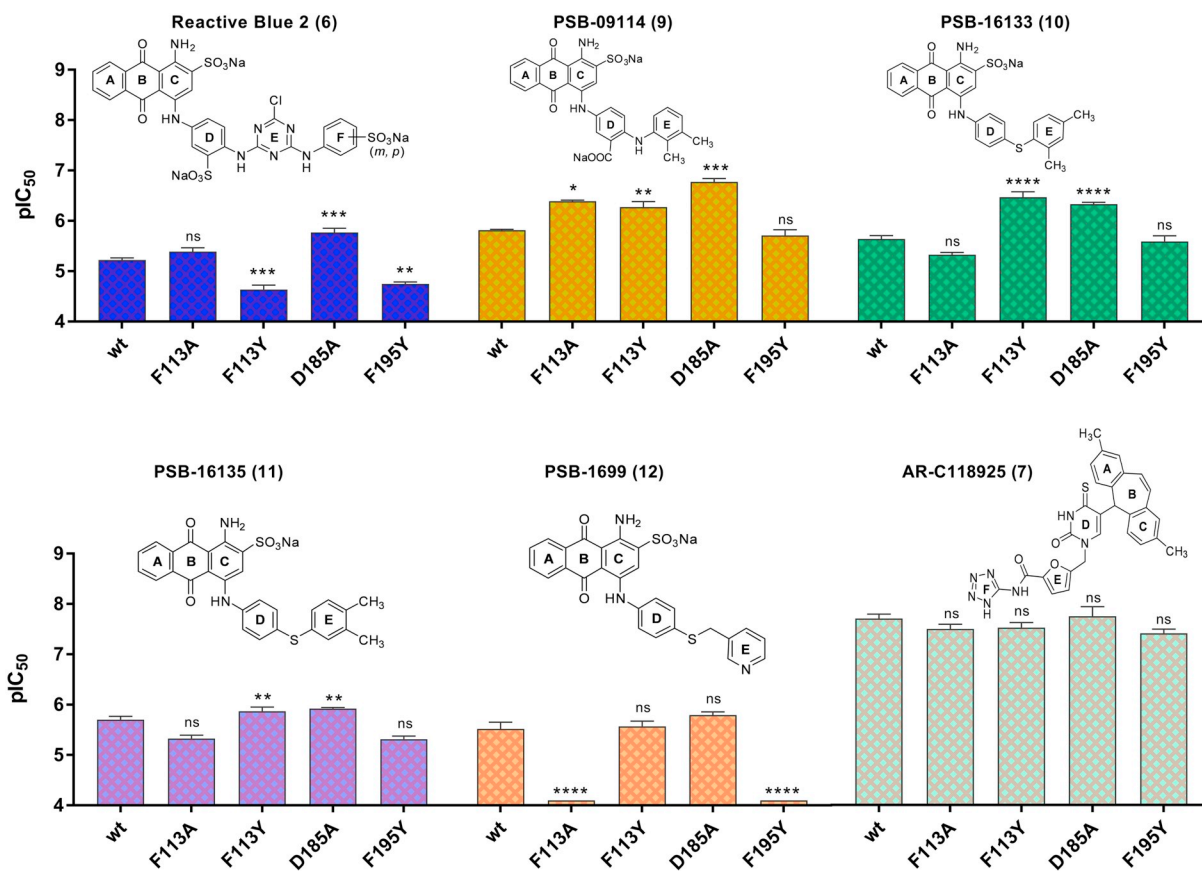


Fig. 12. Potencies of RB-2 (6, purified prior to testing), PSB-09114 (9), and PSB-16133 (10), PSB-16135 (11), PSB-1699 (12) and AR-C118925 (7) determined in calcium mobilization assays at the wt *hP2Y₂R* and its mutants expressed in 1321 N1 astrocytoma cells. Data represent mean pIC₅₀ values \pm SEM of 3–5 independent determinations each in duplicates vs. UTP employed at its EC₈₀ value for the respective cell line. IC₅₀ values are reported in Supplementary Table S4. Concentration–response curves are shown in Supplementary Fig. S2.

interaction partners in the receptor protein have not been confirmed so far. Therefore, we set out to investigate the proposed differing binding modes of the AQ derivatives by our mutational approach (see Figs. 12 and 13 for potencies of the antagonists at the wt and mutant *hP2Y₂R* and *hP2Y₄R*s; see Supplementary Information Fig. S2 and Table S4 for concentration–response curves and IC₅₀ values of antagonists at *hP2Y₂R*; for those at *hP2Y₄R*, see Supplementary Figs. S3 and S4, and Table S5).

3.4.1. Evaluation of antagonists at the *P2Y₂R* mutants

3.4.1.1. Reactive blue 2. At the wt *P2Y₂R*, the *P2Y₂R* antagonist RB-2 displayed a potency in the low micromolar range (IC₅₀ 5.99 \pm 0.563 μ M) consistent with reported values [12,47]. We observed a 3- to 4-fold reduction in RB-2 potency at the mutants F113^{3.32}Y (IC₅₀ 23.5 \pm 4.6 μ M, $p \leq .0001$, ****) and F195^{5.35}Y (IC₅₀ 18.0 \pm 1.5 μ M, $p \leq .01$, **, Fig. 12). In contrast, RB-2 was 3-fold more potent at the D185^{ECL2}A mutant (IC₅₀ 1.73 \pm 0.32 μ M, $p \leq .001$, ***). RB-2 appeared to have a profile of inhibitory potency different from that of the other AQ derivatives at the *P2Y₂R* mutants studied (see Fig. 12).

3.4.1.2. Small anthraquinone derivatives. PSB-09114 (9), PSB-16133 (10) and PSB-16135 (11), showed no significant differences in potency at the wt *P2Y₂R* as compared to the mutant receptors F113^{3.32}A and F195^{5.35}Y. However, at the *P2Y₂R* mutants F113^{3.32}Y and D185^{ECL2}A, the potencies of these AQ derivatives, which are lacking ring F of RB-2, were significantly increased (see Fig. 12). PSB-09114 (9) was 3-fold more potent at the F113^{3.32}Y (IC₅₀ 0.550 \pm 0.134 μ M, $p \leq .05$, *) and 9-fold more potent at the D185^{ECL2}A receptor mutant (IC₅₀ 0.170 \pm 0.025 μ M, $p \leq .01$, **). Similarly, PSB-16133 (10) was 5- to 7-fold more potent, and PSB-16135

(11) was about 2-fold more potent at the F113^{3.32}Y (IC₅₀ 1.38 \pm 0.26 μ M, $p \leq .01$, **) and the D185^{ECL2}A (1.20 \pm 0.06 μ M, $p \leq .01$, **) mutants compared to the wt *P2Y₂R* (Fig. 12 and Table S4). Interestingly, the AQ derivative PSB-1699 (12), with a 2-atom linker between ring D and E, instead of a 1-atom linker as in 9–11, showed a completely different pattern. Contrary to the AQ derivatives 9–11, PSB-1699 (12, IC₅₀ 3.19 \pm 0.97 μ M at the wt *P2Y₂R*) showed no inhibition of UTP-induced receptor activation at the F113^{3.32}A and F195^{5.35}Y receptor mutants while it maintained potency similar to that at the wt *P2Y₂R* for the F113^{3.32}Y and D185^{ECL2}A receptor mutants.

3.4.1.3. AR-C118925. The potency of the UTP-derived *P2Y₂R*-selective antagonist AR-C118925 (7) was in the nanomolar range as previously reported [32]. Interestingly, there was no significant difference in AR-C118925 potency at the investigated *P2Y₂R* mutants (Fig. 12, also see Table S4 of Supplementary Information).

3.4.2. Evaluation of antagonists at the *P2Y₄R* mutants

3.4.2.1. Reactive-blue 2. RB-2 (6) was about 6-fold more potent at the wt *P2Y₄R* (IC₅₀ 1.05 \pm 0.04 μ M) as compared to the wt *P2Y₂R* (IC₅₀ 5.99 \pm 0.563 μ M). In comparison to the wt *P2Y₄R*, RB-2 was 2-fold less potent at the D195^{5.33}C mutant (2.26 \pm 0.40 μ M, $p \leq .05$, *), 3-fold less potent at the Y197^{5.35}F mutant (3.30 \pm 0.65 μ M, $p \leq .001$, ***) and 4-fold less potent at the F200^{5.38}Y mutant (4.17 \pm 0.22 μ M, $p \leq .0001$, ****). At the N170^{4.60}V mutant, RB-2 was 2-fold more potent (0.477 \pm 0.083 μ M, $p \leq .05$, *). There was no significant change in potency of RB-2 at the other investigated *P2Y₄R* mutants (see Fig. 13 and Table S5).

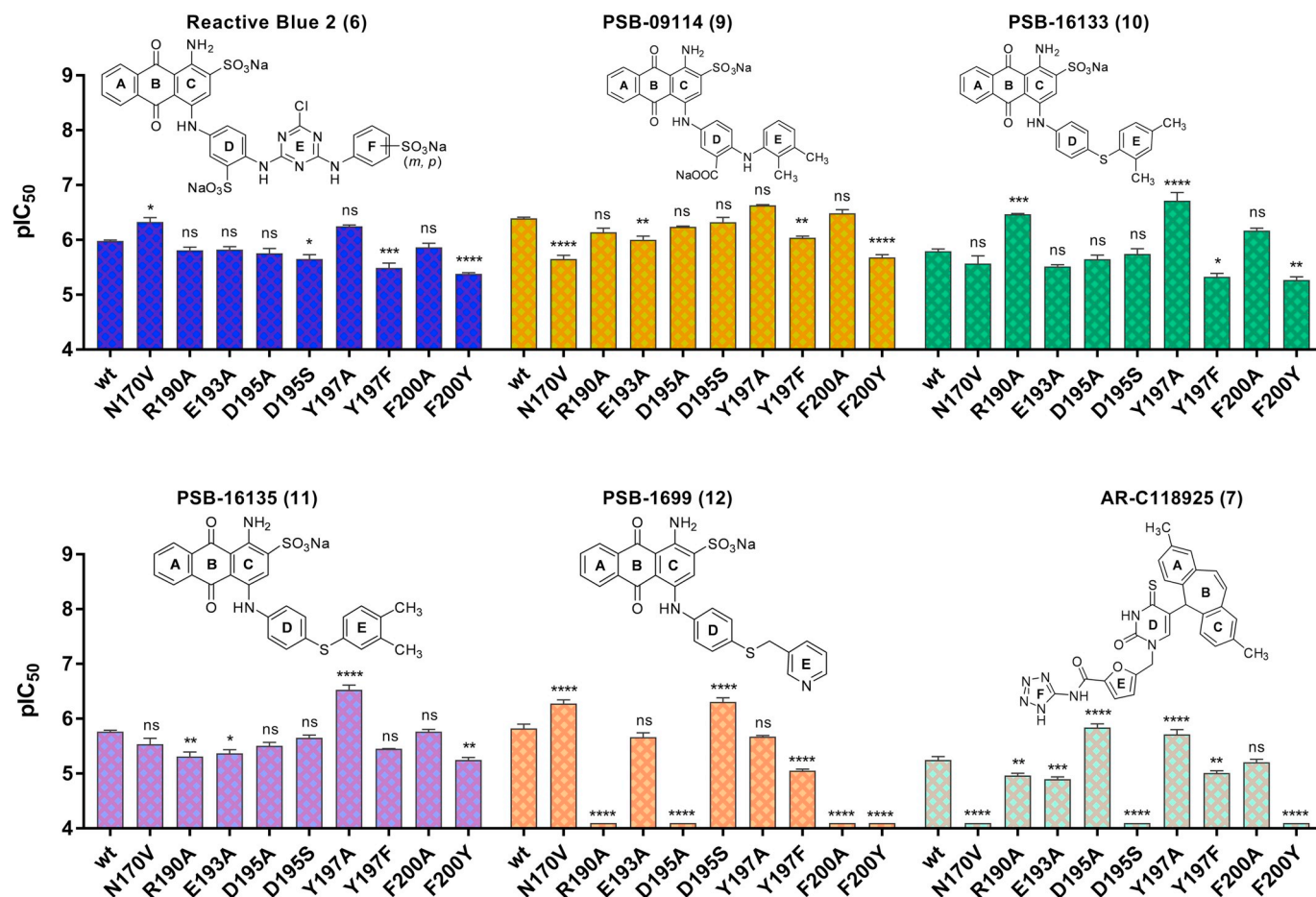


Fig. 13. Potencies of RB-2 (6, purified), PSB-09114 (9), and PSB-16133 (10), PSB-16135 (11), PSB-1699 (12) and AR-C118925 (7) as determined by calcium mobilization assays at the wt *hP2Y₄R* and its mutants expressed in 1321 N1 astrocytoma cells. Data represent mean pIC₅₀ values ± SEM of 3–5 independent determinations each in duplicates vs. UTP (at its EC₈₀ value for the respective cell line). IC₅₀ values are reported in Supplementary Table S5. Concentration–response curves are shown in Supplementary Fig. S3 and S4.

3.4.2.2. Small anthraquinone derivatives. No significant or only moderate differences between the potencies of PSB-09114 (9, IC₅₀ 0.403 ± 0.017 μM, wt *hP2Y₄R*), PSB-16133 (10, IC₅₀ 1.62 ± 0.17 μM, wt *hP2Y₄R*) and PSB-16135 (11, IC₅₀ 1.73 ± 0.11 μM, wt *hP2Y₄R*) at the wt *P2Y₄R* and the investigated *P2Y₄R* mutants were observed (see Fig. 13 and Table S5). PSB-09114 (9) was 5-fold less potent at the N170^{4.60V} (2.26 ± 0.35 μM, *p* ≤ .0001, ****) and the F200^{5.38Y} (2.09 ± 0.24 μM, *p* ≤ .0001, ****) mutants, and 2-fold less potent at the E193^{ECL2A} (1.01 ± 0.16 μM, *p* ≤ .01, **) and the Y197^{5.35F} (0.913 ± 0.059 μM, *p* ≤ .01, **) mutants compared to the wt *P2Y₄R*. PSB-16133 (10) showed a significant, 3-fold decrease in potency at the Y197^{5.35F} (4.77 ± 0.68 μM, *p* ≤ .05, *) and the F200^{5.38Y} (5.43 ± 0.71 μM, *p* ≤ .01, **) receptor mutants, whereas its potency increased by 5-fold at R190^{ECL2A} (0.339 ± 0.010 μM, *p* ≤ .001, ***) and 8-fold at the Y197^{5.35A} mutant (0.205 ± 0.068 μM, *p* ≤ .0001, ****). The potency of PSB-16135 (11) was 3-fold lower at the R190^{ECL2A} (4.98 ± 0.94 μM, *p* ≤ .01, **), the E193^{ECL2A} (4.33 ± 0.65 μM, *p* ≤ .05, *) and the F200^{5.38Y} (5.69 ± 0.62 μM, *p* ≤ .01, **) receptor mutants. At the Y197^{5.35A} mutant, PSB-16135 displayed a 6-fold increase in potency (0.303 ± 0.060 μM, *p* ≤ .0001, ****).

Interestingly, as observed at *P2Y₂R*, PSB-1699 (12) also displayed a different pattern as compared to the other AQ derivatives at the *P2Y₄R* subtype. PSB-1699's inhibitory potency (12, IC₅₀ 1.53 ± 0.27 μM, wt *hP2Y₄R*) was completely abolished at the R190^{ECL2A}, D195^{5.33A}, F200^{5.38A}, and F200^{5.38Y} receptor mutants. At the Y197^{5.35F} receptor mutant, there was a 6-fold decrease in potency while it was 3-fold more potent at the N170^{4.60V} (0.537 ± 0.084 μM, *p* ≤ .0001, ****) and the

D195^{5.33S} *P2Y₄R* mutants (0.504 ± 0.090 μM, *p* ≤ .0001, ****) relative to the wt *P2Y₄R*.

3.4.2.3. AR-C118925. In the current study, AR-C118925 (7) was determined to be about 270-fold selective for *P2Y₂R* (IC₅₀ 0.0212 ± 0.0042 μM) over *P2Y₄R* (IC₅₀ 5.73 ± 0.82 μM). These data confirm the previously published selectivity profile of AR-C118925 (7) [32]. With the exception of F200^{5.38A} which showed no significant difference in potency of AR-C118925 relative to the wt *P2Y₄R*, the introduced mutations significantly affected AR-C118925 potency at *P2Y₄R* (Fig. 13). Most mutations led to a reduction in potency of the antagonist. The inhibitory potency of 7 versus UTP was completely lost in the N170^{4.60V}, D195^{5.33S} and F200^{5.38Y} receptor mutants. AR-C118925 showed a 2-fold decrease in potency at the R190^{ECL2A} (10.9 ± 1.01 μM, *p* ≤ .01, **) and the E193^{ECL2A} mutants (12.7 ± 1.2 μM, *p* ≤ .001, ***), two amino acids predicted to form ionic locks in *P2Y₄R*. In contrast, 7 was about 3- to 4-fold more potent at the D195^{5.33A} and the Y197^{5.35A} mutants than at the wt *P2Y₄R* with IC₅₀ values of 1.47 ± 0.22 μM (*p* ≤ .0001, ****) and 1.96 ± 0.38 μM (*p* ≤ .0001, ****), respectively.

3.5. Docking studies and assessment of mutagenesis data

3.5.1. Agonists at the *hP2Y₂R*

3.5.1.1. UTP. Docking studies of the selected agonists and antagonists were performed based on the X-ray crystal structure of the related *P2Y₁R* also taking into account the published structures of the somewhat more distantly related *P2Y₁₂R* subtype [49,52]. Results of

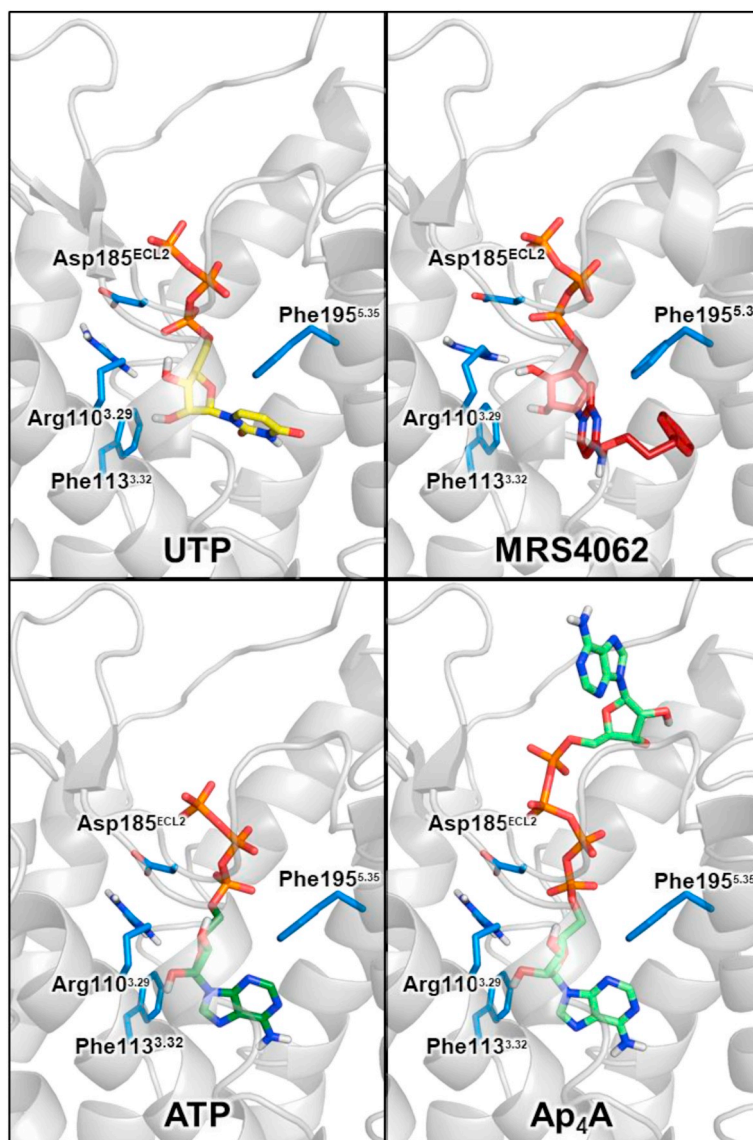


Fig. 14. Interactions of selected P2Y₂R agonists docked into the putative binding pocket of hP2Y₂R with amino acid residues that were exchanged in the present mutagenesis study. Carbon atoms of UTP are colored in yellow, of MRS4062 in dark red, of ATP in dark green, and of Ap₄A in light green. For further color code see Fig. 4.

the present as well as previously published mutagenesis studies provided additional important information to predict ligand–receptor interactions and receptor activation on a molecular level.

Interactions of the phosphate groups with charged amino acids (Arg177^{ECL2}, His184^{ECL2}, Asp185^{ECL2}, Arg265^{6.55}, Arg272^{ECL3}, Lys289^{7.36}, Arg292^{7.39}) and through hydrogen bonds (Tyr268^{6.58}, Tyr269^{6.59}) were predicted by the homology model of hP2Y₂ (see Fig. 4). The hydroxy groups of the ribose moiety likely form hydrogen bonds with Arg110^{3.29} and Asp185^{ECL2}. The uracil base is accommodated in a binding pocket formed by several aromatic residues (Phe113^{3.32}, Tyr114^{3.33}, Tyr118^{3.37}, Phe261^{6.51}), where it is possibly stabilized through π - π -interactions and hydrogen bonding with the hydroxy groups of the tyrosine residues. UTP displayed an EC₅₀ value of 82 nM at hP2Y₂R, which is consistent with previous reports in calcium assays [12,50]. In the present study, mutation of Phe113^{3.32} to alanine resulted in a 300-fold decrease in potency of UTP (EC₅₀ 25 ± 2.7 μ M), while no significant differences were observed for the F113^{3.32}Y mutant (EC₅₀ 52.6 ± 18.3 nM), indicating that Phe113^{3.32} might form π - π -interactions with the nucleobase. The mutation of Asp204^{ECL2} in hP2Y₁R, a residue that is thought to be involved in an ionic lock with an arginine whose agonist-induced breaking contributes to the molecular

receptor activation, had resulted in a 30-fold decrease in potency of the P2Y₁R agonist 2-methylthio-ADP (2-MeSADP) [58]. A similar trend was observed for the analogous residue Asp185^{ECL2} in hP2Y₂R, which resulted in a 7-fold decrease in UTP potency when mutated to alanine (EC₅₀ 606 ± 76 nM). In accordance with our docking studies, the homologous exchange mutant F195^{5.35}Y showed no negative effect on the potency of UTP (EC₅₀ 23.3 ± 6.4 nM), which was predicted to interact with Phe195^{5.35} through π - π -interactions.

3.5.1.2. ATP, Ap₄A. Docking studies suggested a binding mode for ATP similar to that of UTP and its derivative Ap₄A (see Fig. 14). The phosphate chain is supposed to bind in a pocket formed by positively charged residues, the same that were predicted to interact with the phosphate chain of UTP: Arg177^{ECL2}, His184^{ECL2}, Asp185^{ECL2}, Arg265^{6.55}, Arg272^{ECL3}, Arg292^{7.39} (see Fig. 15). Interactions with those residues were previously confirmed [12,50,54]. ATP was about equipotent to UTP at the wt hP2Y₂R (EC₅₀ 102 nM) with nearly the same efficacy (see Table S2). The EC₅₀ value of Ap₄A (3) at the wt P2Y₂R amounted to 69.5 nM with 88% efficacy compared to UTP, similar to the previously reported values [50]. A complete loss of receptor activation had been observed for the R265^{6.55}A and the R292^{7.39}A P2Y₂R mutants [50]. Mutation of

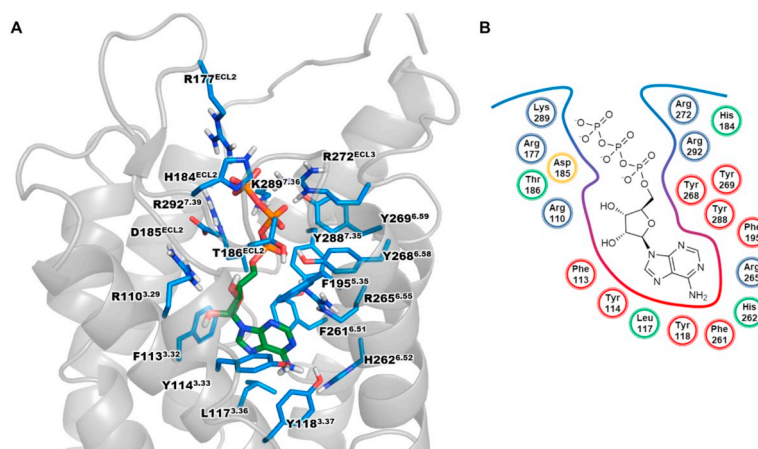


Fig. 15. Putative binding mode of ATP in the homology model of *hP2Y₂R*. **A.** Docked pose of ATP with the important residues in the binding pocket shown. Carbon atoms of ATP are colored in green. **B.** Schematic 2D representation of the binding pocket. For further color code see Fig. 4.

Arg272^{ECL3} to alanine was reported to lead to a 185-fold (ATP) and a > 4000-fold (Ap₄A) decrease in potency, respectively. The larger decrease in potency for Ap₄A versus ATP at the R272^{ECL3}A mutant [50] can be explained by additional interactions of the δ -phosphate group of Ap₄A. His184^{ECL2} may interact with one or several phosphate groups, as its mutation to alanine had resulted in a > 100-fold decrease in UTP and Ap₄A potency [50]. In the present study, differences between ATP and Ap₄A were observed at the D185^{ECL2}A mutant, which resulted in a 21-fold decrease in potency for ATP (EC₅₀ 2160 \pm 454 nM), similar to the results for UTP, but it led to complete abolishment of receptor activation by Ap₄A (EC₅₀ > 10 μ M). Ap₄A possesses an additional δ -phosphate located in close proximity to the putative ionic lock between Asp185^{ECL2} and Arg292^{7.39} possibly allowing additional ionic and hydrogen bonding interactions that are not present in the ATP and UTP complex. Hydrogen bonds between phosphate groups of the nucleotides and tyrosine Tyr268^{6.58}, Tyr269^{6.59} and Tyr288^{7.35} are feasible (see Fig. 15). Previous findings support hydrogen bond interactions for Tyr268^{6.58} and Tyr269^{6.59}, since mutation of those residues to phenylalanine had resulted in a > 10-fold decrease in UTP and Ap₄A potency [50]. Tyr288^{7.35}, on the other hand, might play a role in agonist discrimination. The mutation of Tyr288^{7.35} to alanine had resulted in a > 1000-fold decrease in potency of both UTP and Ap₄A, whereas its mutation to phenylalanine had severely affected the potency of Ap₄A (> 1000-fold decrease) but not so much that of UTP (20-fold decrease) [50]. It had been hypothesized that Tyr288^{7.35} might form interactions with Arg265^{6.55} resulting in a rotamer of Arg265^{6.55} required for agonist binding, or Tyr288^{7.35} itself might recognize and guide the nucleobase of the agonists towards the lipophilic binding pocket through π - π -interactions [50]. Arg110^{3.29} likely forms hydrogen bonds with both hydroxy groups of the ribose moiety, while the backbone of Asp185^{ECL2} possibly forms hydrogen bonds with the 3'-hydroxy group of the ribose moiety. As previously reported for UTP and Ap₄A [50] and presently confirmed, mutation of the key residue Arg110^{3.29} to alanine also led to complete abolishment of ATP activity (EC₅₀ > 10 μ M). According to the model, the adenine moiety of ATP and one adenine moiety of Ap₄A bind in an aromatic binding cavity formed by the previously described aromatic and lipophilic amino acids Phe113^{3.32}, Tyr114^{3.33}, Leu117^{3.37}, Tyr118^{3.38}, Phe195^{5.35}, and Phe261^{6.51}. The nucleobases of ATP and Ap₄A are likely to form π - π -interactions with Phe113^{3.32}, since mutation of this residue to alanine resulted in a 200- and > 1000-fold decrease in potency for ATP (EC₅₀ 20.5 \pm 4.2 μ M) and Ap₄A (EC₅₀ > 10 μ M), respectively. This is supported by the observation that the F113^{3.32}Y mutation had no significant effect on ATP potency (EC₅₀ 219 \pm 44 nM). The decrease in potency for Ap₄A (EC₅₀ > 10 μ M) might be due to different modes of receptor activation (as discussed below). Mutation of Phe195^{5.35} to tyrosine also had no effect ATP potency and efficacy,

whereas potency and efficacy of Ap₄A were slightly decreased (EC₅₀ 194 \pm 43 nM). As we did not observe different interactions of Ap₄A and ATP within the ATP binding site of the model, the small difference in agonist potency might be explained by modulation of ECL2 flexibility resulting in weaker interactions with the larger agonist Ap₄A. The Y114^{3.33}F and F261^{6.51}A mutations had been reported to lead to complete abolishment of receptor activation by Ap₄A but not by UTP, which was explained by different interaction patterns of the nucleobases in the lipophilic binding domain [50]. The proposed ATP binding mode and interactions are presented in Fig. 15 which is consistent with all present and previously published experimental data.

The larger ATP derivative Ap₄A additionally projects into the extracellular domain of P2Y₂R (see Fig. 14). The δ -phosphate group might be involved in ionic interactions with Arg26^{N-terminus} and Arg177^{ECL2} (not shown). Cation- π -interactions are conceivable between Arg24^{N-terminus}, Arg26^{N-terminus}, and Arg177^{ECL2} and the second adenine moiety forming a possible second nucleotide binding pocket close to the N-terminus and the extracellular domain. Mutation of Arg177^{ECL2} to alanine in previous studies had resulted in weaker effects on the potency of ATP (3-fold reduction in potency) as compared to Ap₄A (7-fold reduction) [12]. However, other binding modes of the second adenine group cannot be excluded.

3.5.1.3. MRS4062. The synthetic UTP-derivative MRS4062 (5), a moderately potent P2Y₄R agonist, is proposed to share the same binding site as the endogenous agonists (see Fig. 16). The wt P2Y₂R was activated by the P2Y₄R agonist MRS4062 (5) with an EC₅₀ value of 535 \pm 44 nM and 88% efficacy compared to UTP. The interaction pattern of the phosphate groups is likely shifted due to the large N⁴-substituent on the cytosine heterocycle. The α -phosphate may form ionic and hydrogen bonding interactions with Arg110^{3.29}, Lys289^{7.36} and Arg292^{7.39}. The β -phosphate group possibly interacts with Asp185^{ECL2}, Tyr268^{6.58}, Lys289^{7.36}, and Arg292^{7.39}, and the γ -phosphate may form interactions with Arg177^{ECL2}, Asp185^{ECL2}, Arg272^{ECL3}, Lys289^{7.36}, and Arg292^{7.39}.

The potency of MRS4062 was decreased by > 100-fold at the D185^{ECL2}A mutant (EC₅₀ > 10 μ M) compared to a 21-fold decrease for UTP, which may be explained by stronger interactions of MRS4062 with Asp185^{ECL2} due to its shifted binding mode as compared to UTP. According to the docking study, the ribose moiety of MRS4062 might form hydrogen bonds between the 3'-hydroxy group and Arg110^{3.29}. As observed for UTP, ATP and Ap₄A, MRS4062 also could not activate the R110^{3.29}A mutant (EC₅₀ > 10 μ M). The potency of MRS4062 was decreased by > 100-fold at the F113^{3.32}A mutant (EC₅₀ > 10 μ M) and significantly increased (10-fold) at the F113^{3.32}Y mutant (EC₅₀ 54.6 \pm 14.5 nM), likely due to the closer proximity of the nucleobase

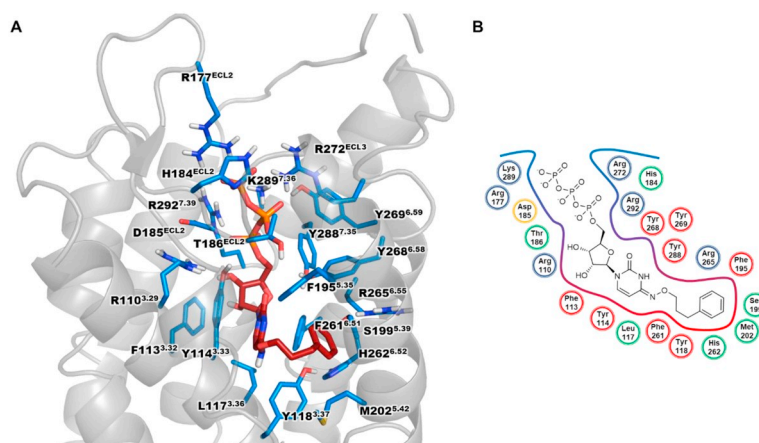


Fig. 16. Putative binding mode of MRS4062 in the homology model of *hP2Y₂R*. **A.** Docked pose of MRS4062 with the important residues in the binding pocket shown. Carbon atoms of MRS4062 are colored in red. **B.** Schematic 2D representation of the binding pocket. For further color code see Fig. 4.

to Phe113^{3.32}. The cytosine core is possibly stabilized through π - π -stacking with an induced rotamer of Tyr114^{3.33}, and the oxime substituent may project towards TM V. Several aromatic (Tyr118, Phe195^{5.35}, Tyr198) and lipophilic (Val168, Met202^{5.42}, Leu203) amino acid residues could be responsible for binding of the phenylpropyl residue through lipophilic interactions. The 3-fold increase in MRS4062 potency at the F195^{5.35}Y mutant (EC_{50} 178 \pm 27 nM) might be rationalized by additional hydrogen bonds between the introduced hydroxy group of the tyrosine and the keto group in position 2 of the cytosine moiety. In our docking studies, the phosphate chain still binds in the same cationic binding cavity as UTP, ATP and Ap₄A, whereas the nucleobase binding pocket of the cognate agonists is now occupied by the phenylpropyl residue of MRS4062, while the pyrimidine moiety is moved towards Phe113^{3.32} and Tyr114^{3.33}.

3.5.1.4. Comparison of agonists. The efficacy profiles at the P2Y₂R mutants were similar between the agonists UTP and ATP on the one hand, and Ap₄A and MRS4062 on the other hand (see Fig. 8). The mutations F113^{3.32}A and D185^{ECL2}A resulted in very different effects as shown in Figs. 7 and 8. The F113^{3.32}A mutation caused a significant increase in efficacy in the case of UTP and ATP (170 \pm 12 and 185 \pm 16%, respectively), and a complete absence of receptor response for Ap₄A and MRS4062. Since ATP and Ap₄A likely share the same binding mode based on the collected data, the difference in their pharmacological profiles can be explained by different modes of receptor activation. This includes additional ionic and hydrogen bond interactions for Ap₄A involving the ionic lock between Asp185^{ECL2} and Arg292^{7.39} and other residues close to the ionic lock. Further support for this hypothesis is provided by a decrease in efficacy of Ap₄A and MRS4062 at the D185^{ECL2}A mutant (9 \pm 7 and 7 \pm 3%, respectively), while no changes in efficacies for UTP and ATP could be observed for that mutant (116 \pm 7 and 100 \pm 9%, respectively). It is possible, that the formation of the ionic lock between Asp185^{ECL2} and Arg292^{7.39} induces a specific rotamer of Arg292^{7.39} which is needed for interaction with the phosphate groups. Since Ap₄A possesses an additional δ -phosphate group, and MRS4062 likely has a slightly different interaction pattern due to its shifted position in the binding pocket, they might form additional interactions with the rotamer of Arg292^{7.39}, which are not present in the case of UTP and ATP.

Although no significant changes in potencies and efficacies of agonists were determined for the F195^{5.35}Y mutant, different trends were observed depending on the agonist structure. When mutated to tyrosine, the potency of UTP and MRS4062 slightly increased while it decreased for ATP and Ap₄A with respect to the wt P2Y₂R. Our docking studies suggest that the nucleobase binds close to Phe195^{5.35} which would allow π - π -interactions of varying magnitudes with the adenine and uracil

derivatives, respectively. Since the space in the investigated lipophilic binding pocket is limited, the size and functionality of residues might be crucial for ligand discrimination. The Phe195^{5.35} residue is conserved in the mouse and rat P2Y₂R, but exchanged for the larger tyrosine residue in the mouse, rat and *hP2Y₄R* (Tyr197^{5.35}). Mutation of Tyr197^{5.35} to alanine introduced ATP-sensitivity into P2Y₄R, probably due to the increase in available space, but since it was not crucial for ATP agonism at P2Y₂R, we expect several residues besides Phe195^{5.35} to be responsible for accepting both ATP and UTP by P2Y₂R.

3.5.2. Antagonists at the *hP2Y₂R*

3.5.2.1. Anthraquinone derivatives. The AQ derivatives are proposed to bind in the upper third part of P2Y₂R (see Fig. 17). While rings A and B of AOs (Fig. 2) are exposed towards the extracellular space, the sulfonate group of ring C likely forms ionic and hydrogen bond interactions with charged residues, such as Arg110^{3.29}, Lys289^{7.36} and Arg292^{7.39}. Increased potencies (2- to 9-fold) of the investigated AQ-derived antagonists were determined at the D185^{ECL2}A mutant. The mutation of Asp185^{ECL2} to alanine would break the ionic lock with Arg292^{7.39} thus allowing rotamers to form additional interactions with the sulfonate of AQ ring C. Ring D probably binds in a cavity formed by the aromatic residues Tyr268^{6.58}, Tyr269^{6.59} and Tyr288^{7.35}. Mutation of Tyr269^{6.59} to phenylalanine had resulted in increased potency for small AQ derivatives with lipophilic substitutions on ring E [50]. Ring E likely projects into the putative orthosteric binding site, overlapping with the nucleobase binding cavity of the agonists. Several lipophilic (Leu117^{3.36}) and aromatic residues (Phe113^{3.32}, Tyr114^{3.33}, Phe261^{6.51}, Tyr269^{6.59}) may be involved in stabilizing ring E in the orthosteric binding site. Additional cation- π -interactions are feasible with Arg265^{6.55}. Mutation of Phe113^{3.32} to alanine had no significant effect on the potency of the antagonists except for PSB-1699 (12), which showed a complete loss of antagonistic activity at the F113^{3.32}A mutant (IC_{50} > 10 μ M). In the case of PSB-1699, the distance between Phe113^{3.32} and ring E amounts to approximately 3.6 Å according to our model, which is a reasonable distance for π - π -interactions. In the complexes of the other AQ antagonists, PSB-16133 (10) and PSB-16135 (11), the distance between ring E and Phe113^{3.32} was estimated to be 5.1 Å, leading to the assumption that no π - π -interactions can be formed. π - π -Interactions between ring E of PSB-1699 and Phe113^{3.32} are further supported by the fact that the F113^{3.32}Y mutant showed no decrease in potency (IC_{50} 2770 \pm 654 nM). In our previously published study [50], the Y114^{3.33}F mutation located deep down in the orthosteric binding pocket, had resulted in increased potency of several AQ derivatives, but had no effect on the larger RB-2. The Y114^{3.33}A mutant, on the other hand, had led to significantly decreased potency of RB-2, but had not shown any effect on the potency of small AQ derivatives [50]. This further supports the

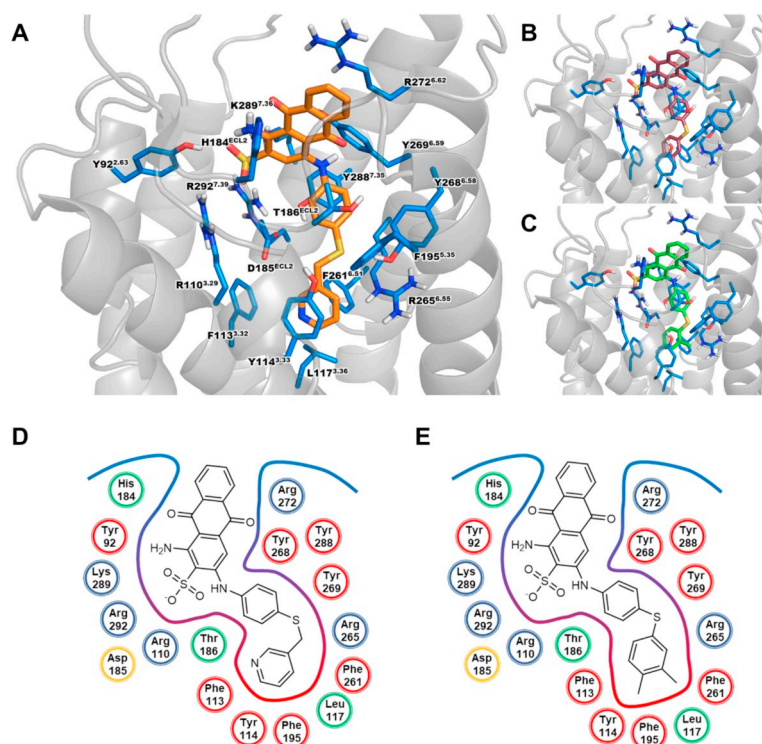


Fig. 17. Putative binding mode of selected AQ-derived antagonists in the homology model of *hP2Y₂R*. **A.** Docked pose of PSB-1699 with the important residues in the binding pocket shown. The *h2Y₂R* (gray) is displayed in cartoon representation, the amino acid residues (blue) and PSB-1699 (orange) are shown as stick models. Oxygen atoms are colored in red, nitrogen atoms in blue, phosphorus atoms in orange, sulfur atoms in yellow. **B.** Binding mode of PSB-16133. **C.** Binding mode of PSB-16135. Schematic 2D representation of the binding pocket of PSB-1699 (**D**) and PSB-16133 (**E**). Charged, basic residues are circled in blue, aromatic residues in red, the conserved aspartic acid residue in ECL2 involved in the ionic lock in yellow, and further residues in the binding pocket in green (in **D**, **E**).

proposed binding mode of small AQ derivatives in the orthosteric binding pocket, but not that of the larger RB-2 having an additional ring F with a charged sulfonate group. A complete loss of inhibitory potency of PSB-1699 was also observed at the F195^{5.35}Y mutant close to the orthosteric binding site ($IC_{50} > 10 \mu\text{M}$), while the potency of RB-2 was decreased (3-fold, $IC_{50} 18.0 \pm 1.54 \mu\text{M}$), and the potency of the other investigated AQ derivatives PSB-09114 (**9**), PSB-16133 (**10**), and PSB-16135 (**11**) remained unaffected ($IC_{50} 2020 \pm 513$, 2660 ± 683 , $4890 \pm 708 \text{ nM}$, respectively). The longer linker in PSB-1699 between ring D and E increases the flexibility of the molecule and may thereby allow π - π -interactions with Phe195^{5.35}. The replacement of the phenylalanine with a tyrosine in the F195^{5.35}Y mutant introduces an additional hydroxy group which reduces the lipophilicity and limits the space in the binding cavity for ring E. As previously proposed by our group, the larger RB-2, with an additional sulfonated ring F, appears to have a different binding mode compared to the smaller AQ derivatives lacking that ring. No final docking predictions for the moderately potent RB-2 at *hP2Y₂R* are provided, as the interactions appear to be complex, and multiple binding modes cannot be excluded.

3.5.3. Agonists at *hP2Y₄R*

3.5.3.1. UTP. UTP displayed an EC_{50} value of $135 \pm 25 \text{ nM}$ at the wt *hP2Y₄R*. UTP is predicted to bind in the upper third part of *P2Y₄R*, close to the ECL2, comparable to its binding mode at *P2Y₂R* (see Fig. 4). According to the model, phosphate groups are accommodated in a negatively charged binding cleft formed by Lys34^{1.31}, Lys289^{7.36}, and Arg292^{7.39}. Residues likely involved in forming hydrogen bonds with the phosphate groups include Asp187^{ECL2}, Tyr268^{6.58}, and Asn285^{7.32}. The 2'- and 3'-hydroxy groups probably form hydrogen bonding interactions with Arg112^{3.29}, and the 5'-hydroxy group might form additional hydrogen bonds with the backbone of Asp185. The oxygen atom of the ribose ring may form a hydrogen bond with Tyr288^{7.35}. The uracil moiety is predicted to bind in a lipophilic region consisting of aromatic (Phe115^{3.32}, Tyr116^{3.33}, Tyr120^{3.37}, Tyr197^{5.35}, Phe200^{5.38}, Phe261^{6.51}) and lipophilic (Leu119^{3.37}, Val204^{5.42}, Met205^{5.43}) residues. Cation- π interactions between the uracil moiety and Arg265^{6.55} are conceivable. Small decreases (2–3-fold, not quite reaching the level of statistical

significance) in UTP potency were observed for the Y197^{5.35}A ($EC_{50} 411 \pm 56 \text{ nM}$) and F200^{5.38}A ($EC_{50} 284 \pm 18 \text{ nM}$) mutants. The Y197^{5.35}F and F200^{5.38}Y mutants with preserved aromatic functionality had no effect on UTP potency, supporting π - π -interactions with the nucleobase (Fig. 4). Arg194^{5.34} of *P2Y₂R* had been reported to be important for agonist potency [50], indicating indirect modulation rather than direct interaction between the agonist and the amino acid side-chain, e.g. by the increased flexibility of the ECL2 resulting in different receptor conformations; it had been proposed to be involved in a second ionic lock distant from Asp185^{ECL2} and Arg292^{7.39}.

A significant change in UTP potency was observed for the mutant of the corresponding amino acid in *P2Y₄R*, R190^{ECL2}A (15-fold decrease in potency, $EC_{50} 1980 \pm 196 \text{ nM}$), while no changes were observed for the E193^{ECL2}A ($EC_{50} 61.6 \pm 5.2 \text{ nM}$) and the D195^{5.33}A/S mutants ($EC_{50} 47.5 \pm 6.6 \text{ nM}$ and $68.6 \pm 12.0 \text{ nM}$, respectively). Although distant from the orthosteric binding site, we could neither confirm Glu193^{ECL2} nor Asp195^{5.33} as major interaction partners for Arg190^{ECL2} to form an ionic lock. Other residues in TM V such as Glu192^{ECL2} might act as ionic interaction partners for Arg190^{ECL2}. Mutation of Asn170^{4.60} of *P2Y₄R*, which is a non-conserved amino acid residue in the *P2Y₂*- and *P2Y₄*Rs, had no effect on UTP potency.

Our docking results support a similar binding mode of UTP at *P2Y₂*- and *P2Y₄*R. In both cases several residues form a highly charged and hydrophilic binding cleft ideally suited for the binding of the phosphate chain, a slightly less hydrophilic binding pocket for the binding of the ribose where Arg^{3.29} (*P2Y₂*-Arg110^{3.29}, *P2Y₄*-Arg112^{3.29}) probably forms bidentate hydrogen bonds with the 2'- and 3'-hydroxy groups, and a lipophilic pocket with an aromatic network as a binding site for the nucleobase.

3.5.3.2. ATP. The wt *hP2Y₄R* is activated by UTP but not by ATP ($EC_{50} > 10 \mu\text{M}$). We were able to introduce ATP-sensitivity into *P2Y₄R* by mutating the large Tyr197^{5.35} to alanine ($EC_{50} 11.9 \pm 1.56 \mu\text{M}$). The tyrosine residue in position 5.35 is conserved in the mouse, rat and human *P2Y₄R*. It is exchanged for a phenylalanine in *P2Y₂R*. However, mutation of Tyr197^{5.35} in *hP2Y₄R* to phenylalanine did not result in ATP recognition. As discussed above, the aromatic side-chain in the 5.35 position might be involved in π - π -interactions with the nucleobase.

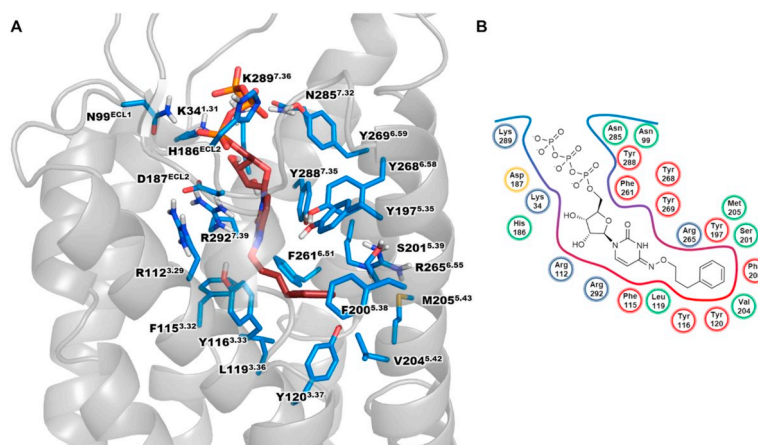


Fig. 18. Putative binding mode of the potent P2Y₄R agonist MRS4062 in the homology model of hP2Y₄R. A. Docked pose of MRS4062 with the important residues in the binding pocket shown. Carbon atoms of MRS4062 are colored in red. B. Schematic 2D representation of the binding pocket. For further color code see Fig. 4.

Similar interactions are likely for Phe195^{5.35} in P2Y₂R with agonists. Our results indicate that Tyr197^{5.35} may be too large and thereby prevent binding of the larger nucleobase adenine of ATP to the P2Y₄R. But Tyr197^{5.35} is not solely responsible for the agonist preferences of the P2Y₄R. ATP-sensitivity of the P2Y₄R-Y197^{5.35}A mutant may also arise from altered flexibility of the ECL2 facilitating the binding of ATP.

The docking results based on the improved homology model indicate that the available space in the orthosteric binding domain is an important factor governing ligand recognition for both investigated receptors. At P2Y₄R, Met205^{5.43} likely appears to be directed towards TM VI, while in P2Y₂R the homologous Met202^{5.42} is directed towards TM IV (see Supplementary Information, Fig. S5). Several rotamer combinations are possible for Met205^{5.43} and Arg265^{6.55} (numbered 265 in both receptors, see Fig. 4), in which they interact through hydrogen bonds resulting in an overall reduced space in the orthosteric binding site. At P2Y₂R, more rotamers of Arg265^{6.55} are conceivable, as Met202^{5.42} projects outwards of the orthosteric binding site, where it can form interactions with Cys164(4.56) and Gln165(4.57). In our previous studies we reported on the role of Arg265^{6.55} and Tyr288^{7.35} of hP2Y₂R in UTP and Ap₄A binding [50]. The R265^{6.55}A and Y288^{7.35}A mutants were both insensitive towards UTP and Ap₄A. Interestingly, UTP was still accepted by the Y288^{7.35}F mutant, while Ap₄A failed to activate that mutant. We measured a volume of 310 Å³ available in the binding site of P2Y₂R, and 220 Å³ in the case of P2Y₄R, which leads to the assumption that the triad of Met202^{5.42}-Arg265^{6.55}-Tyr288^{7.35} induces a rotamer of Arg265^{6.55} in P2Y₂R which provides the required space for binding of adenine nucleotides. The larger available space in the P2Y₄R-Y197^{5.35}A mutant could therefore be a reason for accepting the more spacious agonist ATP, which is completely inactive in the wt P2Y₄R.

3.5.3.3. MRS4062. MRS4062 (5) was found in our experiments to be 7-fold selective for the wt P2Y₄R (EC₅₀ 76.1 ± 10 nM, 100 ± 2% efficacy) versus the wt P2Y₂R (EC₅₀ 535 ± 44 nM, 88 ± 4% efficacy) essentially confirming originally published data [44]. According to the hP2Y₄R model, MRS4062 (5) occupies the same binding pocket as UTP (see Fig. 18). The phosphate groups are proposed to form ionic or hydrogen bonding interactions with Glu31^{N-term}, Lys34^{1.31}, Asn99^{ECL1}, His186^{ECL2}, Asp187^{ECL2}, Tyr268^{6.58}, Arg272^{ECL3}, Asn285^{7.32}, Lys289^{7.36}, and Arg292^{7.39}. In the model, the ribose moiety binds close to TM I and VII, where the 5'-hydroxy group might form hydrogen bonding interactions with Lys34^{1.31}. The uracil moiety likely forms hydrogen bond interactions with Arg292^{7.39}, while other aromatic residues (Phe115^{3.32}, Phe261^{6.51}, Tyr288^{7.35}) may stabilize the nucleobase through π-π-interactions. The phenylpropyl residue is predicted to occupy the nucleobase binding cavity at the bottom of the orthosteric binding site. According to the model, the phenyl group binds close to

several aromatic residues, including Tyr116^{3.33}, Tyr120^{3.37}, Tyr197^{5.35} and Phe200^{5.38}, whereas other residues (Leu119^{3.37}, Val204^{5.42}, Phe261^{6.51}) increase the lipophilicity in the binding cavity. The phenylpropyl group of MRS4062 is accommodated in the putative nucleobase binding domain, and the pyrimidine moiety is shifted in P2Y₄R as in P2Y₂R, leading to similar binding modes in both receptor subtypes. In the P2Y₄R docking studies, MRS4062 displayed a somewhat larger shift towards TM VII than in P2Y₂R. The R190^{ECL2}A mutant showed a significant decrease (16-fold, EC₅₀ 1240 ± 279 nM) in agonist potency compared to the wt P2Y₄R, most likely due to the altered flexibility of the ECL2. Larger decreases in potency were also observed for the Y197^{5.35}A (10-fold, EC₅₀ 757 ± 68 nM) and F200^{5.38}A mutants (9-fold, EC₅₀ 694 ± 69 nM), indicating that the phenylpropyl substitution might contribute to stronger π-π-interactions with the two residues as compared to UTP. This is supported by the Y197^{5.35}F and F200^{5.38}Y mutations, which had no effect on the potency of MRS4062.

Previously, Marouka, Jacobson *et al.*, who had developed MRS4062, reported on its selectivity for hP2Y₄ over P2Y₂R. Based on a homology model of the two receptors generated based on the X-ray crystal structure of the CXCR4 chemokine receptor, they predicted that the phenyl moiety of the N⁴-phenylpropoxy group of MRS4062 projects from the P2Y₄R binding pocket into a cavity formed by the ECL2 surrounded by Thr182^{ECL2} and Leu184^{ECL2}. According to that study, the cavity is surrounded by bulky amino acids, Arg180^{ECL2} and Thr182^{ECL2}, in P2Y₂R which was put forward as a possible explanation for the P2Y₄R-selectivity of MRS4062 [44]. Our current results, based on the recently published X-ray structure of the more closely related P2Y₁R, indicate that MRS4062, like UTP, has a binding mode similar to that observed for nucleotide agonists in the X-ray structure of hP2Y₁₂R [52]. The previous and current mutagenesis data, however, cannot completely explain the P2Y₄R-selectivity of MRS4062.

3.5.4. Antagonists at hP2Y₄R

3.5.4.1. Anthraquinone derivatives. As previously reported, the AQ derivatives had been predicted to bind in the upper third part of hP2Y₄R [47]. The small AQ derivatives were proposed to bind close to the ECL2 where the 2-sulfonate of ring C can interact with charged residues (Lys34^{1.31}, Asp187^{ECL2}, Arg292^{7.39}) comparable to the binding position of the same 2-sulfonate group in P2Y₂R (see Fig. 19). Ring D of AOs is presumably stabilized by interactions with His186^{ECL2} and Tyr288^{7.35}. Ring E may bind close to TM V and VI in a highly aromatic binding pocket formed by Tyr116^{3.33}, Tyr197^{5.35}, Phe200^{5.38}, Tyr269^{6.59}, where it is stabilized through π-π-stacking with, and probably through cation-π-interactions with Arg265^{6.55}. In the case of RB-2, a similar binding mode was proposed. The 3-sulfonate of ring D likely interacts with charged residues (Lys34^{1.31}, Asp187^{ECL2}, Arg292^{7.39}) and ring F was

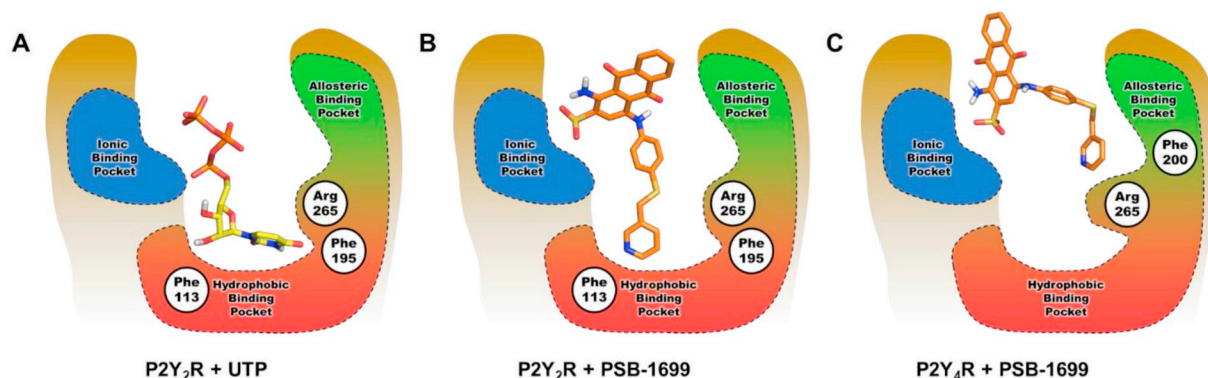


Fig. 19. Comparison of agonist (A) and antagonist binding modes in the P2Y₂- (B) and P2Y₄R pocket (C). Carbon atoms of UTP are colored in yellow, those of PSB-1699 in orange. Negatively charged groups of the ligands interact with a binding cavity consisting of positively charged amino acid residues denoted as 'ionic binding pocket'. The putative orthosteric binding pocket is located beneath ECL2 and consists of lipophilic and aromatic residues of TM III, V, and VI (valine, leucine, phenylalanine, tyrosine). The allosteric binding pocket is formed by residues of the ECL2, TM V and VI and separated by Arg265^{6,55} from the orthosteric binding site. At P2Y₂R, the AQ antagonist can reach the hydrophobic binding pocket, while at P2Y₄R, ring E is predicted to be prevented from reaching the hydrophobic binding site due to steric hindrance, and therefore to bind to an allosteric pocket.

predicted to project towards the aromatic binding pocket where the sulfonate can form ionic interactions with Arg265^{6,55}.

RB-2 as well as its smaller derivatives showed significant decreases in potency at the F200^{5,38}Y-P2Y₄R mutant (3- to > 200-fold). Phe200 is located deep in the aromatic binding pocket where ring E of small AQ derivatives and sulfonate-substituted ring F of RB-2 may bind. The introduction of a hydroxy group in the binding pocket in the case of the F200^{5,38}Y mutant limits the available space and increases the ratio of hydrophilic, solvent-accessible surface area. This is consistent with the proposed docking studies, as the investigated smaller AQ derivatives possess lipophilic substituents at ring E which benefit from hydrophobic interactions with Phe200^{5,38}. The potency of PSB-1699 (12), which contains a longer linker, was most strongly decreased (> 200-fold, IC₅₀ > 10 μM) at the F200^{5,38}Y mutant, since the pyridylmethylthio group may bind deeper in the aromatic binding pocket, thus forming π-π-interactions. Space limitations by the hydroxy group of the F200^{5,38}Y mutant therefore resulted in a much larger decrease in the potency of PSB-1699 as compared to the other AQ derivatives. The mutation of Tyr197^{5,35} to alanine had no negative impact on the potencies of the investigated antagonists. Therefore, we assume that no strong π-π-interactions between Tyr197^{5,35} and aromatic rings of the AQ core structure are formed, which is consistent with our proposed docking position. The Y197^{5,35}F mutation led to a decrease of potency of RB-2 (6), PSB-16133 (10), PSB-16135 (11) and PSB-1699 (12) (4-, 3- to 6-fold). Therefore, hydrogen bond interactions between the hydroxy group of Tyr197^{5,35} and the linker between ring D and E are feasible. The results indicated that the larger RB-2 interacts similarly as the smaller AQ derivatives 9–11 with the P2Y₄R, while it likely has a different binding mode at P2Y₂R.

Again, PSB-1699 (12) shows a different profile than the other AQ derivatives. Here, R190^{ECL2}A and D195^{5,33}A mutation led to a complete loss of potency. The main difference between PSB-1699 and the other investigated AQ antagonists is a longer linker connecting the thioether with ring E, resulting in higher flexibility and at the same time requiring more space in the binding site. Therefore, changes in the flexibility of the ECL2 could greatly affect the potency of PSB-1699. As mentioned above, Arg190^{ECL2} is possibly involved in an ionic lock close to the extracellular space modulating the flexibility of the ECL2. Although only the mutation of Arg190^{ECL2} but not that of Asp195^{5,33} affected the potency of agonists, it is possible that Asp195^{5,33} affects antagonist potency through interactions with other residues by modulating the flexibility of the ECL2. These results, in addition to those described for the Y197^{5,35}A/F and F200^{5,38}A/Y mutants, indicate that PSB-1699 may bind closer to the aromatic binding site based on its longer linker. The orthosteric or allosteric binding mode of small AQ derivatives at P2Y₂- and P2Y₄Rs may thereby be determined by

the structure of ring D and E. Ring E of AQ derivatives can be accommodated in the larger orthosteric site of P2Y₂R, whereas space restrictions likely by a rotamer of Arg265^{6,55} impede the access to the orthosteric binding site of P2Y₄R. Increased flexibility of ring E (in PSB-1699) may allow interactions with amino acid residues close to the orthosteric binding site since the molecule can adapt to the steric constraints.

To confirm the binding mode of PSB-1699 in the P2Y₄R ligand pocket, the mechanism of inhibition was determined by Schild analysis using calcium mobilization assays. With increasing concentrations, competitive antagonists are expected to display a parallel rightward shift of the concentration–response curve of an agonist. In contrast, allosteric, noncompetitive antagonists will decrease the maximal effect of the agonist with or without a significant rightward shift [32,47,61]. Our data suggests PSB-1699 may be an allosteric (non-competitive) inhibitor of hP2Y₄R activation by UTP as increasing concentrations of the antagonist (0.500–50.0 μM) significantly decreased the maximal effect of UTP at the wt hP2Y₄R (from 100 ± 4% to 34 ± 4%) showing little to no significant change in its EC₅₀ value (Fig. 20; see Supplementary Table S6 for EC₅₀ values).

3.5.4.2. AR-C118925. Large decreases in potency of the antagonist AR-C118925 (7), which is moderately potent at P2Y₄R (IC₅₀ 5730 ± 821 nM), were observed at the N170^{4,60}V, D195^{5,33}S and F200^{5,38}Y mutants (> 15-fold, IC₅₀ > 10 μM) of P2Y₄R, minor changes resulted from the R190^{ECL2}A, E193^{ECL2}A, Y197^{5,35}F, and F200^{5,38}A mutations. An increase in potency was seen for the D195^{5,33}A and Y197^{5,35}A mutants (3- to 4-fold). Asn170^{4,60} is placed in TM IV very close to the nucleotide binding pocket. The homology model and docking results suggest that hydrogen bonds may be formed with Tyr116^{3,33}, leading to the assumption that Asn170^{4,60} is involved in regulation of the aromatic network. Increases in space in the binding pocket through mutation of Tyr197^{5,35} or Phe200^{5,38} to alanine had no negative impact on the potency of AR-C118925. The substitution with the respective other aromatic amino acid (Y197^{5,35}F, F200^{5,38}Y) led to a 2-fold (IC₅₀ 9790 ± 884 nM) and > 20-fold (IC₅₀ > 10 μM) decrease in potency, respectively, indicating that hydrogen bonds affected the binding of AR-C118925 to the P2Y₄R. Tyr197^{5,35} and Phe200^{5,38} may modulate the flexibility of the ECL2, which could also explain the effects of charged amino acids present in the ECL2 (Arg190^{ECL2}, Glu193^{ECL2}, Asp195^{5,33}) on the potency of AR-C118925. The selectivity of AR-C118925 for P2Y₂R versus P2Y₄R may be explained through increased lipophilicity or favorable aromatic stacking in the binding cavity for the dibenzocycloheptenyl moiety, as Asn170^{4,60} of P2Y₄R is replaced by a valine, and Tyr197^{5,35} by phenylalanine in P2Y₂R.

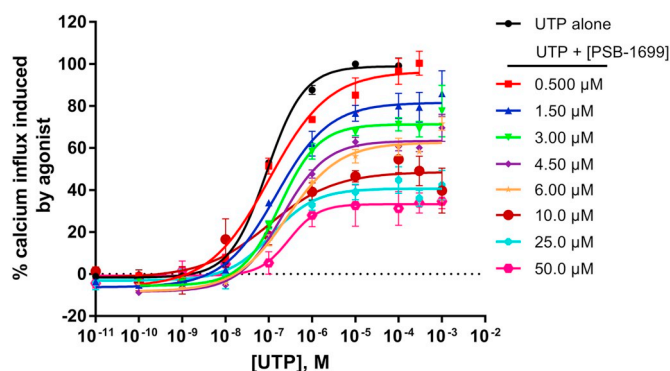


Fig. 20. Concentration–response curves of UTP at the wt *hP2Y₄R* after preincubation with fixed concentrations of PSB-1699 determined using the calcium mobilization assay. The receptor was stably expressed in 1321 N1 astrocytoma cells. Each data point represents mean \pm SEM of 3–4 independent determinations each in duplicates. In the presence of increasing concentrations of PSB-1699, the maximal effect of UTP was decreased whereas the EC_{50} values were hardly affected (one-way ANOVA with Dunnett's post-hoc test). The EC_{50} values and maximum effects of UTP are shown in Supporting Information Table S6.

4. Conclusions

Docking and mutagenesis results suggest a binding mode of agonists at *P2Y₂*- and *P2Y₄R* comparable to that of agonists in the crystal structure of *hP2Y₁₂R* [52], where the phosphate groups interact with negatively charged residues, and a lipophilic binding pocket accommodates the nucleobase. The putative agonist binding mode of *P2Y₂*- and *P2Y₄R* differs from the one observed in the crystal structure of *hP2Y₁R* in complex with the nucleotide antagonist MRS2500 (13) [49]. The agonists UTP (1) and ATP (2) contain a 5'-triphosphate chain, while the *P2Y₁R* antagonist MRS2500 (13) of the crystal structure bears single phosphate groups in the 3'- and 5'-position of the ribose moiety, which is the probable reason for different binding modes. We were able to elucidate the role of Asp185^{ECL2} of *P2Y₂R*, which likely forms an ionic lock with an arginine in TM VII. UTP and ATP share a common pharmacological profile of full agonists at *P2Y₂R*, while Ap₄A (3) and MRS4062 (5) acting as partial agonists, appear to induce a different active receptor conformer. Phe113^{3,32} and Asp185^{ECL2} play a key role in receptor activation by Ap₄A and MRS4062, since mutation of both amino acid residues resulted in a complete loss of receptor activation by agonists 3 and 5, in contrast to UTP and ATP. The charged residues Arg190^{ECL2}, Glu193^{ECL2} and Asp195^{5,33}, predicted to be distant from the putative ligand binding site of *P2Y₄R*, affected the potency of agonists and antagonists when mutated to alanine, which is consistent with previous observations for *hP2Y₂R*. Ligand recognition is therefore not only limited to the orthosteric binding site but can also be altered through interactions between residues close to the ECL2, which may affect loop flexibility. The binding mode of both, agonists and antagonists, may be determined through an aromatic network consisting of residues of TM III, V and VI. The *P2Y₂R* may be privileged to accept ATP and other adenine nucleotide-derived agonists due to a more spacious nucleobase binding cavity, as the increase in space in the orthosteric binding site of the *P2Y₄R*-Y197^{5,35}A mutant resulted in reintroduction of ATP-sensitivity.

The investigated AQ antagonists share a similar binding cavity for the AQ core, whereas substituents (rings D and E) of PSB-1699, PSB-16133 and PSB-16135 project towards an allosteric binding domain in *P2Y₄R*. The antagonist PSB-1699 appears to form additional interactions with aromatic residues of *P2Y₄R* (Phe200^{5,38}), and with aromatic residues close to the putative orthosteric binding site (Phe113^{3,32}) and close to the ECL2 (Phe195^{5,35}) of *P2Y₂R* due to its longer linker in comparison to the other investigated AQ derivatives. The binding modes of smaller AQ derivatives at *P2Y₂*- and *P2Y₄R*s might therefore be dependent on the structure and flexibility of ring E, as well as the available space in the

binding cavities resulting in either orthosteric or allosteric binding.

The antagonist AR-C118925 likely binds to the orthosteric site of both receptor subtypes. The ECL2 possibly plays a key role in binding of AR-C118925 in the case of *P2Y₄R* while no similar observation has been made for the investigated mutants of *P2Y₂R*. The selectivity for *P2Y₂R* could be explained by increased lipophilicity in the binding pocket resulting in tighter binding and stronger π - π -stacking.

Altogether, the data from the current work provides further insights into the architecture of ligand–receptor interactions and ligand selectivity of *P2Y₂*- and *P2Y₄R*s. Docking studies at homology models predicted key residues with direct ligand interactions and those remote to the orthosteric binding site for developing novel therapeutics. These findings, supported by mutagenesis and pharmacological studies, and the refined homology models will aid future rational structure-based ligand design for *P2Y₂*- and *P2Y₄R*s for both of which potent and selective ligands are badly needed to perform target validation studies.

Declaration of Competing Interests

The authors declare that they have no known competing financial interests or personal relationships that could have appeared to influence the work reported in this paper.

Acknowledgements

This study was supported by the German Research Foundation (DFG, Research Training group GRK 1873) and by the Federal Ministry of Education and Research (BMBF, project BIGS DrugS). I.A. obtained a PhD scholarship by the Deutscher Akademischer Austauschdienst (DAAD). Y.B. is grateful for an SQU grant (SR/SCI/CHEM/15/01).

Appendix A. Supplementary data

Supplementary material.

References

- [1] G. Burnstock, M. Williams, P2 purinergic receptors: modulation of cell function and therapeutic potential, *J. Pharmacol. Exp. Ther.* 295 (2000) 862–869.
- [2] A. Brunschweiler, C.E. Müller, P2 receptors activated by uracil nucleotides—an update, *Curr. Med. Chem.* 13 (2006) 289–312.
- [3] K.A. Jacobson, C.E. Müller, Medicinal chemistry of adenosine, P2Y and P2X receptors, *Neuropharmacology* 104 (2016) 31–49.
- [4] G. Burnstock, Purinergic receptors, *J. Theor. Biol.* 62 (1976) 491–503.
- [5] K.A. Jacobson, J.M. Boeynaems, P2Y nucleotide receptors: promise of therapeutic applications, *Drug Discov. Today* 15 (2010) 570–578.
- [6] P. Savi, J.M. Herbert, Clopidogrel and ticlopidine: P2Y₁₂ adenosine diphosphate-receptor antagonists for the prevention of atherothrombosis, *Semin. Thromb. Hemost.* 31 (2005) 174–183.
- [7] D.J. Angiolillo, J.L. Ferreira, Platelet adenosine diphosphate P2Y₁₂ receptor antagonism: benefits and limitations of current treatment strategies and future directions, *Rev. Esp. Cardiol.* 63 (2010) 60–76.
- [8] Y. Baqi, C.E. Müller, Antithrombotic P2Y₁₂ receptor antagonists: recent developments in drug discovery, *Drug Discov. Today* 6446 (2018).
- [9] M. Rafehi, C.E. Müller, Tools and drugs for uracil nucleotide-activated P2Y receptors, *Pharmacol. Ther.* 190 (2018) 24–80.
- [10] G.P. Connolly, P.J. Harrison, T.W. Stone, Action of purine and pyrimidine nucleotides on the rat superior cervical ganglion, *Br. J. Pharmacol.* 110 (1993) 1297–1304.
- [11] G.P. Connolly, N.J. Abbott, C. Demaine, J.A. Duley, Investigation of receptors responsive to pyrimidines, *Trends Pharmacol. Sci.* 18 (1997) 413–414.
- [12] P. Hillmann, G.Y. Ko, A. Spinrath, A. Raulf, I. von Kügelgen, S.C. Wolff, R.A. Nicholas, E. Kostenis, H.D. Höltje, C.E. Müller, Key determinants of nucleotide-activated G protein-coupled P2Y₂ receptor function revealed by chemical and pharmacological experiments, mutagenesis and homology modeling, *J. Med. Chem.* 52 (2009) 2762–2775.
- [13] J. Pintor, A. Peral, C.H.V. Hoyle, C. Redick, J. Douglass, I. Sims, B. Yerxa, Effects of diadenosine polyphosphates on tear secretion in new zealand white rabbits, *J. Pharmacol. Exp. Ther.* 300 (2002) 291–297.
- [14] D.J. Moore, J.K. Chambers, J.P. Wahlin, K.B. Tan, G.B. Moore, O. Jenkins, P.C. Emson, P.R. Murdock, Expression pattern of human P2Y receptor subtypes: a quantitative reverse transcription-polymerase chain reaction study, *Biochim. Biophys. Acta* 1521 (2001) 107–119.
- [15] A.M. Wong, A.W. Chow, S.C. Au, C.C. Wong, W.H. Ko, Apical versus basolateral P2Y₆ receptor-mediated Cl⁻ secretion in immortalized bronchial epithelia, *Am. J.*

- Respir. Cell Mol. Biol. 40 (2009) 733–745.
- [16] J.B. Regard, I.T. Sato, S.R. Coughlin, Anatomical profiling of G protein-coupled receptor expression, *Cell* 135 (2009) 561–571.
- [17] M. León-Otegui, R. Gómez-Villafuertes, J.I. Díaz-Hernández, M. Díaz-Hernández, M.T. Miras-Portugal, J. Gualix, Opposite effects of P2X7 and P2Y2 nucleotide receptors on α -secretase-dependent APP processing in Neuro-2a cells, *FEBS Lett.* 585 (2011) 2255–2262.
- [18] B.R. Yerxa, J.R. Sabater, C.W. Davis, M.J. Stutts, M. Picher, A.C. Jones, M. Cowlen, Pharmacology of INS37217 [P^1 -(uridine 5')- P^1 -(2'-deoxycytidine 5') tetraphosphate, tetrasodium salt], a next-generation P2Y2 receptor agonist for the treatment of cystic fibrosis, *J. Pharmacol. Exp. Ther.* 302 (2002) 871–880.
- [19] K.K. Nichols, B. Yerxa, D.J. Kellerman, Diquafosol tetrasodium: a novel dry eye therapy, *Expert Opin. Investig. Drugs* 13 (2004) 47–54.
- [20] R. Deterding, G. Retsch-Bogart, L. Milgram, R. Gibson, C. Daines, P.L. Zeitlin, C. Milla, B. Marshall, L. LaVange, J. Engels, D. Mathews, J. Gorden, A. Schaberg, J. Williams, B. Ramsey, Safety and tolerability of denofosol tetrasodium inhalation solution, a novel P2Y2 receptor agonist: results of a phase 1/phase 2 multicenter study in mild to moderate cystic fibrosis, *Pediatr. Pulmonol.* 39 (2005) 339–348.
- [21] G.M. Keating, Diquafosol ophthalmic solution 3%: a review of its use in dry eye, *Drugs* 75 (2015) 911–922.
- [22] R.B. Moss, Pitfalls of drug development: lessons learned from trials of denofosol in cystic fibrosis, *J. Pediatr.* 162 (2013) 676–680.
- [23] L. Erb, C. Cao, D. Ajit, G.A. Weisman, P2Y receptors in Alzheimer's disease, *Biol. Cell.* 107 (2015) 1–21.
- [24] E. Hochhauser, R. Cohen, M. Waldman, A. Maksin, A. Isak, D. Aravot, P.S. Jayasekara, C.E. Müller, K.A. Jacobson, A. Shainberg, P2Y2 receptor agonist with enhanced stability protects the heart from ischemic damage in vitro and in vivo, *Purinergic Signal* 9 (2013) 633–642.
- [25] R. Cohen, A. Shainberg, E. Hochhauser, Y. Cheporoko, A. Tobar, E. Birk, L. Pinhas, J. Leipziger, J. Don, E. Porat, UTP reduces infarct size and improves mice heart function after myocardial infarct via P2Y2 receptor, *Biochem. Pharmacol.* 82 (9) (2011) 1126–1133.
- [26] D. Schumacher, B. Strilic, K.K. Sivaraj, N. Wettschreck, S. Offermanns, Platelet-derived nucleotides promote tumor-cell transendothelial migration and metastasis via P2Y2 receptor, *Cancer Cell* 24 (2013) 130–137.
- [27] D. Ajit, L.T. Woods, J.M. Camden, C.N. Thebeau, F.G. El-Sayed, G.W. Greeson, L. Erb, M.J. Petris, D.C. Miller, G.Y. Sun, G.A. Weisman, Loss of P2Y2 nucleotide receptors enhances early pathology in the TgCRND8 mouse model of Alzheimer's disease, *Mol. Neurobiol.* 49 (2014) 1031–1042.
- [28] C. S  r, M.-T. Melki, F. Subra, S.Q. Raza, M. Bras, H. Saïdi, R. Nardacci, L. Voisin, A. Paoletti, F. Law, I. Martins, A. Amendola, A.A. Abdul-Sater, F. Ciccosanti, O. Delelis, F. Niedergang, S. Thierry, N. Said-Sadier, C. Lamaze, D. M  tivier, J. Estaquier, G.M. Fimia, L. Falasca, R. Casetti, N. Modjtahedi, J. Kanellopoulos, J.-F. Mouscadet, D.M. Ojcius, M. Piacentini, M.-L. Gougeon, G. Kroemer, J.-L. Perfettini, Extracellular ATP acts on P2Y2 purinergic receptors to facilitate HIV-1 infection, *J. Exp. Med.* 208 (2011) 1823–1834.
- [29] S.A. Pothoff, J. Stegbauer, J. Becker, P.J. Wagnenhaus, B. Duvnjak, L.C. Rump, O. Vonend, P2Y2 receptor deficiency aggravates chronic kidney disease progression, *Front. Physiol.* 4 (2013) 1–9.
- [30] B.K. Kishore, N.G. Carlson, C.M. Ecelbarger, D.E. Kohan, C.E. M  ller, R.D. Nelson, J. Peti-Peterdi, Y. Zhang, Targeting renal purinergic signalling for the treatment of lithium-induced nephrogenic diabetes insipidus, *Acta Physiol.* 214 (2015) 176–188.
- [31] J. Merz, P. Albrecht, S. von Garlen, I. Ahmed, D. Dimanski, D. Wolf, I. Hilgendorf, C. H  rdtner, K. Grotius, F. Willecke, T. Heidt, H. Bugger, N. Hoppe, U. Kintscher, C. von zur M  hlen, M. Idzko, C. Bode, A. Zirlirk, P. Stachon, Purinergic receptor Y2 (P2Y2)-dependent VCAM-1 expression promotes immune cell infiltration in metabolic syndrome, *Basic Res. Cardiol.* 113 (2018) 45.
- [32] M. Rafehi, J.C. Burbiel, I.Y. Attah, A. Abdelrahman, C.E. M  ller, Synthesis, characterization, and in vitro evaluation of the selective P2Y2 receptor antagonist AR-C118925, *Purinergic Signal* 13 (2016) 89–103.
- [33] P.A. Kemp, R.A. Sugar, A.D. Jackson, Nucleotide-mediated mucin secretion from differentiated human bronchial epithelial cells, *Am. J. Respir. Cell Mol. Biol.* 31 (2004) 446–455.
- [34] N. Kinton, A. Davis, I. Dougall, J. Dixon, T. Johnson, I. Walters, S. Thom, K. McKechnie, P. Meghani, M.J. Stocks, From utp to ar-c118925, the discovery of a potent non nucleotide antagonist of the p2y2receptor, *Bioorganic Med. Chem. Lett.* 27 (2017) 4849–4853.
- [35] J.E. Matos, B. Robaye, J.M. Boeynaems, R. Beauwens, J. Leipziger, K⁺ secretion activated by luminal P2Y2 and P2Y4 receptors in mouse colon, *J. Physiol.* 564 (2005) 269–279.
- [36] E. Ghanem, B. Robaye, T. Leal, J. Leipziger, W. Van Driessche, R. Beauwens, J.-M. Boeynaems, The role of epithelial P2Y2 and P2Y4 receptors in the regulation of intestinal chloride secretion, *Br. J. Pharmacol.* 146 (2005) 364–369.
- [37] M.M. Ward, T. Puthussery, E.L. Fletcher, Localization and possible function of P2Y4 receptors in the rodent retina, *Neuroscience* 155 (2008) 1262–1274.
- [38] M.D. Tran, P2 receptor stimulation induces amyloid precursor protein production and secretion in rat cortical astrocytes, *Neurosci. Lett.* 492 (2011) 155–159.
- [39] B. Robaye, E. Ghanem, F. Wilkin, D. Fokan, W. Van Driessche, S. Schurmans, J.-M. Boeynaems, R. Beauwens, Loss of nucleotide regulation of epithelial chloride transport in the jejunum of P2Y4-null mice, *Mol. Pharmacol.* 63 (2003) 777–783.
- [40] H. Li, C. Chen, Y. Dou, H. Wu, Y. Liu, H.-F. Lou, J. Zhang, X. Li, H. Wang, S. Duan, P2Y4 receptor-mediated pycnosis contributes to amyloid beta-induced self-up-take by microglia, *Mol. Cell. Biol.* 33 (2013) 4282–4293.
- [41] F. Cavaliere, S. Amadio, D.F. Angelini, G. Sancesario, G. Bernardi, C. Volont  , Role of the metabotropic P2Y4 receptor during hypoglycemia: cross talk with the ionotropic NMDAR1 receptor, *Exp. Cell Res.* 300 (2004) 149–158.
- [42] M. Horckmans, H. Esfahani, C. Beauloye, S. Clouet, L. di Pietrantonio, B. Robaye, J.-L. Balligand, J.-M. Boeynaems, C. Dessy, D. Communi, Loss of Mouse P2Y4 nucleotide receptor protects against myocardial infarction through endothelin-1 downregulation, *J. Immunol.* 194 (2015) 1874–1881.
- [43] A. Lemaire, M. Vanorl  , M. Horckmans, L. di Pietrantonio, S. Clouet, B. Robaye, J.-M. Boeynaems, D. Communi, Mouse P2Y4 nucleotide receptor is a negative regulator of cardiac adipose-derived stem cell differentiation and cardiac fat maturation, *Stem Cells Dev.* 26 (2017) 363–373.
- [44] H. Maruoka, M.P.S. Jayasekara, M.O. Barrett, D.A. Franklin, S. De Castro, N. Kim, S. Costanzi, T.K. Harden, K.A. Jacobson, Pyrimidine nucleotides with 4-alkyloxymino and terminal tetraphosphate δ -ester modifications as selective agonists of the P2Y4 receptor, *J. Med. Chem.* 54 (2011) 4018–4033.
- [45] G. Lambrecht, K. Braun, M. Damer, M. Ganso, C. Hildebrandt, H. Ullmann, M.U. Kassack, P. Nickel, Structure-activity relationships of suramin and pyridoxal-5'-phosphate derivatives as P2 receptor antagonists, *Curr. Pharm. Des.* 8 (2002) 2371–2399.
- [46] I. von K  gelgen, K. Hoffmann, Pharmacology and structure of P2Y receptors, *Neuropharmacology* 104 (2016) 50–61.
- [47] M. Rafehi, E.M. Malik, A. Neumann, A. Abdelrahman, T. Hanck, V. Namasivayam, C.E. M  ller, Y. Baqi, Development of potent and selective antagonists for the UTP-activated P2Y4 receptor, *J. Med. Chem.* 60 (2017) 3020–3038.
- [48] K. Zhang, Z.-G. Gao, D. Zhang, L. Zhu, G.W. Han, S.M. Moss, S. Paoletta, E. Kiselev, W. Lu, G. Fenalti, W. Zhang, C.E. M  ller, H. Yang, H. Jiang, V. Cherezov, V. Katritch, K.A. Jacobson, R.C. Stevens, B. Wu, Q. Zhao, Structure of the human P2Y12 receptor in complex with an antithrombotic drug, *Nature* 509 (2014) 115–118.
- [49] D. Zhang, Z.-G. Gao, K. Zhang, E. Kiselev, S. Crane, J. Wang, S. Paoletta, C. Yi, L. Ma, W. Zhang, G.W. Han, H. Liu, V. Cherezov, V. Katritch, H. Jiang, R.C. Stevens, K.A. Jacobson, Q. Zhao, B. Wu, Two disparate ligand-binding sites in the human P2Y1 receptor, *Nature* 520 (2015) 317–321.
- [50] M. Rafehi, A. Neumann, Y. Baqi, E.M. Malik, M. Wiese, V. Namasivayam, C.E. M  ller, Molecular recognition of agonists and antagonists by the nucleotide-activated G protein-coupled P2Y2 receptor, *J. Med. Chem.* 60 (2017) 8425–8440.
- [51] B. Webb, A. Sali, Protein structure modeling with modeller, *Humana Press*, New York, NY, 2017, pp. 39–54.
- [52] J. Zhang, K. Zhang, Z.-G. Gao, S. Paoletta, D. Zhang, G.W. Han, T. Li, L. Ma, W. Zhang, C.E. M  ller, H. Yang, H. Jiang, V. Cherezov, V. Katritch, K.A. Jacobson, R.C. Stevens, B. Wu, Q. Zhao, Agonist-bound structure of the human P2Y12 receptor, *Nature* 509 (2014) 119–122.
- [53] A. Bateman, M.J. Martin, C. O'Donovan, M. Magrane, E. Alpi, R. Antunes, B. Bely, M. Bingley, C. Bonilla, R. Britto, B. Bursteinas, H. Bye-AJee, A. Cowley, A. Da Silva, M. De Giorgi, T. Dogan, F. Fazzini, L.G. Castro, L. Figueira, P. Garmiri, G. Georghiou, D. Gonzalez, E. Hatton-Ellis, W. Li, W. Liu, R. Lopez, J. Luo, Y. Lussi, A. MacDougall, A. Nightingale, B. Palka, K. Pichler, D. Poggioli, S. Pundir, L. Purga, G. Qi, S. Rosanoff, R. Saidi, T. Sawford, A. Shyptsyna, E. Speretta, E. Turner, N. Tyagi, V. Volynkin, T. Wardell, K. Warner, X. Watkins, R. Zaru, H. Zellner, I. Xenarios, L. Bougueleret, A. Bridge, S. Poux, N. Redaschi, L. Aimo, G. Argoud-Puy, A. Auchincloss, K. Axelsen, P. Bansal, D. Baratin, M.C. Blatter, B. Boeckmann, J. Bolleman, E. Boutet, L. Breuza, C. Casal-Casas, E. De Castro, E. Coudert, B. Cuche, M. Doche, D. Dornevil, S. Duvaud, A. Estreicher, L. Famiglietti, M. Feuermann, E. Gasteiger, S. Gehant, V. Gerritsen, A. Gos, N. Gruaz-Gumowski, U. Hinz, C. Hulo, F. Junco, G. Keller, V. Lara, P. Lemercier, D. Lieberherr, T. Lombardot, X. Martin, P. Masson, A. Morgat, T. Neto, N. Nouspikel, S. Paesano, I. Pedruzzi, S. Pilbout, M. Pozzato, M. Pruess, C. Rivoire, B. Roehert, M. Schneider, C. Sigrist, K. Sonesson, S. Staehli, A. Stutz, S. Sundaram, M. Tognolli, L. Verbregue, A.L. Veuthey, C.H. Wu, C.N. Arighi, L. Arminski, C. Chen, Y. Chen, J.S. Garavelli, H. Huang, K. Laiho, P. McGarvey, D.A. Natale, K. Ross, C.R. Vinayaka, Q. Wang, Y. Wang, L.S. Yeh, J. Zhang, UniProt: the universal protein knowledgebase, *Nucleic Acids Res.* 45 (2017) D158–D169.
- [54] L. Erb, R. Garrad, Y. Wang, T. Quinn, J.T. Turner, G.A. Weisman, Site-directed mutagenesis of P2U purinoceptors: positively charged amino acids in transmembrane helices 6 and 7 affect agonist potency and specificity, *J. Biol. Chem.* (1995) 4185–4188.
- [55] C.L. Herold, A.D. Qi, T.K. Harden, R.A. Nicholas, Agonist versus antagonist action of ATP at the P2Y4 receptor is determined by the second extracellular loop, *J. Biol. Chem.* 279 (2004) 11456–11464.
- [56] P.J. Conn, A. Christopoulos, C.W. Lindsley, Allosteric modulators of GPCRs: a novel approach for the treatment of CNS disorders, *Nat. Rev. Drug Discov.* 8 (2009) 41–54.
- [57] S. Yuan, H.C.S. Chan, H. Vogel, S. Filipek, R.C. Stevens, K. Palczewski, The molecular mechanism of P2Y1 receptor activation, *Angew. Chemie Int. Ed.* 55 (2016) 10331–10335.
- [58] C. Hoffmann, S. Moro, R.A. Nicholas, T.K. Harden, K.A. Jacobson, C. Hill, N. Carolina, The role of amino acids in extracellular loops of the human P2Y1 receptor in surface expression and activation processes, *J. Biol. Chem.* 274 (1999) 14639–14647.
- [59] T. Kenakin, Differences between natural and recombinant G-protein-coupled receptor systems with varying receptor G-protein stoichiometry, *Trends Pharmacol. Sci.* 18 (1997) 456–464.
- [60] T.L. Kinzer-Ursem, J.J. Linderman, Both ligand- and cell-specific parameters control ligand agonism in a kinetic model of G protein-coupled receptor signaling, *PLoS Comput. Biol.* 3 (2007) 0084–0094.
- [61] T. Kenakin, S. Jenkinson, C. Watson, Determining the potency and molecular mechanism of action of insurmountable antagonists, *J. Pharmacol. Exp. Ther.* 319 (2006) 710–723.

5.3. Supporting Information

Supplementary information

Ligand binding and activation of UTP-activated G protein-coupled P2Y₂ and P2Y₄ receptors elucidated by mutagenesis, pharmacological and computational studies

Isaac Y. Attah,^{1,x,#} Alexander Neumann,^{1,#} Haneen Al-Hroub,¹ Muhammad Rafehi,¹ Younis Baqi,^{1,2} Vigneshwaran Namasivayam¹ and Christa E. Müller^{1*}

¹PharmaCenter Bonn, Pharmaceutical Institute, Pharmaceutical Sciences Bonn (PSB),
Pharmaceutical & Medicinal Chemistry, University of Bonn, Germany

²Department of Chemistry, Faculty of Science, Sultan Qaboos University, PO Box 36, Postal Code
123, Muscat, Oman

^xPresent address: Department of Biomedical Sciences, School of Health and Allied Sciences,
University of Cape Coast, Cape Coast, Ghana

[#]Equal contribution

*Address correspondence to:

Dr. Christa E. Müller,

Pharmazeutisches Institut, Pharmazeutische Chemie I,

An der Immenburg 4, D-53121 Bonn, Germany.

Phone: +49-228-73-2301. Fax: +49-228-73-2567.

E-mail address: christa.mueller@uni-bonn.de

Table of Contents

Supplementary Table S1. Cell surface expression of P2Y ₂ and P2Y ₄ receptors.....	3
Supplementary Table S2. Potencies of agonists at the <i>h</i> P2Y ₂ receptor mutants.....	3
Supplementary Table S3. Potencies of agonists at the <i>h</i> P2Y ₄ receptor mutants.....	4
Supplementary Table S4. Potencies of antagonists at the <i>h</i> P2Y ₂ receptor mutants.....	6
Supplementary Table S5. Potencies of antagonists at the <i>h</i> P2Y ₄ receptor mutants.....	7
Supplementary Table S6. Potencies and maximal efficacy for the UTP concentration-response curves determined by calcium assay at the wt <i>h</i> P2Y ₄ receptor after pre-incubation with fixed concentration of PSB-1699.....	9
Supplementary Figure S1. Sequence alignment of the <i>h</i> P2Y ₂ and the <i>h</i> P2Y ₄ receptors.....	10
Supplementary Figure S2. Antagonist-induced inhibition curves of P2Y ₂ receptor (wt and mutants) activation by UTP.....	11
Supplementary Figure S3. Reactive blue-2, AR-C118925 and PSB-09114 inhibition curves of UTP-induced P2Y ₄ receptor (wt and mutants) activation.....	12
Supplementary Figure S4. PSB-16133, PSB-16135 and PSB-1699 inhibition curves of UTP-induced P2Y ₄ receptor (wt and mutants) activation.....	13
Supplementary Figure S5. Comparison of selected residues close to the putative orthosteric binding site in the homology models of <i>h</i> P2Y ₂ and <i>h</i> P2Y ₄ receptors.....	14

Supplementary Table S1. Cell surface expression of P2Y₂ and P2Y₄ receptors ^a

Cell line	% Expression ± SEM (%) ^b	n
P2Y ₂		
wt	100	3
R110A	74 ± 4 **	3
F113A	125 ± 10 **	3
F113Y	16 ± 1 ****	3
D185A	105 ± 9 ^{ns}	3
F195Y	95 ± 8 ^{ns}	3
P2Y ₄		
wt	100	3
N170V	73 ± 13 **	3
R190A	65 ± 6 ****	4
E193A	86 ± 7 ^{ns}	4
D195A	132 ± 14 **	4
D195S	90 ± 15 ^{ns}	3
Y197A	56 ± 2 ****	4
Y197F	65 ± 5 ****	4
F200A	84 ± 7 ^{ns}	3
F200Y	144 ± 6 ****	3

^a Data represent means ± SEM of 3-4 independent experiments (n). Cell surface receptor expression levels were determined by ELISA using antibodies that interacted with the receptors' N-terminal-HA tag. Expression of the respective wildtype (wt) receptor was set at 100 %. ^b One-way ANOVA with Dunnett's post-hoc test: ^{ns} not significant; * p ≤ 0.05; ** p ≤ 0.01; *** p ≤ 0.001; **** p ≤ 0.0001.

Supplementary Table S2. Potencies of agonists at the hP2Y₂ receptor mutants as determined in intracellular calcium mobilization assays. ^a

Cell line	EC ₅₀ (μM) ± SEM ^b	n	% Efficacy (± SEM) ^b	EC ₅₀ mutant/EC ₅₀ wt
UTP (1)				
P2Y ₂ -wt	0.0822 ± 0.0059	5	100	1
R110A	>100	6	n.d ^c	>1200
F113A	25.0 ± 2.7 ****	3	170 ± 12 ****	304
F113Y	0.0526 ± 0.0183 ^{ns}	5	33 ± 2 ****	0.6
D185A	0.606 ± 0.076 ***	4	116 ± 7 ^{ns}	7

F195Y	0.0233 ± 0.0064 **	4	104 ± 3 ^{ns}	0.3
ATP (2)				
P2Y ₂ -wt	0.102 ± 0.010	6	100 ± 2	1
R110A	>100	6	n.d. ^c	>980
F113A	20.5 ± 4.2****	3	185 ± 16****	201
F113Y	0.219 ± 0.044 ^{ns}	5	31 ± 7****	2
D185A	2.160 ± 0.454 ****	5	100 ± 9 ^{ns}	21
F195Y	0.203 ± 0.057 ^{ns}	4	92 ± 7 ^{ns}	2
Ap₄A (3)				
P2Y ₂ -wt	0.0695 ± 0.0065	4	88 ± 3	1
R110A	>100	6	n.d. ^c	>1400
F113A	>100	5	n.d. ^c	>1400
F113Y	>100	5	16 ± 4****	>1400
D185A	>100	5	9 ± 7****	>1400
F195Y	0.194 ± 0.043 ***	5	67 ± 8 *	3
MRS4062 (5)				
P2Y ₂ -wt	0.535 ± 0.044	4	88 ± 4	1
R110A	>100	6	n.d. ^c	>187
F113A	>100	5	n.d. ^c	>187
F113Y	0.0546 ± 0.0145 ****	4	20 ± 2 ****	0.1
D185A	>100	5	7 ± 3 ****	>187
F195Y	0.178 ± 0.027 ***	5	71 ± 3 ***	0.3

^a Data represent means ± SEM of 3-6 independent experiments each in duplicates. ^b Results of One-way ANOVA with Dunnett's post-hoc test: ^{ns} not significant; * p ≤ 0.05; ** p ≤ 0.01; *** p ≤ 0.001; **** p ≤ 0.0001. ^c no concentration-dependent activation up to 100 μM; n.d. = not determined.

Supplementary Table S3. Potencies of agonists at the hP2Y₄ receptor mutants as determined in intracellular calcium mobilization assays.^a

Cell line	EC ₅₀ (μM) ± SEM ^b	n	% Efficacy (± SEM) ^b	EC ₅₀ mutant/EC ₅₀ wt
UTP (1)				
P2Y ₄ - wt	0.135 ± 0.025	3	100	1
N170V	0.259 ± 0.075 ^{ns}	5	72 ± 8 *	2
R190A	1.98 ± 0.20 ****	3	53 ± 6 ***	15
E193A	0.0616 ± 0.0052 ^{ns}	3	100 ± 8 ^{ns}	0.5
D195A	0.0475 ± 0.0066 ^{ns}	3	83 ± 5 ^{ns}	0.4

D195S	0.0686 ± 0.0120 ^{ns}	4	80 ± 6 ^{ns}	0.5
Y197A	0.411 ± 0.056 ^{ns}	4	56 ± 6 ^{***}	3
Y197F	0.0844 ± 0.0120 ^{ns}	3	75 ± 1 ^{ns}	0.6
F200A	0.284 ± 0.018 ^{ns}	3	24 ± 5 ^{****}	2
F200Y	0.0471 ± 0.0064 ^{ns}	3	106 ± 9 ^{ns}	0.3
ATP (2)				
P2Y ₄ - wt	>100	3	n.d ^c	n.d ^c
N170V	>100	5	4 ± 2 ^{ns}	n.d ^c
R190A	>100	4	n.d ^c	n.d ^c
E193A	>100	4	n.d ^c	n.d ^c
D195A	>100	4	n.d ^c	n.d ^c
D195S	>100	5	5 ± 3 ^{ns}	n.d ^c
Y197A	11.9 ± 1.6 ^{****}	4	32 ± 3 ^{****}	n.d ^c
Y197F	>100	4	n.d ^c	n.d ^c
F200A	>100	5	n.d ^c	n.d ^c
F200Y	>100	4	5 ± 1 ^{ns}	n.d ^c
Ap₄A (3)				
P2Y ₄ - wt	>100	5	n.d ^c	n.d ^c
N170V	>100	4	n.d ^c	n.d ^c
R190A	>100	5	n.d ^c	n.d ^c
E193A	>100	4	n.d ^c	n.d ^c
D195A	>100	4	n.d ^c	n.d ^c
D195S	>100	4	n.d ^c	n.d ^c
Y197A	>100	5	n.d ^c	n.d ^c
Y197F	>100	6	n.d ^c	n.d ^c
F200A	>100	4	n.d ^c	n.d ^c
F200Y	>100	5	n.d ^c	n.d ^c
MRS4062 (5)				
P2Y ₄ - wt	0.0761 ± 0.0100	3	100 ± 2	1
N170V	0.0776 ± 0.0096 ^{ns}	5	56 ± 7 ^{****}	1
R190A	1.24 ± 0.28 ^{****}	3	57 ± 3 ^{***}	16
E193A	0.0831 ± 0.0091 ^{ns}	3	94 ± 5 ^{ns}	1
D195A	0.0825 ± 0.0107 ^{ns}	3	88 ± 5 ^{ns}	1
D195S	0.154 ± 0.014 ^{ns}	5	84 ± 6 ^{ns}	2
Y197A	0.757 ± 0.068 ^{***}	4	57 ± 5 ^{***}	10
Y197F	0.0866 ± 0.0122 ^{ns}	3	75 ± 2 ^{ns}	1
F200A	0.694 ± 0.069 ^{**}	3	21 ± 5 ^{****}	9
F200Y	0.0359 ± 0.0017 ^{ns}	3	89 ± 8 ^{ns}	0.5

^a Data represents means \pm SEM of 3-6 independent experiments each in duplicates. ^b Results of One-way ANOVA with Dunnett's post-hoc test: ^{ns} not significant; * $p \leq 0.05$; ** $p \leq 0.01$; *** $p \leq 0.001$; **** $p \leq 0.0001$. ^c no concentration-dependent activation up to 100 μ M; n.d. = not determined.

Supplementary Table S4. Potencies of antagonists at the *h*P2Y₂ receptor mutants.^a

Cell line	IC ₅₀ (μ M) \pm SEM ^b	n
RB-2 purified (6)		
P2Y ₂ -wt	5.99 \pm 0.563	4
F113A	4.13 \pm 0.71 ^{ns}	4
F113Y	23.5 \pm 4.6 ^{***}	4
D185A	1.73 \pm 0.32 ^{****}	4
F195Y	18.0 \pm 1.5 ^{**}	5
AR-C118925 (7)		
P2Y ₂ -wt	0.0212 \pm 0.0042	5
F113A	0.0340 \pm 0.0071 ^{ns}	4
F113Y	0.0324 \pm 0.0075 ^{ns}	5
D185A	0.0204 \pm 0.0082 ^{ns}	3
F195Y	0.0416 \pm 0.0081 ^{ns}	5
PSB-09114 (9)		
P2Y ₂ -wt	1.54 \pm 0.06	4
F113A	0.710 \pm 0.020 ^{ns}	4
F113Y	0.550 \pm 0.134 [*]	4
D185A	0.170 \pm 0.025 ^{**}	3
F195Y	2.02 \pm 0.51 ^{ns}	4
PSB-16133 (10)		
P2Y ₂ -wt	2.31 \pm 0.34	4
F113A	4.74 \pm 0.52 ^{ns}	3
F113Y	0.351 \pm 0.087 ^{****}	3
D185A	0.467 \pm 0.039 ^{****}	4
F195Y	2.66 \pm 0.68 ^{ns}	3
PSB-16135 (11)		
P2Y ₂ -wt	2.01 \pm 0.31	4
F113A	4.78 \pm 0.74 ^{ns}	3
F113Y	1.38 \pm 0.26 ^{**}	5
D185A	1.20 \pm 0.063 ^{**}	4
F195Y	4.89 \pm 0.71 ^{ns}	5

PSB-1699 (12)		
P2Y ₂ -wt	3.19 ± 0.97	5
F113A	>100 ****	3
F113Y	2.77 ± 0.65 ^{ns}	4
D185A	1.62 ± 0.22 ^{ns}	4
F195Y	>100 ****	4

^aData represents means ± SEM of 3-5 independent experiments each in duplicates. ^bResults of One-way ANOVA with Dunnett's post-hoc test: ^{ns} not significant; * $p \leq 0.05$; ** $p \leq 0.01$; *** $p \leq 0.001$; **** $p \leq 0.0001$.

Supplementary Table S5. Potencies of antagonists at the *h*P2Y₄ receptor mutants.^a

Cell line	IC ₅₀ (μM) ± SEM ^b	n
RB-2 purified (6)		
P2Y ₄ - wt	1.05 ± 0.04	3
N170V	0.477 ± 0.083 *	3
R190A	1.56 ± 0.20 ^{ns}	3
E193A	1.51 ± 0.18 ^{ns}	3
D195A	1.78 ± 0.35 ^{ns}	3
D195S	2.26 ± 0.40 *	4
Y197A	0.566 ± 0.035 ^{ns}	4
Y197F	3.30 ± 0.65 ***	3
F200A	1.39 ± 0.24 ^{ns}	3
F200Y	4.17 ± 0.22 ****	3
AR-C118925 (7)		
P2Y ₄ - wt	5.73 ± 0.82	3
N170V	>100 ****	5
R190A	10.9 ± 1.01 **	4
E193A	12.7 ± 1.2 ***	4
D195A	1.47 ± 0.22 ****	3
D195S	>100 ****	5
Y197A	1.96 ± 0.38 ****	3
Y197F	9.79 ± 0.88 **	5
F200A	6.28 ± 0.77 ^{ns}	4
F200Y	>100 ****	4
PSB-09114 (9)		
P2Y ₄ - wt	0.403 ± 0.017	3

N170V	2.26 ± 0.35 ****	4
R190A	0.736 ± 0.127 ^{ns}	3
E193A	1.01 ± 0.16 **	3
D195A	0.576 ± 0.017 ^{ns}	2
D195S	0.487 ± 0.098 ^{ns}	3
Y197A	0.234 ± 0.007 ^{ns}	3
Y197F	0.913 ± 0.059 **	3
F200A	0.331 ± 0.051 ^{ns}	3
F200Y	2.09 ± 0.24 ****	3
PSB-16133 (10)		
P2Y ₄ - wt	1.62 ± 0.17	3
N170V	2.84 ± 0.87 ^{ns}	4
R190A	0.339 ± 0.010 ***	3
E193A	3.08 ± 0.24 ^{ns}	3
D195A	2.27 ± 0.37 ^{ns}	3
D195S	1.85 ± 0.41 ^{ns}	4
Y197A	0.205 ± 0.068 ****	3
Y197F	4.77 ± 0.68 *	3
F200A	0.680 ± 0.071 ^{ns}	3
F200Y	5.43 ± 0.71 **	3
PSB-16135 (11)		
P2Y ₄ - wt	1.73 ± 0.11	3
N170V	2.99 ± 0.72 ^{ns}	5
R190A	4.98 ± 0.94 **	3
E193A	4.33 ± 0.65 *	3
D195A	3.16 ± 0.46 ^{ns}	3
D195S	2.24 ± 0.26 ^{ns}	5
Y197A	0.303 ± 0.060 ****	3
Y197F	3.54 ± 0.05 ^{ns}	3
F200A	1.73 ± 0.18 ^{ns}	3
F200Y	5.69 ± 0.62 **	3
PSB-1699 (12)		
P2Y ₄ - wt	1.53 ± 0.27	5
N170V	0.537 ± 0.084 ****	3
R190A	>100 ****	3
E193A	2.19 ± 0.38 ^{ns}	3
D195A	>100 ****	3
D195S	0.504 ± 0.090 ****	4
Y197A	2.13 ± 0.11 ^{ns}	3
Y197F	8.85 ± 0.53 ****	3
F200A	>100 ****	3
F200Y	>100 ****	3

^a Data represent means \pm SEM of 3-5 independent experiments each in duplicates. ^b Results of One-way ANOVA with Dunnett's post-hoc test: ^{ns} not significant; * $p \leq 0.05$; ** $p \leq 0.01$; *** $p \leq 0.001$; **** $p \leq 0.0001$.

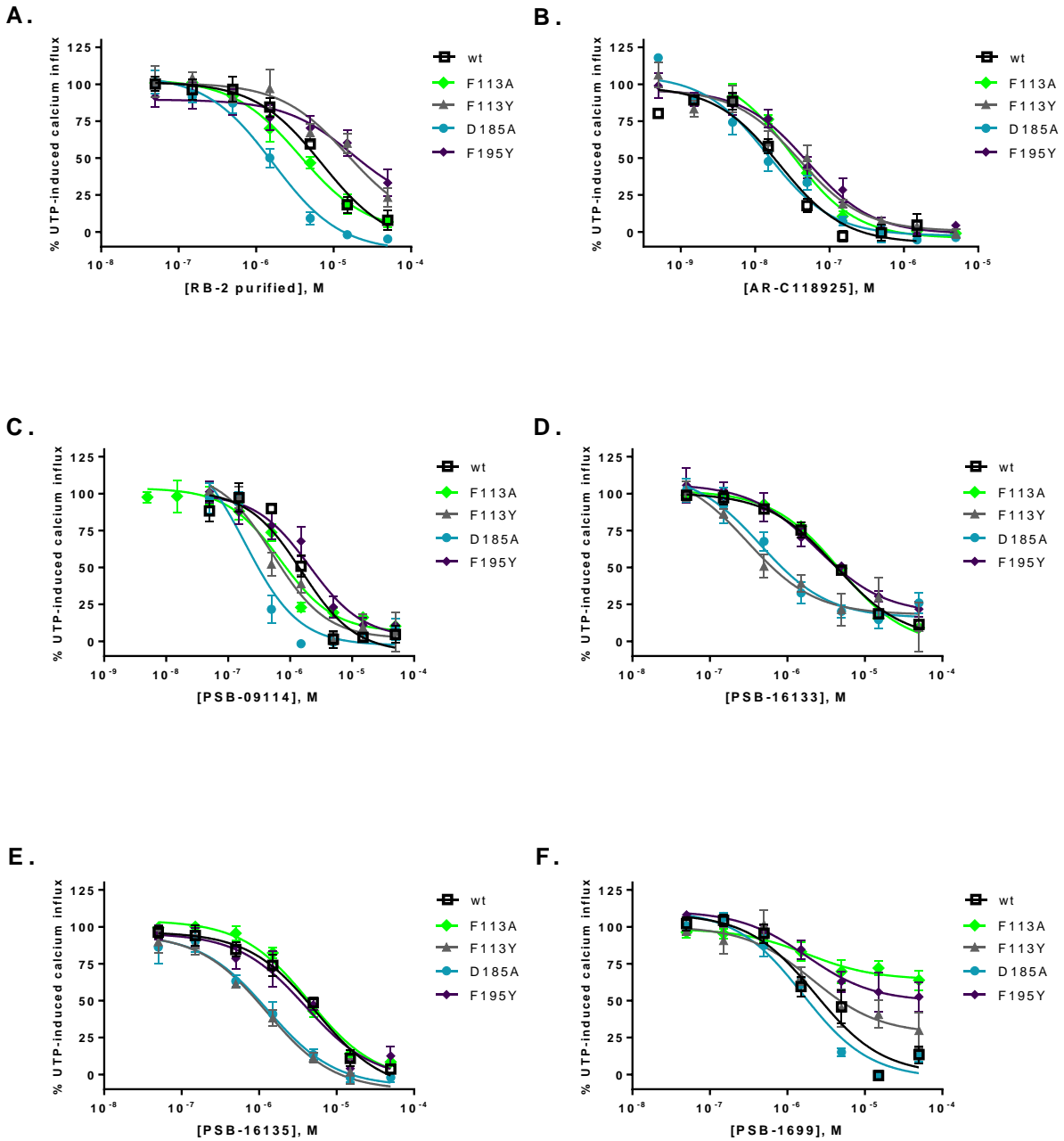
Supplementary Table S6. EC₅₀ values and maximal efficacy for the UTP concentration-response curves determined by calcium assay at the wt hP2Y₄R after pre-incubation with fixed concentration of PSB-1699. ^a

UTP + [PSB-1699], μ M	EC ₅₀ value (μ M) ^b , n = 3-4	Maximal receptor response to 100000 nM UTP (%)
0	0.0896 \pm 0.0031	100 \pm 4
0.500	0.104 \pm 0.006 ^{ns}	100 \pm 6
1.50	0.148 \pm 0.022 ^{ns}	86 \pm 11
3.00	0.198 \pm 0.024 ^{ns}	78 \pm 12
4.50	0.221 \pm 0.045 *	70 \pm 6
6.00	0.308 \pm 0.024 ***	72 \pm 3
10.0	0.129 \pm 0.018 ^{ns}	49 \pm 7
25.0	0.150 \pm 0.045 ^{ns}	42 \pm 7
50.0	0.293 \pm 0.041 ****	34 \pm 4

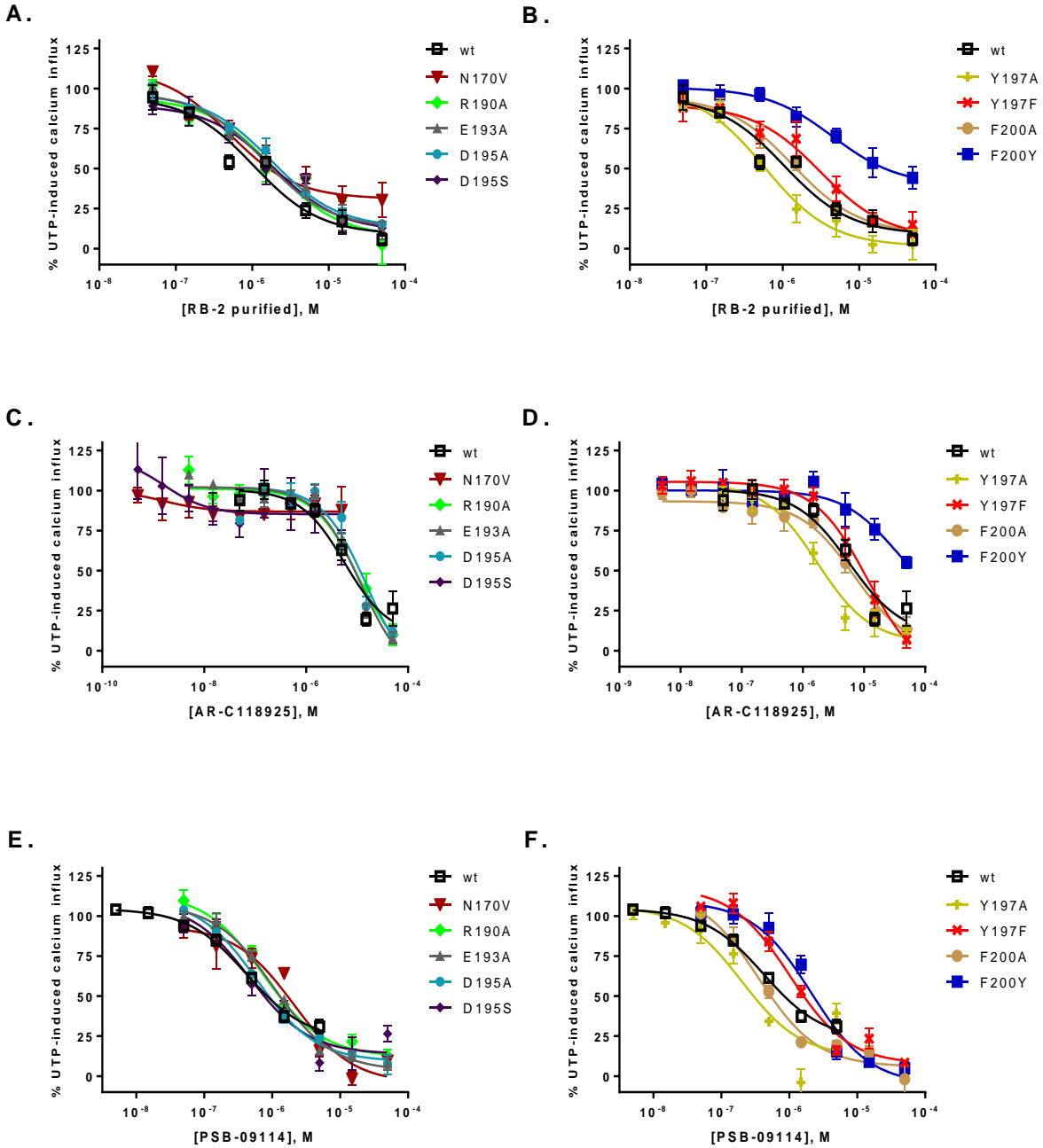
^a Data represent mean \pm SEM of 3-4 independent experiments each in duplicates. ^b Results of one-way ANOVA with Dunnett's post-hoc test: ^{ns} not significant; * $p \leq 0.05$; ** $p \leq 0.01$; *** $p \leq 0.001$; **** $p \leq 0.0001$.

sp P41231 P2RY2_HUMAN	-----MAADLGPWN DINGTWGDDELGYKCRFNEDFKYVLLPVSYGVVCPVGLCLNAV	53
sp P41232 P2RY2_RAT	-----MAAGLDSWNSTINGTWEGDELGYKCRFNEDFKYVLLPVSYGVVCVLGLCLNVV	53
sp P35383 P2RY2_MOUSE	-----MAADLEPWNSTINGTWEGDELGYKCRFNEDFKYVLLPVSYGVVCVLGLCLNVV	53
sp P51582 P2RY4_HUMAN	MASTESSLLRSLGLS----PGPGSSEVELDCWFDEDFKFI LLPVSYAVV FVLGLGNAP	55
sp O35811 P2RY4_RAT	MTSAESLLFTSLGPS----PSS----GDGDCRFNEEFKFI LLPMSYAVV FVLGLALNAP	51
sp Q9JJS7 P2RY4_MOUSE	MTSADSLFTSLGPS----PSS----GDGDCRFNEEFKFI LLPLSYAVV FVLGLALNAP	51
	: . *	
	* * : * : * : * : * : * : * : * : * : * : *	
sp P41231 P2RY2_HUMAN	ALYIFLCRLKTNASTTYMFHLAVSDALYAASLPLLVY YARGDHWPFSTVLCKLVRLEF	113
sp P41232 P2RY2_RAT	ALYIFLCRLKTNASTTYMFHLAVSDSLYAASLPLLVY YAQGDHWPFSTVLCKLVRLEF	113
sp P35383 P2RY2_MOUSE	ALYIFLCRLKTNASTTYMFHLAVSDSLYAASLPLLVY YARGDHWPFSTVLCKLVRLEF	113
sp P51582 P2RY4_HUMAN	TLWLFIFRLRPWDATATYMFHLALSDTLVLSLPTLIVY YAAHNWPFPGTEICKFVRLFF	115
sp O35811 P2RY4_RAT	TLWLFIFRLRPWDATATYMFHLALSDTLVLSLPTLIVY YARNHWPFPGTGLCKFVRLFF	111
sp Q9JJS7 P2RY4_MOUSE	TLWLFIFRLRPWDATATYMFHLALSDTLVLSLPTLIVY YARNHWPFPGTGCKFVRLFF	111
	: * : * : * : * : * : * : * : * : * : * : * : * : * : * : * : * : * : * : *	
sp P41231 P2RY2_HUMAN	NTNLYCSILFLTCISVHRCLGVLRPLRSLRWGRARYARRVAGAVVWLV LACQAPVLYFVT	173
sp P41232 P2RY2_RAT	NTNLYCSILFLTCISVHRCLGVLRPLHLSLWGHARYARRVA AVVWLV LACQAPVLYFVT	173
sp P35383 P2RY2_MOUSE	NTNLYCSILFLTCISVHRCLGVLRPLRSLRWGRARYARRVA AVVWLV LACQAPVLYFVT	173
sp P51582 P2RY4_HUMAN	TWNLYCSVLF LTCISVHRYLGICHPLRALRWGRPRLAGLLCLAVWLV VAGCLVPLFFVT	175
sp O35811 P2RY4_RAT	TWNLYCSVLF LTCISVHRYLGICHPLRAIRWGRPRFASLLCLGVWLV VAGCLVPLFFVT	171
sp Q9JJS7 P2RY4_MOUSE	TWNLYCSVLF LTCISVHRYMGICHPLRAIRWGRPRFAGLLCLGVWLV VAGCLVPLFFVT	171
	* * : * : * : * : * : * : * : * : * : * : * : * : * : * : * : * : * : * : *	
sp P41231 P2RY2_HUMAN	TSVRGGRVTC HDTSAPELSRFVAYS VMLG LLFVAVPFAVILVLCYVLMARRLLKPAYGTS	233
sp P41232 P2RY2_RAT	TSVRGTRITC HDTSARELSHFVAYS VMLG LLFVAVPFSIILVLCYVLMARRLLKPAYGTT	233
sp P35383 P2RY2_MOUSE	TSVRGTRITC HDTSARELSHFVAYS VMLG LLFVAVPFSVILVLCYVLMARRLLKPAYGTT	233
sp P51582 P2RY4_HUMAN	TSNRGTTVLC HDTRPEEDHYVHFS AVMGLLFGVPCLVTLVLCYGLMARRLYQPLPGSA	235
sp O35811 P2RY4_RAT	TNANGTTILC HDTTLPEEDHYVYFS AVMVLLFGLPFLITLVCYGLMARRLYRPLPGAG	231
sp Q9JJS7 P2RY4_MOUSE	TNANGTTILC HDTTLPEEDHYVYFS TIMVLLFGFPFLITLVCYGLMARRLYRPLPGAG	231
	* . * : * * : * * : * * : * * : * * : * * : * * : * * : * * : * * : * * : *	
sp P41231 P2RY2_HUMAN	GGLPRAKRKSVRTIAVLAVFALCFLPFHVT TLVYSFRSLDLSCHTLNAINMAKKTTRP	293
sp P41232 P2RY2_RAT	-GLPRAKRKSVRTIALVLAVFALCFLPFHVT TLVYSFRSLDLSCHTLNAINMAKKTTRP	292
sp P35383 P2RY2_MOUSE	GGLPRAKRKSVRTIALVLAVFALCFLPFHVT TLVYSFRSLDLSCHTLNAINMAKKTTRP	293
sp P51582 P2RY4_HUMAN	Q--SSSRLRSLRTIAVLTVFVAVCFVPHIT TIVYLARLLEADCRV LNIVVVKVTRP	293
sp O35811 P2RY4_RAT	Q--SSSRLRSLRTIAVLTVFVAVCFVPHIT TIVYQARLLQADCHV LNIVVVKVTRP	289
sp Q9JJS7 P2RY4_MOUSE	Q--SSSRLRSLRTIAVLTVFVAVCFVPHIT TIVYLARLLNAECRV LNIVVVKVTRP	289
	: : * : * * : * : * : * : * : * : * : * : * : * : * : * : * : * : * : * : *	
sp P41231 P2RY2_HUMAN	LASANSCLDPVLYFLAGQRLVRFARDAKPPTGPS PATPARRRLGLRRSDRTDMQRIEDVL	353
sp P41232 P2RY2_RAT	LASANSCLDPVLYFLAGQRLVRFARDAKPATEPTPSPQARRKGLHRRPNRTDTRK-DLS	351
sp P35383 P2RY2_MOUSE	LASANSCLDPVLYFLAGQRLVRFARDAKPTEPTPSPQARRKGLHRRPNRT--VRK-DLS	350
sp P51582 P2RY4_HUMAN	LASANSCLDPVLYLLTGDKYRRQLRQLCGGKQPRTAASSL-ALVSLPEDSSCRWAATP	352
sp O35811 P2RY4_RAT	LASANSCLDPVLYLFTGDKYRNQLQQLCRGSKPKPRTAASSL-ALVTLHEESISRWADTH	348
sp Q9JJS7 P2RY4_MOUSE	LASANSCLDPVLYLFTGDKYRNQLQQLCRGSTRPKRRTTASSL-ALVTLHEESISRWADIH	348
	* *	
sp P41231 P2RY2_HUMAN	GSSDSRRTTESTPAGSENTKD IRL	377
sp P41232 P2RY2_RAT	ISSDSRRTTESTPAGSET-KD IRL	374
sp P35383 P2RY2_MOUSE	VSSDSRRTTESTPAGSET-KD IRL	373
sp P51582 P2RY4_HUMAN	---QD--SSCSTPRADRL-----	365
sp O35811 P2RY4_RAT	---QD--STFSAYEGDRL-----	361
sp Q9JJS7 P2RY4_MOUSE	---QD--SIFPAYEGDRL-----	361
	: * : * : * : * : * : * : * : * : * : * : * : * : * : * : * : * : * : * : *	

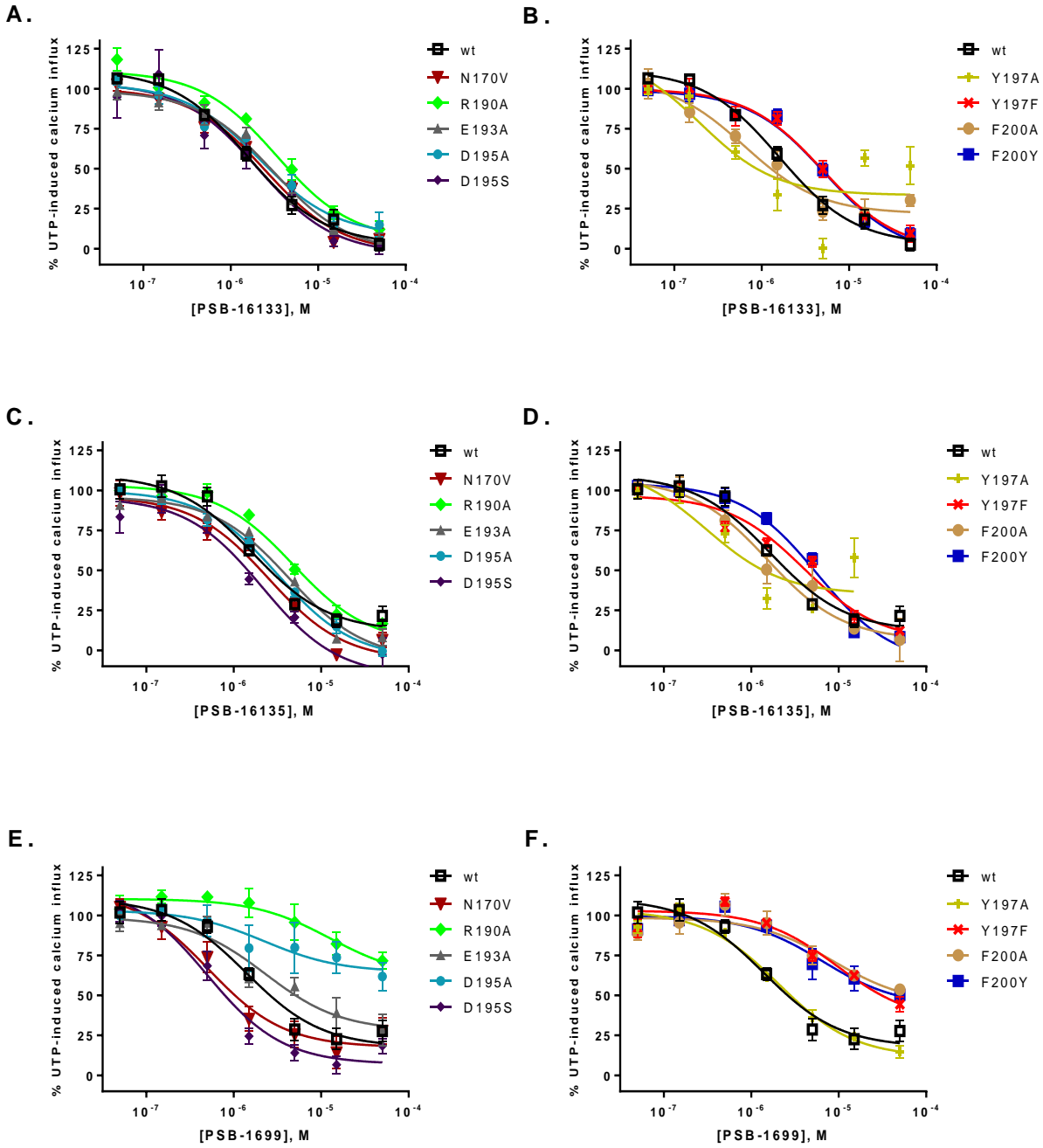
Supplementary Figure S1. Sequence alignment of *hP2Y₂*- and *hP2Y₄*Rs. Conserved residues of the putative orthosteric binding site are highlighted in green, non-conserved residues are highlighted in blue.



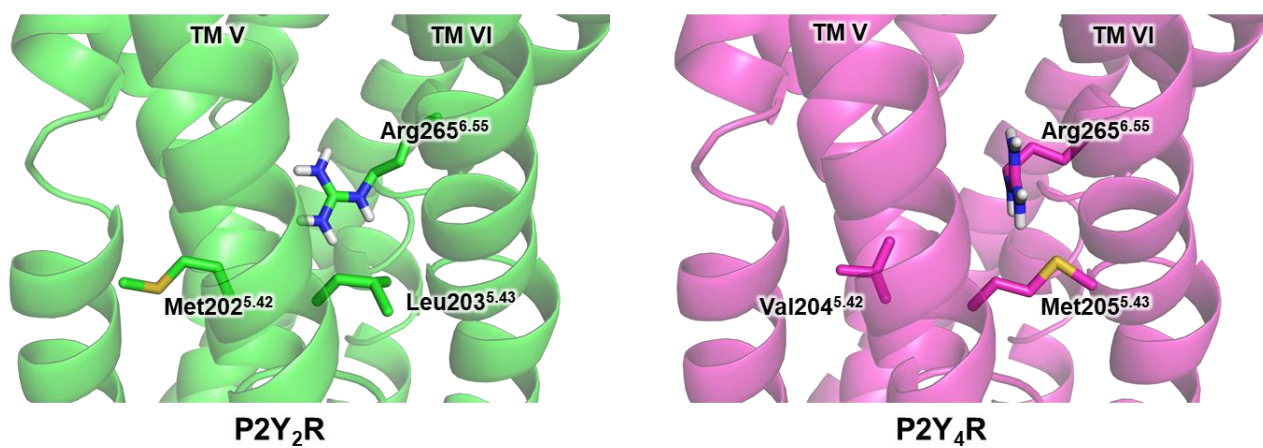
Supplementary Figure S2. Antagonist-induced inhibition curves of P2Y₂R(wt and mutants) activation by UTP using calcium mobilization assay **A.** Reactive blue 2 (RB-2) purified, **B.** AR-C118925, **C.** PSB-09114, **D.** PSB-16133, **E.** PSB-16135 and **F.** YB - 099. Each data point represents mean \pm SEM of 3 – 5 independent determinations each in duplicate vs. UTP employed at its EC₈₀ value for the respective cell line. IC₅₀ values are reported in Table S4.



Supplementary Figure S3. Antagonist-induced inhibition curves of P2Y₄R(wt and mutants) activation by UTP using calcium mobilization. **A.** and **B.** Reactive blue-2, **C.** and **D.** AR-C118925, and **E.** and **F.** PSB-09114. Each data point represents mean \pm SEM of 3 – 5 independent determinations each in duplicate vs. UTP employed at EC₈₀ value for the respective cell line. IC₅₀ values are reported in Table S5.



Supplementary Figure S4. Antagonist-induced inhibition curves of P2Y₄R(wt and mutants) activation by UTP using calcium mobilization. **A.** and **B.** PSB-16133, **C.** and **D.** PSB-16135, and **E.** and **F.** PSB-1699. Each data point represents the mean \pm SEM of 3 – 5 independent determinations each in duplicate vs UTP employed at its EC₈₀ value for the respective cell line. IC₅₀ values are reported in Table S5.



Supplementary Figure S5. Comparison of selected residues close to the putative orthosteric binding site in the homology models of human P2Y₂- (left) and P2Y₄Rs (right).

5.4. Summary and Outlook

The presented work shed a new light on ligand recognition and binding site differences between P2Y₂- and P2Y₄Rs which is a vital element in the design of selective and potent compounds. The data suggests that in the case of P2Y₂R, more space in the nucleobase binding site is available for the ligands. Furthermore, the putative orthosteric binding site of P2Y₂R is more lipophilic compared to P2Y₄R, which results in acceptance of the bulkier nucleotide ATP additionally to UTP. Both factors likely contribute to the distinct P2Y₂R selectivity of AR-C118925. Again, as a follow up of the investigation in **Section 4**, more key residues involved in nucleotide and antagonist binding were identified, fortifying the hypothesis of endogenous ligand binding underneath ECL2 in the case of P2Y₂R. This study represents the first reported SAR analysis supported by mutagenesis data for human P2Y₄R which will function as pioneering work for rational design of potent (tool) compounds in the future. Homologous to P2Y₂- and P2Y₁₂Rs, the results suggest that the nucleobase of agonists interact with buried lipophilic and aromatic residues of TM6. Yet, the space of the P2Y₄R binding site is restricted due to a rotamer of Arg265, resulting in sensitivity towards UTP. Interestingly, ATP sensitivity was introduced at the Y197A P2Y₄R mutant, likely due to the increased space in the putative nucleobase binding site. Investigation of antagonists at the P2Y₄R mutants revealed additional differences between both binding sites: More flexible anthraquinone derivatives (RB-2, PSB-1699) displayed potential to interact with aromatic and residues buried beneath ECL2 that are likely involved in stabilization of the nucleobase of agonists in the orthosteric binding site at both P2Y₂- and P2Y₄Rs – a feature that can be exploited in future drug design and to increase the selectivity of the compounds.

The homology models of P2Y₂- and P2Y₄Rs proved to predict important interactions between receptor and ligands which were confirmed by pharmacological data. The insights on the architecture of both receptors will prove imperative for structure-based drug discovery methods such as in the case of high-throughput virtual screening.

6. Discovery of P2Y₂ Receptor Antagonist Scaffolds through Virtual High-Throughput Screening

6.1. Introduction

Screening for novel drug candidates can be approached from different perspectives and starting points. Among them, SBDD assimilates 3D information of ligand and target to enable rational strategies for compound evolution or the discovery of new active molecules. VS represents a cost-efficient structure-based method as a pre-screening for potential drug candidates which greatly benefits from additional data on features important for proper interaction with the receptor. During VS, a collection of molecules is placed at a target of interest where several conformations of the ligand or the complex are generated and assessed for their interaction qualities. Subsequent quantification in the form of a docking score allows prognosis which pose complements the binding site the best and is therefore the most likely one to be observed in reality.

Section 3 to 5 collected information on P2Y₂R receptor architecture, and, more importantly, the topology of the orthosteric binding site was discussed. In this study, the resulting knowledge was utilized for a VS campaign with the aim to discover novel drug-like molecular scaffolds surpassing the physicochemical properties of the endogenous ligands and available tool compounds. Therefore, complexes of P2Y₂R homology model with the selective antagonist AR-C118925 were used to screen a virtual library of 3.2 million of drug-like compounds from the ZINC database to identify potential binders, also addressed as 'hit' molecules. The top 1,000 scoring compounds were visually inspected, and the most promising candidates were selected. In total, fifty-eight compounds were purchased and assessed for their inhibitory effect at P2Y₂R and, for preliminary selectivity studies, at human acetylcholine M₃ receptor in calcium mobilization studies.

6.2. Publication

Discovery of P2Y₂ Receptor Antagonist Scaffolds through Virtual High-Throughput Screening

Alexander Neumann, Isaac Attah, Haneen Al-Hroub, Vigneshwaran Namasivayam, and Christa E. Müller*



Cite This: <https://doi.org/10.1021/acs.jcim.1c01235>



Read Online

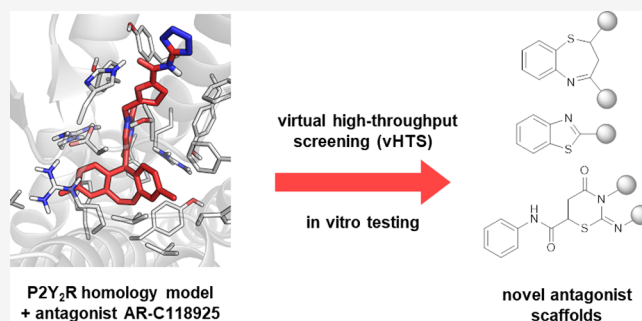
ACCESS |

Metrics & More

Article Recommendations

Supporting Information

ABSTRACT: The human ATP- and UTP-activated P2Y₂ receptor (P2Y₂R) is a G_q protein-coupled receptor involved in several pathophysiological conditions including acute and chronic inflammation, cancer, and pain. Despite its potential as a novel drug target, only few P2Y₂R antagonists have been developed so far, all of which suffer from severe drawbacks. These include (i) high polarity due to one or several negative charges resulting in low oral bioavailability, (ii) metabolic instability and generally poor pharmacokinetic properties, and/or (iii) lack of selectivity, which limits their utility for *in vitro* and *in vivo* studies aimed at target validation. In search of new druglike scaffolds for P2Y₂R antagonists, we employed a structure-based virtual high-throughput screening approach utilizing the complex of a P2Y₂R homology model with one of the most potent and selective orthosteric antagonists described so far, AR-C118925 (**10**). After virtual screening of 3.2 million molecules, 58 compounds were purchased and pharmacologically evaluated. Several novel antagonist scaffolds were discovered, and their binding modes at the human P2Y₂R were analyzed by molecular docking studies. The investigated antagonists likely share a similar binding mode with **10** which includes accommodation of bulky, lipophilic groups in the putative orthosteric binding site of the P2Y₂R. The discovered scaffolds and the elucidated structure–activity relationships provide a basis for the development of future drug candidates for the P2Y₂R which have great potential as novel drugs.



1. INTRODUCTION

G protein-coupled receptors (GPCRs) are ubiquitously expressed membrane receptors involved in various signaling pathways. They represent the largest family of transmembrane receptors and are the most intensively studied class of drug targets. The expression of GPCRs in the plasma membrane, their accessibility from the extracellular compartment, their physiological and pathophysiological relevance, and their accessibility and druggability by small molecules have led to the fact that approximately 35% of approved drugs target GPCRs.¹

The human P2Y₂ receptor (P2Y₂R) is a GPCR belonging to the purinergic P2 or nucleotide-activated receptor family activated equipotently by two different endogenous nucleotides, ATP (adenosine-5'-triphosphate, **1**) and UTP (uridine-5'-triphosphate, **2**).^{2–6} Activation of the G_q protein-coupled P2Y₂ receptor leads to intracellular calcium release. Prolonged activation results in the recruitment of β -arrestin followed by receptor internalization.⁷ P2Y₂Rs are widely expressed in several organs and tissues, including brain, lung, heart, and kidneys.^{8,9} Several studies confirm the crucial involvement of P2Y₂Rs in acute and chronic inflammation.^{10–14} Inhibition of P2Y₂Rs using selective antagonists represents an opportunity

for the treatment of pathologic conditions such as neurodegenerative disorders, asthma, and rheumatoid arthritis.¹⁵ Furthermore, P2Y₂Rs were proposed to be involved in immune responses based on their expression in eosinophils, lymphocytes, macrophages, mast cells, and natural killer cells.^{16,17} Early stages of human immunodeficiency virus-1 (HIV-1) infection were reported to be facilitated by extracellular ATP *via* P2Y₂Rs, indicating that antagonist treatment may open new therapeutic pathways for interrupting the virus entry mechanism.^{18,19} Similarly, a critical role of P2Y₂Rs for human cytomegalovirus infection was described, where inhibition of P2Y₂Rs resulted in low viral load in infected cells.²⁰ Further potential indications for P2Y₂R antagonists comprise, for example, atherosclerosis, psoriasis, osteoporosis, nephrogenic diabetes insipidus, cancer, and pain.²¹

Received: October 13, 2021

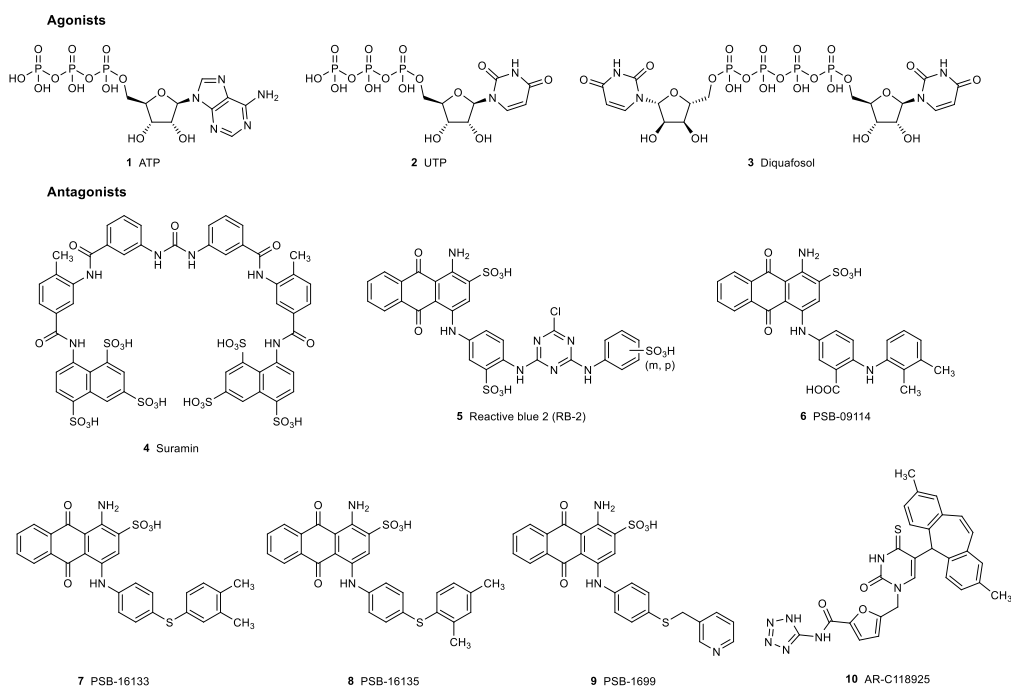


Figure 1. Structures of selected P2Y₂R agonists (1–3) and antagonists (4–10).

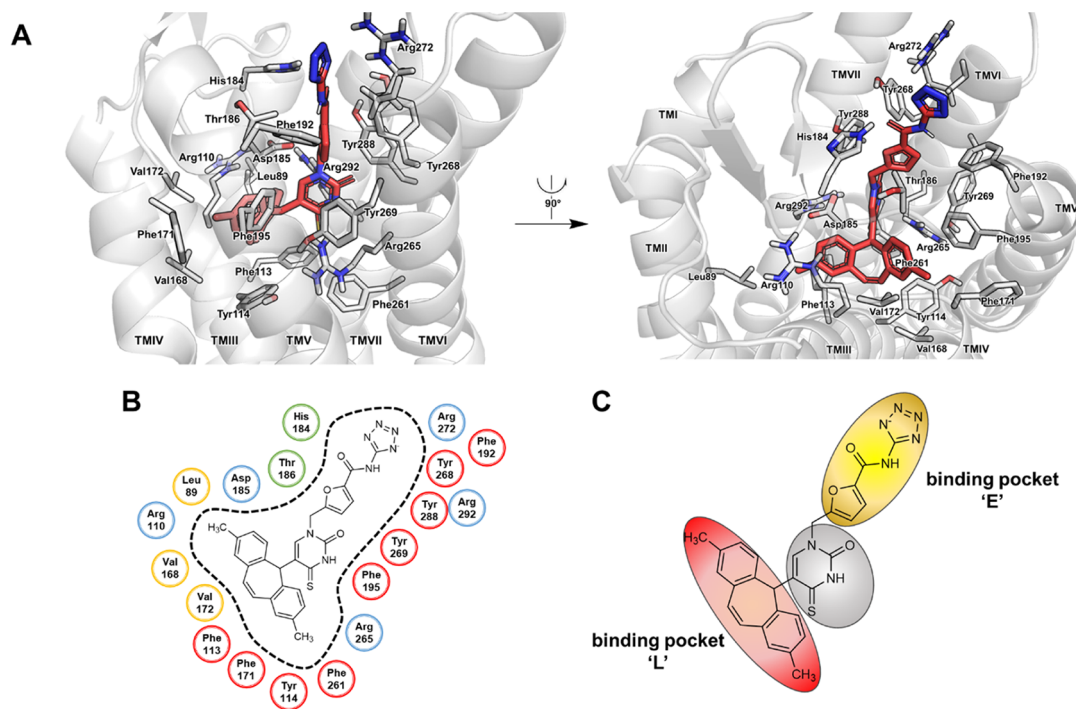


Figure 2. Putative binding mode of P2Y₂R antagonist **10** in the orthosteric binding site of the human P2Y₂R. (A) Docked pose of **10** in complex with the homology model of the human P2Y₂R shown with the residues forming the binding pocket. The receptor is displayed in cartoon representation, and the amino acid residues (white) and compound **10** (red) are shown as stick models. Oxygen atoms are colored in blue, nitrogen atoms in yellow, and sulfur atoms in yellow. (B) Schematic 2D representation of the binding pocket. Lipophilic amino acids are colored in yellow, hydrophilic ones in blue, aromatic ones in red, and amino acid residues with mixed properties in green. (C) Denotation and schematic localization of lipophilic binding pocket L and binding pocket E close to the extracellular lumen.

Although the P2Y₂R poses a potential target for the treatment of various pathological conditions, only few antagonists have been described to date, all of which are not ideal to perform pharmacological studies including target validation.²¹

Rational drug design of P2Y₂R antagonists poses significant challenges: the endogenous nucleotidic agonists ATP and UTP are prone to enzymatic hydrolysis. The triphosphate groups which are negatively charged at a physiological pH value of 7.4 prevent oral bioavailability of the nucleotides and its analogues. Likewise, most of the few described P2Y₂R antagonists suffer

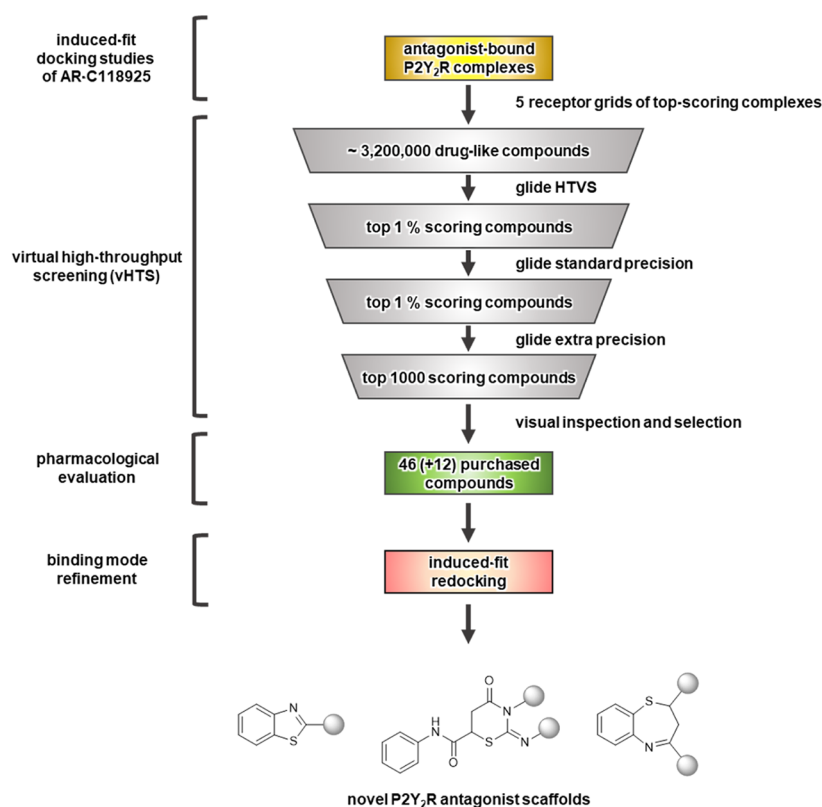


Figure 3. Workflow for the discovery of P2Y₂R antagonists. In the first round of *in vitro* testing, 46 compounds were purchased. In the second round, 12 analogues of initial hits were ordered and tested to elucidate SARs.

from poor physicochemical and pharmacokinetic properties. The replacement of the triphosphate group represents a challenge in the design of analogues due to its multiple interactions within the P2Y₂R binding site and its requirement for high-affinity binding.^{2,3,22,23} So far, the P2Y₂R agonist diquafosol (di-uridine-tetraphosphate, **3**) is the only P2Y₂R ligand that has been approved as a drug, which is applied for the treatment of dry eye disease in Asia.²⁴ The polysulfonated, polyaromatic P2Y₂R antagonists suramin (**4**) and reactive blue 2 (RB-2, **5**), both of which are nonselective, and various somewhat more selective anthraquinone derivatives (**6–9**) possess IC₅₀ values only in the micromolar range (for structures see Figure 1).^{2,3} Their target promiscuity, low potency, metabolic instability, and/or high polarity prevent oral bioavailability and brain penetration and limit their utility as tool compounds for *in vivo* studies. The orthosteric antagonist AR-C118925 (**10**), a structural analogue of the endogenous agonist UTP, exhibited 50- to 500-fold selectivity for P2Y₂R compared to other P2Y_R subtypes with IC₅₀ values in the mid-nanomolar range.^{7,25} However, **10** showed poor oral bioavailability in preclinical studies; nevertheless, it is still a valuable pharmacological tool compound for studying the P2Y₂ receptor.^{26–30}

Recently, we have reported on suramin-derived dual antagonists targeting the human P2Y₂R and the orphan receptor GPR17 that are potentially useful for the treatment of inflammatory diseases.³¹ The reported antagonists containing a sulfonic acid group inhibited both receptors, P2Y₂ and GPR17, with low micromolar potency and selectivity compared to the other P2Y_R subtypes.

P2Y₂R antagonists of herbal origin have also been reported; tangeretin, heptamethoxyflavone, β -oxo-auretiacin, and sev-

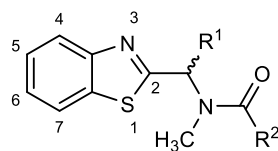
eral other flavonoids were characterized as allosteric inhibitors with IC₅₀ values in the micromolar concentration range (for structures, see Figure S1 in the Supporting Information).³² However, the promiscuity of flavonoids which are multitarget drugs, and the rather complex structure–activity relationships (SARs) of 40 investigated flavonoids impede causal connections for straightforward ligand optimization. Plant extracts of *Joannesia princeps* Vell. (stem) and *Peixotoa* A. Juss (flower and leaf) were reported to inhibit UTP-induced responses *via* P2Y₂R and P2Y₄R, but the identification of the active molecules is still pending.³³

The scarcity of potent, druglike antagonists for the P2Y₂R reflects the obstacles in drug discovery and ligand optimization for this target. In the present study, we report on the first homology model-based approach for the discovery of novel antagonist scaffolds for the P2Y₂R. Based on docking predictions of the orthosteric antagonist **10**, a virtual screening campaign with over 3,200,000 compounds was performed. Best-scoring compounds were visually assessed for their binding modes, and candidates were selected for purchase and *in vitro* testing.

2. METHODS

2.1. Molecular Modeling. **2.1.1. Receptor Grid Generation.** With the aim to identify potential novel P2Y₂R antagonist scaffolds, docking studies with the competitive antagonist **10** into the previously published homology model of the human P2Y₂R were carried out.^{2,6} The P2Y₂R homology model was based on the X-ray crystal structure of the human P2Y₁R.³⁴ The top five scoring complexes of the homology model of the P2Y₂R with **10** were used for receptor grid generation based on their induced-fit docking (IFD) score. No

Table 1. Potencies of Benzothiazole Derivatives Identified by Initial Screening as Antagonists of the P2Y₂R Compared to their Inhibitory Activity at the Acetylcholine M₃R^{a,e}



11 - 13
Benzothiazole derivatives

Compound	Structure		IC ₅₀ ± SEM (μM) ^b (% inhibition at 10 μM)	
	R ¹	R ²	P2Y ₂ R ^c	M ₃ R ^d
11	H		16.6 ± 1.7	> 10 (5 %)
12	H		21.9 ± 0.7	> 10 (1 %)
13	CH ₃		9.26 ± 1.92	(68 % inhibition)

^aBiological assessment of the compounds was performed using calcium mobilization assays. ^bPotencies of antagonists were determined versus an EC₃₀ concentration of the agonist in the respective assay. ^cAntagonism was determined at the human P2Y₂ receptor versus UTP (3 μM). ^dAntagonism was determined at the acetylcholine M₃R versus carbachol (100 μM). ^eAll data are presented as mean from three to four independent assays.

significant deviations between the five complexes were observed. Receptor grids for molecular docking into the putative binding site of antagonist **10** were generated using the receptor grid generator implemented in Maestro Schrödinger software package release 2016. The binding pocket size was set to 10 Å × 10 Å × 10 Å and centered on the centroid of the ligand in each P2Y₂R homology model complex.

2.1.2. Data Set. A chemical library consisting of approximately 3.2 million druglike compounds, according to Lipinski's rule of five (≤5 H-bond donors, ≤10 H-bond acceptors, molecular mass ≤ 500, log *P* ≤ 5), was retrieved from the ZINC database (version ZINC15, accessed in March 2017).^{35,36} Molecules containing reactive functional groups were excluded with the "reactive groups" filter of the LigPrep module to minimize off-target effects and false positives. Molecules were prepared for glide docking at pH 7.4 and desalted if necessary. Tautomers were generated according to standard settings. Stereoisomers were generated for unspecified chiral centers with at the most four per ligand.

2.1.3. Virtual Screening. In the first step of the virtual screening workflow of Maestro, the compound library was docked with the Glide HTVS.³⁷ The ligands were flexible during docking, and nonplanar amide bonds were penalized during the Glide HTVS workflow. The top 1% of the best scoring compounds were taken over to the next step. In the second step, the compounds were docked according to the glide standard precision protocol implemented in Maestro. The top 1% of the best scoring compounds were transferred to

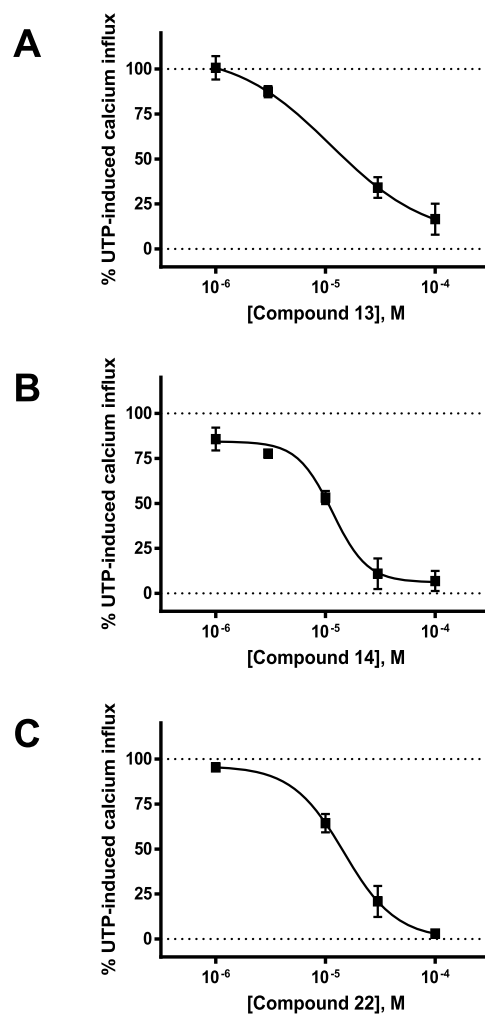


Figure 4. Concentration–response curve of compound **13** (A), **14** (B), and **22** (C) determined in calcium mobilization assays at human P2Y₂Rs expressed in 1321N1 astrocytoma cells. Each data point represents the mean ± SEM of three to four independent determinations, each in duplicate.

the third step for glide XP (extra precision) docking. We decided on the top 1% in each step to increase the chances of finding potent lead structures during the screening process. Docking scores were merged, and only the best scoring pose of duplicates within the ensemble was retained for visual assessment. The top 1000 scoring compounds were visually inspected and individually evaluated for their interactions with the receptor, molecular complexity, interaction quality with target residues, correct protonation states, complementation of the binding site surface, ligand strain and distorted ligand geometry, π -stacking, structural diversity, chemical stability, (potential) toxicity, and commercial availability. A selection of 46 compounds was finally purchased for preliminary *in vitro* screening, measuring inhibition of UTP-mediated P2Y₂R activation. Hits from *in vitro* screening were evaluated and cherry-picked. Subsequently, 12 additional compounds were purchased and subjected to a second round of *in vitro* screening. This second set of compounds consisted of analogues of the selected hits from the first *in vitro* screening at the P2Y₂R. In the present report, we discuss three selected active scaffolds. An overview of compounds purchased in each

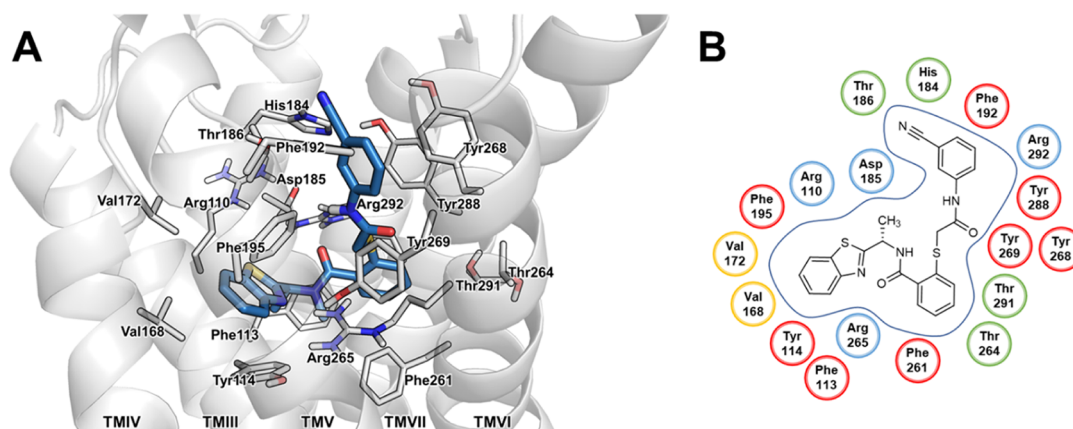


Figure 5. Putative binding mode of antagonist **13** in complex with the homology model of the human P2Y₂R. (A) Docked pose of **13** into the homology model of the human P2Y₂R shown with the residues forming the binding pocket. The receptor is displayed in cartoon representation, and the amino acid residues (white) and compound **13** (blue) are shown as stick models. Oxygen atoms are colored in red, nitrogen atoms in blue, and sulfur atoms in yellow. (B) Schematic 2D representation of the binding pocket. For color code, see Figure 2.

round is given in Tables S1 and S2 of the [Supporting Information](#).

2.1.4. Docking Studies. In order to refine the initial docking prediction based on glide docking, a method where the structure is maintained rigid during the docking procedure, we decided to redock *in vitro* hits using the IFD module implemented in Maestro Schrödinger.³⁸ The docking procedure was previously published.^{2,6,23} Ligands and receptor were prepared at pH 7.4. Ligands were docked into the homology model of the human P2Y₂R. The ligand binding mode of **10** was selected as a center for the docking procedure. Binding modes of antagonists with the highest IFD scores were selected.

2.2. Materials. Dulbecco's modified Eagle medium (DMEM), penicillin G, streptomycin, and trypsin–EDTA (ethylenediaminetetraacetic acid) were obtained from Life Technologies GmbH (Darmstadt, Germany). Fluo-4 acetoxy-methyl ester (Fluo-4-AM) was obtained from Invitrogen/Thermo Fisher (Merelbeke, Belgium), and geneticin (G418) was purchased from PAN Biotech (Aidenbach, Germany). Fetal calf serum (FCS) and Pluronic F-127 were purchased from Sigma-Aldrich (Taufkirchen, Germany). UTP was obtained from Sigma-Aldrich (Steinheim, Germany), and carbachol was obtained from Alfa Aesar Thermo Fisher GmbH (Kandel, Germany). Corning 3340 microplates were purchased from Corning Life Sciences (Tewksbury, MA, USA), and 24-well plates were purchased for ELISA assays from Sarstedt AG & Co. (Nuembrecht, Germany). Compounds for *in vitro* screening were purchased at MolPort (Riga, Latvia).

2.3. Calcium Mobilization Assays. Calcium mobilization assays were performed to screen the selected compounds at P2Y₂R and other P2YR subtypes recombinantly expressed in 1321N1 astrocytoma cells.^{2,6,23} 1321N1 Astrocytoma cells natively express the muscarinic M₃ receptor (M₃R); therefore, the VS hits were counter-screened at the M₃R against the agonist carbachol utilizing calcium mobilization assays. Compounds which were also hits on the M₃R were considered to potentially display off-target effects and were hence discarded as possible artifacts. The compounds were screened at 10 μM as potential antagonists at the P2Y₂R versus UTP. The threshold for selection of *in vitro* screening hits was set to 30% inhibition at 10 μM. Concentration inhibition

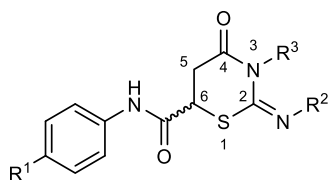
curves for the most potent compound of each scaffold series were determined.

The calcium measurements were performed as previously described.^{2,6,23} One day before the assay, the growth medium was removed from a T175 flask with approximately 80–90% cell confluency. The cells were washed with phosphate-buffered saline (containing 137 mM NaCl, 2.7 mM KCl, 4.3 mM Na₂HPO₄, and 1.47 mM KH₂PO₄ at pH 7.3). The cells were then detached with trypsin–EDTA and resuspended in DMEM supplemented with 10% FCS, 100 U/mL penicillin G, 100 μg/mL streptomycin, and 800 μg/mL geneticin (G418). About 60,000 cells in 200 μL of DMEM growth medium were seeded into each well of the sterile black 96-well polystyrene plate with a transparent flat bottom (Corning 3340) and incubated at 37 °C, 96% humidity, and 10% CO₂. Prior to the assay, the growth medium was removed completely, and the adherent cells were incubated for 1 h with 40 μL of loading dye consisting of 15 μL of Fluo-4-AM (1 mM solution in dimethyl sulfoxide, DMSO) and 15 μL of Pluronic F-127 (25% w/v in DMSO) in 4970 μL of Hank's balanced salt solution (HBSS) buffer in each well. After incubation, excess dye was removed, and the cells were further incubated in HBSS buffer at rt for 30 min before the addition of agonist. For assessment of antagonist potencies, the cells were preincubated with the antagonist in HBSS buffer during the 30 min incubation before addition of the agonist UTP at its EC₈₀ concentration (3 μM). All dilutions used for dose–response curves were performed on a log-scale (10⁻⁷ to 10⁻⁴ M). The final volume in each well was 200 μL, and the final DMSO concentration was maintained at 0.5% (v/v). The measurement of fluorescence intensity was performed on a Novostar plate reader (BMG LabTechnologies, Offenburg, Germany) at 520 nm for 30 s at 0.4 s intervals after excitation at 485 nm. For all assays, 100 μM carbachol, inducing intracellular Ca²⁺ release by activating the natively expressed G_q protein-coupled muscarinic M₃ receptor (M₃R) in 1321N1 astrocytoma cells, was used as a positive control. The maximal carbachol response was set at 100% and employed for normalization of all other responses.

3. RESULTS

Recently, we developed a homology model of the human P2Y₂R and investigated its structure in detail by utilizing site-directed mutagenesis studies.^{2,6} Meanwhile, with the develop-

Table 2. Potency of 1,3-Thiazinane Derivative 14 Identified by Screening as P2Y₂R Antagonist Compared to Its Inhibitory Activity at the Acetylcholine M₃R, along with Some Analogues^{a,e}



14 - 21

2-Imino-4-oxo-N-phenyl-1,3-thiazinane-6-carboxamide derivatives

Compound	Structure			IC ₅₀ ± SEM (μM) ^b (% inhibition at 10 μM)	
	R ¹	R ²	R ³	P2Y ₂ R ^c	M ₃ R ^d
14	COOH			9.87 ± 0.68	> 10 (21%)
15	COOH			> 10 (15%)	> 10 (25%)
16	COOH			> 10 (1%)	> 10 (-23%)
17	COOH			> 10 (16%)	> 10 (2%)
18	COOH		CH ₃	> 10 (-7%)	> 10 (-20%)
19	COOH			> 10 (-15%)	> 10 (-29%)
20	COOC ₂ H ₅			> 10 (-1%)	> 10 (-14%)
21	F		CH ₃	> 10 (13%)	> 10 (-2%)

^aBiological assessment of the compounds was performed using calcium mobilization assays. ^bPotencies of antagonists were determined versus an EC₈₀ concentrations of the agonist in the respective assays. ^cAntagonism was determined at the human P2Y₂ receptor versus UTP (3 μM). ^dAntagonism was determined at the acetylcholine M₃R versus carbachol (100 μM). ^eAll data are presented as means from three to four independent assays. The observed negative values for some compounds may be artifacts, for example, due to autofluorescence, or reflect very minor positive allosteric receptor modulation.

ment of AlphaFold for predicting protein structures by artificial intelligence (<https://alphafold.com/>), an additional resource for model comparison and validation became available. Based on the binding site selection (Leu89, Arg110, Phe113, Tyr114, Val168, Phe171, Val172, His184, Asp185, Thr186, Phe192, Phe195, Phe261, Arg265, Tyr268, Tyr269, Arg272, Tyr288, and Arg292), the RMSD between the homology model and

the AlphaFold structure amounts to 0.75 Å indicating an equivalent prediction quality. RMSD values above 1 Å were observed for residues Asp185 and Phe192, which are part of the extracellular loop (ECL2) (1.09 and 1.21 Å, respectively), and for Tyr269 (1.28 Å). Since the ECL2 is a highly flexible structure that can undergo several conformational changes, we believe that those differences would not have a significant impact on the docking predictions. The overall RMSD of both structures amounts to 1.73 Å. Greater differences were observed for residues which are not part of the defined binding site (tips of ECL2, ECL3, ICL2, and ICL3) and therefore likely could not significantly affect the docking predictions.

The reported top scoring proposed binding mode of **10** at the P2Y₂R is presented in Figure 2. The predicted binding poses indicate that the tricyclic dibenzocycloheptenyl moiety of **10** binds in a binding pocket created by several lipophilic and aromatic residues (Leu89, Phe113, Tyr114, Val168, Phe171, Val172, Phe195, and Phe261), designated as binding pocket L (lipophilic). The methyl substituents of **10** may act as “dowels”^{39–41} in the lipophilic binding site through lipophilic interactions with Leu89, Phe113, Val168, Phe171, and Phe195. Phe113, Tyr114, Phe195, and Phe261 in binding pocket L were confirmed to interact with the nucleobase of the agonists ATP and UTP which supports the orthosteric binding mode of antagonist **10**.^{2,3,6} The thiouracil group likely binds in a subpocket formed by two arginine residues (Arg110 and Arg292), and lipophilic residues (Phe113, Phe261, and Tyr269). Residues of ECL 2 and transmembrane region (TM) VI, namely, His184, Thr186, Tyr268, and Tyr288, are predicted to form a binding cavity accommodating the furan moiety of **10**, designated as binding pocket E (ECL). The tetrazolate group, which is deprotonated at physiological pH value of 7.4, was predicted to form salt bridges with His184 and Arg272. Compared to the apo homology model structure, minor conformational changes (<1 Å RMSD) of Leu89, Tyr114, His184, Asp185, and Arg265 were observed.

Based on the IFD predictions of the orthosteric antagonist **10** into the homology model of the human P2Y₂R, five top scoring complexes were selected for receptor grid generation for structure-based virtual high-throughput screening (vHTS). Even though the top five scoring complexes showed only negligible differences in their binding modes, we decided to perform the vHTS as ensemble docking to increase the positive hit rate. We take into account that our approach limits docking to the putative orthosteric binding site of compound **10**, while other binding modes of the discussed compounds might be feasible.

A virtual library containing 3.2 million druglike molecules was retrieved from the ZINC database and was subsequently docked into the rigid receptors resulting in five sets of 1000 compounds.^{35,36} The top 1000 scoring compounds were evaluated individually for their molecular complexity, interaction quality with target residues, correct protonation states, complementation of the binding site surface, ligand strain and disorted ligand geometry, π-stacking, structural diversity, chemical stability, and toxicity.

Binding modes of promising candidates were additionally assessed among all five ensemble complexes to take the impact of the flexibility of side chains on the docking score and spatial clashes into account. Subsequently, 46 compounds were purchased and tested for their ability to inhibit UTP-mediated P2Y₂R activation. Their inhibitory potency was determined by

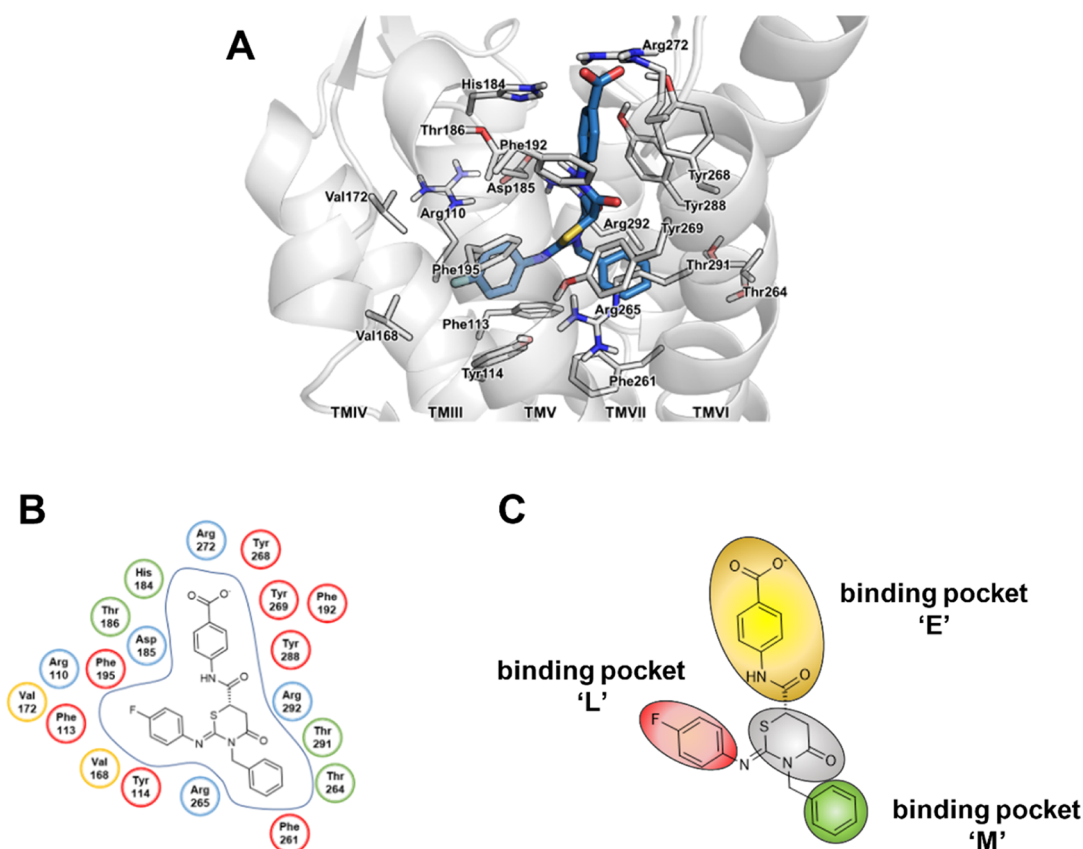


Figure 6. Putative binding mode of antagonist **14** in complex with the homology model of the human P2Y₂R. (A) Docked pose of **14** with the homology model of the human P2Y₂R shown with the residues forming the binding pocket. The receptor is displayed in cartoon representation, and the amino acid residues (white) and compound **14** (blue) are shown as stick models. Oxygen atoms are colored in red, nitrogen atoms in blue, and sulfur atoms in yellow, fluorine atoms in cyan. (B) Schematic 2D representation of the binding pocket. For color code, see Figure 2. (C) Denotation and schematic localization of lipophilic binding pocket L, binding pocket E close to the extracellular lumen, and binding pocket M with mixed properties.

a fluorescence-based calcium mobilization assay. The screening results were analyzed, and additional 12 analogues based on the initial hit compounds were purchased and pharmacologically evaluated. Compounds inhibiting the P2Y₂R were redocked into the homology model of the P2Y₂R using the induced-fit protocol to refine the binding mode prediction. The workflow of the lead structure discovery is schematically presented in Figure 3.

This approach led to the discovery of several druglike antagonist scaffolds, which likely share binding sites with the orthosteric antagonist **10**. The threshold for the selection of *in vitro* screening hits was set at 30% inhibition of UTP-(3 μM)-induced calcium mobilization assays at a test concentration of 10 μM. The hit rate for the first round of screening was 7% after exclusion of ligands which also showed ≥30% inhibition in the counterscreen assay using the same calcium mobilization assay at the muscarinic M₃R. In the second round, the hit rate increased to 17%. The relatively low screening hit rate in the first round, for example, as compared to X-ray crystal structure-based virtual screening approaches, can be explained by the low homology between the P2Y₂R and the P2Y₁R used as the template (34% sequence identity), but it was in the same range as previously published homology model-based virtual screening approaches.^{42–45} GPCRs with several X-ray crystal structures in different activation states and defined binding sites certainly allow more reliable prediction of screening hits.^{46,47} In fact, previous virtual screening studies for other

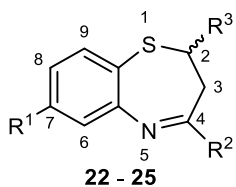
P2Y receptor subtypes were reported with hit rates ranging between <1% up to more than 50%.^{48,49}

In this study, three of the discovered active scaffolds will be discussed, whose binding modes have been analyzed. The *in vitro* hit structures do not belong to the classes of pan-assay interference compounds as assessed by available online tools.^{50,51} Excluded compounds that showed less than 30% inhibition of P2Y₂R activation at a test concentration of 10 μM, or that were equally potent in blocking the P2Y₂ and the muscarinic M₃R, are collected in Table S1 of the Supporting Information, while the selected hit compounds were further characterized.

3.1. Benzothiazole Derivatives. Pharmacological evaluation of the purchased screening hits led to the discovery of benzothiazole derivatives as P2Y₂R antagonists. The results of pharmacological evaluation are summarized in Table 1. Antagonists **11** and **12** inhibited the P2Y₂R with micromolar potency (**11**, IC₅₀ 16.6 ± 1.7 μM; **12**, 21.9 ± 0.7 μM) without displaying antagonistic activity at the muscarinic M₃R (5% and 1% inhibition at 10 μM). Compound **13** inhibited UTP-induced P2Y₂R activation with the highest potency (IC₅₀ 9.26 ± 1.92 μM) but also blocked the M₃R (68% inhibition at 10 μM). Concentration-inhibition curves of selected P2Y₂R inhibitors are shown in Figure 4.

In the virtual screening workflow, we applied the glide docking method to predict hit structures. During glide docking, the receptor is kept rigid, which facilitates calculations and

Table 3. Potencies of 1,4-Thiazepine Derivative 22 Identified by Initial Screening as Antagonist of the P2Y₂R Compared to Its Inhibitory Activity at the Acetylcholine M₃R, along with Some Inactive Analogues^{a,c}



Compound	Structure			IC ₅₀ ± SEM (μM) ^b (% inhibition at 10 μM)	
	R ¹	R ²	R ³	P2Y ₂ R ^c	M ₃ R ^d
22	CF ₃			10.9 ± 0.8	> 10 (30 %)
23	CF ₃			> 10 (-6 %)	> 10 (-14 %)
24	H			> 10 (10 %)	> 10 (-36 %)
25	H			> 10 (-20 %)	> 10 (10 %)

^aBiological assessment of the compounds was performed using calcium mobilization assays. ^bPotencies of antagonists were determined versus an agonist EC₈₀ concentrations of the agonist in the respective assays. ^cAntagonism was determined at the human P2Y₂ receptor versus UTP (3 μM). ^dAntagonism was determined at the acetylcholine M₃R versus carbachol (100 μM). ^eAll data are presented as means from three to four independent assays.

eventually reduces program runtime, disregarding adaptation of the receptor to ligand binding. In order to address this initial simplification and to refine the binding mode prediction, we redocked screening hits using IFD which allows conformational adjustments of the receptor. The redocked putative binding mode of antagonist 11 is presented in Figure 5.

The benzothiazole core of 13 is predicted to bind in the binding pocket L of the P2Y₂R (Figure 5; also see Figure 2 for designation of the binding pockets). Arg265 can form H-bonds with the nitrogen atom of the heterocycle. The *S*-enantiomer scored higher, most likely due to additional lipophilic interactions of the methyl group with Phe113. The phenylsulfane moiety is observed to be accommodated in a binding cleft formed by Phe261, Thr264, Arg265, Tyr269, Thr291, and Arg292. The nitrogen atom of the amide group is predicted to form a H-bond with the backbone of Asp185. The terminal phenyl group likely binds in pocket E, where π - π interactions with Phe195, Tyr268, and Tyr288 are feasible. The *meta*-nitrile group is likely exposed to the extracellular space, with His184 as a potential partner for H-bond interactions.

The benzothiazole was predicted to occupy the same binding pocket L as the orthosteric antagonist 10, indicating that more bulky aryl groups might be tolerated. Substitutions in positions 4 and 5 may increase antagonistic potency as the phenylsulfane does not completely fill the available space in the binding pocket which features mixed properties.

3.2. 1,3-Thiazinane Derivatives. *In vitro* screening results of the subset of discovered 2-imino-4-oxo-*N*-phenyl-1,3-thiazinane-6-carboxamide derivatives 14–21 and their structures are collected in Table 2. The chiral compounds were tested as racemates. Antagonist 14 displayed potency in the micromolar range (IC₅₀ 9.87 μM), whereas several related derivatives, 15–21, did not exhibit inhibitory effects at P2Y₂R. Compound 14 was able to fully inhibit UTP-induced P2Y₂R activation. For the concentration–response curve, see Figure 4B.

The putative binding mode of antagonist 14 at the human P2Y₂R is presented in Figure 6. The *S*-enantiomer scored higher during redocking. The 4-fluorophenylimino group may project toward the lipophilic binding pocket L. The 1,3-thiazinane moiety likely binds between Arg265 and Arg292, and close to Tyr269, with possible H-bond formation between the carbonyl oxygen atom of the 4-oxo-1,3-thiazinane hetero-

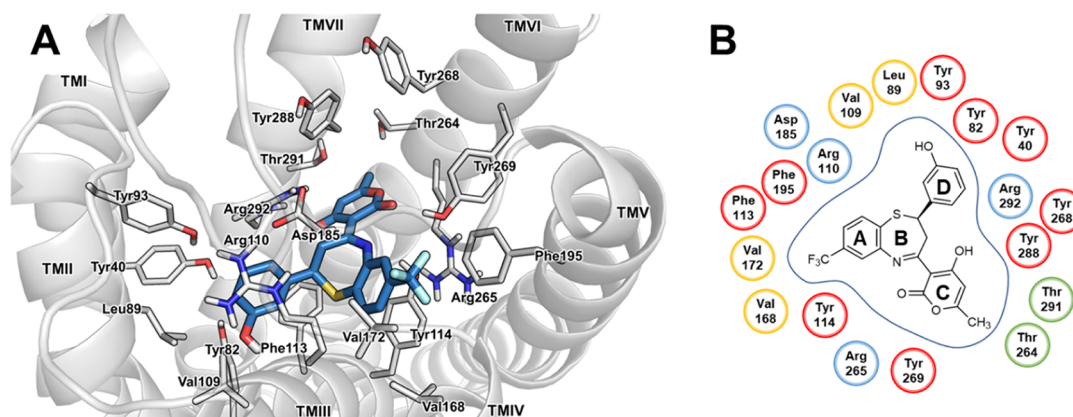


Figure 7. Putative binding mode of antagonist 22 in complex with the homology model of the human P2Y₂R. (A) Docked pose of 22 in the homology model of the human P2Y₂R shown with the residues forming the binding pocket. The receptor is displayed in cartoon representation, and the amino acid residues (white) and compound 22 (blue) are shown as stick models. Oxygen atoms are colored in red, nitrogen atoms in blue, sulfur atoms in yellow, and fluorine atoms in cyan. (B) Schematic 2D representation of the binding pocket. For color code, see Figure 2.

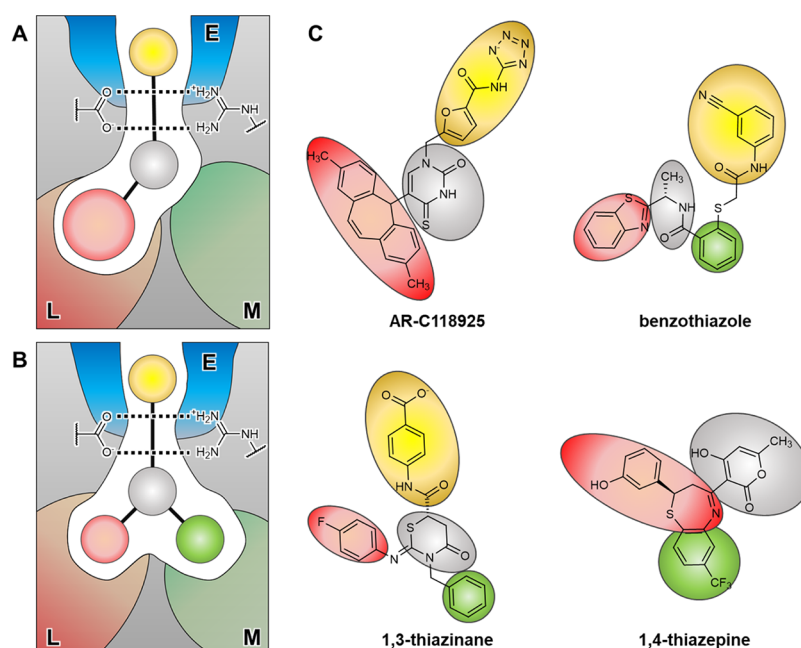


Figure 8. Schematic presentation of putative binding modes of antagonists at the human P2Y₂R. (A) Schematic diagram of the binding mode of the competitive, selective antagonist **10**. (B) Binding mode of antagonists discovered in this study. The lipophilic binding site L, denoted as “L,” is colored in red. The binding site M with mixed properties, denoted as “M,” is colored in green. The binding site E close to the extracellular compartment, denoted as “E,” is colored in blue. (C) Spheres highlighting the functional groups implicate their binding position in the P2Y₂R. The core structure (colored in gray) connects the moiety binding in binding pocket L (colored in red) with the moiety binding in binding pocket M (colored in green). Several linkers connecting the core structure with an aryl group (colored in yellow) are accepted. Asp185 and Arg292, forming an ionic lock likely involved in receptor activation, are present in proximity to the gray- and yellow-colored moieties.

cycle and Arg292. The benzyl group in position 3 is predicted to bind in a subpocket with mixed properties formed by Phe261, Thr264, Arg265, and Thr291 (binding pocket M). The amide was observed to form a H-bond with the backbone of Asp185 in the model. The 4-carboxyphenyl residue likely binds close to several aromatic residues of binding pocket E (Phe195, Tyr268, Tyr288), stabilized through π - π interactions. The carboxylate may form a salt bridge with Arg272 and a H-bond with Tyr268.

Our results suggest that binding pocket M (see Figure 6) has spatial restrictions regarding the size of substituents in position 3 of the 1,3-thiazinane ring, resulting in loss of antagonistic activity for **15** and **16**. Decreased antagonistic activity of compounds **17**–**21** may be due to the lacking of aromatic groups which allow proper π - π interactions with Phe261 and Tyr269 and/or cation- π interactions with Arg265. The redocked binding mode of antagonist **14** suggests an additional occupation of binding pocket M compared to the predicted binding mode of the selective, orthosteric antagonist **10**. The lipophilic binding pocket L accommodating the tricyclic group of **10** is not completely filled by the comparatively smaller aryl group of the investigated antagonists and may therefore provide space for modification and expansion by introduction of larger lipophilic groups.

3.4. 1,4-Thiazepine Derivatives. The investigated antagonists were pharmacologically evaluated as racemic mixtures. Among the investigated 2,3-dihydrobenzo[*b*][1,4]-thiazepine derivatives, compound **22** was the only one to display a high potency (IC₅₀ 10.9 μ M) showing full inhibition of P2Y₂R (for structures see Table 3). The concentration–inhibition curve of **22** as an antagonist of the P2Y₂R is presented in Figure 4C. Compounds **23**–**25** did not exhibit

significant inhibition in calcium mobilization assays, neither at the human P2Y₂R nor at the muscarinic M₃R.

The *R*-enantiomer of **22** scored higher during the induced-fit redocking. The aromatic system consisting of rings A and B is predicted to bind in binding pocket L, where it can be stabilized through lipophilic interactions and/or cation- π interactions with Arg265 (for ring numbering see Figure 7). The nitrogen atom possibly forms a H-bond with Tyr114. The trifluoromethyl group in position 7 of the 2,3-dihydrobenzo[*b*][1,4]-thiazepine likely projects toward Val172 and Phe195, where lipophilic interactions may contribute to antagonistic activity. The 1,4-thiazepine heterocycle binds in a chairlike conformation close to ECL2, Phe113, and Tyr114. The sulfur atom is pointing downward toward Phe113. The 2*H*-pyran-2-one moiety (ring C) likely binds in binding pocket M. H-Bond interactions between the carbonyl O atom of the lactone and Tyr269 are feasible. Possible interaction partners for the hydroxy group in position 5 include Asp185 and Arg292. Ring C of **22** is predicted to bind in a distant binding pocket created by Tyr40, Tyr82, Tyr93, Val109, Arg110, Phe113, and Arg292, where the hydroxyl group can form a H-bond with the backbone of Val109.

The putative binding mode of **22** appears to be different when compared to those of the previously discussed scaffolds. It lacks an aromatic moiety which is exposed to the extracellular domain. Rings A, B, and C likely bind similarly to the tricyclic system of **10**. The trifluoromethyl (ring A) and hydroxy (ring D) groups may therefore interact as “dowels,” like the methyl groups of **10**. The *R*-enantiomer which scored higher during redocking, likely has better interaction potential of ring D with the receptor. Loss of inhibitory activity of compound **23** may be explained by unfavorable interactions or clashes of the nitro group with the hydroxy group of the

tyrosine residues in the distant binding pocket. In the cases of **24** and **25**, lacking of the trifluoromethyl group, the loss of potential interactions of the 2*H*-pyran-2-one moiety, sterical clashes with the 2,4-dimethoxyphenyl moiety, or all of the above changes may be responsible for the loss of antagonistic activity.

Our results suggest that the discussed scaffolds share a similar binding pocket as the competitive antagonist **10**. Compared to **10**, they lack a bulky, lipophilic tricyclic group and partially occupy binding pocket L formed by residues of TM IV and V. Additional stabilization of the novel scaffolds can be ascribed to additional interactions resulting from occupation of binding pocket M, which is not occupied by **10**. In most cases, a terminal aryl group is predicted to bind in binding pocket E and to be exposed to the extracellular space. The acceptance of diverse linkers connecting the core buried in the P2Y₂R with the terminal aryl group suggests high flexibility and adaptation of ECL2. We suggest that the investigated antagonists inhibit the P2Y₂R through stabilization of an ionic lock between Asp185 and Arg292, similar to that postulated for the P2Y₁R.^{34,52} Anchoring of antagonists in the orthosteric binding site and the binding pocket M having mixed properties, as well as additional interactions with residue side chains of ECL2, will increase the stability of the ionic lock, thus impeding receptor activation. A schematic presentation of our results is presented in Figure 8. It is noteworthy that antagonist **10** bears the largest group binding in the orthosteric binding site, namely, the tricyclic moiety, which contributes to its high potency and selectivity for the P2Y₂R.

4. CONCLUSIONS

Virtual screening studies have proven to be cost- and time-efficient methods for the discovery of hit compounds and drugs.^{53,54} In this study we identified several druglike molecular scaffolds with P2Y₂R-antagonistic activity showing IC₅₀ values at low micromolar concentrations. Contrary to available tool compounds, the discovered scaffolds lacking negatively charged groups (benzothiazole, thiazepine derivatives) or containing a single carboxylate function (thiazine derivatives) have potential for oral bioavailability. Predicted binding modes of antagonists can be divided into two types: antagonist **10** which fills the putative orthosteric binding site with the tricyclic moiety and those which partly reach the lipophilic binding site (**13**, **14**, and **22**). Displaying already low micromolar potency, the structures represent good starting points for further optimization by rational drug design.

Our results will provide useful insights for future drug design of potent P2Y₂R inhibitors including ligands for the treatment of cancer, (neuro-)inflammation, and other complex diseases.

SOFTWARE AND DATA AVAILABILITY

Schrödinger Suite Maestro is available for Linux, macOS, and Windows for free for academic use and evaluation purposes at <https://www.schrodinger.com/products/maestro>. Schrödinger Suite Glide is available for Linux, macOS, and Windows for licensed users and evaluation purposes at <https://www.schrodinger.com/products/glide>. Pymol is available for Linux, macOS, and Windows for free for academic use and evaluation purposes at <https://pymol.org/2/>.

ASSOCIATED CONTENT

Supporting Information

The Supporting Information is available free of charge at <https://pubs.acs.org/doi/10.1021/acs.jcim.1c01235>.

Structures and results of inactive analogues; overview of the compound acquisition steps; structures of additional P2Y₂R antagonists as well as the following PDB files: homology model of the human P2Y₂R; AlphaFold structure of the human P2Y₂R used for RMSD calculations; five top-scoring IFD complexes of human P2Y₂R homology model with compound **10**; and IFD binding modes of compounds **13**, **14**, and **22** (PDF)

AUTHOR INFORMATION

Corresponding Author

Christa E. Müller – PharmaCenter Bonn, Pharmaceutical Institute, Pharmaceutical Sciences Bonn (PSB), Pharmaceutical & Medicinal Chemistry, University of Bonn, 53121 Bonn, Germany; Research Training Group 1873, University of Bonn, 53127 Bonn, Germany; orcid.org/0000-0002-0013-6624; Phone: +49-228-73-2301; Email: christa.mueller@uni-bonn.de; Fax: +49-228-73-2567

Authors

Alexander Neumann – PharmaCenter Bonn, Pharmaceutical Institute, Pharmaceutical Sciences Bonn (PSB), Pharmaceutical & Medicinal Chemistry, University of Bonn, 53121 Bonn, Germany; Research Training Group 1873, University of Bonn, 53127 Bonn, Germany

Isaac Attah – PharmaCenter Bonn, Pharmaceutical Institute, Pharmaceutical Sciences Bonn (PSB), Pharmaceutical & Medicinal Chemistry, University of Bonn, 53121 Bonn, Germany

Haneen Al-Hroub – PharmaCenter Bonn, Pharmaceutical Institute, Pharmaceutical Sciences Bonn (PSB), Pharmaceutical & Medicinal Chemistry, University of Bonn, 53121 Bonn, Germany

Vigneshwaran Namasivayam – PharmaCenter Bonn, Pharmaceutical Institute, Pharmaceutical Sciences Bonn (PSB), Pharmaceutical & Medicinal Chemistry, University of Bonn, 53121 Bonn, Germany; orcid.org/0000-0003-3031-3377

Complete contact information is available at: <https://pubs.acs.org/doi/10.1021/acs.jcim.1c01235>

Funding

A.N. and C.E.M. were funded by the Deutsche Forschungsgemeinschaft (DFG, German Research Foundation, 214362475/GRK1873/2). A.N., I.A., H.A.H., and C.E.M. were supported by the BMBF-funded Bonn International Graduate School Drug Sciences (BIGS DrugS). I.A. received a PhD scholarship from the Deutscher Akademischer Austauschdienst (DAAD, German Academic Exchange Service)

Notes

The authors declare the following competing financial interest(s): C.E.M. is Chair of the Board of Directors of ePURINES, a biotech company that is working in the field of P2Y₂ receptor antagonists.

■ ABBREVIATIONS

ATP, adenosine-5'-triphosphate; BPTU, 1-[2-(2-*tert*-butylphenoxy)pyridin-3-yl]-3-[4-(trifluoromethoxy)phenyl]-urea; CHO, Chinese hamster ovary; DMEM, Dulbecco's modified Eagle's medium; DMSO, dimethyl sulfoxide; DNA, deoxyribonucleic acid; ECLX, extracellular loop X ($X = 1-3$); FCS, fetal calf serum; FDA, Food and Drug Administration; GPCR(s), G protein-coupled receptor(s); HBSS, Hank's balanced salt solution; HIV, Human immunodeficiency virus; HTS, high-throughput screening; IFD, Induced-fit docking; M_3R , muscarinic M_3 receptor; PAINS, pan-assay interference compounds; PBS, phosphate-buffered saline; $P2Y_nR(s)$, $P2Y_n$ receptor(s) ($n = 1, 2, 4, 6, 11, 12, 13$ or 14); RB-2, reactive blue 2; rt, room temperature; SAR(s), structure-activity relationship(s); SP, standard precision; TMX, transmembrane region X ($X = I-VII$); UTP, uridine-5'-triphosphate; vHTS, virtual high-throughput screening; VS, virtual screening; XP, extra precision

■ REFERENCES

- (1) Sriram, K.; Insel, P. A. G Protein-Coupled Receptors as Targets for Approved Drugs: How Many Targets and How Many Drugs? *Mol. Pharmacol.* **2018**, *93*, 251–258.
- (2) Attah, I. Y.; Neumann, A.; Al-Hroub, H.; Rafehi, M.; Baqi, Y.; Namasivayam, V.; Müller, C. E. Ligand binding and activation of UTP-activated G protein-coupled P2Y2 and P2Y4 receptors elucidated by mutagenesis, pharmacological and computational studies. *Biochim. Biophys. Acta Gen. Subj.* **2020**, *1864*, 129501.
- (3) Hillmann, P.; Ko, G.-Y.; Spinrath, A.; Raulf, A.; von Kügelgen, I.; Wolff, S. C.; Nicholas, R. A.; Kostenis, E.; Höltje, H.-D.; Müller, C. E. Key determinants of nucleotide-activated G protein-coupled P2Y(2) receptor function revealed by chemical and pharmacological experiments, mutagenesis and homology modeling. *J. Med. Chem.* **2009**, *52*, 2762–2775.
- (4) Jacobson, K. A.; Costanzi, S.; Ivanov, A. A.; Tchilibon, S.; Besada, P.; Gao, Z. G.; Maddileti, S.; Harden, T. K. Structure activity and molecular modeling analyses of ribose- and base-modified uridine 5'-triphosphate analogues at the human P2Y2 and P2Y4 receptors. *Biochem. Pharmacol.* **2006**, *71*, 540–549.
- (5) Nicholas, R. A.; Watt, W. C.; Lazarowski, E. R.; Li, Q.; Harden, K. Uridine nucleotide selectivity of three phospholipase C-activating P2 receptors: identification of a UDP-selective, a UTP-selective, and an ATP- and UTP-specific receptor. *Mol. Pharmacol.* **1996**, *50*, 224–229.
- (6) Rafehi, M.; Neumann, A.; Baqi, Y.; Malik, E. M.; Wiese, M.; Namasivayam, V.; Müller, C. E. Molecular Recognition of Agonists and Antagonists by the Nucleotide-Activated G Protein-Coupled P2Y2 Receptor. *J. Med. Chem.* **2017**, *60*, 8425–8440.
- (7) Rafehi, M.; Burbiel, J. C.; Attah, I. Y.; Abdelrahman, A.; Müller, C. E. Synthesis, characterization, and in vitro evaluation of the selective P2Y2 receptor antagonist AR-C118925. *Purinergic Signal.* **2017**, *13*, 89–103.
- (8) von Kügelgen, I.; Hoffmann, K. Pharmacology and structure of P2Y receptors. *Neuropharmacology* **2016**, *104*, 50–61.
- (9) Peterson, T. S.; Camden, J. M.; Wang, Y.; Seye, C. I.; Wood, W. G.; Sun, G. Y.; Erb, L.; Petris, M. J.; Weisman, G. A. P2Y2 Nucleotide Receptor-Mediated Responses in Brain Cells. *Mol. Neurobiol.* **2010**, *41*, 356–366.
- (10) Adamson, S. E.; Montgomery, G.; Seaman, S. A.; Peirce-Cottler, S. M.; Leitinger, N. Myeloid P2Y2 receptor promotes acute inflammation but is dispensable for chronic high-fat diet-induced metabolic dysfunction. *Purinergic Signal.* **2018**, *14*, 19–26.
- (11) Chen, J.; Zhao, Y.; Liu, Y. The role of nucleotides and purinergic signaling in apoptotic cell clearance - implications for chronic inflammatory diseases. *Front. Immunol.* **2014**, *5*, 656.
- (12) Le, T.-T. T.; Berg, N. K.; Harting, M. T.; Li, X.; Eltzschig, H. K.; Yuan, X. Purinergic Signaling in Pulmonary Inflammation. *Front. Immunol.* **2019**, *10*, 1633.
- (13) Wan, H.-X.; Hu, J.-H.; Xie, R.; Yang, S.-M.; Dong, H. Important roles of P2Y receptors in the inflammation and cancer of digestive system. *Oncotarget* **2016**, *7*, 28736–28747.
- (14) Zhu, H.; Yu, Y.; Zheng, L.; Wang, L.; Li, C.; Yu, J.; Wei, J.; Wang, C.; Zhang, J.; Xu, S.; Wei, X.; Cui, W.; Wang, Q.; Chen, X. Chronic inflammatory pain upregulates expression of P2Y2 receptor in small-diameter sensory neurons. *Metab. Brain Dis.* **2015**, *30*, 1349–1358.
- (15) Dosch, M.; Gerber, J.; Jebbawi, F.; Beldi, G. Mechanisms of ATP Release by Inflammatory Cells. *Int. J. Mol. Sci.* **2018**, *19*, 1222.
- (16) Jacob, F.; Novo, C. P.; Bachert, C.; van Crombruggen, K. Purinergic signaling in inflammatory cells: P2 receptor expression, functional effects, and modulation of inflammatory responses. *Purinergic Signal.* **2013**, *9*, 285–306.
- (17) Le Duc, D.; Schulz, A.; Lede, V.; Schulze, A.; Thor, D.; Brüser, A.; Schöneberg, T. P2Y Receptors in Immune Response and Inflammation. *Adv. Immunol.* **2017**, *136*, 85–121.
- (18) Paoletti, A.; Allouch, A.; Caillet, M.; Saïdi, H.; Subra, F.; Nardacci, R.; Wu, Q.; Muradova, Z.; Voisin, L.; Raza, S. Q.; Law, F.; Thoreau, M.; Dakhli, H.; Delelis, O.; Poirier-Beaudouin, B.; Dereuddre-Bosquet, N.; Le Grand, R.; Lambotte, O.; Saez-Cirion, A.; Pancino, G.; Ojcius, D. M.; Solary, E.; Deutsch, E.; Piacentini, M.; Gougeon, M.-L.; Kroemer, G.; Perfettini, J.-L. HIV-1 Envelope Overcomes NLRP3-Mediated Inhibition of F-Actin Polymerization for Viral Entry. *Cell Rep.* **2019**, *28*, 3381–3394.
- (19) Séror, C.; Melki, M.-T.; Subra, F.; Raza, S. Q.; Bras, M.; Saïdi, H.; Nardacci, R.; Voisin, L.; Paoletti, A.; Law, F.; Martins, I.; Amendola, A.; Abdul-Sater, A. A.; Ciccosanti, F.; Delelis, O.; Niedergang, F.; Thierry, S.; Said-Sadier, N.; Lamaze, C.; Métivier, D.; Estaquier, J.; Fimia, G. M.; Falasca, L.; Casetti, R.; Modjtahedi, N.; Kanellopoulos, J.; Mouscadet, J.-F.; Ojcius, D. M.; Piacentini, M.; Gougeon, M.-L.; Kroemer, G.; Perfettini, J.-L. Extracellular ATP acts on P2Y2 purinergic receptors to facilitate HIV-1 infection. *J. Exp. Med.* **2011**, *208*, 1823–1834.
- (20) Chen, S.; Shen, T.; Nogalski, M. T. P2Y2 purinergic receptor modulates virus yield, calcium homeostasis, and cell motility in human cytomegalovirus-infected cells. *Proc. Natl. Acad. Sci. U.S.A.* **2019**, *116*, 18971–18982.
- (21) Rafehi, M.; Müller, C. E. Tools and drugs for uracil nucleotide-activated P2Y receptors. *Pharmacol. Ther.* **2018**, *190*, 24–80.
- (22) Neumann, A.; Müller, C. E.; Namasivayam, V. P2Y 1-like nucleotide receptors—Structures, molecular modeling, mutagenesis, and oligomerization. *WIREs Comput. Mol. Sci.* **2020**, *10*, 491.
- (23) Rafehi, M.; Malik, E. M.; Neumann, A.; Abdelrahman, A.; Hanck, T.; Namasivayam, V.; Müller, C. E.; Baqi, Y. Development of Potent and Selective Antagonists for the UTP-Activated P2Y4 Receptor. *J. Med. Chem.* **2017**, *60*, 3020–3038.
- (24) Xu, P.; Feng, X.; Luan, H.; Wang, J.; Ge, R.; Li, Z.; Bian, J. Current knowledge on the nucleotide agonists for the P2Y2 receptor. *Bioorg. Med. Chem.* **2018**, *26*, 366–375.
- (25) Kindon, N.; Davis, A.; Dougall, I.; Dixon, J.; Johnson, T.; Walters, I.; Thom, S.; McKechnie, K.; Meghani, P.; Stocks, M. J. From UTP to AR-C118925, the discovery of a potent non nucleotide antagonist of the P2Y2 receptor. *Bioorg. Med. Chem. Lett.* **2017**, *27*, 4849–4853.
- (26) Ali, S.; Turner, J.; Fountain, S. J. P2Y2 and P2Y6 receptor activation elicits intracellular calcium responses in human adipose-derived mesenchymal stromal cells. *Purinergic Signal.* **2018**, *14*, 371–384.
- (27) Hu, L.-P.; Zhang, X.-X.; Jiang, S.-H.; Tao, L.-Y.; Li, Q.; Zhu, L.-L.; Yang, M.-W.; Huo, Y.-M.; Jiang, Y.-S.; Tian, G.-A.; Cao, X.-Y.; Zhang, Y.-L.; Yang, Q.; Yang, X.-M.; Wang, Y.-H.; Li, J.; Xiao, G. G.; Sun, Y.-W.; Zhang, Z.-G. Targeting Purinergic Receptor P2Y2 Prevents the Growth of Pancreatic Ductal Adenocarcinoma by Inhibiting Cancer Cell Glycolysis. *Clin. Cancer Res.* **2019**, *25*, 1318–1330.

- (28) Kemp, P. A.; Sugar, R. A.; Jackson, A. D. Nucleotide-mediated mucin secretion from differentiated human bronchial epithelial cells. *Am. J. Respir. Cell Mol. Biol.* **2004**, *31*, 446–455.
- (29) Muoboghare, M. O.; Drummond, R. M.; Kennedy, C. Characterisation of P2Y2 receptors in human vascular endothelial cells using AR-C118925XX, a competitive and selective P2Y2 antagonist. *Br. J. Pharmacol.* **2019**, *176*, 2894–2904.
- (30) Perera, L. M. B.; Sekiguchi, A.; Uchiyama, A.; Uehara, A.; Fujiwara, C.; Yamazaki, S.; Yokoyama, Y.; Ogino, S.; Torii, R.; Hosoi, M.; Ishikawa, O.; Motegi, S.-I. The Regulation of Skin Fibrosis in Systemic Sclerosis by Extracellular ATP via P2Y2 Purinergic Receptor. *J. Invest. Dermatol.* **2019**, *139*, 890–899.
- (31) Pillaiyar, T.; Funke, M.; Al-Hroub, H.; Weyler, S.; Ivanova, S.; Schlegel, J.; Abdelrahman, A.; Müller, C. E. Design, synthesis and biological evaluation of suramin-derived dual antagonists of the proinflammatory G protein-coupled receptors P2Y2 and GPR17. *Eur. J. Med. Chem.* **2020**, *186*, 111789.
- (32) Kaulich, M.; Streicher, F.; Mayer, R.; Müller, I.; Müller, C. E. Flavonoids—novel lead compounds for the development of P2Y2 receptor antagonists. *Drug Dev. Res.* **2003**, *59*, 72–81.
- (33) Ferreira, N. C. d. S.; Soares-Bezerra, R. J.; da Silveira, R. F. C.; da Silva, C. M.; Oliveira, C. S.; Calheiros, A. S.; Alves, T. M.; Zani, C. L.; Alves, L. A. New Insights in Purinergic Therapy: Novel Antagonists for Uridine 5'-Triphosphate-Activated P2Y Receptors from Brazilian Flora. *J. Med. Food* **2019**, *22*, 211–224.
- (34) Zhang, D.; Gao, Z.-G.; Zhang, K.; Kiselev, E.; Crane, S.; Wang, J.; Paoletta, S.; Yi, C.; Ma, L.; Zhang, W.; Han, G. W.; Liu, H.; Cherezov, V.; Katritch, V.; Jiang, H.; Stevens, R. C.; Jacobson, K. A.; Zhao, Q.; Wu, B. Two disparate ligand-binding sites in the human P2Y1 receptor. *Nature* **2015**, *520*, 317–321.
- (35) Irwin, J. J.; Sterling, T.; Mysinger, M. M.; Bolstad, E. S.; Coleman, R. G. ZINC: a free tool to discover chemistry for biology. *J. Chem. Inf. Model.* **2012**, *52*, 1757–1768.
- (36) Sterling, T.; Irwin, J. J. ZINC 15—Ligand Discovery for Everyone. *J. Chem. Inf. Model.* **2015**, *55*, 2324–2337.
- (37) Friesner, R. A.; Murphy, R. B.; Repasky, M. P.; Frye, L. L.; Greenwood, J. R.; Halgren, T. A.; Sanschagrin, P. C.; Mainz, D. T. Extra precision glide: docking and scoring incorporating a model of hydrophobic enclosure for protein-ligand complexes. *J. Med. Chem.* **2006**, *49*, 6177–6196.
- (38) Sherman, W.; Day, T.; Jacobson, M. P.; Friesner, R. A.; Farid, R. Novel procedure for modeling ligand/receptor induced fit effects. *J. Med. Chem.* **2006**, *49*, 534–553.
- (39) Kuschak, M.; Namasivayam, V.; Rafehi, M.; Voss, J. H.; Garg, J.; Schlegel, J. G.; Abdelrahman, A.; Kehraus, S.; Reher, R.; Küppers, J.; Sylvester, K.; Hinz, S.; Matthey, M.; Wenzel, D.; Fleischmann, B. K.; Pfeifer, A.; Inoue, A.; Gütschow, M.; König, G. M.; Müller, C. E. Cell-permeable high-affinity tracers for Gq proteins provide structural insights, reveal distinct binding kinetics and identify small molecule inhibitors. *Br. J. Pharmacol.* **2020**, *177*, 1898–1916.
- (40) Schlegel, J. G.; Tahoun, M.; Seidinger, A.; Voss, J. H.; Kuschak, M.; Kehraus, S.; Schneider, M.; Matthey, M.; Fleischmann, B. K.; König, G. M.; Wenzel, D.; Müller, C. E. Macrocyclic Gq Protein Inhibitors FR900359 and/or YM-254890-Fit for Translation? *ACS Pharmacol. Transl. Sci.* **2021**, *4*, 888–897.
- (41) Voss, J. H.; Nagel, J.; Rafehi, M.; Guixà-González, R.; Malfacini, D.; Patt, J.; Kehraus, S.; Inoue, A.; König, G. M.; Kostenis, E.; Deupi, X.; Namasivayam, V.; Müller, C. E. Unraveling binding mechanism and kinetics of macrocyclic Gαq protein inhibitors. *Pharmacol. Res.* **2021**, *173*, 105880.
- (42) Carlsson, J.; Coleman, R. G.; Setola, V.; Irwin, J. J.; Fan, H.; Schlessinger, A.; Sali, A.; Roth, B. L.; Shoichet, B. K. Ligand discovery from a dopamine D3 receptor homology model and crystal structure. *Nat. Chem. Biol.* **2011**, *7*, 769–778.
- (43) Kooistra, A. J.; Vischer, H. F.; McNaught-Flores, D.; Leurs, R.; de Esch, I. J. P.; de Graaf, C. Function-specific virtual screening for GPCR ligands using a combined scoring method. *Sci. Rep.* **2016**, *6*, 28288.
- (44) Mysinger, M. M.; Weiss, D. R.; Ziarek, J. J.; Gravel, S.; Doak, A. K.; Karpiak, J.; Heveker, N.; Shoichet, B. K.; Volkman, B. F. Structure-based ligand discovery for the protein-protein interface of chemokine receptor CXCR4. *Proc. Natl. Acad. Sci. U.S.A.* **2012**, *109*, 5517–5522.
- (45) Vass, M.; Schmidt, É.; Horti, F.; Keserü, G. M. Virtual fragment screening on GPCRs: a case study on dopamine D3 and histamine H4 receptors. *Eur. J. Med. Chem.* **2014**, *77*, 38–46.
- (46) Kooistra, A. J.; Leurs, R.; de Esch, I. J. P.; de Graaf, C. From three-dimensional GPCR structure to rational ligand discovery. *Adv. Exp. Med. Biol.* **2014**, *796*, 129–157.
- (47) Senderowitz, H.; Marantz, Y. G Protein-Coupled Receptors: target-based in silico screening. *Curr. Pharm. Des.* **2009**, *15*, 4049–4068.
- (48) Costanzi, S.; Santhosh Kumar, T.; Balasubramanian, R.; Kendall Harden, T.; Jacobson, K. A. Virtual screening leads to the discovery of novel non-nucleotide P2Y1 receptor antagonists. *Bioorg. Med. Chem.* **2012**, *20*, 5254–5261.
- (49) Wang, W.; Liu, C.; Li, H.; Tian, S.; Liu, Y.; Wang, N.; Yan, D.; Li, H.; Hu, Q. Discovery of novel and potent P2Y14R antagonists via structure-based virtual screening for the treatment of acute gouty arthritis. *J. Adv. Res.* **2020**, *23*, 133–142.
- (50) Baell, J. B.; Holloway, G. A. New substructure filters for removal of pan assay interference compounds (PAINS) from screening libraries and for their exclusion in bioassays. *J. Med. Chem.* **2010**, *53*, 2719–2740.
- (51) Lagorce, D.; Bouslama, L.; Becot, J.; Miteva, M. A.; Villoutreix, B. O. FAF-Drugs4: free ADME-tox filtering computations for chemical biology and early stages drug discovery. *Bioinformatics* **2017**, *33*, 3658–3660.
- (52) Yuan, S.; Chan, H. C. S.; Vogel, H.; Filipek, S.; Stevens, R. C.; Palczewski, K. The Molecular Mechanism of P2Y1 Receptor Activation. *Angew. Chem., Int. Ed. Engl.* **2016**, *55*, 10331–10335.
- (53) Lionta, E.; Spyrou, G.; Vassilatis, D. K.; Cournia, Z. Structure-Based Virtual Screening for Drug Discovery: Principles, Applications and Recent Advances. *Curr. Top. Med. Chem.* **2014**, *14*, 1923–1938.
- (54) Neves, B. J.; Braga, R. C.; Melo-Filho, C. C.; Moreira-Filho, J. T.; Muratov, E. N.; Andrade, C. H. QSAR-Based Virtual Screening: Advances and Applications in Drug Discovery. *Front. Pharmacol.* **2018**, *9*, 1275.

6.3. Supporting Information

The Supporting Information can be accessed free of charge online at <https://pubs.acs.org/doi/10.1021/acs.jcim.1c01235?goto=supporting-info>.

Supporting Information
**Discovery of P2Y₂ Receptor Antagonist Scaffolds through Virtual High
Throughput Screening**

Alexander Neumann^{1,2}, Isaac Attah¹, Haneen Al-Hroub¹, Vigneshwaran Namasivayam¹ and
Christa E. Müller^{1,2,*}

¹ PharmaCenter Bonn, Pharmaceutical Institute, Pharmaceutical Sciences Bonn (PSB),
Pharmaceutical & Medicinal Chemistry, University of Bonn, 53121 Bonn, Germany.

² Research Training Group 1873, University of Bonn, 53127 Bonn, Germany.

§Address correspondence to:

Prof. Dr. Christa E. Müller,

Pharmazeutisches Institut

Pharmazeutische & Medizinische Chemie

An der Immenburg 4, D-53121 Bonn, Germany.

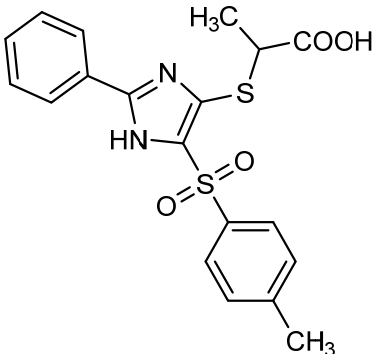
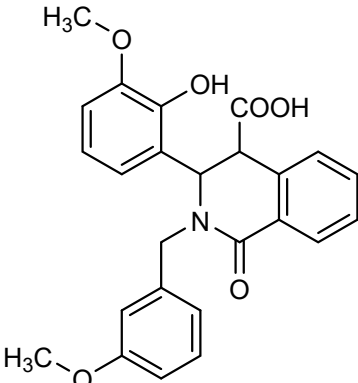
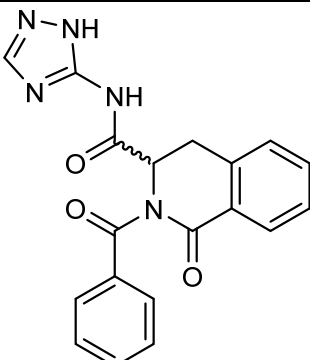
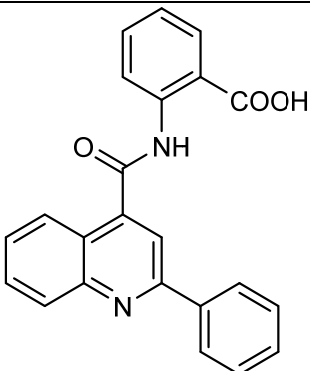
Phone: +49-228-73-2301. Fax: +49-228-73-2567.

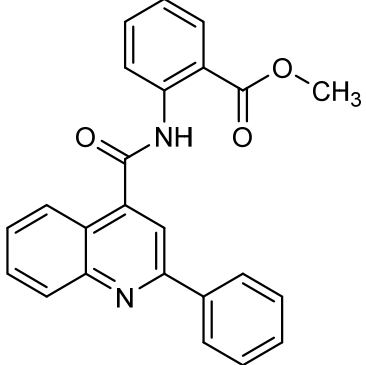
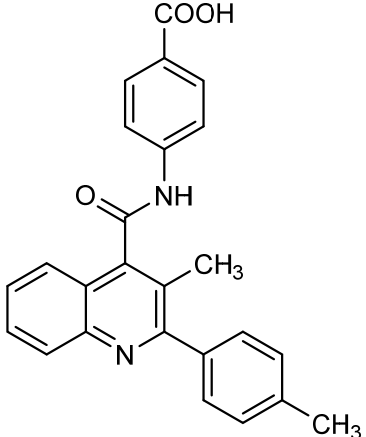
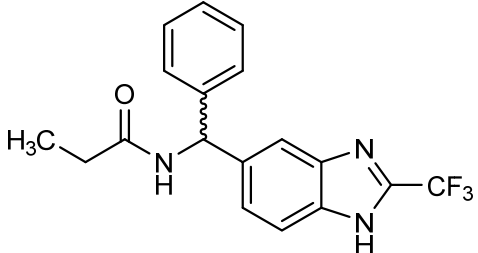
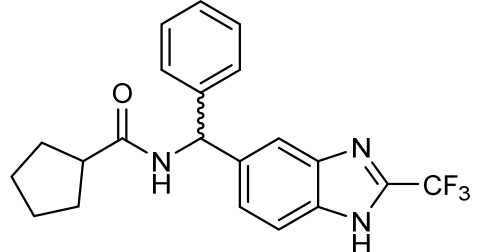
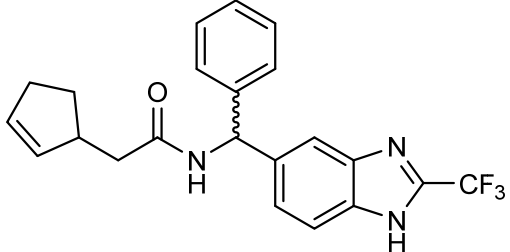
E-mail address: christa.mueller@uni-bonn.de

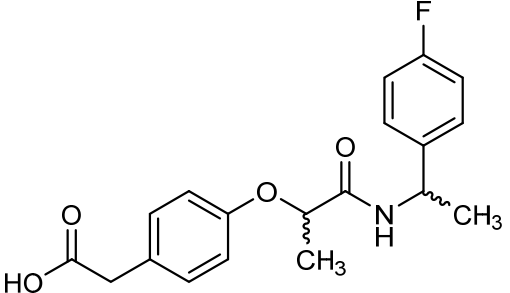
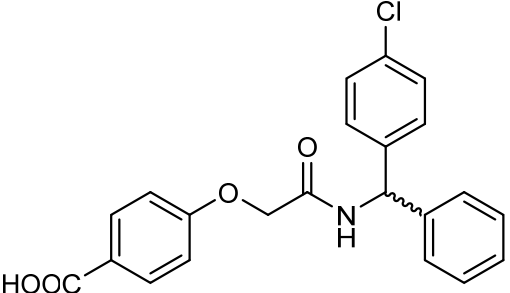
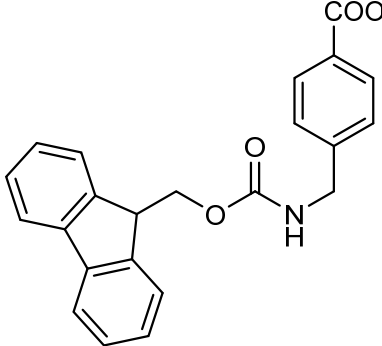
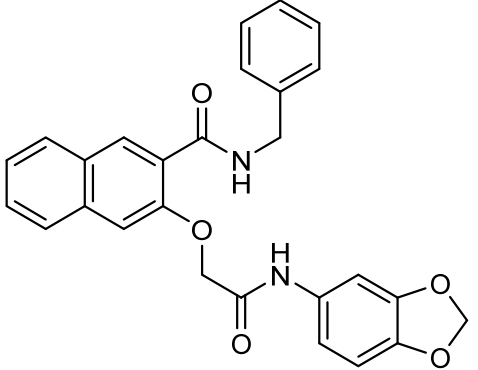
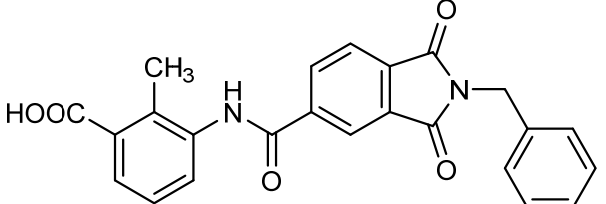
Table of Contents

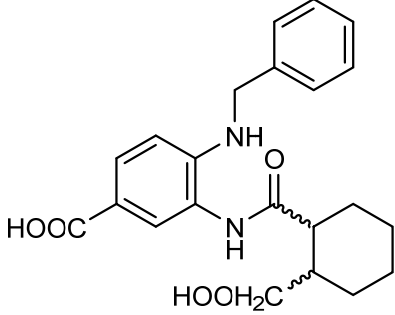
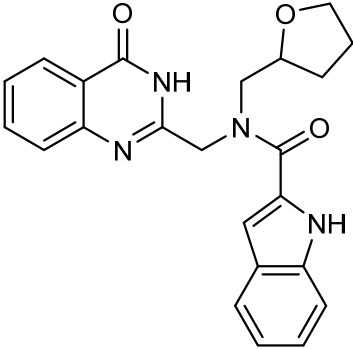
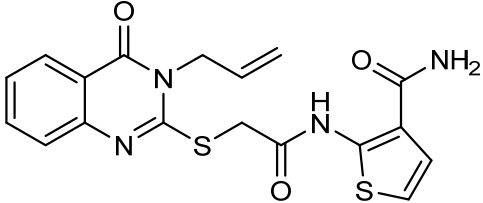
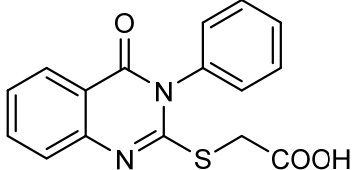
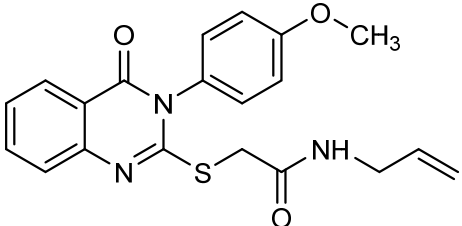
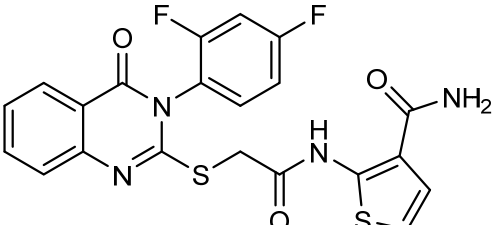
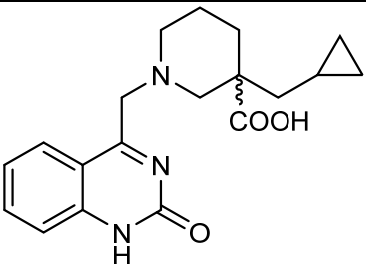
Table S1. Structures and results of inactive analogs of screening hits at the human P2Y ₂ R and at the human acetylcholine M ₃ R	3
Table S2. Overview of compound acquisition steps.....	11
Figure S1. Structures of selected flavonoids that act as allosteric P2Y ₂ R antagonists.....	12
Reference	12

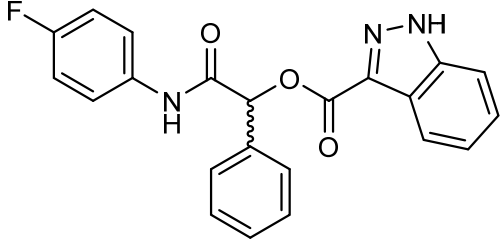
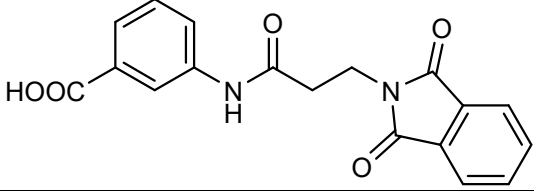
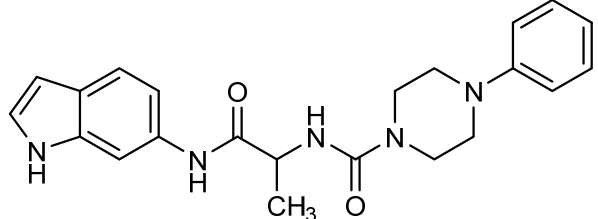
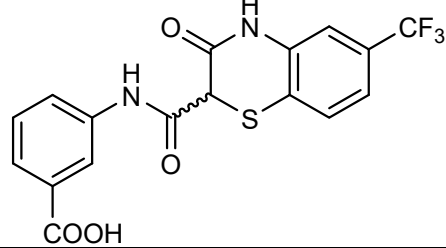
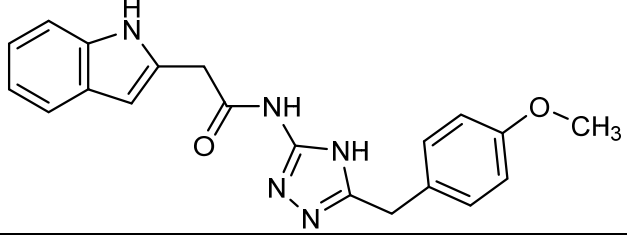
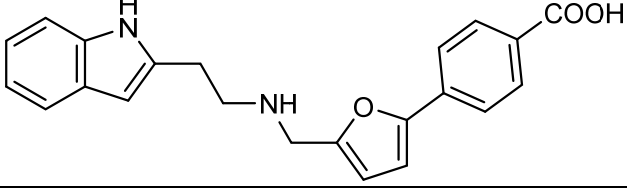
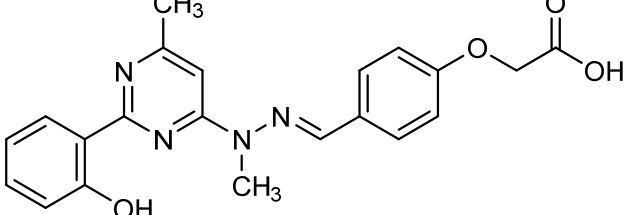
Table S1. Structures and results of inactive analogs of screening hits at the human P2Y₂R and at the human acetylcholine M₃R. Biological assessment of the compounds was performed using calcium mobilization assays.

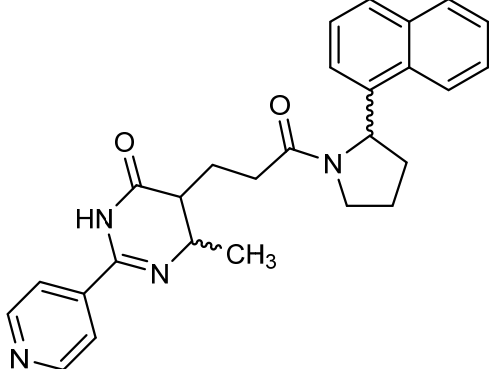
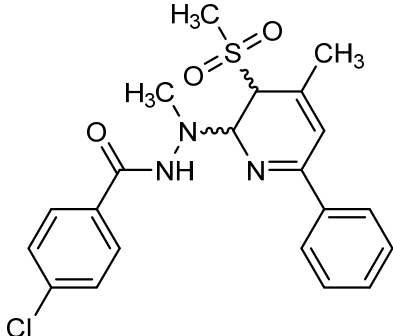
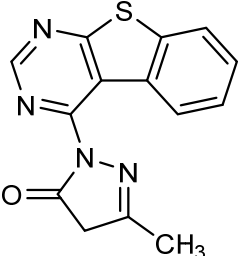
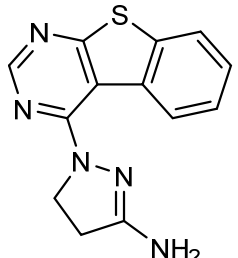
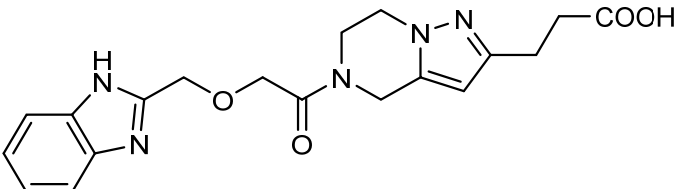
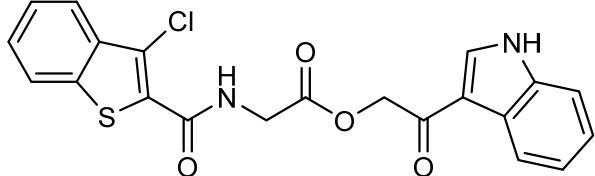
Compound	Structure	IC ₅₀ ± SEM (μM) (% inhibition at 10 μM) ^a	
		P2Y ₂ R ^a	M ₃ R ^b
26		> 10 (-11 %)	> 10 (-7 %)
27		> 10 (-9 %)	> 10 (-1 %)
28		> 10 (-23 %)	> 10 (4 %)
29		> 10 (5 %)	ca.10 (64 %)

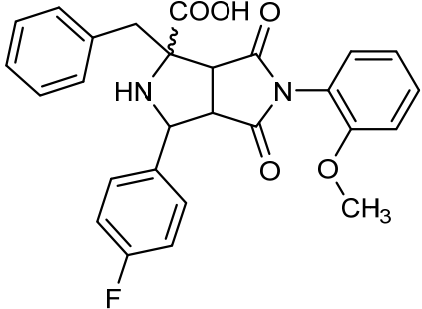
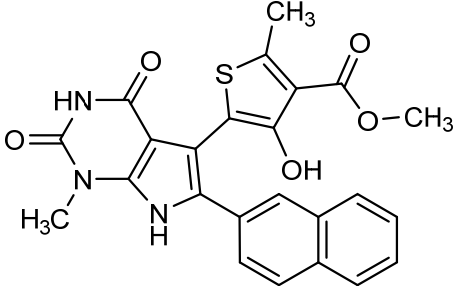
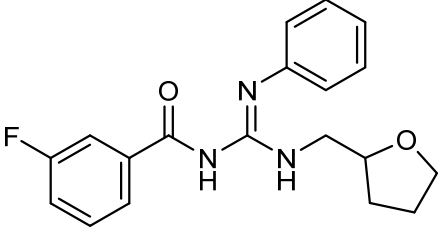
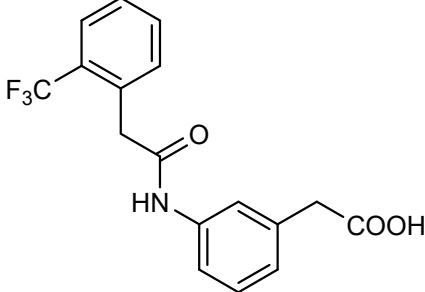
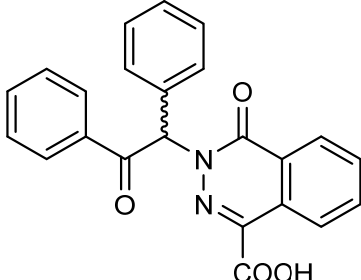
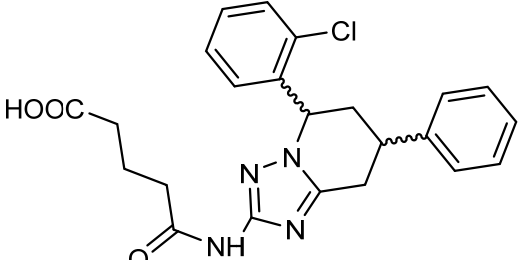
30		> 10 (-12 %)	> 10 (-35 %)
31		> 10 (7 %)	> 10 (-15 %)
32		> 10 (1 %)	> 10 (-8 %)
33		> 10 (1 %)	> 10 (1 %)
34		> 10 (-52 %)	> 10 (5 %)

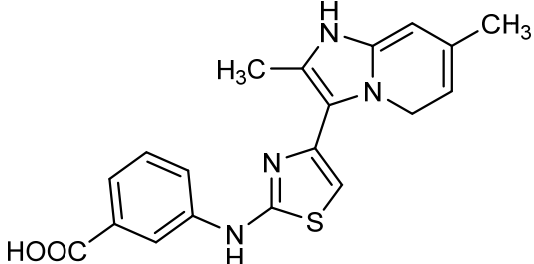
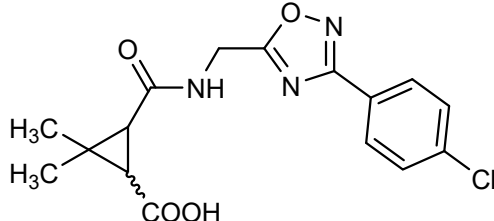
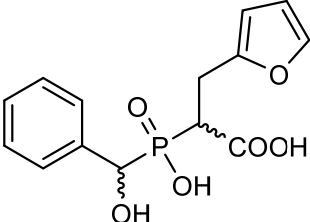
35		> 10 (-33 %)	> 10 (10 %)
36		> 10 (-37 %)	> 10 (-29 %)
37		> 10 (-62 %)	> 10 (3 %)
38		> 10 (22 %)	> 10 (15 %)
39		> 10 (4 %)	> 10 (-17 %)

40		> 10 (-4 %)	> 10 (1 %)
41		> 10 (-19 %)	> 10 (23 %)
42		> 10 (21 %)	> 10 (21 %)
43		> 10 (6 %)	> 10 (1 %)
44		> 10 (-7 %)	> 10 (1 %)
45		> 10 (6 %)	> 10 (-24 %)
46		> 10 (-11 %)	> 10 (11 %)

47		> 10 (4 %)	> 10 (12 %)
48		> 10 (-20 %)	> 10 (-19 %)
49		> 10 (-34 %)	> 10 (-18 %)
50		> 10 (-1 %)	> 10 (-33 %)
51		> 10 (-12 %)	> 10 (11 %)
52		> 10 (1 %)	> 10 (-8 %)
53		Colored, interference with test system	

54		> 10 (-32 %)	> 10 (16 %)
55		> 10 (-10 %)	> 10 (-5 %)
56		> 10 (-5 %)	> 10 (-5 %)
57		> 10 (10 %)	> 10 (15 %)
58		> 10 (-15 %)	> 10 (6 %)
59		> 10 (14 %)	> 10 (6 %)

60		> 10 (-11 %)	> 10 (22 %)
61		> 10 (26 %)	> 10 (-5 %)
62		> 10 (-22 %)	> 10 (7 %)
63		> 10 (-15 %)	> 10 (-14 %)
64		> 10 (23 %)	> 10 (-16 %)
65		> 10 (-10 %)	> 10 (-10 %)

66		> 10 (-2 %)	> 10 (-7 %)
67		> 10 (5 %)	> 10 (-5 %)
68		> 10 (-39 %)	> 10 (-3 %)

^aPotencies of antagonists were determined against EC₈₀ concentrations of agonist (3 μM UTP at the P2Y₂ receptor, 100 μM carbachol at the muscarinic M₃ receptor). All data are means from 3-4 independent experiments.

Table S2. Overview of compound acquisition steps. In the first round 47 chemically diverse compounds were purchased for in vitro assessment. In the second round 11 commercially available analogs of hits from the first round were purchased.

Compound	Round		Compound	Round
11	1		40	1
12	2		41	1
13	2		42	1
14	1		43	1
15	2		44	1
16	2		45	1
17	2		46	1
18	2		47	1
19	2		48	1
20	2		49	1
21	2		50	1
22	1		51	1
23	2		52	1
24	2		53	1
25	2		54	1
26	1		55	1
27	1		56	1
28	1		57	1
29	1		58	1
30	1		59	1
31	1		60	1
32	1		61	1
33	1		62	1
34	1		63	1
35	1		64	1
36	1		65	1
37	1		66	1
38	1		67	1
39	1		68	1

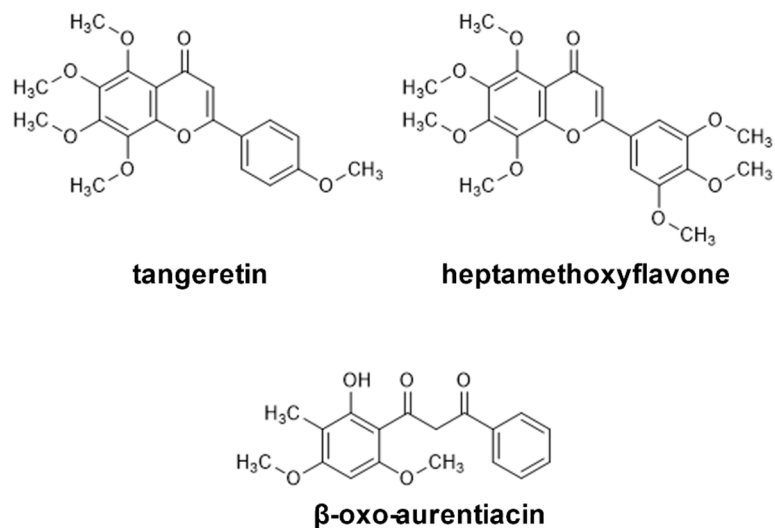


Figure S1. Structures of selected flavonoids that act as allosteric P2Y₂R antagonists.^[1]

Reference

[1] Kaulich, M.; Streicher, F.; Mayer, R.; Müller, I.; Müller, C. E. Flavonoids - novel lead compounds for the development of P2Y₂ receptor antagonists. *Drug Dev. Res.* **2003**, *59*, 72–81. DOI: 10.1002/ddr.10203.

6.4. Summary and Outlook

Although tool compounds such as the anthraquinone derivatives and the orthosteric antagonist AR-C118925 are available for target validation studies of the pharmaceutically relevant P2Y₂R, development of those to drug-like compounds represents an arduous challenge. Deduced from molecular docking studies, key interaction motifs such as the sulfonic acid groups mimic the negatively charged nature of the phosphate groups of the endogenous agonists and are therefore necessary for ligand binding. While the specified functionalities are important for proper interaction with the receptor, they lower the oral bioavailability leading to a developmental dead end for those structures if no adequate bioisoster can be found. Hence, a chemically diverse portfolio of drug-like alternatives can improve the likelihood of success to find a novel scaffold surviving the preclinical process and making it to therapeutic approval.

Utilizing the updated homology model of human P2Y₂R, a VS campaign was conducted and retrieved three novel chemically diverse inhibitor scaffolds: Benzothiazole, 2-imino-4-oxo-*N*-phenyl-1,3-thiazinane-6-carboxamide, and 1,4-thiazepine. The discovered antagonists share analogous interaction features to AR-C118925 as they are predicted to occupy the lipophilic orthosteric nucleobase binding site likely leading to the stabilization of an inactive receptor conformation. Just as importantly, the putative binding modes of the antagonists are located close to the previously discussed ionic lock between Asp185^{ECL2}-Arg292^{TM7} likely involved in agonist-induced receptor activation presumably contributing to receptor inhibition. Finally, the compounds also lack functional groups known to be metabolically unstable or accompanied by unfavorable physicochemical properties elevating them to excellent starting points for hit-to-lead optimization. The results emphasize the power of SBDD to retrieve relevant chemistry from a virtual compound library through synergistic effects of computational predictions and iterative improvement of the receptor model with biological assay data.

7. Development of Potent and Selective Antagonists for the UTP-Activated P2Y₄ Receptor

7.1. Introduction

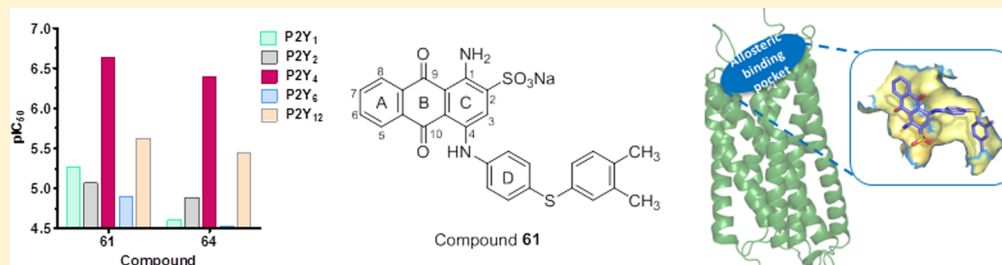
The anthraquinone derivative RB-2 belongs to one of the oldest P2YR antagonists and was even involved in characterization of receptors involved in purinergic signaling finally leading to differentiation of its members.^{87,88} It displays affinity for a broad range of proteins which usually interact with adenine nucleotides as substrate or cofactor resulting in unappealing target promiscuity. Consequently, it became an alluring template for the design of selective compounds targeting particular structures, such as P2YR subtypes, with improved potency.⁸⁹⁻⁹² Still, its potential to interact with several binding sites impedes the development of tool compounds.

The work presented in this section deals with the assessment of anthraquinones as potential inhibitors of human P2Y₄R for which only few compounds for pharmacological investigation exist. The motive of this study was the development of potent and selective P2Y₄R antagonists, as well as the elucidation of the anthraquinone binding site to distill key interactions with the receptor for future structure-based practices. For this, a library of compounds based on the anthraquinone derivative RB-2 was synthesized and assessed in calcium mobilization assays. A homology model of human P2Y₄R was created with the X-ray crystal structure of the related P2Y₁R in complex with the nucleotide-derived antagonist MRS2500 as template. Subsequently, the most potent antagonists and RB-2 were docked, and poses were assessed with the experimental data to deduce SARs for the anthraquinone derivatives. Binding mode differences between smaller molecules and the bulky RB-2 were discussed.

7.2. Publication

Development of Potent and Selective Antagonists for the UTP-Activated P2Y₄ ReceptorMuhammad Rafehi,^{†,§} Enas M. Malik,^{†,§} Alexander Neumann,[†] Aliaa Abdelrahman,[†] Theodor Hanck,[†] Vigneshwaran Namasivayam,[†] Christa E. Müller,^{*,†} and Younis Baqi^{*,‡}[†]PharmaCenter Bonn, Pharmaceutical Institute, Pharmaceutical Chemistry I, Pharmaceutical Sciences Bonn (PSB), University of Bonn, An der Immenburg 4, D-53121 Bonn, Germany[‡]Department of Chemistry, Faculty of Science, Sultan Qaboos University, PO Box 36, Postal Code 123, Muscat, Oman

Supporting Information



ABSTRACT: P2Y₄ is a G_q protein-coupled receptor activated by uridine-5'-triphosphate (UTP), which is widely expressed in the body, e.g., in intestine, heart, and brain. No selective P2Y₄ receptor antagonist has been described so far. Therefore, we developed and optimized P2Y₄ receptor antagonists based on an anthraquinone scaffold. Potency was assessed by a fluorescence-based assay measuring inhibition of UTP-induced intracellular calcium release in 1321N1 astrocytoma cells stably transfected with the human P2Y₄ receptor. The most potent compound of the present series, sodium 1-amino-4-[4-(2,4-dimethylphenylthio)phenylamino]-9,10-dioxo-9,10-dihydroanthracene-2-sulfonate (PSB-16133, **61**) exhibited an IC₅₀ value of 233 nM, selectivity versus other P2Y receptor subtypes, and is thought to act as an allosteric antagonist. A receptor homology model was built and docking studies were performed to analyze ligand–receptor interactions. Compound **64** (PSB-1699, sodium 1-amino-4-[4-(3-pyridin-3-ylmethylthio)phenylamino]-9,10-dioxo-9,10-dihydroanthracene-2-sulfonate) represents the most selective P2Y₄ receptor antagonist known to date. Compounds **61** and **64** are therefore anticipated to become useful tools for studying this scarcely investigated receptor.

INTRODUCTION

The G protein-coupled P2Y receptors represent, together with the ATP-gated ion channels known as P2X receptors, the nucleotide-activated P2 receptor family. Eight subtypes of P2Y receptors are known to exist: P2Y₁, P2Y₂, P2Y₄, P2Y₆, and P2Y₁₁ belonging to the P2Y₁-like subgroup, and P2Y₁₂, P2Y₁₃, and P2Y₁₄ that are members of the P2Y₁₂-like subgroup of P2Y receptors.^{1,2}

P2Y receptors are present in almost all human tissues, where they exert various biological functions. They are of great interest as (potential) therapeutic targets for several indications, including neurodegenerative disorders, pain, cancer, and cardiovascular diseases.^{3,4} In fact, several antithrombotic drugs on the market, namely clopidogrel, prasugrel, and ticagrelor, achieve their effect through inhibiting the human platelet P2Y₁₂ receptor.^{5–7} Despite a generally strong interest in the P2Y receptor family, relatively little is known regarding the P2Y₄ subtype. This uridine-5'-triphosphate (UTP)-activated receptor shows a wide distribution in the body, including heart, gastrointestinal tract (GIT), central nervous system (CNS), skin, and ear (cochlea).^{8–12} In the GIT, P2Y₄ receptors were

demonstrated to mediate chloride (Cl[−]) secretion in the jejunal epithelium and therefore represent possible targets for the treatment of cystic fibrosis (P2Y₄ receptor agonists) and diarrhea (P2Y₄ receptor antagonists).^{13–16} P2Y₄ receptors also appear to be involved in the regulation of amyloid precursor protein (APP) production and its release in the brain.¹⁷ Because APP accumulation is associated with the progression of Alzheimer's disease, P2Y₄ receptor antagonists might be useful as therapeutic agents for this debilitating and yet incurable disorder.¹⁷ In the heart, P2Y₄ receptors are expressed on cardiac endothelial cells; they were found to be important for cardiac endothelial cell growth and migration as well as secretion of platelet-derived growth factor B (PDGF-B). Moreover, P2Y₄ receptor-knockout mice showed defective postnatal cardiac development, including reduced heart weight. It has thus been postulated that P2Y₄ receptors could be possible targets to modulate angiogenesis and regulate cardiac remodeling and postischemic revascularization.¹⁸ In the cochlea, P2Y₄ receptors

Received: January 12, 2017

Published: March 17, 2017

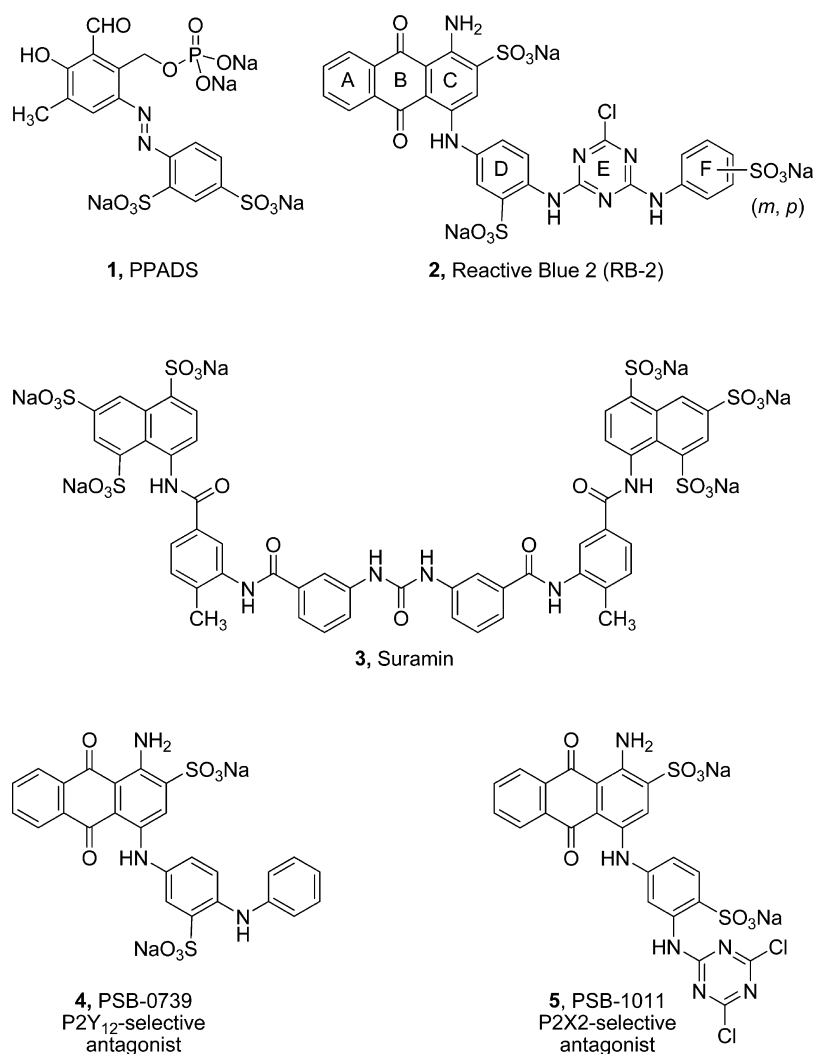


Figure 1. Structures of the classical P2 receptor antagonists PPADS, Reactive Blue 2 (RB-2), suramin, and receptor subtype-selective tool compounds derived from RB-2.

are expressed in the epithelial cells of Reissner's membrane, where they regulate Na⁺ absorption upon noise exposure,⁸ and in the apical membrane, where they are involved in K⁺ secretion across strial marginal cell epithelium during stimulation of the cochlea by sound.⁹

So far, no selective antagonists for the P2Y₄ receptor have been described.¹ However, such a compound is required as a pharmacological tool for receptor characterization and for studies aimed at target validation.¹⁹ Mouse and rat P2Y₄ receptors, which share 51% and 83% sequence identity with the human P2Y₄ receptor,^{12,20} are noncompetitively antagonized by PPADS (pyridoxal phosphate-6-azophenyl-2',4'-disulfonic acid, **1**, Figure 1) and also blocked by Reactive Blue 2 (RB-2, **2**, Figure 1).^{21,22} Rat P2Y₄ receptors, expressed in *Xenopus* oocytes, were found to be weakly antagonized by suramin (**3**, Figure 1).²³ On the other hand, human P2Y₄ receptors expressed in 1321N1 cells were ineffectively inhibited by PPADS and were insensitive to suramin²³ but were inhibited by RB-2 at micromolar concentrations.²⁴

RB-2 is a well-known nonselective P2 receptor antagonist that has served as an important pharmacological tool in the field of purinergic signaling.^{25,26} Our laboratory has been extensively working on the development of anthraquinone derivatives structurally related to RB-2 as potent and selective

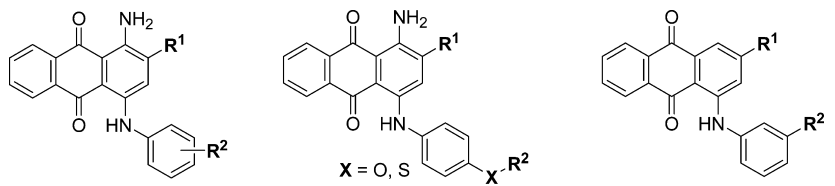
antagonists of purine receptors and ectonucleotidases.^{24,27–36}

For example, we have previously developed PSB-0739 (**4**, Figure 1),³⁰ an extremely potent and selective competitive P2Y₁₂ receptor antagonist (pA₂ of 9.8),³⁷ and PSB-1011 (**5**, Figure 1), a competitive inhibitor of the rat P2X₂ receptor with a K_i value of 79 nM.³¹

High potency and selectivity could be attained, for example, by optimizing the residue at the 4-position of the anthraquinone core. Structure–activity relationships (SARs) were found to be very different at the different purine receptor subtypes, and the anthraquinone core structure can thus be described as a “privileged structure” in medicinal chemistry.²⁶

The aim of this study was to specifically design and develop the first potent and selective P2Y₄ receptor antagonist. To this end, a library of RB-2-related anthraquinone derivatives was synthesized using recently developed methods,^{27–29,39} and the compounds were tested for their potency to block P2Y₄ receptors using a Ca²⁺-mobilization assay.⁵⁹ This data served as a basis for subsequent structure–activity relationship analyses and receptor docking studies aimed at enhancing our knowledge with respect to P2Y₄ receptor ligand preferences and for further optimizing the structures. Modifications of the substituents at the 4-position of the anthraquinone core led to

Table 1. Yields, Molecular Weights, UV Absorption, Color, and Purity of the Newly Synthesized Anthraquinone Derivatives



compd	R ¹	R ² (A,C) or R ² -X (B)	yield (%) ^a	MW (g/mol)	absorption λ _{max} (nm)	color	purity by LC-MS/UV (%) ^b
Structure A							
14	SO ₃ Na	2-chloro	36	450.83	590	blue	99.0
19	SO ₃ Na	2-methyl	80	430.41	624	blue	99.0
20	SO ₃ Na	3-methyl	70	430.41	626	blue	99.1
21	SO ₃ Na	4-methyl	72	430.41	626	blue	100.0
24	SO ₃ Na	4-ethyl	64	444.44	626	blue	99.0
25	SO ₃ Na	3-propyl	35	458.46	628	blue	97.7
33	SO ₃ Na	2,3-dimethyl	49	444.44	624	blue	99.0
34	SO ₃ Na	2,4-dimethyl	60	444.44	624	blue	99.0
35	SO ₃ Na	2,5-dimethyl	50	444.44	624	blue	99.5
37	SO ₃ Na	3,4-dimethoxy	46	476.43	624	blue	98.5
39	SO ₃ Na	3-methoxy-4-methyl	44	460.43	626	blue	98.3
40	SO ₃ Na	4-chloro-2-methyl	36	464.85	626	blue	99.0
41	SO ₃ Na	4-chloro-3-methyl	40	464.85	624	blue	99.0
42	SO ₃ Na	4-hydroxy-3-methyl	40	446.41	626	blue	96.0
43	SO ₃ Na	4-fluoro-3-methoxy	43	464.40	624	blue	99.3
44	SO ₃ Na	4-chloro-3-methoxy	40	480.85	624	blue	99.7
49	SO ₃ Na	2-carboxy-3-fluoro	40	478.38	594	blue	98.0
52	SO ₃ Na	2-carboxy-4-hydroxy	68	476.39	630	blue	100.0
53	SO ₃ Na	2-carboxy-4-nitro	21	505.39	584	blue	95.7
67	CH ₃	2-carboxy-4-fluoro	21	390.36	612	blue	99.7
Structure B							
58	SO ₃ Na	4-fluorophenoxy	41	526.47	630	blue	99.5
59	SO ₃ Na	4-chlorophenoxy	25	542.92	630	blue	98.6
60	SO ₃ Na	4-bromophenoxy	17	587.38	625	blue	96.1
61	SO ₃ Na	2,4-dimethylphenylthio	10	552.59	640	blue	96.1
62	SO ₃ Na	2,5-dimethylphenylthio	7	552.59	640	blue	98.0
63	SO ₃ Na	3,4-dimethylphenylthio	7	552.59	640	blue	95.9
64	SO ₃ Na	3-pyridylmethylthio	14	539.56	640	blue	98.6
Structure C							
68	SO ₃ H	fluoro	97	397.38	500	purple	98.5
69	SO ₃ H	methoxy	38	409.41	506	purple	95.2

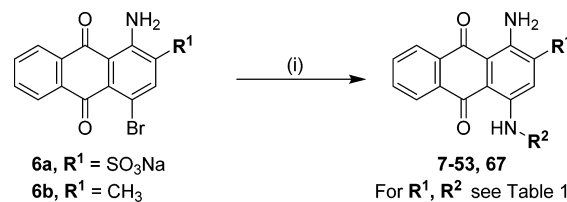
^aIsolated yield. ^bPurity of the compounds was determined using LC-MS coupled to a diode array detector (220–900 nm).

an increase in potency at the P2Y₄ receptor and resulted in selectivity for P2Y₄ over other P2Y receptor subtypes.

RESULTS AND DISCUSSION

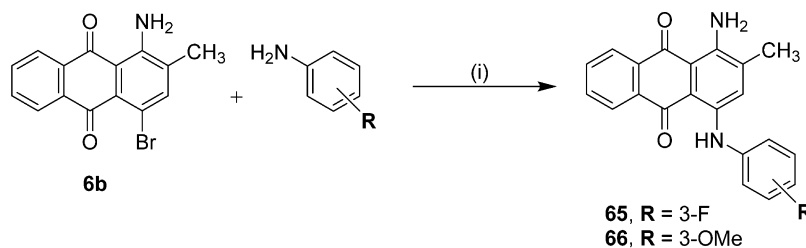
Chemistry. The target compounds were synthesized as depicted in Schemes 1–3. The syntheses of several compounds had been previously described.^{24,27–30,33,36,38–40} Some of the known anthraquinone derivatives (19–21, 24, and 33–35 (Table 1)) have now been obtained by improved synthetic procedures. In addition to known compounds, a series of 21 new compounds was prepared. Condensation of bromaminic acid (R¹ = SO₃H (**6a**)) or 1-amino-4-bromo-2-methylantraquinone (R¹ = CH₃ (**6b**)) with the appropriate amine yielded the target compounds in satisfactory to excellent isolated yields (Scheme 1). Reactions were conducted in phosphate buffer (pH 6–7) in the presence of copper powder (Cu⁰) under microwave irradiation at 80–120 °C.

Scheme 1. General Synthesis of 4-Substituted Anthraquinone Derivatives (7–53 and 67)^a



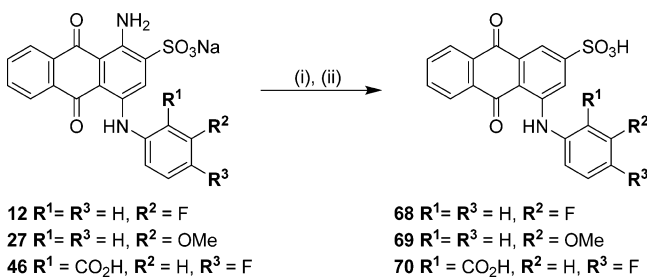
^aReagents and conditions: (i) R²-NH₂, phosphate buffer (pH 6–7), Cu⁰, microwave, 80–120 °C, 5–24 min.

Compounds **65** and **66** were synthesized from 1-amino-4-bromo-2-methylantraquinone (**6b**) by treatment with an excess of the appropriate aniline derivative (15 equiv) under argon in the presence of potassium acetate and a catalytic amount of copper(I) acetate at 110 °C for 6–15 h (Scheme 2).

Scheme 2. Synthesis of Anthraquinone Derivatives 65 and 66^a

^aReagents and conditions: (i) CuOAc, KOAc, 110 °C, argon, 6–15 h.

Three anilinoanthraquinone derivatives, **12**, **27**, and **46**, which bear a primary amino group in the 1-position of the anthraquinone moiety, were treated with sodium nitrite in hydrochloric acid solution (1 M) at 0 °C for 5 min, then allowed to warm up to room temperature followed by the addition of ethanol and an excess of zinc powder (10 equiv) to achieve deamination,³⁹ affording the desired products **68–70** (Scheme 3).

Scheme 3. Synthesis of Deaminated Anthraquinone Derivatives 68–70^a

^aReagents and conditions: (i) NaNO₂, HCl (1 M), 0–5 °C, 5 min; (ii) Zn (10 equiv), ethanol, rt, 30 s.

Purification of Reactive Blue 2. RB-2 has been used for decades as a valuable pharmacological tool for studying nucleotide receptors. Most studies relied on commercially available products. However, there has always been some doubt regarding the identity and purity of commercial products, making it difficult to obtain reliable pharmacological results.^{41–43} RB-2 is a mixture of two isomers bearing a sulfonate group either in position 3 or 4 of ring F (compound **2**, Figure 1). Thus, we decided to investigate the purity of commercially available RB-2. The purity of the investigated RB-2 was declared to be 88.2% as determined by HPLC-UV. However, the employed technique is not suitable to detect inorganic impurities, e.g., inorganic salts. Therefore, we purified commercially available RB-2 by reversed phase-18 flash column chromatography (RP-18 FCC, for details see Experimental Section). Subsequent analysis showed that the commercial product only contained 54% of RB-2, while the main organic contaminant was found to be the precursor of RB-2, namely disodium 1-amino-4-[4-(4,6-dichloro-[1,3,5]triazin-2-ylamino)-3-sulfonatophenylamino]-9,10-dioxo-9,10-dihydroanthracene-2-sulfonate (ca. 12%). Moreover, it was found to be contaminated with ca. 34% of inorganic salts, presumably NaCl and Na₃PO₄, which were washed out during the purification step using RP-18 column chromatography.

Biological Assays. The potencies of the compounds were determined using a fluorescence-based Ca²⁺-mobilization assay

according to the following principle: monoclonal colonies of 1321N1 astrocytoma cells stably transfected with the human P2Y₄ receptor were loaded with the acetoxymethyl ester of the calcium-sensitive fluorescent dye fluo-4. The P2Y₄ receptor is coupled to G_q protein. Thus, receptor activation with the endogenous ligand UTP will lead to an increase in the intracellular calcium ion concentration and a rise in the intensity of fluorescent light emitted by the dye. Test compounds that act as P2Y₄ receptor antagonists inhibit the increase in fluorescence intensity, which is monitored using a microplate fluorescence reader. Prior to evaluating the antagonistic activity of the anthraquinone derivatives, a concentration–response curve of the agonist UTP at the human P2Y₄ receptor was obtained (Figure 2). The EC₈₀ of

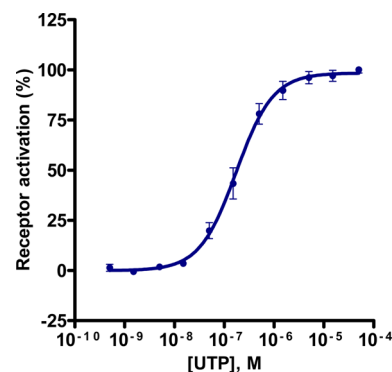


Figure 2. Concentration–response curve of the agonist UTP determined by calcium mobilization assays on recombinant 1321N1 astrocytoma cells stably expressing the human P2Y₄ receptor. Data points shown are the mean values of eight independent experiments, each performed in duplicate. The determined EC₅₀ of UTP is 203 ± 41 nM. The calculated EC₈₀ value is 565 nM.

UTP at this cell line was determined to be 565 nM. A UTP concentration of 500 nM, close to its EC₈₀ value, was subsequently used for receptor activation for the determination of antagonist potency using the calcium mobilization assay.

A total of 64 synthesized anthraquinone derivatives including 21 new compounds not previously described in the literature along with the commercially obtained and the purified RB-2 were tested for their inhibitory activity at the human P2Y₄ receptor. The IC₅₀ values are summarized in Tables 2–4.

Structure–Activity Relationships. Purified RB-2 (2′) displayed an IC₅₀ value of 0.625 μM and hence was more potent than the commercially available RB-2 (IC₅₀ = 1.14 μM, Figure 3 and Table 2). This is very reasonable, because the dye content of commercially available RB-2 was found to be only 54%. While the Hill slope of the concentration–inhibition curve for purified RB-2 (2′) was found to be close to unity,

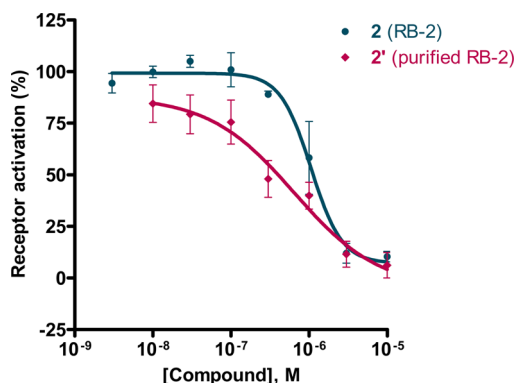


Figure 3. Concentration–response curves of the commercially available RB-2 (**2**) and purified RB-2 (**2'**), determined using the calcium-mobilization assay on recombinant 1321N1 astrocytoma cells stably expressing the human P2Y₄ receptor. UTP at a concentration of 500 nM (\sim EC₈₀) was used for receptor activation. Data points shown are the mean values of at least three independent experiments, each performed in duplicate. The IC₅₀ values are 1.14 ± 0.31 for the commercially available RB-2 (**2**), Hill slope -2.20 , and 0.625 ± 0.198 for the purified RB-2 (**2'**), Hill slope -0.80 .

crude RB-2 had a much steeper Hill slope of -2.20 . This might be due to allosteric modulatory effects of the contaminants present in the nonpurified material, e.g., inorganic salts.⁴⁴

Regarding the synthesized compounds, the structurally simple 1-amino-4-phenylamino-2-sulfoanthraquinone, acid blue-25 (AB-25, **7**), showed inhibitory activity at low micromolar concentrations (IC₅₀ = 3.10 μ M), being almost as potent as the much larger RB-2 (IC₅₀ = 1.14 μ M). Replacing the phenylamino ring by benzylamino, phenethylamino, or α -naphthylamino (**8**–**10**) decreased the activity by more than 2-fold (Table 2).

Table 2. Antagonistic Activity of Anthraquinone Derivatives at the Human P2Y₄ Receptor, Part I

Compound	R	IC ₅₀ \pm SEM (μ M) ^a
7		3.10 ± 0.35
8		14.4 ± 3.5
9		7.18 ± 0.80
10		7.42 ± 2.77
2 (RB-2)	For structure, see Figure 1	1.14 ± 0.31
2' (RB-2 purified)	For structure, see Figure 1	0.625 ± 0.198

^aPotency to inhibit calcium mobilization following receptor activation with 500 nM UTP (EC₈₀) in 1321N1 astrocytoma cells stably transfected with the human P2Y₄ receptor.

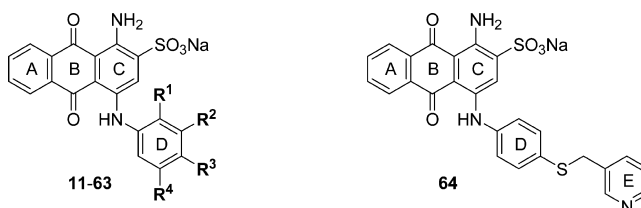
These results suggested that a phenylamino substituent at the 4-position of the anthraquinone core structure is preferred for P2Y₄ receptor inhibitory potency over a benzyl or phenethyl residue. Therefore, a library consisting of 60 derivatives of lead structure **7** with various mono- and di-substitutions on the phenyl ring attached to the 4-amino group was investigated for inhibitory potency at the P2Y₄ receptor (see Table 3).

Introducing different lipophilic substituents in the *ortho*-, *meta*-, and *para*-positions in ring D, e.g. a halogen atom (F, Cl, Br), an alkyl (CH₃, C₂H₅, C₃H₇), or a methoxy group, did not alter the activity, which ranged between 1 and 9 μ M (compounds **11**–**28**, Table 3). On the other hand, introducing hydrophilic moieties led to a reduction in potency by over a 10-fold in the case of *meta*- and *para*-carboxy, while *ortho*-carboxy and *para*-hydroxy substitutions were tolerated (compounds **29**–**32**, Table 3).

In the next step, we assessed di-substitution in ring D (Table 3): di-substitution with lipophilic residues did not alter the compounds' potency (compounds **33**–**41** and **43**–**45**, Table 3). However, a combination of lipophilic and hydrophilic substituents affected the activity in three different directions: 3-methyl-4-hydroxy (**42**; IC₅₀ = 0.746) enhanced the antagonistic activity by over 4-fold, 2-carboxy-5-chloro (**51**; IC₅₀ = 2.76) was tolerated, whereas any other combination, 2-carboxy-4-fluoro (**46**), 2-carboxy-4-chloro (**47**), 2-carboxy-4-bromo (**48**), 2-carboxy-3-fluoro (**49**), 2-carboxy-5-fluoro (**50**), 2-carboxy-3-hydroxy (**52**), and 2-carboxy-3-nitro (**53**), dramatically decreased the inhibitory activity up to over a hundred-fold (Table 3).

To investigate the effect of the presence of an additional ring E, 11 new compounds (**54**–**64**) were synthesized. In the first step, different bridges (CH₂, O, NH, S) in the *para*-position of ring D were investigated. All four linkers were tolerated (compounds **54**–**57**, IC₅₀ = 3.45, 1.94, 1.91, and 1.18 μ M, respectively, Table 3). In the next step, different substituents were introduced into ring E, including halogen (F, Cl, Br) and methyl groups. 4-Fluorophenoxy and 4-bromophenoxy residues were found to have no influence on the antagonistic activity (compounds **58** and **60**, IC₅₀ = 1.69 and 1.76, respectively, Table 3), while 4-chlorophenoxy substitution increased the potency by >8-fold (**59**, IC₅₀ = 0.373). Di-methylation in ring E with a sulfide linker between ring D and E improved potency by more than 13-fold (compounds **61**–**64**, IC₅₀ = 0.233, 0.395, 0.482, and 0.409 μ M, respectively, Table 3 and Figure 4). Indeed, compound **61** (IC₅₀ = 0.233 μ M) can be considered as the most potent P2Y₄ receptor antagonist known to date.

As a next step, we were interested in investigating the effects of other substituents on the anthraquinone core, namely the amino group in the 1-position and the sulfonate group in the 2-position. Therefore, we developed six new analogues (**65**–**70**, Table 4) of selected anthraquinone derivatives (**12**, **27**, and **46**). No improvement in the activity of compound **46** (IC₅₀ > 100, Table 3) was observed upon replacement of the sulfonate group with a methyl group (compound **67**) or upon deamination at the 1-position (compound **70**). Moreover, replacement of the 2-sulfonate group of compounds **12** and **27** (IC₅₀ = 1.39 and 1.70 μ M, respectively, Table 3) with a methyl group completely abolished the activity (compounds **65** and **66**, respectively, Table 4). Similar results were obtained with the deaminated compounds **68** and **69** (Table 4). These results indicate that the presence of an amino group in the 1-position and a sulfonate function in the 2-position of the anthraquinone core are essential for antagonistic activity at the P2Y₄ receptor.

Table 3. Antagonistic Activity of Anthraquinone Derivatives at the Human P2Y₄ Receptor, Part II

compd	R ¹	R ²	R ³	R ⁴	IC ₅₀ ± SEM (μM) ^a (or % inhibition at indicated concentration)
11	F	H	H	H	1.97 ± 0.42
12	H	F	H	H	1.39 ± 0.36
13	H	H	F	H	4.04 ± 1.01
14	Cl	H	H	H	9.34 ± 2.07
15	H	Cl	H	H	2.34 ± 0.71
16	H	H	Cl	H	3.03 ± 0.66
17	H	Br	H	H	6.96 ± 0.73
18	H	H	Br	H	3.30 ± 0.09
19	CH ₃	H	H	H	3.49 ± 0.29
20	H	CH ₃	H	H	2.22 ± 0.31
21	H	H	CH ₃	H	2.82 ± 0.92
22	C ₂ H ₅	H	H	H	3.53 ± 1.21
23	H	C ₂ H ₅	H	H	1.51 ± 0.48
24	H	H	C ₂ H ₅	H	3.21 ± 0.91
25	H	C ₃ H ₇	H	H	2.99 ± 0.12
26	OMe	H	H	H	3.98 ± 1.39
27	H	OMe	H	H	1.70 ± 0.24
28	H	H	OMe	H	2.59 ± 0.72
29	H	H	OH	H	3.16 ± 0.58
30	CO ₂ H	H	H	H	6.10 ± 1.72
31	H	CO ₂ H	H	H	23.4 ± 3.6
32	H	H	CO ₂ H	H	≈30 (57%) ^b
33	CH ₃	CH ₃	H	H	2.63 ± 0.59
34	CH ₃	H	CH ₃	H	3.58 ± 0.25
35	CH ₃	H	H	CH ₃	11.2 ± 1.2
36	H	CH ₃	H	CH ₃	6.45 ± 2.22
37	H	OMe	OMe	H	4.98 ± 0.99
38	H	OMe	H	OMe	9.25 ± 4.56
39	H	OMe	CH ₃	H	4.13 ± 0.99
40	CH ₃	H	Cl	H	2.20 ± 0.52
41	H	CH ₃	Cl	H	1.65 ± 0.37
42	H	CH ₃	OH	H	0.746 ± 0.076
43	H	OMe	F	H	1.54 ± 0.66
44	H	OMe	Cl	H	3.37 ± 1.09
45	H	F	H	F	12.5 ± 2.3
46 ²⁴	CO ₂ H	H	F	H	>100 (17%) ^c
47	CO ₂ H	H	Cl	H	>100 (31%) ^c
48	CO ₂ H	H	Br	H	>100 (30%) ^b
49	CO ₂ H	F	H	H	>100 (10%) ^c
50	CO ₂ H	H	H	F	>100 (33%) ^c
51	CO ₂ H	H	H	Cl	2.76 ± 0.75
52	CO ₂ H	H	OH	H	21.1 ± 7.1
53	CO ₂ H	H	NO ₂	H	>30 (30%) ^b
54	H	H	benzyl	H	3.45 ± 0.41
55	H	H	phenoxy	H	1.94 ± 0.54
56	H	H	phenylamino	H	1.91 ± 0.28
57	H	H	phenylthio	H	1.18 ± 0.09
58	H	H	4-fluorophenoxy	H	1.69 ± 0.38
59	H	H	4-chlorophenoxy	H	0.373 ± 0.112
60	H	H	4-bromophenoxy	H	1.76 ± 0.49
61	H	H	2,4-dimethylphenylthio	H	0.233 ± 0.079
62	H	H	2,5-dimethylphenylthio	H	0.395 ± 0.082
63	H	H	3,4-dimethylphenylthio	H	0.482 ± 0.137

Table 3. continued

compd	R ¹	R ²	R ³	R ⁴	IC ₅₀ ± SEM (μM) ^a (or % inhibition at indicated concentration)
64			see structure above		0.409 ± 0.138

^aPotency to inhibit calcium mobilization following receptor activation with 500 nM UTP (EC₈₀) in 1321N1 astrocytoma cells stably transfected with the human P2Y₄ receptor. ^b% Inhibition at 30 μM. ^c% Inhibition at 100 μM.

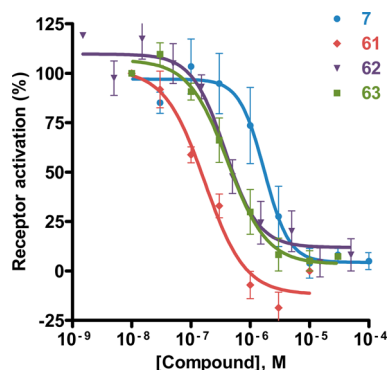


Figure 4. Concentration–response curves of selected anthraquinone derivatives, determined using the calcium mobilization assay with recombinant 1321N1 astrocytoma cells stably expressing the human P2Y₄ receptor. UTP at a concentration of 500 nM (EC₈₀) was used for receptor activation. Data points shown are the mean values of at least three independent experiments, each performed in duplicate. The IC₅₀ values are found in Tables 2 and 3.

Comparison of Structure–Activity Relationships of Anthraquinone Derivatives at Different Targets. An overview of the structure–activity relationships (SARs) of the investigated anthraquinone derivatives at the human P2Y₄ receptor is depicted in Figure 5. The ABCDE aromatic ring system proved to be important for high inhibitory potency. The amino function in the 1-position and the sulfonate group in the 2-position of the anthraquinone scaffold were found to be essential for the activity. This is in accordance with previous

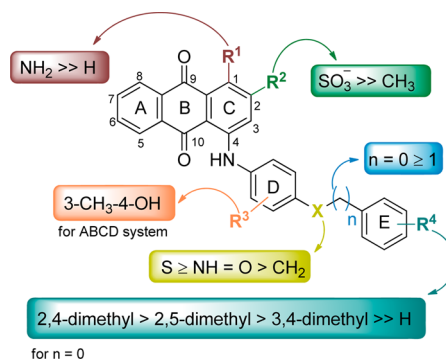


Figure 5. Summary of structure–activity relationships of anthraquinone derivatives as P2Y₄ receptor antagonists.

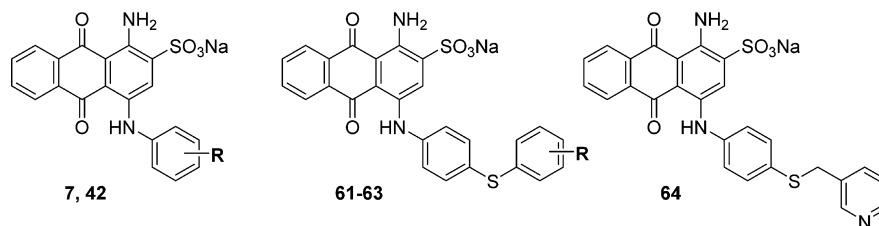
studies on the SARs of RB-2 and related dyes, which showed that AB-25 is the minimum structural requirement for biological activity of this class of compounds.^{24,29,30,33,45–52} Moreover, the activity on the P2Y₄ receptor was strongly affected by the substituents present on ring E, e.g., a lipophilic substitution in the *ortho*-, *meta*-, or *para*-position increased the activity, while an unsubstituted ring E with an –SCH₂– linker was also tolerated.

It is interesting to compare the results of the SAR analysis at the human P2Y₄ receptor with that at other purinergic targets (Figure 53, Supporting Information). The main difference between the human P2Y₄ receptor and both the human P2Y₁₂ receptor and P2Y₁-like receptors of the guinea-pig taenia coli (receptor was not cloned but found to be pharmacologically

Table 4. Inhibitory Potencies at the Human P2Y₄ Receptor of Selected Anthraquinone Derivatives Modified in the 1- and 2-Positions

compd	R ¹	R ²	R ³	IC ₅₀ ± SEM (μM) ^a (or % inhibition at indicated concentration)
Structure A				
12	H	F	H	1.39 ± 0.36
27	H	OMe	H	1.70 ± 0.28
46	CO ₂ H	H	F	>100 (17%) ^c
Structure B				
65	H	F	H	>30 (–4%) ^b
66	H	OMe	H	>30 (38%) ^b
67	CO ₂ H	H	F	≈100 (57%) ^c
Structure C				
68	H	F	H	≈30 (49%) ^b
69	H	OMe	H	>10 (77%) ^b
70	CO ₂ H	H	F	>100 (25%) ^c

^aPotency to inhibit calcium mobilization following receptor activation with 500 nM UTP (EC₈₀) in 1321N1 astrocytoma cells stably transfected with the human P2Y₄ receptor. ^bPercent inhibition at 30 μM. ^cPercent inhibition at 100 μM.

Table 5. Selectivity of the Most Potent P2Y₄ Receptor Antagonists versus Other P2Y Receptor Subtypes^a

compd	R	IC ₅₀ ± SEM (μM) or (% inhibition at 50 μM)				
		hP2Y ₄	hP2Y ₁	hP2Y ₂	hP2Y ₆	hP2Y ₁₂
7	H	3.10 ± 0.35	17.6 ± 6.5	17.1 ± 6.3	2.79 ± 0.17	3.12 ± 1.17
42	3-methyl-4-hydroxy	0.746 ± 0.076	7.65 ± 1.90	16.4 ± 4.5	4.75 ± 1.49	0.0604 ± 0.0147
61	2,4-dimethyl	0.233 ± 0.079	5.48 ± 0.34	8.54 ± 1.45	12.5 ± 3.9	2.41 ± 0.45
62	2,5-dimethyl	0.395 ± 0.082	2.72 ± 0.59	6.52 ± 1.04	2.67 ± 0.91	2.96 ± 0.24
63	3,4-dimethyl	0.482 ± 0.137	4.55 ± 0.42	10.2 ± 1.5	4.36 ± 0.60	2.34 ± 0.10
64	see structure above	0.409 ± 0.138	~25 (61 ± 4%)	13.1 ± 2.6	>> 100 (12 ± 19%)	3.59 ± 0.38

^aPotency to inhibit calcium mobilization in 1321N1 astrocytoma cells recombinantly expressing human P2Y receptors following receptor activation with 500 nM ADP (P2Y₁), 500 nM UTP (P2Y₂, P2Y₄), or 750 nM UDP (P2Y₆). Potency at the G_i-coupled P2Y₁₂ receptor was determined using a β-arrestin translocation assay.

similar to the recombinant P2Y₁-receptor subtype⁴¹ is that substitution of ring D with a sulfonate group at the *meta*-position (for P2Y₁₂ receptors)^{30,37} and at the *ortho*-position (for the P2Y₁-like receptors) was essential for the inhibitory activity of the compounds. An additional ring F was also important in case of the P2Y₁-like receptor.^{32,42} For activity at the AMP-hydrolyzing enzyme *ecto*-5'-nucleotidase, ring system ABCD was sufficient for the inhibitory activity.²⁴ In contrast, a triazine or pyrimidine as ring E was preferred by the P2X₂ receptor.³¹ On the other hand, development of anthraquinone compounds as large conductance Ca²⁺-activated K⁺ channel openers showed a preference for a bulky and hydrophobic ring D.⁵³ Interestingly, the amino group at ring C was not essential for activity at that target.⁵³

These differences in SARs emphasize the influence of the nature of substituents at the 4-position of the anthraquinone ring on the potency and target selectivity of the compounds, and allow the development of receptor (subtype)-selective ligands.

Selectivity. To gain insights into the selectivity of these compounds, we assessed the most potent compounds of this series, 61–64, on the receptor subtypes that share the greatest sequence homology with the P2Y₄ receptor, namely P2Y₁, P2Y₂, and P2Y₆, which belong to the subgroup of G_q protein-coupled P2Y₁-like P2Y receptors. In addition, we investigated selected compounds at the P2Y₁₂ receptor that had previously been shown to be potently blocked by anthraquinone derivatives.³⁰ Table 5 and Figure 6 summarize the results. Of this series of compounds, 64 is the most selective one, with particularly high selectivity versus the P2Y₁ and P2Y₆ receptors, where it showed only low potency. Selectivity against the P2Y₁₂ receptor was also observed. It can therefore be concluded that these compounds display P2Y₄ receptor selectivity, and it is not only the potency but also the selectivity of lead structure 7 that has been significantly enhanced (see Figure 6).

The Binding Mode of Anthraquinone Derivatives at the P2Y₄ Receptor. The mode of antagonism, competitive or noncompetitive, at the P2Y₄ receptor was determined using the most potent compound (61) of the present series. Concentration–response curves of the endogenous ligand UTP after a preincubation with fixed concentrations of 61 were obtained.

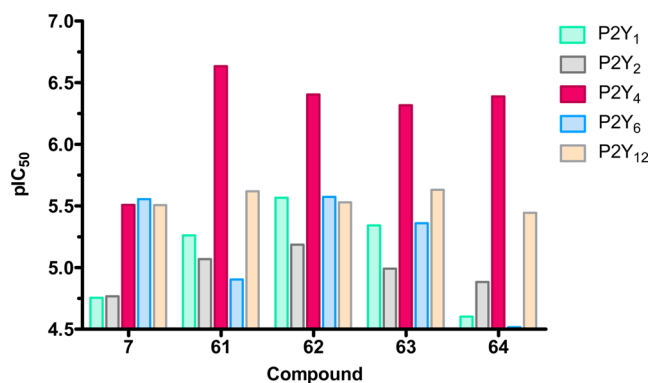


Figure 6. Potencies of selected anthraquinone derivatives on different human P2Y receptors determined using the calcium mobilization assay (P2Y_{1–6} receptors) or β-arrestin translocation assay (P2Y₁₂ receptor). Shown are the pIC₅₀ values of at least three independent experiments performed in duplicate.

For a competitive antagonist, a parallel rightward shift of the curves toward higher concentrations of UTP would be expected with increasing concentrations of 61. The upper plateaus of the curves, corresponding to the maximum receptor activation, should remain unaltered. A corresponding Schild plot would show a straight line with a slope of approximately 1. Noncompetitive antagonism, on the other hand, is characterized by a suppression of the maximum receptor activation with increasing antagonist concentrations, while the EC₅₀ remains largely unaffected. Our results, summarized in Figure 7, show a significant depression of the upper plateaus of the UTP curves with increasing concentrations of 61. The reduction in the maximum receptor activation is successively more pronounced with rising concentrations of 61, and a complete blockade of UTP-mediated receptor activation is observed at a concentration of 15 μM of 61. In the calcium mobilization assay, the cells were first incubated with the antagonist 61 for 30 min. The agonist UTP was subsequently injected into the cell suspension, and the assay signal was read immediately thereafter. Because there is no simultaneous incubation with both agonist and antagonist and the measurement of the signal is very fast, the assay conditions are likely to

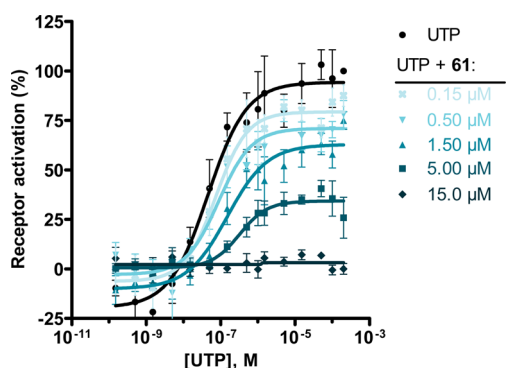


Figure 7. Concentration–response curves of UTP on the P2Y₄ receptor after preincubation with fixed concentrations of **61**. The results were obtained using the calcium mobilization assay with 1321N1 astrocytoma cells recombinantly expressing the human P2Y₄ receptor. EC₅₀ values are not significantly different from each other ($p > 0.05$, unpaired t -test). The EC₅₀ values and maximum receptor activation are shown in the [Supporting Information](#).

be under nonequilibrium conditions. Nevertheless, our data indicate that **61** may achieve P2Y₄ receptor antagonism via a noncompetitive mechanism, but competitive antagonism cannot be completely ruled out at present. Interestingly, on the P2Y₁₂ receptor, we previously found that anthraquinone derivatives of this series act as competitive antagonists.³⁰ However, the percentage of sequence shared by the P2Y₄ and P2Y₁₂ receptors is only 25% and, consequently, significant differences exist between these two receptors (also with respect to orthosteric ligand preferences and G protein coupling).

To get more insight into the interaction of the anthraquinone derivatives with the P2Y₄ receptor on a molecular level, we decided to perform docking studies.

Analysis of the Human P2Y₄ Receptor Model. Two P2Y receptor subtypes, the more distantly related P2Y₁₂ and the more closely related P2Y₁ receptors, had been crystallized and X-ray structures were obtained in complex with agonists (P2Y₁₂) and antagonists (P2Y₁, P2Y₁₂).^{54–56} On the basis of these structures, the molecular mechanism of activation of the human P2Y₁ receptor was recently analyzed by molecular dynamics simulations, which explained the essential role of the amino acids Asp204 in extracellular loop 2 (ECL2) and Arg310 in the transmembrane region 7 (TM VII).⁵⁷ The two amino acids Asp204 and Arg310 form an ionic lock and are stabilized in the inactive state by P2Y₁ antagonists. The ionic lock is broken during the activation of the receptor by the agonist adenosine diphosphate (ADP). We constructed a homology model of the P2Y₄ receptor based on the P2Y₁ receptor. In our inactive state homology model of the human P2Y₄ receptor, an ionic lock between Asp187 and Arg292 was formed, suggesting a similar mechanism of activation as in the human P2Y₁ receptor.

Two ligand binding sites located toward the extracellular regions of the P2Y₄ receptor were identified in the homology model ([Figure 8](#)). The binding site denoted as “A” with a volume of 190 Å³ was observed upon the downward movement of the ECL2. This binding site “A” is comparable to the binding site of the noncompetitive antagonist 2-iodo-*N*⁶-methyl-(*N*)-methanocarba-2'-deoxyadenosine-3',5'-bisphosphate (MRS2500, **72**) in the human P2Y₁ receptor with a size of 214 Å³. The second binding site in the homology model of the P2Y₄ receptor, denoted as “O”, is formed in the region comparable to the orthosteric binding site identified in the crystal structure of the human P2Y₁₂ receptor in complex with the agonist 2-methylthioadenosine-5'-diphosphate (2MeSADP, **71**) and in the molecular dynamics simulation study of the human P2Y₁

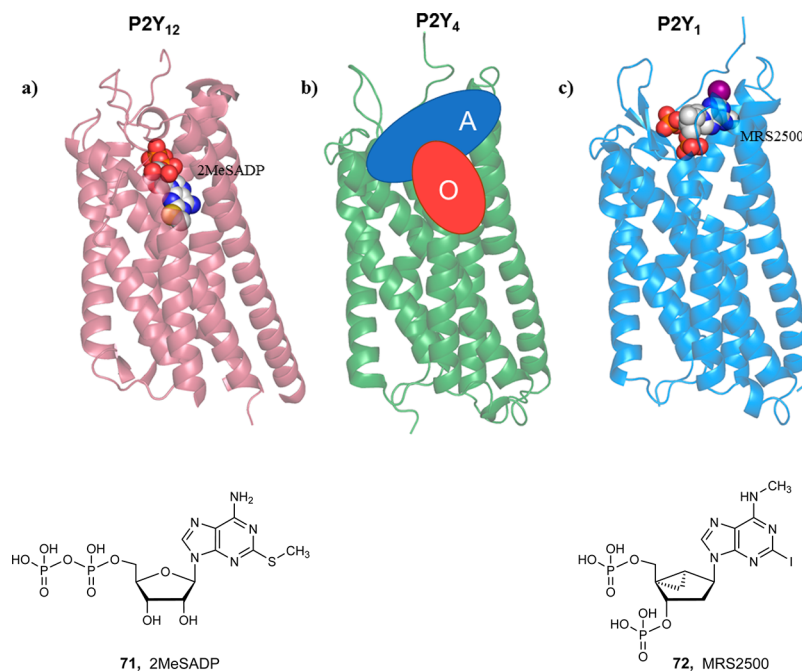


Figure 8. (a) Crystal structure of the human P2Y₁₂ receptor (light red) in complex with the agonist 2-methylthio-ADP (2MeSADP, **71**). (b) Homology model of the human P2Y₄ receptor (light green) with the schematic representation of the orthosteric binding site (denoted “O”) and the allosteric binding site (denoted “A”). (c) Crystal structure of the human P2Y₁ receptor (light blue) in complex with the noncompetitive antagonist 2-iodo-*N*⁶-methyl-(*N*)-methanocarba-2'-deoxyadenosine-3',5'-bisphosphate (MRS2500, **72**). The receptors are represented as cartoon models, and the small molecules **71** and **72** are represented as space fill models.

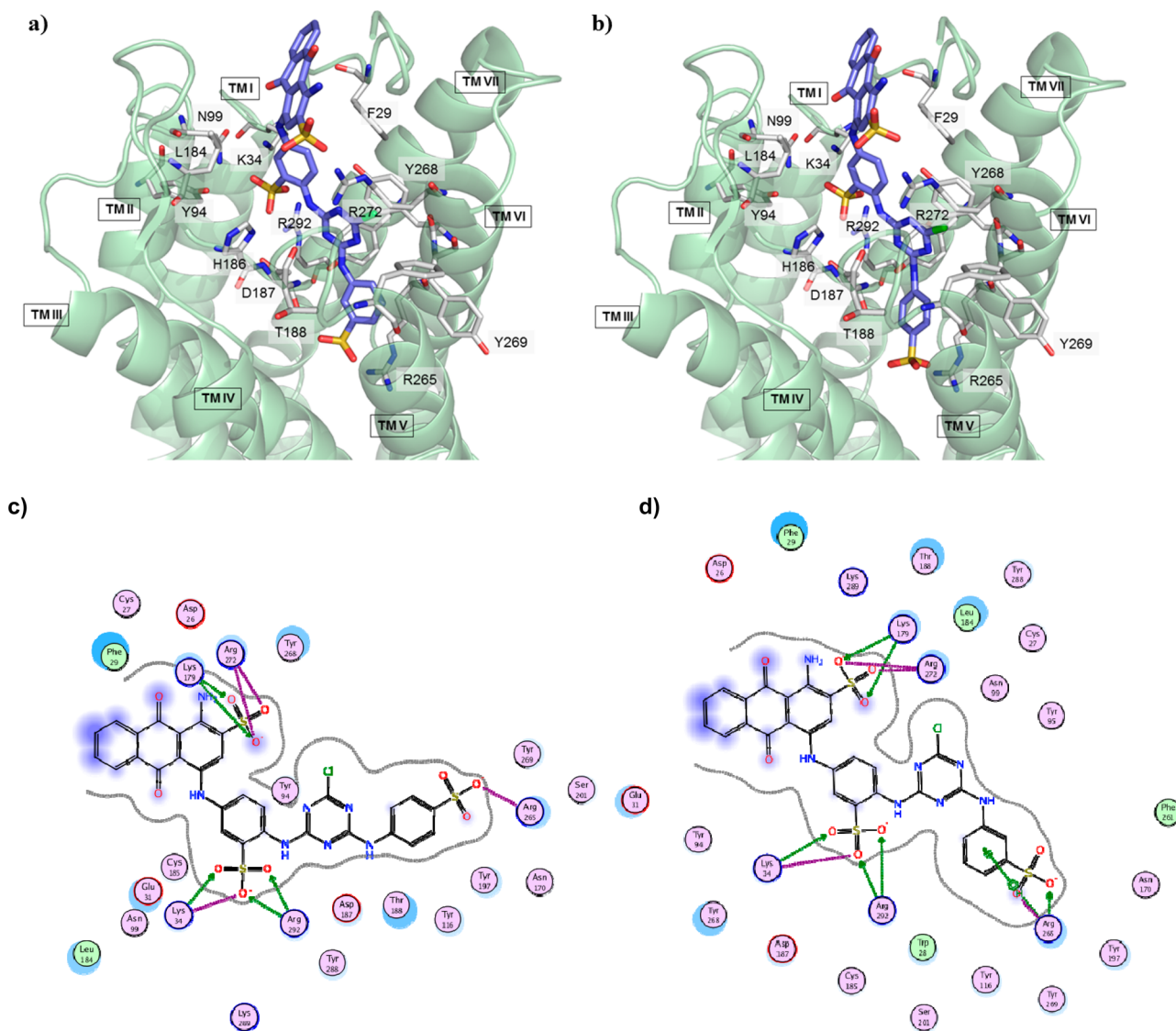


Figure 9. Proposed binding modes of Reactive Blue 2 (RB-2) in our homology model of the P2Y₄ receptor. Docked poses of RB-2 (a) *para*-substituted and (b) *meta*-substituted with the important residues in the putative binding pocket of the human P2Y₄ receptor and their 2D interaction diagrams shown in (c) and (d). The human P2Y₄ receptor model (dark cyan) is depicted in cartoon representation, and the amino acid residues (white) and RB-2 (marine blue) are presented as stick models. The oxygen atoms are colored in red, nitrogen atoms in blue and sulfur atoms in orange. None of the interacting residues are highly conserved for the subtypes analyzed in selectivity studies (P2Y₁, P2Y₂, P2Y₄, P2Y₆, and P2Y₁₂; see Supporting Information, Figure 61).

receptor with the agonist ADP.^{56,57} In our inactive state model of the human P2Y₄ receptor, the binding site “O” is limited in size due to the downward movement of the ECL2. However, after its upward movement, it could accommodate the endogenous agonists UTP and ATP, respectively. The experimental data for the P2Y₄ receptor antagonists developed in this study suggested a noncompetitive mode of inhibition. Hence, we selected binding site “A” for compound docking to probe whether **61** and analogues may display a similar mode of receptor inactivation as MRS2500 (**72**) in the P2Y₁ receptor.

Docking Studies of Reactive Blue 2 (RB-2). The putative binding modes of the *para*- and *meta*-sulfo-substituted isomers (ring F) of RB-2 are shown in Figure 9. The binding poses showed that the two derivatives have the same orientation in the binding pocket “A” formed between ECL2 and TM regions V, VI, and VII. Ring A of RB-2 appears to be completely exposed to the extracellular space of the human P2Y₄ receptor.

Ring B may be stabilized by π - π -stacking with Phe29 from the N-terminal region of the receptor. The sulfonate group in position 2 of ring C likely binds to Lys179 and Arg272, forming strong electrostatic and hydrogen bonding interactions. The carbonyl groups at positions 9 and 10 of the anthraquinone core, the amino group at position 1, and the amine linker between rings C and D were not observed to form any specific interactions with the amino acids of the human P2Y₄ receptor. However, the amino group at position 1 of the anthraquinone ring system probably forms intramolecular H-bond interactions with the carbonyl group at position 9. The sulfonate group at ring D forms strong electrostatic interactions with Lys34, Lys289, and Arg292, and possibly with Asp187, according to our model. Ring E was found to occupy the binding pocket formed by His186 and Thr188 of ECL2, Tyr268 and Arg272 of TM VI, and Tyr288 of TM VII. Ring F is bound by the aromatic residues Tyr116, Tyr197, and Tyr269 between TM

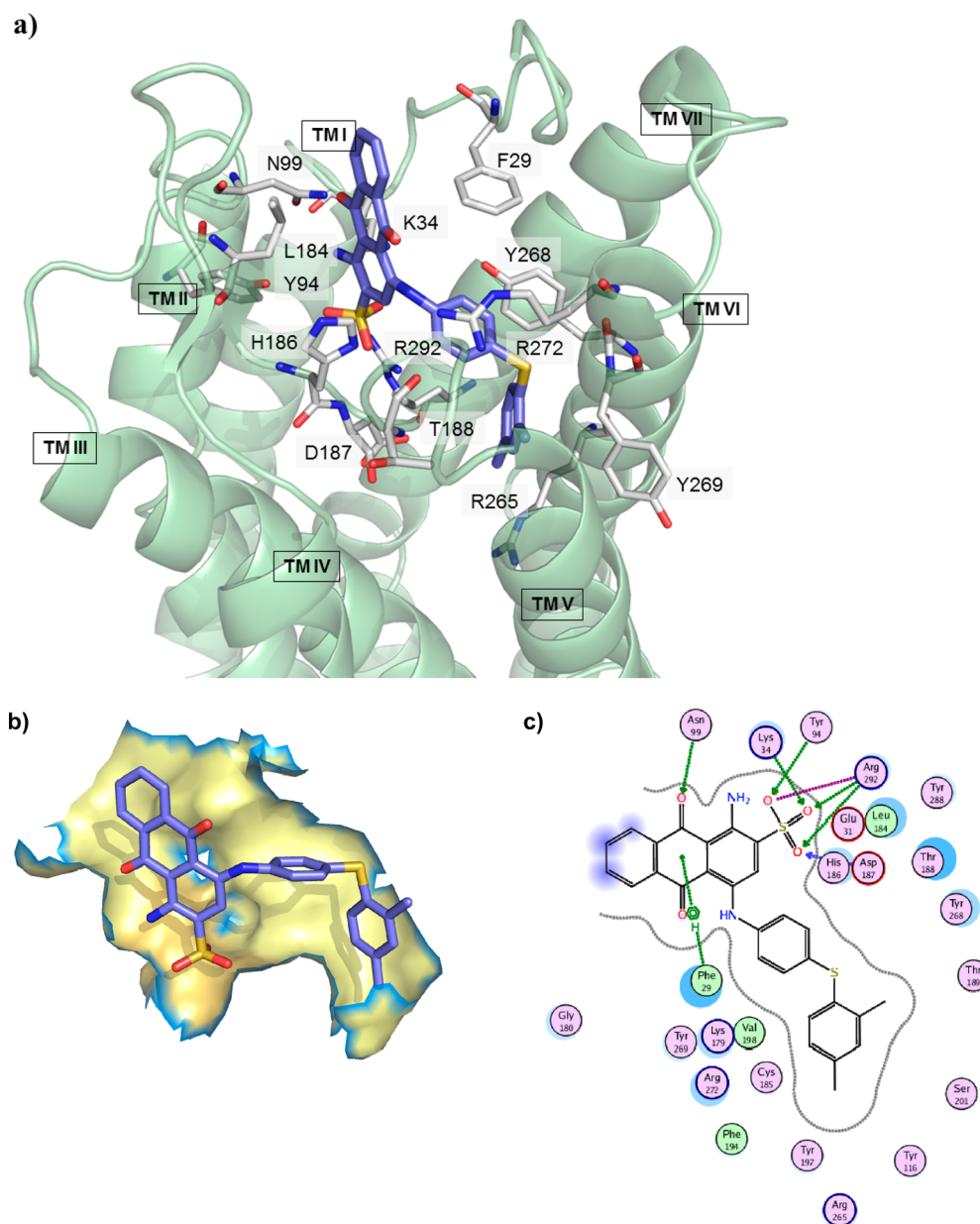


Figure 10. Proposed binding mode of **61** in our homology model of the P2Y₄ receptor. (a) Docked pose of **61** with the important residues in the putative binding pocket of the human P2Y₄ receptor. (b) The putative binding pocket is shown in a surface model; the 2D interaction diagram is shown in (c). The human P2Y₄ receptor model (dark cyan) is displayed in cartoon representation, and the amino acid residues (white) and compound **61** (marine blue) are shown as stick models. The oxygen atoms are colored in red, nitrogen atoms in blue, and sulfur atoms in orange. As for RB-2, none of the residues interacting with **61** are highly conserved for the subtypes analyzed in selectivity studies (P2Y₁, P2Y₂, P2Y₄, P2Y₆, and P2Y₁₂; see Supporting Information, Figure 61).

regions V and VI. The sulfonate group on ring F (*para*- or *meta*-substituted) interacts with Arg265 through electrostatic interactions and additionally stabilizes the ring in the binding pocket through cation- π interactions as observed in the docking study.

Docking Studies of the New, Potent P2Y₄ Receptor Antagonists. To propose binding modes for the anthraquinone derivatives that were optimized for P2Y₄ receptor blockade, and to rationalize the determined potency values, we selected compounds **7**, **42**, and **61–64** for performing molecular docking studies on the homology model of the human P2Y₄ receptor. The putative binding pose of the most potent antagonist **61** in the binding pocket and its 2D interaction diagram are shown in Figure 10. Similar to RB-2,

compound **61** can be well accommodated in binding pocket “A”. Ring A of **61** faces toward the extracellular space and rings B and C form hydrophobic interactions with Phe29 and Leu184. The sulfonate group in ring C could make strong electrostatic interactions with Lys34, Asp187, and Arg292 present in the pocket formed by Lys34, Tyr94, Asp187, Lys289, and Arg292 of the ECL2 and TMs I, VI, and VII. Through its strong electrostatic interactions, the sulfonate group may act as an anchor for the compound and stabilize it in a vertical position through hydrophobic interactions of ring B and C with Phe29 and Leu184. The carbonyl group at position 9 of the anthraquinone ring system likely interacts with Asn99 through hydrogen bonding, and the carbonyl group at position 10 and the amino group at position 1 may form weak hydrogen bond

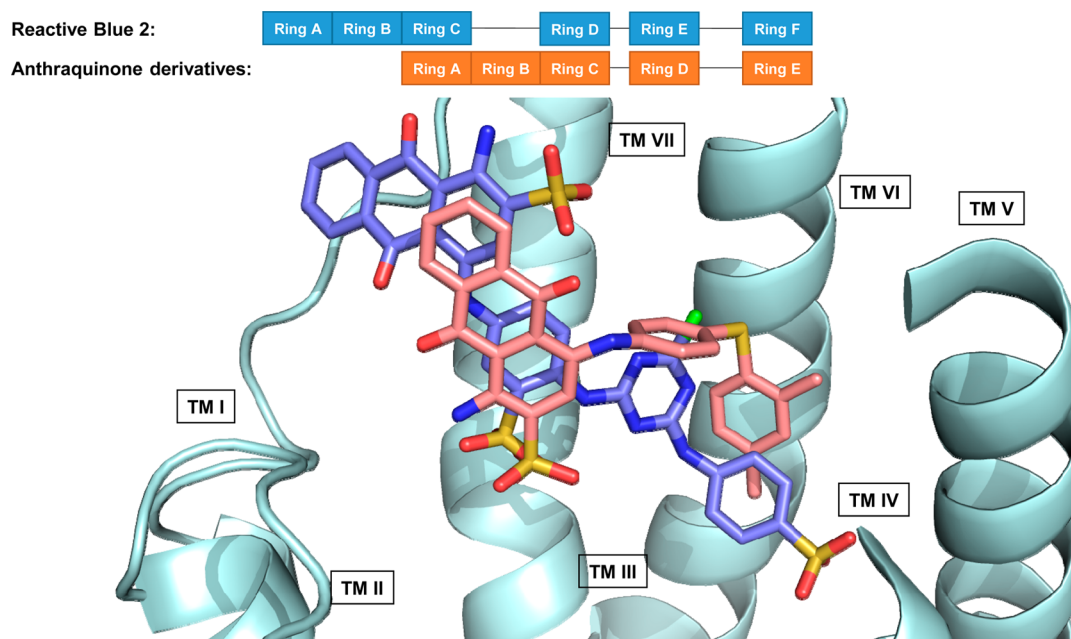


Figure 11. Comparative overlay of the docked poses of *para*-substituted RB-2 (in blue) and compound **61** (in red) in the binding pocket of the human P2Y₄ receptor model. The overlap of the ring system of RB-2 and **61** is shown in the schematic representation on the top.

interactions with Arg272 and Lys34, respectively. Additionally, the amino group at position 1 of the anthraquinone probably forms intramolecular interactions with the carbonyl group at position 9 and the sulfonate oxygen at ring C. The importance of the amino group at position 1 was confirmed for compounds **68–70** by replacing the amino group with a hydrogen atom. This led to a significant drop in inhibitory potency. The amine linker between ring C and D may form weak hydrogen bond interactions with His186. We hypothesize that the sulfonate group at ring C forms strong electrostatic interactions with Arg292; it is essential for high potency of the anthraquinone derivatives. The presence of an acidic (carboxylic) group at ring D decreased potency (see **30–32**, **46**, **67**, and **70**). A possible explanation is that both acidic structures compete for the same binding subpocket interacting with Arg292, which might lead to different binding modes. Furthermore, the binding pocket of ring D appears to be limited in space with the subpocket formed by His186, Thr188 of ECL2, and Tyr268, Arg272 and Tyr288 of TMs VI and VII. In this pocket, phenyl substitution is well tolerated, as opposed bulky groups, for example, the naphthyl group (compounds **8–10**). This was additionally supported by the linker preferences between rings D and E: S > O > NH > CH₂. Thiophenoxy derivatives were most potent, likely because the orientation provided by a sulfur linker is required for positioning ring E into the hydrophobic pocket. Except for compound **62**, ring D of the docked compounds showed the same orientation within the subpocket (Supporting Information, Figure S4).

The terminal ring E present in **61–63** and **64** was found to occupy the pocket formed by Tyr116 of TM III, Phe194, Tyr197, and Val198 of TM V, and Arg265, Tyr268, and Tyr269 of TM IV. Because of a large number of aromatic residues, compounds with a ring E may be tightly packed within the pocket, resulting in somewhat improved potency in comparison to the compounds without ring E. The putative binding modes of compounds **7** and **42** without ring E, and their 2D interaction diagrams are shown in Supporting Information, Figure S5. The dimethyl substitutions at ring E are thought to

increase the hydrophobic interactions with the aromatic residues and promote the tight binding of the compound inside the binding pocket of the P2Y₄ receptor. Among different substituents, 2,4-dimethylphenylthio-substitution (**61**, 0.233 μM) showed slightly higher potency as compared to 2,5- and 3,4-dimethylphenylthio-substituted derivatives (**62**, 0.395 μM; **63**, 0.482 μM). The putative binding poses and 2D interaction diagrams of **62** and **63** are shown in Supporting Information, Figure S6. In case of **64**, tight binding was achieved with an extended linker. Additionally, Arg265 is located at the bottom of the pocket occupied by ring E and might interact with the pyridine group of **64**. The putative binding pose and 2D interaction diagram of **64** are shown in Supporting Information, Figure S7.

As a next step, we compared the binding poses of RB-2 and compound **61** (see overlay of RB-2 and **61** in Figure 11). Ring B of RB-2 and ring A of **61** form hydrophobic aromatic interactions with Phe29. The sulfonate groups in ring D of RB-2 correlates with the sulfonate group in ring C of **61**; they are believed to interact with Lys34 and Arg292. Ring E of RB-2 and ring D of **61** occupy the same binding pocket formed by the amino acid residues His186, Thr188, Tyr268, Arg272, and Tyr288. A comparison of ring F of RB-2 with ring E of **61** shows that the sulfonate group in ring F probably displays electrostatic interactions with Arg265 in the bottom part of the hydrophobic pocket. The dimethyl substitution of **61** may lead to a tightening of the binding pocket through hydrophobic interactions with the aromatic residues instead. Thus, our homology model explains the positive contributions of lipophilic terminal moieties on the anthraquinone derivatives as well as those of a polar sulfonate moiety as in RB-2.

A further important observation regarding the binding poses of the antagonists in the binding pocket of the human P2Y₄ receptor relate to the orientation and interactions of Asp187 and Arg292, which correspond to Asp204 and Arg310 in the human P2Y₁ receptor. This supports the hypothesis that the mode of P2Y₄ receptor inhibition by anthraquinone derivatives is similar to that described for **72** at the P2Y₁ receptor. They

stabilize the ionic lock and prevent the movement of TMs VI and VII required for receptor activation. Our docking results are consistent with the experimental data and the SARs of anthraquinone derivatives. The homology model of the human P2Y₄ receptor will be useful for future compound optimization and allow rational ligand design and virtual screening approaches.

CONCLUSIONS

In conclusion, we have synthesized a library of RB-2-related anthraquinone derivatives and successfully optimized them as selective antagonists of the human P2Y₄ receptor. To the best of our knowledge, compound **61** (sodium 1-amino-4-[4-(2,4-dimethylphenylthio)-phenylamino]-9,10-dioxo-9,10-dihydroanthracene-2-sulfonate) represents the most potent P2Y₄ receptor antagonist known to date, with an IC₅₀ value of 233 nM. Our results suggest that **61** exerts its antagonistic effect on the P2Y₄ receptor through a noncompetitive mechanism. This was rationalized by the docking of **61** to a homology model of the human P2Y₄ receptor based on the recently published X-ray structure of the P2Y₁ receptor in complex with allosteric antagonists. As a continuation of our previous work on anthraquinone derivatives, the current results confirm the validity of RB-2 as a privileged structure in the field of purinergic signaling. Furthermore, by fine-tuning the structure, it is possible to develop subtype-specific ligands as valuable pharmacological tool compounds.

EXPERIMENTAL SECTION

Chemistry. Material and Methods. All materials were used as purchased (Acros, Alfa Aesar, Merck, or Sigma-Aldrich, Germany). 3-Propylaniline was prepared according to the method of Rasmussen et al.⁵⁸ Thin-layer chromatography was performed using TLC aluminum sheets silica gel 60 F₂₅₄ or TLC aluminum sheets reversed phase (RP) silica gel 18 F₂₅₄ (Merck, Darmstadt, Germany). Colored compounds were visible at daylight; other compounds were visualized under UV light (254 nm). Flash chromatography was performed on a Büchi system using silica gel RP-18 (Merck, Darmstadt, Germany). ¹H and ¹³C NMR data were collected on either a Bruker Avance 500 MHz NMR spectrometer at 500 MHz (¹H) or 126 MHz (¹³C), respectively, or a 600 MHz NMR spectrometer at 600 MHz (¹H) or 151 MHz (¹³C), respectively. DMSO-*d*₆ was used as a solvent. Chemical shifts are reported in parts per million (ppm) relative to the deuterated solvent, i.e., DMSO, δ ¹H 2.49 ppm; ¹³C 39.7 ppm, coupling constants *J* are given in hertz, and spin multiplicities are given as s (singlet), d (doublet), t (triplet), q (quartet), sext (sextet), m (multiplet), and br (broad).

The purities of isolated products were determined by ESI-mass spectra obtained on an LC-MS instrument (Applied Biosystems API 2000 LC-MS/MS, HPLC Agilent 1100) using the following procedure: the compounds were dissolved at a concentration of 0.5 mg/mL in H₂O:MeOH = 1:1, containing 2 mM NH₄CH₃COO. Then, 10 μ L of the sample was injected into an HPLC column (Phenomenex Luna 3 μ C18, 50 mm \times 2.00 mm). Elution was performed with a gradient of water:methanol (containing 2 mM NH₄CH₃COO) from 90:10 to 0:100 starting the gradient immediately at a flow rate of 250 μ L/min for 15 min, followed by washing with 100% methanol for another 15 min. UV absorption was detected from 200 to 950 nm using a diode array detector. The purity of the compounds proved to be \geq 95%. For microwave reactions, a CEM Focused Microwave Synthesis Type Discover apparatus was used. A freeze-dryer (CHRIST ALPHA 1-4 LSC) was used for lyophilization. The synthesis and analysis of compounds **7–12**, **13**, **15–18**, **22**, **23**, **26–32**, **36**, **38**, **45–48**, **50**, **51**, **65–66**, and **70** were previously described.^{24,27–29,33,36,38–40} All other compounds (**14**, **19–21**, **24**, **25**, **33–35**, **37**, **39–44**, **49**, **52**,

53, **58–64**, and **67–69**) were newly prepared in analogy to described methods^{27–29,39} with modifications as described below.

Purification of Reactive Blue 2 (RB-2). RB-2 (200 mg) was dissolved in 10 mL of deionized water and injected into a flash column chromatography type Sepacore glass column C-690 (ID 26 mm \times 500 mm) two-thirds filled with reversed phase-18 silica gel (40–63 μ m, Merck) using water as eluent. The polarity was gradually decreased by increasing the concentration of methanol (5, 10, 20, 40, and 60%). The pooled blue-colored fractions were collected and evaporated under vacuum to remove the methanol, and the remaining water was subsequently removed by lyophilization to yield 108 mg (54%) of RB-2 P (2') as a blue powder. The chemical structure and purity were confirmed by RP-TLC, LC-MS (>96%), and NMR.

General Procedure A: Preparation of 4-Substituted 1-Aminoanthraquinone-2-sulfonate Derivatives (14, 19–21, 24, 25, 33–35, 37, 39–44, 49, 52, 53, 58–64, and 67). To a 5 mL microwave reaction vial, equipped with a magnetic stirring bar, were added 1-amino-4-bromo substituted anthraquinone compounds (bromamic acid sodium salt **6a**, or 1-amino-4-bromo-2-methylanthraquinone **6b**) (0.1–0.3 mmol) and the appropriate aniline or amine derivative (1.5–9.0 equiv), followed by a buffer solution of Na₂HPO₄ (pH 9.6) (4.5 mL) and NaH₂PO₄ (pH 4.2) (0.5 mL) and a finely powdered elemental copper (0.002–0.003 g, 5–10 mol %). The mixture was capped and irradiated in the microwave oven (80–100 W) for 5–24 min at 100–120 °C. The reaction mixture was cooled down to room temperature (rt), and the product was purified using the following procedure. The contents of the vial were filtered to remove the elemental copper. Then ca. 200 mL of water was added to the filtrate and the aqueous solution was extracted with dichloromethane (200 mL). The extraction procedure was repeated until the dichloromethane layer became colorless (2–3 times). The aqueous layer was reduced by rotary evaporation to a volume of 10–20 mL, which was subsequently submitted to flash column chromatography using RP-18 silica gel and water as an eluent. The polarity of the eluent was then gradually decreased by the addition of acetone in the following steps: 5, 10, 20, 40, and 60%. Fractions containing blue product were collected. For some compounds the last step of purification (RP-18 flash chromatography) had to be repeated two to three times to obtain pure product (\geq 95% purity as determined by LC-MS, Table 1). The pooled product-containing fractions were evaporated under vacuum to remove the acetone and reduce water volume. The remaining water was subsequently removed by lyophilization to yield (up to 80%) of the product as blue powder (Scheme 1 and Table 1).

General Procedure B: Preparation of 4-Substituted Anthraquinone-2-sulfonate Derivatives (68 and 69). To a 50 mL round-bottom flask equipped with a magnetic stirring bar, 0.1 mmol of 1-aminoanthraquinone derivative (**12** or **27**) were added, followed by 5 mL of 1 molar hydrochloric acid. The solution was cooled to 0–5 °C in an ice bath, and a previously cooled solution of NaNO₂ (13.8 mg, 0.2 mmol, 2 equiv) in 0.5 mL of distilled water was added dropwise. After 5 min, the mixture was allowed to warm up to rt followed by addition of 30 mg of zinc powder (1.0 mmol, 10 equiv) and 5 mL of ethanol. The resulting mixture was then allowed to stir at rt for ca. 30 s. The mixture was filtered off, and the purple-colored filtrate was then purified by flash column chromatography on a reversed phase silica gel (RP-18) using a gradient of acetone in water (5% and 20%) as the eluent. Fractions containing the purple product were collected and evaporated in vacuum to remove acetone and decrease the volume of water to ca. 20 mL. Complete drying was achieved with a freeze-dryer, affording purple-colored products **68** and **69** in 97% and 38 yield, respectively (Scheme 3 and Table 1).

Sodium 1-Amino-4-(2-chlorophenylamino)-9,10-dioxo-9,10-dihydroanthracene-2-sulfonate (14). Reaction conditions according to general procedure A: Compound **6a** (81 mg, 0.2 mmol), 2-chloroaniline (51 mg, 0.4 mmol). MW conditions: 5 min, 120 °C, 100 W; pressure up to 10 bar. Analytical data: blue powder (36% yield), mp >300 °C. ¹H NMR (500 MHz): δ 7.20 (m, 1H, 4'-H), 7.42 (m, 2H, 5'-H, 6'-H), 7.61 (dd, 1H, 3'-H), 7.86 (m, 2H, 6-H, 7-H), 7.91 (s, 1H, 3-H), 8.27 (m, 2H, 5-H, 8-H), 10.00 (br, 2H, 1-NH₂), 11.95 (s, 1H, 4-NH). ¹³C NMR (126 MHz): δ 109.61, 112.91, 122.79, 123.81,

125.48, 126.24, 126.50, 128.30, 130.48, 133.06, 133.56, 133.64, 134.32, 136.77, 139.32, 142.66, 144.70, 182.20, 183.47. LC-MS (m/z): 446 [M - Na⁺ + NH₄⁺]⁺, 429 [M - Na⁺ + H⁺]⁺, 427 [M - Na⁺ + H⁺]⁻. Purity by HPLC-UV (254 nm) ESI-MS: 99%.

Sodium 1-Amino-4-(2-methylphenylamino)-9,10-dioxo-9,10-dihydroanthracene-2-sulfonate (19). Reaction conditions according to general procedure A: Compound **6a** (81 mg, 0.2 mmol), 2-methylaniline (43 mg, 0.4 mmol). MW conditions: 10 min, 120 °C, 100 W; pressure up to 10 bar. Yield 80%. Purity by HPLC-UV (254 nm) ESI-MS: 99%.

Sodium 1-Amino-4-(3-methylphenylamino)-9,10-dioxo-9,10-dihydroanthracene-2-sulfonate (20). Reaction conditions according to general procedure A: Compound **6a** (81 mg, 0.2 mmol), 3-methylaniline (43 mg, 0.4 mmol). MW conditions: 10 min, 120 °C, 100 W; pressure up to 10 bar. Yield 70%. Purity by HPLC-UV (254 nm) ESI-MS: 99.1%.

Sodium 1-Amino-4-(4-methylphenylamino)-9,10-dioxo-9,10-dihydroanthracene-2-sulfonate (21). Reaction conditions according to general procedure A: Compound **6a** (121.3 mg, 0.3 mmol), 4-methylaniline (64.3 mg, 0.6 mmol). MW conditions: 5 min, 120 °C, 100 W; pressure up to 10 bar. Yield 72%. Purity by HPLC-UV (254 nm) ESI-MS: 100%.

Sodium 1-Amino-4-(4-ethylphenylamino)-9,10-dioxo-9,10-dihydroanthracene-2-sulfonate (24). Reaction conditions according to general procedure A: Compound **6a** (81 mg, 0.2 mmol), 4-ethylphenylamine (48.5 mg, 0.4 mmol). MW conditions: 5 min, 120 °C, 100 W; pressure up to 10 bar. Analytical data: blue powder (64% yield), mp >300 °C. ¹H NMR (500 MHz): δ 1.22 (t, 3H, 4'-CH₂CH₃), 2.64 (q, 2H, 4'-CH₂CH₃), 7.20 (d, 2H, 2'-H, 6'-H), 7.29 (d, 2H, 3'-H, 5'-H), 7.84 (m, 2H, 6-H, 7-H), 7.98 (s, 1H, 3-H), 8.27 (m, 2H, 5-H, 8-H), 10.10 (br, 2H, 1-NH₂), 12.07 (s, 1H, 4-NH). ¹³C NMR (126 MHz): δ 15.64, 27.75, 109.18, 111.03, 122.73, 123.61, 126.05, 126.15, 129.12, 132.85, 133.18, 133.76, 134.28, 136.81, 140.43, 141.59, 143.04, 144.39, 181.84, 182.30. LC-MS (m/z): 440 [M - Na⁺ + NH₄⁺]⁺, 423 [M - Na⁺ + H⁺]⁺, 421 [M - Na⁺ + H⁺]⁻. Purity by HPLC-UV (254 nm) ESI-MS: 99%.

Sodium 1-Amino-4-(3-propylphenylamino)-9,10-dioxo-9,10-dihydroanthracene-2-sulfonate (25). Reaction conditions according to general procedure A: Compound **6a** (121.3 mg, 0.3 mmol), 3-propylaniline (61 mg, 0.45 mmol). MW conditions: 15 min, 120 °C, 100 W; pressure up to 10 bar. Analytical data: blue powder (35% yield), mp >300 °C. ¹H NMR (500 MHz): δ 0.91 (t, 3H, -CH₂CH₂CH₃), 1.63 (sext, 2H, -CH₂CH₂CH₃), 2.58 (t, 2H, -CH₂CH₂CH₃), 7.03 (d, 1H, 6'-H), 7.10 (m, 2H, 2'-H, 4'-H), 7.35 (t, 1H, 5'-H), 7.85 (m, 2H, 6-H, 7-H), 8.05 (s, 1H, 3-H), 8.28 (m, 2H, 5-H, 8-H), 12.07 (s, 1H, 4-NH). ¹³C NMR (126 MHz): δ 13.65, 23.91, 37.91, 109.06, 111.19, 120.32, 122.79, 123.02, 124.59, 125.90, 126.00, 129.41, 132.71, 133.09, 133.57, 134.12, 139.05, 140.93, 142.79, 143.94, 144.30, 181.72, 182.32. LC-MS (m/z): 454 [M - Na⁺ + NH₄⁺]⁺, 437 [M - Na⁺ + H⁺]⁺, 435 [M - Na⁺ + H⁺]⁻. Purity by HPLC-UV (220–700 nm) ESI-MS: 97.7%.

Sodium 1-Amino-4-(2,3-dimethylphenylamino)-9,10-dioxo-9,10-dihydroanthracene-2-sulfonate (33). Reaction conditions according to general procedure A: Compound **6a** (81 mg, 0.2 mmol), 2,3-dimethylaniline (48.5 mg, 0.4 mmol). MW conditions: 5 min, 120 °C, 100 W; pressure up to 10 bar. Yield 49%. Purity by HPLC-UV (254 nm) ESI-MS: 99%.

Sodium 1-Amino-4-(2,4-dimethylphenylamino)-9,10-dioxo-9,10-dihydroanthracene-2-sulfonate (34). Reaction conditions according to general procedure A: Compound **6a** (81 mg, 0.2 mmol), 2,4-dimethylaniline (48.5 mg, 0.4 mmol). MW conditions: 5 min, 120 °C, 100 W; pressure up to 10 bar. Yield 60%. Purity by HPLC-UV (254 nm) ESI-MS: 99%.

Sodium 1-Amino-4-(2,5-dimethylphenylamino)-9,10-dioxo-9,10-dihydroanthracene-2-sulfonate (35). Reaction conditions according to general procedure A: Compound **6a** (81 mg, 0.2 mmol), 2,5-dimethylaniline (48.5 mg, 0.4 mmol). MW conditions: 5 min, 120 °C, 100 W; pressure up to 10 bar. Yield 50%. Purity by HPLC-UV (254 nm) ESI-MS: 99.5%.

Sodium 1-Amino-4-(3,4-dimethoxyphenylamino)-9,10-dioxo-9,10-dihydroanthracene-2-sulfonate (37). Reaction conditions ac-

ording to general procedure A: Compound **6a** (121.3 mg, 0.3 mmol), 3,4-dimethoxyaniline (92 mg, 0.6 mmol). MW conditions: 5 min, 120 °C, 100 W; pressure up to 10 bar. Analytical data: blue powder (46% yield), mp >300 °C. ¹H NMR (500 MHz): δ 3.78 (s, 3H, -OCH₃), 3.80 (s, 3H, -OCH₃), 6.83 (dd, 1H, 6'-H, J_{2',6'}: 2.45 Hz, J_{5',6'}: 8.5 Hz), 6.94 (d, 1H, 2'-H, J_{2',6'}: 2.45 Hz), 7.03 (d, 1H, 5'-H, J_{5',6'}: 8.5 Hz), 7.85 (m, 2H, 6-H, 7-H), 7.98 (s, 1H, 3-H), 8.28 (m, 1H, 5-H, 8-H), 12.08 (s, 1H, 4-NH). ¹³C NMR (126 MHz): δ 55.60, 55.74, 108.88, 110.34 (C-4a), 112.55, 115.94, 122.79, 125.82, 125.97, 131.96, 132.63, 132.90, 133.65, 134.12, 142.21, 142.91, 144.14, 146.42, 149.49, 181.57, 181.80. LCMS (m/z): 472 [M - Na⁺ + NH₄⁺]⁺, 455 [M - Na⁺ + H⁺]⁺, 453 [M - Na⁺ + H⁺]⁻. Purity by HPLC-UV (220–700 nm) ESI-MS: 98.5%.

Sodium 1-Amino-4-(3-methoxy-4-methylphenylamino)-9,10-dioxo-9,10-dihydroanthracene-2-sulfonate (39). Reaction conditions according to general procedure A: Compound **6a** (121.3 mg, 0.3 mmol), 3-methoxy-4-methylaniline (82.3 mg, 0.6 mmol). MW conditions: 5 min, 120 °C, 100 W; pressure up to 10 bar. Analytical data: blue powder (44% yield), mp >300 °C. ¹H NMR (500 MHz): δ 2.17 (s, 1H, -CH₃), 3.81 (s, 3H, -OCH₃), 6.77 (dd, 1H, 6'-H, J_{2',6'}: 2.0 Hz, J_{5',6'}: 7.9 Hz), 6.89 (d, 1H, 2'-H, J_{2',6'}: 2.0 Hz), 7.19 (d, 1H, 5'-H, J_{5',6'}: 7.9 Hz), 7.85 (m, 2H, 6-H, 7-H), 8.10 (s, 1H, 3-H), 8.28 (m, 1H, 5-H, 8-H), 12.10 (s, 1H, 4-NH). ¹³C NMR (126 MHz): δ 15.69, 55.49, 106.40, 109.16, 111.05, 115.03, 122.20, 123.15, 126.03, 126.14, 131.08, 132.84, 133.18, 133.75, 134.28, 138.15, 141.46, 142.93, 144.40, 158.21, 181.83, 182.28. LCMS (m/z): 456 [M - Na⁺ + NH₄⁺]⁺, 439 [M - Na⁺ + H⁺]⁺, 437 [M - Na⁺ + H⁺]⁻. Purity by HPLC-UV (220–700 nm) ESI-MS: 98.3%.

Sodium 1-Amino-4-(4-chloro-2-methylamino)-9,10-dioxo-9,10-dihydroanthracene-2-sulfonate (40). Reaction conditions according to general procedure A: Compound **6a** (81 mg, 0.2 mmol), 4-chloro-2-methylaniline (56.6 mg, 0.4 mmol). MW conditions: 24 min, 120 °C, 100 W; pressure up to 10 bar. Analytical data: blue powder (36% yield), mp >300 °C. ¹H NMR (500 MHz): δ 2.28 (s, 3H, 2'-CH₃), 7.27 (d, 1H, 6'-H, J_{5',6'}: 8.5 Hz), 7.33 (dd, 1H, 5'-H, J_{3',5'}: 2.4 Hz, J_{5',6'}: 8.5 Hz), 7.46 (d, 1H, 3'-H, J_{3',5'}: 2.4 Hz), 7.70 (s, 1H, 3-H), 7.84 (m, 2H, 6-H, 7-H), 8.26 (m, 2H, 5-H, 8-H), 10.05 (br, 2H, 1-NH₂), 11.88 (s, 1H, 4-NH). ¹³C NMR (126 MHz): δ 17.69, 109.31, 111.46, 122.53, 125.89, 126.11, 126.20, 126.91, 129.03, 130.85, 132.92, 133.36, 133.67, 134.31, 134.70, 136.97, 131.40, 143.01, 144.36, 181.95, 182.83. LC-MS (m/z): 460 [M - Na⁺ + NH₄⁺]⁺, 443 [M - Na⁺ + H⁺]⁺, 441 [M - Na⁺ + H⁺]⁻. Purity by HPLC-UV (254 nm) ESI-MS: 99%.

Sodium 1-Amino-4-(4-chloro-3-methylphenylamino)-9,10-dioxo-9,10-dihydroanthracene-2-sulfonate (41). Reaction conditions according to general procedure A: Compound **6a** (81 mg, 0.2 mmol), 4-chloro-3-methylaniline (56.6 mg, 0.4 mmol). MW conditions: 5 min, 120 °C, 100 W; pressure up to 10 bar. Analytical data: blue powder (40% yield), mp >300 °C. ¹H NMR (500 MHz): δ 2.34 (s, 3H, CH₃), 7.13 (dd, 1H, 6'-H, J_{2',6'}: 2.7 Hz, J_{5',6'}: 8.5 Hz), 7.27 (d, 1H, 2'-H, J_{2',6'}: 2.7 Hz), 7.44 (d, 1H, 5'-H, J_{5',6'}: 8.5 Hz), 7.84 (m, 2H, 6-H, 7-H), 7.96 (s, 1H, 3-H), 8.25 (m, 2H, 5-H, 8-H), (br, 2H, 1-NH₂ not detectable), 11.90 (br, 1H, 4-NH). ¹³C NMR (126 MHz): δ 19.80, 109.38, 111.96, 122.16, 122.86, 125.82, 126.09, 126.18, 128.69, 129.94, 132.96, 133.40, 133.63, 134.27, 137.02, 138.47, 140.48, 142.84, 144.52, 182.02, 182.82. LC-MS (m/z): 460 [M - Na⁺ + NH₄⁺]⁺, 443 [M - Na⁺ + H⁺]⁺, 441 [M - Na⁺ + H⁺]⁻. Purity by HPLC-UV (254 nm) ESI-MS: 99%.

Sodium 1-Amino-4-(4-hydroxy-3-methylphenylamino)-9,10-dioxo-9,10-dihydroanthracene-2-sulfonate (42). Reaction conditions according to general procedure A: Compound **6a** (121.3 mg, 0.3 mmol), 4-amino-2-methylphenol (111 mg, 0.9 mmol). MW conditions: 20 min, 100 °C, 100 W; pressure up to 10 bar. Analytical data: blue powder (40% yield), mp >300 °C. ¹H NMR (500 MHz): δ 2.15 (s, 3H, CH₃), 6.86 (d, 1H, 5'-H, J_{5',6'}: 8.4 Hz), 6.93 (dd, 1H, 6'-H, J_{5',6'}: 8.4 Hz, J_{2',6'}: 2.6 Hz), 7.01 (d, 1H, 2'-H, J_{2',6'}: 2.6 Hz), 7.81 (s, 1H, 3-H), 7.84 (m, 2H, 6-H, 7-H), 8.28 (m, 2H, 5-H, 8-H). ¹³C NMR (126 MHz): δ 15.94, 108.73, 109.68, 115.32, 122.57, 123.39, 125.23, 125.79, 125.94, 127.37, 129.58, 132.54, 132.73, 133.74, 134.11, 143.07, 143.28, 143.97, 153.42, 181.41, 181.46. LC-MS (m/z): 425 [M - Na⁺ + H⁺]⁺, 423 [M - Na⁺ + H⁺]⁻. Purity by HPLC-UV (254 nm) ESI-MS: 96%.

Sodium 1-Amino-4-(4-fluoro-3-methoxyphenylamino)-9,10-dioxo-9,10-dihydroanthracene-2-sulfonate (43). Reaction conditions according to general procedure A: Compound **6a** (121.3 mg, 0.3 mmol), 4-fluoro-3-methoxyaniline (84.7 mg, 0.6 mmol). MW conditions: 5 min, 120 °C, 100 W; pressure up to 10 bar. Analytical data: blue powder (43% yield), mp >300 °C. ¹H NMR (500 MHz): δ 3.86 (s, 3H, -OCH₃), 6.85 (m, 1H, 6'-H), 7.14 (dd, 1H, 2'-H, ⁴J_{H-F} 7.8 Hz, ⁴J_{2',6'} 2.5 Hz), 7.27 (dd, 1H, 5'-H, ³J_{H-F} 11.35 Hz, ⁴J_{5',6'} 8.6 Hz), 7.86 (m, 2H, 6-H, 7-H), 8.00 (s, 1H, 3-H), 8.28 (m, 1H, 5-H, 8-H), 11.96 (s, 1H, 4-NH). ¹³C NMR (126 MHz): δ 56.52, 109.07, 109.79, 111.22, 115.36, 116.37, 122.72, 125.88, 126.01, 132.74, 133.14, 133.52, 134.12, 135.89, 141.06, 142.77, 144.26, 147.78, 149.65, 181.77, 182.40. LCMS (*m/z*): 460 [M - Na⁺ + NH₄⁺]⁺, 443 [M - Na⁺ + H⁺]⁺, 441 [M - Na⁺ + H⁺]⁻. Purity by HPLC-UV (220–700 nm) ESI-MS: 99.3%.

Sodium 1-Amino-4-(4-chloro-3-methoxyphenylamino)-9,10-dioxo-9,10-dihydroanthracene-2-sulfonate (44). Reaction conditions according to general procedure A: Compound **6a** (121.3 mg, 0.3 mmol), 4-chloro-3-methoxyaniline (94.6 mg, 0.6 mmol). MW conditions: 5 min, 120 °C, 100 W; pressure up to 10 bar. Analytical data: blue powder (40% yield), mp >300 °C. ¹H NMR (500 MHz): δ 3.88 (s, 3H, -OCH₃), 6.87 (dd, 1H, 6'-H, ²J_{2',6'} 2.4 Hz, ¹J_{5',6'} 8.45 Hz), 7.10 (d, 1H, 2'-H, ²J_{2',6'} 2.4 Hz), 7.44 (d, 1H, 5'-H, ¹J_{5',6'} 8.45 Hz), 7.86 (m, 2H, 6-H, 7-H), 8.10 (s, 1H, 3-H), 8.27 (m, 1H, 5-H, 8-H), 11.90 (s, 1H, 4-NH). ¹³C NMR (126 MHz): δ 56.14, 107.60, 109.26, 112.08, 115.13, 116.00, 123.08, 125.92, 126.03, 130.31, 132.81, 133.28, 133.43, 134.10, 139.67, 139.80, 142.51, 144.43, 155.23, 181.88, 182.74. LC-MS (*m/z*): 476 [M - Na⁺ + NH₄⁺]⁺, 459 [M - Na⁺ + H⁺]⁺, 457 [M - Na⁺ + H⁺]⁻. Purity by HPLC-UV (220–700 nm) ESI-MS: 99.7%.

Sodium 1-Amino-4-(2-carboxy-3-fluorophenylamino)-9,10-dioxo-9,10-dihydroanthracene-2-sulfonate (49). Reaction conditions according to general procedure A: Compound **6a** (121.3 mg, 0.3 mmol), 2-amino-6-fluorobenzoic acid (93 mg, 0.6 mmol). MW conditions: 15 min, 120 °C, 100 W; pressure up to 10 bar. Analytical data: blue powder (40% yield), mp >300 °C. ¹H NMR (500 MHz): δ 6.78 (dd, 1H, 5'-H), 6.94 (d, 1H, 6'-H), 7.15 (dd, 1H, 4'-H), 7.82 (m, 2H, 6-H, 7-H), 8.10 (s, 1H, 3-H), 8.25 (m, 2H, 5-H, 8-H), 10.05 (br, 2H, 1-NH₂), 12.07 (s, 1H, 4-NH). ¹³C NMR (126 MHz): δ 109.67, 110.09, 113.18, 116.83, 124.46, 126.27, 126.04, 127.18, 127.22, 132.82, 133.13, 133.86, 134.22, 138.59, 139.03, 141.96, 144.59, 159.54, 166.02, 181.9, 182.2. (*m/z*): 474 [M - Na⁺ + NH₄⁺]⁺, 457 [M - Na⁺ + H⁺]⁺, 455 [M - Na⁺ + H⁺]⁻. Purity by HPLC-UV (254 nm) ESI-MS: 98%.

Sodium 1-Amino-4-(2-carboxy-4-hydroxyphenylamino)-9,10-dioxo-9,10-dihydroanthracene-2-sulfonate (52). Reaction conditions according to general procedure A: Compound **6a** (81 mg, 0.2 mmol), 2-amino-5-hydroxybenzoic acid (61.3 mg, 0.4 mmol). MW conditions: 5 min, 120 °C, 100 W; pressure up to 10 bar. Analytical data: blue powder, (68% yield), mp >300 °C. ¹H NMR (500 MHz): δ 7.00 (dd, 1H, 5'-H, ¹J_{3',5'} 2.9 Hz, ¹J_{5',6'} 8.7 Hz), 7.17 (d, 1H, 6'-H, ¹J_{5',6'} 8.7 Hz), 7.33 (d, 1H, 3'-H, ¹J_{3',5'} 2.9 Hz), 7.83 (m, 2H, 6-H, 7-H), 7.90 (s, 1H, 3-H), 8.24 (m, 2H, 5-H, 8-H), 9.7 (br, 2H, 1-NH₂), 12.27 (s, 1H, 4-NH). ¹³C NMR (126 MHz): δ 109.54, 112.69, 117.20, 120.36, 123.80, 124.19, 125.33, 126.03, 126.11, 132.04, 132.84, 133.09, 133.90, 134.24, 140.03, 142.17, 144.44, 153.4, 167.33, 181.88, 182.06. LC-MS (*m/z*): 555 [M - Na⁺ + H⁺]⁺, 553 [M - Na⁺ + H⁺]⁻. Purity by HPLC-UV (254 nm) ESI-MS: 100%.

Sodium 1-Amino-4-(2-carboxy-4-nitrophenylamino)-9,10-dioxo-9,10-dihydroanthracene-2-sulfonate (53). Reaction conditions according to general procedure A: Compound **6a** (60.6 mg, 0.15 mmol), 2-amino-5-nitrobenzoic acid (246 mg, 1.35 mmol). MW conditions: 20 min, 110 °C, 100 W; pressure up to 10 bar. Analytical data: blue powder (21% yield), mp >300 °C. ¹H NMR (500 MHz): δ 7.10 (d, 1H, 6'-H, ¹J_{5',6'} 9.2 Hz) 7.86 (m, 2H, 6-H and 7-H) 8.09 (s, 1H, 3-H), 8.11 (dd, 1H, 5'-H, ¹J_{3',5'} 2.9 Hz, ¹J_{5',6'} 9.2 Hz), 8.15 (m, 1H, 5-H or 8-H), 8.24 (m, 1H, 5-H or 8-H), 8.77 (d, 1H, 3'-H, ¹J_{3',5'} 2.9 Hz). ¹³C NMR (126 MHz): δ 111.28, 115.34, 121.37, 126.03, 126.10, 126.58, 128.03, 128.06, 130.95, 133.18, 133.42, 133.73, 133.92, 137.78, 139.84, 146.07, 149.67, 167.63, 182.93, 183.22. LC-MS (*m/z*): 501 [M - Na⁺ + NH₄⁺]⁺, 484 [M - Na⁺ + H⁺]⁺, 482 [M - Na⁺ + H⁺]⁻. Purity by HPLC-UV (254 nm) ESI-MS: 95.7%.

Sodium 1-Amino-4-[4-(4-fluorophenoxy)phenylamino]-9,10-dioxo-9,10-dihydroanthracene-2-sulfonate (58). Reaction conditions according to general procedure A: Compound **6a** (121.3 mg, 0.3 mmol), 4-(4-fluorophenoxy)aniline (131.5 mg, 0.6 mmol). MW conditions: 15 min, 120 °C, 100 W; pressure up to 10 bar. Analytical data: blue powder (41% yield), mp >300 °C. ¹H NMR (500 MHz): δ 7.06 (d, 2H, 3'-H, 5'-H), 7.13 (dd, 2H, 2''-H, 6''-H), 7.24 (dd, 2H, 3''-H, 5''-H), 7.30 (d, 2H, 2'-H, 6'-H), 7.84 (m, 2H, 6-H, 7-H), 7.94 (s, 1H, 3-H), 8.27 (m, 2H, 5-H, 8-H), 10.11 (br, 2H, 1-NH₂), 12.03 (s, 1H, 4-NH). ¹³C NMR (126 MHz): δ 109.2, 111.1, 116.6, 116.8, 119.4, 120.8, 120.9, 122.6, 125.5, 126.0, 126.1, 132.9, 133.2, 133.7, 134.0, 134.6, 141.6, 143.1, 144.4, 152.7, 154.3, 157.4, 159.4, 181.9, 182.4. LC-MS (*m/z*): 522 [M - Na⁺ + NH₄⁺]⁺, 505 [M - Na⁺ + H⁺]⁺, 503 [M - Na⁺ + H⁺]⁻. Purity by HPLC-UV (254 nm) ESI-MS: 99.5%.

Sodium 1-Amino-4-[4-(4-chlorophenoxy)phenylamino]-9,10-dioxo-9,10-dihydroanthracene-2-sulfonate (59). Reaction conditions according to general procedure A: Compound **6a** (121.3 mg, 0.3 mmol), 4-(4-chlorophenoxy)aniline (141.4 mg, 0.6 mmol). MW conditions: 15 min, 120 °C, 100 W; pressure up to 10 bar. Analytical data: blue powder (25% yield), mp >300 °C. ¹H NMR (500 MHz): δ 7.10 (m, 4H, 3'-H, 5'-H, 2''-H, 6''-H), 7.32 (dd, 2H, 3''-H, 5''-H), 7.44 (d, 2H, 2'-H, 6'-H), 7.85 (m, 2H, 6-H, 7-H), 7.96 (s, 1H, 3-H), 8.27 (m, 2H, 5-H, 8-H), 10.11 (br, 2H, 1-NH₂), 12.03 (s, 1H, 4-NH). ¹³C NMR (126 MHz): δ 109.3, 111.3, 120.2, 120.4, 122.6, 125.4, 126.1, 126.2, 127.4, 130.1, 132.9, 133.3, 133.7, 134.3, 135.2, 141.4, 143.1, 144.4, 153.2, 155.9, 181.9, 182.5. LC-MS (*m/z*): 519 [M - Na⁺ + H⁺]⁻. Purity by HPLC-UV (254 nm) ESI-MS: 98.6%.

Sodium 1-Amino-4-[4-(4-bromophenoxy)phenylamino]-9,10-dioxo-9,10-dihydroanthracene-2-sulfonate (60). Reaction conditions according to general procedure A: Compound **6a** (121.3 mg, 0.3 mmol), 4-(4-bromophenoxy)aniline (190 mg, 0.6 mmol). MW conditions: 15 min, 120 °C, 100 W; pressure up to 10 bar. Analytical data: blue powder (17% yield), mp >300 °C. ¹H NMR (500 MHz): δ 7.03 (d, 2H, 3'-H, 5'-H) 7.12 (d, 2H, 2''-H, 6''-H), 7.33 (dd, 2H, 3''-H, 5''-H), 7.56 (d, 2H, 2'-H, 6'-H), 7.85 (m, 2H, 6-H, 7-H), 7.96 (s, 1H, 3-H), 8.27 (m, 2H, 5-H, 8-H), 10.10 (br, 2H, 1-NH₂), 12.03 (s, 1H, 4-NH). ¹³C NMR (126 MHz): δ 109.3, 111.3, 115.2, 120.3, 120.7, 122.6, 125.3, 126.1, 126.2, 132.9, 133.0, 133.3, 135.3, 141.4, 144.4, 153.1, 156.5, 181.9, 182.5. LC-MS (*m/z*): 565 [M - Na⁺ + H⁺]⁺, 563 [M - Na⁺ + H⁺]⁻. Purity by HPLC-UV (254 nm) ESI-MS: 96.1%.

Sodium 1-Amino-4-[4-(2,4-dimethylphenylthio)phenylamino]-9,10-dioxo-9,10-dihydroanthracene-2-sulfonate (61). Reaction conditions according to general procedure A: Compound **6a** (121.3 mg, 0.3 mmol), 4-[(2,4-dimethylphenyl)thio]aniline (137.6 mg, 0.6 mmol). MW conditions: 15 min, 120 °C, 100 W; pressure up to 10 bar. Analytical data: blue powder (10% yield), mp >300 °C. ¹H NMR (500 MHz): δ 2.31, 2.28 (2s, 6H, 2CH₃), 7.04, 7.20 (m, 7H, 2'-H, 3'-H, 5'-H, 6'-H, 3''-H, 5''-H, 6''-H), 7.84 (m, 2H, 6-H, 7-H), 7.98 (s, 1H, 3-H), 8.25 (m, 2H, 5-H, 8-H), 10.05 (br, 2H, 1-NH₂), 11.95 (s, 1H, 4-NH). ¹³C NMR: δ 20.2, 20.7, 109.4, 112.0, 122.9, 123.7, 126.1, 126.2, 127.9, 129.5, 130.4, 130.9, 131.7, 132.9, 133.3, 133.6, 134.2, 138.1, 138.2, 139.5, 140.2, 142.8, 144.5, 182.0, 182.7. LC-MS (*m/z*): 531 [M - Na⁺ + H⁺]⁺, 529 [M - Na⁺ + H⁺]⁻. Purity by HPLC-UV (254 nm) ESI-MS: 96.1%.

Sodium 1-Amino-4-[4-(2,5-dimethylphenylthio)phenylamino]-9,10-dioxo-9,10-dihydroanthracene-2-sulfonate (62). Reaction conditions according to general procedure A: Compound **6a** (121.3 mg, 0.3 mmol), 4-[(2,5-dimethylphenyl)thio]aniline (137.6 mg, 0.6 mmol). MW conditions: 15 min, 120 °C, 100 W; pressure up to 10 bar. Analytical data: blue powder (7% yield), mp >300 °C. ¹H NMR (500 MHz): δ 2.23, 2.30 (2s, 6H, 2CH₃), 7.08, 7.23 (m, 7H, 2'-H, 3'-H, 5'-H, 6'-H, 3''-H, 4''-H, 6''-H), 7.84 (m, 2H, 6-H, 7-H), 8.00 (s, 1H, 3-H), 8.25 (m, 2H, 5-H, 8-H), 10.07 (br, 2H, 1-NH₂), 11.94 (s, 1H, 4-NH). ¹³C NMR: δ 19.8, 20.6, 109.4, 112.2, 123.0, 123.7, 126.1, 126.2, 128.9, 129.9, 130.7, 131.4, 132.6, 133.0, 133.2, 133.4, 133.6, 134.3, 135.9, 136.4, 138.6, 140.1, 142.8, 144.6, 182.0, 182.8. LC-MS (*m/z*): 531 [M - Na⁺ + H⁺]⁺, 529 [M - Na⁺ + H⁺]⁻. Purity by HPLC-UV (254 nm) ESI-MS: 98.0%.

Sodium 1-Amino-4-[4-(3,4-dimethylphenylthio)phenylamino]-9,10-dioxo-9,10-dihydroanthracene-2-sulfonate (63). Reaction con-

ditions according to general procedure A: Compound **6a** (121.3 mg, 0.3 mmol), 4-[(3,4-dimethylphenyl)thio]aniline (137.6 mg, 0.6 mmol). MW conditions: 15 min, 120 °C, 100 W; pressure up to 10 bar. Analytical data: blue powder (7% yield), mp >300 °C. ¹H NMR (500 MHz): δ 2.21 (s, 6H, 2CH₃), 7.21 (m, 7H, 2'-H, 3'-H, 5'-H, 6'-H, 3''-H, 4''-H, 6''-H), 7.84 (m, 2H, 6-H, 7-H), 8.00 (s, 1H, 3-H), 8.25 (m, 2H, 5-H, 8-H), 10.06 (br, 2H, 1-NH₂), 11.93 (s, 1H, 4-NH). ¹³C NMR: δ 19.1, 19.4, 109.4, 112.1, 122.9, 123.6, 126.1, 126.2, 129.3, 130.8, 130.9, 131.1, 131.5, 132.7, 132.9, 133.4, 133.6, 134.2, 136.4, 137.9, 138.5, 140.1, 142.7, 144.6, 182.0, 182.8. LC-MS (*m/z*): 531 [M - Na⁺ + H⁺]⁺, 529 [M - Na⁺ + H⁺]⁻. Purity by HPLC-UV (254 nm) ESI-MS: 95.6%.

Sodium 1-Amino-4-[4-(3-pyridin-3-ylmethylthio)phenylamino]-9,10-dioxo-9,10-dihydroanthracene-2-sulfonate (64). Reaction conditions according to general procedure A: Compound **6a** (121.3 mg, 0.3 mmol), 4-[(pyridin-3-ylmethyl)thio]aniline (129.8 mg, 0.6 mmol). MW conditions: 15 min, 120 °C, 100 W; pressure up to 10 bar. Analytical data: blue powder (14% yield), mp >300 °C. ¹H NMR (500 MHz): δ 4.33 (s, 2H, CH₂), 7.21 (d, 2H, 2'-H, 6'-H), 7.39 (d, 2H, 3'-H, 5'-H), 7.64 (m, 1H, 5''-H), 7.84 (m, 2H, 6-H, 7-H), 7.97 (s, 1H, 3-H), 8.03 (s, 1H, 6''-H), 8.26 (m, 2H, 5-H, 8-H), 8.60 (2s, 2H, 2''-H, 4''-H), 11.89 (s, 1H, 4-NH). ¹³C NMR: δ 34.7, 109.4, 112.2, 123.0, 123.4, 125.2, 126.1, 126.2, 129.1, 132.6, 133.0, 133.4, 133.6, 134.3, 136.1, 138.7, 140.2, 140.8, 142.7, 144.6, 145.0, 146.2, 182.0, 182.8. LC-MS (*m/z*): 518 [M - Na⁺ + H⁺]⁺, 516 [M - Na⁺ + H⁺]⁻. Purity by HPLC-UV (254 nm) ESI-MS: 98.6%.

1-Amino-4-(2-carboxy-4-fluorophenylamino)-2-methyl-9,10-dioxo-9,10-dihydroanthracene (67). Reaction conditions according to general procedure A: Compound **6b** (31.6 mg, 0.1 mmol), 2-amino-5-fluorobenzoic acid (31 mg, 0.2 mmol). MW conditions: 5 min, 120 °C, 100 W; pressure up to 10 bar. Analytical data: blue powder (21 % yield), mp > 300 °C. ¹H NMR (500 MHz): δ 2.22 (s, 3H, -CH₃), 7.02 (m, 1H, 6'-H), 7.17 (m, 1H, 5'-H), 7.50 (m, 2H, 3-H, 3'-H), 7.79 (m, 2H, 6-H, 7-H), 8.24 (m, 2H, 5-H, 8-H). ¹³C NMR (126 MHz): δ 18.34, 108.74, 111.85, 114.83, 115.02, 116.56, 116.72, 121.77, 121.84, 125.74, 125.86, 126.37, 132.35, 132.49, 133.84, 134.23, 135.24, 135.93, 139.43, 141.12, 146.98, 155.93, 157.82, 168.08, 180.26, 182.27. LC-MS (*m/z*): 391 [M]⁺, 389 [M]⁻. Purity by HPLC-UV (254 nm)-ESI-MS: 99.7 %.

4-(3-Fluorophenylamino)-9,10-dioxo-9,10-dihydroanthracene-2-sulfonic Acid (68). Reaction conditions: Compound **12** (41 mg, 0.1 mmol) was reacted according to general procedure C. Analytical data: reddish-purple powder (97% yield), mp >300 °C. ¹H NMR (600 MHz): δ 7.07 (td, 1H, 6'-H), 7.23 (m, 2H, 2'-H, 5'-H), 7.51 (m, 1H, 4'-H), 7.80 (d, 1H, 1-H or 3-H, *J*_{1,3} 1.47 Hz), 7.86 (d, 1H, 1-H or 3-H, *J*_{1,3} 1.47 Hz), 7.90 (td, 1H, 6-H or 7-H), 7.94 (td, 1H, 6-H or 7-H), 8.20 (dd, 1H, 5-H or 8-H), 8.25 (dd, 1H, 5-H or 8-H), 11.21 (s, 1H, 4-NH). ¹³C NMR (151 MHz) δ 39.52, 110.16, 110.32, 111.46, 111.60, 113.94, 115.53, 116.05, 119.18, 119.20, 126.51, 126.66, 131.26, 131.33, 132.49, 133.98, 134.17, 134.30, 134.68, 140.94, 141.01, 147.72, 154.35, 161.98, 163.60, 182.30, 184.50. LC-MS (*m/z*): 415 [M - H⁺ + NH₄⁺]⁺, 398 [M]⁺, 396 [M]⁻. Purity by HPLC-UV (220–650 nm) ESI-MS: 98.5%.

4-(3-Methoxyphenylamino)-9,10-dioxo-9,10-dihydroanthracene-2-sulfonic Acid (69). Reaction conditions: Compound **27** (42 mg, 0.1 mmol) was reacted according to general procedure C. Analytical data: reddish-purple powder (38% yield), mp >300 °C. ¹H NMR (500 MHz) δ 3.80 (s, 1H, -OCH₃), 6.84 (m, 1H, 6'-H), 6.94 (m, 2H, 2'-H, 4'-H), 7.39 (m, 1H, 5'-H), 7.81 (d, 1H, 1-H or 3-H, *J*_{1,3} 1.5 Hz), 7.83 (d, 1H, 1-H or 3-H, *J*_{1,3} 1.5 Hz), 7.90 (td, 1H, 6-H or 7-H), 7.95 (td, 1H, 6-H or 7-H), 8.20 (dd, 1H, 5-H or 8-H), 8.27 (dd, 1H, 5-H or 8-H), 11.24 (s, 1H, 4-NH). ¹³C NMR (126 MHz) δ 55.20, 109.27, 110.86, 113.28, 115.08, 115.70, 116.14, 126.46, 126.61, 130.47, 132.51, 133.84, 134.15, 134.61, 140.03, 148.47, 154.31, 160.36, 182.35, 184.35. LC-MS (*m/z*): 427 [M - H⁺ + NH₄⁺]⁺, 410 [M]⁺, 408 [M]⁻. Purity by HPLC-UV (220–600 nm) ESI-MS: 95.2%.

Retroviral Transfection of 1321N1 Astrocytoma Cells with Human P2Y₁, P2Y₄, and P2Y₆ Receptors. Transfection of 1321N1 astrocytoma cells with human P2Y₁, P2Y₄, and P2Y₆ receptors was performed as previously described.⁵⁹ Transfection with the human

P2Y₂ receptor was done in analogy (see Supporting Information). Briefly, the coding sequence of the respective receptor was cloned into the pQCXIN or pLXSN retroviral vector, amplified, purified, and sequenced prior to the transfection of GP⁺env AM-12 packaging cells together with vesicular stomatitis virus G (VSV-G) protein DNA using lipofectamine 2000. After 16 h, 3 mL of Dulbecco's Modified Eagle's Medium (DMEM) containing 10% fetal calf serum, 1% of a penicillin/streptomycin solution (final concentrations: penicillin = 100 U/mL, streptomycin = 0.1 mg/mL), and sodium butyrate (5 mM) was given to the packaging cells and these were kept at 32 °C and 5% CO₂ for 48 h, during which the viral vectors containing the receptor sequence were produced and released into the surrounding medium. These were harvested, filtered (45 μm filter pore diameter), and given to 1321N1 astrocytoma cells that do not intrinsically express P2 receptors at a detectable level. Polybrene solution (6 μL, 4 mg/mL in H₂O, filtered) was added. After 2.5 h, the virus-containing medium was discarded and DMEM supplemented with 10% fetal calf serum and 1% of a penicillin/streptomycin solution (final concentrations: penicillin = 100 U/mL, streptomycin = 0.1 mg/mL) was given to the cells. These were incubated for 2 days, followed by selection of successfully transfected cells with Geneticin resistance by adding G418 (200 μg/mL) to the medium. Single cells were selected and grown into monoclonal colonies in case of the P2Y₂ and P2Y₄ receptor expressing cells.

Pharmacological Evaluation of the Compounds at Human P2Y₁, P2Y₂, P2Y₄, and P2Y₆ Receptors. All experiments were performed using 1321N1 human astrocytoma cells stably expressing the respective human P2Y receptor subtype. The cells were grown in T175 tissue culture flasks (175 cm² area) containing 25–30 mL DMEM supplemented with 10% fetal calf serum, 200 μg/mL G418, and 1% of a penicillin/streptomycin solution (final concentrations: penicillin = 100 U/mL, streptomycin = 0.1 mg/mL). DMEM and supplements were purchased from Invitrogen (Life Technologies GmbH, Darmstadt, Germany). The flasks were kept at 37 °C in a humidified atmosphere (96% relative humidity) containing 5% CO₂. Cells were maintained in the exponential growth phase throughout and regularly tested for mycoplasma contamination.

Calcium Mobilization Assays. Calcium measurements were performed as previously described.⁶⁰ Briefly, 1321N1 human astrocytoma cells stably transfected with the coding sequence for the respective human P2Y receptor were used. Approximately 24 h prior to testing, the nutrient medium was discarded and the cells rinsed with phosphate-buffered saline before detachment using 0.05% trypsin/0.6 mM EDTA. The cells were then suspended in DMEM with the supplements described above and dispensed into sterile, black, flat, clear-bottom 96-well polystyrene microplates with lid (Corning 3340) at 50000 cells per well. The microplates were incubated at 37 °C in humidified air with 5% CO₂, during which the cells adhered to the coated bottom of the wells. Test compounds were investigated by measuring their inhibition of P2Y₁, P2Y₂, P2Y₄, or P2Y₆ receptor-mediated intracellular calcium mobilization using a FlexStation 3 (Molecular Devices GmbH, Biberach an der Riss, Germany) plate reader. At the start of the assay, the plated cells were loaded with fluo-4 acetoxymethyl ester (Life Technologies GmbH, Darmstadt, Germany) for 1 h. Excess dye was subsequently removed and Hank's Balanced Salt Solution (HBSS) buffer given to the cells. Afterward, the cells were preincubated with the test compound for 30 min. Using the pipetting function of the microplate reader, the physiological ligand was injected at a concentration that corresponds to its EC₈₀: 500 nM ADP for the P2Y₁, 500 nM UTP for the P2Y₂ and P2Y₄, and 750 nM UDP for the P2Y₆ receptor. The final volume was 200 μL per well. Fluorescence was measured at 525 nm following excitation at 488 nm. At least three independent experiments were performed in duplicate. IC₅₀ values were calculated by nonlinear regression using Prism 5.0 (GraphPad Software, San Diego, CA, USA).

Homology Modeling of the Human P2Y₄ Receptor. A homology model of the human P2Y₄ receptor was created based on the X-ray cocrystal structure of the human P2Y₁ receptor with the nucleotide-derived antagonist MRS2500 (PDB-ID: 4XNW, resolution 2.7 Å).⁵⁶ The structure was downloaded from the RSCB (Research Collaboratory for Structural Bioinformatics) Protein Data Bank

(<http://www.rcsb.org/>) and used as a template for generating the homology model of the human P2Y₄ receptor.⁶¹ The amino acid sequence of the human P2Y₄ receptor with the accession number P51582 was retrieved from UniProtKB sequence database.⁶² The sequences of the human P2Y₁ and P2Y₄ receptors were aligned using Clustal Omega and AlignMe (Supporting Information, Figure S8).^{63,64} The resulting alignments were manually adjusted for improving the alignment, particularly in the transmembrane and extracellular loop region 2 (ECL2). An overall sequence identity of 41.8% and a similarity of 60.2% between the human P2Y₁ and P2Y₄ receptors was calculated. The resulting alignment was used as input for generating homology models of the human P2Y₄ receptor using Modeller9.16.^{65,66} From the 750 models generated, the best model was selected on the basis of the Discrete Optimized Protein Energy (DOPE) score included in Modeller, manual visualization of the presence of an ionic lock between Asp187 and Arg292, and analysis of the binding sites. The overall structural quality was confirmed by a Ramachandran plot (Supporting Information, Figure S9),⁶⁷ and sequence–structure compatibility of the model was ensured using PROSA II profile analysis (Supporting Information, Figure 60).⁶⁸ Possible binding sites were identified using the SiteFinder module from Molecular Operating Environment (MOE 2014.09).⁶⁹

Docking Studies. Docking simulations were performed using Induced Fit Docking (IFD) and Glide as implemented in Schrödinger release 2016.^{70–72} Prior to docking, the homology model of the human P2Y₄ receptor was prepared using the Protein Preparation Wizard at pH 7.4 and with force field Optimized Potentials for Liquid Simulations Version 3 (OPLS3) implemented in Schrödinger. The ligands were prepared using the implemented LigPrep module and the OPLS3 force field in possible states at pH 7.4 ± 1.0. The conformations of the docked ligands within an energy window of 2.5 kcal/mol were considered. For Glide docking, the following standard parameters were selected: receptor van der Waals scaling, 0.50; ligand van der Waals scaling, 0.50; a maximum of 20 poses per ligand. Residues within 5.0 Å of the ligand poses were refined, and the side chains were optimized. The best docking pose was selected based on the IFD score and Prime Energy values. The compounds were subsequently docked to the best scoring complex obtained for compound 61. A receptor grid center was specified on the basis of the transformed position of the allosteric antagonist MRS2500 from the human P2Y₁ receptor structure, with a cubic grid side length of 10 Å. As precision setting, XP (extra precision) was chosen. Following Glide docking, the resulting poses were selected using the IFD scores and Prime Energy as representative values.

■ ASSOCIATED CONTENT

Supporting Information

The Supporting Information is available free of charge on the ACS Publications website at DOI: 10.1021/acs.jmedchem.7b00030.

LC-MS spectra of RB-2 P (2'); ¹H NMR, ¹³C NMR, and DEPT 135 NMR spectra of the newly synthesized anthraquinone derivatives; description of the β-arrestin recruitment assay used for measuring P2Y₁₂ receptor antagonism; multiple sequence alignment of P2Y receptor subtypes (PDF)

Molecular formula strings (CSV)

■ AUTHOR INFORMATION

Corresponding Authors

*For C.E.M.: phone, +49-228-73-2301; fax, +49-228-73-2567; E-mail, christa.mueller@uni-bonn.de.

*For Y.B.: phone, +968-24141473; fax, +968-24141469; E-mail, baqi@sq.edu.om.

ORCID

Enas M. Malik: 0000-0003-4563-3584

Christa E. Müller: 0000-0002-0013-6624

Younis Baqi: 0000-0002-9659-8419

Author Contributions

[§]These authors contributed equally to this work

Notes

The authors declare no competing financial interest.

■ ACKNOWLEDGMENTS

Y.B. is grateful for an SQU grant (SR/SCI/CHEM/15/01). E.M.M. thanks The Deutscher Akademischer Austauschdienst (DAAD) for a Ph.D. scholarship. M.R. and C.E.M. are grateful to the NRW International Graduate Research School Biotech-Pharma for financial support. A.N. and C.E.M. were supported by the Deutsche Forschungsgemeinschaft (DFG, Research Training group GRK 1873). We thank Schrödinger Inc., for providing the evaluation license.

■ ABBREVIATIONS USED

2MeSADP, 2-methylthioadenosine-5'-diphosphate; APP, amyloid precursor protein; DMEM, Dulbecco's Modified Eagle's Medium; ECL, extracellular loop; GIT, gastrointestinal tract; IFD, induced fit docking; MRS2500, 2-iodo-N⁶-methyl-(N)-methanocarpa-2'-deoxyadenosine-3',5'-bisphosphate; PPADS, pyridoxalphosphate-6-azophenyl-2',4'-disulfonic acid; RB-2, reactive blue 2; SEM, standard error of the mean; TM, transmembrane region; UTP, uridine-5'-triphosphate

■ REFERENCES

- (1) Jacobson, K. A.; Müller, C. E. Medicinal chemistry of adenosine, P2Y and P2X receptors. *Neuropharmacology* **2016**, *104*, 31–49.
- (2) King, B. F.; Burnstock, G. Purinergic receptors. In *Understanding G Protein-Coupled Receptors and Their Role in the CNS*; Pangalos, M., Davies, C., Eds.; Oxford University Press: Oxford, UK, 2002; pp 422–438.
- (3) Burnstock, G. Introduction: P2 receptors. *Curr. Top. Med. Chem.* **2004**, *4*, 793–803.
- (4) Jacobson, K.; Jarvis, M. F.; Williams, M. Purine and pyrimidine (P2) receptors as drug targets. *J. Med. Chem.* **2002**, *45*, 4057–4093.
- (5) Savi, P.; Herbert, J. M. Clopidogrel and ticlopidine: P2Y₁₂ adenosine diphosphate-receptor antagonists for the prevention of atherothrombosis. *Semin. Thromb. Hemostasis* **2005**, *31*, 174–183.
- (6) Angiolillo, D. J.; Luis Ferreiro, J. Platelet adenosine diphosphate P2Y₁₂ receptor antagonism: benefits and limitations of current treatment strategies and future directions. *Rev. Esp. Cardiol.* **2010**, *63*, 60–76.
- (7) Teng, R.; Oliver, S.; Hayes, M.; Butler, K. Absorption, distribution, metabolism, and excretion of ticagrelor in healthy subjects. *Drug Metab. Dispos.* **2010**, *38*, 1514–1521.
- (8) Kim, C.-H.; Kim, H.-Y.; Lee, H. S.; Chang, S. O.; Oh, S.-H.; Lee, J. H. P2Y₄-mediated regulation of Na⁺ absorption in the reissner's membrane of the cochlea. *J. Neurosci.* **2010**, *30*, 3762–3769.
- (9) Marcus, D. C.; Liu, J.; Lee, J. H.; Scherer, E. Q.; Scofield, M. A.; Wangemann, P. Apical membrane P2Y₄ purinergic receptor controls K⁺ secretion by strial marginal cell epithelium. *Cell Commun. Signaling* **2005**, *3*, 13.
- (10) Burrell, H. E.; Bowler, W. B.; Gallagher, J. A.; Sharpe, G. R. Human keratinocytes express multiple P2Y-receptors: evidence for functional P2Y₁, P2Y₂, and P2Y₄ receptors. *J. Invest. Dermatol.* **2003**, *120*, 440–447.
- (11) Song, X.; Guo, W.; Yu, Q.; Liu, X.; Xiang, Z.; He, C.; Burnstock, G. Regional expression of P2Y₄ receptors in the rat central nervous system. *Purinergic Signalling* **2011**, *7*, 469–488.
- (12) Communi, D.; Piroton, S.; Parmentier, M.; Boeynaems, J. Cloning and functional expression of a human uridine nucleotide receptor. *J. Biol. Chem.* **1995**, *270*, 30849–30852.

- (13) Robaye, B.; Ghanem, E.; Wilkin, F.; Fokan, D.; Van Driessche, W.; Schurmans, S.; Boeynaems, J.-M.; Beauwens, R. Loss of nucleotide regulation of epithelial chloride transport in the jejunum of p2y₄-null mice. *Mol. Pharmacol.* **2003**, *63*, 777–783.
- (14) Kunzelmann, K.; Mall, M. Electrolyte transport in the mammalian colon: mechanisms and implications for disease. *Physiol. Rev.* **2002**, *82*, 245–289.
- (15) Ghanem, E.; Robaye, B.; Leal, T.; Leipziger, J.; Van Driessche, W.; Beauwens, R.; Boeynaems, J.-M. The role of epithelial P2Y₂ and P2Y₄ receptors in the regulation of intestinal chloride secretion. *Br. J. Pharmacol.* **2005**, *146*, 364–369.
- (16) DuBose, D. R.; Wolff, S. C.; Qi, A.-D.; Naruszewicz, I.; Nicholas, R. A. Apical targeting of the P2Y₄ receptor is directed by hydrophobic and basic residues in the cytoplasmic tail. *Am. J. Physiol. Cell Physiol.* **2013**, *304*, C228–C239.
- (17) Tran, M. D. P2 receptor stimulation induces amyloid precursor protein production and secretion in rat cortical astrocytes. *Neurosci. Lett.* **2011**, *492*, 155–159.
- (18) Horckmans, M.; Robaye, B.; Léon-Gómez, E.; Lantz, N.; Unger, P.; Dol-Gleizes, F.; Clouet, S.; Cammarata, D.; Schaeffer, P.; Savi, P.; Gachet, C.; Balligand, J.-L.; Dessy, C.; Boeynaems, J.-M.; Communi, D. P2Y₄ nucleotide receptor: a novel actor in post-natal cardiac development. *Angiogenesis* **2012**, *15*, 349–360.
- (19) Brunschweiler, A.; Müller, C. E. P2 receptors activated by uracil nucleotides - an update. *Curr. Med. Chem.* **2006**, *13*, 289–312.
- (20) Gachet, C. Regulation of platelet functions by P2 receptors. *Annu. Rev. Pharmacol. Toxicol.* **2006**, *46*, 277–300.
- (21) Schwiebert, E. M.; Zsemberly, A.; Geibel, J. P. Cellular mechanisms and physiology of nucleotide and nucleoside release from cells: current knowledge, novel assays to detect purinergic agonists, and future directions. In *Extracellular Nucleotides and Nucleosides: Release, Receptors, and Physiological & Pathophysiological Effects*; Schwiebert, E. M., Ed.; Academic Press, Elsevier Science: Cambridge, MA, 2003; p 76.
- (22) Bogdanov, Y. D.; Wildman, S. S.; Clements, M. P.; King, B. F.; Burnstock, G. Molecular cloning and characterization of rat P2Y₄ nucleotide receptor. *Br. J. Pharmacol.* **1998**, *124*, 428–430.
- (23) Wildman, S. S.; Unwin, R. J.; King, B. F. Extended pharmacological profiles of rat P2Y₂ and rat P2Y₄ receptors and their sensitivity to extracellular H⁺ and Zn²⁺ ions. *Br. J. Pharmacol.* **2003**, *140*, 1177–1186.
- (24) Baqi, Y.; Lee, S.-Y.; Iqbal, J.; Ripphausen, P.; Lehr, A.; Scheiff, A. B.; Zimmermann, H.; Bajorath, J.; Müller, C. E. Development of potent and selective inhibitors of ecto-5'-nucleotidase based on an anthraquinone scaffold. *J. Med. Chem.* **2010**, *53*, 2076–2086.
- (25) Malik, E. M.; Müller, C. E. Anthraquinones as pharmacological tools and drugs. *Med. Res. Rev.* **2016**, *36*, 705–748.
- (26) Baqi, Y. Anthraquinones as a privileged scaffold in drug discovery targeting nucleotide-binding proteins. *Drug Discovery Today* **2016**, *21*, 1571–1577.
- (27) Baqi, Y.; Müller, C. E. Rapid and efficient microwave-assisted copper (0)-catalyzed ullmann coupling reaction: general access to anilinoanthraquinone derivatives. *Org. Lett.* **2007**, *9*, 1271–1274.
- (28) Baqi, Y.; Müller, C. E. Synthesis of alkyl- and aryl-amino-substituted anthraquinone derivatives by microwave-assisted copper(0)-catalyzed ullmann coupling reactions. *Nat. Protoc.* **2010**, *5*, 945–953.
- (29) Weyler, S.; Baqi, Y.; Hillmann, P.; Kaulich, M.; Hunder, A. M.; Müller, I. A.; Müller, C. E. Combinatorial synthesis of anilinoanthraquinone derivatives and evaluation as non-nucleotide-derived P2Y₂ receptor antagonists. *Bioorg. Med. Chem. Lett.* **2008**, *18*, 223–227.
- (30) Baqi, Y.; Atzler, K.; Köse, M.; Glänzel, M.; Müller, C. E. High-affinity, non-nucleotide-derived competitive antagonists of platelet P2Y₁₂ receptors. *J. Med. Chem.* **2009**, *52*, 3784–3793.
- (31) Baqi, Y.; Hausmann, R.; Rosefort, C.; Rettinger, J.; Schmalzing, G.; Müller, C. E. Discovery of potent competitive antagonists and positive modulators of the P2X₂ receptor. *J. Med. Chem.* **2011**, *54*, 817–830.
- (32) Baqi, Y.; Müller, C. E. Convergent synthesis of the potent P2Y receptor antagonist MG 50–3-1 based on a regioselective ullmann coupling reaction. *Molecules* **2012**, *17*, 2599–2615.
- (33) Baqi, Y.; Weyler, S.; Iqbal, J.; Zimmermann, H.; Müller, C. E. Structure-activity relationships of anthraquinone derivatives derived from bromaminic acid as inhibitors of ectonucleoside triphosphate diphosphohydrolases (E-NTPDases). *Purinergic Signalling* **2009**, *5*, 91–106.
- (34) Baqi, Y. Ecto-nucleotidase inhibitors: recent developments in drug discovery. *Mini-Rev. Med. Chem.* **2015**, *15*, 21–33.
- (35) Malik, E. M.; Baqi, Y.; Müller, C. E. Syntheses of 2-substituted 1-amino-4-bromoanthraquinones (bromaminic acid analogues) – precursors for dyes and drugs. *Beilstein J. Org. Chem.* **2015**, *11*, 2326–2333.
- (36) Malik, E. M.; Rashed, M.; Wingen, L.; Baqi, Y.; Müller, C. E. Ullmann reactions of 1-amino-4-bromoanthraquinones bearing various 2-substituents furnishing novel dyes. *Dyes Pigm.* **2016**, *131*, 33–40.
- (37) Hoffmann, K.; Baqi, Y.; Morena, M. S.; Glänzel, M.; Müller, C. E.; von Kügelgen, I. Von. Interaction of new, very potent non-nucleotide antagonists with arg256 of the human platelet P2Y₁₂ receptor. *J. Pharmacol. Exp. Ther.* **2009**, *331*, 648–655.
- (38) Baqi, Y.; Hausmann, R.; Rosefort, C.; Rettinger, J.; Schmalzing, G.; Müller, C. E. Discovery of potent competitive antagonists and positive modulators of the P2X₂ receptor. *J. Med. Chem.* **2011**, *54*, 817–830.
- (39) Baqi, Y.; Müller, C. E. Efficient and mild deamination procedure for 1-aminoanthraquinones yielding a diverse library of novel derivatives with potential biological activity. *Tetrahedron Lett.* **2012**, *53*, 6739–6742.
- (40) Fiene, A.; Baqi, Y.; Malik, E. M.; Newton, P.; Li, W.; Lee, S.; Hartland, E. L.; Müller, C. E. Inhibitors of the bacterial ectonucleotidase LpNTPDase from *Legionella pneumophila*. *Bioorg. Med. Chem.* **2016**, *24*, 4363–4371.
- (41) Glänzel, M.; Bültmann, R.; Starke, K.; Frahm, A. W. Constitutional isomers of Reactive Blue 2 – selective P2Y-receptor antagonists? *Eur. J. Med. Chem.* **2003**, *38*, 303–312.
- (42) Glänzel, M.; Bültmann, R.; Starke, K.; Frahm, A. W. Structure-activity relationships of novel P2-receptor antagonists structurally related to Reactive Blue 2. *Eur. J. Med. Chem.* **2005**, *40*, 1262–1276.
- (43) Burton, S. J.; McLoughlin, S. B.; Stead, C. V.; Lowe, C. R. Design and applications of biomimetic anthraquinone dyes 1. synthesis and characterization of terminal ring isomers of C.T. Reactive Blue 2. *J. Chromatogr. A* **1988**, *435*, 127–137.
- (44) Müller, C. E.; Schiedel, A. C.; Baqi, Y. Allosteric modulators of rhodopsin-like G protein-coupled receptors: opportunities in drug development. *Pharmacol. Ther.* **2012**, *135*, 292–315.
- (45) Böhme, H.-J.; Kopperschläger, G.; Schulz, J.; Hofmann, E. Affinity chromatography of phosphofructokinase using Cibacron Blue F3G-A. *J. Chromatogr. A* **1972**, *69*, 209–214.
- (46) Bornmann, L.; Hess, B. Interaction of cibacron dyes with dehydrogenases and kinases. *Z. Naturforsch. C* **1977**, *32c*, 756–759.
- (47) Ashton, A. R.; Polya, G. M. The specific interaction of cibacron and related dyes with cyclic nucleotide phosphodiesterase and lactate dehydrogenase. *Biochem. J.* **1978**, *175*, 501–506.
- (48) Beissner, R. S.; Rudolph, F. B. Interaction of Cibacron Blue 3G-A and related dyes with nucleotide-requiring enzymes. *Arch. Biochem. Biophys.* **1978**, *189*, 76–80.
- (49) Prestera, T.; Prochaska, H. J.; Talalay, P. Inhibition of NAD(P)H:(quinone-acceptor) oxidoreductase by Cibacron Blue and related anthraquinone dyes: a structure-activity study. *Biochemistry* **1992**, *31*, 824–833.
- (50) Biellmann, J.; Samama, J.; Branden, C. I.; Eklund, H. X-ray studies of the binding of Cibacron Blue F3GA to liver alcohol dehydrogenase. *Eur. J. Biochem.* **1979**, *102*, 107–110.
- (51) Monaghan, C.; Holland, S.; Dale, J. W. The interaction of anthraquinone dyes with the plasmid-mediated OXA-2 beta-lactamase. *Biochem. J.* **1982**, *205*, 413–417.

- (52) Liu, Y. C.; Ledger, R.; Stellwagen, E. Quantitative analysis of protein: immobilized dye interaction. *J. Biol. Chem.* **1984**, *259*, 3796–3799.
- (53) Roy, S.; Large, R. J.; Akande, A. M.; Kshatri, A.; Webb, T. I.; Domene, C.; Sergeant, G. P.; McHale, N. G.; Thornbury, K. D.; Hollywood, M. A. Development of GoSlo-SR-5–69, a potent activator of large conductance Ca^{2+} -activated K^+ (BK) channels. *Eur. J. Med. Chem.* **2014**, *75*, 426–437.
- (54) Zhang, K.; Zhang, J.; Gao, Z. G.; Zhang, D.; Zhu, L.; Han, G. W.; Moss, S. M.; Paoletta, S.; Kiselev, E.; Lu, W.; Fenalti, G.; Zhang, W.; Müller, C. E.; Yang, H.; Jiang, H.; Cherezov, V.; Katritch, V.; Jacobson, K. A.; Stevens, R. C.; Wu, B.; Zhao, Q. Structure of the human P2Y_{12} receptor in complex with an antithrombotic drug. *Nature* **2014**, *509*, 115–118.
- (55) Zhang, J.; Zhang, K.; Gao, Z. G.; Paoletta, S.; Zhang, D.; Han, G. W.; Li, T.; Ma, L.; Zhang, W.; Müller, C. E.; Yang, H.; Jiang, H.; Cherezov, V.; Katritch, V.; Jacobson, K. A.; Stevens, R. C.; Wu, B.; Zhao, Q. Agonist-bound structure of the human P2Y_{12} receptor. *Nature* **2014**, *509*, 119–122.
- (56) Zhang, D.; Gao, Z. G.; Zhang, K.; Kiselev, E.; Crane, S.; Wang, J.; Paoletta, S.; Yi, C.; Ma, L.; Zhang, W.; Han, G. W.; Liu, H.; Cherezov, V.; Katritch, V.; Jiang, H.; Stevens, R. C.; Jacobson, K. A.; Zhao, Q.; Wu, B. Two disparate ligand-binding sites in the human P2Y_1 receptor. *Nature* **2015**, *520*, 317–321.
- (57) Yuan, S.; Chan, H. C.; Vogel, H.; Filipek, S.; Stevens, R. C.; Palczewski, K. The molecular mechanism of P2Y_1 receptor activation. *Angew. Chem., Int. Ed.* **2016**, *55*, 10331–10335.
- (58) Rasmussen, C. R.; Gardocki, J. F.; Plampin, J. N.; Twardzik, B. L.; Reynolds, B. E.; Molinari, A. J.; Schwartz, N.; Bennetts, W. W.; Price, B. E.; Marakowski, J. 2-Pyrrolidinylideneureas, a new class of central nervous system agents. *J. Med. Chem.* **1978**, *21*, 1044–1054.
- (59) Hillmann, P.; Ko, G. Y.; Spinrath, A.; Raulf, A.; von Kügelgen, I.; Wolff, S. C.; Nicholas, R. A.; Kostenis, E.; Höltje, H. D.; Müller, C. E. Key determinants of nucleotide-activated G protein-coupled P2Y_2 receptor function revealed by chemical and pharmacological experiments, mutagenesis and homology modeling. *J. Med. Chem.* **2009**, *52*, 2762–2775.
- (60) Hernandez-Olmos, V.; Abdelrahman, A.; El-Tayeb, A.; Freudendahl, D.; Weinhausen, S.; Müller, C. E. N-substituted phenoxazine and acridone derivatives: structure-activity relationships of potent P2X_4 receptor antagonists. *J. Med. Chem.* **2012**, *55*, 9576–9588.
- (61) Berman, H. M.; Westbrook, J.; Feng, Z.; Gilliland, G.; Bhat, T. N.; Weissig, H.; Shindyalov, I. N.; Bourne, P. E. The Protein Data Bank. *Nucleic Acids Res.* **2000**, *28*, 235–242.
- (62) The UniProt Consortium. UniProt: a hub for protein information. *Nucleic Acids Res.* **2015**, *43*, D204–D212.
- (63) Sievers, F.; Wilm, A.; Dineen, D.; Gibson, T. J.; Karplus, K.; Li, W.; Lopez, R.; McWilliam, H.; Remmert, M.; Söding, J.; Thompson, J. D.; Higgins, D. G. Fast, scalable generation of high-quality protein multiple sequence alignments using Clustal Omega. *Mol. Syst. Biol.* **2011**, *7*, 539.
- (64) Stamm, M.; Staritzbichler, R.; Khafizov, K.; Forrest, L. R. AlignMe—a membrane protein sequence alignment web server. *Nucleic Acids Res.* **2014**, *42*, W246–W251.
- (65) Sali, A.; Blundell, T. L. Comparative protein modelling by satisfaction of spatial restraints. *J. Mol. Biol.* **1993**, *234*, 779–815.
- (66) Webb, B.; Sali, A. Protein structure modeling with MODELLER. *Methods Mol. Biol.* **2014**, *1137*, 1–15.
- (67) Ramachandran, G. N.; Ramakrishnan, C.; Sasisekharan, V. Stereochemistry of polypeptide chain configurations. *J. Mol. Biol.* **1963**, *7*, 95–99.
- (68) Wiederstein, M.; Sippl, M. J. ProSA-web: interactive web service for the recognition of errors in three-dimensional structures of proteins. *Nucleic Acids Res.* **2007**, *35*, W407–W410.
- (69) Molecular Operating Environment (MOE), 2014.09; Chemical Computing Group Inc.: 1010 Sherbooke St. West, Suite #910, Montreal, QC, Canada, H3A 2R7, 2016.
- (70) Halgren, T. A.; Murphy, R. B.; Friesner, R. A.; Beard, H. S.; Frye, L. L.; Pollard, W. T.; Banks, J. L. Glide: A new approach for rapid, accurate docking and scoring. 2. Enrichment factors in database screening. *J. Med. Chem.* **2004**, *47*, 1750–1759.
- (71) Friesner, R. A.; Banks, J. L.; Murphy, R. B.; Halgren, T. A.; Klicic, J. J.; Mainz, D. T.; Repasky, M. P.; Knoll, E. H.; Shaw, D. E.; Shelley, M.; Perry, J. K.; Francis, P.; Shenkin, P. S. Glide: A new approach for rapid, accurate docking and scoring. 1. Method and assessment of docking accuracy. *J. Med. Chem.* **2004**, *47*, 1739–1749.
- (72) Sherman, W.; Day, T.; Jacobson, M. P.; Friesner, R. A.; Farid, R. Novel procedure for modeling ligand/receptor induced fit effects. *J. Med. Chem.* **2006**, *49*, 534–553.

7.3. Supporting Information

The Supporting Information can be accessed free of charge online at <http://pubs.acs.org/doi/abs/10.1021/acs.jmedchem.7b00030>.

It contains:

- Spectra of *para*-RB-2 (2'): chromatogram, mass spectrum, UV spectrum, and purity calculation
- ¹H-NMR, ¹³C-NMR, and DEPT135-NMR spectra of the newly synthesized anthraquinone derivatives
- Structure-activity relationships of RB-2-related anthraquinone derivatives at different targets
- Docked poses of compounds 7, 42, 62, 63, and 64 in the proposed allosteric binding pocket of the P2Y₄R model
- Sequence alignment of the human P2Y₁- and P2Y₄Rs
- Ramachandran diagram of the human P2Y₄R homology model
- Multiple sequence alignment of different human P2Y subtypes assessed for the selectivity of the compounds
- Descriptions of the lentiviral transfection of 1321N1 astrocytoma cells with the
- Lentiviral transfection of 1321N1 astrocytoma cells with human P2Y₂R
- Expression of the human P2Y₁₂R CHO cells for the β-arrestin translocation assay
- Procedure of the β-arrestin translocation assay
- EC₅₀ values and maximal receptor activation for the dose-response curves of UTP after pre-incubation with fixed concentrations of compound 61

7.4. Summary and Outlook

As discussed in in **Sections 5** and **6**, design of selective antagonists for P2Y₄R is challenging due to the fact that it shares high sequence similarity with human P2Y₂R. In this study, six novel anthraquinone-derived P2Y₄R antagonists with nanomolar IC₅₀ values were identified and their selectivity profiles at other P2YR subtypes were characterized. The results suggest that the most potent antagonist (sodium 1-amino-4-[4-(2,4-dimethylphenylthio)-phenylamino]-9,10-dioxo-9,10-dihydroanthracene-2-sulfonate, compound number 61 in the publication) displays allosteric inhibition at human P2Y₄R. Moreover, the potent compound 64 displayed a superior selectivity profile versus over P2Y₁-, P2Y₂-, P2Y₆- and P2Y₁₂Rs. Connecting experimental data with molecular docking studies, comprehensive SARs for the compound series were established. While interaction of a sulfonate with positively charged residues predicted to be involved in the binding of the phosphate group of the (**Section 5**) was observed for both RB-2 and the smaller antagonists, different binding motifs of the anthraquinone core were forecasted suggesting different possible binding conformations of anthraquinone derivatives at P2Y₄R.

In total, several potent P2Y₄R antagonists were successfully developed, and their pharmacology was characterized. The results will function as a guiding force for future rational design of drug-like compounds acting at human P2Y₄R and provide fundamental information for virtual screening campaigns.

8. Computational Investigations on the Binding Mode of Ligands for the Cannabinoid-Activated G Protein-Coupled Receptor GPR18

8.1. Introduction

Orphan receptors represent a heterogeneous cluster of proteins where the identity of the physiological signaling molecule, the endogenous ligand, remains unknown. Although their pharmacology is cryptic, they can represent relevant points for therapeutic intervention for the treatment of diseases. One of those potential drug targets is GPR18 which is suggested to belong to the class of cannabinoid receptors due to the agonistic sensitivity towards THC. Unfortunately, no X-ray crystal structure of human GPR18 has been reported yet, impeding advancements in tool compound design and deorphanization of the GPCR. In order to elucidate the architecture of human GPR18, a homology model was constructed and used for computational studies of agonists and antagonists to stimulate SBDD and provide novel insights on receptor functionality. Taking advantage from the knowledge collected in the previous sections covering the investigation of P2YRs, particular interest was given to potential salt bridges that modulate receptor functionality. Furthermore, behavior of imidazothiazinone antagonist complexes was investigated in 200 ns long MD simulations to identify key interactions with the receptors and structural features contributing to the stabilization of the inactive state. To complement the total picture, SARs of the imidazothiazinone series were coupled to the predicted binding modes. Conclusively, the binding mode of the promiscuous agonist THC was examined in detail to elucidate the binding mode of cannabinoids at GPR18 and compared to other cannabinoid-GPCR complexes.

8.2. Publication

Article

Computational Investigations on the Binding Mode of Ligands for the Cannabinoid-Activated G Protein-Coupled Receptor GPR18

Alexander Neumann ^{1,2}, Viktor Engel ¹, Andhika B. Mahardhika ^{1,2}, Clara T. Schoeder ^{1,2}, Vigneshwaran Namasivayam ¹, Katarzyna Kieć-Kononowicz ³ and Christa E. Müller ^{1,2,*}

¹ PharmaCenter Bonn, Pharmaceutical Institute, Pharmaceutical Sciences Bonn (PSB), Pharmaceutical & Medicinal Chemistry, University of Bonn, 53121 Bonn, Germany; alexander-neumann@uni-bonn.de (A.N.); Viktor34@gmx.de (V.E.); mahardhika@uni-bonn.de (A.B.M.); clara.t.schoeder@vanderbilt.edu (C.T.S.); vnamasiv@uni-bonn.de (V.N.)

² Research Training Group 1873, University of Bonn, 53127 Bonn, Germany

³ Department of Technology and Biotechnology of Drugs, Faculty of Pharmacy, Jagiellonian University Medical College, Medyczna 9, 30-688 Krakow, Poland; mfkono@cyf-kr.edu.pl

* Correspondence: christa.mueller@uni-bonn.de; Tel.: +49-228-73-2301; Fax: +49-228-73-2567

Received: 10 March 2020; Accepted: 23 April 2020; Published: 29 April 2020



Abstract: GPR18 is an orphan G protein-coupled receptor (GPCR) expressed in cells of the immune system. It is activated by the cannabinoid receptor (CB) agonist Δ^9 -tetrahydrocannabinol (THC). Several further lipids have been proposed to act as GPR18 agonists, but these results still require unambiguous confirmation. In the present study, we constructed a homology model of the human GPR18 based on an ensemble of three GPCR crystal structures to investigate the binding modes of the agonist THC and the recently reported antagonists which feature an imidazothiazinone core to which a (substituted) phenyl ring is connected via a lipophilic linker. Docking and molecular dynamics simulation studies were performed. As a result, a hydrophobic binding pocket is predicted to accommodate the imidazothiazinone core, while the terminal phenyl ring projects towards an aromatic pocket. Hydrophobic interaction of Cys251 with substituents on the phenyl ring could explain the high potency of the most potent derivatives. Molecular dynamics simulation studies suggest that the binding of imidazothiazinone antagonists stabilizes transmembrane regions TM1, TM6 and TM7 of the receptor through a salt bridge between Asp118 and Lys133. The agonist THC is presumed to bind differently to GPR18 than to the distantly related CB receptors. This study provides insights into the binding mode of GPR18 agonists and antagonists which will facilitate future drug design for this promising potential drug target.

Keywords: cannabinoid; docking studies; GPCR; GPR18; MD simulation; orphan GPCRs

1. Introduction

G protein-coupled receptors (GPCR) represent the largest family of membrane proteins in eukaryotes. They are structurally characterized by seven transmembrane (TM) regions connected by three extracellular (ECL1-3) and three intracellular loops (ICL1-3), an extracellular N-terminal and an intracellular C-terminal domain. Upon binding of the cognate agonist (e.g., biogenic amine neurotransmitter, nucleotide, lipid, amino acid, peptide, glycoprotein) conformational changes are induced. These result in coupling with G proteins, and thereby transducing information from the extracellular to the intracellular compartment and inducing or inhibiting downstream signaling pathways [1,2]. Despite persistent efforts, nearly 100 GPCRs remain orphan, with their endogenous ligands unidentified or unconfirmed [3]. The functionalities and roles of orphan GPCRs under

(patho)physiological conditions are in most cases poorly understood. The identification of the endogenous ligands would be helpful for target validation studies and the design of novel therapeutic drugs for orphan GPCRs.

GPR18 is such an orphan GPCR of therapeutic interest, phylogenetically belonging to the δ -branch of class A, rhodopsin-like GPCRs. GPR18 was first described in 1997 and reported to be highly expressed in different tissues and cell lines of the immune system, including spleen, thymus, and leukocytes [4]. The role of GPR18 is still unclear and controversially debated. GPR18 has been proposed by independent groups to be involved in immunological [5–8] and neurodegenerative processes including Alzheimer’s disease and multiple sclerosis [9–13]. Based on the observation that the activation of GPR18 lowers the intraocular pressure in mice, GPR18 agonists have been proposed for the treatment of glaucoma [14,15]. Antagonists targeting GPR18 may be effective as anticancer drugs [16–18], since the receptor was found to be abundantly overexpressed in melanoma metastases and reported to contribute to tumor cell survival through inhibition of apoptosis [17].

In recent years, several studies aimed at the deorphanization of GPR18 have been published. Due to the lack of selective agonists, the moderately potent cannabinoid (CB) receptor agonist Δ^9 -tetrahydrocannabinol (THC, **1**) has been used in pharmacological studies to activate human GPR18, which led to the suggestion to classify GPR18 as a cannabinoid receptor subtype besides CB₁ and CB₂ [19–22]. *N*-Arachidonoylglycine (NAGly, **2**) and resolvin D2 (RvD2, **3**) were proposed as endogenous agonists of GPR18 [23,24]. However, independent confirmation for both lipids is still lacking, as other groups, including ours, have not been able to confirm their activation of GPR18 [25,26]. We recently described the first GPR18 antagonists based on an imidazothiazinone core structure [21,27]. These were discovered by screening a compound library at the human receptor in a β -arrestin recruitment assay using enzyme complementation technology and THC as an agonist. Based on the screening results, a library of imidazothiazinones was synthesized and their structure–activity relationships (SARs) were investigated. PSB-CB-27 (**4**) and PSB-CB-5 (**5**; for structures, see Figure 1) were reported as the first potent and selective GPR18 antagonists [21].

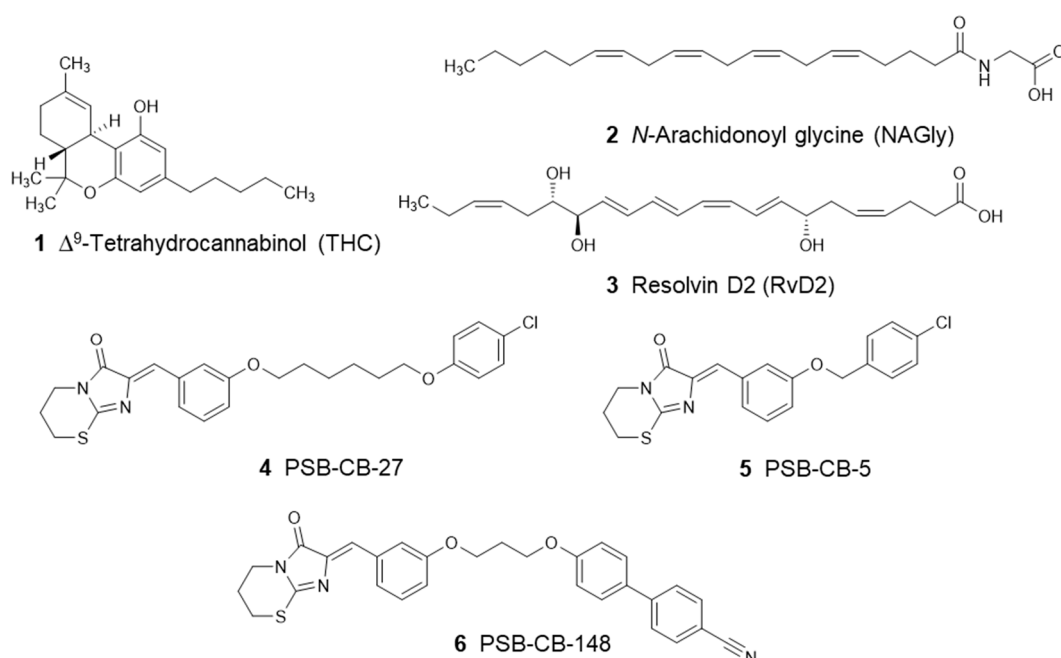


Figure 1. Structures of proposed GPR18 agonists (**1–3**) and antagonists (**4–6**).

In the present study, we constructed a homology model of the human GPR18 to elucidate the binding mode of the only confirmed agonist so far, the natural product THC, and of selected antagonists by docking and molecular dynamics (MD) simulation studies. Insights into the binding interactions of

agonists and antagonists will provide a basis for the rational design of more potent ligands and may eventually contribute to the deorphanization of GPR18.

2. Material and Methods

2.1. Homology Modeling

The crystal structures of the murine μ -opioid receptor in complex with the agonist BU72 (PDB-ID: 5C1M), the human P2Y₁ receptor in complex with the allosteric antagonist BPTU (PDB-ID: 4XNV) and the zebrafish lysophosphatidic acid receptor LPA6 in complex with 1-oleoyl-*R*-glycerol (PDB-ID: 5XSZ) were obtained from the Research Collaboratory for Structural Bioinformatics (RCSB) Protein Data Bank (PDB) [28–30]. The crystal structures of all three receptors were used as templates for generating homology models of the human GPR18 sequence (accession number: Q14330) retrieved from the UniProt sequence database (<http://www.uniprot.org>) [31]. The sequences of the murine μ -opioid receptor, the P2Y₁R, and the zebrafish lysophosphatidic acid receptor LPA6 were aligned with that of the human GPR18 using Clustal Omega [32]. We generated 500 models for the human GPR18 based on the triple template approach using the standard comparative modeling automodel class implemented in MODELLER (version 9.16, University of California, San Francisco, CA, USA). To ensure correct tertiary protein structure prediction, we introduced a disulfide bridge between Cys94 and Cys172. The best model was selected on the basis of Discrete Optimized Protein Energy (DOPE) scores calculated for the models [33,34]. The generated models were analyzed, and the best models for the human GPR18 were used to perform molecular docking studies, based on the DOPE and GA341 score, PROSA II Z score, and Ramachandran plots. We took into account that the X-ray crystal structure of the lysophosphatidic acid receptor LPA6 is missing part of the ECL2, likely due to low resolution and high flexibility of that region. Nevertheless, we decided to include LPA6 as a template for model generation as it might provide valuable information, e.g., regarding the transmembrane domains and the ligand-binding site. Sequences for the cannabinoid receptors CB₁ (P21554) and CB₂ (P34972) were retrieved from UniProt.

2.2. Docking Studies

Prior to docking, the homology model of the human GPR18 was prepared using the Protein Preparation Wizard module implemented in Schrödinger [34,35]. In the first step for protein preparation, we preprocessed the structure using the standard protocol at pH 7.4. Docking was performed using Induced Fit Docking (IFD) and Glide as implemented in Schrödinger release 2016 [35–37]. In the first step of IFD, Glide ligand docking was performed by removing the side chains of the amino acids in the selected binding pocket. In the second phase of docking, Prime was applied to refine the nearby residues and to optimize the side chains. In the final docking phase, the ligand was re-docked into all induced fit protein structures that were within 30 kcal/mol of the lowest energy structure, by using the Glide XP scoring function. A receptor grid center was specified on the basis of preliminary docking studies, resulting in the highest docking scores for the centroid of Lys174 with a cubic grid side length of 10 Å. Preliminary ensemble docking studies provided highest docking scores and consistent SARs explanation for this selection as well as comparison with published cannabinoid receptor X-ray crystal structures [38].

During the docking simulations, the receptor and the ligands were kept flexible. Following docking, the resulting poses of the best model were selected using the IFD scores and Prime Energy as representative values. The conformations of the docked ligands within an energy window of 2.5 kcal/mol were considered. For Glide docking, the following standard parameters were selected: receptor van der Waals scaling, 0.50, ligand van der Waals scaling, 0.50, and a maximum of 20 poses per ligand. Residues within 5.0 Å of the ligand poses were refined, and the side chains were optimized. The best docking pose was selected based on the IFD score and Prime Energy values.

2.3. Compounds

Synthesis of the compounds which are utilized in this computational study as performed in the Department of Technology and Biotechnology of Drugs Jagiellonian University at Kraków, Poland, and potencies of the compounds were determined at the Department of Pharmaceutical & Medicinal Chemistry, Pharmaceutical Institute, University of Bonn, Germany, as previously reported [21,27]. The synthesis and biological evaluation of the new potent GPR18 antagonist 6 will be published elsewhere.

2.4. Molecular Dynamics Simulation

We selected several successful MD simulations as starting points for our runs [39–42]. The GPR18 complexes and the unbound GPR18 structure were prepared using the method described above to determine the protein protonation state at pH 7.4. The obtained structures were processed to the CHARMM-GUI molecular simulation program [43–45]. The forcefield CHARMM36m was applied for all simulation runs. Ligand parameters were obtained separately from Schrödinger. The orientation of the protein in the phosphatidylcholine lipid bilayer (POPC) was determined using the orientation of proteins in membranes (OPM) database [46]. The cubic water box size was adjusted to the structure size of 20 Å and filled with 0.15 M KCl solution. Water molecules were treated with the transferable intermolecular potential with a 3 points (TIP3P) water model [47]. Equilibration steps for all structures were divided into six steps using NAMD2 [48]. For the first three steps, we selected a runtime of 250 ps in 1 fs intervals. For the last three steps, we selected an equilibration runtime of 2 ns in 2 fs intervals. The system was heated from 0 to 303.15 K during equilibration using the NPT ensemble. During production stages, the system was kept at 303.15 K. Temperature was regulated using the Langevin dynamics thermostat. Production runs were performed for 4 × 50 ns with 4 fs intervals (eventually amounting to 200 ns), and frames were collected every 40 ps using ACEMD by Acellera® with the NVT ensemble [49].

3. Results

So far, no X-ray crystal structure of GPR18 has been published. After performing a BLAST search, three crystal structures with highest sequence identity and overall sequence coverage were chosen as templates: the murine μ -opioid receptor (PDB-ID: 5C1M) in complex with an agonist, the human P2Y₁R (PDB-ID: 4XNV) in complex with an allosteric antagonist, and the zebrafish lysophosphatidic acid receptor LPA6 (PDB-ID: 5XSZ) in complex with oleoyl-*R*-glycerol, showing sequence identities of 24.8%, 25.5% and 27.3%, respectively [28–30,50]. Multiple template approaches had been reported to compensate for poor sequence similarity for receptors lacking a template with sequence similarity above 30% [51,52]. Therefore, we decided to include all three templates into the process of homology modeling, although they represent different states of receptor activation. Structures of class A GPCRs belonging to the same δ -branch as GPR18 (P2Y₁, LPA6) and one GPCR that is activated by a lipid like GPR18 (LPA6) were selected. By this approach, we expected to compensate for gaps and mismatching residues which would be present in a single template approach. The multiple sequence alignment is shown in Figure S1 of Supporting Information.

We subsequently investigated the binding modes of imidazothiazinone antagonists and of the agonist THC in the homology model of the human GPR18. To this end, we used the Induced Fit module implemented in Maestro Schrödinger to propose a binding mode for the selected ligands and to rationalize the potency values obtained in biological studies. Imidazothiazinone derivatives 4 and 5 were selected as representative potent antagonist structures. In addition to the imidazothiazinone core, they both possess a 4-chlorophenoxy substituent connected by a linker which differs in length. For the investigated antagonists 4 and 5, IC₅₀ values of 0.650 and 0.279 μ M had been determined [21,27]. In order to investigate whether the proposed antagonist–GPR18 complexes are stable, we performed a 200 ns MD simulation study. Furthermore, we rationalized the SARs of related GPR18 antagonists using a structure-based approach.

3.1. Docking Studies of Antagonists

Recently, several studies on molecular modeling of the human GPR18 have been published [53–57]. However, neither binding mode predictions of THC (or other agonists) nor MD simulations of ≥ 200 ns of antagonist–GPR18 complexes have been published so far. Kuder et al. reported molecular modeling and docking studies, creating a homology model of the human GPR18 based on the crystal structure of the antagonist-bound human P2Y₁ receptor [53]. The imidazothiazinone group of antagonist **5** was predicted to point into a deeper binding pocket towards TM3 where it was hypothesized to form a hydrogen bond with Arg191^{5,42}. The results obtained in the present study indicate a different binding mode which is supported by comprehensive SAR data and based on an ensemble of templates for homology model generation rather than a single, low homology template as in the previous study [53].

The proposed binding mode for antagonist **4** based on the performed docking studies is presented in Figure 2. Antagonist **4** is predicted to bind in the upper third part of the receptor, extending from a hydrophobic cavity formed by ECL2, TM2 and TM3 to an aromatic binding pocket formed by TM6 and TM7, which is a common motif for several GPCRs [58–61]. Compound **4** likely binds with its imidazothiazinone moiety close to the conserved disulfide bridge of Cys94^{3,25} and Cys172^{ECL2}. Both cysteines and Leu97^{3,28} form a lipophilic binding pocket which is predicted to accommodate the thiazine ring. The keto group of the imidazolone ring likely forms an H-bond with Tyr82^{2,64}. Due to the close proximity of Arg78^{2,60}, cation– π interactions with the imidazolone system are feasible. The benzylidene ring may extend towards the center of the receptor, where hydrophobic interactions with Thr272^{7,39} are possible. The hexyloxy linker could bind with several hydrophobic residues (Tyr160^{4,64}, Ile175^{ECL2}, Phe248^{6,51}, Met275^{7,42}) towards an aromatic binding pocket formed by side chains of TM6 and TM7. Additional van der Waals forces for hydrophobic interactions with the benzylidene moiety and the hexyloxy linker may be provided by the alkyl chain of Lys174^{ECL2}. Several aromatic (Phe248^{6,51}, Phe252^{6,55}, Tyr264^{7,31}) and hydrophobic (Cys251^{6,54} and Leu255^{6,58}) residues of TM6 and TM7 are predicted to form the binding pocket accommodating the 4-chlorophenoxy moiety of compound **5** (see Figure 3).

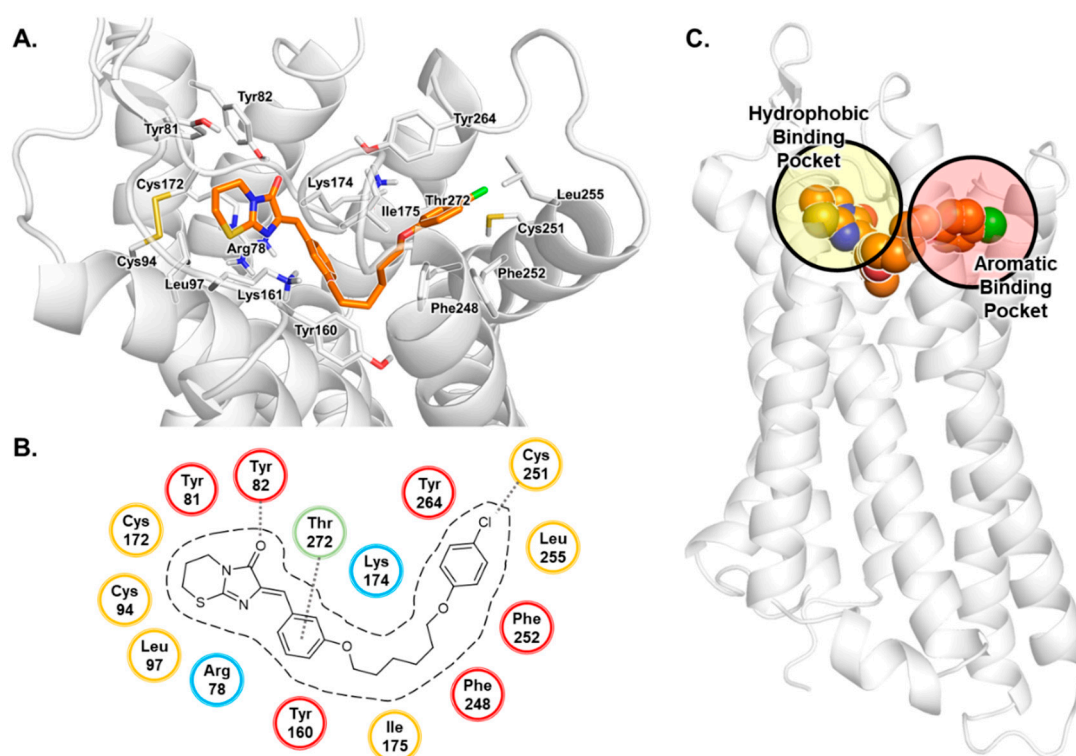


Figure 2. Proposed binding mode of antagonist 4. (A) Docked pose of 4 in complex with the homology model of the human GPR18 shown with the residues forming the binding pocket. The receptor is displayed in cartoon representation, the amino acid residues (white) and compound 4 (orange) are shown as stick models. Oxygen atoms are colored in red, nitrogen atoms in blue, chlorine in green and sulfur atoms in yellow. (B) Schematic 2D representation of the binding pocket. Lipophilic amino acids are colored in yellow, hydrophilic ones in blue, aromatic ones in red, amino acid residues with mixed properties in green. (C) Schematic presentation of the homology model of GPR18 in complex with antagonist 4. The imidazothiazinone moiety is predicted to bind in the hydrophobic binding pocket consisting of residues of TM3 and ECL2. The 4-chlorophenyl moiety binds in the aromatic binding pocket consisting of residues of TM6 and TM7. Cys251^{6,54} in the aromatic binding pocket most likely interacts with hydrophobic substituents in position 4 of the phenoxy (4) or benzyloxy (5) moiety of the antagonists.

The smaller antagonist 5 can occupy the same binding cavity as antagonist 4 (see Figure 3). The imidazothiazinone moiety of both compounds can reach the same binding pose. Due to the missing linker, the benzylidene ring is predicted to exhibit an upward shift towards ECL2 where additional cation– π interactions with Lys161^{ECL2} can be realized. In both cases, the chlorine atoms on the terminal phenyl ring can reach the same binding cavity consisting of aromatic and hydrophobic residues of TM6 and TM7 close to Cys251^{6,54}. Therefore, we expect halogen or methyl substitutions to interact analogously with Cys251^{6,54}. These findings suggest that hydrophobic substituents in position 4 of the terminal phenyl ring of the antagonists are necessary for proper hydrophobic interaction with Cys251^{6,54} resulting in increased potency.

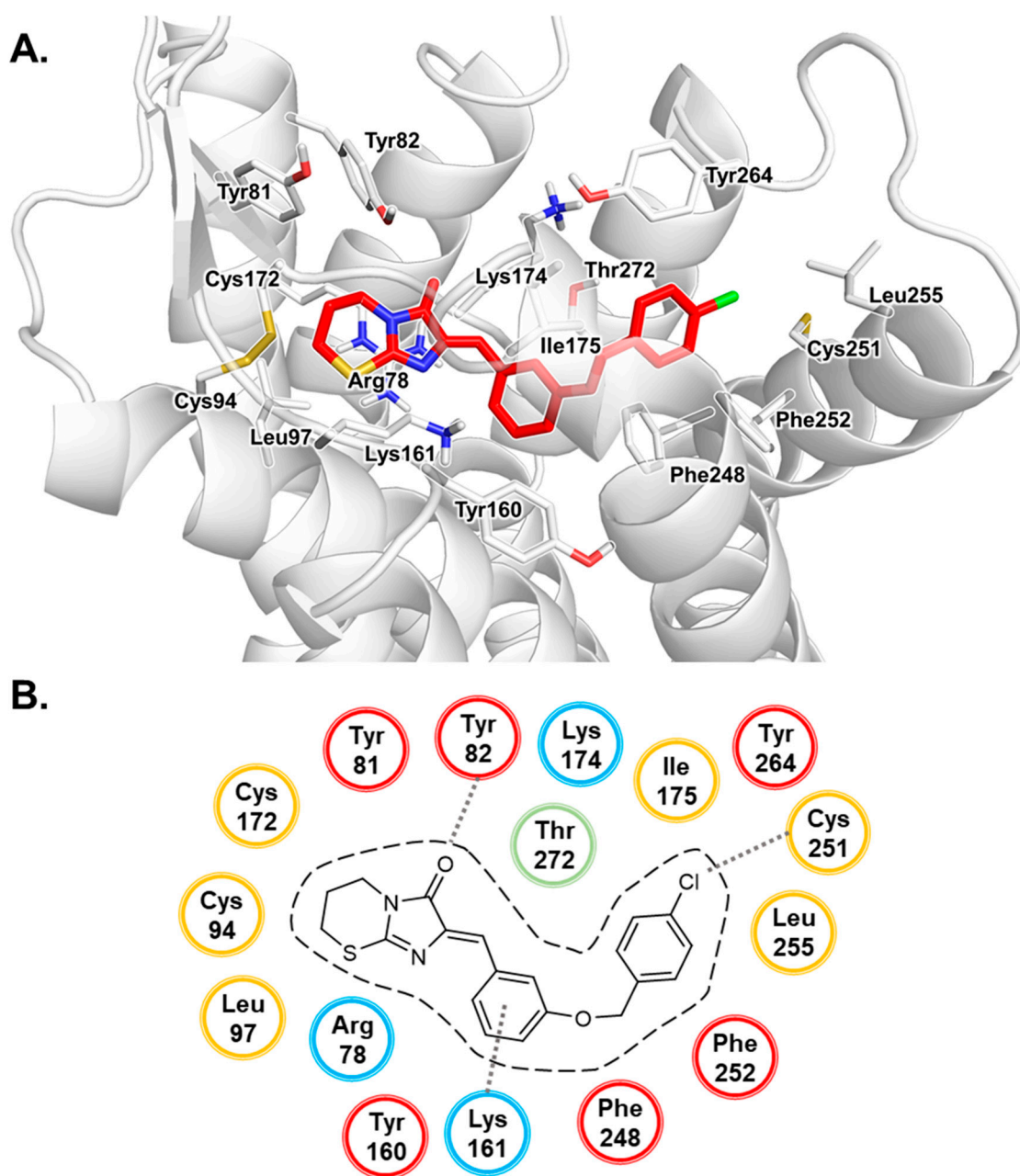


Figure 3. Proposed binding mode of antagonist 5. (A) Docked pose of 5 in complex with the homology model of GPR18 shown with the residues forming the binding pocket. (B) Schematic 2D representation of the binding pocket. For color code, see Figure 2.

3.2. MD Simulation Study of Antagonists

Both antagonist–GPR18 complexes were stable during the 200 ns MD simulation runs, which supports our prediction of the binding pocket based on docking studies. The duration of the MD simulation runs was in accordance with similar studies performed for other GPCRs [62–65]. The behavior of antagonists 4 and 5 in the homology model of GPR18 during the 200 ns MD simulation is presented from a bird’s eye view perspective in Supplementary Information Figures S2 and S3. The 0 ns state refers to the structure of the docked complex after equilibration. The course of the root mean square deviation (RMSD) indicates that the complex of GPR18 with antagonist 5 reached an equilibrated state after approximately 50 ns, and after approximately 100 ns for antagonist 4 (see Figure 4). Compared to the unbound GPR18 structure, the complex of GPR18 with antagonist 5

showed decreased root mean square fluctuation (RMSF) values for TM1, TM2, TM3, TM5 and TM7, and for ECL2 and ECL3, indicating stabilization of these regions upon antagonist binding. Similar results were observed for the complex with the larger antagonist **4**, where decreased RMSF values were observed for TM7, ECL2 and ECL3, and ICL2 and ICL3 when compared to the unbound structure. The concept of stabilization of an inactive conformation of the target GPCR upon antagonist binding was postulated for several receptors and supported by mutagenesis experiments, biophysical studies and MD simulations [58,66–68]. This had also been observed for the P2Y₁ receptor which belongs to the same δ -branch of the class A family of GPCRs. The P2Y₁ receptor can be blocked by structurally distinct antagonists that bind to different binding sites, the nucleotide analog MRS2500 and the urea derivative BPTU—both of which stabilize an ionic lock between an aspartic acid residue of ECL2 and an arginine of TM7 [69]. During MD simulations for 2 μ s, RMSD values had been significantly lower for the complexes with an antagonist as compared to those with the P2Y₁ receptor agonist ADP [69]. A shift in TM3, TM6 and TM7 in the simulation runs with the agonists created a void resulting in receptor activation through a bulk water influx into the binding pocket [69]. Similar observations were reported for several class A family members of GPCRs including μ -opioid receptors and adenosine receptors [70–73].

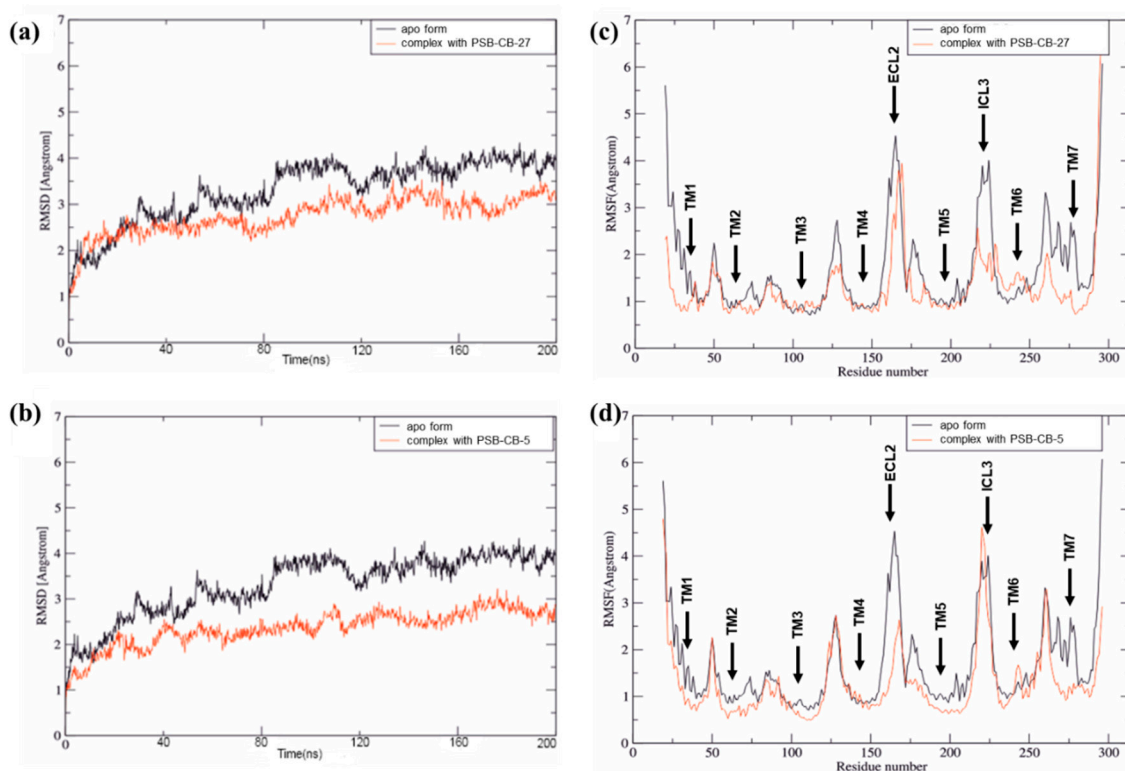


Figure 4. (a,b) Root mean square deviation (RMSD) curves for the 200 ns MD simulation runs of the GPR18 complex with antagonist **4** (a) and antagonist **5** (b). (c,d) Root mean square fluctuation (RMSF) curves of the molecular dynamics (MD) simulation for complexes with antagonist **4** (c) and **5** (d). Curves of the complexes are colored in orange, and the curve of the apo form of the receptor in black.

To further investigate conformational changes in the receptor, RMSD values for each transmembrane-spanning helix were calculated (see Figure 5). Using the OPM database [46] seven transmembrane region segments were determined: TM1 (Ile23^{1.33}–Ser48^{1.58}), TM2 (Ile59^{2.41}–Phe80^{2.62}), TM3 (Glu91^{3.22}–Ala117^{3.53}), TM4 (Val139^{4.43}–Tyr160^{4.64}), TM5 (Ala183^{5.34}–Val209^{5.60}), TM6 (Ile231^{6.34}–Phe254^{6.57}) and TM7 (Trp267^{7.34}–Val289^{7.56}). The RMSD values amounted to 2.8, 1.0, 1.2, 1.2, 1.4, 2.0 and 1.9 Å for TM1–TM7, respectively, when comparing the TM regions of the complex of GPR18 and compound **4** at 0 ns and at 200 ns. For the complex with the larger antagonist **4**, the

RMSD values amounted to 2.2, 2.2, 1.4, 1.9, 2.1, 2.3 and 1.8 Å for TM1–TM7, respectively. The higher RMSD values for antagonist **4** can be explained by the size of the compound when compared to **5**: the larger linker requires adaptation of the receptor, resulting in higher RMSD values. In contrast to the behavior of the antagonist-bound complexes, even higher RMSD values were observed for the unbound apo form of GPR18. Here, RMSD values of 4.6, 1.4, 1.8, 2.4, 1.4, 2.9 and 5.4 Å were calculated for TM1–TM7, respectively. Furthermore, the stabilization of TM1, TM6 and TM7 in the presence of an antagonist supports the theory of stabilization of an inactive state of the receptor upon binding of an antagonist [74–76].

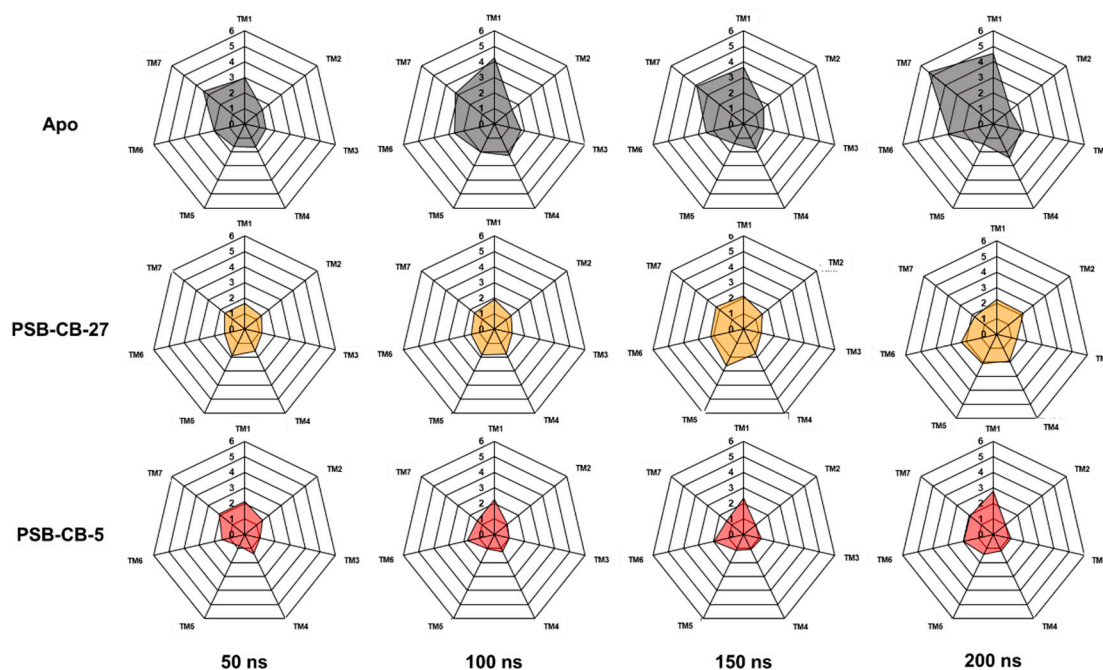


Figure 5. RMSD values for the transmembrane (TM) regions during the 200 ns MD simulation runs. Values were calculated based on the initial complex state after equilibration (0 ns).

Potential salt bridges within the receptor were analyzed to further investigate the mode of inhibition. Arg119^{3.50} of the DRY motif had been proposed to be located in an “arginine cage,” where it forms an ionic lock with Asp118^{3.49}, thus stabilizing the inactive GPR18 [54,77]. Disruption of the ionic lock was postulated to contribute to receptor activation through facilitated movements of TM3 and TM6, resulting in conformational changes towards the intracellular lumen [54]. The authors concluded that stable salt bridges or H-bonds induce a rotamer of Arg119^{3.50}, which is no longer present during receptor activation. The ionic lock between Asp118^{3.49} and Arg119^{3.50} was observed in the apo form of GPR18 during our 200 ns MD simulation run, which is consistent with previous studies [54]. Interestingly, we observed differences in the behavior of Arg119^{3.50} in the apo form as compared to the antagonist-bound complexes: in the apo form, the salt bridge between Arg119^{3.50} and Asp118^{3.49} formed after approximately 75 ns and was stable until the end of the MD simulation, while no similar interaction was observed for the antagonist-bound complexes. Asp118^{3.49} formed a stable salt bridge with Lys133^{ICL2} in the complexes but not in the apo form. This lysine is neither conserved in the three homology model templates nor in the two CB receptor subtypes. Furthermore, we observed stable ionic interactions of Asp85^{ECL1} with Lys22^{N-terminus} and of Asp162^{ECL2} with Lys161^{ECL2} in the antagonist-bound structures, which were not present in the apo form. Interaction of Glu131^{ICL2} with Lys137^{4.41} was observed in all three structures. The salt bridge between Glu228^{6.31} and Arg232^{6.35} was stable in the receptor apo form, which was not the case for the antagonist-bound structures. The trajectory for the salt bridge distances is presented in Supplementary Information (Figure S4).

We conclude that the binding of an antagonist stabilizes several salt bridges within GPR18, resulting in the stabilization of an inactive conformation of the receptor.

We additionally investigated the binding mode of a new potent antagonist, an analog of **4** and **5**, which has a more rigid substituent in position 4 of the phenyl group (a biphenyl derivative). Compound PSB-CB-148 (**6**) contains a *p*-cyano-biphenyl group which is larger and at the same time less flexible than the corresponding substituents in antagonists **4** and **5**. The imidazothiazinone group is predicted to bind in the same binding cavity as for compounds **4** and **5** (see Figure 6). The trajectory of the linker in the docked structure closely resembles the binding mode of compound **4**. Furthermore, the proximity of Arg191^{5,42} to both oxygen atoms in the linker indicates bidental H-bond interactions. The biphenyl moiety likely binds in a lipophilic binding cavity, where π - π interactions between the phenyl groups and the aromatic residues Phe248^{6,51}, Phe252^{6,55} and Tyr264^{7,31} are feasible. Interactions of the terminal phenyl group with Cys251^{6,54} are not observed for **6**. Due to its decreased flexibility, the terminal group does not allow this interaction. The shift in the phenyl group is predicted to place the cyano moiety in close proximity to Asn185^{5,39}. Upon inspection of Asn185^{5,39}, several rotamers were found which could form H-bonds with the nitrile (see Figure S5 in Supplementary Information).

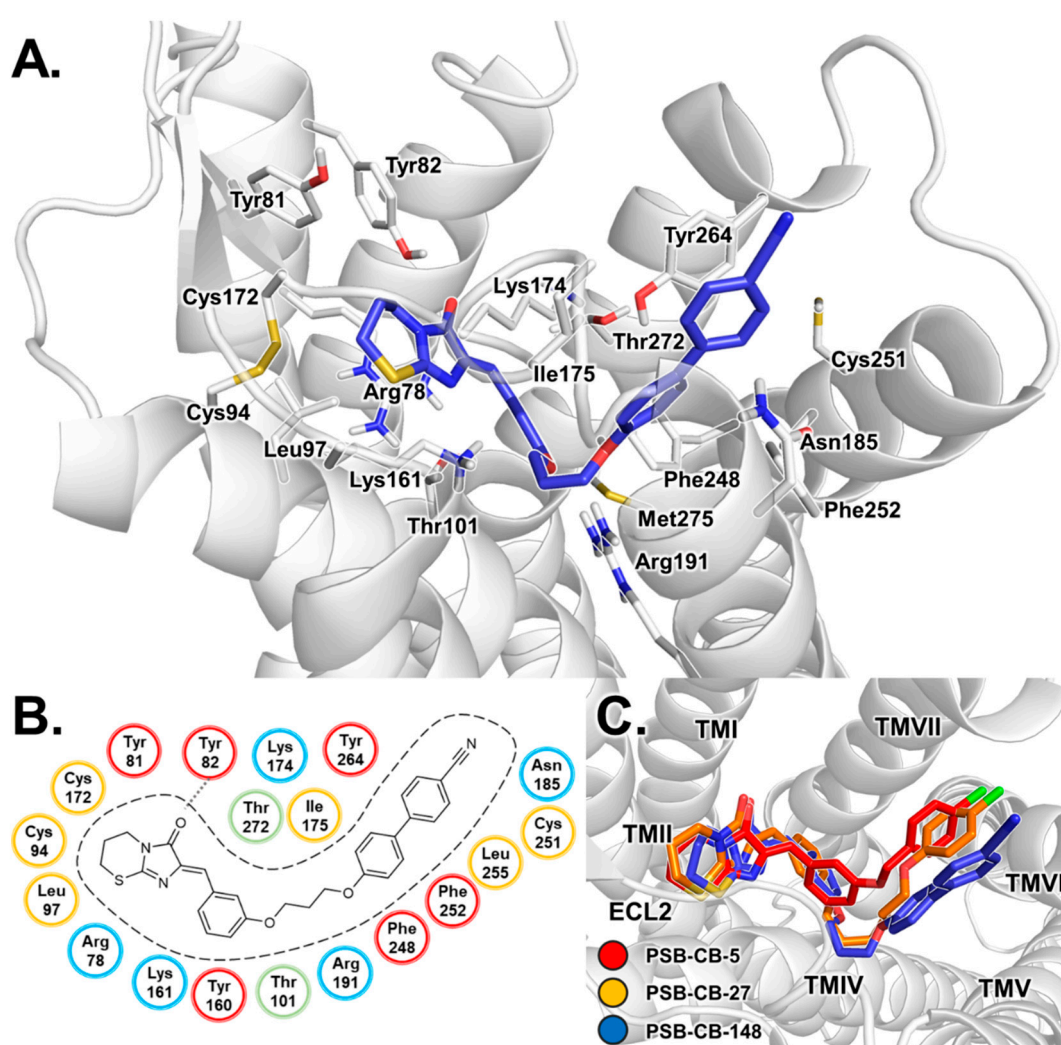


Figure 6. Proposed binding mode of antagonist **6**. (A) Docked pose of **6** in complex with the homology model of human GPR18 shown with the residues forming the binding pocket. (B) Schematic 2D representation of the binding pocket. For color code, see Figure 2. (C) Overlay of the proposed binding modes of GPR18 antagonists. Antagonist **4** is colored in orange, antagonist **5** in red, antagonist **6** in blue.

The obtained data of the docking studies were used to re-analyze the SARs of previously published antagonists [21]. The summarized results are presented in Figure 7 (for structures, see Figures S6 and S7 in Supporting Information). The linker size was found to have an impact on the potency of the tested antagonists. The antagonist containing a hexyloxy linker (**4**) showed an almost 10-fold increase in potency compared to the analog with the shorter ethyloxy linker (**7**) (IC_{50} of 0.650 μ M versus 5.00 μ M). Prolongation of the ethyloxy linker resulted in increased inhibitory potency, with hexyloxy being optimal (IC_{50} = 0.650 μ M), while larger linkers, i.e., heptyloxy (**11**) and octyloxy (**12**), led to slightly less potent antagonists (IC_{50} = 1.71 and 1.15 μ M). Our docking results suggest that the hexyloxy linker is required for the 4-chlorophenoxy moiety to reach the aromatic binding pocket and to form hydrophobic interactions with Cys251^{6,54}. The shorter alkyloxy linker is less well stabilized in the hydrophobic cavity formed by Tyr160^{4,64}, Ile175^{ECL2}, Phe248^{6,51} and Met275^{7,42}. The decrease in potency observed for compounds **11** and **12** despite their higher lipophilicity could be explained by limited space in the binding cavity or unfavorable adaptation of the alkyloxy linker, resulting in a shifted binding position for the 4-chlorophenoxy moiety which prohibits optimal interaction with Cys251^{6,54}. Among the smaller compounds missing an additional linker between the benzylidene and the substituted phenoxy ring, the most potent antagonists contained a hydrophobic substituent in position 4 of the phenyl ring (compounds **5**, **14–16**). Hydrophobic interactions of substituents in position 4 of the phenoxy residue with Cys251^{6,54} are supported by acceptance of both chlorine and methyl groups in compounds **4** and **13**, resulting in comparable IC_{50} values (0.650 and 0.238 μ M). The potency (IC_{50} values) of the compounds decreased in the following rank order Cl (0.279 μ M) > Br (1.73 μ M) \geq CH₃ (3.59 μ M) > F (> 10 μ M), indicating that the size and lipophilicity of the substituent plays a major role. Decreased potency observed for antagonists containing larger substituents in position 4 such as ethyl (**17**) or isopropyl (**18**) can be explained by the limited space of the binding pocket in proximity to Cys251^{6,54}. Moreover, the substitution position on the phenyl ring proved to have an effect on the potency of the compounds. Antagonist **19** (*o,o*-dimethyl-substituted), for example, was inactive (IC_{50} > 10 μ M). Antagonists containing different heterocycles in place of the imidazothiazinone moiety (**20–34**) showed lower potency as compared to antagonist **5**. In our homology model, two aromatic residues close to the hydrophobic binding pocket, Tyr81^{2,63} and Trp87^{ECL1}, may form π - π interactions with antagonists containing an additional aromatic group attached to the heterocycle (see Figure S8 in Supporting Information). The ethylthio linker connecting the imidazolone ring with the phenyl ring in compound **32** might be beneficial to enable proper binding for π - π interactions. The results suggest that the imidazothiazinone heterocycle is optimal to allow hydrophobic packing in the binding pocket close to the disulfide bridge of ECL2.

In conclusion, the docking studies, MD simulations and SARs of imidazothiazinones as well as antagonists containing smaller heterocycles further support our suggested binding mode of an aromatic and lipophilic binding pocket of the human GPR18 for antagonists. The most potent antagonists of this series likely interact with Cys251^{6,54} through lipophilic interactions, and this additional interaction is predicted to be the reason for their high potency.

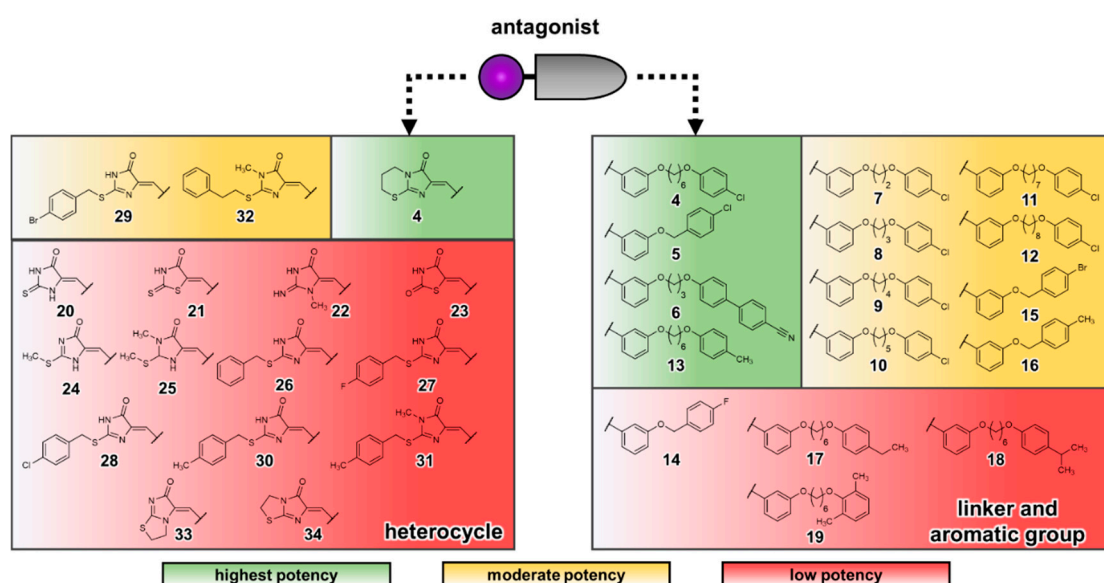


Figure 7. Schematic representation of the structure–activity relationships (SARs) of GPR18 antagonists. The different heterocycles shown contain a 4-chlorophenoxy group, while the compounds with varying aryl substituents and linker lengths contain the imidazothiazinone heterocycle. Compounds were categorized into three groups: highest potency ($IC_{50} < 1 \mu M$), moderate potency ($1 \mu M < IC_{50} < 10 \mu M$) and low potency ($IC_{50} > 10 \mu M$) based on their antagonistic activity.

3.3. Binding Mode of THC

As a next step, we explored the most likely binding pocket for the GPR18 agonist THC (1). The ability of the potent CB receptor agonist THC to activate GPR18 with moderate potency had led to the suggestion to classify GPR18 as a novel CB receptor subtype [19]. Lipophilicity is a feature shared by GPR18 agonists and antagonists [78,79]. THC is regarded as a promiscuous ligand acting not only at cannabinoid but also at several non-cannabinoid receptors [80–85]. Studies on the binding mode of cannabinoids at the cannabinoid receptors CB₁ and CB₂ proposed a binding portal between TM6 and TM7 from the lipid-facing side of the receptor for the entrance of agonists [86–88]. Such entry is unique among GPCRs, as ligands typically reach the binding pocket between TM3 and TM7 from the extracellular lumen.

To date, two crystal structures of the CB₁ receptor bound to THC-related compounds are available (PDB-ID: 5XR8, 5XRA) [38]. As observed for many other GPCRs, the agonist binding site, which is very lipophilic in the case of the CB₁ receptor, is located between a highly conserved Trp^{6.48} and ECL2 [89,90]. The tricyclic THC ring system is stabilized through lipophilic as well as π – π interactions with an aromatic cluster (Phe170^{2.57}, Phe174^{2.61}, Phe177^{2.64}, Phe189^{3.25}, Phe268^{ECL2}, Phe379^{7.35}). Several previous mutagenesis studies have confirmed the key role of the aromatic residues for the binding of cannabinoids [38,91–93]. The alkyl chain of the agonists extends towards a binding cleft formed by several lipophilic residues (Leu193^{3.29}, Val196^{3.32}, Tyr275^{5.39}, Leu276^{5.40}, Leu359^{6.51} and Met363^{6.55}).

Given the low sequence similarity between the cannabinoid receptors CB₁, CB₂, and GPR18 (18.7 and 23.7%, respectively), similar binding of the THC ring system in GPR18 cannot be taken for granted. Amino acid residues Val196^{3.32}, Phe268^{ECL2}, Tyr275^{5.39}, Met363^{6.55} and Phe379^{7.35} are conserved in both CB receptor subtypes but replaced in GPR18 by leucine, serine, arginine, phenylalanine and glycine, respectively (see Figure S9 in Supplementary Information for multiple sequence alignment). Phe174^{2.61} and Leu193^{3.29}, but not Leu359^{6.51}, are conserved among all three receptors. The absence of the aromatic network responsible for the binding of the THC ring system in the CB receptors suggests a different binding mode for the agonist THC at GPR18.

Docking studies of THC were performed using the generated homology model of the human GPR18. We observed that THC appears to bind closer to TM4 and TM5 as compared to the cannabinoids

in the X-ray crystal structures of the CB₁ receptor (see Figure 8). The phenyl group of the tricyclic THC ring system is predicted to bind in a cleft formed by several lipophilic (Val102^{3,33}, Ile175^{ECL2}, Phe248^{6,51}, Phe252^{6,55}) and hydrophilic (Lys161^{ECL2}, Lys174^{ECL2}, Asn188^{5,39}, Arg191^{5,42}, His249^{6,52}) amino acid residues. H-bond interactions are feasible for the oxygen atoms of the chromene moiety and Lys161^{ECL2}, as well as the hydroxy group and Asn188^{5,39} and Arg191^{5,42}. The cyclohexenyl moiety is likely accommodated in a lipophilic binding pocket formed by Thr152^{4,56}, Pro155^{4,59}, Leu156^{4,60}, Val184^{5,35} and the alkyl side chain of Arg191^{5,42}. The alkyl group of the agonist likely projects towards TM7, where it can be stabilized through lipophilic interactions with Phe248^{6,51}, Phe252^{6,55} and Met275^{7,42}. The binding modes of THC in the CB₁ receptor as compared to GPR18 are shown in Figure S10 of Supporting Information.

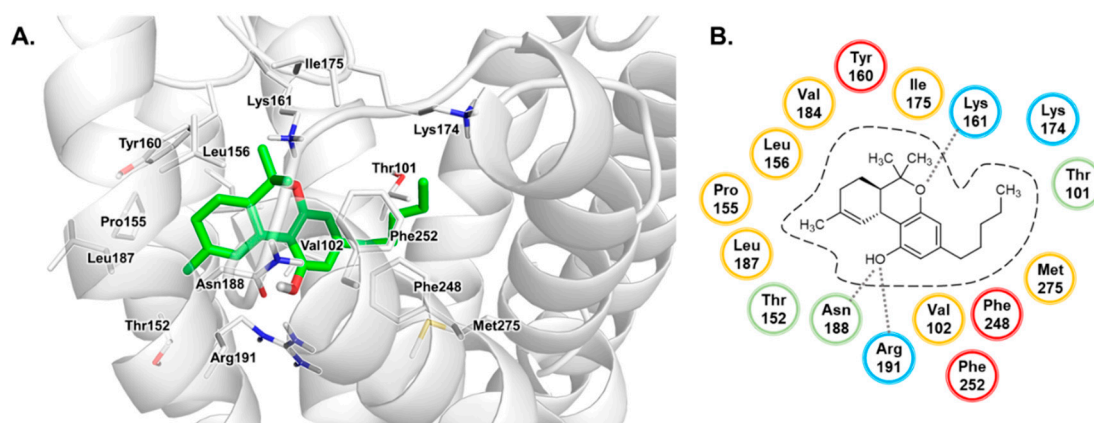


Figure 8. Proposed binding mode of Δ^9 -tetrahydrocannabinol (THC) in the homology model of human GPR18. (A) The receptor is displayed in cartoon representation, the amino acid residues (white) and THC (1, green) are shown as stick models. Oxygen atoms are colored in red, nitrogen atoms in blue, sulfur atoms in yellow. (B) Schematic 2D representation of the binding pocket. For color code, see Figure 2.

We propose that the tricyclic THC ring system binds in a binding cavity of GPR18 distant to the orthosteric binding site of the CB₁ receptor. The absence of aromatic residues in ECL2 of GPR18 may contribute to the proposed shifted binding mode of THC, as π - π stacking with a phenylalanine in position 2.57 is not possible. However, the binding cleft for the alkyl chain is predicted to be overlapping in both receptors. It should be pointed out that THC displays much higher potency at CB₁ (and CB₂) receptors as compared to GPR18.

Our results suggest that THC shares a common binding pocket with the imidazothiazinone antagonists (see Figure 9). While the imidazothiazinone moiety of the antagonists is predicted to bind in a lipophilic pocket formed by amino acid residues of TM2 and TM7, the benzylidene group is suggested to project towards the putative binding site of the chromene and alkyl group of THC. This is supported by experimental data showing that imidazothiazinone antagonists containing lipophilic residues act as competitive antagonists versus THC [21].

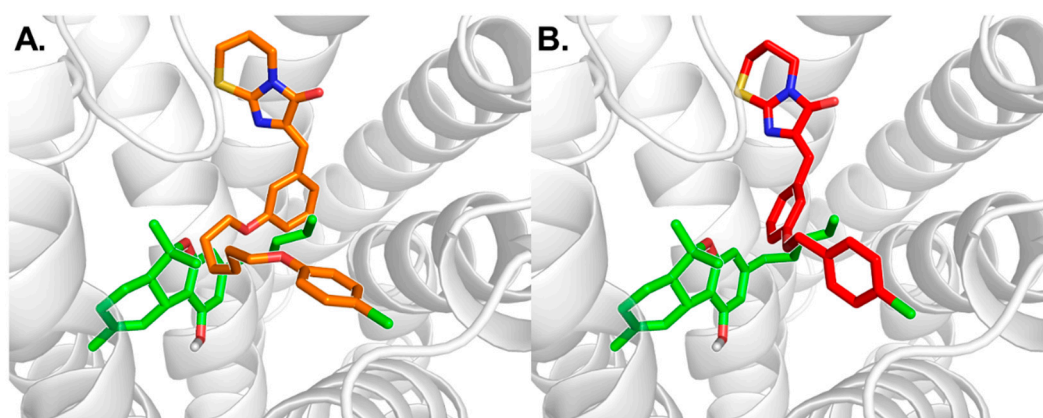


Figure 9. (A) Comparison of the proposed binding mode of THC (green) and antagonist 4 (orange) at human GPR18. (B) Comparison of the proposed binding modes of THC and antagonist 5 (red).

4. Conclusions

Since only approximately 10% of the non-olfactory GPCRs are covered by structural studies, meaningful prediction of ligand-binding modes represents one of the greatest challenges in molecular modeling [94]. In particular, homology modeling assessment of receptors with no resolved closely related crystal structures requires further experimental validation. In the present study, we generated a homology model of the orphan GPR18 and predicted the binding modes of the confirmed agonist THC as well as the most potent class of antagonists containing an imidazothiazinone scaffold. Despite the lack of closely related X-ray crystal structures, we successfully performed docking and MD simulation studies of antagonist complexes which were in agreement with the extensive published SAR data. The investigated potent antagonists are predicted to share the same binding site for the imidazothiazinone core. The linker of the antagonists is likely accommodated in a lipophilic binding cleft shared by the alkyl chain of the agonist THC. The 200 ns MD simulation runs suggested stabilization of a receptor conformation by antagonists which was not observed for the unbound receptor structure. Stabilization of a salt bridge between Asp118^{3.49} and Lys133^{ICL2} through imidothiazinone-based antagonists may play a role in the inhibition mechanism. Our docking studies suggest a different binding mode of the agonist THC in GPR18 as compared to that observed in cannabinoid receptors. However, future structural studies will be required to confirm the proposed interactions. The presented data provide a well-founded hypothesis that will support the rational design of new ligands for this poorly investigated receptor which has potential as a future drug target.

Supplementary Materials: The following are available online at <http://www.mdpi.com/2218-273X/10/5/686/s1>, Figure S1: Multiple sequence alignment of GPR18 for homology modeling, Figure S2: Time scale of the molecular dynamics simulation of antagonist 4, Figure S3: Time scale of the molecular dynamics simulation of antagonist 5, Figure S4: Trajectories of salt bridges, Figure S5: Possible interaction of antagonist 6 with Asn185, Figure S6: Structures of GPR18 imidazothiazinone antagonists, Figure S7: Structures of GPR18 antagonists with modification of the core structure, Figure S8: Comparison of the binding modes of antagonists 5 and 32, Figure S9: Multiple sequence alignment of human GPR18 and the cannabinoid receptors CB1 and CB2, Figure S10: Comparison of the binding mode of THC to GPR18 with the binding of THC derivatives to the CB1 receptor, Figure S11: Multiple Sequence alignment of top 10 scoring BLAST sequences, Figure S12: Residues considered to be important for the binding of antagonists, Table S1: Results for 10 scoring BLAST sequences for GPR18.

Author Contributions: Conceptualization, A.N. and C.E.M.; methodology, A.N., V.E., A.B.M., C.T.S., V.N. and K.K.-K.; first draft preparation, A.N.; writing of manuscript, A.N. and C.E.M. with contributions of all co-authors; review and editing, all co-authors; supervision, C.E.M. and V.N.; project administration and funding acquisition, C.E.M. All authors have read and agreed to the published version of the manuscript.

Funding: A.N., A.B.M., C.T.S., and C.E.M. were funded by the Deutsche Forschungsgemeinschaft (DFG, German Research Foundation) - 214362475 / GRK1873/2 and the BMBF-funded Bonn International Graduate School Drug Sciences (BIGS DrugS). C.T.S. received a BAYER PhD fellowship through BIGS DrugS. A.B.M. was funded by the Ministry of Finance of Indonesia in the scheme of Indonesia Endowment Fund for Education (Lembaga Pengelola Dana Pendidikan (LPDP)).

Conflicts of Interest: The authors declare no conflict of interest.

References

1. Hilger, D.; Masureel, M.; Kobilka, B.K. Structure and dynamics of GPCR signaling complexes. *Nat. Struct. Mol. Biol.* **2018**, *25*, 4–12. [[CrossRef](#)] [[PubMed](#)]
2. Kobilka, B.K. G protein coupled receptor structure and activation. *Biochim. Biophys. Acta* **2007**, *1768*, 794–807. [[CrossRef](#)] [[PubMed](#)]
3. Tang, X.-L.; Wang, Y.; Li, D.-L.; Luo, J.; Liu, M.-Y. Orphan G protein-coupled receptors (GPCRs): Biological functions and potential drug targets. *Acta Pharmacol. Sin.* **2012**, *33*, 363–371. [[CrossRef](#)] [[PubMed](#)]
4. Gantz, I.; Muraoka, A.; Yang, Y.K.; Samuelson, L.C.; Zimmerman, E.M.; Cook, H.; Yamada, T. Cloning and chromosomal localization of a gene (GPR18) encoding a novel seven transmembrane receptor highly expressed in spleen and testis. *Genomics* **1997**, *42*, 462–466. [[CrossRef](#)] [[PubMed](#)]
5. Sumida, H.; Cyster, J.G. G-Protein Coupled Receptor 18 Contributes to Establishment of the CD8 Effector T Cell Compartment. *Front. Immunol.* **2018**, *9*, 660. [[CrossRef](#)] [[PubMed](#)]
6. Wang, X.; Sumida, H.; Cyster, J.G. GPR18 is required for a normal CD8 $\alpha\alpha$ intestinal intraepithelial lymphocyte compartment. *J. Exp. Med.* **2014**, *211*, 2351–2359. [[CrossRef](#)]
7. Becker, A.M.; Callahan, D.J.; Richner, J.M.; Choi, J.; DiPersio, J.F.; Diamond, M.S.; Bhattacharya, D. GPR18 controls reconstitution of mouse small intestine intraepithelial lymphocytes following bone marrow transplantation. *PLoS ONE* **2015**, *10*, e0133854. [[CrossRef](#)]
8. Pridgeon, J.W.; Klesius, P.H. G-protein coupled receptor 18 (GPR18) in channel catfish: Expression analysis and efficacy as immunostimulant against *Aeromonas hydrophila* infection. *Fish Shellfish Immunol.* **2013**, *35*, 1070–1078. [[CrossRef](#)]
9. Morales, P.; Reggio, P.H. An update on non-CB1, non-CB2 cannabinoid related G-protein-coupled receptors. *Cannabis Cannabinoid Res.* **2017**, *2*, 265–273. [[CrossRef](#)]
10. Reyes-Resina, I.; Navarro, G.; Aguinaga, D.; Canela, E.I.; Schoeder, C.T.; Załuski, M.; Kieć-Kononowicz, K.; Saura, C.A.; Müller, C.E.; Franco, R. Molecular and functional interaction between GPR18 and cannabinoid CB2 G-protein-coupled receptors. Relevance in neurodegenerative diseases. *Biochem. Pharmacol.* **2018**, *157*, 169–179. [[CrossRef](#)]
11. McHugh, D. GPR18 in microglia: Implications for the CNS and endocannabinoid system signalling. *Br. J. Pharmacol.* **2012**, *167*, 1575–1582. [[CrossRef](#)]
12. Walter, L.; Franklin, A.; Witting, A.; Wade, C.; Xie, Y.; Kunos, G.; Mackie, K.; Stella, N. Nonpsychotropic cannabinoid receptors regulate microglial cell migration. *J. Neurosci.* **2003**, *23*, 1398–1405. [[CrossRef](#)]
13. Haugh, O.; Penman, J.; Irving, A.J.; Campbell, V.A. The emerging role of the cannabinoid receptor family in peripheral and neuro-immune interactions. *Curr. Drug Targets* **2016**, *17*, 1834–1840. [[CrossRef](#)]
14. Miller, S.; Leishman, E.; Oehler, O.; Daily, L.; Murataeva, N.; Wager-Miller, J.; Bradshaw, H.; Straiker, A. Evidence for a GPR18 role in diurnal regulation of intraocular pressure. *Investig. Ophthalmol. Vis. Sci.* **2016**, *57*, 6419–6426. [[CrossRef](#)]
15. Caldwell, M.D.; Hu, S.S.-J.; Viswanathan, S.; Bradshaw, H.; Kelly, M.E.M.; Straiker, A. A GPR18-based signalling system regulates IOP in murine eye. *Br. J. Pharmacol.* **2013**, *169*, 834–843. [[CrossRef](#)]
16. Haskó, J.; Fazakas, C.; Molnár, J.; Nyúl-Tóth, Á.; Herman, H.; Hermenean, A.; Wilhelm, I.; Persidsky, Y.; Krizbai, I.A. CB2 receptor activation inhibits melanoma cell transmigration through the blood-brain barrier. *Int. J. Mol. Sci.* **2014**, *15*, 8063–8074. [[CrossRef](#)]
17. Qin, Y.; Verdegaal, E.M.E.; Siderius, M.; Bebelman, J.P.; Smit, M.J.; Leurs, R.; Willemze, R.; Tensen, C.P.; Osanto, S. Quantitative expression profiling of G-protein-coupled receptors (GPCRs) in metastatic melanoma: The constitutively active orphan GPCR GPR18 as novel drug target. *Pigment Cell Melanoma Res.* **2011**, *24*, 207–218. [[CrossRef](#)]
18. Noreen, N.; Muhammad, F.; Akhtar, B.; Azam, F.; Anwar, M.I. Is cannabidiol a promising substance for new drug development? A review of its potential therapeutic applications. *Crit. Rev. Eukaryot. Gene Expr.* **2018**, *28*, 73–86. [[CrossRef](#)]
19. Console-Bram, L.; Brailoiu, E.; Brailoiu, G.C.; Sharir, H.; Abood, M.E. Activation of GPR18 by cannabinoid compounds: A tale of biased agonism. *Br. J. Pharmacol.* **2014**, *171*, 3908–3917. [[CrossRef](#)]

20. Pertwee, R.G.; Howlett, A.C.; Abood, M.E.; Alexander, S.P.H.; Di Marzo, V.; Elphick, M.R.; Greasley, P.J.; Hansen, H.S.; Kunos, G.; Mackie, K.; et al. International Union of Basic and Clinical Pharmacology. LXXIX. Cannabinoid receptors and their ligands: Beyond CB1 and CB2. *Pharmacol. Rev.* **2010**, *62*, 588–631. [[CrossRef](#)]
21. Schoeder, C.T.; Kaleta, M.; Mahardhika, A.B.; Olejarz-Maciej, A.; Łażewska, D.; Kieć-Kononowicz, K.; Müller, C.E. Structure-activity relationships of imidazothiazinones and analogs as antagonists of the cannabinoid-activated orphan G protein-coupled receptor GPR18. *Eur. J. Med. Chem.* **2018**, *155*, 381–397. [[CrossRef](#)] [[PubMed](#)]
22. Schoeder, C.T.; Hess, C.; Madea, B.; Meiler, J.; Müller, C.E. Pharmacological evaluation of new constituents of “Spice”: Synthetic cannabinoids based on indole, indazole, benzimidazole and carbazole scaffolds. *Forensic Toxicol.* **2018**, *36*, 385–403. [[CrossRef](#)] [[PubMed](#)]
23. Kohno, M.; Hasegawa, H.; Inoue, A.; Muraoka, M.; Miyazaki, T.; Oka, K.; Yasukawa, M. Identification of N-arachidonylglycine as the endogenous ligand for orphan G-protein-coupled receptor GPR18. *Biochem. Biophys. Res. Commun.* **2006**, *347*, 827–832. [[CrossRef](#)]
24. Chiang, N.; Dalli, J.; Colas, R.A.; Serhan, C.N. Identification of resolvin D2 receptor mediating resolution of infections and organ protection. *J. Exp. Med.* **2015**, *212*, 1203–1217. [[CrossRef](#)]
25. Yin, H.; Chu, A.; Li, W.; Wang, B.; Shelton, F.; Otero, F.; Nguyen, D.G.; Caldwell, J.S.; Chen, Y.A. Lipid G protein-coupled receptor ligand identification using beta-arrestin PathHunter assay. *J. Biol. Chem.* **2009**, *284*, 12328–12338. [[CrossRef](#)]
26. van Lu, B.; Puhl, H.L.; Ikeda, S.R. N-Arachidonyl glycine does not activate G protein-coupled receptor 18 signaling via canonical pathways. *Mol. Pharmacol.* **2013**, *83*, 267–282.
27. Rempel, V.; Atzler, K.; Behrenswerth, A.; Karcz, T.; Schoeder, C.; Hinz, S.; Kaleta, M.; Thimm, D.; Kieć-Kononowicz, K.; Müller, C.E. Bicyclic imidazole-4-one derivatives: A new class of antagonists for the orphan G protein-coupled receptors GPR18 and GPR55. *Med. Chem. Commun.* **2014**, *5*, 632–649. [[CrossRef](#)]
28. Huang, W.; Manglik, A.; Venkatakrisnan, A.J.; Laeremans, T.; Feinberg, E.N.; Sanborn, A.L.; Kato, H.E.; Livingston, K.E.; Thorsen, T.S.; Kling, R.C.; et al. Structural insights into μ -opioid receptor activation. *Nature* **2015**, *524*, 315–321. [[CrossRef](#)]
29. Taniguchi, R.; Inoue, A.; Sayama, M.; Uwamizu, A.; Yamashita, K.; Hirata, K.; Yoshida, M.; Tanaka, Y.; Kato, H.E.; Nakada-Nakura, Y.; et al. Structural insights into ligand recognition by the lysophosphatidic acid receptor LPA6. *Nature* **2017**, *548*, 356–360. [[CrossRef](#)]
30. Zhang, D.; Gao, Z.-G.; Zhang, K.; Kiselev, E.; Crane, S.; Wang, J.; Paoletta, S.; Yi, C.; Ma, L.; Zhang, W.; et al. Two disparate ligand-binding sites in the human P2Y1 receptor. *Nature* **2015**, *520*, 317–321. [[CrossRef](#)]
31. UniProt Consortium. UniProt: A hub for protein information. *Nucleic Acids Res.* **2015**, *43*, D204–D212. [[CrossRef](#)] [[PubMed](#)]
32. Sievers, F.; Wilm, A.; Dineen, D.; Gibson, T.J.; Karplus, K.; Li, W.; Lopez, R.; McWilliam, H.; Remmert, M.; Söding, J.; et al. Fast, scalable generation of high-quality protein multiple sequence alignments using Clustal Omega. *Mol. Syst. Biol.* **2011**, *7*, 539. [[CrossRef](#)] [[PubMed](#)]
33. Sali, A.; Blundell, T.L. Comparative protein modelling by satisfaction of spatial restraints. *J. Mol. Biol.* **1993**, *234*, 779–815. [[CrossRef](#)]
34. Webb, B.; Sali, A. Protein structure modeling with MODELLER. *Methods Mol. Biol.* **2014**, *1137*, 1–15.
35. Friesner, R.A.; Banks, J.L.; Murphy, R.B.; Halgren, T.A.; Klicic, J.J.; Mainz, D.T.; Repasky, M.P.; Knoll, E.H.; Shelley, M.; Perry, J.K.; et al. Glide: A new approach for rapid, accurate docking and scoring. 1. Method and assessment of docking accuracy. *J. Med. Chem.* **2004**, *47*, 1739–1749. [[CrossRef](#)]
36. Halgren, T.A.; Murphy, R.B.; Friesner, R.A.; Beard, H.S.; Frye, L.L.; Pollard, W.T.; Banks, J.L. Glide: A new approach for rapid, accurate docking and scoring. 2. Enrichment factors in database screening. *J. Med. Chem.* **2004**, *47*, 1750–1759. [[CrossRef](#)]
37. Sherman, W.; Day, T.; Jacobson, M.P.; Friesner, R.A.; Farid, R. Novel procedure for modeling ligand/receptor induced fit effects. *J. Med. Chem.* **2006**, *49*, 534–553. [[CrossRef](#)]
38. Hua, T.; Vemuri, K.; Nikas, S.P.; Laprairie, R.B.; Wu, Y.; Qu, L.; Pu, M.; Korde, A.; Jiang, S.; Ho, J.-H.; et al. Crystal structures of agonist-bound human cannabinoid receptor CB1. *Nature* **2017**, *547*, 468–471. [[CrossRef](#)]
39. Abdelrahman, A.; Yerande, S.G.; Namasivayam, V.; Klapschinski, T.A.; Alnouri, M.W.; El-Tayeb, A.; Müller, C.E. Substituted 4-phenylthiazoles: Development of potent and selective A1, A3 and dual A1/A3 adenosine receptor antagonists. *Eur. J. Med. Chem.* **2020**, *186*, 111879. [[CrossRef](#)]

40. Ciancetta, A.; O'Connor, R.D.; Paoletta, S.; Jacobson, K.A. Demystifying P2Y1 Receptor Ligand Recognition through Docking and Molecular Dynamics Analyses. *J. Chem. Inf. Model.* **2017**, *57*, 3104–3123. [[CrossRef](#)]
41. Liang, Y.-L.; Belousoff, M.J.; Fletcher, M.M.; Zhang, X.; Khoshouei, M.; Deganutti, G.; Koole, C.; Furness, S.G.B.; Miller, L.J.; Hay, D.L.; et al. Structure and Dynamics of Adrenomedullin Receptors AM1 and AM2 Reveal Key Mechanisms in the Control of Receptor Phenotype by Receptor Activity-Modifying Proteins. *ACS Pharmacol. Transl. Sci.* **2020**, *3*, 263–284. [[CrossRef](#)]
42. Tosh, D.K.; Rao, H.; Bitant, A.; Salmaso, V.; Mannes, P.; Lieberman, D.I.; Vaughan, K.L.; Mattison, J.A.; Rothwell, A.C.; Auchampach, J.A.; et al. Design and in Vivo Characterization of A1 Adenosine Receptor Agonists in the Native Ribose and Conformationally Constrained (N)-Methanocarba Series. *J. Med. Chem.* **2019**, *62*, 1502–1522. [[CrossRef](#)] [[PubMed](#)]
43. Brooks, B.R.; Brooks, C.L.; Mackerell, A.D.; Nilsson, L.; Petrella, R.J.; Roux, B.; Won, Y.; Archontis, G.; Bartels, C.; Boresch, S.; et al. CHARMM: The biomolecular simulation program. *J. Comput. Chem.* **2009**, *30*, 1545–1614. [[CrossRef](#)] [[PubMed](#)]
44. Jo, S.; Kim, T.; Iyer, V.G.; Im, W. CHARMM-GUI: A web-based graphical user interface for CHARMM. *J. Comput. Chem.* **2008**, *29*, 1859–1865. [[CrossRef](#)] [[PubMed](#)]
45. Lee, J.; Cheng, X.; Swails, J.M.; Yeom, M.S.; Eastman, P.K.; Lemkul, J.A.; Wei, S.; Buckner, J.; Jeong, J.C.; Qi, Y.; et al. CHARMM-GUI Input Generator for NAMD, GROMACS, AMBER, OpenMM, and CHARMM/OpenMM Simulations Using the CHARMM36 Additive Force Field. *J. Chem. Theory Comput.* **2016**, *12*, 405–413. [[CrossRef](#)] [[PubMed](#)]
46. Lomize, M.A.; Pogozheva, I.D.; Joo, H.; Mosberg, H.I.; Lomize, A.L. OPM database and PPM web server: Resources for positioning of proteins in membranes. *Nucleic Acids Res.* **2012**, *40*, D370–D376. [[CrossRef](#)] [[PubMed](#)]
47. Jorgensen, W.L.; Chandrasekhar, J.; Madura, J.D.; Impey, R.W.; Klein, M.L. Comparison of simple potential functions for simulating liquid water. *J. Chem. Phys.* **1983**, *79*, 926–935. [[CrossRef](#)]
48. Phillips, J.C.; Braun, R.; Wang, W.; Gumbart, J.; Tajkhorshid, E.; Villa, E.; Chipot, C.; Skeel, R.D.; Kalé, L.; Schulten, K. Scalable molecular dynamics with NAMD. *J. Comput. Chem.* **2005**, *26*, 1781–1802. [[CrossRef](#)]
49. Harvey, M.J.; Giupponi, G.; Fabritiis, G.D. ACEMD: Accelerating Biomolecular Dynamics in the Microsecond Time Scale. *J. Chem. Theory Comput.* **2009**, *5*, 1632–1639. [[CrossRef](#)]
50. Altschul, S.F.; Gish, W.; Miller, W.; Myers, E.W.; Lipman, D.J. Basic local alignment search tool. *J. Mol. Biol.* **1990**, *215*, 403–410. [[CrossRef](#)]
51. Chaudhari, R.; Heim, A.J.; Li, Z. Improving homology modeling of G-protein coupled receptors through multiple-template derived conserved inter-residue interactions. *J. Comput. Aided Mol. Des.* **2015**, *29*, 413–420. [[CrossRef](#)] [[PubMed](#)]
52. Larsson, P.; Wallner, B.; Lindahl, E.; Elofsson, A. Using multiple templates to improve quality of homology models in automated homology modeling. *Protein Sci.* **2008**, *17*, 990–1002. [[CrossRef](#)] [[PubMed](#)]
53. Kuder, K.J.; Karcz, T.; Kaleta, M.; Kieć-Kononowicz, K. Molecular Modeling of an Orphan GPR18 Receptor. *Letts. Drug Des. Discov.* **2019**, *16*, 1167–1174. [[CrossRef](#)]
54. Sotudeh, N.; Morales, P.; Hurst, D.P.; Lynch, D.L.; Reggio, P.H. Towards a molecular understanding of the cannabinoid related orphan receptor GPR18: A focus on its constitutive activity. *Int. J. Mol. Sci.* **2019**, *20*, 2300. [[CrossRef](#)]
55. Schmeisser, M.G.; Pearsall, E.A.; Reggio, P.H. Construction of a GPR18 receptor model using conformational memories. *Biophys. J.* **2013**, *104*, 409a. [[CrossRef](#)]
56. Reynolds, J.L. Inhibition of GPR18 through docking of known antagonists using a homology model. *Biophys. J.* **2015**, *108*, 513a. [[CrossRef](#)]
57. Kothandan, G.; Cho, S.J. Homology modeling of GPR18 Receptor, an orphan G-protein-coupled receptor. *J. Chosun Nat. Sci.* **2013**, *6*, 16–20. [[CrossRef](#)]
58. Rosenbaum, D.M.; Rasmussen, S.G.F.; Kobilka, B.K. The structure and function of G-protein-coupled receptors. *Nature* **2009**, *459*, 356–363. [[CrossRef](#)]
59. Weis, W.I.; Kobilka, B.K. The molecular basis of G protein-coupled receptor activation. *Annu. Rev. Biochem.* **2018**, *87*, 897–919. [[CrossRef](#)]
60. Gacasan, S.B.; Baker, D.L.; Parrill, A.L. G protein-coupled receptors: The evolution of structural insight. *AIMS Biophys.* **2017**, *4*, 491–527. [[CrossRef](#)]

61. Zhang, D.; Zhao, Q.; Wu, B. Structural studies of G protein-coupled receptors. *Mol. Cells* **2015**, *38*, 836–842. [[PubMed](#)]
62. Grossfield, A. Recent progress in the study of G protein-coupled receptors with molecular dynamics computer simulations. *Biochim. Biophys. Acta* **2011**, *1808*, 1868–1878. [[CrossRef](#)] [[PubMed](#)]
63. Chen, H.; Fu, W.; Wang, Z.; Wang, X.; Lei, T.; Zhu, F.; Li, D.; Chang, S.; Xu, L.; Hou, T. Reliability of docking-based virtual screening for GPCR ligands with homology modeled structures: A case study of the angiotensin II type I receptor. *ACS Chem. Neurosci.* **2019**, *10*, 677–689. [[CrossRef](#)]
64. Ciancetta, A.; Rubio, P.; Lieberman, D.I.; Jacobson, K.A. A3 adenosine receptor activation mechanisms: Molecular dynamics analysis of inactive, active, and fully active states. *J. Comput. Aided Mol. Des.* **2019**, *33*, 983–996. [[CrossRef](#)] [[PubMed](#)]
65. Kashani-Amin, E.; Sakhteman, A.; Larijani, B.; Ebrahim-Habibi, A. Presence of carbohydrate binding modules in extracellular region of class C G-protein coupled receptors (C GPCR): An in silico investigation on sweet taste receptor. *J. Biosci.* **2019**, *44*, 138. [[CrossRef](#)]
66. Wacker, D.; Stevens, R.C.; Roth, B.L. How ligands illuminate GPCR molecular pharmacology. *Cell* **2017**, *170*, 414–427. [[CrossRef](#)]
67. Heydenreich, F.M.; Vuckovic, Z.; Matkovic, M.; Vepintsev, D.B. Stabilization of G protein-coupled receptors by point mutations. *Front. Pharmacol.* **2015**, *6*, 82. [[CrossRef](#)]
68. Deganutti, G.; Moro, S.; Reynolds, C.A. Peeking at G-protein-coupled receptors through the molecular dynamics keyhole. *Future Med. Chem.* **2019**, *11*, 599–615. [[CrossRef](#)]
69. Yuan, S.; Chan, H.C.S.; Vogel, H.; Filipek, S.; Stevens, R.C.; Palczewski, K. The molecular mechanism of P2Y1 receptor activation. *Angew. Chem.* **2016**, *55*, 10331–10335. [[CrossRef](#)]
70. Ribeiro, J.M.L.; Filizola, M. Insights from molecular dynamics simulations of a number of G-Protein coupled receptor targets for the treatment of pain and opioid use disorders. *Front. Mol. Neurosci.* **2019**, *12*, 207. [[CrossRef](#)]
71. An, X.; Bai, Q.; Bing, Z.; Zhou, S.; Shi, D.; Liu, H.; Yao, X. How does agonist and antagonist binding lead to different conformational ensemble equilibria of the κ -opioid receptor: Insight from long-time gaussian accelerated molecular dynamics simulation. *ACS Chem. Neurosci.* **2019**, *10*, 1575–1584. [[CrossRef](#)] [[PubMed](#)]
72. Tautermann, C.S.; Seeliger, D.; Kriegl, J.M. What can we learn from molecular dynamics simulations for GPCR drug design? *Comput. Struct. Biotechnol. J.* **2015**, *13*, 111–121. [[CrossRef](#)] [[PubMed](#)]
73. Renault, P.; Louet, M.; Marie, J.; Labesse, G.; Floquet, N. Molecular dynamics simulations of the allosteric modulation of the adenosine A2a receptor by a mini-G Protein. *Sci. Rep.* **2019**, *9*, 1–12. [[CrossRef](#)] [[PubMed](#)]
74. Bartuzi, D.; Kaczor, A.A.; Matosiuk, D. Molecular mechanisms of allosteric probe dependence in μ opioid receptor. *J. Biomol. Struct. Dyn.* **2019**, *37*, 36–47. [[CrossRef](#)]
75. Dalton, J.A.R.; Lans, I.; Giraldo, J. Quantifying conformational changes in GPCRs: Glimpse of a common functional mechanism. *BMC Bioinform.* **2015**, *16*, 124. [[CrossRef](#)]
76. Lee, Y.; Basith, S.; Choi, S. Recent advances in structure-based drug design targeting class A G protein-coupled receptors utilizing crystal structures and computational simulations. *J. Med. Chem.* **2018**, *61*, 1–46. [[CrossRef](#)]
77. Ballesteros, J.; Kitanovic, S.; Guarnieri, F.; Davies, P.; Fromme, B.J.; Konvicka, K.; Chi, L.; Millar, R.P.; Davidson, J.S.; Weinstein, H.; et al. Functional microdomains in G-protein-coupled receptors. The conserved arginine-cage motif in the gonadotropin-releasing hormone receptor. *J. Biol. Chem.* **1998**, *273*, 10445–10453. [[CrossRef](#)]
78. Wiley, J.L.; Marusich, J.A.; Thomas, B.F. Combination chemistry: Structure-activity relationships of novel psychoactive cannabinoids. *Curr. Top. Behav. Neurosci.* **2017**, *32*, 231–248.
79. Morales, P.; Hurst, D.P.; Reggio, P.H. Molecular targets of the phytocannabinoids—a complex picture. *Prog. Chem. Org. Nat. Prod.* **2017**, *103*, 103–131.
80. Ryberg, E.; Larsson, N.; Sjögren, S.; Hjorth, S.; Hermansson, N.-O.; Leonova, J.; Elebring, T.; Nilsson, K.; Drmota, T.; Greasley, P.J. The orphan receptor GPR55 is a novel cannabinoid receptor. *Br. J. Pharmacol.* **2007**, *152*, 1092–1101. [[CrossRef](#)]
81. de Petrocellis, L.; Di Marzo, V. Non-CB1, non-CB2 receptors for endocannabinoids, plant cannabinoids, and synthetic cannabimimetics: Focus on G-protein-coupled receptors and transient receptor potential channels. *J. Neuroimmune Pharmacol.* **2010**, *5*, 103–121. [[CrossRef](#)] [[PubMed](#)]

82. Qin, N.; Neeper, M.P.; Liu, Y.; Hutchinson, T.L.; Lubin, M.L.; Flores, C.M. TRPV2 is activated by cannabidiol and mediates CGRP release in cultured rat dorsal root ganglion neurons. *J. Neurosci.* **2008**, *28*, 6231–6238. [[CrossRef](#)] [[PubMed](#)]
83. de Petrocellis, L.; Vellani, V.; Schiano-Moriello, A.; Marini, P.; Magherini, P.C.; Orlando, P.; Di Marzo, V. Plant-derived cannabinoids modulate the activity of transient receptor potential channels of ankyrin type-1 and melastatin type-8. *J. Pharmacol. Exp. Ther.* **2008**, *325*, 1007–1015. [[CrossRef](#)] [[PubMed](#)]
84. Xiong, W.; Cheng, K.; Cui, T.; Godlewski, G.; Rice, K.; Xu, Y.; Zhang, L. Cannabinoid potentiation of glycine receptors contributes to cannabis-induced analgesia. *Nat. Chem. Biol.* **2011**, *7*, 296–303. [[CrossRef](#)]
85. Anavi-Goffer, S.; Baillie, G.; Irving, A.J.; Gertsch, J.; Greig, I.R.; Pertwee, R.G.; Ross, R.A. Modulation of L- α -lysophosphatidylinositol/GPR55 mitogen-activated protein kinase (MAPK) signaling by cannabinoids. *J. Biol. Chem.* **2012**, *287*, 91–104. [[CrossRef](#)]
86. Hurst, D.P.; Grossfield, A.; Lynch, D.L.; Feller, S.; Romo, T.D.; Gawrisch, K.; Pitman, M.C.; Reggio, P.H. A lipid pathway for ligand binding is necessary for a cannabinoid G protein-coupled receptor. *J. Biol. Chem.* **2010**, *285*, 17954–17964. [[CrossRef](#)]
87. Picone, R.P.; Khanolkar, A.D.; Xu, W.; Ayotte, L.A.; Thakur, G.A.; Hurst, D.P.; Abood, M.E.; Reggio, P.H.; Fournier, D.J.; Makriyannis, A. (-)-7'-Isothiocyanato-11-hydroxy-1',1'-dimethylheptylhexahydrocannabinol (AM841), a high-affinity electrophilic ligand, interacts covalently with a cysteine in helix six and activates the CB1 cannabinoid receptor. *Mol. Pharmacol.* **2005**, *68*, 1623–1635. [[CrossRef](#)]
88. Pei, Y.; Mercier, R.W.; Anday, J.K.; Thakur, G.A.; Zvonok, A.M.; Hurst, D.; Reggio, P.H.; Janero, D.R.; Makriyannis, A. Ligand-binding architecture of human CB2 cannabinoid receptor: Evidence for receptor subtype-specific binding motif and modeling GPCR activation. *Chem. Biol.* **2008**, *15*, 1207–1219. [[CrossRef](#)]
89. Palczewski, K.; Kumasaka, T.; Hori, T.; Behnke, C.A.; Motoshima, H.; Fox, B.A.; Le Trong, I.; Teller, D.C.; Okada, T.; Stenkamp, R.E.; et al. Crystal structure of rhodopsin: A G protein-coupled receptor. *Science* **2000**, *289*, 739–745. [[CrossRef](#)]
90. Ring, A.M.; Manglik, A.; Kruse, A.C.; Enos, M.D.; Weis, W.I.; Garcia, K.C.; Kobilka, B.K. Adrenaline-activated structure of β 2-adrenoceptor stabilized by an engineered nanobody. *Nature* **2013**, *502*, 575–579. [[CrossRef](#)]
91. Shim, J.-Y.; Bertalovitz, A.C.; Kendall, D.A. Identification of essential cannabinoid-binding domains: Structural insights into early dynamic events in receptor activation. *J. Biol. Chem.* **2011**, *286*, 33422–33435. [[CrossRef](#)] [[PubMed](#)]
92. McAllister, S.D.; Tao, Q.; Barnett-Norris, J.; Buehner, K.; Hurst, D.P.; Guarnieri, F.; Reggio, P.H.; Nowell Harmon, K.W.; Cabral, G.A.; Abood, M.E. A critical role for a tyrosine residue in the cannabinoid receptors for ligand recognition. *Biochem. Pharmacol.* **2002**, *63*, 2121–2136. [[CrossRef](#)]
93. Murphy, J.W.; Kendall, D.A. Integrity of extracellular loop 1 of the human cannabinoid receptor 1 is critical for high-affinity binding of the ligand CP 55,940 but not SR 141716A. *Biochem. Pharmacol.* **2003**, *65*, 1623–1631. [[CrossRef](#)]
94. Munk, C.; Mutt, E.; Isberg, V.; Nikolajsen, L.F.; Bibbe, J.M.; Flock, T.; Hanson, M.A.; Stevens, R.C.; Deupi, X.; Gloriam, D.E. An online resource for GPCR structure determination and analysis. *Nat. Methods* **2019**, *16*, 151–162. [[CrossRef](#)] [[PubMed](#)]



© 2020 by the authors. Licensee MDPI, Basel, Switzerland. This article is an open access article distributed under the terms and conditions of the Creative Commons Attribution (CC BY) license (<http://creativecommons.org/licenses/by/4.0/>).

8.3. Supporting Information

The Supporting Information can be accessed free of charge online at <https://www.mdpi.com/2218-273X/10/5/686/s1>.

Computational Investigations on the Binding Mode of Ligands for the Cannabinoid-Activated G Protein-Coupled Receptor GPR18

Alexander Neumann,^{1,2} Viktor Engel,¹ Andhika B. Mahardhika,^{1,2} Clara T. Schoeder,^{1,2} Vigneshwaran Namasivayam,¹ Katarzyna Kieć-Kononowicz,³ and Christa E. Müller^{1,2*}

¹ PharmaCenter Bonn, Pharmaceutical Institute, Pharmaceutical Sciences Bonn (PSB), Pharmaceutical & Medicinal Chemistry, University of Bonn, Bonn 53121, Germany

² Research Training Group 1873, University of Bonn, Bonn 53127, Germany

³ Department of Technology and Biotechnology of Drugs, Faculty of Pharmacy, Jagiellonian University Medical College, Medyczna 9, 30 - 688 Krakow, Poland.

* Correspondence: christa.mueller@uni-bonn.de; Tel.: +49-228-73-2301. Fax: +49-228-73-2567

Table of Contents

Figure S1. Multiple sequence alignment of GPR18 for homology modeling.....	2
Figure S2. Time scale of the molecular dynamics simulation of antagonist 4	3
Figure S3. Time scale of the molecular dynamics simulation of antagonist 5	4
Figure S4. Trajectories of salt bridges.....	5
Figure S5. Possible interaction of antagonist 6 with Asn185.....	6
Figure S6. Structures of GPR18 imidazothiazinone antagonists	7
Figure S7. Structures of GPR18 antagonists with modification of the core structure	8
Figure S8. Comparison of the binding modes of antagonists 5 and 32	9
Figure S9. Multiple sequence alignment of human GPR18 and the cannabinoid receptors CB ₁ and CB ₂	10
Figure S10. Comparison of the binding mode of THC to GPR18 with the binding of THC derivatives to the CB ₁ receptor.....	11
References	12

4xnv	1	TGFQF-YYLPAVYILVFIIGFLGNSVAIWMFVFMKPPWGSISVYMFNLALADFLYVLTLP	59
5c1m	1	PSMVTAITIMALYSIVCVVGLFGNFLVMYVIVRYTKMKTATNIYIFNLALADALATSTLP	60
5xsz	1	DNFKYPLYSM-VFSIVFMVGLITNVAAMYIFMCSLKLNRNETTTYMMNLVVSDDLFLVLTLP	59
GPR18	1	--DEYKIAALVFYSCIFIIGLGVNITALWVFSCTTKKRRTVTIYMMNVALVDLIFIMTLP	58
4xnv	60	ALIFYYFNKTDWIFGDAMCKLQRFIFHVNLYGSILFLTCISAHRYSGVVYP-KSLGRLKK	118
5c1m	61	FQSVNYLMGT-WPFGNILCKIVISIDYNNMFTSIFTLCTMSVDRIYVCHPVKALDFRTP	119
5xsz	60	LRVFYFVQQN-WPFGSLLCKLSVSLFYTNMYGSILFLTCISVDRFLAIVYPFRSRGLRTK	118
GPR18	59	FRMFYYAKDE-WPFGYFCQILGALTVFYPSIALWLLAFISADRYMAIVQPKYAKELKNT	117
4xnv	119	KNAICISVLVWLVVVAISPILFY-SGTGVRKNKTITCYDTTSDEYLRSYFIYSMCTTV-	176
5c1m	120	RNAKIVNVCNWILSSAIGLPVMFM--ATTKYRQGSIDCTLTFSHPTWYWENLLKICVFI-	176
5xsz	119	RNAKIVCAAVWLVLSGSLPTGFMLNSTNKLENNISCF-----EWK-SHLSKVVFIE	171
GPR18	118	CKAVLACVGVWIMTLTTTTPLLLLYKDPDK-DSTPATCLKISDIYLKAVNVNLNLRLT-	175
4xnv	177	-AMFCVPLVLILGCYGLIVRALIYKEPL-----RRKSIYLVIIIVLTVFAVSYIPFH	226
5c1m	177	-FAFIMPVLIIITVCYGLMILRLKSVRMLSGSKEKDRNLRRITRMVLVVAVFIVCWTPIH	235
5xsz	172	TVGFLLIPLMLNVVCSAMVLQTLRRPNTVL-----NKKKILRMIIVHLFIFCFPIYN	224
GPR18	176	-FFFLIPLFIMIGCYLVIIHNLHGRGTSK---LKPVKKEKSIRIITLLVQVLVCFMPPH	231
4xnv	227	VMKTMNLRARLDFQTPAMCAFNDRVYAT-YQVTRGLASLNSCVNPILYFLAGDTFRRR	283
5c1m	236	I--YVIIKALI---TIP----ETTFQTVSWHFCIALGYTNSCLNPVLYAFLDENFKRC	284
5xsz	225	V--NLVFYSLVRTNTLKGCAAESVVRTI-YPIALCIAVSNCCFDPVIVYFTSETIQNS	279
GPR18	232	I--CFAFLMLGT-----GENSYNPWGAFTTFLMNLSTCLDVILYYIVSKQFQAR	278

Figure S1. Multiple sequence alignment of the human GPR18 and the templates chosen for homology modeling.

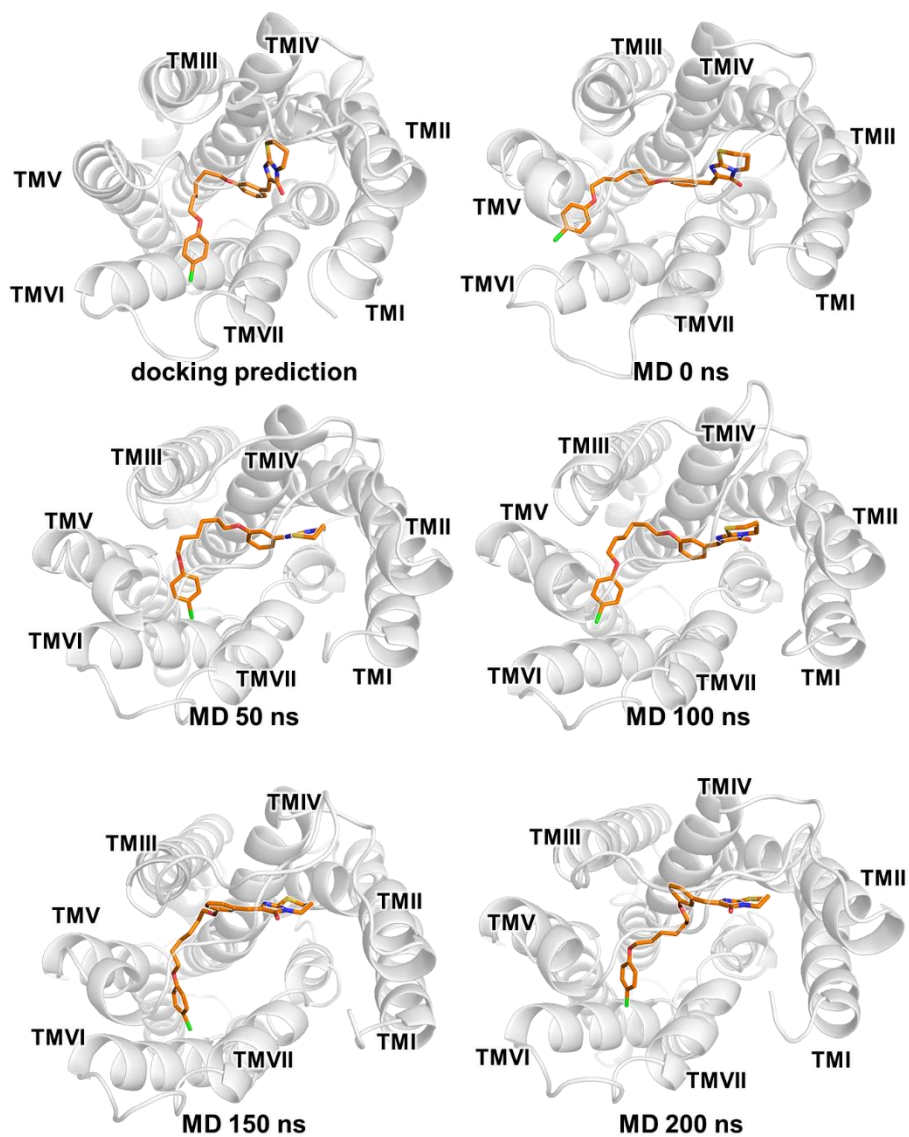


Figure S2. Time scale of the molecular dynamics (denoted 'MD') simulation of GPR18 homology model complex with antagonist 4. The docking prediction which was used for the simulation run is shown at the top left corner. 0 ns presents the complex after relaxation steps.

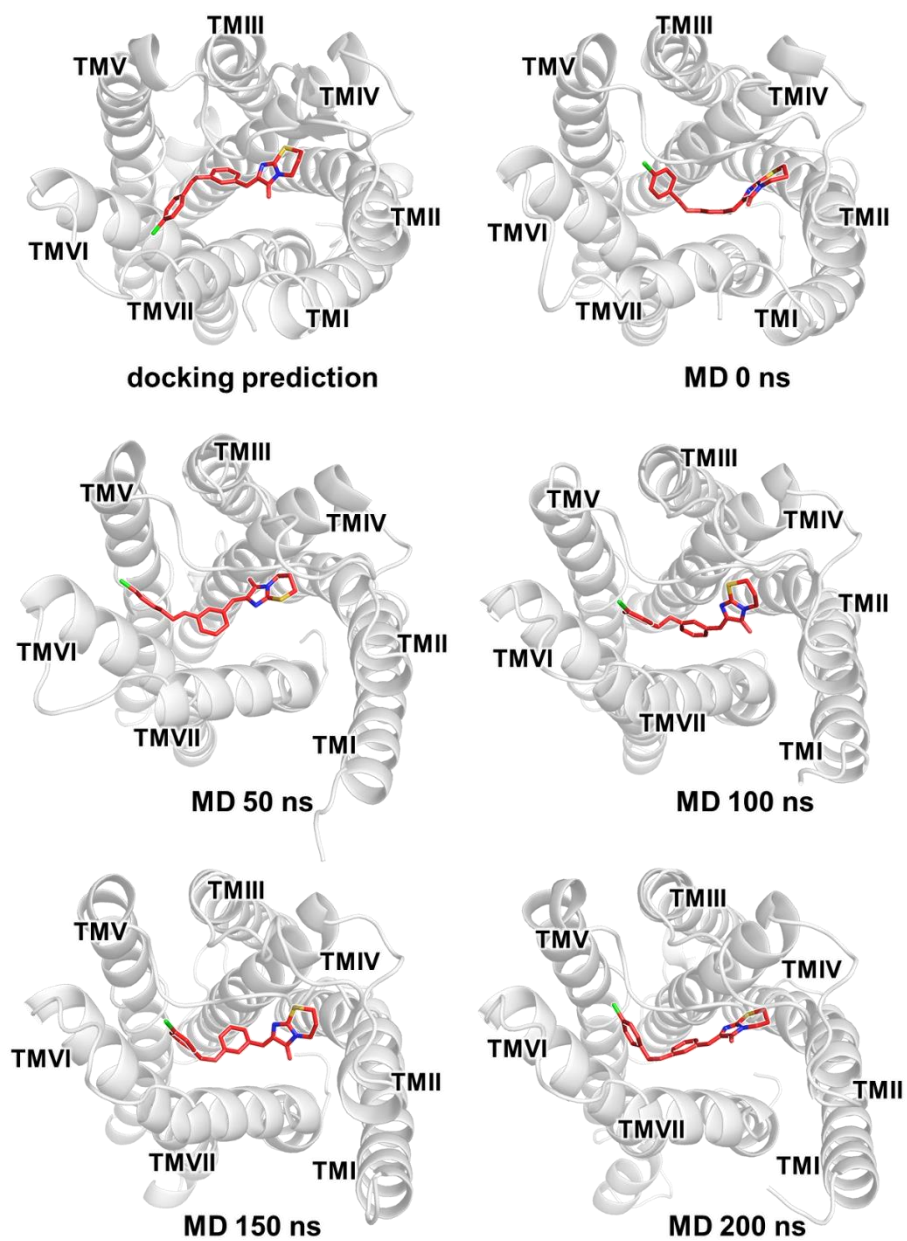


Figure S3. Time scale of the molecular dynamics (denoted 'MD') simulation of GPR18 homology model complex with antagonist 5. The docking prediction which was used for the simulation run is shown at the top left corner. 0 ns presents the complex after relaxation steps.

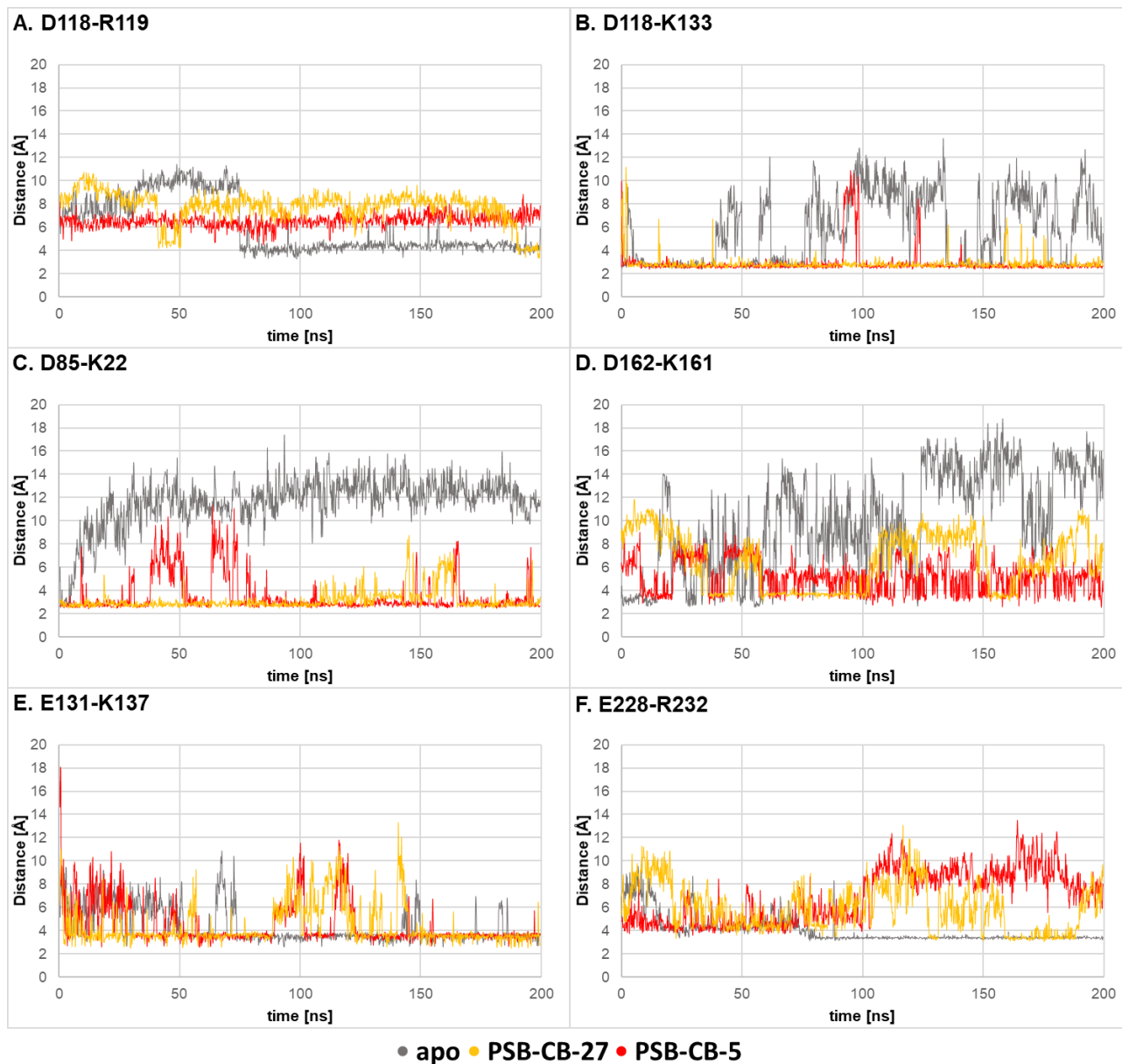


Figure S4. Trajectories of salt bridges during the 200 ns MD simulation runs.

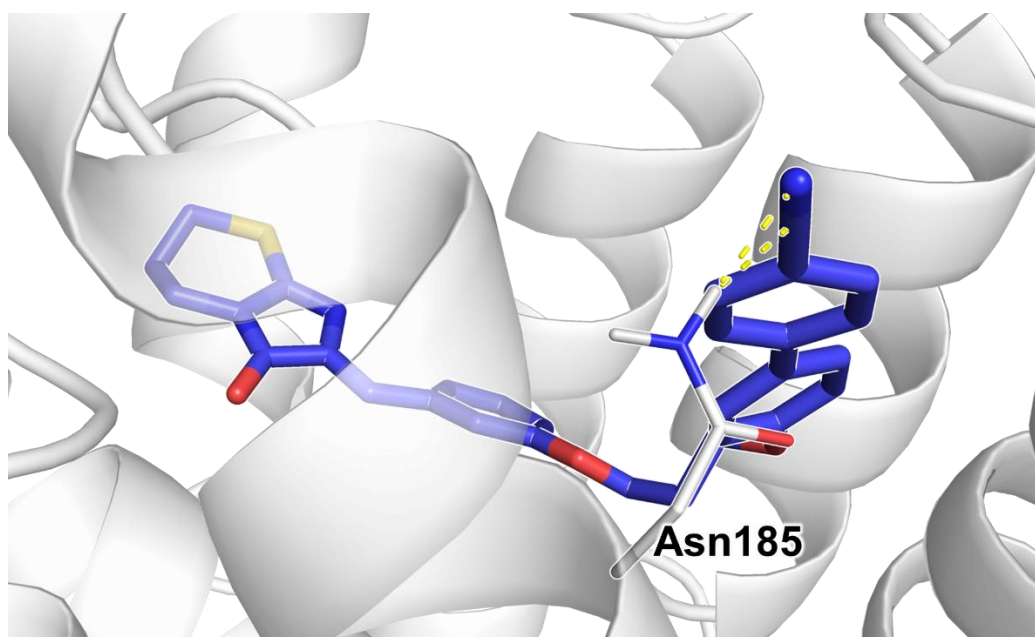


Figure S5. Possible interaction of antagonist 6 with a rotamer of Asn185.

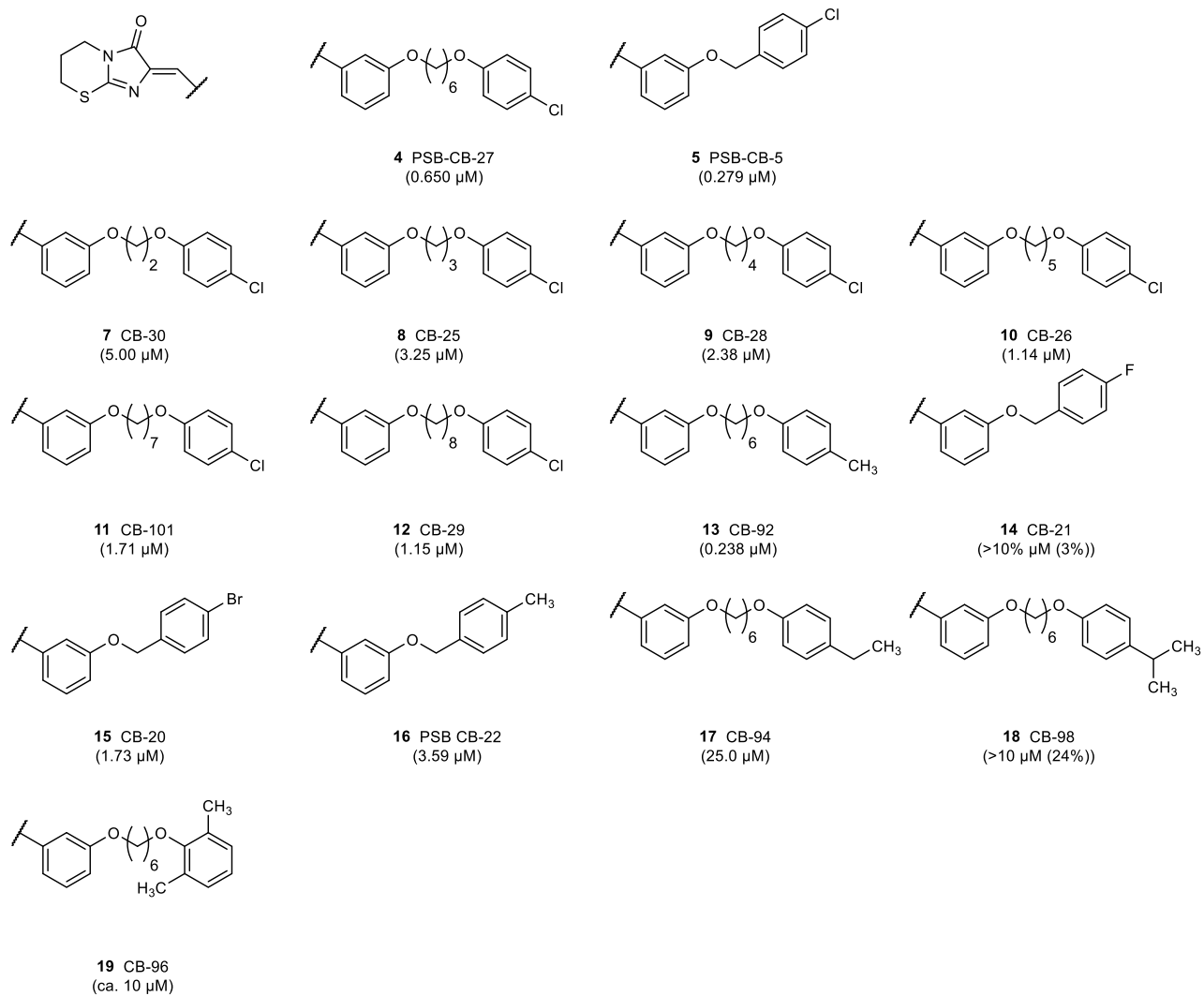


Figure S6. Structures of GPR18 imidazothiazinone antagonists with their respective IC_{50} values in brackets. For IC_{50} values $> 10\ \mu\text{M}$ the percent inhibition of agonist-induced luminescence signal at $10\ \mu\text{M}$ is given. Biological results were taken from published studies [1].

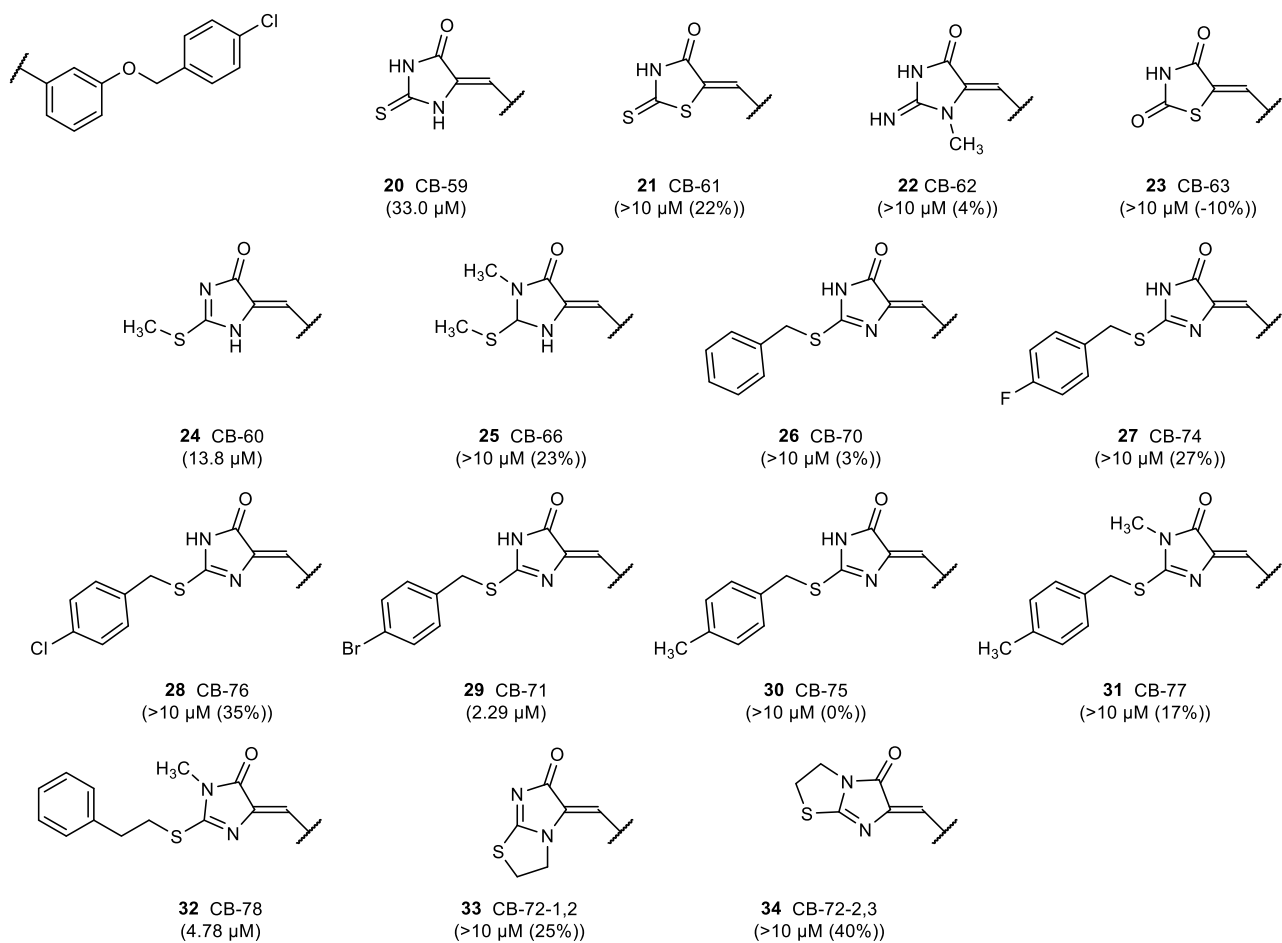


Figure S7. Structures of GPR18 antagonists with modification of the core structure with their respective IC_{50} values in brackets. For IC_{50} values $> 10 \mu M$ the percent inhibition of agonist-induced luminescence signal at $10 \mu M$ is given. Biological results were taken from published studies [1].

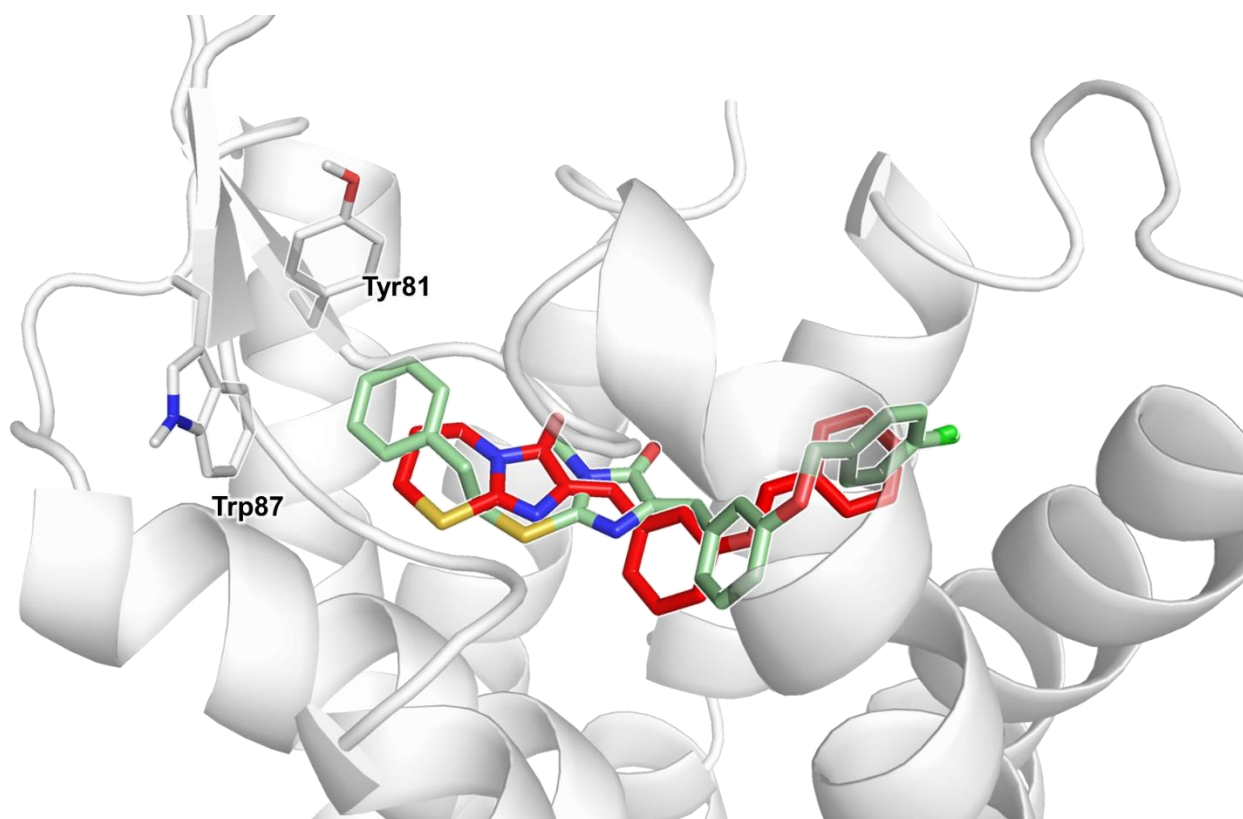


Figure S8. Comparison of the putative binding mode of antagonist 32 (green) and predicted binding mode of antagonist 5.

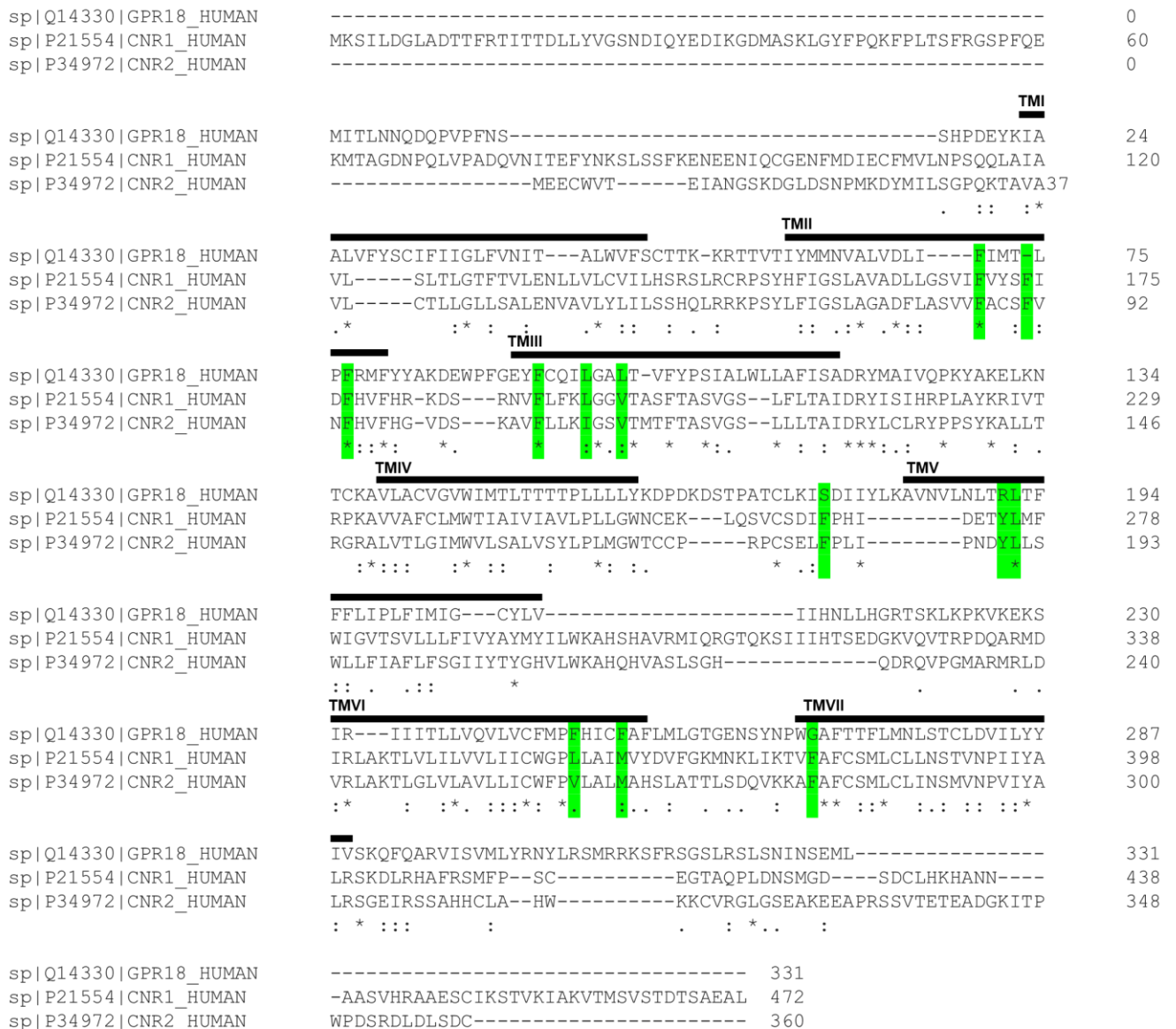


Figure S9. Multiple sequence alignment of human GPR18 and the cannabinoid receptors CB₁ and CB₂. Residue positions involved in the binding of cannabinoid agonists in the X-ray crystal structure of CB₁ receptor are highlighted.

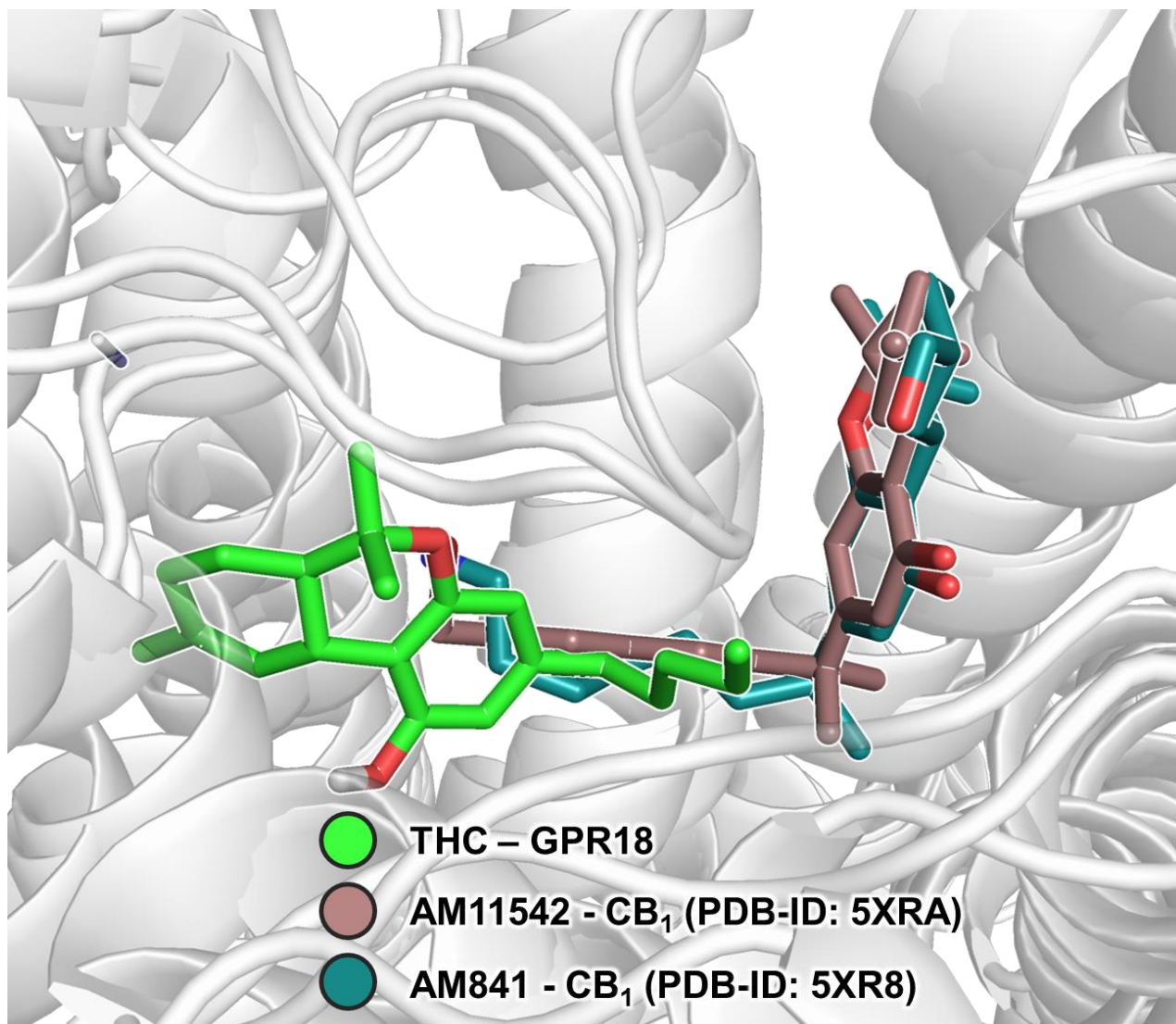


Figure S10. Comparison of the proposed binding mode of THC to GPR18 with the binding of THC derivatives to the CB₁ receptor as observed in the crystal structure [2].

References

1. Schoeder, C. T.; Kaleta, M.; Mahardhika, A. B.; Olejarz-Maciej, A.; Łażewska, D.; Kieć-Kononowicz, K.; Müller, C. E. Structure-activity relationships of imidazothiazinones and analogs as antagonists of the cannabinoid-activated orphan G protein-coupled receptor GPR18. *Eur. J. Med. Chem.* **2018**, *155*, 381–397.
2. Hua, T.; Vemuri, K.; Nikas, S. P.; Laprairie, R. B.; Wu, Y.; Qu, L.; Pu, M.; Korde, A.; Jiang, S.; Ho, J.-H.; *et al.* Crystal structures of agonist-bound human cannabinoid receptor CB1. *Nature* **2017**, *547*, 468–471.

8.4. Summary and Outlook

As a member of the GPCR family, GPR18 was expected to display complex conformational changes. Therefore, information collected and processed in **Section 3-7** greatly contributed to understanding and interpretation of the multilayered MD simulation data. Antagonist-induced stabilization of the inactive receptor state was observed in both MD simulation runs, likely resulting from an interplay between salt bridges in separate locations. A similar phenomenon was proposed for the P2Y₁-, P2Y₂- and P2Y₄R subtypes. The discussed SARs and presented binding modes of the imidazothiazinone antagonists were consistent with experimental data and are therefore of major value for future optimization of the compound series. Study of THC binding mode at GPR18 yielded new insights on the promiscuity of the cannabinoid: The explicit lipophilicity of the molecule contributes to the binding event and ligand recognition which is not limited to conserved residues observed at other cannabinoid receptors or target structures associated with them (e.g., GPR55).

The findings represent a stimulus for future studies focused on the deorphanization of GPR18. Elucidated interactions between target and ligands will be of significant value as pharmacophore constraints for virtual screening campaigns aiming to discover novel molecular scaffolds addressing this relevant receptor.

9. Conclusions

The initiative of this work was to elucidate the architecture of δ -branch GPCRs and the binding modes of their respective ligands as a starting point for the development, design, and discovery of potent and selective drugs by applying computational methods (**Section 2**). The generated homology models were evaluated for their quality and used for molecular docking studies. Subsequent mutagenesis studies, complemented with previously published data^{93,94}, and MD simulations fortified the binding mode hypotheses, and key interactions of ligands with the receptor were identified.

For P2YRs, challenges originated from the physicochemical properties of the endogenous nucleotide ligands of the investigated receptors. The triphosphate chain of ATP and UTP is negatively charged at physiological pH 7.4 resulting in poor oral bioavailability but is required for proper interactions with the receptor impeding potential replacement of the functional group. Further, selectivity issues have to be addressed during the development of potential drug candidates due the conserved binding site hosting the nucleobase.

Unfortunately, no agonist-bound X-ray crystal structure of a P2Y₁-like receptor has been published to perform structure-based computational methods for the design and discovery of compounds. Yet, the related P2Y₁R X-ray crystal structure bound to antagonist represented a viable starting point for template-based homology modeling of the related P2Y₂- and P2Y₄Rs. The PDB structure 4XNW contains a nucleotide antagonist which binds at the upper third part of the receptor close to the extracellular lumen.⁹³ In contrast, two agonist-bound structures of the more distantly-related P2Y₁₂R revealed an alternating binding mode for the co-complexed nucleotides with the nucleobase buried inside a lipophilic binding pocket formed by the surrounding transmembrane regions.⁹⁵ This raised the question on how the endogenous nucleotide ligands bind to P2Y₂- and P2Y₄Rs (**Section 3**). Therefore, in order to determine the orthosteric binding site, extensive analysis of potential binding modes of agonists and antagonists was performed.

Docking studies successfully predicted important key interactions and differences between ATP and UTP recognition taking subpockets distant to the putative orthosteric binding site into consideration (**Section 4 and 5**). Several lipophilic residues of P2Y₂R

were discovered to participate in the ligand recognition: Phe113, Tyr114, Tyr118, Phe195, Phe261, and Tyr269, were found to interact with the nucleobase of the agonists. Compared to P2Y₄R, the putative orthosteric binding site, and especially the subpocket likely involved in the binding of the nucleobase, were found to be more lipophilic in the case of P2Y₂R. Furthermore, the results suggest that the putative nucleobase binding site of P2Y₂R is more spacious than the one at P2Y₄R. Interestingly, mutation of Tyr197 to alanine introduced ATP-sensitivity in P2Y₄R likely due to the increased available space in the orthosteric binding site. Additional insights on binding mode differences were gained during the investigation of *N*⁴-phenylpropoxy-substituted cytidine-5'-triphosphate derivative MRS4062. MRS4062 acts as agonist on several UTP-activated P2YRs but displays moderate P2Y₄R-selectivity.⁹⁶ The collected data for both receptors proposes a binding mode similar to UTP in which the cytidine and phenylpropoxy group are hosted in the orthosteric nucleobase binding site. This is supported by the fact that mutation of the deeply buried Phe113 to alanine resulted in complete loss of P2Y₂R activation, whereas mutation to tyrosine increased the potency of MRS4062. In the case of P2Y₄R, aromatic interactions of MRS4062 with Tyr197 and Phe200 were observed as mutation of said residues to alanine resulted in decreased potency which was not observed at the respective phenylalanine and tyrosine mutants.

Correspondingly, the topology of the binding pocket likely plays a crucial role in the behavior of antagonist binding. Although multiple binding modes of individual anthraquinone derivatives at P2YRs are feasible, both allosteric and orthosteric inhibition was observed for different subtypes (**Section 7**). In the case of P2Y₂R, access to the lipophilic nucleobase binding site for anthraquinone derivative PSB-1699 was observed in docking and confirmed by mutagenesis studies. There, aromatic interactions with Phe113 were observed as mutation of said residue to alanine resulted in complete loss of potency, whereas the mutation to tyrosine maintained potency compared to the wild type. Compared to the other investigated anthraquinone derivatives PSB-1699 contains an additional linker atom resulting in increased flexibility of ring E (see **Figure 2** for ring numbering) allowing to interact with the buried residue Phe113. The loss of PSB-1699 inhibition at the F195Y mutant can be accounted for the additional hydroxy group of the tyrosine which results in clashes with the linker of ring E. Similarly, complete loss of RB-2 inhibition was observed for the P2Y₂R mutants F111A, Y114A, Y198A, and F261A.⁹⁴ The docking studies suggested

the binding of ring E in the orthosteric nucleobase binding site which includes π - π stacking and lipophilic interactions with said residues with and is therefore consistent with the mutagenesis data. Additionally, the sulfonic acid group likely engages in hydrogen bond interactions within the binding site as the mutation of Tyr269 to phenylalanine resulted in loss of RB-2 inhibition, and decreased potency at the F113Y and F195Y mutants. Rearrangement of hydrogen bond partners in the nucleobase subpocket could therefore interfere with the interaction pattern of the sulfonic acid leading to the decreased potency. Those effects were not observed for the other investigated anthraquinones at P2Y₂R mutants as those do not contain hydrogen bond partners at the respective rings.

For P2Y₄R, a rotamer of Arg265 was observed that limits the space and the access to the lipophilic nucleobase binding site which may contribute to the allosteric mode of inhibition of anthraquinone derivatives. Future development of drug candidates could therefore profit from addressing the space availability in the orthosteric binding site and the increased lipophilicity in case of P2Y₂R to design selective compounds. Seemingly, the presence of the highly lipophilic and bulky 2,8-dimethyl-5*H*-dibenzo[*a,d*][7]annulene group in AR-C118925 exploits the lipophilic nature and the available space of the orthosteric binding site resulting in increased P2Y₂R selectivity.

Alongside the orthosteric nucleobase binding site, the allosteric binding site addressed by anthraquinone antagonists in P2Y₄R, an ionic binding pocket present in both P2YR subtypes was investigated. This binding pocket consists of hydrophilic and charged residues, namely Arg110, His184, Asp185, Lys289, and Arg292 (P2Y₂R), and Arg112, His186, Asp187, Lys289, and Arg292 (P2Y₄R). Those residues were predicted in interacting with the phosphate groups of the endogenous ligands and the sulfonic acid group(s) of the investigated anthraquinone derivatives. As several of those residues were found to be important for the interaction with the agonists, assessment of their role in antagonist binding remains unanswered due to the accompanying absence of receptor activation in the performed assays. Yet, mutation of Asp185 to alanine (P2Y₂R) resulted in increased potency of the anthraquinone derivatives. This can originate from the replacement of a negatively charged residue which would repel the sulfonic acid group of the antagonists allowing proper interaction with the positively charged residues in the ionic binding pocket, or the increased potency can be a consequence of removal of the ionic lock mentioned in the next paragraph.

MD simulations of the P2Y₁R X-ray crystal structure with agonist ADP and antagonists proposed the involvement of an ionic lock between an asparagine in ECL2 and an arginine in TM6.⁸⁶ While both antagonists stabilized the Asp-Arg salt bridge in the 20 μ s all-atom long-timescale MD simulation, agonist ADP was found to break the ionic lock resulting in receptor activation through conformational changes. Analogous residues were observed in the generated homology models of P2Y₂R (Asp185-Arg292) and P2Y₄R (Asp187-Arg292), respectively. The role of the ionic lock was elucidated by docking and mutagenesis studies of this work. For P2Y₂R, mutation of both residues to alanine resulted in decreased agonist potency (D185A) and complete loss of potency (R292A), supporting their involvement of both residues in receptor activation and ligand recognition. Furthermore, involvement of a second salt bridge between Glu190 and Arg194 in agonist-induced receptor activation was discovered in P2Y₂R. Mutation of Arg194 to alanine resulted in reduced potency of ATP and to a absent activation by Ap₄A, whereas mutation of Arg194 to histidine resulted only in a decrease in Ap₄A potency. The observations could occur from modulation of ECL2 flexibility by the formed salt bridge as mutation to a basic amino acid preserved receptor response to Ap₄A. In the case of P2Y₄R, a second ionic lock distant to proposed binding sites between Arg190 and Asp195 in ECL2 of P2Y₄R was found to affect the potency and efficacy of agonists likely due to modification of flexibility.

In summary, the presented data supports similar binding modes of agonists at P2Y₂-, P2Y₄- and P2Y₁₂Rs. The nucleobase likely binds in a lipophilic and aromatic cavity buried between the TM regions underneath ECL2 distant to the binding spot of the P2Y₁R nucleotide antagonist.⁹³ ATP-sensitivity of P2Y₂R can result from more available space inside the nucleobase binding cavity. Finally, antagonists likely stabilize an ionic lock between an aspartic acid in ECL2 and an arginine in TM6.

The gained insights were taken over to the VS campaign for P2Y₂R antagonists (**Section 6**). Proper interaction patterns are important for the assessment of potential binders and increase the likelihood of finding active compounds. Hence, approximately 3.2 million drug-like compounds retrieved from the ZINC database were docked at an ensemble of the homology model of P2Y₂R in complex with AR-C118925. The resulting top one thousand ranked compounds were visually inspected and purchased at Molport. Although the replacement of the essential triphosphate for drug-like groups to stabilize the ionic lock by interacting with surrounding residues posed a major

challenge, three novel antagonist scaffolds with selectivity towards P2Y₂R were discovered. The antagonists were predicted to occupy the orthosteric nucleobase binding site with lipophilic groups. Additional stabilization may result from interactions of antagonists with residues in the extracellular compartment or with residues forming a binding site with mixed (hydrophilic and lipophilic) properties. Most importantly, the discovered antagonists contained drug-like groups that were predicted to bind in the region hosting the triphosphate chain of the nucleotide agonists opening alternative future routes for the development and optimization of novel drug candidates.

Incorporating the accumulated insights on the architecture of δ -branch rhodopsin-like GPCRs, behavior of ligands at the orphan receptor GPR18 was investigated (**Section 8**). Due to close conformational resemblance of GPR18 to the validated P2Y₂- and P2Y₄R structures resulting from the use of same template X-ray crystal structures for the generation of the homology model, effort was taken to elucidate unique or conserved interaction motifs. For this, 200 ns MD simulations were run for the apo state human GPR18 homology model, as well as for two selected antagonists, PSB-CB-5 and PSB-CB-27, and the occurring inter- and intramolecular interactions were analyzed.

Several salt bridges were of particular interest as an inactive receptor conformation resulting from the binding of an antagonist was expected, analogous to the inhibition mechanism of P2Y₁R and therefore to that of P2Y₂- and P2Y₄Rs.⁸⁶ The apo state of GPR18 was considered as the active conformation of the receptor due to its reported constitutive activity.^{26,97,98} During the 200 ns MD simulations, a previously proposed salt bridge between Asp118 and Arg119 was confirmatively observed at the apo structure after 75 ns, whereas the binding of an antagonist broke the salt bridge and induced a new ionic lock between Asp118 and Lys133.⁹⁹ The salt bridge between Glu131-Lys137 was conserved in all three simulation runs and is therefore unlikely to be involved in the receptor activation process. Further, the ionic lock between Glu228 and Arg232 was observed at the apo state only. Lastly, two additional salt bridges were observed exclusive to antagonist-bound complexes: Lys22-Asp185 and Lys161-Asp162. In conclusion, it appears that one or more ionic locks are involved in receptor functionality of GPR18. Ligands that modulate the stability of the proposed ionic interactions therefore represent enormous potential as novel tool compounds or drug candidates.

Antagonist-bound complexes of PSB-CB-5 and PSB-CB-27 both stabilized a receptor conformation during the 200 ns MD simulation runs. Especially TM1, TM6 and TM7 displayed reduced root mean square fluctuations compared to the apo state, indicating conformational constraints induced by the antagonists. Both antagonists bind in the upper third part of the receptor – a the binding cavity shared by many δ -branch GPCRs.¹⁰⁰ The imidazothiazinone moiety was found to bind underneath ECL2 and close to the disulfide bridge Cys94-Cys172, where it is stabilized by lipophilic interactions and H-bonds with Tyr82. The 4-chlorophenoxy group of both antagonists binds in a lipophilic and aromatic subpocket formed by residues of TM6 and TM7. The superior potency of the selected antagonists was accounted for the interactions of the chlorine atom with the side chain of Cys251 which is consistent with published SAR data.⁸⁴

The promiscuity of THC can be attributed to the high lipophilicity of the molecule as the driving force for the binding at GPR18. Compared to the binding modes of other cannabinoids, THC displays a turned conformation at GPR18 where the tricyclic ring system binds underneath ECL2 in a lipophilic binding cavity formed by residues of TM4 and TM5.^{101,102} This can be accounted to sequence differences between GPR18 and CB₁- and CB₂Rs such as the absence of aromatic residues in ECL2 of GPR18: While a phenylalanine was discovered to form aromatic interactions with the phenyl moiety of the cannabinoids at CBRs, no analog residue as interaction partner was discovered at GPR18. This finding is of foremost importance as it enables rational design of selective ligands targeting individual receptors thus lowering the risk of adverse side effects.

Finally, the proposed binding mode of the GPR18 antagonist was successfully reproduced in a recent independent computational study.¹⁰³ Taken this together with the previously mentioned consistency with previous computational and pharmacological studies, the validity and utility of the generated homology model was confirmed. Therefore, the collected knowledge will contribute to the understanding of GPR18 behavior and help to deorphanize this therapeutically relevant receptor.

To summarize the preceding paragraphs, it can be said that molecular modeling is a powerful and cost-efficient method for lead generation and optimization that relies on feed-back and support from experimental validation of the predictions. The symbiotic interplay between computational and pharmacological methods provides invaluable

insights into SARs which fosters understanding of key interactions required for successful design and discovery of novel therapeutics. Although great advances related to the development of P2YR antagonists and tool compounds were reported, expansion of the medicinal chemistry tool box is still required to appropriately address those difficult targets.^{104,105} With this work several novel drug-like scaffolds for P2Y₂R were identified based on information gained from structure-guided investigation of known binders. Those structures represent excellent drug-like starting points surpassing the properties of the endogenous ligands and available tool compounds. The overall picture of P2Y₂R, P2Y₄R and GPR18 architecture and the ligand binding sites will facilitate rational development of therapeutic drug candidates and pave the way to GPR18 deorphanization.

10. Abbreviations

ADP	Adenosine-5'-diphosphate
Ap ₄ A	<i>P</i> ¹ , <i>P</i> ⁴ -di(adenosine-5')-tetraphosphate
AR-C118925	5-[[5-(2,8-Dimethyl-5 <i>H</i> dibenzo[<i>a,d</i>]cyclohepten-5-yl)-3,4-dihydro-2-oxo-4-thioxo-1(2 <i>H</i>)-pyrimidinyl]methyl]- <i>N</i> -(1 <i>H</i> -tetrazol-5-yl)-2-furancarboxamide
ATP	Adenosine-5'-triphosphate
β-arrestin-EA	enzyme acceptor-tagged β-arrestin
CADD	Computer-aided drug discovery
CB _x R	Cannabinoid receptor subtype X
cryo-EM	Electron cryo-microscopy
DAG	Diacyl glycerol
ECL	Extracellular loop
EA	Enzyme acceptor fragment
FDA	Food and Drug Administration
GPCR	G protein-coupled receptor
GPCR-PK	ProLink™-tagged GPCR
GPR18	G protein-coupled receptor 18
HTS	High-throughput screening
IFD	Induced-fit docking
IP ₃	Inositol 1,4,5-trisphosphate
LBDD	Ligand-based drug discovery
MD	Molecular dynamics
NAGly	<i>N</i> -arachidonoylglycine

P2Y _x R	P2Y receptor subtype X
PAINS	Pan-assay interference compounds
PIP ₂	Phosphatidylinositol 4,5-bisphosphate r
PK	ProLink™ fragment
PLC	Phospholipase C
RB-2	Reactive Blue 2
RMSD	Root-mean-square deviation
SAR	Structure-activity relationship
SBDD	Structure-based drug discovery
THC	Δ^9 -tetrahydrocannabinol
TM	Transmembrane
UDP	Uridine-5'-diphosphate
UTP	Uridine-5'-triphosphate
VS	Virtual screening

11. References

- (1) Hauser, A. S.; Attwood, M. M.; Rask-Andersen, M.; Schiöth, H. B.; Gloriam, D. E. Trends in GPCR Drug Discovery: New Agents, Targets and Indications. *Nat. Rev. Drug Discov.* **2017**, *16* (12), 829–842. <https://doi.org/10.1038/nrd.2017.178>.
- (2) Santos, R.; Ursu, O.; Gaulton, A.; Bento, A. P.; Donadi, R. S.; Bologa, C. G.; Karlsson, A.; Al-Lazikani, B.; Hersey, A.; Oprea, T. I.; Overington, J. P. A Comprehensive Map of Molecular Drug Targets. *Nat. Rev. Drug Discov.* **2017**, *16* (1), 19–34. <https://doi.org/10.1038/nrd.2016.230>.
- (3) Jacobson, K. A.; Delicado, E. G.; Gachet, C.; Kennedy, C.; von Kügelgen, I.; Li, B.; Miras-Portugal, M. T.; Novak, I.; Schöneberg, T.; Perez-Sen, R.; Thor, D.; Wu, B.; Yang, Z.; Müller, C. E. Update of P2Y Receptor Pharmacology: IUPHAR Review 27. *Br. J. Pharmacol.* **2020**, *177* (11), 2413–2433. <https://doi.org/10.1111/bph.15005>.
- (4) Moore, D. J.; Chambers, J. K.; Wahlin, J.-P.; Tan, K. B.; Moore, G. B.; Jenkins, O.; Emson, P. C.; Murdock, P. R. Expression Pattern of Human P2Y Receptor Subtypes: A Quantitative Reverse Transcription–Polymerase Chain Reaction Study. *Biochim. Biophys. Acta - Gene Struct. Expr.* **2001**, *1521* (1–3), 107–119. [https://doi.org/10.1016/S0167-4781\(01\)00291-3](https://doi.org/10.1016/S0167-4781(01)00291-3).
- (5) Knight, G. E. Receptors on Autonomic Neurons and Neuroeffector Cells: Purinergic Receptors. In *Reference Module in Neuroscience and Biobehavioral Psychology*; Elsevier, **2017**. <https://doi.org/10.1016/B978-0-12-809324-5.02358-0>.
- (6) Wan, H.-X.; Hu, J.-H.; Xie, R.; Yang, S.-M.; Dong, H. Important Roles of P2Y Receptors in the Inflammation and Cancer of Digestive System. *Oncotarget* **2016**, *7* (19), 28736–28747. <https://doi.org/10.18632/oncotarget.7518>.
- (7) Förster, D.; Reiser, G. Supportive or Detrimental Roles of P2Y Receptors in Brain Pathology?—The Two Faces of P2Y Receptors in Stroke and Neurodegeneration Detected in Neural Cell and in Animal Model Studies. *Purinergic Signal.* **2015**, *11* (4), 441–454. <https://doi.org/10.1007/s11302-015-9471-6>.
- (8) Woods, L. T.; Forti, K. M.; Shanbhag, V. C.; Camden, J. M.; Weisman, G. A. P2Y Receptors for Extracellular Nucleotides: Contributions to Cancer Progression and Therapeutic Implications. *Biochem. Pharmacol.* **2021**, *187*, 114406. <https://doi.org/10.1016/j.bcp.2021.114406>.
- (9) Burnstock, G. Purinergic Receptors. *J. Theor. Biol.* **1976**, *62* (2), 491–503. [https://doi.org/10.1016/0022-5193\(76\)90133-8](https://doi.org/10.1016/0022-5193(76)90133-8).
- (10) Burnstock, G. Do Some Nerve Cells Release More than One Transmitter? *Neuroscience* **1976**, *1* (4), 239–248. [https://doi.org/10.1016/0306-4522\(76\)90054-3](https://doi.org/10.1016/0306-4522(76)90054-3).
- (11) Drury, A. N.; Szent-Györgyi, A. The Physiological Activity of Adenine Compounds with Especial Reference to Their Action upon the Mammalian Heart1. *J. Physiol.* **1929**, *68* (3), 213–237. <https://doi.org/10.1113/jphysiol.1929.sp002608>.
- (12) Sabe, V. T.; Ntombela, T.; Jhamba, L. A.; Maguire, G. E. M.; Govender, T.; Naicker, T.; Kruger, H. G. Current Trends in Computer Aided Drug Design and a Highlight of Drugs Discovered via Computational Techniques: A Review. *Eur. J. Med. Chem.* **2021**, *224*, 113705. <https://doi.org/10.1016/j.ejmech.2021.113705>.

- (13) Illes, P.; Müller, C. E.; Jacobson, K. A.; Grutter, T.; Nicke, A.; Fountain, S. J.; Kennedy, C.; Schmalzing, G.; Jarvis, M. F.; Stojilkovic, S. S.; King, B. F.; Di Virgilio, F. Update of P2X Receptor Properties and Their Pharmacology: IUPHAR Review 30. *Br. J. Pharmacol.* **2021**, *178* (3), 489–514. <https://doi.org/10.1111/bph.15299>.
- (14) McHugh, D.; Hu, S. S.; Rimmerman, N.; Juknat, A.; Vogel, Z.; Walker, J. M.; Bradshaw, H. B. N-Arachidonoyl Glycine, an Abundant Endogenous Lipid, Potently Drives Directed Cellular Migration through GPR18, the Putative Abnormal Cannabidiol Receptor. *BMC Neurosci.* **2010**, *11* (1), 44. <https://doi.org/10.1186/1471-2202-11-44>.
- (15) McHugh, D.; Wager-Miller, J.; Page, J.; Bradshaw, H. B. SiRNA Knockdown of GPR18 Receptors in BV-2 Microglia Attenuates N-Arachidonoyl Glycine-Induced Cell Migration. *J. Mol. Signal.* **2012**, *7*, 10. <https://doi.org/10.1186/1750-2187-7-10>.
- (16) Kohno, M.; Hasegawa, H.; Inoue, A.; Muraoka, M.; Miyazaki, T.; Oka, K.; Yasukawa, M. Identification of N-Arachidonoylglycine as the Endogenous Ligand for Orphan G-Protein-Coupled Receptor GPR18. *Biochem. Biophys. Res. Commun.* **2006**, *347* (3), 827–832. <https://doi.org/10.1016/j.bbrc.2006.06.175>.
- (17) Chiang, N.; Dalli, J.; Colas, R. A.; Serhan, C. N. Identification of Resolvin D2 Receptor Mediating Resolution of Infections and Organ Protection. *J. Exp. Med.* **2015**, *212* (8), 1203–1217. <https://doi.org/10.1084/jem.20150225>.
- (18) Schoeder, C. T.; Mahardhika, A. B.; Drabczyńska, A.; Kieć-Kononowicz, K.; Müller, C. E. Discovery of Tricyclic Xanthines as Agonists of the Cannabinoid-Activated Orphan G-Protein-Coupled Receptor GPR18. *ACS Med. Chem. Lett.* **2020**, *11* (10), 2024–2031. <https://doi.org/10.1021/acsmchemlett.0c00208>.
- (19) Irving, A.; Abdulrazzaq, G.; Chan, S. L. F.; Penman, J.; Harvey, J.; Alexander, S. P. H. Cannabinoid Receptor-Related Orphan G Protein-Coupled Receptors; **2017**; pp 223–247. <https://doi.org/10.1016/bs.apha.2017.04.004>.
- (20) Gantz, I.; Muraoka, A.; Yang, Y.-K.; Samuelson, L. C.; Zimmerman, E. M.; Cook, H.; Yamada, T. Cloning and Chromosomal Localization of a Gene (GPR18) Encoding a Novel Seven Transmembrane Receptor Highly Expressed in Spleen and Testis. *Genomics* **1997**, *42* (3), 462–466. <https://doi.org/10.1006/geno.1997.4752>.
- (21) Becker, A. M.; Callahan, D. J.; Richner, J. M.; Choi, J.; DiPersio, J. F.; Diamond, M. S.; Bhattacharya, D. GPR18 Controls Reconstitution of Mouse Small Intestine Intraepithelial Lymphocytes Following Bone Marrow Transplantation. *PLoS One* **2015**, *10* (7), e0133854. <https://doi.org/10.1371/journal.pone.0133854>.
- (22) Lee, Y.; Jo, J.; Chung, H. Y.; Pothoulakis, C.; Im, E. Endocannabinoids in the Gastrointestinal Tract. *Am. J. Physiol. Liver Physiol.* **2016**, *311* (4), G655–G666. <https://doi.org/10.1152/ajpgi.00294.2015>.
- (23) Wang, X.; Sumida, H.; Cyster, J. G. GPR18 Is Required for a Normal CD8 α Intestinal Intraepithelial Lymphocyte Compartment. *J. Exp. Med.* **2014**, *211* (12), 2351–2359. <https://doi.org/10.1084/jem.20140646>.
- (24) Sumida, H.; Cyster, J. G. G-Protein Coupled Receptor 18 Contributes to Establishment of the CD8 Effector T Cell Compartment. *Front. Immunol.* **2018**, *9*. <https://doi.org/10.3389/fimmu.2018.00660>.
- (25) Morales, P.; Lago-Fernandez, A.; Hurst, D. P.; Sotudeh, N.; Brailoiu, E.; Reggio, P. H.; Abood, M. E.; Jagerovic, N. Therapeutic Exploitation of GPR18: Beyond the Cannabinoids? *J. Med. Chem.* **2020**, *63* (23), 14216–14227. <https://doi.org/10.1021/acs.jmedchem.0c00926>.
- (26) Qin, Y.; Verdegaal, E. M. E.; Siderius, M.; Bebelman, J. P.; Smit, M. J.; Leurs,

- R.; Willemze, R.; Tensen, C. P.; Osanto, S. Quantitative Expression Profiling of G-Protein-Coupled Receptors (GPCRs) in Metastatic Melanoma: The Constitutively Active Orphan GPCR GPR18 as Novel Drug Target. *Pigment Cell Melanoma Res.* **2011**, *24* (1), 207–218. <https://doi.org/10.1111/j.1755-148X.2010.00781.x>.
- (27) Qiao, G.; Chen, L.; Wu, J.; Li, Z. Identification of an Eight-Gene Signature for Survival Prediction for Patients with Hepatocellular Carcinoma Based on Integrated Bioinformatics Analysis. *PeerJ* **2019**, *7*, e6548. <https://doi.org/10.7717/peerj.6548>.
- (28) Fabisiak, A.; Fabisiak, N.; Mokrowiecka, A.; Malecka-Panas, E.; Jacenik, D.; Kordek, R.; Zielińska, M.; Kieć-Kononowicz, K.; Fichna, J. Novel Selective Agonist of GPR18, PSB-KK-1415 Exerts Potent Anti-inflammatory and Antinociceptive Activities in Animal Models of Intestinal Inflammation and Inflammatory Pain. *Neurogastroenterol. Motil.* **2021**, *33* (3). <https://doi.org/10.1111/nmo.14003>.
- (29) Cowan, S. W.; Newcomer, M. E.; Jones, T. A. Crystallographic Refinement of Human Serum Retinol Binding Protein at 2Å Resolution. *Proteins Struct. Funct. Genet.* **1990**, *8* (1), 44–61. <https://doi.org/10.1002/prot.340080108>.
- (30) Elliott, T. S.; Slowey, A.; Ye, Y.; Conway, S. J. The Use of Phosphate Bioisosteres in Medicinal Chemistry and Chemical Biology. *Medchemcomm* **2012**, *3* (7), 735. <https://doi.org/10.1039/c2md20079a>.
- (31) Prasher, P.; Sharma, M. Medicinal Chemistry of Pyrophosphate Mimics: A Mini Review. *Drug Dev. Res.* **2022**, *83* (1), 3–15. <https://doi.org/10.1002/ddr.21877>.
- (32) Rye, C. S.; Baell, J. B. Phosphate Isosteres in Medicinal Chemistry. *Curr. Med. Chem.* **2005**, *12* (26), 3127–3141. <https://doi.org/10.2174/092986705774933452>.
- (33) Meanwell, N. A. Synopsis of Some Recent Tactical Application of Bioisosteres in Drug Design. *J. Med. Chem.* **2011**, *54* (8), 2529–2591. <https://doi.org/10.1021/jm1013693>.
- (34) Johnson, T. W.; Gallego, R. A.; Edwards, M. P. Lipophilic Efficiency as an Important Metric in Drug Design. *J. Med. Chem.* **2018**, *61* (15), 6401–6420. <https://doi.org/10.1021/acs.jmedchem.8b00077>.
- (35) Hughes, J. D.; Blagg, J.; Price, D. A.; Bailey, S.; DeCrescenzo, G. A.; Devraj, R. V.; Ellsworth, E.; Fobian, Y. M.; Gibbs, M. E.; Gilles, R. W.; Greene, N.; Huang, E.; Krieger-Burke, T.; Loesel, J.; Wager, T.; Whiteley, L.; Zhang, Y. Physicochemical Drug Properties Associated with in Vivo Toxicological Outcomes. *Bioorg. Med. Chem. Lett.* **2008**, *18* (17), 4872–4875. <https://doi.org/10.1016/j.bmcl.2008.07.071>.
- (36) Peng, J.; Fan, M.; An, C.; Ni, F.; Huang, W.; Luo, J. A Narrative Review of Molecular Mechanism and Therapeutic Effect of Cannabidiol (CBD). *Basic Clin. Pharmacol. Toxicol.* **2022**, *130* (4), 439–456. <https://doi.org/10.1111/bcpt.13710>.
- (37) Cogan, P. S. Regarding the Mechanisms of Promiscuous Cannabinoid Pharmacology: An Elephant Has Entered the Room. *Cannabis Cannabinoid Res.* **2021**, *6* (6), 457–461. <https://doi.org/10.1089/can.2020.0115>.
- (38) Zhou, J.; Jiang, X.; He, S.; Jiang, H.; Feng, F.; Liu, W.; Qu, W.; Sun, H. Rational Design of Multitarget-Directed Ligands: Strategies and Emerging Paradigms. *J. Med. Chem.* **2019**, *62* (20), 8881–8914. <https://doi.org/10.1021/acs.jmedchem.9b00017>.
- (39) Talevi, A. Multi-Target Pharmacology: Possibilities and Limitations of the “Skeleton Key Approach” from a Medicinal Chemist Perspective. *Front. Pharmacol.* **2015**, *6*. <https://doi.org/10.3389/fphar.2015.00205>.

- (40) Kumar, A.; Tiwari, A.; Sharma, A. Changing Paradigm from One Target One Ligand Towards Multi-Target Directed Ligand Design for Key Drug Targets of Alzheimer Disease: An Important Role of In Silico Methods in Multi-Target Directed Ligands Design. *Curr. Neuropharmacol.* **2018**, *16* (6), 726–739. <https://doi.org/10.2174/1570159X16666180315141643>.
- (41) Kiriiri, G. K.; Njogu, P. M.; Mwangi, A. N. Exploring Different Approaches to Improve the Success of Drug Discovery and Development Projects: A Review. *Futur. J. Pharm. Sci.* **2020**, *6* (1), 27. <https://doi.org/10.1186/s43094-020-00047-9>.
- (42) Zsoldos, Z.; Szabo, I.; Szabo, Z.; Peter Johnson, A. Software Tools for Structure Based Rational Drug Design. *J. Mol. Struct. THEOCHEM* **2003**, 666–667, 659–665. <https://doi.org/10.1016/j.theochem.2003.08.105>.
- (43) Montanari, F.; Knasmüller, B.; Kohlbacher, S.; Hillisch, C.; Baierová, C.; Grandits, M.; Ecker, G. F. Vienna LiverTox Workspace—A Set of Machine Learning Models for Prediction of Interactions Profiles of Small Molecules With Transporters Relevant for Regulatory Agencies. *Front. Chem.* **2020**, *7* (January), 1–8. <https://doi.org/10.3389/fchem.2019.00899>.
- (44) Yang, H.; Sun, L.; Li, W.; Liu, G.; Tang, Y. In Silico Prediction of Chemical Toxicity for Drug Design Using Machine Learning Methods and Structural Alerts. *Front. Chem.* **2018**, *6* (February), 1–12. <https://doi.org/10.3389/fchem.2018.00030>.
- (45) Stumpfe, D.; Ripphausen, P.; Bajorath, J. Virtual Compound Screening in Drug Discovery. *Future Med. Chem.* **2012**, *4* (5), 593–602. <https://doi.org/10.1073/pnas.44.2.98>.
- (46) Truchon, J.-F.; Bayly, C. I. Evaluating Virtual Screening Methods: Good and Bad Metrics for the “Early Recognition” Problem. *J. Chem. Inf. Model.* **2007**, *47* (2), 488–508. <https://doi.org/10.1021/ci600426e>.
- (47) Shun, T. Y.; Lazo, J. S.; Sharlow, E. R.; Johnston, P. A. Identifying Actives from HTS Data Sets: Practical Approaches for the Selection of an Appropriate HTS Data-Processing Method and Quality Control Review. *SLAS Discov.* **2011**, *16* (1), 1–14. <https://doi.org/10.1177/10870571110389039>.
- (48) Hevener, K. E.; Zhao, W.; Ball, D. M.; Babaoglu, K.; Qi, J.; White, S. W.; Lee, R. E. Validation of Molecular Docking Programs for Virtual Screening against Dihydropteroate Synthase. *J. Chem. Inf. Model.* **2009**, *49* (2), 444–460. <https://doi.org/10.1021/ci800293n>.
- (49) Fischer, A.; Smieško, M.; Sellner, M.; Lill, M. A. Decision Making in Structure-Based Drug Discovery: Visual Inspection of Docking Results. *J. Med. Chem.* **2021**, *64* (5), 2489–2500. <https://doi.org/10.1021/acs.jmedchem.0c02227>.
- (50) Koshland, D. E. Application of a Theory of Enzyme Specificity to Protein Synthesis. *Proc. Natl. Acad. Sci.* **1958**, *44* (2), 98–104. <https://doi.org/10.1073/pnas.44.2.98>.
- (51) Pagadala, N. S.; Syed, K.; Tuszynski, J. Software for Molecular Docking: A Review. *Biophys. Rev.* **2017**, *9* (2), 91–102. <https://doi.org/10.1007/s12551-016-0247-1>.
- (52) Sherman, W.; Day, T.; Jacobson, M. P.; Friesner, R. A.; Farid, R. Novel Procedure for Modeling Ligand/Receptor Induced Fit Effects. *J. Med. Chem.* **2006**, *49* (2), 534–553. <https://doi.org/10.1021/jm050540c>.
- (53) Desta, I. T.; Porter, K. A.; Xia, B.; Kozakov, D.; Vajda, S. Performance and Its Limits in Rigid Body Protein-Protein Docking. *Structure* **2020**, *28* (9), 1071–1081.e3. <https://doi.org/10.1016/j.str.2020.06.006>.
- (54) García-Nafría, J.; Tate, C. G. Structure Determination of GPCRs: Cryo-EM

- Compared with X-Ray Crystallography. *Biochem. Soc. Trans.* **2021**, *49* (5), 2345–2355. <https://doi.org/10.1042/BST20210431>.
- (55) Gurevich, V.; Gurevich, E. Molecular Mechanisms of GPCR Signaling: A Structural Perspective. *Int. J. Mol. Sci.* **2017**, *18* (12), 2519. <https://doi.org/10.3390/ijms18122519>.
- (56) Ishchenko, A.; Gati, C.; Cherezov, V. Structural Biology of G Protein-Coupled Receptors: New Opportunities from XFELs and CryoEM. *Curr. Opin. Struct. Biol.* **2018**, *51*, 44–52. <https://doi.org/10.1016/j.sbi.2018.03.009>.
- (57) Rosenbaum, D. M.; Rasmussen, S. G. F.; Kobilka, B. K. The Structure and Function of G-Protein-Coupled Receptors. *Nature* **2009**, *459* (7245), 356–363. <https://doi.org/10.1038/nature08144>.
- (58) Wu, M.; Lander, G. C. Present and Emerging Methodologies in Cryo-EM Single-Particle Analysis. *Biophys. J.* **2020**, *119* (7), 1281–1289. <https://doi.org/10.1016/j.bpj.2020.08.027>.
- (59) Nygaard, R.; Kim, J.; Mancina, F. Cryo-Electron Microscopy Analysis of Small Membrane Proteins. *Curr. Opin. Struct. Biol.* **2020**, *64*, 26–33. <https://doi.org/10.1016/j.sbi.2020.05.009>.
- (60) Liang, Y.-L.; Khoshouei, M.; Radjainia, M.; Zhang, Y.; Glukhova, A.; Tarrasch, J.; Thal, D. M.; Furness, S. G. B.; Christopoulos, G.; Coudrat, T.; Danev, R.; Baumeister, W.; Miller, L. J.; Christopoulos, A.; Kobilka, B. K.; Wootten, D.; Skiniotis, G.; Sexton, P. M. Phase-Plate Cryo-EM Structure of a Class B GPCR–G-Protein Complex. *Nature* **2017**, *546* (7656), 118–123. <https://doi.org/10.1038/nature22327>.
- (61) Berman, H. M. The Protein Data Bank. *Nucleic Acids Res.* **2000**, *28* (1), 235–242. <https://doi.org/10.1093/nar/28.1.235>.
- (62) Trindade Maia, R.; de Araújo Campos, M.; Maciel de Moraes Filho, R. Introductory Chapter: Homology Modeling. In *Homology Molecular Modeling - Perspectives and Applications*; IntechOpen, **2021**. <https://doi.org/10.5772/intechopen.95446>.
- (63) Muhammed, M. T.; Aki-Yalcin, E. Homology Modeling in Drug Discovery: Overview, Current Applications, and Future Perspectives. *Chem. Biol. Drug Des.* **2019**, *93* (1), 12–20. <https://doi.org/10.1111/cbdd.13388>.
- (64) McGinnis, S.; Madden, T. L. BLAST: At the Core of a Powerful and Diverse Set of Sequence Analysis Tools. *Nucleic Acids Res.* **2004**, *32* (Web Server), W20–W25. <https://doi.org/10.1093/nar/gkh435>.
- (65) Altschul, S. F.; Gish, W.; Miller, W.; Myers, E. W.; Lipman, D. J. Basic Local Alignment Search Tool. *J. Mol. Biol.* **1990**, *215* (3), 403–410. [https://doi.org/10.1016/S0022-2836\(05\)80360-2](https://doi.org/10.1016/S0022-2836(05)80360-2).
- (66) Sievers, F.; Higgins, D. G. Clustal Omega for Making Accurate Alignments of Many Protein Sequences. *Protein Sci.* **2018**, *27* (1), 135–145. <https://doi.org/10.1002/pro.3290>.
- (67) Jumper, J.; Evans, R.; Pritzel, A.; Green, T.; Figurnov, M.; Ronneberger, O.; Tunyasuvunakool, K.; Bates, R.; Žídek, A.; Potapenko, A.; Bridgland, A.; Meyer, C.; Kohl, S. A. A.; Ballard, A. J.; Cowie, A.; Romera-Paredes, B.; Nikolov, S.; Jain, R.; Adler, J.; Back, T.; Petersen, S.; Reiman, D.; Clancy, E.; Zielinski, M.; Steinegger, M.; Pacholska, M.; Berghammer, T.; Bodenstein, S.; Silver, D.; Vinyals, O.; Senior, A. W.; Kavukcuoglu, K.; Kohli, P.; Hassabis, D. Highly Accurate Protein Structure Prediction with AlphaFold. *Nature* **2021**, *596* (7873), 583–589. <https://doi.org/10.1038/s41586-021-03819-2>.
- (68) Baek, M.; DiMaio, F.; Anishchenko, I.; Dauparas, J.; Ovchinnikov, S.; Lee, G. R.; Wang, J.; Cong, Q.; Kinch, L. N.; Schaeffer, R. D.; Millán, C.; Park, H.; Adams,

- C.; Glassman, C. R.; DeGiovanni, A.; Pereira, J. H.; Rodrigues, A. V.; van Dijk, A. A.; Ebrecht, A. C.; Opperman, D. J.; Sagmeister, T.; Buhlheller, C.; Pavkov-Keller, T.; Rathinaswamy, M. K.; Dalwadi, U.; Yip, C. K.; Burke, J. E.; Garcia, K. C.; Grishin, N. V.; Adams, P. D.; Read, R. J.; Baker, D. Accurate Prediction of Protein Structures and Interactions Using a Three-Track Neural Network. *Science* **2021**, *373* (6557), 871–876. <https://doi.org/10.1126/science.abj8754>.
- (69) Humphreys, I. R.; Pei, J.; Baek, M.; Krishnakumar, A.; Anishchenko, I.; Ovchinnikov, S.; Zhang, J.; Ness, T. J.; Banjade, S.; Bagde, S. R.; Stancheva, V. G.; Li, X.-H.; Liu, K.; Zheng, Z.; Barrero, D. J.; Roy, U.; Kuper, J.; Fernández, I. S.; Szakal, B.; Branzei, D.; Rizo, J.; Kisker, C.; Greene, E. C.; Biggins, S.; Keeney, S.; Miller, E. A.; Fromme, J. C.; Hendrickson, T. L.; Cong, Q.; Baker, D. Computed Structures of Core Eukaryotic Protein Complexes. *Science* **2021**, *374* (6573). <https://doi.org/10.1126/science.abm4805>.
- (70) Thornton, J. M.; Laskowski, R. A.; Borkakoti, N. AlphaFold Heralds a Data-Driven Revolution in Biology and Medicine. *Nat. Med.* **2021**, *27* (10), 1666–1669. <https://doi.org/10.1038/s41591-021-01533-0>.
- (71) Yin, R.; Feng, B. Y.; Varshney, A.; Pierce, B. G. Benchmarking AlphaFold for Protein Complex Modeling Reveals Accuracy Determinants. *Protein Sci.* **2022**, *31* (8). <https://doi.org/10.1002/pro.4379>.
- (72) Bæk, K. T.; Kepp, K. P. Assessment of AlphaFold2 for Human Proteins via Residue Solvent Exposure. *J. Chem. Inf. Model.* **2022**, *62* (14), 3391–3400. <https://doi.org/10.1021/acs.jcim.2c00243>.
- (73) Lee, C.; Su, B.-H.; Tseng, Y. J. Comparative Studies of AlphaFold, RoseTTAFold and Modeller: A Case Study Involving the Use of G-Protein-Coupled Receptors. *Brief. Bioinform.* **2022**, *23* (5). <https://doi.org/10.1093/bib/bbac308>.
- (74) Taylor, C. W.; Tovey, S. C. IP3 Receptors: Toward Understanding Their Activation. *Cold Spring Harb. Perspect. Biol.* **2010**, *2* (12), a004010–a004010. <https://doi.org/10.1101/cshperspect.a004010>.
- (75) Unal, H. Calcium Mobilization Assay to Measure the Activity of Gq-Coupled Receptors. *BIO-PROTOCOL* **2013**, *3* (12). <https://doi.org/10.21769/BioProtoc.790>.
- (76) DeWire, S. M.; Ahn, S.; Lefkowitz, R. J.; Shenoy, S. K. β -Arrestins and Cell Signaling. *Annu. Rev. Physiol.* **2007**, *69* (1), 483–510. <https://doi.org/10.1146/annurev.physiol.69.022405.154749>.
- (77) Gurevich, E. V.; Gurevich, V. V. Arrestins: Ubiquitous Regulators of Cellular Signaling Pathways. *Genome Biol.* **2006**, *7* (9), 236. <https://doi.org/10.1186/gb-2006-7-9-236>.
- (78) Rominger, D. H.; Cowan, C. L.; Gowen-MacDonald, W.; Violin, J. D. Biased Ligands: Pathway Validation for Novel GPCR Therapeutics. *Curr. Opin. Pharmacol.* **2014**, *16*, 108–115. <https://doi.org/10.1016/j.coph.2014.04.002>.
- (79) Van Der Lee, M. M. C.; Bras, M.; Van Koppen, C. J.; Zaman, G. J. R. β -Arrestin Recruitment Assay for the Identification of Agonists of the Sphingosine 1-Phosphate Receptor EDG1. *SLAS Discov.* **2008**, *13* (10), 986–998. <https://doi.org/10.1177/1087057108326144>.
- (80) Giordano, D.; Biancaniello, C.; Argenio, M. A.; Facchiano, A. Drug Design by Pharmacophore and Virtual Screening Approach. *Pharmaceuticals* **2022**, *15* (5), 646. <https://doi.org/10.3390/ph15050646>.
- (81) Peach, M. L.; Nicklaus, M. C. Combining Docking with Pharmacophore Filtering for Improved Virtual Screening. *J. Cheminform.* **2009**, *1* (1), 6. <https://doi.org/10.1186/1758-2946-1-6>.

- (82) Rafehi, M.; Müller, C. E. Tools and Drugs for Uracil Nucleotide-Activated P2Y Receptors. *Pharmacol. Ther.* **2018**, *190*, 24–80. <https://doi.org/10.1016/j.pharmthera.2018.04.002>.
- (83) Rafehi, M.; Burbiel, J. C.; Attah, I. Y.; Abdelrahman, A.; Müller, C. E. Synthesis, Characterization, and in Vitro Evaluation of the Selective P2Y2 Receptor Antagonist AR-C118925. *Purinergic Signal.* **2017**, *13* (1), 89–103. <https://doi.org/10.1007/s11302-016-9542-3>.
- (84) Schoeder, C. T.; Kaleta, M.; Mahardhika, A. B.; Olejarz-Maciej, A.; Łażewska, D.; Kieć-Kononowicz, K.; Müller, C. E. Structure-Activity Relationships of Imidazothiazinones and Analogs as Antagonists of the Cannabinoid-Activated Orphan G Protein-Coupled Receptor GPR18. *Eur. J. Med. Chem.* **2018**, *155*, 381–397. <https://doi.org/10.1016/j.ejmech.2018.05.050>.
- (85) Rempel, V.; Atzler, K.; Behrenswerth, A.; Karcz, T.; Schoeder, C.; Hinz, S.; Kaleta, M.; Thimm, D.; Kiec-Kononowicz, K.; Müller, C. E. Bicyclic Imidazole-4-One Derivatives: A New Class of Antagonists for the Orphan G Protein-Coupled Receptors GPR18 and GPR55. *Med. Chem. Commun.* **2014**, *5* (5), 632–649. <https://doi.org/10.1039/C3MD00394A>.
- (86) Yuan, S.; Chan, H. C. S.; Vogel, H.; Filipek, S.; Stevens, R. C.; Palczewski, K. The Molecular Mechanism of P2Y1 Receptor Activation. *Angew. Chemie Int. Ed.* **2016**, *55* (35), 10331–10335. <https://doi.org/10.1002/anie.201605147>.
- (87) Burnstock, G. Classification and Characterization of Purinoceptors. In *Purines in Cellular Signaling*; Springer New York: New York, NY, **1990**; pp 241–253. https://doi.org/10.1007/978-1-4612-3400-5_36.
- (88) Malik, E. M.; Müller, C. E. Anthraquinones As Pharmacological Tools and Drugs. *Med. Res. Rev.* **2016**, *36* (4), 705–748. <https://doi.org/10.1002/med.21391>.
- (89) Baqi, Y. Anthraquinones as a Privileged Scaffold in Drug Discovery Targeting Nucleotide-Binding Proteins. *Drug Discov. Today* **2016**, *21* (10), 1571–1577. <https://doi.org/10.1016/j.drudis.2016.06.027>.
- (90) El-Tayeb, A.; Griessmeier, K. J.; Müller, C. E. Synthesis and Preliminary Evaluation of [3H]PSB-0413, a Selective Antagonist Radioligand for Platelet P2Y12 Receptors. *Bioorg. Med. Chem. Lett.* **2005**, *15* (24), 5450–5452. <https://doi.org/10.1016/j.bmcl.2005.08.104>.
- (91) Weyler, S.; Baqi, Y.; Hillmann, P.; Kaulich, M.; Hunder, A. M.; Müller, I. A.; Müller, C. E. Combinatorial Synthesis of Anilinoanthraquinone Derivatives and Evaluation as Non-Nucleotide-Derived P2Y2 Receptor Antagonists. *Bioorg. Med. Chem. Lett.* **2008**, *18* (1), 223–227. <https://doi.org/10.1016/j.bmcl.2007.10.082>.
- (92) Baqi, Y.; Atzler, K.; Köse, M.; Glänzel, M.; Müller, C. E. High-Affinity, Non-Nucleotide-Derived Competitive Antagonists of Platelet P2Y12 Receptors. *J. Med. Chem.* **2009**, *52* (12), 3784–3793. <https://doi.org/10.1021/jm9003297>.
- (93) Zhang, D.; Gao, Z.-G.; Zhang, K.; Kiselev, E.; Crane, S.; Wang, J.; Paoletta, S.; Yi, C.; Ma, L.; Zhang, W.; Han, G. W.; Liu, H.; Cherezov, V.; Katritch, V.; Jiang, H.; Stevens, R. C.; Jacobson, K. A.; Zhao, Q.; Wu, B. Two Disparate Ligand-Binding Sites in the Human P2Y1 Receptor. *Nature* **2015**, *520* (7547), 317–321. <https://doi.org/10.1038/nature14287>.
- (94) Hillmann, P.; Ko, G.-Y.; Spinrath, A.; Raulf, A.; von Kügelgen, I.; Wolff, S. C.; Nicholas, R. A.; Kostenis, E.; Höltje, H.-D.; Müller, C. E. Key Determinants of Nucleotide-Activated G Protein-Coupled P2Y2 Receptor Function Revealed by Chemical and Pharmacological Experiments, Mutagenesis and Homology Modeling. *J. Med. Chem.* **2009**, *52* (9), 2762–2775. <https://doi.org/10.1021/jm801442p>.

- (95) Zhang, J.; Zhang, K.; Gao, Z.-G.; Paoletta, S.; Zhang, D.; Han, G. W.; Li, T.; Ma, L.; Zhang, W.; Müller, C. E.; Yang, H.; Jiang, H.; Cherezov, V.; Katritch, V.; Jacobson, K. A.; Stevens, R. C.; Wu, B.; Zhao, Q. Agonist-Bound Structure of the Human P2Y12 Receptor. *Nature* **2014**, *509* (7498), 119–122. <https://doi.org/10.1038/nature13288>.
- (96) Maruoka, H.; Jayasekara, M. P. S.; Barrett, M. O.; Franklin, D. A.; de Castro, S.; Kim, N.; Costanzi, S.; Harden, T. K.; Jacobson, K. A. Pyrimidine Nucleotides with 4-Alkyloxyimino and Terminal Tetrphosphate δ -Ester Modifications as Selective Agonists of the P2Y4 Receptor. *J. Med. Chem.* **2011**, *54* (12), 4018–4033. <https://doi.org/10.1021/jm101591j>.
- (97) Martin, A. L.; Steurer, M. A.; Aronstam, R. S. Constitutive Activity among Orphan Class-A G Protein Coupled Receptors. *PLoS One* **2015**, *10* (9), e0138463. <https://doi.org/10.1371/journal.pone.0138463>.
- (98) Finlay, D. B.; Joseph, W. R.; Grimsey, N. L.; Glass, M. GPR18 Undergoes a High Degree of Constitutive Trafficking but Is Unresponsive to N-Arachidonoyl Glycine. *PeerJ* **2016**, *4*, e1835. <https://doi.org/10.7717/peerj.1835>.
- (99) Sotudeh, N.; Morales, P.; Hurst, D. P.; Lynch, D. L.; Reggio, P. H. Towards A Molecular Understanding of The Cannabinoid Related Orphan Receptor GPR18: A Focus on Its Constitutive Activity. *Int. J. Mol. Sci.* **2019**, *20* (9), 2300. <https://doi.org/10.3390/ijms20092300>.
- (100) Chan, H. C. S.; Li, Y.; Dahoun, T.; Vogel, H.; Yuan, S. New Binding Sites, New Opportunities for GPCR Drug Discovery. *Trends Biochem. Sci.* **2019**, *44* (4), 312–330. <https://doi.org/10.1016/j.tibs.2018.11.011>.
- (101) Hua, T.; Li, X.; Wu, L.; Iliopoulos-Tsoutsouvas, C.; Wang, Y.; Wu, M.; Shen, L.; Brust, C. A.; Nikas, S. P.; Song, F.; Song, X.; Yuan, S.; Sun, Q.; Wu, Y.; Jiang, S.; Grim, T. W.; Benchama, O.; Stahl, E. L.; Zvonok, N.; Zhao, S.; Bohn, L. M.; Makriyannis, A.; Liu, Z.-J. Activation and Signaling Mechanism Revealed by Cannabinoid Receptor-Gi Complex Structures. *Cell* **2020**, *180* (4), 655-665.e18. <https://doi.org/10.1016/j.cell.2020.01.008>.
- (102) Hua, T.; Vemuri, K.; Nikas, S. P.; Laprairie, R. B.; Wu, Y.; Qu, L.; Pu, M.; Korde, A.; Jiang, S.; Ho, J.-H.; Han, G. W.; Ding, K.; Li, X.; Liu, H.; Hanson, M. A.; Zhao, S.; Bohn, L. M.; Makriyannis, A.; Stevens, R. C.; Liu, Z.-J. Crystal Structures of Agonist-Bound Human Cannabinoid Receptor CB1. *Nature* **2017**, *547* (7664), 468–471. <https://doi.org/10.1038/nature23272>.
- (103) Michalik, I.; Kuder, K. J.; Kieć-Kononowicz, K.; Handzlik, J. Structure Prediction, Evaluation, and Validation of GPR18 Lipid Receptor Using Free Programs. *Int. J. Mol. Sci.* **2022**, *23* (14), 7917. <https://doi.org/10.3390/ijms23147917>.
- (104) Conroy, S.; Kindon, N. D.; Glenn, J.; Stoddart, L. A.; Lewis, R. J.; Hill, S. J.; Kellam, B.; Stocks, M. J. Synthesis and Evaluation of the First Fluorescent Antagonists of the Human P2Y2 Receptor Based on AR-C118925. *J. Med. Chem.* **2018**, *61* (7), 3089–3113. <https://doi.org/10.1021/acs.jmedchem.8b00139>.
- (105) Pillaiyar, T.; Funke, M.; Al-Hroub, H.; Weyler, S.; Ivanova, S.; Schlegel, J.; Abdelrahman, A.; Müller, C. E. Design, Synthesis and Biological Evaluation of Suramin-Derived Dual Antagonists of the Proinflammatory G Protein-Coupled Receptors P2Y2 and GPR17. *Eur. J. Med. Chem.* **2020**, *186*, 111789. <https://doi.org/10.1016/j.ejmech.2019.111789>.

12. Acknowledgments

Beginnend mit der Person, ohne die die Anfertigung dieser Doktorarbeit nicht möglich wäre, möchte ich vom ganzen Herzen Prof. Dr. Christa E. Müller danken. Dein Arbeitskreis bot mir die Möglichkeit an, mich als Wissenschaftler und Mensch weiterzuentwickeln. In der heutigen Perspektive stelle ich immer wieder fest, wie unglaublich viel ich in dieser Zeit gelernt habe, was mich beruflich unterstützt und weiterbringt. Es war mir immer eine Freude mit Dir zusammen an den Publikationen zu arbeiten, Ideen auszutauschen, und auch mal einfach nur sich über die Welt in- und außerhalb der Universität auszutauschen. Deine freundliche und menschliche Art hat mich niemals daran zweifeln lassen die Richtige Entscheidung getroffen zu haben.

Zudem möchte ich der gesamten Prüfungskommission für die Bewertung der Arbeit und der damit verbundenen Diskussion danken. Besonderer Dank gilt hierbei Prof. Dr. Finn Hansen, für die Anfertigung des Zweitgutachtens.

Dr. Vigneshwaran Namasivayam möchte ich für die exzellente Betreuung, die hilfreichen Ratschläge, und die wundervolle Zusammenarbeit danken. Seine Motivationsfähigkeit und Einsatz von Druck an den passenden Stellen ermöglichten schließlich diese Arbeit.

Dr. Isaac Attah, Dr. Mohammad Rafehi, Dr. Clara T. Schöder, Dr. Enas Malik, Dr. Younis Baqi, Haneen Al-Hroub und Andhika Mahardhika möchte ich für die äußerst fruchtbare Zusammenarbeit danken, ohne die die präsentierten Publikationen nicht möglich gewesen wären.

Dr. Ralf Mayer, Dr. Dominik Thimm, Dr. Martin Schlesinger und dem gesamten Assistententeam möchte ich für die hervorragende Zusammenarbeit und Organisation des vierten und siebten Semesters danken. Euer Einsatz ermöglicht es, die Lehre am Institut aufrecht zu erhalten und ich würdige die damit verbundene Mühe.

Beate Ponatowski und Tatjana Müller möchte ich für die organisatorische Unterstützung im Vorder- und Hintergrund, ebenso wie für die nette, freundliche Art danken.

Marion Schneider und Christin Vielmuth möchte ich für die helfenden Hände im Probenmanagement danken.

Dem gesamten Arbeitskreis Müller möchte ich für die einzigartige Atmosphäre, die wissenschaftlichen Diskussionen, die Unterstützung im Labor, und die Arbeitskreiseminare danken, in denen ich sehr viel lernen durfte. Besonderer Dank gilt hierbei Dr. Constanze Schmies, die mich in ihrem Labor aufgenommen hat.

Der Deutschen Forschungsgesellschaft und dem Graduiertenkolleg 1873 möchte ich für die finanzielle Unterstützung sowie für die Kostenübernahme bei Kongressreisen innerhalb der Promotion danken.

Meinem Bürokollegen Fabian Balthes, Katja Silbermann, Vladlena Pfeifer und Dr. Mathias Weigt möchte ich für die wunderschönste Zeit am Institut danken. Es war mir immer ein Fest Euch morgens zu begrüßen und Teil Eures Lebens sein zu dürfen.

Den Arbeitskreisen Bendas, Wiese und Hansen möchte ich für die freundliche Aufnahme in ihren Räumen und Stockwerken danken, ebenso wie für die gemeinsamen Mittagessen und Bürounterhaltungen.

Jan Schomaker möchte ich für seine Gelassenheit und seine Geduld während der Promotion danken.

Am Ende möchte ich mich bei meiner Mutter bedanken, die sehr viele Opfer bringen musste, damit ich heute dort stehen kann, wo ich bin.